**UNIVERSIDAD AUTÓNOMA DE MADRID**
**Facultad de Ciencias Físicas**
**Departamento de Física Teórica**

# THE LAMBDA ORIONIS STAR FORMING REGION.

## Spectroscopic Characterization.

**Amelia Bayo Arán**
**Madrid, 2009**

**UNIVERSIDAD AUTÓNOMA DE MADRID**
Facultad de Ciencias Físicas
(Departamento de Física Teórica)

# THE LAMBDA ORIONIS STAR FORMING REGION.

## Spectroscopic Characterization.

Memoria para obtener el título de Doctor en Ciencias Físicas que presenta

**Amelia Bayo Arán**
dirigido por el
**Dr. David Barrado y Navascués**
en el
Laboratorio de Astrofísica Espacial y Física Fundamental
(INSTITUTO NACIONAL DE TÉCNICA AEROESPACIAL)

y supervisado por
**Dr. Carlos Eiroa de San Francisco**

Madrid, Junio 2009

*A Carlos y a mis padres...*
*y a esa particular familia del LAEFF.*

# Agradecimientos

Una vez me dijo un amigo muy sabio que no debería esperar hasta el último momento para escribir los agradecimientos de la tesis; que al fin y al cabo es un trabajo (el realizado durante el doctorado) que uno desarrolla en última instancia para uno mismo, y durante el cual las implicaciones personales son constantes. Por todo esto, él pensaba que los agradecimientos no deberían de escribirse simplemente para “salir del paso” sino para realmente reflejar esa componente humana que toda tesis tiene detrás.

También es cierto que al margen de darme este consejo tan bueno no me advirtió del respeto que impone sentarse frente al papel y ordenar todas las ideas que vienen a la cabeza cuando uno piensa en la gente que ha contrubuido de uno u otro modo al desarrollo de esta tesis. Y el temor más que considerable a olvidarse de nombrar diréctamente a alguien que claramente merezca agradecimiento.

Lógicamente tengo que empezar por mi familia, mis padres, que con su ejemplo me han demostrado que para conseguir lo que realmente uno quiere (una vez que sepa qué es exactamente lo que quiere) “sólo” son necesarios dos ingredientes: la ilusión y el trabajo duro. Gracias por confiar tanto en mí y por apoyarme en decisiones no muy estándares que puede que no encajen en el ideal de vida que la mayoría de los padres tienen para sus hijos. Pero sobre todo gracias por hacerme saber cuado creíais que estaba equivocada con el mismo cariño con el que habéis celebrado mis decisiones acertadas.

La siguiente persona en la ”lista” resulta obvio; gracias Carlos por ser mi compañero, mi mejor amigo, mi crítico más duro, el que conoce todas mis caras y aun así no se mueve de mi lado, quien sabe pintarlo todo de colores.

Gracias también a David, por ser mucho más que mi director, por trasmitir la pasión que sientes por lo que haces, por haber sabido sacar lo mejor de mí fomentando al mismo tiempo mi independencia y porque claramente sin tí esta tesis no existiría.

Gracias a este grupo tan completo y divertido que ha sabido ensamblar David: María, Nuria, Aina, Pablo y Belén. María, mi hermana desde hace casi cinco años; gracias por las charlas más interesantes que he tenido en este tiempo tanto de ciencia como de la vida; gracias por ser una compañera de despacho excepcional y una persona de la que aprender a cómo tomarse las cosas con buen ánimo. Gracias Nuria por ser tan especial, por todo el entusiasmo que trasmites, por contestar a mis preguntas con la sencillez del que entiende lo realmente importante de las cosas. Gracias Aina y Belén por tener siempre comentarios positivos, por valorar mi optinión y mis preguntas y por tener siempre que lo he necesitado un momento para mi. Gracias Pablo por inyectar una dosis de inocencia e ilusión que a veces uno pierde cuando se agobia con fechas límite y demás aspectos que no son tan importantes cuando uno recuerda como bien dices que nuestro trabajo es muy bonito.

Gracias a Benjamín por tantas cosas... porque combinas un corazón enorme con una sabiduría reposada, eres el maestro que todos deberíamos encontrarnos en la escuela y luego de

adultos, para poder aprovechar todas tus cualidades. Gracias principalmente por haberme dado ejemplo para ser mejor persona.

Gracias a todos los que hicísteis del LAEFF un sitio tan especial (Bruno, Concha, Itziar, Daniel y tantos otros) y a los que así lo seguís manteniendo (Margie, Ignacio, Raúl, Sergio, Carlos, Albert, Miriam, Santi, Mauro, Iñaki, Julia, María, Enrique, Miguel, Daid, Jorge, no quisera dejarme a nadie). Cuando uno llega a trabajar aqui por primera vez bastan unas horas para que se sienta relajado y con la confianza de pedir ayuda en cualquier momento... y eso, se agradece mucho.

A mi parecer, durante la tesis, especialmente al final de la misma, uno necesita que la gente de su alrededor sea paciente y, en cierto modo, le mimen. No puedo pasar por alto el apoyo que mis amigas “del cole” me han dado todo este tiempo. Muchas gracias Lara, Esther y Marian, por ser mi familia en Madrid.

Por último, y con la pena y la seguridad de que olvido dar las gracias a gente a la que debiera; muchas gracias a la gente que ha hecho que mis dos visitas de trabajo a Pasadena se hayan convertido probablemente en dos de las mejores experiencias vitales que he tenido. En especial muchas gracias a John por lo tantísimo que he aprendido de él; por enseñarme con su ejemplo que en este trabajo hay que ser concienzudo y estar muy seguro de poder explicar bien todas las conclusiones a las que uno llegue. Muchas gracias a Sylvain, porque desde el primer momento me brindó su ayuda y por ser una de esas personas que sabes que te acompañarán para toda la vida.

Amelia Bayo Arán,

14 de Junio de 2009

# List of contents

# List of Figures

# List of Tables

# Resumen

La región de formación estelar $\lambda$ Orionis, situada en la cabeza de Orión, forma parte de la nube molecular de Orión pero situado a unos 15 grados al Norte del centro del complejo (con una declinación $\sim 10^o$). La estrella $\lambda$ Ori es el miembro más brillante del cúmulo central Collinder 69. Éste es un cúmulo abierto compacto y bien definido. Otras dos asociaciones algo menores se encuentran situadas cerca de Collinder 69 y están asociados a las nubes moleculares Barnard 30 y Barnard 35.

En el infrarrojo medio y a 21 cm, $\lambda$ Ori marca el centro de burbuja circular de cuatro grados de diámetro formada por polvo y gas y que se cree que es el resultado de los vientos estelares procedentes de los miembros más masivos del cúmulo o por una explosión de supernova cuyo progenitor habría sido el miembro más masivo del cúmulo.

Las propiedades de estas tres asociaciones son muy diversas. Collinder 69 es un cúmulo muy rico con una estrella de tipo espectral O (la propia $\lambda$ Ori – O8III), aproximadamente una docena de estrellas tipo B y un buen número de estrellas de baja masa y enanas marrones; sin embargo Barnard 30 y Barnard 35 parecen estar formados exclusivamente de estrellas de baja masa. Además la frecuencia de estrellas TTauri Clásicas en las asociaciones en torno a Barnard 30 y Barnard 35 parece ser mucho más elevada que la de Collinder 69. Así, la región de formación estelar $\lambda$ Ori conforma el perfecto laboratorio para estudiar los procesos formación estelar.

La motivación de esta tesis es estudiar y comparar las propiedades de los miembros individuales de estas tres regiones, en particular la evolución de los discos y su dependencia con la masa estelar.

Hemos recopilado una gran variedad de observaciones espectroscópicas a muy diferentes resoluciones que nos han permitido establecer la pertenencia al cúmulo de un gran número de fuentes y el estudio detallado de las propiedades de las fuentes que albergan discos, así como de aquellas (mas evolucionadas) que ya carecen de ellos. Hemos estudiado objetos desde Clase I/II (cuando la protoestrella central está rodeada de un disco y embebida en una envoltura de gas y polvo)) a Clase II (CTTs, en las que la envoltura ya ha desaparecido pero el disco de acrecimiento aun perdura), y Clase III (WTTs, cuando el disco ya ha desaparecido). Al comparar estos resultados para las distintas asociaciones queremos abordar cuestiones que pudieran tener dependencia con el entorno como la frecuencia de discos y la estructura radial de los mismos en función del entorno.

# Abstract

The Lambda Orionis Star Forming Region is part of the Orion molecular cloud complex, it is located about 15 degree north of the center of the complex ($\delta \sim 10$ degrees). $\lambda$ Ori, itself is the brightest member of Collinder 69, a well-defined, compact open cluster at the center of the star forming region. Two other already identified and somewhat smaller clusters lie near Collinder 69 and are associated with the Barnard 30 and Barnard 35 molecular clouds.

At mid-infrared wavelengths and 21 cm, $\lambda$ Ori marks the center of a four degree diameter circular shell of gas and dust thought to be the result of winds from the high mass stars in the cluster or from a supernova whose progenitor was the highest mass member of the cluster.

The properties of these three associations are quite diverse. Collinder 69 is quite rich, with one O star ($\lambda$ Ori itself) and of order a dozen B stars and a well-populated sequence of low-mass stars and brown dwarfs whereas the Barnard 30 and Barnard 35 associations appear to be almost entirely composed of low-mass stars. Moreover, the fraction of Classical TTauri low-mass stars in the Barnard 30 and Barnard 35 clusters seems to be much higher than that of Collinder 69. Thus, we believe that the $\lambda$ Ori star-forming region can serve as a valuable testbed for star formation studies.

It is the comparative properties of the individual members of these three regions what leads the work presented here. In particular, the evolution of the disks and its dependence with the stellar mass.

We have gathered a wide variety of spectroscopic observations with very different resolutions. These spectra have allowed us to stablish membership to the various associations and the detailed study of the properties of sources harbouring disks as well as those (more evolved) that have cleared them. We have analyzed spectra from sources at different evolutionary stages; from Class I/II (when the central protostar is surrounded by a disk and still embedded within a dust/gas envelope), to Class II (or Classical T Tauri stars, where the envelope has disappeared but the accretion disk remains), and Class III (weak line T Tauri stars, when only a fast rotating star remains). By comparing these results for the three associations, we aim to address the questions of the frequency and radial structure of circumstellar disks as a function of environment.

# Chapter 1

# Introduction

*"...one is forced to wonder where it will lead to,*
*if everyone who works on stellar spectra*
*also introduces a new classification..."*
(Nils Duner, 1899).

## 1.1 Star Formation Theory

The formation of stars and planetary systems constitutes one of the basic problems of modern Astrophysics. The development of new instrumentation and observational techniques has provided a large body of observational data, allowing a deeper understanding of earlier stages of the evolution of stars and planets. Nevertheless, there still remain many open questions.

Whilst there is a generally accepted evolutionary scheme (see Section 1.1.1) for the formation of low mass stars (more numerous than high-mass stars, perhaps with longer formation phases, and closer parent molecular clouds), the analogue processes involving both ends of the Initial Mass Function (hereafter IMF) are not well understood yet.

The discovery of the first brown dwarfs in 1995 (very low mass objects characterized by the lack of stable hydrogen burning in their interior, typically masses below $0.072 M_{\odot}$) led to a debate on the formation mechanism of this type of objects that is still open nowadays. Padoan & Nordlund (2002) argued that brown dwarfs form via "turbulent fragmentation" (the same mechanism as more massive stars), while Reipurth & Clarke (2001) suggested that brown dwarfs may be stellar embryos ejected from newborn multiple systems before they accreted enough mass to start hydrogen burning (in this model, the truncation of the disks is explained by dynamical interactions). Studies of disk accretion, rotation and activity (and the relationship between classic indicators of activity such as H$\alpha$ and these phenomena) in young brown dwarfs could help to distinguish between the former scenarios.

On the other edge of the mass spectrum, high-mass star formation plays a very important role from the perspective of the momentum, mass, and energy input to the interstellar medium by

such stars (see Massey 2003 and Bromm & Larson 2004); they take part in both the heating and cooling of the ISM but the question of their mechanism of formation remains open (from an observational point of view, the high dust extinction makes it difficult to observe high-mass stars during critical early formation phases, besides, they are rare and evolve quickly). Do massive stars form similarly to low-mass stars but with enhanced accretion rates, or are there different processes taking place, like the coalescence and merging of intermediate-mass protostars in the very center of star-forming clusters?

### 1.1.1 Low-mass Star Formation and Young Stellar Objects classification

In the current paradigm, stars are born within molecular clouds, which are accumulations of gas and dust. These clouds are initially supported against gravitational collapse by a combination of thermal, magnetic, and turbulent pressures (Shu et al. 1987; Mouschovias 1991). Nevertheless, molecular clouds can fragment in smaller and denser cores, where the presence of gravitational instabilities yields a collapse of the cloud material (Shu et al. 1987, and references therein).

The processes that take place after the initial gravitational collapse are very likely to depend on the mass of the system. Focussing on the low-mass regime; the gas of molecular clouds contains an initial amount of angular momentum (Goodman 1993), which must be conserved during the collapse of the core. Due to this conservative phenomenon, the infalling matter encounters a centrifugal barrier in a plane perpendicular to the angular momentum vector, and the cloud material tends to be deposited on a that plane, yielding the formation of a rotating disk and a central protostar (Terebey et al. 1984; Shu et al. 1987). After the collapse phase, where most of the infalling material is deposited onto the disk, an accretion phase begins, in which part of the disk mass is accreted onto the central protostar. This step requires both the transfer of mechanical energy (to keep the stability in a Keplerian disk when material fall onto the protostar) and the transfer of angular momentum (to make possible that disk material falls onto orbits located closer to the protostar). See an schematic overview of the complete process of formation of low-mass stars and a time scale estimation of the different phases in Fig. 1.1

This thesis concerns the study of the spectroscopic properties of Young Stellar Objects (hereafter YSOs) at different evolutionary states. The first attempt to empirically study the nature of youngest/embedded low-mass YSOs relied on infrared observations. The dust conforming the surrounding envelope reprocesses the energy emitted by the central pre-stellar object, and therefore a significant fraction of their luminosity is emitted in the infrared.

Lada (1987) and Adams et al. (1987) proposed a classification scheme of low-mass YSOs based on the morphology of their Spectral Energy Distributions (SEDs) in contrast with blackbodies at these long wavelengths (between $\lambda$ = 2.2 and 100 $\mu$m). The observed slope $\alpha_{IR} = d\log(\lambda F_\lambda)/d\log(lambda)$ was interpreted as a proxy of the evolutionary status of the object under study from Class I (deeply embedded objects) to Class III objects (young- or pre-main sequence

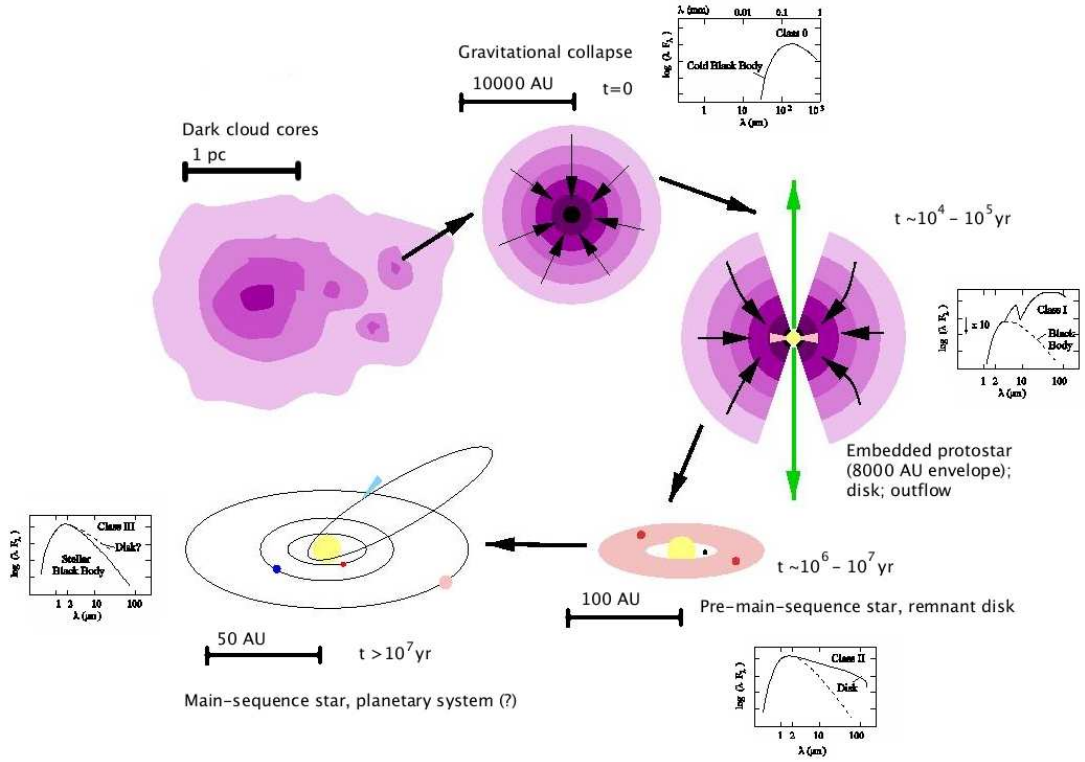


**Figure 1.1**: Evolution from Pre-Stellar Cores to Class III sources. On the sides of the cartoon (after Shu et al. 1987), we have represented typical SEDs of the objects at different stages of their evolution (Lada 1987; Andre & Montmerle 1994).

stars).

Several years later, Andre et al. (1993) extended this classification scheme to even younger sources. They proposed to study the relation of the bolometric luminosity of the embedded YSOs with their submillimeter and millimeter continuum emission ($L_{smm}/L_{bol}$ and $L_{mm}/L_{bol}$) as a proxy for the ratio of stellar and envelope masses ($M_{env}/M_*$, which decreases with protostellar age). The new category of sources, the Class 0 (with largest $L_{smm}/L_{bol}$ and $L_{mm}/L_{bol}$ ratios), would correspond therefore to the youngest protostars, and might have a phase lifetime of $\sim 10^4$ years according to Andre & Montmerle (1994).

In this context, the definition of the Bolometric Temperature ($T_{bol}$) by Myers & Ladd (1993); the temperature of a blackbody having the same mean frequency as the observed SED; allowed a parametrization of this evolutionary scheme. Chen et al. (1995) proposed the following ranges of $T_{bol}$ for each evolutionary stage: $T_{bol} < 70$ K for Class 0 sources (characterized by the presence of powerful and collimated molecular outflows and compact centimeter radiocontinuum emission, Margulis & Snell 1989 and Bontemps et al. 1996), $70 < T_{bol} < 650$ K for Class I

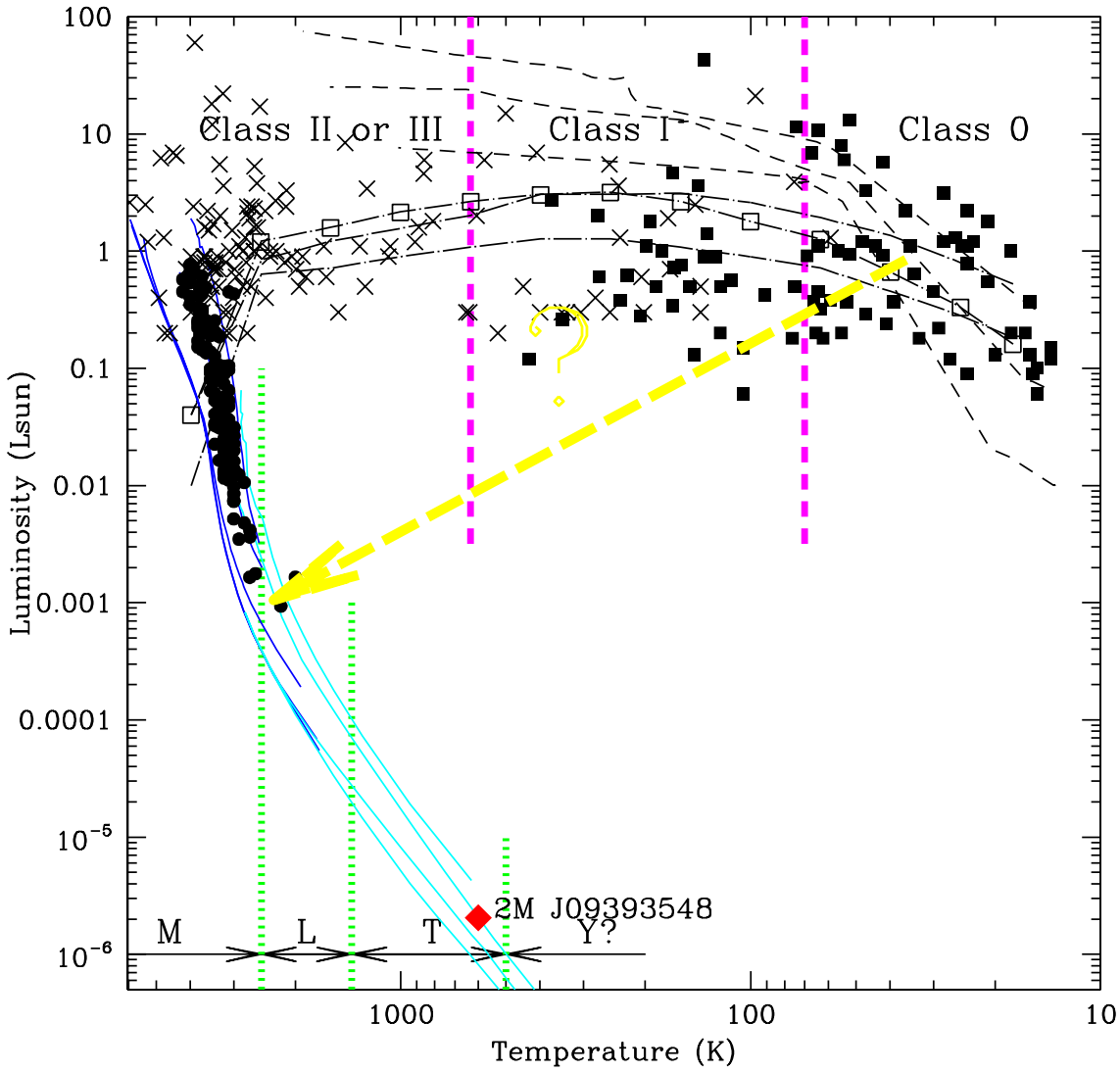


**Figure 1.2**: Bolometric luminosity vs. temperature ($T_{bol}$ or $T_{eff}$) diagram after Young et al. (2005); Dunham et al. (2008). The 50 sources compiled by Dunham et al. (2008) showing some evidence for being embedded low luminosity sources, are shown as filled black squares. The black dot-dashed lines show the evolutionary tracks for the three models considered by Young et al. (2005). The short-dashed black lines show the evolutionary tracks for three models considered by Myers et al. (1998). The crosses correspond to Taurus members and the vertical magenta dashed lines show the Class 0–I and Class I–II $T_{bol}$ boundaries from Chen et al. (1995). Members from the 5 Myr Collinder 69 cluster are included as solid circles (Barrado y Navascués et al. 2007b), as well as isochrones from Baraffe et al. (1998), blue lines. The red diamond coresponds to the coldest and least luminous brown dwarf binary candidate by Burgasser et al. (2008).

sources (invisible in the optical, with less powerful and collimated outflows than the previous phase and faint near-infrared emission associated to hotter dust closer to the central protostar), $650 < T_{bol} < 2800$ K for Class II sources (characterized by showing near-IR emission and H$\alpha$ emission lines) and higher temperatures for Class III sources (post- T Tauri stars where the gas of theirs disks has already been disipated almos completely). See Fig. 1.1 for a representation of the typical SEDs associated to each of these classes, and Fig 1.2 for a $\log(L_{bol})$ vs. $\log(T_{bol})$ evolutionary diagram for embedded objects (Myers & Ladd 1993).

## 1.2 Stellar Spectral Classification

Classification is an important first step in the characterization of any population. It enables us to study the global properties of a group of similar objects and generalize to larger, and perhaps undetected, members. A fundamental attribute of astronomical classification is that it is based on observations; i.e., the way objects appear morphologically, photometrically, or spectroscopically.

Stellar spectral classification has been in practice for nearly 150 years, and calibration of spectral classes to temperature and luminosity scales has provided both crucial insight into the internal physics of stars, their history and evolution, and into the properties of the Galaxy and extragalactic systems.

The classical stellar sequence of Morgan et al. (1943), the most widely accepted classification scheme, originates from the temperature-based sequence first used in the Henry Draper catalog (Pickering 1890), and luminosity discriminants initially identified by Maury & Pickering (1897). It extends the main sequence from hot O–type stars to cool M dwarfs. With the advent of more sensitive optical and near-infrared detectors and large-scale surveys, including the Two Micron All Sky Survey (Skrutskie et al. 2006, hereafter 2MASS), the Sloan Digital Sky Survey (York et al. 2000, hereafter SDSS), and the Deep Near-Infrared Survey of the Southern Sky (Epchtein et al. 1999, hereafter DENIS), cooler stars and brown dwarfs have now been identified. As a result, two new spectral classes have been introduced, the L (Kirkpatrick et al. 1999 and Martín et al. 1999) and T (Burgasser 2002; Burgasser et al. 2002) classes, which are extensions of the main stellar sequence into the brown dwarf regime.

This Thesis is focused on the study of the coolest candidate members of the Lambda Orionis Star Forming Region. These objects (photometrically selected) are expected to have spectral types in the range from M dwarfs to even T dwarfs (although some K dwarfs are also present in our sample). Therefore we present below a description of the typical features that characterize each of these spectral types:

- M dwarfs:

  The most obvious features in the optical spectra of these sources are the molecular bands of TiO (and VO for the latest types, M7 and later) and the atomic lines of Ca II, Na I, and K I.

In the case of M dwarfs, the Ca II triplet is much weaker than in M supergiant spectra but on the other hand, they present much stronger lines of the Na I and K I doublets (Kirkpatrick et al. 1999). The latter, at 0.7665 and 0.7699 $\mu$m, shows two trends, broadening with later spectral type down to M7/7.5, but becoming narrower (lower equivalent widths) at spectral types M8 and M9.

On the other hand, the spectra in the near-infrared domain are dominated by deep broad absorption bands of $H_2O$ (particularly at 1.4 and 1.85 $\mu$m), but have many other strong features, both molecular and atomic. The spectral identifications shown in Fig. 1.3 have been extracted from Jones et al. (1994). There are some features that scale with temperature (Jones et al. 1994), such as the water bandhead at 1.34$\mu$m, the 2.05-2.15 $\mu$m gradient and the CO bandhead at 2.29 $\mu$m; the FeH at 0.99 $\mu$m and VO at 1.2 $\mu$m. The fact that water vapour in the Earth's atmosphere also contributes with a substantial absorption at these wavelengths hampers the analysis to some extent. However, the higher temperatures in the stellar atmospheres mean that the associated steam bands are broader than the terrestrial absorption, so the wings are accessible for measurement (and will be used in Section 3.4.1 with infrared spectral typing purposes). The loci of the deep telluric atmospheric absorptions in Fig. 1.3 are labelled with an asterisk, these parts of the spectrum have been flattened for graphical purpouses. Other features are gravity sensitive such as the K I 1.169 and 1.177 $\mu$m and 1.244 and 1.252 $\mu$m doublets, and Na I 1.138 and 1.140 $\mu$m (Reid et al. 2001).

M dwarfs cover an effective temperature ($T_{\rm eff}$) range from $\sim$ 4500 K down to $\sim$ 2000 K (Casagrande et al. 2008), and although they are among the most common stars in our stellar neighbourhood, they are also among the least understood; in particular, the evolution of the angular momentum and their internal structures are still open questions.

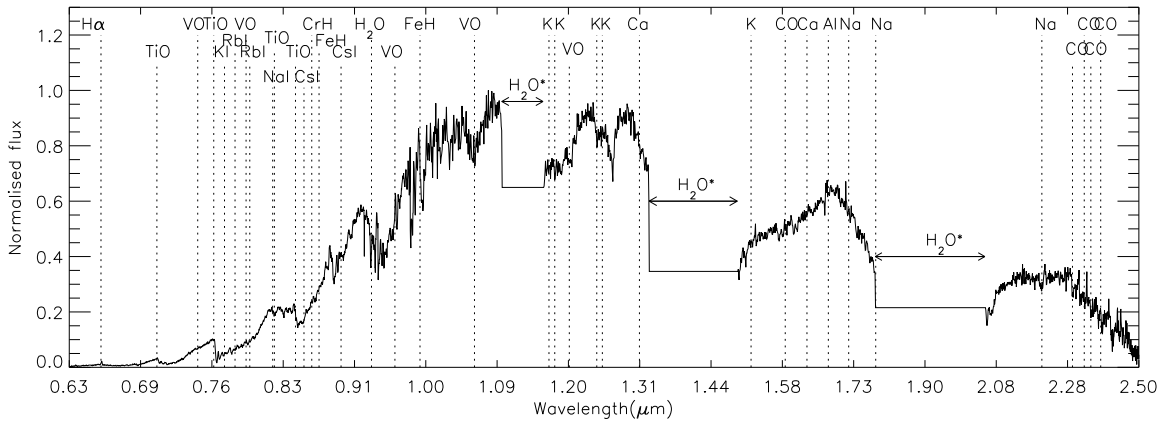


**Figure 1.3**: Spectral identifications for a M dwarf member of the Chamaleon I Dark Cloud.

- L dwarfs:

The L spectral class is comprised of a mix of stars and brown dwarfs (depending on the age). This class covers a $T_{\rm eff}$ range from ~ 2000–2200 K down to ~ 1300–1700 K (Kirkpatrick et al. 1999, 2000; Basri et al. 2000; Leggett et al. 2001), corresponding to luminosities $L_{bol}$ ~ $4 \times 10^{-4}$ to $3 \times 10^{-5}$ $L_{\odot}$ (Burrows et al. 1997).

In the optical, the spectra are characterized by weakening bands of TiO and VO (dominant features in previously described M dwarfs, become progressively weaker still detectable in L3 dwarfs and mostly disappear by L5-6) and strengthening bands of FeH, CrH, CaH, as the dominant molecular features. Those bands reach maximum strengths at mid-L types, before weakening in the latest L dwarfs, where $H_2O$ provides the most prominent molecular absorption at ~9300 Å.

As the molecular bands decrease in strength, a number of atomic lines become significantly more prominent. The resonance lines due to Rb (0.7800/0.7948 $\mu$m) and Cs (0.8521/0.8943 $\mu$m) are discernible in the early L dwarfs, and grow in strength throughout the sequence (Kirkpatrick et al. 1999; Martín et al. 1999). The same tendency has been observed for the K I doublet at 0.7665 and 0.7699 $\mu$m. As stated before, these lines become narrower at spectral types M8 and M9. However, that trend reverses between M9.5 and L0, and the lines broaden substantially until, by spectral type L5, the separate cores are indistinguishable (Reid et al. 2000).

Li I (doublet at 0.6708 $\mu$m) is also evident in L dwarfs (and M dwarfs) with masses below 0.065 $M_{\odot}$ (see Rebolo et al. 1992 for a detailed explanation of the *lithium test*).

As stated before, classification schemes for L dwarfs in the red optical have been defined by Kirkpatrick et al. (1999); Martín et al. (1999), see Fig. 1.4.

The near-infrared spectra of these objects show similarities with those of M dwarfs; they also are dominated by broad absorption bands of $H_2O$ and CO, with the water bands increasing in strength through spectral type L.

The main atomic line features are due to neutral Na (1.14 $\mu$m) and K (two doublets at 1.169/1.177 $\mu$m and 1.244/1.253 $\mu$m). The Na I line shows relatively little variation in strength with increasing spectral type from M8 to at least L5. The 1.17 $\mu$m K lines have individual equivalent widths rising steadely from M8 to L5, before dropping sharply in strength in the later L dwarfs. The 1.25 $\mu$m doublet is somewhat stronger, but shows identical behaviour (Reid et al. 2000).

- T dwarfs:

  As brown dwarfs cool through spectral types M and L, their spectra change reflecting differences in the composition of their atmospheres. The most dramatic change at near-infrared wavelengths occurs at temperatures between 1400 and 1200 K, where methane takes over from carbon monoxide as the dominant repository of carbon. In this very cool domain, the

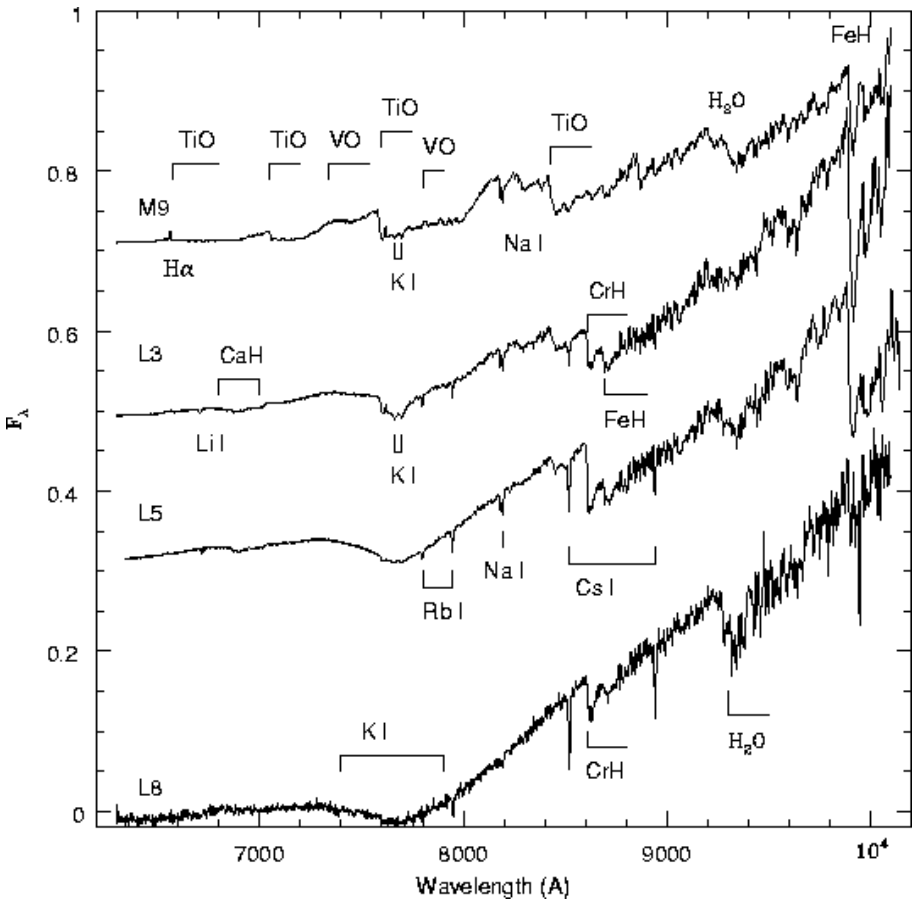


**Figure 1.4**: Optical spectral sequence of L dwarf types (Kirkpatrick et al. 1999, 2000).

T spectral class is comprised of brown dwarfs that exhibit $CH_4$ absorption bands between 1.0 and 2.2 $\mu$m (see 1.5).

The presence of the methane bands, broad $H_2O$ features, and collision-induced (CIA) $H_2$ absorption radically alter the spectral energy distributions of T dwarfs, and near-infrared colours become increasingly blue (J-Ks ~ 0 ±0.1 mag, similar to those of A stars) as compared to L dwarfs. These distinctions led Kirkpatrick et al. (1999) to propose a second class, which at that time was solely occupied by the first unequivocal brown dwarf, Gliese 229B (Nakajima et al. 1995; Oppenheimer et al. 1995).

A series of flux ratios designed to measure the strengths of the more prominent near-infrared features, notably $CH_4$ and $H_2O$ have been devised independently by Burgasser (2002) and Geballe et al. (2002). The two T dwarf spectral classification schemes derived from those indices are almost identical.

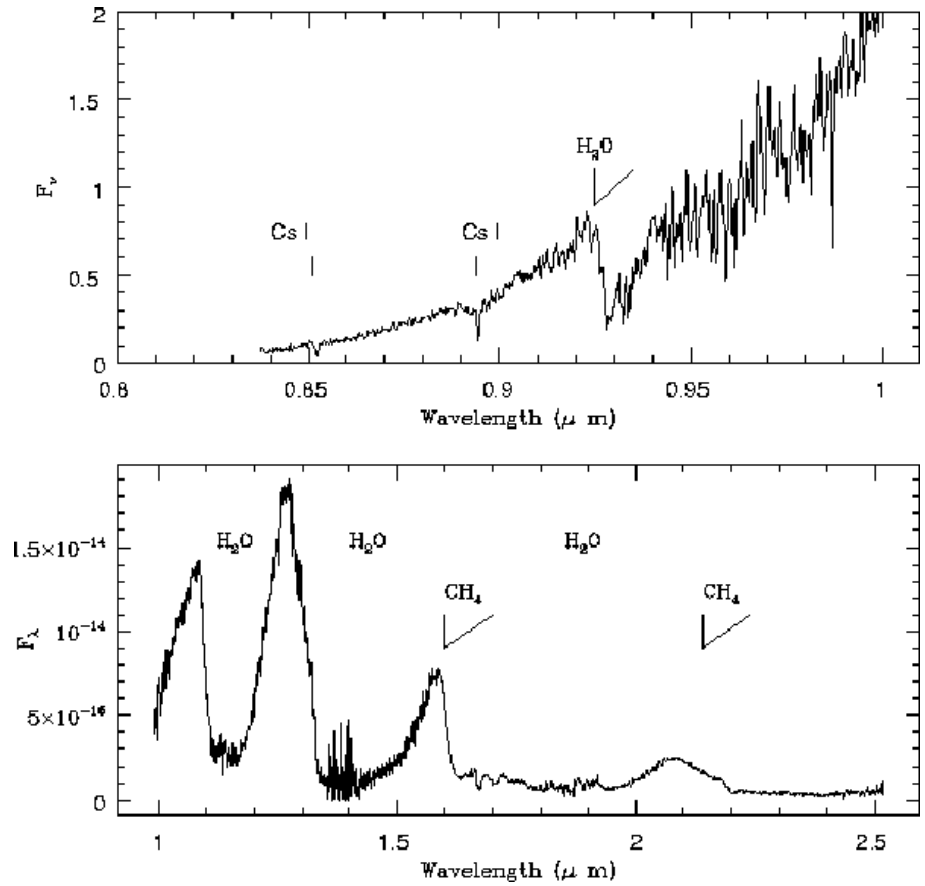


**Figure 1.5**: The optical/near-infrared spectrum of Gl 229B (from Oppenheimer et al. 1995).

## 1.3 The Lambda Orionis Star Forming Region

One of the most interesting Star Forming Regions (SFR) is associated to the O8III star $\lambda$ Orionis (located at ~400 pc, Murdin & Penston 1977), the head of the Orion giant. It comprises both recently formed stars from 0.2 $M_\odot$ to 24 $M_\odot$ (beloging to the central cluster Collinder 69) and dark clouds actively forming stars (Barnard 30 and Barnard 35). Although due to its properties (morphology, distance, reddening, size), the Lambda Orionis Star Forming Region (LOSFR) seems to be an ideal laboratory to test star formation theories, until recently, it had not been very well studied.

The $\lambda$ Orionis OB association lies at $\sim 15^\circ$ North of the center of the complex inside a fossil giant molecular cloud, and it anchors a tight knot of 11 OB stars, centered within a 40 pc diameter ring of dense molecular gas and dust (detected by Zhang et al. 1989 making use of the Infrared Astronomical Satellite, IRAS, see Fig 1.6 for a false colour image created from the IRAS images). This ring is complementary to a shell of neutral hydrogen discovered previously by Wade (1958). Estimates for the total mass of the ring are of the order $10^4 M_\odot$.

At the begining of the 80s, Duerr et al. (1982) carried out an H$\alpha$ emission survey identifying three stellar clusters centered around the dark clouds Barnard 30 and Barnard 35 (located whithin this ring and separated from $\lambda$ Ori by 2.°2 and 2.°7), and $\lambda$ Ori, respectively. Those clusters were later confirmed from a statistical point of view by Gomez & Lada (1998). These three regions have been studied intensively by our group during the last five years (see Fig 1.6 for an scheme of their location and Fig 1.7 for a clear view of the abundant H$\alpha$ emission detected in the Region). Collinder 69 is a well-defined, compact open cluster. It is quite rich, with one O star ($\lambda$ Ori itself) and of order a dozen B stars (Duerr et al. 1982) and a well-populated sequence of low-mass stars and brown dwarfs whereas Barnard 30 and Barnard 35 are somewhat smaller and mainly formed by low mass stars.

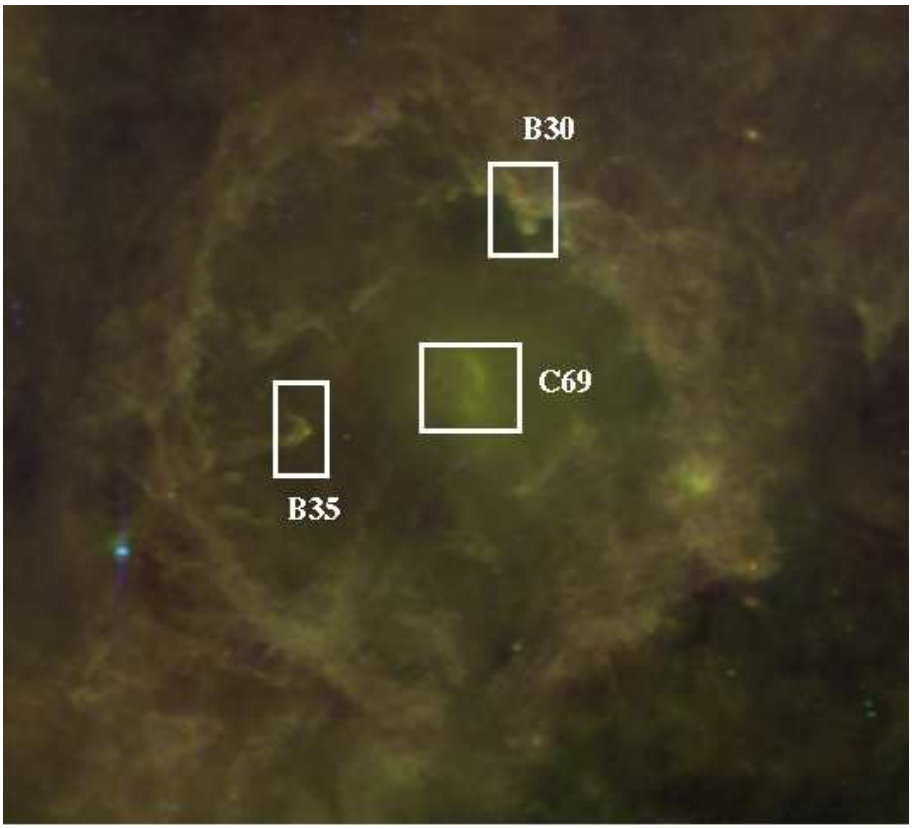


**Figure 1.6**: IRAS false colour image of the Lambda Orionis Star Formin Region (100 $\mu$m red, 60 $\mu$m green, 12 $\mu$m blue). The loci of the three regions studied in this thesis have been highlighted.

## 1.4 Previous Observations

Prior to our study, several groups have published different studies focused on a variety of aspects of the SFR, such as the initial discovery, studies on the distance, an H$\alpha$ survey, analysis of

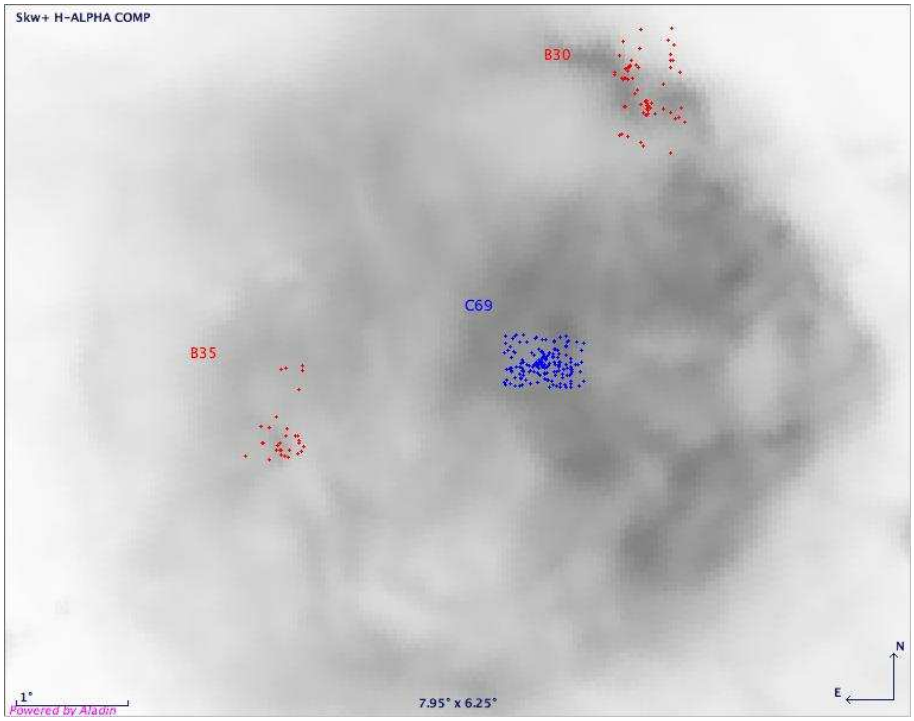


**Figure 1.7**: An image of the Lambda Orionis Star Forming Region taken with a narrow filter cetered in H$\alpha$. The positions of the candidates members of Colinder 69, Barnard 30 and Barnard 35 studied in this thesis have been highlighted with blue and red dots. The image has been taken from the "H-alpha Full Sky Map" (see Finkbeiner 2003); a composite of the Virginia Tech Spectral line Survey (VTSS) in the north and the Southern H-Alpha Sky Survey Atlas (SHASSA) in the south with a pixel scale of 2.5' and a resolution (FWHM) of 6'. Note the complex structure seen in H$\alpha$ due to a large extent to the ionizan front induced bu Lambda Orionis itself.

the IRAS data and photometric and spectrospic searches. Regarding photometry and spectroscopy, a summary follows:

- Photometry: Morales-Calderón (2008), Dolan & Mathieu (1999, 2001, 2002) among others. In this last set of studies, the authors collected moderately deep photometry (VRI filters) reaching $I_C = 14.5$ (about 0.5 $M_\odot$ for 5 Myr age) in an area about 8 squared degrees centered on the OB association, discovering a significant population of low-mass stellar members.

- Spectroscopy: The first comprehensive surveys for PMS stars in the $\lambda$Ori region were based on H$\alpha$ objective prism surveys. As an example, Duerr et al. (1982) surveyed about 100 square degrees centered on $\lambda$Ori.

  More spatially limited spectroscopic surveys have detected a few H$\alpha$ emission stars not previously found in the objective prism surveys. Dolan & Mathieu (2001) found ~25 new stars with large H$\alpha$ equivalent widths and strong H$\alpha$ emission has also been detected from can-

didate substellar members in the very deep survey for young stars of Barrado y Navascués et al. (2004b).

Other surveys with the goal to study youth (based on the presence of Li I absorption line at 6707 Å for late-type stars) and kinematics (via radial velocities determination) of the possble members of the Lambda Orionis Star forming region have been carried out. Dolan & Mathieu (2001) surveyed ~3600 stars located radially in the LOSFR; and based on the lithium absorption and radial velocities of the sources in their sample, thay concluded that the stars showing strong Li I absorption were kinematically associated with a mean velocity typical of the Orion association.

More recently, Sacco et al. (2008) and Maxted et al. (2008), performed parallel studies of members of the $\sigma$ Ori and $\lambda$ Ori clusters (both simmilar clusters the first one thoughtly studied by González Hernández et al. 2008; Zapatero Osorio et al. 2008; Scholz et al. 2009; Caballero et al. 2009; Bouy et al. 2009b, and references therein). With very high resolution optical spectroscopy (different instrumental set-ups and slightly different sample of candidates), they derived radial velocities and combined that information with the study of Li I absorption and H$\alpha$ emission to establish membership to the clusters. Whilst the Sacco et al. (2008) study was mainly focused on the comparison of the properties of the accretion and disk population on both clusters (concluding that the differences might be caused either by the high–mass stars present in the $\lambda$ Ori cluster or differences in age). Maxted et al. (2008) focused on the determination of the fraction of spectroscopic binaries in the young very low mass domain (a key issue when trying to understand which physical mechanism rules the formation of these very low mass stars); which was found to be significantly different from the one estimated for more massive stars in the same Star Forming Region.

Further and more detailed discussion on the results achieved with these surveys will be provided in Chapters 2, 3 and 4.

The distance derived by Dolan & Mathieu (1999) for the LOSFR is 450± 50 pc; larger than both the distance derived by Murdin & Penston (1977) and the value derived from Hipparcos (Perryman et al. 1997) for the five stars in the central area, 380± 30 pc. According to Dolan & Mathieu (2002), the turnoff age for the massive stars is of order 6 Myr (see also Murdin & Penston 1977 for another age determination based on the massive stars, 4 Myr), although the star formation history might be more complex as suggested by Dolan & Mathieu (2001).

According to Dolan & Mathieu, the star formation rate was relatively slow for a few million years, then accelerated up until about 1 to 2 Myr ago. At that point, the highest mass star in Collinder 69 became a supernova and dispersed the molecular gas in the immediate vicinity of Collinder 69, and partially disrupted the nearby molecular clouds associated with Barnard 35 and to a lesser extent Barnard 30. The ring of gas and dust is then the current location of the swept up gas from the SN and O star winds. Over the lifetime of the Collinder 69 cluster (but particularly

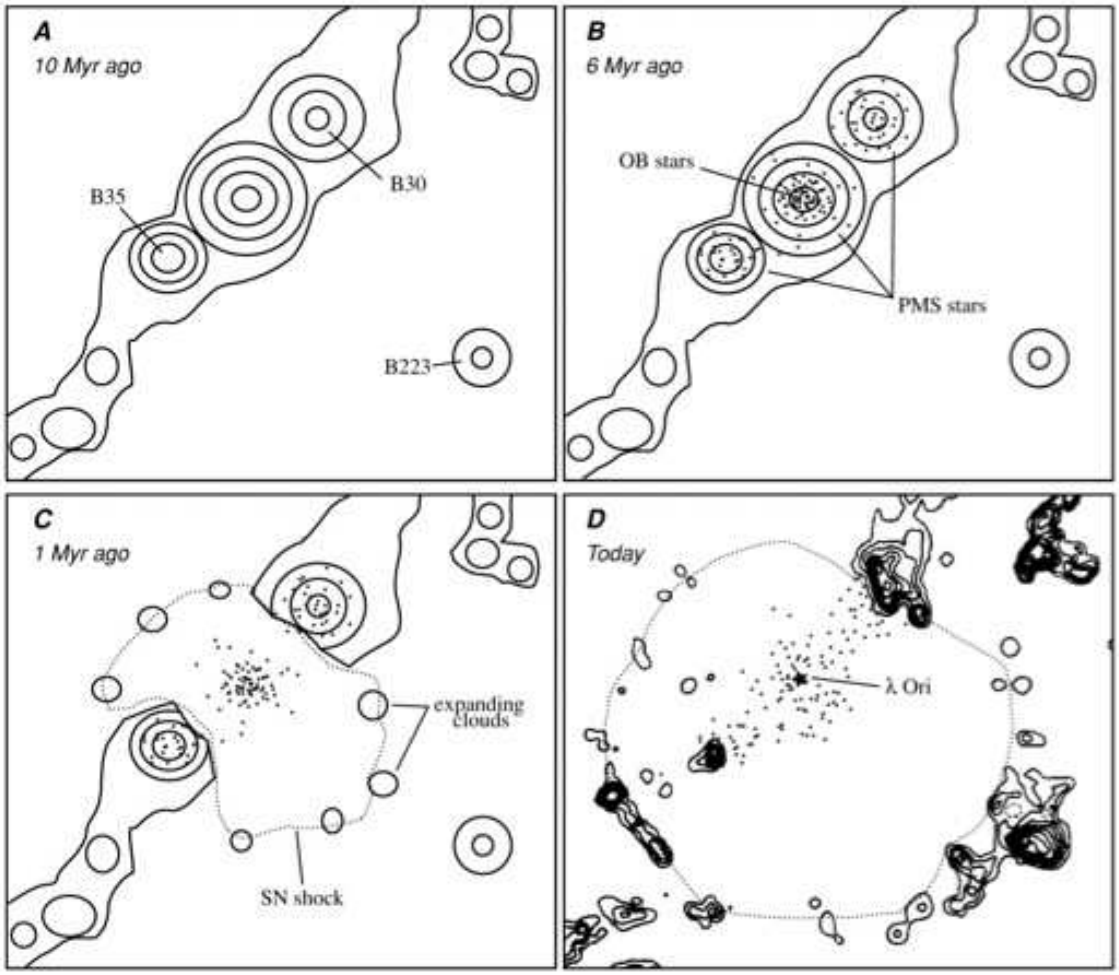


**Figure 1.8**: Cartoon, taken from Dolan & Mathieu (2002), showing the possible evolution of the Lambda Orionis Star Forming Region. If this hypothesis is correct, the star formation in the external dark clouds, was induced by a SN which took place few million years ago in the central region fo the Orionâs Head, in Collinder 69.

in its earliest phase), the OB stars photoevaporated much of the circumstellar material around the low-mass stars in the cluster such that by the present time, few of them have active accretion disks. The low-mass stars else where in the region did not have their circumstellar gas "cooked" in this fashion, thus explaining the higher rate of CTTs in Barnard 30 and Barnard 35 found by these authors. Figure 1.8 shows a cartoon from Dolan & Mathieu (2002) showing this scenario.

However, as emphasized by Lada et al. (2000), even for the Trapezium cluster which is denser and has a larger population of OB stars, 80-85 have circumstellar disks as inferred from L-band excesses (as opposed to a significantly lower apparent disk fraction using JHK or using H$\alpha$ as a disk surrogate, as was done by Dolan & Mathieu). Therefore, are the low mass stars in the Collinder 69 cluster completely diskless, or do they have disks which are not detectable by an H$\alpha$ survey such as 1 AU inner holes?

### 1.4.1 The Aim of this Thesis

If the supernova hypothesis is correct, the $\lambda$ Ori complex shows interesting peculiarities since there might be a direct link between spatial location in the complex and the history of star formation.

Besides, $\lambda$ Orionis represents an unique environment to study star formation due to its diversity, proximity (~400 pc), age range (~2–6 Myr), and the low extinction affecting the internal area of the ring (E(B-V)=0.12).

Thus we have conducted several observational campaigns to carry out a comprehensive study in three of its associations (Collinder 69, Barnard 35 and Barnard 30). The observations on which this thesis is based include optical and near-infrared spectroscopy at very different resolutions of candidate members photometrically selected by Morales-Calderón (2008). In particular, we have collected medium and high resolution optical spectroscopy and low resolution infrared spectroscopy for candidate members to Collinder 69. Medium and high resolution optical spectroscopy for candidate members to Barnard 35 and Barnard 30 was also carried out.

With this wealth of data we want to study a number of properties, namely the membership and the Initial Mass Function, accretion and circumstellar disk evolution of very low-mass stars and brown dwarfs. All the collected data will allow us to: (a) build the most complete census of members of the three regions up to date; (b) study possible differences in the properties between the disks in the three clusters (study disk evolution); (c) confirm members in the different regions to well below the hydrogen burning mass limit (HBL, the substellar border line at ~0.072 $M_{\odot}$, Baraffe et al. 1998); (d) try to shed some light on the formation mechanism of brown dwarfs.

This thesis is organized as follows: in the next chapter we briefly present the photometric surveys that led to the main part of the lists of candidate members studied spectroscopically as well as the most recent X-ray survey of Collinder 69. In chapter 3 we analyze the candidate members to Collinder 69 establishing their membership and studying their properties. In chapters 4 and 5 we follow a similar scheme, this time targeting the dark clouds Barnard 35 and Barnard 30. Finally,

in chapter 6 we present the conclusions achieved.

With this thesis we intend to improve our understanding of the star formation, in particular the evolution of the disks around low mass stars.

# Chapter 2

# The Photometric and X-Ray Surveys

Our group has been involved in the past ten years in a very ambitious project to study the different associations within the Lambda Orionis Star Forming Region. The first step to be performed in order to achieve this goal is the characterization of the physical properties of the objects that have been formed in those associations.

Thus, a comprehensive photometric study of this complex Star Forming Region is mandatory to select the most probable candidate members belonging to each association. While this kind of study can be biased towards members showing infrared excess (specially when basing our selection criteria on IRAC data); the analysis of X-rays data has revealed to be a very efficient tool to unveil the weak-line TTaury population of star forming regions. Therefore, the combination of both kinds of analysis should provide us with a fairly complete list os candidate members. Once this step has been accomplished, a detailed spectroscopic analysis of the individual sources will provide us with estimations of their physical properties (such as effective temperatures, surface gravities, presence of outflows, accretion rates, etc.).

The details of the exhaustive photometric surveys performed on the three regions studied in this thesis can be found in Morales-Calderón (2008), and those of the Collinder 69 X-ray data on Barrado et al 2009, in prep. A brief summary follows:

## 2.1 Colinder 69

Collinder 69 is the central cluster of the Lambda Orionis Star Forming Region, it is associated to the eponymous $\lambda$ Ori star, and it is also the most thoroughly studied association within the SFR. We have carried out a number of photometric observations in this region, from the optical to mid-IR, using different ground-based and space observatories. Figure 2.1 shows the layout of these observations.

- Optical data:

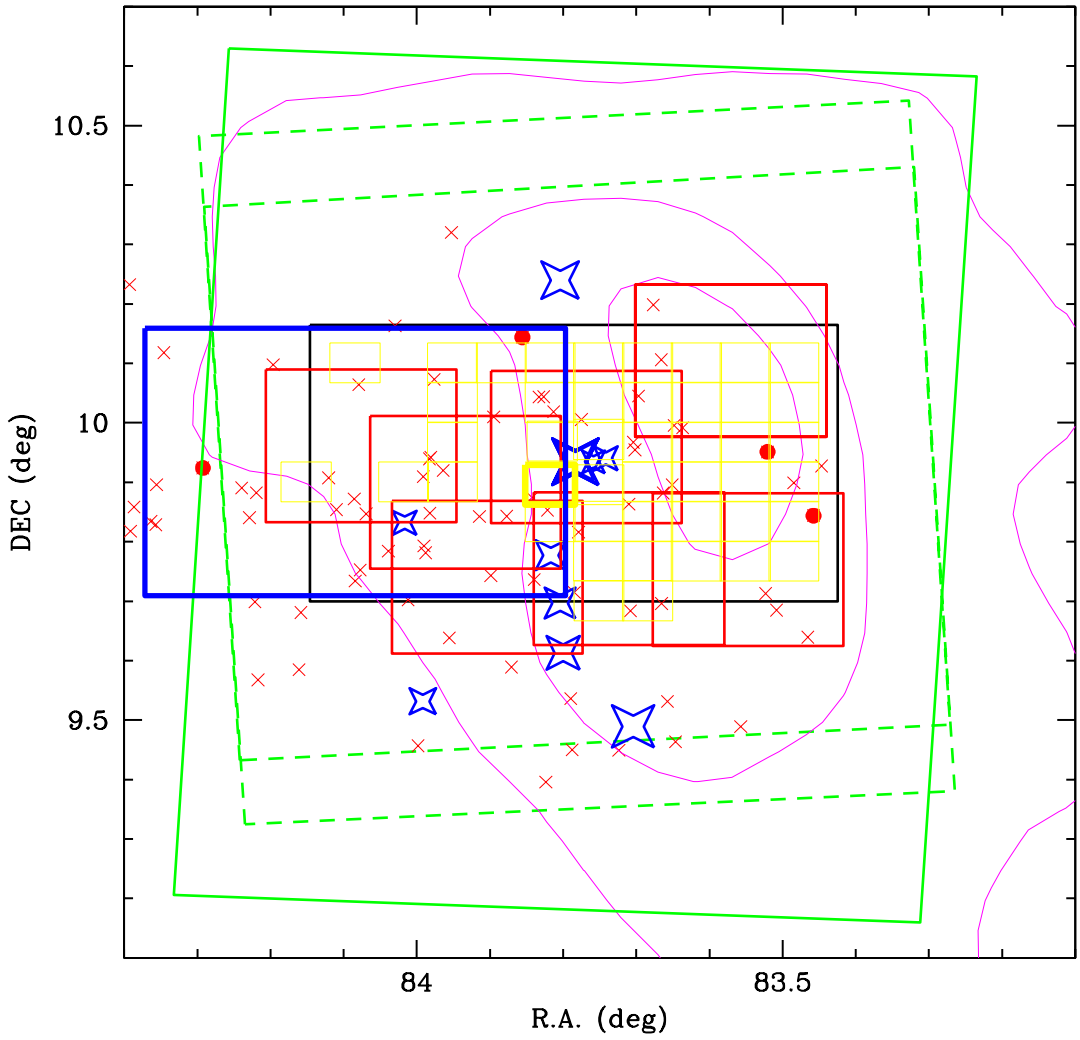


**Figure 2.1**: Layout of observations in Collinder 69. Thick green rectangles represent the Spitzer fields obtained with Spitzer (long-dashed: IRAC, and short-dashed: MIPS). Black rectangle define the area covered by our optical CFHT1999 survey. Red and yellow boxes represent the near-IR surveys for Omega 2000 and INGRID respectively. Blue thick rectangle represents the Subaru survey. Young stars, identified by Dolan & Mathieu (1999, 2001), appear as crosses (WTTs) and solid circles (CTTs). IRAS 100 $\mu$m contours are plotted in magenta.

– The CFHT1999 Survey: On September 29th and 30th, 1999, we used the Canada-France-Hawaii Telescope (CFHT) 12K mosaic camera and the Cousins R and I filters to perform a survey around the star $\lambda$ Orionis. This instrument covers a projected area on the sky of $42' \times 28'$, with a scale of about 0.2 $''$/pix (black rectangle in Figure 2.1).

  The data were collected under photometric conditions. The reduction was performed with the standard pipeline, and the extraction of the aperture photometry was carried out within the IRAF[1] environment. Two different sets of exposures were obtained, with short and long exposure times. In the first case, we exposed during 10 seconds for each filter, whereas the exposure times were 600 and 900 seconds, Cousins I and R filters, respectively, for the second set. With this method, we increased the dynamical range, and our photometry overlaps with previously published data in these filters.

  The limiting magnitude for these data is $I_{Limit}$~24.0 mag while completeness is achieved at $R_{Complete}$~22.75 mag and $I_{Complete}$~22.75 mag, based on the drop in the number of detected objects for each interval in the Ic and Rc filters (Wainscoat et al. 1992; Santiago et al. 1996). For cluster members, the faint limit is set by $R_{Complete}$~22.75 mag at (R - I) = 2.5, corresponding then to $I_{Complete,cluster}$~20.2 mag.

– The Subaru2006 Survey: In addition to the CFHT1999 survey, in November 2006 we performed a very deep survey using the Subaru Prime Focus Camera (Suprime-Cam – Miyazaki et al. (2002)) mounted at the Subaru 8 m telescope at the summit of Mauna Kea, Hawaii. Suprime-Cam is a mosaic of ten 2048×4096 CCDs, located at the prime focus of Subaru Telescope, which covers a $34' \times 27'$ field of view with a pixel scale of $0.20''$ (blue rectangle in Figure 2.1). The aim of the survey was to perform a very deep search of the less massive members of Collinder 69 with the goal of trying to detect the end of the IMF (ie, the minimum mass for direct collapse, fragmentation and formation of a "pre-stelar" core).

  Observations were performed in service mode in the i' and z' filters. We obtained 9 cycles of 5 positions and 136 sec/position in the i' band totalling 6120 sec of observation and 3 cycles of 6 positions and 180 sec/position in the z' band totalling 3240 sec of observation. The images were reduced in the standard way using IRAF but we did use a routine inside the data reduction package for Suprime-Cam (SDFRED) to fix the distortion found in the images. We have performed aperture photometry with an aperture of 2 pixels and, since no standard stars were observed during the run, we used our CFHT1999 data to calibrate our photometry. Only the I data were calibrated. The completeness limits can be estimated at $I_{Complete}$ ~25.5 mag, and $Z_{Inst,Complete}$ ~24.5 mag. For a DUSTY 5Myr isochrone (Chabrier et al. 2000), and the distance and stan-

[1]IRAF is distributed by National Optical Astronomy Observatories, which is operated by the Association of Universities for Research in Astronomy, Inc., under contract to the National Science Foundation, USA

dard extinction for the cluster, an I magnitude of 25.5 mag corresponds to ~7 $M_{Jupiter}$ for a COND 5Myr isochrone, more appropriate for this range of temperatures, the completeness limit is located at 3 $M_{Jupiter}$.

- Near Infrared photometry: 2MASS provides near infrared data down to a limiting magnitude of $J$=16.8, $H$=16.1, and $Ks$=15.3 mag. We have performed additional near-IR surveys to provide deeper photometry for objects with large errors in 2MASS JHKs, or without this type of data due to their intrinsic faintness.

  - INGRID Survey: This survey was performed in November 2002 and February 2003 with the 4.5 m William Herschel Telescope (El Roque de los Muchachos Observatory at La Palma, Spain), and the near-IR camera, INGRID which has a field-of-view of ~4.1′×4.1′. Observations were designed with a double goal, on the one hand, we wanted to obtain deep near-IR photometry and we observed the area around $\lambda$ Orionis creating a grid (See Figure 2.1 where the yellow boxes represent the INGRID pointings) and, for each position, we took five individual exposures of 60 seconds each, with small offsets of a few arcsec, thus totalling 5 minutes. Essentially, we have observed about 2/3 of the CFHT 1999 optical survey region in J (in the area around the star and west of it), with some coverage in H and K. On the other hand, as our second goal, we devoted a whole night in the 2003 run, with a five-hour time-span, to observe a small area just South of the $\lambda$ Ori star in the J band (thick yellow box in Figure 2.1), looking for short term variability. The individual 60 seconds exposures were processed, aligned and combined into single 5 minutes frames. In total, we collected 51 of such five-minute images.

    All the data were processed and analyzed with IRAF, using aperture photometry. The detection limit can be estimated as $J_{Limit}$=21.1 mag and the completeness limit as $J_{Complete}$=19.5 mag. For a DUSTY 5 Myr isochrone (Chabrier et al. 2000), and the distance and standard extinction for the cluster, this limit correspond to 10 $M_{Jupiter}$.

  - Omega2000 Survey: In October 2005 observations focused on the faint candidate members were obtained under a Director Discretionary program using the Calar Alto 3.5m telescope (CAHA, Almeria, Spain) and Omega2000 (15.36′×15.36′ FOV). We collected observations in the J, H and Ks filters taking five individual exposures of 60 seconds each, with small offsets of a few arcseconds, totalling 5 minutes. The seeing was 1.2 arcsec. The areas observed are represented by red squares in Figure 2.1.

    All the data were processed and analyzed with IRAF, using aperture photometry. The completeness limits for the survey are: $J_{Complete}$=20 mag, $H_{Complete}$=19, and $Ks_{Complete}$=18. For a DUSTY 5Myr isochrone (Chabrier et al. 2000), and the distance and standard extinction for the cluster, this limit correspond to 8 $M_{Jupiter}$.

- Spitzer mid-IR imaging: Our Spitzer data were collected during March 15 (Multiband Imaging Photometer for Spitzer – MIPS Rieke et al. (2004)) and October 11 (InfraRed Array Camera – IRAC Fazio et al. (2004)), 2004, as part of a Guaranteed Time Observation program (GTO, PID:37).

  IRAC is a four channel camera which takes images at 3.6, 4.5, 5.8, and 8.0 $\mu$m with a field of view that covers ~5.2′×5.2′. IRAC imaging was performed in mapping mode with individual exposures of 12 seconds "frametime" (corresponding to 10.4 seconds exposure times) and three dithers at each map step. In order to keep the total observation time for a given map under three hours, the Lambda Ori map was broken into two segments, each of size 28.75′×61.5′ - one offset west of the star $\lambda$ Ori and the other offset to the east, with the combined image covering an area of 57′×61.5′, leaving the star $\lambda$ Orionis approximately at the center. Each of the IRAC images from the Spitzer Science Center pipeline were corrected for instrumental artifacts using the IDL code provided by the Spitzer Science Center and then combined into mosaics at each of the four bandpasses using the MOPEX package (Makovoz & Khan 2005). Figure 2.1 shows the IRAC and MIPS pointings as green dashed and solid lines respectively.

  The MIPS instrument was used to map the cluster with a medium rate scan mode and 12 legs separated by 302″ in the cross scan direction. The total effective integration time per point on the sky at 24 $\mu$m for most points in the map was 40 seconds, and the mosaic covered an area of 60.5′×98.75′ centered around the star $\lambda$ Orionis. Since there were no visible artifacts in the pipeline mosaics for MIPS 24 $\mu$m we used them as our starting point to extract the photometry.

The new candidates to the cluster selected with these surveys, are shown in the tables from 2.6 to 2.7.

**Table 2.1**: Photometry for the DM members of Collinder 69 not in common with Barrado y Navascués et al. (2004b, 2007b).

| Dolan ID | RA (J2000) | DEC (J2000) | V | R | I | J error | H error | Ks error | [3.6] error | [4.5] error | [5.8] error | [8.0] error | [24] error |
|---|---|---|---|---|---|---|---|---|---|---|---|---|---|
| 3 | 05:33:51.70 | +09:38:21.5 | 14.629 | 13.744 | 12.826 | 11.488 0.023 | 10.865 0.026 | 10.631 0.019 | 10.439 0.011 | – – | – – | 10.428 0.068 | – – |
| 5 | 05:34:02.00 | +09:41:06.2 | 13.388 | 12.687 | 12.039 | 11.08 0.024 | 10.483 0.024 | 10.347 0.024 | 10.21 0.002 | 10.257 0.003 | 10.232 0.006 | 10.141 0.007 | 9.187 0.192 |
| 6 | 05:34:04.94 | +09:57:03.8 | 16.064 | 15.05 | 13.947 | 12.5 0.022 | 11.727 0.024 | 11.336 0.021 | 10.879 0.002 | 10.598 0.003 | 10.229 0.006 | 9.538 0.005 | 6.935 0.023 |
| 7 | 05:34:05.53 | +09:42:46.8 | 12.751 | 12.162 | 11.609 | 10.801 0.023 | 10.262 0.024 | 10.125 0.021 | 10.036 0.008 | 10.113 0.012 | – – | 10.049 0.048 | 9.643 0.278 |
| 8 | 05:34:13.69 | +09:29:19.8 | 13.573 | 12.965 | 12.388 | 11.403 0.026 | 10.9 0.023 | 10.731 0.021 | – – | 10.648 0.003 | – – | 10.56 0.009 | – – |
| 9 | 05:34:32.81 | +09:59:30.9 | 14.211 | 13.463 | 12.776 | 11.839 0.027 | 11.227 0.026 | 11.059 0.021 | 10.91 0.003 | 10.929 0.004 | 10.92 0.009 | 10.894 0.012 | – – |
| 10 | 05:34:35.16 | +09:27:49.2 | 16.907 | 15.772 | 14.374 | 12.77 0.024 | 12.067 0.024 | 11.857 0.025 | – – | 11.591 0.005 | – – | 11.573 0.025 | – – |
| 13 | 05:34:37.78 | +09:31:52.9 | 15.438 | 14.53 | 13.63 | 12.325 0.026 | 11.659 0.026 | 11.437 0.022 | 11.29 0.003 | 11.315 0.004 | 11.27 0.011 | 11.197 0.013 | – – |
| 14 | 05:34:39.19 | +09:52:55.4 | 15.091 | 14.167 | 13.307 | 12.072 0.027 | 11.36 0.023 | 11.186 0.022 | 11.0 0.003 | 11.039 0.003 | 10.96 0.009 | 10.915 0.013 | – – |
| 15 | 05:34:39.69 | +09:41:46.1 | 15.845 | 14.818 | 13.877 | 12.656 0.023 | 11.974 0.023 | 11.808 0.027 | 11.63 0.003 | 11.66 0.005 | 11.6 0.014 | 11.58 0.019 | – – |
| 16 | 05:34:39.79 | +10:06:22.1 | 16.079 | 15.017 | 13.859 | 12.366 0.024 | 11.663 0.023 | 11.429 0.019 | 11.22 0.003 | 11.248 0.004 | 11.13 0.01 | 11.136 0.017 | – – |
| 17 | 05:34:42.46 | +10:11:54.3 | 13.529 | 12.746 | 12.029 | 10.973 0.024 | 10.324 0.024 | 10.182 0.021 | 10.079 0.009 | 10.128 0.013 | – – | 10.553 0.065 | – – |
| 18 | 05:34:47.24 | +10:02:43.0 | 14.009 | 13.254 | 12.517 | 11.436 0.023 | 10.804 0.026 | 10.636 0.023 | 10.53 0.002 | 10.544 0.003 | 10.52 0.007 | 10.434 0.009 | 11.001 0.725 |
| 19 | 05:34:48.44 | +09:57:15.7 | 15.791 | 14.777 | 13.721 | 12.42 0.027 | 11.718 0.026 | 11.54 0.025 | 11.28 0.003 | 11.265 0.004 | 11.19 0.009 | 11.199 0.015 | – – |
| 21 | 05:34:49.91 | +09:41:01.8 | 14.543 | 13.683 | 12.842 | 11.656 0.024 | 11.015 0.026 | 10.835 0.025 | 10.65 0.002 | 10.641 0.003 | 10.61 0.007 | 10.616 0.01 | – – |
| 22 | 05:34:50.44 | +09:51:47.6 | 15.583 | 14.699 | 13.744 | 12.434 0.027 | 11.767 0.026 | 11.56 0.025 | 11.42 0.003 | 11.405 0.004 | 11.32 0.012 | 11.288 0.016 | – – |
| 23 | 05:34:53.74 | +09:26:57.0 | 15.822 | 14.848 | 13.914 | 12.642 0.026 | 11.907 0.026 | 11.752 0.024 | – – | 11.561 0.005 | – – | 11.495 0.017 | – – |
| 24 | 05:35:06.04 | +10:00:19.9 | 12.772 | 12.238 | 11.752 | 11.007 0.026 | 10.528 0.024 | 10.437 0.021 | 10.35 0.003 | 10.386 0.003 | 10.33 0.008 | 10.317 0.009 | – – |
| 25 | 05:35:06.93 | +09:48:57.6 | 15.396 | 14.421 | 13.472 | 12.258 0.027 | 11.56 0.026 | 11.296 0.021 | 11.12 0.003 | 11.2 0.004 | 11.09 0.011 | 11.005 0.018 | – – |
| 26 | 05:35:08.31 | +09:42:53.9 | 12.921 | 12.335 | 11.806 | 10.953 0.026 | 10.433 0.022 | 10.301 0.024 | 10.119 0.009 | – – | 10.185 0.048 | 9.948 0.04 | 11.294 0.797 |
| 27 | 05:35:09.03 | +09:26:59.7 | 16.381 | 15.219 | 13.877 | 12.442 0.026 | 11.734 0.022 | 11.489 0.021 | – – | 11.243 0.004 | – – | 11.17 0.015 | – – |
| 28 | 05:35:09.53 | +09:32:09.1 | 14.066 | 13.376 | 12.727 | 11.725 0.024 | 11.115 0.022 | 10.99 0.024 | 10.841 0.003 | 10.861 0.003 | 10.852 0.008 | 10.789 0.013 | – – |
| 30 | 05:35:17.15 | +09:51:11.5 | 16.46 | 15.317 | 14.156 | 12.798 0.023 | 12.056 0.024 | 11.835 0.021 | 11.694 0.004 | 11.604 0.004 | 11.616 0.016 | 11.671 0.025 | – – |
| 31 | 05:35:17.72 | +09:23:44.6 | 13.495 | 12.808 | 12.174 | 11.385 – | 10.951 0.051 | 10.712 – | – – | 10.572 0.003 | – – | – – | 10.513 0.387 |
| 32 | 05:35:18.37 | +10:02:38.5 | 16.725 | 15.709 | 14.493 | 13.067 0.027 | 12.417 0.027 | 12.162 0.021 | 11.95 0.004 | 11.94 0.005 | 11.862 0.016 | 11.871 0.031 | – – |
| 34 | 05:35:21.46 | +09:44:10.3 | 16.803 | 15.684 | 14.387 | 12.894 0.024 | 12.14 0.023 | 11.919 0.021 | 11.657 0.003 | 11.669 0.005 | 11.629 0.015 | 11.62 0.024 | – – |
| 35 | 05:35:22.18 | +09:52:27.6 | 15.429 | 14.481 | 13.612 | 12.309 0.023 | 11.629 0.026 | 11.459 0.024 | 11.285 0.003 | 11.341 0.004 | 11.288 0.011 | 11.218 0.015 | – – |
| 37 | 05:35:28.96 | +09:35:21.0 | 14.811 | 14.004 | 13.313 | 12.266 0.024 | 11.627 0.022 | 11.468 0.021 | 11.358 0.003 | 11.412 0.004 | 11.33 0.012 | 11.351 0.019 | – – |
| 40 | 05:35:35.71 | +09:44:35.5 | 17.23 | 16.013 | 14.664 | 13.23 0.026 | 12.518 0.025 | 12.27 0.026 | 12.083 0.005 | 12.079 0.006 | 12.022 0.023 | 12.12 0.043 | – – |
| 42 | 05:35:48.60 | +10:19:12.3 | 16.768 | 15.645 | 14.359 | 12.983 0.023 | 12.228 0.023 | 12.038 0.026 | 11.826 0.004 | 11.842 0.005 | 11.733 0.016 | 11.748 0.023 | – – |
| 43 | 05:35:49.35 | +09:38:18.1 | 15.967 | 14.959 | 13.893 | 12.644 0.023 | 11.939 0.023 | 11.709 0.021 | 11.572 0.003 | 11.574 0.004 | 11.569 0.013 | 11.454 0.018 | – – |
| 45 | 05:35:54.32 | +10:04:23.4 | 12.886 | 12.272 | 11.68 | 10.936 0.023 | 10.378 0.022 | 10.235 0.021 | 10.166 0.01 | 10.195 0.012 | 10.39 0.085 | 10.226 0.05 | 10.713 0.481 |
| 48 | 05:35:55.84 | +09:56:21.8 | 16.851 | 15.69 | 14.392 | 13.011 0.024 | 12.237 0.025 | 11.94 0.024 | 11.418 0.005 | 11.188 0.005 | 10.905 0.009 | 10.313 0.008 | 7.624 0.032 |
| 52 | 05:35:59.54 | +09:27:23.8 | 13.873 | 13.352 | 12.839 | 12.076 0.027 | 11.598 0.022 | 11.462 0.023 | – – | 11.337 0.004 | – – | 11.086 0.014 | – – |
| 53 | 05:36:02.87 | +09:42:07.6 | 15.219 | 14.304 | 13.391 | 12.151 0.023 | 11.455 0.022 | 11.25 0.023 | 11.028 0.003 | 11.011 0.003 | 10.924 0.008 | 10.748 0.01 | 8.658 0.077 |
| 57 | 05:36:18.56 | +09:45:08.9 | 13.255 | 12.681 | 12.13 | 11.34 0.023 | 10.796 0.022 | 10.676 0.019 | 10.54 0.002 | 10.57 0.003 | 10.521 0.008 | 10.481 0.009 | 11.729 1.042 |
| 61 | 05:36:26.30 | +09:51:14.0 | 16.313 | 15.294 | 14.189 | 12.866 0.026 | 12.153 0.022 | 11.931 0.027 | 11.824 0.004 | 11.808 0.005 | 11.737 0.013 | 11.791 0.023 | – – |
| 62 | 05:36:28.88 | +09:54:27.1 | 16.573 | 15.461 | 14.204 | 12.893 0.029 | 12.108 0.023 | 11.945 0.024 | 11.749 0.003 | 11.745 0.005 | 11.642 0.016 | 11.703 0.024 | – – |
| 63 | 05:36:38.03 | +09:40:50.8 | 13.768 | 13.023 | 12.338 | 11.285 0.023 | 10.655 0.025 | 10.383 0.019 | 9.931 0.008 | 9.813 0.01 | 9.731 0.036 | 8.978 0.023 | 5.714 0.004 |
| 64 | 05:36:38.60 | +09:35:05.3 | 16.026 | 14.937 | 13.665 | 12.413 0.029 | 11.691 0.035 | 11.418 0.024 | 11.115 0.003 | 11.002 0.003 | 10.784 0.008 | 10.412 0.006 | 8.271 0.053 |
| 65 | 05:36:47.10 | +10:05:51.8 | 15.738 | 14.757 | 13.746 | 12.454 0.026 | 11.744 0.022 | 11.546 0.026 | 11.36 0.003 | 11.363 0.004 | 11.332 0.013 | 11.28 0.018 | – – |
| 66 | 05:36:52.06 | +09:34:02.4 | 13.174 | 12.496 | 11.805 | 10.809 0.023 | 10.212 0.022 | 10.046 0.021 | 9.937 0.002 | 9.961 0.002 | 9.918 0.005 | 9.866 0.005 | 9.673 0.207 |
| 67 | 05:36:52.65 | +09:52:56.3 | 16.69 | 15.498 | 14.062 | 12.512 0.023 | 11.841 0.022 | 11.665 0.024 | 11.407 0.004 | 11.382 0.005 | 11.367 0.012 | 11.382 0.018 | – – |
| 68 | 05:36:53.07 | +09:41:55.7 | 13.759 | 13.054 | 12.397 | 11.651 0.037 | 11.096 0.047 | 10.823 0.027 | 10.553 0.002 | 10.599 0.003 | 10.599 0.007 | 10.499 0.01 | 10.397 0.467 |
| 69 | 05:36:54.84 | +09:50:25.0 | 15.536 | 14.565 | 13.627 | 12.418 0.024 | 11.717 0.023 | 11.522 0.021 | 11.374 0.003 | 11.421 0.004 | 11.311 0.011 | 11.257 0.018 | – – |
| 70 | 05:36:57.49 | +09:53:26.0 | 16.05 | 15.024 | 13.911 | 12.695 0.028 | 11.958 0.023 | 11.767 0.021 | 11.574 0.004 | 11.58 0.005 | 11.551 0.014 | 11.484 0.017 | – – |

**Table 2.2**: Disk properties of the DM members not in common with Barrado y Navascués et al. (2004b, 2007b).

| DM ID | Mass ($M_\odot$)[4] | Teff (K)[4] | IRAC class[1] | SED slope | Disk Type[2] | $W_\lambda$(H$\alpha$) (Å)[3] | $W_\lambda$(Li) (Å)[3] |
|---|---|---|---|---|---|---|---|
| 3 | 0.34 | 3400 | III | – | Diskless | 3.18 | 0.44 |
| 5 | 1.30 | 4000 | III | -2.75 | Diskless | 0.06 | 0.46 |
| 6 | 0.09 | 4000 | II | -1.295 | Thick | 72.64 | 0.43 |
| 7 | 1.58 | 4000 | III | – | Diskless | -0.12 | 0.42 |
| 8 | 1.30 | 3500 | III | – | Diskless | -0.09 | 0.41 |
| 9 | 1.30 | 4400 | III | -2.816 | Diskless | 0.74 | 0.40 |
| 10 | 0.29 | 4250 | III | – | Diskless | 5.97 | 0.51 |
| 13 | 0.73 | 3600 | III | -2.721 | Diskless | 1.29 | 0.53 |
| 14 | 0.73 | 4000 | III | -2.719 | Diskless | 2.28 | 0.57 |
| 15 | 0.73 | 3750 | III | -2.764 | Diskless | 1.07 | 0.49 |
| 16 | 0.34 | 3750 | III | -2.711 | Diskless | 5.45 | 0.61 |
| 17 | 1.19 | 5000 | III | – | Diskless | 0.25 | 0.47 |
| 18 | 1.01 | 4000 | III | -2.725 | Diskless | 2.64 | 0.52 |
| 19 | 0.39 | 4750 | III | -2.731 | Diskless | 2.07 | 0.56 |
| 21 | 0.73 | 3400 | III | -2.794 | Diskless | 1.73 | 0.50 |
| 22 | 0.49 | 4500 | III | -2.672 | Diskless | 2.37 | 0.54 |
| 23 | 0.49 | 3500 | III | – | Diskless | 2.04 | 0.53 |
| 24 | 1.72 | 3500 | III | -2.783 | Diskless | -1.07 | 0.30 |
| 25 | 0.73 | 4500 | III | -2.672 | Diskless | 1.47 | 0.54 |
| 26 | 1.53 | 3600 | III | – | Diskless | -0.39 | 0.35 |
| 27 | 0.28 | 3500 | III | – | Diskless | 3.64 | 0.59 |
| 28 | 1.30 | 4000 | III | -2.777 | Diskless | -0.35 | 0.47 |
| 30 | 0.34 | 4250 | III | -2.828 | Diskless | 1.0 | 0.61 |
| 31 | 1.30 | 3600 | III | – | Diskless | -0.01 | 0.42 |
| 32 | 0.39 | 3750 | III | -2.732 | Diskless | 5.5 | 0.42 |
| 34 | 0.34 | 3700 | III | -2.786 | Diskless | 2.64 | 0.49 |
| 35 | 0.73 | 4800 | III | -2.744 | Diskless | 1.68 | 0.55 |
| 37 | 1.01 | 3000 | III | -2.802 | Diskless | 0.08 | 0.43 |
| 40 | 0.39 | 4500 | III | -2.865 | Diskless | 3.63 | 0.55 |
| 42 | 0.49 | 4750 | III | -2.722 | Diskless | 2.94 | 0.58 |
| 43 | 0.46 | 3600 | III | -2.707 | Diskless | 2.6 | 0.57 |
| 45 | 1.58 | 4750 | III | -2.953 | Diskless | -0.12 | 0.46 |
| 48 | 0.09 | 3000 | II | -1.572 | Thick | 8.61 | 0.58 |
| 52 | 1.53 | 3750 | III | – | Diskless | -0.36 | 0.25 |
| 53 | 0.39 | 3700 | III | -2.509 | Transition | 3.62 | 0.52 |
| 57 | 1.53 | 3500 | III | -2.757 | Diskless | -0.15 | 0.39 |
| 61 | 0.49 | 3300 | III | -2.786 | Diskless | 4.23 | 0.56 |
| 62 | 0.46 | 3700 | III | -2.761 | Diskless | 4.05 | 0.61 |
| 63 | 0.34 | 4500 | II | -1.78 | Thick | 4.76 | 0.54 |
| 64 | 0.23 | 3500 | II | -2.019 | Thin | 2.52 | 0.45 |
| 65 | 0.46 | 4250 | III | -2.742 | Diskless | 2.67 | 0.58 |
| 66 | 1.30 | 4000 | III | -2.746 | Diskless | 1.0 | 0.55 |
| 67 | 0.34 | 4800 | III | -2.811 | Diskless | 4.88 | 0.66 |
| 68 | 1.01 | 3750 | III | -2.773 | Diskless | -0.04 | 0.44 |
| 69 | 0.73 | 4500 | III | -2.674 | Diskless | 0.49 | 0.51 |
| 70 | 0.49 | 4500 | III | -2.731 | Diskless | 0.9 | 0.58 |

[1]IRAC Class based on the IRAC [3.6]-[4.5] vs. [5.8]-[8.0] color-color diagram and in the SED of each object.

[2]Disk type based on the IRAC slope and SED shape

[3]$W_\lambda$(H$\alpha$) and $W_\lambda$(Li) from Dolan & Mathieu (1999)

[4]Teff comes from the SED fitting performed with VOSA. The mass is estimated with Teff and a 5Myr Siess et al. isochrone

**Table 2.3**: Candidate members of the Collinder 69 cluster from Barrado y Navascués et al. (2007b).

| Name[3] | R error | I error | J error | H error | Ks error | [3.6] error | [4.5] error | [5.8] error | [8.0] error | [24] error | Mem[1] |
|---|---|---|---|---|---|---|---|---|---|---|---|
| LOri001 | 13.21 0.00 | 12.52 0.00 | 11.297 0.022 | 10.595 0.022 | 10.426 0.021 | 10.228 0.003 | 10.255 0.004 | 10.214 0.009 | 10.206 0.010 | – – | Y |
| LOri002 | 13.44 0.00 | 12.64 0.00 | 11.230 0.024 | 10.329 0.023 | 10.088 0.019 | 9.935 0.003 | 10.042 0.003 | 9.930 0.009 | 9.880 0.008 | – – | Y |
| LOri003 | 13.39 0.00 | 12.65 0.00 | 11.416 0.023 | 10.725 0.022 | 10.524 0.023 | 10.262 0.003 | 10.318 0.004 | 10.239 0.010 | 10.171 0.010 | – – | Y |
| LOri004 | 13.71 0.00 | 12.65 0.00 | 11.359 0.022 | 10.780 0.023 | 10.548 0.021 | 10.287 0.003 | 10.249 0.004 | 10.185 0.009 | 10.127 0.009 | – – | Y |
| LOri005 | 13.38 0.00 | 12.67 0.00 | 11.378 0.022 | 10.549 0.022 | 10.354 0.023 | 10.204 0.003 | 10.321 0.004 | 10.218 0.009 | 10.158 0.009 | – – | Y |
| LOri006 | 13.55 0.00 | 12.75 0.00 | 11.542 0.026 | 10.859 0.026 | 10.648 0.021 | 10.454 0.003 | 10.454 0.004 | 10.399 0.011 | 10.319 0.010 | – – | Y |
| LOri007 | 13.72 0.00 | 12.78 0.00 | 11.698 0.027 | 11.101 0.024 | 10.895 0.030 | 10.668 0.004 | 10.636 0.004 | 10.615 0.012 | 10.482 0.013 | – – | Y |
| LOri008 | 13.60 0.00 | 12.79 0.00 | 11.548 0.029 | 10.859 0.023 | 10.651 0.024 | 10.498 0.003 | 10.495 0.004 | 10.440 0.011 | 10.256 0.012 | – – | Y |
| LOri009 | 13.70 0.00 | 12.95 0.00 | 11.843 0.024 | 11.109 0.024 | 10.923 0.023 | 10.834 0.004 | 10.873 0.005 | 10.788 0.012 | 10.743 0.014 | – – | Y |
| LOri010 | 13.70 0.00 | 12.96 0.00 | 11.880 0.026 | 11.219 0.026 | 11.041 0.023 | 10.916 0.004 | 10.953 0.005 | 10.733 0.012 | 10.839 0.016 | – – | Y |
| LOri011 | 13.84 0.00 | 13.01 0.00 | 11.604 0.026 | 10.784 0.024 | 10.554 0.024 | 10.378 0.003 | 10.521 0.004 | 10.444 0.011 | 10.326 0.011 | – – | Y |
| LOri012 | 13.80 0.00 | 13.03 0.00 | 11.816 0.026 | 10.971 0.024 | 10.795 0.023 | 10.619 0.003 | 10.758 0.005 | 10.627 0.012 | 10.543 0.012 | – – | Y |
| LOri013 | 14.21 0.00 | 13.03 0.00 | 11.656 0.022 | 10.918 0.022 | 10.719 0.023 | 10.511 0.003 | 10.480 0.004 | 10.467 0.011 | 10.344 0.012 | – – | Y |
| LOri014 | 13.84 0.00 | 13.03 0.00 | 11.941 0.024 | 11.278 0.027 | 11.092 0.023 | 10.902 0.004 | 10.904 0.005 | 10.839 0.014 | 10.797 0.014 | – – | Y |
| LOri015 | 13.83 0.00 | 13.05 0.00 | 11.870 0.024 | 11.127 0.024 | 10.912 0.019 | 10.808 0.004 | 10.886 0.005 | 10.824 0.013 | 10.882 0.015 | – – | Y |
| LOri016 | 14.07 0.00 | 13.18 0.00 | 11.958 0.024 | 11.284 0.027 | 11.053 0.024 | 10.833 0.004 | 10.817 0.006 | 10.378 0.011 | 10.700 0.014 | – – | Y |
| LOri017 | 13.99 0.00 | 13.19 0.00 | 12.188 0.024 | 11.482 0.023 | 11.323 0.021 | 11.165 0.005 | 11.206 0.006 | 11.173 0.017 | 11.072 0.019 | – – | Y |
| LOri018 | 14.21 0.00 | 13.26 0.00 | 11.991 0.024 | 11.284 0.022 | 11.090 0.023 | 10.804 0.004 | 10.798 0.005 | 10.722 0.012 | 10.636 0.014 | – – | Y |
| LOri019 | 14.33 0.00 | 13.31 0.00 | 12.019 0.026 | 11.316 0.024 | 11.067 0.021 | 10.880 0.004 | 10.866 0.005 | 10.767 0.013 | 10.788 0.018 | – – | Y |
| LOri020 | 14.65 0.00 | 13.31 0.00 | 11.856 0.028 | 11.214 0.026 | 11.025 0.027 | 10.676 0.003 | 10.609 0.004 | 10.573 0.012 | 10.485 0.012 | – – | N |
| LOri021 | 14.26 0.00 | 13.38 0.00 | 12.258 0.027 | 11.560 0.026 | 11.296 0.021 | 11.129 0.004 | 11.107 0.005 | 11.081 0.016 | 11.065 0.019 | – – | Y |
| LOri022 | 14.41 0.00 | 13.38 0.00 | 12.102 0.023 | 11.411 0.022 | 11.156 0.019 | 11.010 0.004 | 10.985 0.005 | 10.895 0.014 | 10.683 0.014 | – – | Y |
| LOri023 | 14.43 0.00 | 13.44 0.00 | 12.221 0.027 | 11.471 0.022 | 11.290 0.024 | 11.090 0.004 | 11.114 0.005 | 11.071 0.015 | 10.928 0.018 | – – | Y |
| LOri024 | 14.43 0.00 | 13.45 0.00 | 12.139 0.030 | 11.446 0.026 | 11.223 0.028 | 11.018 0.004 | 11.019 0.005 | 10.972 0.015 | 10.877 0.016 | – – | Y |
| LOri025 | 14.36 0.00 | 13.45 0.00 | 12.163 0.044 | 11.409 0.051 | 11.090 0.033 | 10.668 0.003 | 10.674 0.004 | 10.613 0.012 | 10.576 0.012 | – – | Y |
| LOri026 | 14.57 0.00 | 13.47 0.00 | 12.046 0.028 | 11.324 0.024 | 11.092 0.025 | 10.882 0.004 | 10.833 0.005 | 10.811 0.014 | 10.742 0.013 | – – | Y |
| LOri027 | 14.49 0.00 | 13.50 0.00 | 12.378 0.026 | 11.718 0.023 | 11.503 0.021 | 11.305 0.005 | 11.306 0.006 | 11.237 0.016 | 11.179 0.025 | – – | Y |
| LOri028 | 14.86 0.00 | 13.65 0.00 | 12.488 0.024 | 11.872 0.022 | 11.687 0.021 | 11.439 0.005 | 11.417 0.006 | 11.348 0.017 | 11.297 0.021 | – – | Y |
| LOri029 | 14.89 0.00 | 13.69 0.00 | 12.210 0.026 | 11.460 0.027 | 11.071 0.019 | 10.259 0.003 | 9.830 0.003 | 9.321 0.006 | 8.416 0.003 | 5.684 0.007 | Y |
| LOri030 | 14.95 0.00 | 13.74 0.00 | 12.427 0.027 | 11.686 0.026 | 11.428 0.021 | 11.208 0.007 | 11.157 0.007 | 11.119 0.019 | 10.997 0.023 | – – | Y |
| LOri031 | 14.90 0.00 | 13.75 0.00 | 12.412 0.028 | 11.654 0.023 | 11.442 0.028 | 11.206 0.004 | 11.188 0.006 | 11.150 0.015 | 11.079 0.016 | – – | Y |
| LOri032 | 15.04 0.00 | 13.80 0.00 | 12.410 0.029 | 11.714 0.023 | 11.493 0.021 | 11.252 0.004 | 11.215 0.006 | 11.178 0.016 | 11.080 0.019 | – – | Y |
| LOri033 | 14.82 0.00 | 13.81 0.00 | 12.455 0.033 | 11.800 0.042 | 11.502 0.027 | 11.146 0.004 | 11.149 0.005 | 11.060 0.015 | 11.020 0.019 | – – | Y |
| LOri034 | 15.10 0.00 | 13.97 0.00 | 12.442 0.026 | 11.639 0.026 | 11.184 0.023 | 10.068 0.003 | 9.734 0.003 | 9.314 0.007 | 8.325 0.003 | 5.738 0.007 | Y |
| LOri035 | 15.25 0.00 | 13.97 0.00 | 12.546 0.024 | 11.842 0.027 | 11.609 0.019 | 11.371 0.005 | 11.349 0.006 | 11.283 0.017 | 11.259 0.021 | – – | Y |
| LOri036 | 15.47 0.00 | 13.98 0.00 | 12.576 0.024 | 11.936 0.023 | 11.706 0.021 | 11.395 0.005 | 11.378 0.006 | 11.287 0.018 | 11.260 0.019 | – – | N |
| LOri037 | 15.17 0.00 | 13.99 0.00 | 12.459 0.024 | 11.727 0.026 | 11.492 0.021 | 11.302 0.005 | 11.309 0.006 | 11.198 0.016 | 11.180 0.018 | – – | Y |
| LOri038 | 15.10 0.00 | 14.01 0.00 | 12.684 0.030 | 11.954 0.029 | – – | 11.455 0.005 | 11.320 0.006 | 10.970 0.014 | 9.857 0.008 | 6.211 0.010 | Y |
| LOri039 | 15.25 0.00 | 14.02 0.00 | 12.755 0.030 | 12.004 0.023 | 11.775 0.023 | 11.523 0.005 | 11.534 0.007 | 11.434 0.018 | 11.373 0.025 | – – | Y |
| LOri040 | 15.38 0.00 | 14.06 0.00 | 12.553 0.024 | 11.877 0.022 | 11.594 0.024 | 11.364 0.005 | 11.319 0.006 | 11.231 0.017 | 11.218 0.025 | – – | Y |
| LOri041 | 15.55 0.00 | 14.10 0.00 | 12.500 0.024 | 11.856 0.023 | 11.587 0.027 | 11.255 0.004 | 11.187 0.006 | 11.131 0.015 | 11.123 0.021 | – – | Y |
| LOri042 | 15.31 0.00 | 14.14 0.00 | 12.813 0.027 | 12.099 0.026 | 11.853 0.023 | 11.604 0.005 | 11.633 0.007 | 11.546 0.019 | 11.479 0.025 | – – | Y |
| LOri043 | 15.46 0.00 | 14.16 0.00 | 12.707 0.024 | 12.021 0.026 | 11.741 0.024 | 11.512 0.005 | 11.496 0.007 | 11.408 0.019 | 11.393 0.024 | 8.479 0.102 | Y |
| LOri044 | 15.39 0.00 | 14.17 0.00 | 12.924 0.024 | 12.318 0.024 | 12.065 0.023 | 11.837 0.006 | 11.804 0.007 | 11.751 0.023 | 11.674 0.024 | – – | N |

Continued on next page…

Table 2.3 – Continued

| Name[3] | R error | I error | J error | H error | Ks error | [3.6] error | [4.5] error | [5.8] error | [8.0] error | [24] error | Mem[1] |
|---|---|---|---|---|---|---|---|---|---|---|---|
| LOri045 | 15.56 0.00 | 14.23 0.00 | 12.768 0.023 | 12.102 0.026 | 11.844 0.023 | 11.602 0.005 | 11.596 0.007 | 12.023 0.039 | 11.474 0.026 | – – | Y |
| LOri046 | 15.64 0.00 | 14.36 0.00 | 13.033 0.023 | 12.478 0.026 | 12.252 0.026 | 11.906 0.006 | 11.852 0.008 | 11.787 0.024 | 11.763 0.032 | – – | N |
| LOri047 | 15.91 0.00 | 14.38 0.00 | 12.732 0.026 | 12.097 0.031 | 11.827 0.026 | 11.474 0.005 | 11.400 0.006 | 11.303 0.017 | 11.342 0.025 | – – | Y |
| LOri048 | 15.78 0.00 | 14.41 0.00 | 12.887 0.027 | 12.196 0.029 | 11.932 0.026 | 11.612 0.006 | 11.521 0.008 | 11.448 0.020 | 10.920 0.018 | 8.119 0.087 | Y |
| LOri049 | 15.77 0.00 | 14.50 0.00 | 13.173 0.027 | 12.592 0.029 | 12.253 0.023 | 12.004 0.006 | 11.992 0.009 | 12.043 0.027 | 12.427 0.057 | – – | Y |
| LOri050 | 15.90 0.00 | 14.54 0.00 | 12.877 0.027 | 12.236 0.027 | 11.955 0.031 | 11.471 0.005 | 11.089 0.005 | 10.529 0.011 | 9.537 0.007 | 7.268 0.029 | Y |
| LOri051 | 15.91 0.00 | 14.60 0.00 | 13.266 0.024 | 12.559 0.022 | 12.285 0.021 | 12.017 0.006 | 11.995 0.008 | 11.969 0.024 | 11.919 0.035 | – – | Y |
| LOri052 | 15.93 0.00 | 14.63 0.00 | 13.117 0.023 | 12.454 0.024 | 12.192 0.019 | 11.917 0.006 | 11.863 0.008 | 11.764 0.022 | 11.791 0.029 | – – | Y |
| LOri053 | 16.08 0.00 | 14.72 0.00 | 13.173 0.032 | 12.521 0.023 | 12.278 0.027 | 11.995 0.006 | 11.954 0.008 | 11.886 0.022 | 11.862 0.034 | – – | Y |
| LOri054 | 16.19 0.00 | 14.73 0.00 | 13.189 0.024 | 12.509 0.022 | 12.271 0.027 | 11.974 0.006 | 11.948 0.009 | 11.805 0.025 | 11.862 0.038 | – – | Y |
| LOri055 | 16.12 0.00 | 14.76 0.00 | 13.184 0.026 | 12.477 0.026 | 12.253 0.026 | 12.044 0.006 | 12.038 0.009 | 12.015 0.029 | 11.902 0.038 | – – | Y |
| LOri056 | 16.43 0.00 | 14.87 0.00 | 13.211 0.029 | 12.567 0.026 | 12.267 0.029 | 12.011 0.004[2] | 11.906 0.005[2] | 11.913 0.019[2] | 11.853 0.032[2] | – – | Y |
| LOri057 | 16.63 0.00 | 15.04 0.00 | 13.412 0.024 | 12.773 0.023 | 12.487 0.030 | 12.177 0.007 | 12.078 0.009 | 11.988 0.030 | 11.992 0.033 | – – | Y |
| LOri058 | 16.57 0.00 | 15.06 0.00 | 13.521 0.024 | 12.935 0.022 | 12.643 0.027 | 12.332 0.007 | 12.269 0.010 | 12.172 0.032 | 12.637 0.072 | – – | Y |
| LOri059 | 16.57 0.00 | 15.10 0.00 | 13.574 0.026 | 12.884 0.026 | 12.682 0.032 | 12.317 0.007 | 12.270 0.009 | 12.218 0.030 | 12.679 0.066 | – – | Y |
| LOri060 | 16.56 0.00 | 15.14 0.00 | 13.598 0.030 | 12.961 0.030 | 12.663 0.029 | 12.423 0.008 | 12.418 0.011 | 12.408 0.041 | 12.377 0.051 | – – | Y |
| LOri061 | 16.58 0.00 | 15.15 0.00 | 13.533 0.023 | 12.833 0.026 | 12.525 0.027 | 12.052 0.006 | 11.851 0.008 | 11.519 0.019 | 10.730 0.015 | 8.047 0.046 | Y |
| LOri062 | 16.62 0.00 | 15.16 0.00 | 13.634 0.029 | 13.005 0.030 | 12.725 0.027 | 12.370 0.007 | 12.246 0.009 | 12.153 0.030 | 11.306 0.021 | 7.834 0.035 | Y |
| LOri063 | 16.80 0.01 | 15.34 0.00 | 13.756 0.029 | 13.066 0.029 | 12.663 0.030 | 11.666 0.006 | 11.368 0.007 | 11.768 0.028 | 10.397 0.014 | 6.055 0.010 | Y |
| LOri064 | 16.78 0.01 | 15.34 0.00 | 13.782 0.026 | 13.098 0.025 | 12.846 0.029 | 12.486 0.008 | 12.489 0.011 | 12.378 0.034 | 12.245 0.053 | – – | Y |
| LOri065 | 16.89 0.01 | 15.37 0.00 | 13.820 0.024 | 13.123 0.029 | 12.843 0.027 | 12.526 0.008 | 12.504 0.011 | 12.494 0.032 | 12.641 0.063 | 8.424 0.075 | Y |
| LOri066 | 17.12 0.01 | 15.40 0.00 | 13.506 0.024 | 12.901 0.026 | 12.654 0.029 | 12.221 0.007 | 12.170 0.010 | 12.196 0.039 | 12.578 0.072 | – – | Y |
| LOri067 | 17.05 0.01 | 15.53 0.00 | 14.000 0.033 | 13.356 0.027 | 13.102 0.036 | 12.794 0.010 | 12.727 0.014 | 12.702 0.046 | 12.786 0.071 | – – | Y |
| LOri068 | 16.76 0.01 | 15.20 0.00 | 13.521 0.027 | 12.902 0.026 | 12.628 0.027 | 12.348 0.005[2] | 12.246 0.006[2] | 12.029 0.016[2] | 12.145 0.036[2] | – – | Y |
| LOri069 | 16.89 0.01 | 15.20 0.00 | 13.384 0.027 | 12.774 0.027 | 12.425 0.027 | 12.089 0.006 | 12.015 0.008 | 12.034 0.026 | 11.903 0.042 | – – | Y |
| LOri070 | 17.18 0.01 | 15.61 0.00 | 14.042 0.032 | 13.405 0.029 | 13.067 0.031 | 12.809 0.009 | 12.779 0.013 | 12.799 0.041 | 12.559 0.060 | – – | Y |
| LOri071 | 17.13 0.00 | 15.63 0.00 | 13.749 0.030 | 13.129 0.024 | 12.839 0.031 | 12.470 0.008 | 12.382 0.010 | 12.276 0.031 | 12.250 0.044 | – – | Y |
| LOri072 | 17.00 0.00 | 15.35 0.00 | 13.554 0.026 | 12.944 0.032 | 12.631 0.027 | 11.993 0.006 | 11.860 0.008 | 11.836 0.026 | 11.718 0.037 | – – | N |
| LOri073 | 16.84 0.01 | 15.28 0.00 | 13.644 0.028 | 12.992 0.023 | 12.715 0.027 | 12.376 0.007 | 12.274 0.009 | 12.187 0.029 | 12.162 0.031 | – – | Y |
| LOri074 | 17.03 0.01 | 15.39 0.00 | 13.663 0.026 | 13.088 0.025 | 12.720 0.024 | 12.312 0.007 | 12.310 0.010 | 12.290 0.030 | 12.259 0.046 | – – | Y |
| LOri075 | 16.95 0.01 | 15.23 0.00 | 13.396 0.026 | 12.794 0.026 | 12.526 0.024 | 12.089 0.006 | 11.990 0.008 | 11.924 0.026 | 11.936 0.038 | – – | Y |
| LOri076 | 17.39 0.01 | 15.81 0.00 | 14.216 0.027 | 13.527 0.027 | 13.201 0.032 | 12.916 0.010 | 12.843 0.014 | 12.669 0.048 | 12.754 0.072 | – – | Y |
| LOri077 | 17.45 0.00 | 15.89 0.00 | 14.031 0.027 | 13.416 0.027 | 13.109 0.035 | 12.761 0.009 | 12.717 0.012 | 12.700 0.046 | 12.650 0.073 | – – | Y |
| LOri078 | 17.35 0.00 | 15.92 0.00 | 14.227 0.041 | 13.593 0.053 | 13.286 0.040 | 12.766 0.009 | 12.844 0.014 | 12.789 0.046 | 12.554 0.069 | – – | Y |
| LOri079 | 17.51 0.00 | 16.00 0.00 | 14.221 0.032 | 13.536 0.032 | 13.338 0.039 | 13.002 0.006[2] | 12.970 0.008[2] | 12.876 0.078[2] | 12.724 0.048[2] | – – | Y |
| LOri080 | 17.51 0.00 | 16.01 0.00 | 13.804 0.023 | 13.196 0.022 | 12.891 0.033 | 12.504 0.008 | 12.424 0.010 | 12.597 0.041 | 12.190 0.031 | – – | Y |
| LOri081 | 17.61 0.00 | 16.02 0.00 | 14.669 0.032 | 13.692 0.032 | 13.209 0.037 | 12.620 0.008 | 12.360 0.010 | 12.050 0.030 | 11.632 0.028 | 8.062 0.056 | Y |
| LOri082 | 17.57 0.00 | 16.02 0.00 | 14.200 0.033 | 13.570 0.025 | 13.281 0.033 | 13.008 0.011 | 12.954 0.015 | 13.586 0.100 | 12.830 0.100 | – – | Y |
| LOri083 | 17.56 0.00 | 16.02 0.00 | 14.265 0.030 | 13.638 0.035 | 13.375 0.040 | 13.012 0.010 | 12.946 0.013 | 12.947 0.057 | 13.017 0.074 | – – | Y |
| LOri084 | 17.48 0.00 | 16.03 0.00 | 14.077 0.024 | 13.448 0.027 | 13.188 0.034 | 12.888 0.010 | 12.800 0.013 | 12.863 0.061 | 12.745 0.067 | – – | Y |
| LOri085 | 17.65 0.01 | 16.04 0.00 | 14.189 0.026 | 13.622 0.037 | 13.233 0.027 | 12.584 0.008 | 12.315 0.010 | 12.090 0.028 | 11.510 0.029 | 8.089 0.056 | Y |
| LOri086 | 17.59 0.00 | 16.09 0.00 | 14.482 0.032 | 13.867 0.032 | 13.503 0.040 | 13.251 0.011 | 13.205 0.016 | 13.160 0.057 | 13.277 0.098 | – – | Y |
| LOri087 | 17.54 0.00 | 16.09 0.00 | 14.186 0.039 | 13.601 0.030 | 13.279 0.035 | 12.978 0.010 | 12.894 0.013 | 13.002 0.064 | 12.669 0.060 | – – | Y |
| LOri088 | 17.78 0.00 | 16.10 0.00 | 14.140 0.031 | 13.543 0.037 | 13.228 0.039 | 12.923 0.009 | 12.853 0.013 | 12.865 0.040 | 12.676 0.051 | – – | Y |
| LOri089 | 17.79 0.00 | 16.15 0.00 | 14.380 0.032 | 13.839 0.035 | 13.512 0.039 | 13.156 0.011 | 13.123 0.015 | 13.682 0.086 | 12.877 0.081 | – – | Y |
| LOri090 | 17.77 0.00 | 16.17 0.00 | 14.515 0.041 | 13.881 0.023 | 13.651 0.051 | 13.226 0.011 | 13.116 0.015 | 12.930 0.047 | 13.126 0.100 | – – | Y |
| LOri091 | 18.01 0.00 | 16.18 0.00 | 14.184 0.032 | 13.556 0.032 | 13.289 0.031 | 12.868 0.009 | 12.803 0.013 | 13.087 0.062 | 12.462 0.054 | – – | Y |

Continued on next page…

Table 2.3 – Continued

| Name[3] | R error | I error | J error | H error | Ks error | [3.6] error | [4.5] error | [5.8] error | [8.0] error | [24] error | Mem[1] |
|---|---|---|---|---|---|---|---|---|---|---|---|
| LOri092 | 17.84 0.00 | 16.19 0.00 | 14.441 0.030 | 13.841 0.038 | 13.537 0.040 | 13.158 0.011 | 13.053 0.014 | 13.517 0.087 | 12.992 0.089 | – – | Y |
| LOri093 | 17.82 0.00 | 16.21 0.00 | 14.462 0.030 | 13.836 0.039 | 13.604 0.052 | 13.169 0.011 | 13.104 0.015 | 13.256 0.073 | 12.982 0.098 | – – | Y |
| LOri094 | 18.03 0.00 | 16.28 0.00 | 14.404 0.034 | 13.802 0.030 | 13.425 0.038 | 12.955 0.009 | 12.994 0.014 | 13.184 0.058 | 12.894 0.085 | – – | Y |
| LOri095 | 17.96 0.00 | 16.35 0.00 | 14.564 0.033 | 13.913 0.029 | 13.613 0.048 | 13.247 0.012 | 13.278 0.017 | 13.176 0.067 | 13.340 0.138 | – – | Y |
| LOri096 | 18.02 0.02 | 16.37 0.00 | 14.627 0.038 | 13.965 0.037 | 13.638 0.047 | 13.039 0.010 | 12.732 0.013 | 12.527 0.045 | 12.029 0.039 | – – | Y |
| LOri098 | 18.12 0.00 | 16.40 0.00 | 14.647 0.037 | 13.985 0.045 | 13.682 0.039 | 13.393 0.012 | 13.301 0.016 | 13.284 0.075 | 13.182 0.115 | – – | Y |
| LOri099 | 18.14 0.00 | 16.42 0.00 | 14.709 0.034 | 14.074 0.035 | 13.676 0.043 | 13.421 0.013 | 13.335 0.018 | 13.211 0.069 | 13.352 0.124 | – – | Y |
| LOri100 | 18.08 0.00 | 16.43 0.00 | 14.768 0.044 | 14.044 0.042 | 13.821 0.044 | 13.446 0.012 | 13.325 0.017 | 13.163 0.066 | 13.318 0.123 | – – | Y |
| LOri101 | 18.14 0.00 | 16.48 0.00 | 15.019 0.038 | 14.372 0.044 | 14.110 0.066 | 13.763 0.015 | 13.627 0.021 | 13.860 0.105 | 13.475 0.153 | – – | N |
| LOri102 | 18.24 0.00 | 16.50 0.00 | 14.634 0.047 | 14.083 0.050 | 13.809 0.057 | 13.296 0.012 | 13.213 0.015 | 13.275 0.073 | 13.101 0.108 | – – | Y |
| LOri103 | 18.30 0.00 | 16.55 0.00 | 14.643 0.029 | 14.126 0.029 | 13.833 0.055 | 13.425 0.013 | 13.387 0.018 | 13.140 0.067 | 13.628 0.151 | – – | Y |
| LOri104 | 18.48 0.03 | 16.71 0.01 | 14.667 0.030 | 14.136 0.036 | 13.721 0.042 | 13.143 0.011 | 12.877 0.014 | 12.694 0.055 | 11.762 0.035 | – – | Y |
| LOri105 | 18.58 0.00 | 16.75 0.00 | 14.922 0.040 | 14.340 0.052 | 13.993 0.053 | 13.621 0.016 | 13.593 0.021 | 13.601 0.093 | 13.536 0.159 | – – | Y |
| LOri106 | 18.48 0.00 | 16.76 0.00 | 14.776 0.043 | 14.161 0.057 | 13.743 0.045 | 13.295 0.012 | 12.967 0.014 | 12.558 0.045 | 11.832 0.034 | 8.849 0.151 | Y |
| LOri107 | 18.85 0.00 | 16.78 0.00 | 14.656 0.036 | 13.987 0.035 | 13.621 0.052 | 13.213 0.017 | 13.152 0.019 | 13.215 0.082 | 13.046 0.160 | – – | Y |
| LOri108 | 18.64 0.00 | 16.80 0.00 | 14.840 0.033 | 14.256 0.048 | 13.918 0.050 | 13.498 0.013 | 13.464 0.018 | 13.387 0.073 | 13.303 0.124 | – – | Y |
| LOri109 | 18.67 0.00 | 16.81 0.00 | 14.96 0.01 | 14.47 0.01 | 14.18 0.01 | 13.699 0.015 | 13.654 0.022 | 13.519 0.077 | 13.708 0.190 | – – | Y |
| LOri110 | 18.54 0.00 | 16.82 0.00 | 15.043 0.051 | 14.475 0.056 | 14.144 0.060 | 13.798 0.016 | 13.796 0.026 | 14.017 0.130 | 13.454 0.177 | – – | N |
| LOri111 | 18.88 0.00 | 16.86 0.00 | 14.801 0.038 | 14.165 0.043 | 13.786 0.051 | 13.419 0.012 | 13.330 0.017 | 13.601 0.082 | 13.664 0.185 | – – | Y |
| LOri112 | 18.72 0.00 | 16.87 0.00 | 14.991 0.042 | 14.358 0.048 | 14.148 0.062 | 13.412 0.013 | 13.335 0.017 | 13.334 0.079 | 13.299 0.145 | – – | Y |
| LOri113 | 18.71 0.00 | 16.99 0.00 | 15.18 0.01 | 14.62 0.01 | 14.30 0.01 | 13.723 0.017 | 13.579 0.021 | 13.263 0.070 | 12.448 0.054 | – – | Y |
| LOri114 | 18.99 0.00 | 17.06 0.00 | 15.092 0.044 | 14.389 0.053 | 14.006 0.064 | 13.502 0.015 | 13.414 0.020 | 13.525 0.096 | 13.051 0.108 | – – | Y |
| LOri115 | 18.80 0.00 | 17.08 0.00 | 15.449 0.047 | 14.821 0.068 | 14.594 0.104 | 14.083 0.017 | 14.012 0.030 | 13.942 0.119 | 13.346 0.131 | – – | Y |
| LOri116 | 19.05 0.01 | 17.17 0.00 | 15.343 0.057 | 14.573 0.055 | 14.411 0.082 | 13.977 0.017 | 13.847 0.024 | 14.340 0.190 | 13.614 0.141 | – – | Y |
| LOri117 | 19.24 0.01 | 17.21 0.00 | 15.10 0.01 | 14.36 0.01 | 14.17 0.01 | 13.418 0.018 | 13.102 0.024 | 13.063 0.105 | – – | – – | Y |
| LOri118 | 19.10 0.01 | 17.23 0.00 | 15.269 0.044 | 14.686 0.064 | 14.181 0.057 | 13.430 0.013 | 13.251 0.016 | 12.844 0.045 | 12.178 0.043 | – – | Y |
| LOri119 | 19.11 0.00 | 17.30 0.00 | 15.26 0.01 | 14.74 0.01 | 14.41 0.01 | 13.568 0.014 | 13.492 0.019 | 13.408 0.088 | 13.590 0.170 | – – | Y |
| LOri120 | 19.23 0.00 | 17.34 0.00 | 15.335 0.050 | 14.770 0.059 | 14.337 0.087 | 13.878 0.015 | 13.688 0.020 | 13.458 0.086 | 12.783 0.070 | – – | Y |
| LOri121 | 19.12 0.00 | 17.37 0.00 | 15.533 0.060 | 15.093 0.086 | 14.748 0.099 | 14.336 0.019 | 14.310 0.031 | 14.053 0.144 | – – | – – | Y |
| LOri122 | 19.31 0.00 | 17.38 0.00 | 15.428 0.066 | 14.852 0.060 | 14.462 0.080 | 14.096 0.018 | 13.973 0.027 | 14.315 0.190 | 13.659 0.174 | – – | Y |
| LOri124 | 19.30 0.04 | 17.45 0.01 | 15.661 0.073 | 15.059 0.082 | 14.778 0.112 | 14.353 0.012[2] | 14.235 0.018[2] | 14.303 0.086[2] | 13.976 0.126[2] | – – | Y |
| LOri126 | 19.52 0.01 | 17.52 0.00 | 15.62 0.01 | 15.04 0.01 | 14.67 0.01 | 13.709 0.014 | 13.577 0.021 | 13.118 0.063 | 12.352 0.049 | – – | Y |
| LOri127 | 19.87 0.10 | 17.53 0.01 | 13.016 0.023 | 12.606 0.027 | 12.468 0.024 | 12.401 0.007 | 12.348 0.010 | 12.301 0.033 | 12.352 0.037 | – – | N |
| LOri128 | 19.53 0.01 | 17.58 0.00 | 15.624 0.077 | 15.099 0.087 | 14.769 0.109 | 14.150 0.021 | 14.115 0.031 | 14.327 0.254 | 13.956 0.209 | – – | Y |
| LOri129 | 19.51 0.01 | 17.59 0.00 | 15.383 0.056 | 14.816 0.072 | 14.526 0.102 | 13.625 0.014 | 13.317 0.016 | 13.194 0.058 | 12.598 0.057 | – – | Y |
| LOri130 | 19.44 0.01 | 17.63 0.00 | 15.731 0.059 | 15.265 0.092 | 14.735 0.110 | 14.408 0.013[2] | 14.382 0.020[2] | 14.041 0.077[2] | 14.348 0.256[2] | – – | Y |
| LOri131 | 19.79 0.01 | 17.78 0.00 | 15.429 0.054 | 14.900 0.063 | 14.380 0.090 | 13.991 0.017 | 13.909 0.025 | 13.865 0.119 | 13.344 0.106 | – – | Y |
| LOri132 | 19.99 0.01 | 17.82 0.00 | 15.583 0.067 | 14.962 0.078 | 14.913 0.145 | 14.173 0.019 | 14.087 0.025 | 14.076 0.140 | 13.630 0.129 | – – | Y |
| LOri133 | 19.68 0.01 | 17.83 0.00 | 16.290 0.101 | 15.900 0.167 | 15.378 0.203 | 15.066 0.032 | 14.941 0.041 | 15.077 0.312 | – – | – – | N |
| LOri134 | 19.91 0.01 | 17.90 0.00 | 15.543 0.057 | 14.937 0.074 | 14.666 0.107 | 14.321 0.020 | 14.071 0.027 | 13.880 0.113 | 13.884 0.154 | – – | Y |
| LOri135 | 19.91 0.01 | 17.90 0.00 | 15.671 0.072 | 15.082 0.087 | 14.908 0.138 | 14.334 0.014[2] | 14.166 0.018[2] | 14.171 0.113[2] | 13.871 0.108[2] | – – | Y |
| LOri136 | 20.06 0.12 | 17.92 0.01 | 15.560 0.085 | 14.828 0.090 | 14.576 0.108 | 14.139 0.016[2] | 14.224 0.023[2] | 13.948 0.083[2] | 13.607 0.107[2] | – – | Y |
| LOri137 | 19.89 0.08 | 17.96 0.09 | – – | – – | – – | 16.454 0.073 | 16.789 0.270 | – – | – – | – – | N |
| LOri138 | 20.01 0.01 | 17.96 0.00 | 15.821 0.078 | 15.204 0.083 | 14.971 0.133 | 14.527 0.022 | 14.469 0.035 | 14.150 0.123 | – – | – – | Y |
| LOri139 | 20.04 0.01 | 18.16 0.00 | 16.16 0.01 | 15.53 0.01 | 15.06 0.01 | 14.054 0.017 | 13.658 0.019 | 13.151 0.056 | 12.663 0.062 | – – | Y |
| LOri140 | 20.34 0.01 | 18.21 0.00 | 15.981 0.078 | 15.224 0.089 | 14.750 0.113 | 14.030 0.017 | 13.704 0.023 | 13.299 0.066 | 12.786 0.078 | – – | Y |
| LOri141 | 20.44 0.01 | 18.25 0.00 | 16.61 0.01 | 15.89 0.01 | 15.68 0.02 | 15.100 0.034 | 15.668 0.089 | – – | – – | – – | N |

Continued on next page…

Table 2.3 – Continued

| Name[3] | R error | I error | J error | H error | Ks error | [3.6] error | [4.5] error | [5.8] error | [8.0] error | [24] error | Mem[1] |
|---|---|---|---|---|---|---|---|---|---|---|---|
| LOri142 | 20.34 0.01 | 18.27 0.00 | 16.25 0.01 | 15.58 0.01 | 15.26 0.01 | 14.705 0.028 | 14.674 0.041 | – – | – – | – – | Y |
| LOri143 | 20.32 0.01 | 18.30 0.00 | 16.11 0.01 | 15.61 0.02 | 15.23 0.01 | 14.835 0.015 | 14.896 0.023 | 14.765 0.089 | 14.553 0.126 | – – | Y |
| LOri144 | 20.24 0.11 | 18.30 0.11 | 17.69 0.02 | 16.90 0.02 | 16.55 0.03 | 16.476 0.094 | 16.424 0.184 | – – | – – | – – | N? |
| LOri146 | 20.88 0.26 | 18.60 0.02 | 16.230 0.107 | 15.470 0.110 | 14.936 0.128 | 14.404 0.022[2] | 14.199 0.035[2] | 13.836 0.103[2] | 13.614 0.175[2] | – – | Y |
| LOri147 | 20.54 0.01 | 18.60 0.00 | 16.58 0.02 | 15.93 0.02 | 15.62 0.02 | 15.348 0.023[2] | 15.675 0.048[2] | 15.128 0.224[2] | – – | – – | Y? |
| LOri148 | 20.77 0.02 | 18.62 0.00 | 16.39 0.01 | 16.12 0.01 | 15.98 0.02 | 14.869 0.030 | 14.989 0.051 | 14.530 0.210 | – – | – – | Y? |
| LOri149 | 21.07 0.02 | 18.95 0.00 | 99.99 0.00 | 88.88 0.00 | 16.97 0.02 | 17.135 0.132[2] | 16.829 0.099[2] | – – | – – | – – | N |
| LOri150 | 21.29 0.03 | 19.00 0.00 | 16.656 0.152 | 16.134 0.197 | 15.560 0.214 | 15.015 0.032 | 15.133 0.070 | 14.942 0.390 | – – | – – | Y |
| LOri151 | 20.98 0.02 | 19.00 0.00 | 17.40 0.02 | 16.76 0.02 | 16.52 0.04 | 15.801 0.056 | 15.716 0.103 | – – | – – | – – | N |
| LOri152 | 21.43 0.04 | 19.05 0.00 | 16.773 0.173 | 16.657 0.295 | 15.870 0.285 | 16.313 0.086 | 16.316 0.158 | – – | – – | – – | N? |
| LOri153 | 21.30 0.03 | 19.17 0.00 | 17.09 0.01 | 16.37 0.01 | 16.09 0.03 | 15.223 0.036 | 15.139 0.072 | – – | – – | – – | Y |
| LOri154 | 21.79 0.05 | 19.31 0.00 | 16.804 0.169 | 16.143 0.192 | 15.513 0.219 | 15.071 0.035 | 15.953 0.141 | – – | – – | – – | Y |
| LOri155 | 21.87 0.06 | 19.36 0.00 | 16.97 0.01 | 16.30 0.01 | 15.84 0.02 | 15.085 0.019[2] | 15.412 0.045[2] | 14.878 0.163[2] | 14.517 0.183[2] | – – | Y |
| LOri156 | 22.05 0.06 | 19.59 0.01 | 17.06 0.02 | 16.34 0.02 | 15.89 0.02 | 14.942 0.029 | 14.688 0.038 | 14.127 0.148 | 13.870 0.146 | – – | Y |
| LOri157 | 22.09 0.06 | 19.63 0.01 | 18.08 0.03 | 17.42 0.03 | 17.00 0.04 | 16.907 0.103 | 16.719 0.161 | – – | – – | – – | N |
| LOri158 | 22.07 0.05 | 19.67 0.01 | 18.59 0.03 | 17.86 0.05 | 17.61 0.08 | 17.627 0.123[2] | 17.565 0.245[2] | – – | – – | – – | N? |
| LOri159 | 22.25 0.06 | 20.01 0.01 | 18.21 0.02 | 17.62 0.05 | 17.47 0.09 | 16.422 0.089 | 16.627 0.207 | – – | – – | – – | N? |
| LOri160 | 22.82 0.13 | 20.29 0.02 | 18.11 0.03 | 17.14 0.02 | 16.38 0.03 | 15.669 0.052 | 15.384 0.079 | – – | – – | – – | Y |
| LOri161 | 23.09 0.19 | 20.34 0.01 | 17.71 0.02 | 16.90 0.02 | 16.51 0.03 | 16.361 0.122 | 16.451 0.249 | – – | – – | – – | Y |
| LOri162 | 23.22 0.51 | 20.42 0.02 | 17.64 0.03 | 16.90 0.09 | 16.52 0.04 | 15.675 0.062 | 15.733 0.112 | – – | – – | – – | Y |
| LOri163 | 22.96 0.24 | 20.42 0.02 | 17.86 0.04 | 17.02 0.08 | 16.76 0.05 | 15.666 0.062 | 15.904 0.119 | – – | – – | – – | Y |
| LOri164 | 23.11 0.17 | 20.44 0.01 | 18.75 0.04 | 18.17 0.05 | 18.31 0.13 | – – | – – | – – | – – | – – | N |
| LOri165 | 23.12 0.22 | 20.73 0.02 | 18.77 0.08 | 18.11 0.16 | 17.90 0.09 | 16.377 0.112 | 16.130 0.189 | – – | – – | – – | N? |
| LOri166 | 23.33 0.18 | 20.75 0.02 | 18.26 0.03 | 88.88 0.00 | 17.38 0.04 | 16.655 0.055[2] | 17.232 0.237[2] | – – | – – | – – | Y? |
| LOri167 | 23.86 0.64 | 20.90 0.02 | 18.01 0.03 | 17.17 0.07 | 16.83 0.09 | 15.935 0.063 | 16.060 0.129 | – – | – – | – – | Y |
| LOri168 | 24.15 0.62 | 21.54 0.04 | 19.39 0.09 | 18.58 0.08 | 18.70 0.25 | – – | – – | – – | – – | – – | N? |
| LOri169 | 24.83 1.10 | 21.88 0.05 | 20.10 0.10 | 19.47 0.15 | 018.93 0.42 | – – | – – | – – | – – | – – | Y? |
| LOri170 | 25.41 2.61 | 22.06 0.07 | 20.35 0.20 | 19.20 0.20 | 019.39 0.46 | – – | – – | – – | – – | – – | N? |

[1]Final membership.

[2]2-pixel aperture radius used for the photometry due to the presence of nearby objects or hot pixels.

[3]LOri097 and LOri145 are artifacts. LOri123 is a non member and has uncertainties in its photometry.

**Table 2.4**: Membership for the previously selected candidate members of Collinder 69 from Barrado y Navascués et al. (2007b).

| Name | SpT | Phot.Mem[1] | Mem[2] | Mem[3] | IRAC class[4] | SED slope[5] | Disk Type | Comment[6] |
|---|---|---|---|---|---|---|---|---|
| LOri001 | – | Y Y Y Y Y Y | Mem | Y | III | -2.8 | Diskless | Ha- WHa(DM)=2.51 DM#01 |
| LOri002 | – | Y Y Y Y Y Y | NM- | Y | III | -2.74 | Diskless | – |
| LOri003 | – | Y Y Y Y Y Y | Mem | Y | III | -2.71 | Diskless | Ha- WHa(DM)=3.35 DM#46 S08 |
| LOri004 | – | Y Y Y Y Y Y | Mem | Y | III | -2.65 | Diskless | – |
| LOri005 | – | Y Y Y Y Y Y | NM- | Y | III | -2.75 | Diskless | – |
| LOri006 | – | Y Y Y Y Y Y | Mem | Y | III | -2.68 | Diskless | – |
| LOri007 | – | Y Y Y Y Y Y | Mem | Y | III | -2.63 | Diskless | – |
| LOri008 | – | Y Y Y Y Y Y | Mem | Y | III | -2.56 | Diskless | Ha- WHa(DM)=1.65 DM#51 |
| LOri009 | – | Y Y Y Y Y Y | Mem | Y | III | -2.71 | Diskless | – |
| LOri010 | – | Y Y Y Y Y Y | Mem | Y | III | -2.69 | Diskless | – |
| LOri011 | – | Y Y Y Y Y Y | NM- | Y | III | -2.70 | Diskless | – |
| LOri012 | – | Y Y Y Y Y Y | NM- | Y | III | -2.70 | Diskless | – |
| LOri013 | – | Y Y Y Y Y Y | Mem | Y | III | -2.66 | Diskless | Ha- WHa(DM)=4.41 DM#04 |
| LOri014 | – | Y Y Y Y Y Y | Mem | Y | III | -2.71 | Diskless | Ha- WHa(DM)=1.45 DM#58 |
| LOri015 | – | Y Y Y Y Y Y | Mem | Y | III | -2.89 | Diskless | – |
| LOri016 | – | Y Y Y Y Y Y | Mem | Y | III | -2.58 | Diskless | S08 |
| LOri017 | – | Y Y Y Y Y Y | Mem | Y | III | -2.72 | Diskless | Ha- WHa(DM)=0.80 DM#60 |
| LOri018 | – | Y Y Y Y Y Y | Mem | Y | III | -2.63 | Diskless | Ha- WHa(DM)=2.02 DM#56 |
| LOri019 | – | Y Y Y Y Y Y | Mem | Y | III | -2.71 | Diskless | – |
| LOri020 | – | Y Y Y Y Y Y | Mem | N[7] | III | -2.63 | Diskless | – |
| LOri021 | – | Y Y Y Y Y Y | Mem | Y | III | -2.76 | Diskless | Ha- WHa(DM)=1.47 DM#25 |
| LOri022 | – | Y Y Y Y Y Y | Mem | Y | III | -2.65 | Diskless | Ha- WHa(DM)=4.39 DM#44 S08 |
| LOri023 | – | Y Y Y Y Y Y | Mem | Y | III | -2.65 | Diskless | Ha- WHa(DM)=1.95 DM#50 |
| LOri024 | – | Y Y Y Y Y Y | Mem | Y | III | -2.67 | Diskless | S08 |
| LOri025 | – | Y Y Y Y Y Y | Mem? | Y | III | -2.72 | Diskless | Ha- WHa(DM)=3.95 DM#59 |
| LOri026 | – | Y Y Y Y Y Y | Mem | Y | III | -2.69 | Diskless | Ha- WHa(DM)=6.07 DM#12 S08 |
| LOri027 | – | Y Y Y Y Y Y | Mem | Y | III | -2.68 | Diskless | – |
| LOri028 | – | Y Y Y Y Y Y | Mem? | Y | III | -2.67 | Diskless | – |
| LOri029 | – | Y Y Y Y Y Y | NM- | Y | II | -0.72 | Thick | Ha+ WHa(DM)=30.00 DM#36 |
| LOri030 | – | Y Y Y Y Y Y | Mem | Y | III | -2.60 | Diskless | S08 |
| LOri031 | M4.0 | Y Y Y Y Y Y | Mem | Y | III | -2.69 | Diskless | Ha- WHa=3.8 DM#20 WHa(DM)= 3.45 |
| LOri032 | – | Y Y Y Y Y Y | Mem | Y | III | -2.64 | Diskless | Ha- WHa(DM)=6.83 DM#55 |
| LOri033 | – | Y Y Y Y Y Y | Mem | Y | III | -2.68 | Diskless | Ha- WHa(DM)=3.14 DM#39 |
| LOri034 | – | Y Y Y Y Y Y | NM- | Y | II | -0.85 | Thick | Ha+ WHa(DM)=10.92 DM#33 S08 |
| LOri035 | – | Y Y Y Y Y Y | Mem | Y | III | -2.70 | Diskless | Ha- WHa(DM)=4.13 DM#29 S08 |
| LOri036 | – | Y Y Y Y Y Y | Mem | N[7] | III | -2.67 | Diskless | – |
| LOri037 | – | Y Y Y Y Y Y | Mem | Y | III | -2.67 | Diskless | Ha- WHa(DM)=3.63 DM#11 S08 |
| LOri038 | – | Y – Y Y Y – – | Mem | Y | II | -1.00 | Thick | Ha+ WHa(DM)=24.95 DM#02 |
| LOri039 | – | Y Y Y Y Y Y | Mem | Y | III | -2.65 | Diskless | Ha- WHa(DM)=3.59 DM#49 M08 |
| LOri040 | – | Y Y Y Y Y Y | Mem | Y | III | -2.66 | Diskless | Ha- WHa(DM)=3.90 DM#41 S08,M08 |
| LOri041 | – | Y Y Y Y Y Y | Mem | Y | III | -2.69 | Diskless | Ha- WHa(DM)=8.20 DM#38 S08,M08 |
| LOri042 | M4.0 | Y Y Y Y Y Y | Mem | Y | III | -2.67 | Diskless | Ha- WHa=4.3 DM#54 WHa(DM)= 4.22 |
| LOri043 | – | Y Y Y Y Y Y | Mem | Y | III | -2.69 | Transition | M08 |
| LOri044 | – | Y Y Y Y Y Y | Mem | N[7] | III | -2.65 | Diskless | – |

Continued on next page…

Table 2.4 – Continued

| Name | SpT | Phot.Mem[1] | Mem[2] | Mem[3] | IRAC class[4] | SED slope[5] | Disk Type | Comment[6] |
|---|---|---|---|---|---|---|---|---|
| LOri045 | – | Y Y Y Y Y Y | Mem | Y | III | -2.68 | Diskless | S08 |
| LOri046 | – | Y Y Y Y Y Y | Mem? | N[7] | III | -2.67 | Diskless | – |
| LOri047 | – | Y Y Y Y Y Y | Mem | Y | III | -2.68 | Diskless | Ha- WHa(DM)=8.65 DM#47 M08 |
| LOri048 | – | Y Y Y Y Y Y | Mem | Y | II | -2.07 | Thin | S08,M08 |
| LOri049 | – | Y Y Y Y Y Y | Mem | Y | III | -3.32 | Diskless | – |
| LOri050 | M4.5 | Y Y Y Y Y Y | Mem | Y | II | -0.60 | Thick | 200km WHa=15.6 S08,M08 |
| LOri051 | – | Y Y Y Y Y Y | Mem | Y | III | -2.73 | Diskless | M08 |
| LOri052 | – | Y Y Y Y Y Y | Mem | Y | III | -2.68 | Diskless | M08 |
| LOri053 | – | Y Y Y Y Y Y | Mem | Y | III | -2.68 | Diskless | S08,M08 |
| LOri054 | – | Y Y Y Y Y Y | Mem | Y | III | -2.68 | Diskless | M08 |
| LOri055 | M4.5: | Y Y Y Y Y Y | Mem | Y | III | -2.68 | Diskless | Ha- WHa=8.2 S08,M08 |
| LOri056 | M4.5: | Y Y Y Y Y Y | Mem | Y | III | -2.68 | Diskless | Ha- WHa=7.2 S08,M08 |
| LOri057 | M5.5 | Y Y Y Y Y Y | Mem | Y | III | -2.62 | Diskless | Ha- WHa=8.4 S08 |
| LOri058 | M4.5: | Y Y Y Y Y Y | Mem | Y | III | -3.16 | Diskless | Ha- WHa=7.3 M08 |
| LOri059 | M4.5 | Y Y Y Y Y Y | Mem | Y | III | -3.23 | Diskless | Ha- WHa=8.7 M08 |
| LOri060 | M4.5: | Y Y Y Y Y Y | Mem | Y | III | -2.79 | Diskless | Ha- WHa=4.1 S08,M08 |
| LOri061 | – | Y Y Y Y Y Y | Mem | Y | II | -1.32 | Thick | S08,M08 |
| LOri062 | – | Y Y Y Y Y Y | Mem | Y | II | -1.66 | Thick | S08,M08 |
| LOri063 | M4.5: | Y Y Y Y Y Y | Mem? | Y | II | -1.58 | Thick | Ha+FL WHa=12.8 S08,M08 |
| LOri064 | – | Y Y Y Y Y Y | Mem | Y | III | -2.54 | Diskless | M08 |
| LOri065 | – | Y Y Y Y Y Y | Mem | Y | III | -2.97 | Transition | M08 |
| LOri066 | – | Y Y Y Y Y Y | Mem | Y | III | -3.25 | Diskless | M08 |
| LOri067 | – | Y Y Y Y Y Y | Mem | Y | III | -2.83 | Diskless | M08 |
| LOri068 | M5.0 | Y Y Y Y Y Y | Mem? | Y | III | -2.57 | Diskless | Ha+ WHa=16.6 S08,M08 |
| LOri069 | – | Y Y Y Y Y Y | Mem? | Y | III | -2.65 | Diskless | S08,M08 |
| LOri070 | – | Y Y Y Y Y Y | Mem | Y | III | -2.57 | Diskless | – |
| LOri071 | M5.0 | Y Y Y Y Y Y | Mem | Y | III | -2.58 | Diskless | Ha- WHa=8.0 |
| LOri072 | – | Y Y Y Y Y Y | Mem? | N[7] | III | -2.55 | Diskless | – |
| LOri073 | M5.0 | Y Y Y Y Y Y | Mem? | Y | III | -2.59 | Diskless | Ha+? WHa=12.0 M08 |
| LOri074 | – | Y Y Y Y Y Y | Mem? | Y | III | -2.78 | Diskless | M08 |
| LOri075 | M5.5 | Y Y Y Y Y Y | Mem? | Y | III | -2.67 | Diskless | Ha- WHa=9.4 WHa=9.4 S08,M08 |
| LOri076 | – | Y Y Y Y Y Y | Mem | Y | III | -2.62 | Diskless | S08,M08 |
| LOri077 | M5.0 | Y Y Y Y Y Y | Mem | Y | III | -2.72 | Diskless | Ha- WHa=8.8 M08 |
| LOri078 | – | Y Y Y Y Y Y | Mem | Y | III | -2.58 | Diskless | M08 |
| LOri079 | – | Y Y Y Y Y Y | Mem? | Y | III | -2.51 | Diskless | S08,M08 |
| LOri080 | M5.5 | Y Y Y Y Y Y | Mem | Y | III | -2.55 | Diskless | Ha+? WHa=14.3 S08,M08 |
| LOri081 | M5.5 | N Y Y Y Y Y | Mem+ | Y | II | -1.70 | Thick | Ha- WHa=4.2 |
| LOri082 | M4.5 | Y Y Y Y Y Y | Mem+ | Y | III | -2.82 | Diskless | Ha- WHa=8.6 M08 |
| LOri083 | – | Y Y Y Y Y Y | Mem | Y | III | -2.85 | Diskless | S08,M08 |
| LOri084 | – | Y Y Y Y Y Y | Mem | Y | III | -2.71 | Diskless | – |
| LOri085 | – | Y Y Y Y Y Y | Mem | Y | II | -1.63 | Thick | M08 |
| LOri086 | – | Y Y Y Y Y Y | Mem | Y | III | -2.86 | Diskless | M08 |
| LOri087 | M4.5 | Y Y Y Y Y Y | Mem+ | Y | III | -2.54 | Diskless | Ha- WHa=6.7 S08,M08 |
| LOri088 | – | Y Y Y Y Y Y | Mem | Y | III | -2.58 | Diskless | S08,M08 |
| LOri089 | M5.0 | Y Y Y Y Y Y | Mem | Y | III | -2.50 | Diskless | Ha- WHa=5.1 |
| LOri090 | – | Y Y Y Y Y Y | Mem | Y | III | -2.69 | Diskless | M08 |
| LOri091 | M5.5 | Y Y Y Y Y Y | Mem | Y | III | -2.48 | Diskless | Ha+? WHa=14.7 M08 |

Continued on next page…

Table 2.4 – Continued

| Name | SpT | Phot.Mem[1] | Mem[2] | Mem[3] | IRAC class[4] | SED slope[5] | Disk Type | Comment[6] |
|---|---|---|---|---|---|---|---|---|
| LOri092 | – | Y Y Y Y Y Y Y | Mem | Y | III | -2.79 | Diskless | S08,M08 |
| LOri093 | – | Y Y Y Y Y Y Y | Mem | Y | III | -2.68 | Diskless | S08,M08 |
| LOri094 | M5.5 | Y Y Y Y Y Y Y | Mem | Y | III | -2.82 | Diskless | Ha- WHa=10.4 S08,M08 |
| LOri095 | M6.0 | Y Y Y Y Y Y Y | Mem+ | Y | III | -2.91 | Diskless | Ha- WHa=7.3 S08,M08 |
| LOri096 | – | Y Y Y Y Y Y Y | Mem | Y | II | -1.71 | Thick | S08,M08 |
| LOri098 | M5.0 | Y Y Y Y Y Y Y | Mem+ | Y | III | -2.61 | Diskless | Ha- WHa=12.9 M08 |
| LOri099 | M5.25 | Y Y Y Y Y Y Y | Mem | Y | III | -2.74 | Diskless | Ha- WHa=6.6 |
| LOri100 | M5.5 | Y Y Y Y Y Y Y | Mem | Y | III | -2.67 | Diskless | Ha+? WHa=13.1 S08,M08 |
| LOri101 | – | N N ? ? Y Y Y | Mem? | N | III | -2.6 | Diskless | – |
| LOri102 | – | Y Y Y Y Y Y Y | Mem? | Y | III | -2.65 | Diskless | S08,M08 |
| LOri103 | – | Y Y Y Y Y Y Y | Mem? | Y | III | -2.31 | Thin | M08 |
| LOri104 | – | Y Y Y Y Y Y Y | Mem | Y | II | -1.30 | Thick | M08 |
| LOri105 | – | Y Y Y Y Y Y Y | Mem | Y | III | -2.75 | Diskless | S08,M08 |
| LOri106 | M5.5 | Y Y Y Y Y Y Y | Mem | Y | II | -1.16 | Thick | Ha+ WHa=54.0 S08,M08 |
| LOri107 | M6.0 | Y Y Y Y Y Y Y | Mem+ | Y | III | -2.68 | Diskless | Ha- WHa=11.7 M08 |
| LOri108 | – | Y Y Y Y Y Y Y | Mem | Y | III | -2.61 | Diskless | – |
| LOri109 | M5.5 | Y Y Y Y Y Y Y | Mem | Y | III | -2.82 | Diskless | Ha- WHa=10.1 M08 |
| LOri110 | M5.5 | Y Y Y Y Y Y Y | Mem | N[7] | III | -2.52 | Diskless | Ha- WHa=9.1 |
| LOri111 | – | Y Y Y Y Y Y Y | Mem | Y | III | -3.19 | Diskless | – |
| LOri112 | – | Y Y Y Y Y Y Y | NM- | Y | III | -2.72 | Diskless | – |
| LOri113 | M5.5 | Y Y Y Y Y Y Y | Mem | Y | II | -1.37 | Thick | Ha+ WHa=22.0 |
| LOri114 | M6.5 | Y Y Y Y Y Y Y | Mem+ | Y | II | -2.38 | Thin | Ha- WHa=10.9 M08 |
| LOri115 | M5.0 | Y Y Y Y Y Y Y | NM+ | Y | II | -2.02 | Thin | Ha- WHa=8.5 |
| LOri116 | M5.5 | Y Y Y Y Y Y Y | Mem+ | Y | III | -2.43 | Diskless | Ha- WHa=11.1 M08 |
| LOri117 | M6.0 | Y Y Y Y Y Y Y | Mem | Y | – | -2.20 | Thin | Ha+? WHa=22.9 |
| LOri118 | M5.5 | Y Y Y Y Y Y Y | Mem+ | Y | II | -1.37 | Thick | Ha- WHa=10.1 M08 |
| LOri119 | M5.5 | Y Y Y Y Y Y Y | NM? | Y | III | -2.85 | Diskless | Ha+? WHa=12.7 |
| LOri120 | M5.5 | Y Y Y Y Y Y Y | Mem+ | Y | II | -1.59 | Thick | Ha- WHa=7.4 M08 |
| LOri121 | – | Y Y Y Y ? Y Y | NM- | Y | – | -2.31 | Diskless | – |
| LOri122 | – | Y Y Y Y Y Y Y | Mem | Y | III | -2.46 | Diskless | M08 |
| LOri124 | M5.5 | Y Y Y Y Y Y Y | Mem? | Y | III | -2.56 | Diskless | Ha- WHa=8.4 M08 |
| LOri126 | M6.5 | Y Y Y Y Y Y Y | Mem+ | Y | II | -1.24 | Thick | Ha+? WHa=26.2 M08 |
| LOri127 | – | N N N N N N N | NM- | N | III | -2.78 | Diskless | – |
| LOri128 | – | Y Y Y Y Y Y Y | Mem? | Y | III | -2.69 | Diskless | – |
| LOri129 | M6.0 | Y Y Y Y Y Y Y | Mem? | Y | II | -1.71 | Thick | Ha+? WHa=12.1 M08 |
| LOri130 | M5.5 | Y Y Y Y Y ? Y | Mem+ | Y | III | -2.69 | Diskless | Ha- WHa=8.7 M08 |
| LOri131 | – | Y Y Y Y Y Y Y | Mem? | Y | II | -2.12 | Thin | M08 |
| LOri132 | – | Y Y Y Y Y Y N | NM- | Y | II | -2.25 | Thin | – |
| LOri133 | M4.5 | N N N ? ? N Y | NM+ | N | – | -2.91 | Diskless | – |
| LOri134 | M5.0 | Y Y Y Y ? ? Y | NM+ | Y | III | -2.34 | Thin? | – |
| LOri135 | M7.0 | Y Y Y Y Y Y ? | Mem? | Y | III | -2.56 | Diskless | Ha- WHa=15.5 M08 |
| LOri136 | – | Y Y Y Y Y Y Y | Mem? | Y | III | -2.17 | Thin | – |
| LOri137 | – | – – N N – – – | ? | N | – | – | – | – |
| LOri138 | – | Y Y Y Y Y Y Y | NM- | Y | – | -2.13 | Thin | – |
| LOri139 | M6.0 | Y Y Y Y Y Y Y | Mem+ | Y | II | -1.22 | Thick | Ha+? WHa=19.7 |
| LOri140 | M7.0 | Y Y Y Y Y Y Y | Mem+ | Y | II | -1.40 | Thick | Ha+ WHa=72.8 M08 |
| LOri141 | M4.5 | N N ? N Y Y Y | NM+ | N | – | -5.35 | Diskless | – |

Continued on next page…

Table 2.4 – Continued

| Name | SpT | Phot.Mem[1] | Mem[2] | Mem[3] | IRAC class[4] | SED slope[5] | Disk Type | Comment[6] |
|---|---|---|---|---|---|---|---|---|
| LOri142 | – | Y Y Y Y Y Y Y | Mem? | Y | – | – | – | – |
| LOri143 | M6.5 | Y Y Y Y Y Y Y | Mem+ | Y | III | -2.59 | Diskless | Ha+ WHa=35.7 M08 |
| LOri144 | – | N N N N N N Y | ? | N? | – | – | – | – |
| LOri146 | – | Y Y Y Y Y Y Y | Mem | Y | III | -1.90 | Thin | M08 |
| LOri147 | M5.5 | Y Y ? N ? N Y | NM+ | Y? | – | -2.41 | Thin | – |
| LOri148 | – | Y N Y Y Y Y N | NM- | Y? | – | -2.19 | Thin | – |
| LOri149 | – | – N N N – N – | ? | N | – | – | – | – |
| LOri150 | M8.0 | Y Y Y Y Y Y Y | Mem+ | Y | – | -2.72 | Diskless | Ha- WHa=15.6 |
| LOri151 | M5.5 | N N N ? Y Y Y | NM? | N | – | – | – | – |
| LOri152 | – | Y Y N N N N Y | NM- | N? | – | – | – | – |
| LOri153 | – | ? Y Y Y Y Y Y | ? | Y | – | – | – | – |
| LOri154 | M8.0 | Y Y Y ? Y Y Y | Mem+ | Y | – | – | – | Ha- WHa=16.9 |
| LOri155 | M8.0 | Y Y Y Y Y Y Y | Mem+ | Y | III | -2.03 | Thin | Ha+? WHa=38.0 |
| LOri156 | M8.0 | Y Y Y Y Y Y Y | Mem+ | Y | III | -1.54 | Thick | Ha+ WHa=101.7 |
| LOri157 | – | N N N N N N Y | ? | N | – | – | – | – |
| LOri158 | – | N N N N N N Y | ? | N? | – | – | – | – |
| LOri159 | – | N N N N Y Y N | ? | N? | – | – | – | – |
| LOri160 | – | N Y Y Y Y Y Y | ? | Y | – | – | – | – |
| LOri161 | M8.5 | Y Y Y Y Y Y Y | Mem+ | Y | – | – | – | Ha+ WHa=123 |
| LOri162 | – | Y Y Y Y Y Y Y | ? | Y | – | – | – | – |
| LOri163 | – | Y Y Y Y Y Y Y | ? | Y | – | – | – | – |
| LOri164 | – | N N – – – – N | ? | N | – | – | – | – |
| LOri165 | M7.5 | N N Y Y Y Y ? | NM? | N? | – | – | – | – |
| LOri166 | – | ? ? Y N Y Y ? | ? | Y? | – | – | – | – |
| LOri167 | – | Y Y Y Y Y Y Y | ? | Y | – | – | – | – |
| LOri168 | – | N N – – – – Y | ? | N? | – | – | – | – |
| LOri169 | – | N N – – – – – | ? | Y? | – | – | – | – |
| LOri170 | – | N N – – – – – | ? | N? | – | – | – | – |

[1]Membership is Ivs(I-J); Ivs(I-K); Ivs(I-3.6); Ivs(I-4.5); Jvs(J-3.6);Kvs(K-3.6); Jvs(J-K).

[2]Membership as in Barrado y Navascués et al. (2004b).

[3]Final membership.

[4]Final classification after IRAC CCD –[3.6]-[4.5] vs. [5.8]-[8.0] and visual inspection of the SED.

[5]IRAC slope after Lada et al. (2006)

[6]Ha+ = W(Halpha) above the saturation criterion. Ha- = W(Halpha) below the saturation criterion. 200km = width of Halpha equal or larger than this value. WHa(DM) = from Dolan & Mathieu. S08 = confirmed membership in Sacco et al. (2008). M08 = confirmed membership in Maxted et al. (2008)

[7]Non member based on Maxted et al. (2008); Sacco et al. (2008)

**Table 2.5**: Photometry for the new candidate members of Collinder 69. 1°×1° Spitzer survey.

| Name | RA (J2000) | DEC (J2000) | V | R error | I error | J error | H error | Ks error | [3.6] error | [4.5] error | [5.8] error | [8.0] error | [24] error |
|---|---|---|---|---|---|---|---|---|---|---|---|---|---|
| C69EI1-10336 | 05:35:50.93 | +09:38:56.8 | 18.699 | 17.176 0.0 | 15.55 0.0 | 13.994 0.028 | 13.285 0.033 | 13.057 0.038 | 12.491 0.0050 | 12.301 0.0060 | 12.119 0.02 | 11.702 0.026 | 9.072 0.102 |
| C69EI1-10963 | 05:35:55.56 | +10:15:12.4 | 17.578 | 16.648 0.0 | 15.702 0.0 | 14.794 0.076 | 13.939 0.078 | 13.429 0.066 | 12.828 0.0090 | 12.825 0.012 | 12.801 0.032 | 12.168 0.033 | – |
| C69EI1-114 | 05:36:56.16 | +09:31:22.8 | 16.341 | 15.118 0.0 | 13.781 0.0 | 12.212 0.026 | 11.521 0.023 | 11.301 0.023 | 10.742 0.0030 | 10.547 0.0030 | 10.223 0.0070 | 9.632 0.0040 | 7.034 0.019 |
| C69EI1-11529 | 05:35:49.35 | +10:05:39.3 | 17.757 | 16.962 0.001 | 16.383 0.001 | 15.25 0.054 | 14.627 0.067 | 14.382 0.099 | 13.784 0.0090 | 13.443 0.011 | 13.21 0.036 | 12.834 0.046 | – |
| C69EI1-11541 | 05:35:44.43 | +09:45:52.1 | – | 16.94 0.001 | 15.774 0.001 | 13.807 0.026 | 13.085 0.025 | 12.705 0.027 | 12.38 0.0050 | 12.157 0.0060 | 11.91 0.017 | 11.181 0.016 | 7.888 0.041 |
| C69EI1-11637 | 05:35:45.14 | +09:51:37.9 | – | 20.498 0.008 | 19.551 0.007 | 18.358 0.033 | 17.35 0.036 | 16.53 0.038 | 14.787 0.016 | 14.043 0.014 | 13.319 0.035 | 12.514 0.045 | 8.939 0.084 |
| C69EI1-12304 | 05:35:41.24 | +09:53:24.1 | 16.249 | 15.648 0.002 | 15.037 0.002 | 14.158 0.032 | 13.725 0.039 | 13.482 0.041 | 13.057 0.0070 | 12.989 0.0090 | 12.692 0.034 | 10.058 0.0080 | 7.219 0.02 |
| C69EI1-12787 | 05:35:39.76 | +10:01:27.5 | 17.566 | 16.608 0.0 | 15.734 0.0 | 14.779 0.101 | 13.973 0.115 | 13.432 0.083 | 12.622 0.02 | 12.578 0.019 | 11.156 0.015 | 9.358 0.0080 | 5.471 0.0050 |
| C69EI1-13002 | 05:35:37.21 | +09:56:51.7 | 18.541 | 17.057 0.0 | 15.602 0.0 | 13.723 0.026 | 13.027 0.023 | 12.538 0.024 | 11.717 0.0040 | 11.442 0.0040 | 11.287 0.011 | 10.756 0.011 | 7.884 0.04 |
| C69EI1-13542 | 05:35:28.27 | +09:36:04.5 | 15.207 | 14.65 0.0 | 14.165 0.0 | 13.342 0.029 | 12.984 0.022 | 12.847 0.029 | 12.817 0.0060 | 12.721 0.0070 | 13.506 0.054 | 12.757 0.04 | – |
| C69EI1-13667 | 05:35:31.81 | +09:54:01.9 | 14.991 | 14.193 0.001 | 13.534 0.001 | 12.579 0.026 | 11.994 0.025 | 11.82 0.026 | 11.703 0.0040 | 11.721 0.0050 | 11.641 0.019 | 11.568 0.022 | 9.182 0.116 |
| C69EI1-13824 | 05:35:34.96 | +10:11:07.9 | – | – | – | – | – | – | 13.535 0.0080 | 12.418 0.0070 | 11.574 0.013 | 10.565 0.011 | 7.1 0.019 |
| C69EI1-14424 | 05:35:28.45 | +10:02:27.5 | 17.18 | 15.686 0.003 | 14.472 0.001 | 13.151 0.029 | 12.446 0.025 | 12.157 0.029 | 11.721 0.0040 | 11.5 0.0040 | 11.126 0.01 | 10.297 0.0070 | 7.052 0.023 |
| C69EI1-14609 | 05:35:25.34 | +09:54:47.7 | – | 17.274 0.008 | 15.816 0.003 | 14.095 0.024 | 13.47 0.023 | 13.136 0.034 | 12.614 0.0060 | 12.333 0.0060 | 11.989 0.019 | 11.108 0.012 | 6.721 0.019 |
| C69EI1-15980 | 05:35:16.48 | +09:54:37.3 | – | 20.08 0.074 | 18.91 0.033 | 16.714 0.164 | 15.345 0.117 | 14.611 0.108 | 13.547 0.012 | 13.381 0.015 | 12.496 0.027 | 9.848 0.0070 | 7.775 0.047 |
| C69EI1-16121 | 05:35:09.73 | +09:30:37.0 | 18.444 | 17.773 0.0 | 16.915 0.0 | 16.214 0.113 | 15.349 0.125 | 14.651 0.112 | 13.632 0.01 | 13.289 0.012 | 12.63 0.03 | 10.418 0.0090 | 7.199 0.028 |
| C69EI1-16472 | 05:35:08.33 | +09:35:53.6 | – | – | – | 14.314 0.029 | 13.727 0.033 | 13.406 0.038 | 12.948 0.0070 | 12.767 0.0080 | 12.816 0.035 | 11.884 0.025 | 8.247 0.054 |
| C69EI1-16578 | 05:35:12.27 | +09:55:13.2 | – | – | 16.069 0.005 | 14.183 0.036 | 13.45 0.04 | 13.014 0.036 | 12.064 0.0090 | 11.714 0.0080 | 11.422 0.017 | 10.938 0.015 | 7.339 0.081 |
| C69EI1-16821 | 05:35:14.88 | +10:12:29.0 | – | – | – | – | – | – | 14.944 0.025 | 13.941 0.018 | 13.253 0.049 | 12.421 0.045 | 8.599 0.093 |
| C69EI1-2229 | 05:36:48.88 | +09:55:42.4 | – | – | – | 14.222 0.037 | 13.6 0.051 | 13.316 0.047 | 12.804 0.0060 | 12.542 0.0070 | 12.169 0.018 | 11.38 0.018 | 8.799 0.116 |
| C69EI1-3042 | 05:36:43.56 | +09:55:13.8 | – | – | – | 15.894 0.077 | 15.132 0.097 | 14.747 0.106 | 14.118 0.012 | 13.719 0.013 | 13.359 0.04 | 12.556 0.039 | 10.843 0.514 |
| C69EI1-3154 | 05:36:43.29 | +09:57:01.8 | – | – | – | 16.812 0.19 | 15.646 0.146 | 14.84 0.139 | 13.985 0.013 | 13.791 0.017 | 13.338 0.043 | 10.455 0.0080 | 7.572 0.044 |
| C69EI1-3465 | 05:36:36.04 | +09:34:54.6 | – | – | – | 14.833 0.032 | 14.319 0.051 | 14.011 0.062 | 13.516 0.0080 | 13.34 0.01 | 13.182 0.042 | 12.432 0.034 | 10.279 0.321 |
| C69EI1-3574 | 05:36:37.72 | +09:44:43.3 | – | – | – | – | – | – | 16.77 0.071 | 13.972 0.021 | 11.579 0.015 | 9.221 0.0040 | – |
| C69EI1-4761 | 05:36:32.17 | +09:53:16.7 | 13.099 | 12.727 0.001 | 12.319 0.001 | 11.607 0.026 | 11.237 0.022 | 11.154 0.023 | 11.114 0.0030 | 11.115 0.0030 | 11.121 0.01 | 11.085 0.015 | 9.224 0.122 |
| C69EI1-6036 | 05:36:20.09 | +09:39:31.7 | – | – | – | 14.36 0.032 | 13.693 0.033 | 13.43 0.046 | 12.936 0.0060 | 12.678 0.0070 | 12.548 0.024 | 12.121 0.023 | 10.537 0.47 |
| C69EI1-6539 | 05:36:15.48 | +09:34:45.5 | – | – | – | – | – | – | 14.416 0.016 | 13.289 0.011 | 12.242 0.026 | 11.105 0.014 | 7.455 0.023 |
| C69EI1-7021 | 05:36:23.84 | +10:21:25.9 | – | – | – | – | – | – | 13.358 0.0080 | 12.412 0.0070 | 11.514 0.015 | 10.556 0.01 | 7.426 0.025 |
| C69EI1-7070 | 05:36:13.97 | +09:42:17.2 | – | 19.361 0.004 | 18.722 0.004 | – | – | – | 15.152 0.027 | 14.363 0.022 | 13.437 0.047 | 11.851 0.027 | 8.093 0.045 |
| C69EI1-7312 | 05:36:19.27 | +10:10:24.5 | – | – | – | – | – | – | 14.097 0.011 | 13.22 0.011 | 12.323 0.022 | 11.305 0.019 | 8.093 0.04 |
| C69EI1-7620 | 05:36:11.23 | +09:46:26.4 | 18.39 | 17.28 0.0 | 15.856 0.0 | 13.596 0.029 | 12.553 0.027 | 12.063 0.024 | 11.403 0.0030 | 11.037 0.0030 | 10.715 0.0080 | 10.399 0.008 | 8.306 0.058 |
| C69EI1-790 | 05:36:55.33 | +09:46:48.0 | 17.515 | 16.358 0.0 | 14.95 0.0 | 13.571 0.032 | 12.875 0.035 | 12.497 0.03 | 12.081 0.0040 | 11.871 0.0050 | 11.629 0.013 | 10.89 0.013 | 8.631 0.071 |
| C69SEI1-2889 | 05:36:09.38 | +10:01:25.4 | 10.301 | 9.977 0.0 | 9.646 0.0 | 9.11 0.021 | 8.826 0.046 | 8.69 0.021 | 8.556 0.0040 | 8.535 0.0060 | 8.547 0.017 | 8.348 0.012 | 6.718 0.015 |
| C69SEI1-4253 | 05:35:19.03 | +09:54:55.4 | 11.848 | 11.288 0.0 | 10.769 0.0 | 9.887 0.027 | 9.378 0.026 | 9.141 0.024 | 8.808 0.0050 | 8.714 0.0060 | 8.627 0.018 | 8.367 0.011 | 5.87 0.0080 |
| C69SEI1-4263 | 05:35:16.68 | +09:46:39.6 | – | – | – | 7.83 0.024 | 7.851 0.033 | 7.941 0.034 | 7.93 0.0030 | 7.99 0.0040 | 7.992 0.014 | 7.984 0.01 | 5.732 0.0090 |
| C69SWI1-496 | 05:35:02.98 | +09:56:04.8 | 8.307 | 8.146 0.0 | 8.141 0.0 | 10.026 0.0010 | 9.833 0.0010 | 9.616 0.0010 | 9.413 0.0070 | 9.479 0.0090 | 9.454 0.032 | 9.363 0.025 | 7.34 0.036 |
| C69SWI1-937 | 05:34:48.56 | +09:30:57.2 | 10.437 | 10.282 0.0 | 10.12 0.0 | 9.864 0.023 | 9.788 0.024 | 9.729 0.024 | 9.677 0.0070 | 9.654 0.011 | 10.074 0.048 | 9.587 0.031 | 6.984 0.104 |
| C69WI1-10971 | 05:33:49.38 | +09:46:19.3 | 13.97 | 13.534 0.001 | 13.046 0.001 | 12.513 0.023 | 12.27 0.022 | 12.193 0.024 | 12.123 0.0040 | 12.105 0.0060 | 12.094 0.017 | 12.038 0.024 | 10.379 0.524 |
| C69WI1-12378 | 05:33:42.56 | +10:03:48.0 | – | – | – | 16.667 0.155 | 15.675 0.149 | 14.77 0.112 | 13.806 0.01 | 13.166 0.011 | 12.573 0.025 | 11.113 0.016 | 8.076 0.053 |
| C69WI1-1322 | 05:34:55.61 | +09:32:02.7 | – | – | – | 14.819 0.043 | 14.228 0.052 | 13.951 0.068 | 13.28 0.0080 | 13.18 0.011 | 13.02 0.041 | 12.199 0.035 | – |
| C69WI1-1388 | 05:34:55.24 | +09:32:04.1 | – | – | – | 12.65 0.032 | 12.002 0.027 | 11.819 0.033 | 11.59 0.0040 | 11.554 0.0050 | 11.55 0.015 | 11.503 0.02 | 8.698 0.235 |
| C69WI1-14892 | 05:33:21.96 | +10:02:02.0 | – | – | – | 14.222 0.035 | 13.596 0.039 | 13.312 0.039 | 12.911 0.0060 | 12.704 0.0080 | 12.426 0.025 | 11.864 0.025 | 9.836 0.282 |
| C69WI1-15281 | 05:33:22.12 | +10:15:51.9 | 17.508 | 16.98 0.0 | 16.36 0.0 | 15.557 0.084 | 15.204 0.115 | 14.631 0.108 | 13.831 0.01 | 13.542 0.013 | 13.022 0.046 | 10.4 0.012 | 6.783 0.016 |
| C69WI1-15377 | 05:33:15.14 | +09:50:30.1 | 17.505 | 16.291 0.0 | 14.706 0.0 | 12.949 0.028 | 12.287 0.029 | 11.876 0.028 | 11.446 0.0030 | 11.238 0.0040 | 11.071 0.01 | 10.608 0.011 | 8.162 0.053 |
| C69WI1-15404 | 05:33:11.77 | +09:36:58.6 | 17.371 | 16.586 0.0 | 15.968 0.0 | 14.972 0.062 | 14.329 0.076 | 13.802 0.077 | 13.264 0.0080 | 13.341 0.014 | 13.137 0.049 | 12.719 0.05 | – |
| C69WI1-15496 | 05:33:19.45 | +10:11:57.0 | – | – | – | – | – | – | 15.009 0.024 | 14.131 0.02 | 13.141 0.046 | 12.2 0.043 | 8.937 0.138 |

Continued on next page…

Table 2.5 – Continued

| Name | RA (J2000) | DEC (J2000) | V | R error | I error | J error | H error | Ks error | [3.6] error | [4.5] error | [5.8] error | [8.0] error | [24] error |
|---|---|---|---|---|---|---|---|---|---|---|---|---|---|
| C69WI1-2261 | 05:35:00.38 | +10:16:35.8 | 15.03 | 14.513 0.0 | 14.018 0.0 | 13.325 0.029 | 13.021 0.03 | 12.884 0.03 | 12.82 0.0060 | 12.804 0.0090 | 13.22 0.049 | 12.806 0.048 | – |
| C69WI1-2303 | 05:34:55.63 | +09:57:58.2 | – | 16.593 0.006 | 15.197 0.002 | 13.708 0.032 | 12.959 0.026 | 12.735 0.035 | 12.49 0.0050 | 12.427 0.0060 | 13.08 0.046 | 12.314 0.037 | – |
| C69WI1-2708 | 05:34:52.59 | +09:55:50.0 | – | – | – | 13.407 0.03 | 12.563 0.027 | 12.164 0.022 | 11.3 0.0030 | 10.967 0.0040 | 10.66 0.0080 | 10.151 0.008 | 7.102 0.019 |
| C69WI1-306 | 05:35:03.89 | +09:41:09.5 | 15.384 | 14.704 0.0 | 14.018 0.0 | 13.001 0.027 | 12.441 0.025 | 12.316 0.026 | 12.18 0.0050 | 12.237 0.0060 | 12.15 0.025 | 11.283 0.015 | – |
| C69WI1-3226 | 05:34:43.82 | +09:34:09.8 | – | – | – | 15.838 0.092 | 15.082 0.096 | 14.431 0.104 | 13.7 0.014 | 13.591 0.017 | 13.64 0.045 | 13.165 0.062 | – |
| C69WI1-4232 | 05:34:45.88 | +10:08:01.5 | 14.348 | 13.488 0.001 | 12.791 0.001 | 11.742 0.027 | 11.118 0.023 | 10.951 0.023 | 10.82 0.0030 | 10.888 0.0040 | 10.82 0.0090 | 10.752 0.012 | 8.893 0.097 |
| C69WI1-4614 | 05:34:40.12 | +09:56:43.7 | – | 19.261 0.009 | 18.424 0.008 | 16.363 0.165 | 15.455 0.142 | 14.631 0.126 | 13.47 0.01 | 13.341 0.014 | 12.41 0.031 | 9.619 0.006 | 6.767 0.012 |
| C69WI1-4897 | 05:34:32.18 | +09:31:58.0 | 14.957 | 14.486 0.0 | 14.04 0.0 | 13.313 0.024 | 12.907 0.027 | 12.868 0.035 | 12.78 0.0060 | 12.433 0.0060 | 13.46 0.058 | 12.747 0.048 | – |
| C69WI1-6018 | 05:34:27.62 | +09:46:33.9 | 18.471 | 17.728 0.0 | 16.944 0.0 | 16.429 0.125 | 15.662 0.188 | 14.798 0.127 | 13.74 0.012 | 13.565 0.015 | 13.23 0.043 | 10.443 0.009 | 8.817 0.086 |
| C69WI1-6412 | 05:34:22.95 | +09:39:52.1 | – | – | – | – | – | – | 14.34 0.014 | 13.319 0.011 | 13.07 0.045 | 11.202 0.017 | 7.758 0.031 |
| C69WI1-6820 | 05:34:23.33 | +09:52:15.2 | 14.821 | 14.218 0.001 | 13.605 0.001 | 12.85 0.023 | 12.444 0.03 | 12.288 0.024 | 12.21 0.0040 | 12.22 0.0060 | 12.18 0.024 | 12.232 0.04 | 8.983 0.109 |
| C69WI1-7152 | 05:34:17.70 | +09:39:22.4 | – | – | – | 14.094 0.032 | 13.512 0.03 | 13.157 0.034 | 12.57 0.0050 | 12.298 0.0060 | 11.95 0.018 | 11.271 0.019 | 9.685 0.28 |
| C69WI1-718 | 05:35:07.76 | +10:06:28.2 | 18.196 | 17.495 0.0 | 16.677 0.0 | 16.462 0.15 | 15.306 0.136 | 15.089 0.158 | 13.78 0.01 | 13.677 0.018 | 12.93 0.035 | 10.259 0.009 | 6.755 0.014 |
| C69WI1-7809 | 05:34:21.38 | +10:15:56.7 | – | – | – | 14.817 0.039 | 14.267 0.048 | 13.833 0.054 | 13.26 0.0070 | 12.978 0.0090 | 12.75 0.035 | 12.303 0.037 | – |
| C69WI1-9288 | 05:34:03.91 | +09:52:12.3 | 17.394 | 16.116 0.003 | 14.96 0.002 | 13.001 0.024 | 12.05 0.024 | 11.551 0.024 | 10.775 0.0020 | 10.585 0.0030 | 10.422 0.0070 | 9.873 0.006 | 7.635 0.042 |
| C69WI1-9696 | 05:34:02.05 | +09:58:16.5 | – | 20.593 0.009 | 19.8 0.009 | 17.62 0.015 | – | – | 14.671 0.017 | 14.103 0.02 | 13.518 0.046 | 12.489 0.04 | 8.577 0.069 |
| C69WI1-9847 | 05:33:55.00 | +09:33:05.3 | 16.271 | 15.342 0.0 | 14.41 0.0 | 13.232 0.023 | 12.607 0.026 | 12.357 0.029 | 12.195 0.0040 | 12.221 0.0060 | 12.188 0.021 | 10.947 0.011 | – |

**Table 2.6**: Membership for the new sources with IR excess from the 1°×1° Spitzer Survey in Collinder 69.

| Name | Mass[5] | Phot.Mem[1] | Mem[3] | IRAC class[4] | SED slope | Disk Type |
|---|---|---|---|---|---|---|
| C69EI1-114 | 0.70 | Y Y Y Y Y Y Y | Y | II | -1.552 | Thick |
| C69EI1-790 | 0.28 | Y Y Y Y Y Y Y | Y | II | -1.486 | Thick |
| C69EI1-2229 | 0.17 | Y Y Y Y Y Y - | Y | II | -1.2 | Thick |
| C69EI1-3042 | 0.04 | Y Y Y Y Y Y - | Y | II | -1.069 | Thick |
| C69EI1-3154 | – | N? Y Y G G G - | N | I/II | 1.156 | Thick |
| C69EI1-3465 | 0.11 | Y Y Y Y Y Y - | Y | II | -1.622 | Thick |
| C69EI1-3574 | – | N? - - Y Y G - | N | I | 5.778 | Thick |
| C69EI1-4761 | – | ? ? T Y Y Y N | N? | III | -2.808 | Thin |
| C69EI1-6036 | 0.16 | Y ? Y Y Y Y - | Y | II | -1.937 | Thin |
| C69EI1-6539 | – | N? - Y Y Y G - | N | I | 0.953 | Thick |
| C69EI1-7021 | 0.16 | N? - Y Y Y Y - | Y? | I | 0.374 | Thick |
| C69EI1-7070 | – | N? - Y Y Y G N | N | I | 0.953 | Thick |
| C69EI1-7312 | – | N? - Y Y Y G - | N | I | 0.372 | Thick |
| C69EI1-7620 | 0.27 | Y T T Y Y Y Y | Y | II | -1.691 | Thin |
| C69EI1-10336 | 0.20 | Y Y Y Y Y Y Y | Y | II | -1.943 | Thin |
| C69EI1-10963 | – | Y - - Y Y Y N | N | II | -2.104 | Thin |
| C69EI1-11529 | – | Y - - Y Y Y N | N | III | -1.771 | Thick |
| C69EI1-11541 | – | Y Y Y Y Y Y N | N? | II | -1.477 | Thick |
| C69EI1-11637 | – | N? - Y Y Y G N | N | II | -0.231 | Thick |
| C69EI1-12304 | – | N? Y Y G G Y N | N | I/II | 0.544 | Thick |
| C69EI1-12787 | – | N? Y Y Y G Y N | N | I/II | 1.14 | Thick |
| C69EI1-13002 | 0.25 | Y Y Y Y Y Y Y | Y | II | -1.771 | Thick |
| C69EI1-13542 | – | ? - - - - Y N | N | II | -2.994 | Diskless |
| C69EI1-13667 | – | ? ? T Y Y Y N | N | III | -2.666 | Diskless |
| C69EI1-13824 | 0.1 | N? - Y Y Y Y - | Y? | I | 0.523 | Thick |
| C69EI1-14424 | 0.37 | Y Y Y Y Y Y Y | Y | II | -1.195 | Thick |
| C69EI1-14609 | 0.19 | Y Y Y Y Y Y N? | Y | II | -1.12 | Thick |
| C69EI1-15980 | – | N? Y Y G G G - | N | I/II | 1.461 | Thick |
| C69EI1-16121 | – | N? Y Y G G G N | N | I/II | 0.843 | Thick |
| C69EI1-16472 | 0.16 | Y Y Y Y Y Y - | Y | II | -1.7 | Thick |
| C69EI1-16578 | 0.18 | Y Y Y Y Y Y - | Y | II | -1.562 | Thick |
| C69EI1-16821 | – | N? - Y Y Y G - | N | I | 0.0030 | Thick |
| C69SEI1-2889 | 3.05 | ? ? T Y Y Y Y | Y | III | -2.615 | Transition |
| C69SEI1-4253 | 1.94 | ? T T Y Y Y Y | Y | III | -2.341 | Transition |
| C69SEI1-4263 | 5.68 | ? ? T Y Y Y - | Y? | III | -2.891 | Transition |
| C69WI1-10971 | – | ? ? T Y Y Y N | N | III | -2.744 | Diskless |
| C69WI1-12378 | – | N? Y Y Y Y G - | N | I | 0.212 | Thick |
| C69WI1-1322 | 0.11 | Y - - Y Y Y - | Y | II | -1.615 | Thick |
| C69WI1-1388 | 0.52 | ? T T Y Y Y - | Y | III | -2.746 | Transition |
| C69WI1-14892 | 0.17 | Y Y Y Y Y Y - | Y | II | -1.635 | Thick |
| C69WI1-15281 | – | N? Y Y G G G N | N | I/II | 1.052 | Thick |
| C69WI1-15377 | 0.42 | Y Y Y Y Y Y Y | Y | II | -1.896 | Thin |
| C69WI1-15404 | – | Y - - Y Y Y N | N | III | -2.173 | Thin |
| C69WI1-15496 | – | N? - Y Y Y G - | N | I | 0.415 | Thick |
| C69WI1-2261 | – | ? - - Y Y Y N | N | III | -2.936 | Diskless |
| C69WI1-2303 | – | ? - - Y Y Y N | N | III | -2.827 | Diskless |
| C69WI1-2708 | 0.31 | Y Y Y Y Y Y - | Y | II | -1.531 | Thick |
| C69WI1-306 | – | Y - - Y Y Y N | N | III | -1.818 | Thin |
| C69WI1-3226 | – | - - - - - - - | N | II | -2.275 | Thin |
| C69WI1-4232 | 1.05 | ? ? T Y Y Y Y | Y | III | -2.737 | Transition |
| C69WI1-4614 | – | N? Y Y G G G N | N | I/II | 1.646 | Thick |
| C69WI1-4897 | – | ? - - - - Y N | N | - | -3.121 | Diskless |
| C69WI1-6018 | – | N? Y Y G G G N | N | I/II | 0.87 | Thick |
| C69WI1-6412 | – | N? - Y G Y G - | N | I | 0.563 | Thick |
| C69WI1-6820 | – | ? T T Y Y Y N | N | III | -2.851 | Diskless |
| C69WI1-7152 | 0.19 | Y Y Y Y Y Y - | Y | II | -1.346 | Thick |
| C69WI1-718 | – | N? Y Y G G G N | N | I/II | 1.236 | Thick |
| C69WI1-7809 | 0.11 | Y - - Y Y Y - | Y | II | -1.757 | Thick |
| C69WI1-9288 | 0.41 | Y Y Y Y Y Y Y | Y | II | -1.824 | Thin |
| C69WI1-9696 | – | N? - Y Y Y G N | N | II | -0.346 | Thick |
| C69WI1-9847 | – | Y - - G G Y N | N | I/II | -1.448 | – |
| C69SWI1-496 | 1.90 | ? - T Y Y Y Y | Y | III | -2.769 | Transition |
| C69SWI1-937 | 1.94 | ? - - Y Y Y N | Y? | III | -2.854 | Transition |

Continued on next page…

Table 2.6 – Continued

| Name[1] | Mass[5] | Phot.Mem[2] | Mem[3] | IRAC class[4] | SED slope | Disk Type |
|---|---|---|---|---|---|---|

[1]IDs of our targets. E: East part; W: West part; S: photometry from shallow mosaics; I1: coordinates taken from the first IRAC band.

[2]Membership is 3.6vs(3.6-8.0); H-Ksvs(Ks-24.0); (3.6-8.0)vs(8.0-24.0); (4.5-5.8)vs(5.8-8.0);(3.6-5.8)vs(4.5-8.0); 4.5vs(4.5-8.0); IvsR-I. Y: probable member; Y?: possible member; N:non member; N?: possible non member; G: contaminant; -: not enought data for evaluation.

[3]Final membership.

[4]Final YSO classification based on the (3.6-4.5)vs(5.8-8.0) diagram and the SED.

[5]Mass estimate using the J magnitude and a 5 Myr isochrone from Baraffe et al. (1998). The [3.6] magnitude was used for objects that lack 2MASS information and for objects with brighter than J~10 mag, the 5 Myr Siess et al. (2000) isochrone was used.

**Table 2.7**: Photometry for the new candidate members of Collinder 69 from the SUBARU Survey.

| ID | RA(J2000) | DEC(J2000) | Ic eIc | Ic - Z | eZ | J eJ | H eH | Ks eKs | [3.6] e[3.6] | [4.5] e[4.5] | [5.8] e[5.8] | [8.0] e[8.0] |
|---|---|---|---|---|---|---|---|---|---|---|---|---|
| ccd1-016078 | 05:36:53.18 | +10:01:57.7 | 19.011 0.002 | 1.205 | 0.002 | - - | - - | - - | 16.369 0.042 | 15.825 0.055 | - - | - - |
| ccd2-009766 | 05:36:03.33 | +09:44:51.6 | 18.476 0.002 | 1.206 | 0.002 | 17.047 0.218 | 15.759 0.156 | 17.009 0.0 | 15.638 0.025 | 15.826 0.044 | - - | - - |
| ccd2-024918 | 05:36:10.63 | +09:52:48.4 | 18.969 0.002 | 1.256 | 0.002 | 17.366 0.006 | 16.817 0.008 | 16.59 0.009 | 15.999 0.038 | 16.123 0.076 | - - | - - |
| ccd3-005774 | 05:35:36.32 | +09:43:16.0 | 19.463 0.003 | 1.324 | 0.003 | 17.226 0.011 | 16.579 0.011 | 16.282 0.026 | 16.759 0.093 | 16.228 0.127 | - - | - - |
| ccd3-006362 | 05:35:54.10 | +09:43:36.4 | 20.317 0.004 | 1.562 | 0.003 | - - | - - | - - | 16.321 0.057 | 16.279 0.084 | - - | - - |
| ccd3-007031 | 05:35:55.71 | +09:43:58.0 | 20.105 0.004 | 1.322 | 0.004 | 18.163 0.033 | 17.46 0.044 | 17.747 0.126 | 16.606 0.109 | 16.564 0.148 | - - | - - |
| ccd4-005127 | 05:35:57.43 | +09:56:24.5 | 21.252 0.007 | 1.585 | 0.005 | 18.549 0.013 | 17.793 0.017 | 17.225 0.014 | 16.451 0.037 | 16.228 0.065 | - - | - - |
| ccd5-002230 | 05:36:33.33 | +09:54:58.1 | 22.054 0.012 | 1.59 | 0.01 | 19.808 0.083 | 19.617 0.169 | 18.757 0.237 | - - | - - | - - | - - |
| ccd5-008530 | 05:36:24.19 | +09:58:43.1 | 21.417 0.008 | 1.632 | 0.005 | 18.948 0.039 | 17.988 0.045 | 17.513 0.087 | 16.693 0.05 | 16.487 0.073 | - - | - - |
| ccd8-005864 | 05:35:18.79 | +09:43:36.6 | 21.505 0.008 | 1.459 | 0.006 | 18.565 0.037 | 18.004 0.041 | 17.548 0.087 | 16.959 0.09 | 16.676 0.121 | - - | - - |
| ccd8-014467 | 05:35:07.49 | +09:49:33.4 | 18.957 0.002 | 1.351 | 0.002 | 16.591 0.009 | 16.018 0.01 | 15.567 0.013 | 15.107 0.025 | 15.159 0.04 | - - | - - |
| ccd8-021927 | 05:35:14.16 | +09:54:08.1 | 20.778 0.016 | 1.53 | 0.005 | 17.93 0.027 | 17.073 0.022 | 16.672 0.031 | 16.042 0.034 | 16.385 0.091 | - - | - - |
| ccd9-001365 | 05:35:09.10 | +09:54:36.1 | 18.845 0.006 | 1.391 | 0.002 | 16.443 0.007 | 15.853 0.006 | 15.557 0.01 | 15.081 0.023 | 15.001 0.031 | 14.659 0.143 | - - |
| ccd9-005320 | 05:35:10.76 | +09:56:06.5 | 18.426 0.027 | 1.166 | 0.009 | 16.101 0.016 | 15.503 0.011 | 15.039 0.009 | 13.975 0.047 | 13.913 0.06 | 12.385 0.166 | 13.347 0.224 |
| ccd9-007028 | 05:35:18.34 | +09:56:51.6 | 20.469 0.008 | 1.495 | 0.005 | 17.706 0.009 | 16.919 0.009 | 16.516 0.01 | 15.988 0.045 | 15.965 0.068 | - - | - - |

- X-ray data:

  We obtained two *XMM-Newton* observations of Collinder 69. The observations were centered East and West of the bright star $\lambda$ Ori (see Fig.2.2).

  The prime instrument EPIC (*European Photon Imaging Camera*; see Jansen et al. (2001), Turner et al. (2001), and Strüder et al. (2001)) was operated in full-frame mode. The Optical Monitor (OM; Mason et al. (2001)) was scheduled for several consecutive imaging exposures in the $V$ and $B$ bands.

  – EPIC:

    Both observations were analysed with the *XMM-Newton* Science Analysis System (SAS) pipeline, version 7.0.0. We created a photon events list with the metatasks EPCHAIN and EMCHAIN for EPIC/pn and EPIC/MOS respectively. There was some loss of observing time due to high background. We selected good time intervals (GTIs) using a filter that cuts out times of high background maximizing the overall signal-to-noise. The C69 E field is almost unaffected, but the effective exposure time reduces to only $\sim 15$ ksec for C69 W. The data were further filtered for pixel patterns, and events at the boundary of individual CCD chips or near bad pixels or outside the field-of-view (FOV) were removed.

    Images with a pixel size of $5''$ were binned from the cleaned events list. We performed source detection on the images in four energy bands using standard SAS tools. The most suitable boundaries of the energy bands depend on the spectral shape of the X-ray sources which is not known a priori. We have tested various bounds for the energy bands, and after inspection of the results from source detection made the following choice for the soft ($S$), medium ($M$), hard ($H$) and broad ($B$) bands: $S = 0.5 - 1.0$ keV, $M = 1.0 - 2.0$ keV, $H = 2.0 - 7.3$ keV, and $B = S + M + H$.

    For the source detection process we proceeded in two steps. First, all EPIC instruments were analysed separately as described above. To evaluate the relative sensitivity of the detectors we computed separately for each energy band the ratio of count rates measured by EPIC/pn and EPIC/MOS, $(C_{\rm pn}/C_{\rm MOS})_{\rm i}$ with $i = S, M, H, B$, for bright sources detected with all three instruments. The median of these values were used to scale the exposure maps of EPIC/pn for the joint analysis of all three instruments. Then, the source detection procedure was applied to the combined files of all three instruments.

    Our final X-ray catalog contains all sources detected in the merged data ('EPIC sources'), plus all sources detected in the individual instruments that are not within $10''$ of an EPIC source. Detection in one detector but not in the combined data may occur, e.g. if the source is located outside the FOV, near a chip gap, or in a region of low exposure (such as a bad column) in one or more of the instruments. This yields 112

sources in the merged EPIC data of C69-E and 52 sources for C69-W. The X-ray coordinates of the final source list have been cross-correlated with the 2MASS catalog, and a boresight correction was computed as the median of the astrometric offsets in RA and DEC.

– OM:

The OM was operated in Full Frame imaging mode at high/low-resolution. For the C69-W field one *V* band exposure is available, and for the C69-E field there are five consecutive exposures with the *V* and *B* filters.

The OM data were reduced with the SAS metatask OMICHAIN with default parameters. This task performs all basic data reduction steps, including flat-fielding, identification of bad pixels, modulo-8 fixed pattern correction, and source detection with aperture photometry. The final output of the pipeline is a combined OM source list that contains for each source the average Johnson magnitude of all exposures in a given filter, i.e. in our case the average *B* magnitude of exposures 007, 008 and 010 and the average *V* magnitude of exposures 006 and 009.

We corrected the absolute positions of the detections by cross-correlating the OM source list with the 2MASS catalog (Skrutskie et al. 2006). A search radius of 3″ was used and only OM sources with $\geq 15\,\sigma$ detection significance were considered for the astrometry. Subsequently, the OM coordinates of all detected sources were shifted by the median position offset. Each exposure yielded approximately 1000 detections.

Standard (Johnson) magnitudes are automatically extracted by the SAS tools if observations are performed in more than one band, allowing to calculate the colour. Since we obtained only *V* band data for C69-W, the OMICHAIN pipeline does not provide standard magnitudes. However, we can make use of the C69-E data to calibrate the *V* band photometry for the OM detections in C69-W. For the OM sources in the C69-E field we verified that a linear transformation with the $B-V$ colour reproduces the standard magnitudes derived by the SAS tools, $V_{\rm ins} = V_{\rm std} + \kappa_{\rm V} \cdot (B-V)_{\rm std} = V_{\rm std} + CF_{\rm V}$, and we determined the average coefficient $\langle \kappa_{\rm V} \rangle$. In order to compute standard magnitudes $V_{\rm std}$ from the instrumental magnitudes $V_{\rm ins}$ measured in the C69-W field, we assume for all objects the mean colour observed in the East field, $\langle B-V \rangle = 1.04 \pm 0.35$. The conversion factor derived in this way is $CF_{\rm V} = 0.03 \pm 0.02$, where the uncertainty reflects the statistical errors of $\langle \kappa \rangle$ and $\langle B-V \rangle$ of the C69-E field. Note that the transformation factor $CF_{\rm V}$ is almost negligible.

For the search for optical/IR counterparts to the X-ray sources we used the previously mentioned surveys as well as published data from Dolan & Mathieu (1999, 2001, 2002).This compilation includes all presently known solar-type and low-mass members of C69, and a large catalog of photometric measurements ($VR_cI_c$) carried out in the field around the

cluster, without any membership selection (Table 4 of Dolan & Mathieu 2002).

We have searched for optical and infrared counterparts for our X-ray detections, using a radius of 5.1 arcsec. Since the XMM-Newton positions have a moderate uncertainty, we have included the optical and infrared photometry of all sources within this radius from the nominal position of the X-ray source, and extracted accurate positions for all these objects. When there was ambiguity in the optical or infrared identification, after visual inspection, these possibilities were identified by a letter denoting whether the optical or infrared source is close to the fiducial center –c, or south –s, north –n, west –w– or east –e. Therefore, we have compiled a master catalog with all the sources which are present in at least one of the mappings (optical, near-IR or mid-IR) and extrated the photometry from these surveys. This information is provided in Tables 2.8 and 2.10 (East and West fields, respectively).

We have found multiple counterparts for several X-ray sources within our search radius. Although we are confident that the closest optical/IR counterpart provides the correct identification of the X-ray source, we have considered these secondary counterparts and assessed both the cluster membership and the source of the X-ray emission. For the selection of counterparts that were detected in a given passband in more than one of the catalogs and/or surveys we proceed as follows: For the blue side of the optical range ($B$ and $V$), we listed first the data coming form the OM; otherwise, the $V$ magnitude from D&M is listed. For the reddest portion of the optical range ($R_c$ and $I_c$), we have chosen first the data from Barrado y Navascués et al. (2007b) (i.e., candidate members detected in Barrado y Navascués et al. 2004b). Then, we have selected the photometry from Dolan & Mathieu (1999, 2001) (i.e., members based on photometry and spectroscopy). If the X-ray source is not present in any of those catalogs, we first look for an optical counterpart in the CFHT1999 survey (only for objects with $I_c$>13.2 mag, and if it does not appear there, at the database from Dolan & Mathieu (2002), which is shallower but covers a much larger area. For the near-infrared photometry ($JHKs$), we have prioritized the data coming from deep image acquired with Omega2000 in November 2007 ($J$>17.2 mag). If no data have been recored, we selected the photometry coming from Omega2000 taken in October 2000, shallower ($J$>13.0 mag) but covering a much larger area. Otherwise, data from the 2MASS All Sky Survey are listed.

We have applied different criteria to our X-ray sources to assess membership; the process is explained in detail in Barrado y Navascués et al (2009), in prep. In short, our criteria are based on combinations of optical and near-infrared color-color and color-magnitude diagrams (see Fig. 2.3 for an example); analysis of the overall shape of the Spectral Energy Distributions (SED) built, and theoretical model fits to those SEDs. The final list of good candidate members contains 70 objects which correspond to 67 X-ray sources (four have possible companions within the XMM-Newton pointing uncertainty, which might be the actual source of the X-ray emission). Out of these 67 detections, 31 were already presented in Barrado y Navascués et al. (2004b, 2007b), whereas another 16 where listed in Dolan & Mathieu (1999, 2001). Thus, we have uncovered

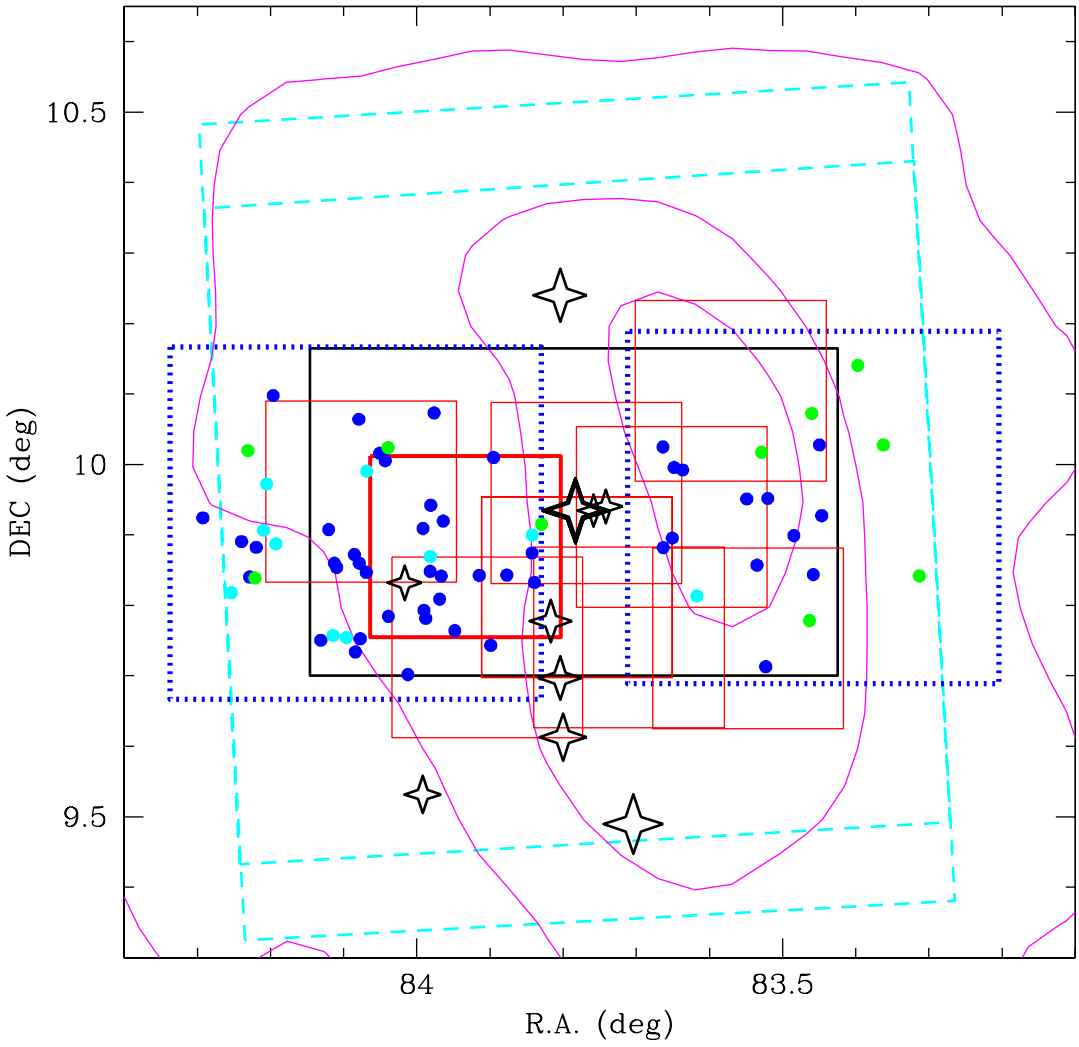


**Figure 2.2**: The young cluster Collinder 69, with all the collected data. The black retangle respresents the CFHT1999 $RI_c$ survey, the red squares the near-IR data ($JHKs$) from Omega2000 (thick lines for the deep image), whereas the IRAC mapping is represented with dashed, cyan lines. Finally, our two XMM-Newton FOVs are located with blue, dotted squares. O and B stars are represented by four-point stars, with increasing size related to increasing brightness. Our final cluster candidate members are represented as solid circles (blue for Y+ or confirmed, cyan for Y or probable, and green for Y? or possible).

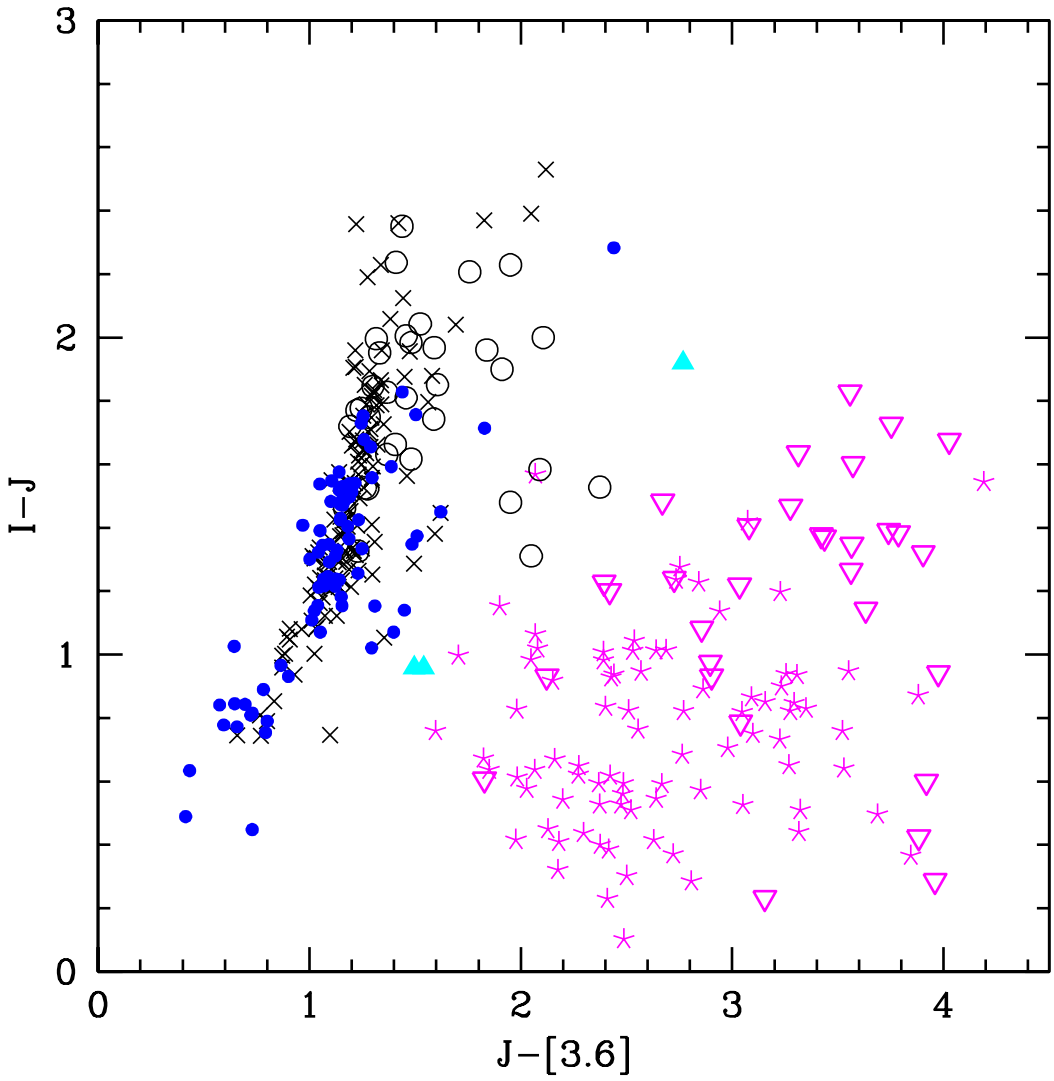


**Figure 2.3**: I-J vs. J- [3.6] color-color diagram that allows the identification of contamination by quasars. Previously known members of Collinder 69 from Dolan & Mathieu (1999) and Barrado y Navascués et al. (2004b, 2007b) are displayed as crosses and open cirles (for Class II members). Quasars observed by the SWIRE team (Lonsdale et al. 2003) appear as magenta asterisks. Data corresponding to our XMM study are shown as open magenta inverted triangle (for quasars), solid blue triangle (for possible quasars) and solid blue circles (others, probable stars). This effective diagram, nicknamed quasar-killer, was first defined in Bouy et al. (2009a).

20 new candidate members plus the three possible companions to more massive objects. One of them, namely LOri025, is a confirmed members of the cluster with a possible fainter companion.

The known cluster member LOri113 is very close to the source C69-X-W032, although it is not the closest. Since our general criterion to identify the X-ray detection with an optical and/or infrared source is the proximity, we do not believe they correspond to the same source and assumed that this source does not belong to the Collinder 69 cluster.

We note that there is a dichotomy in the distribution of X-ray sources (clearly visible on Fig. 2.2 and 3.31. While 48 members are located to the East of the central star $\lambda$ Ori, there are only 20 to the West of this O8III star. This fact was already discussed in Barrado y Navascués et al. (2007b) in the context of the distribution of members with circumstellar disks and will be revisited in Section 4.3. In any event, our final cluster members have been displayed on Figure 2.2 as solid circles (blue for Y+ or spectroscopically confirmed, cyan for Y or probable based on photometric criteria, and green for Y? or possible also based on photometry).

**Table 2.8**: Optical and infrared photometry for the X-ray sources of Collinder 69 East.

| Name | RA (J2000) | DEC (J2000) | *B* | *V* | *Rc* | *Ic* | *J* | *H* | *K* | [3.6] | [4.5] | [5.8] | [8.0] | [24] |
|---|---|---|---|---|---|---|---|---|---|---|---|---|---|---|
| C69-X-E-001 I | 05:35:55.43 | +09:56:31.5 | 15.730 0.010 | 14.43 0.00 | 13.50 0.00 | 12.57 0.00 | 11.416 0.023 | 10.725 0.022 | 10.524 0.023 | 10.262 0.003 | 10.318 0.004 | 10.239 0.010 | 10.171 0.010 | – – |
| C69-X-E-002 I | 05:36:32.03 | +09:44:20.3 | – – | – – | 20.040 0.049 | 19.440 0.052 | – – | – – | – – | 16.471 0.071 | 15.587 0.049 | 14.446 0.131 | 13.186 0.058 | – – |
| C69-X-E-003 M | 05:37:00.84 | +09:49:04.5 | – – | 12.409 0.000 | 11.869 0.000 | 11.357 0.000 | 10.585 0.024 | 10.152 0.025 | 9.990 0.023 | 9.928 0.002 | 9.924 0.002 | 9.908 0.005 | 9.846 0.005 | – – |
| C69-X-E-004 I | 05:35:57.97 | +09:54:32.8 | 16.144 0.010 | 14.855 0.010 | 13.913 0.010 | 12.939 0.010 | 11.548 0.029 | 10.859 0.023 | 10.651 0.024 | 10.498 0.003 | 10.495 0.004 | 10.440 0.011 | 10.256 0.012 | – – |
| C69-X-E-005 c | 05:36:27.90 | +09:55:27.5 | – – | – – | 21.556 0.021 | 20.688 0.019 | 19.311 0.056 | 18.085 0.046 | 17.472 0.079 | 15.89 0.042 | 15.608 0.053 | 14.677 0.121 | 14.006 0.134 | – – |
| ” w | 05:36:27.69 | +09:55:27.1 | – – | – – | 22.394 0.047 | 21.401 0.036 | 20.258 0.144 | 19.194 0.121 | 19.055 0.345 | 16.626 0.089 | 16.815 0.146 | – – | – – | – – |
| C69-X-E-006 I | 05:36:20.49 | +09:52:19.3 | 16.472 0.010 | 15.036 0.000 | 14.163 0.000 | 13.326 0.000 | 12.188 0.024 | 11.482 0.023 | 11.323 0.021 | 11.165 0.005 | 11.206 0.006 | 11.173 0.017 | 11.072 0.019 | – – |
| C69-X-E-007 c | 05:36:19.02 | +10:03:50.9 | – – | 14.872 0.000 | 13.980 0.000 | 13.096 0.000 | 11.941 0.024 | 11.278 0.027 | 11.092 0.023 | 10.902 0.004 | 10.904 0.005 | 10.839 0.014 | 10.797 0.014 | – – |
| C69-X-E-008 I | 05:36:18.55 | +09:45:09.4 | – – | 13.255 0.000 | 12.681 0.000 | 12.130 0.000 | 11.340 0.023 | 10.796 0.022 | 10.676 0.019 | 10.540 0.002 | 10.570 0.003 | 10.521 0.008 | 10.481 0.009 | – – |
| C69-X-E-009 I | 05:35:19.07 | +09:54:54.5 | – – | – – | – – | – – | 9.887 0.027 | 9.378 0.026 | 9.141 0.024 | 8.894 0.002 | 8.727 0.002 | 8.626 0.003 | 8.354 0.002 | 5.871 0.009 |
| C69-X-E-010 c | 05:35:54.31 | +10:04:23.3 | – – | 12.890 0.000 | 12.280 0.000 | 11.690 0.000 | 10.936 0.023 | 10.378 0.022 | 10.235 0.021 | 10.144 0.002 | 10.132 0.002 | 10.099 0.006 | 10.053 0.008 | – – |
| C69-X-E-011 c | 05:36:20.18 | +09:44:02.1 | – – | 15.188 0.000 | 14.201 0.000 | 13.122 0.000 | 12.163 0.044 | 11.409 0.051 | 11.090 0.033 | 10.668 0.003 | 10.674 0.004 | 10.613 0.012 | 10.576 0.012 | – – |
| ” e | 05:36:20.31 | +09:44:02.7 | – – | – – | 15.307 0.003 | 14.181 0.001 | – – | – – | – – | – – | – – | – – | – – | – – |
| C69-X-E-012 I | 05:36:09.42 | +10:01:26.1 | 14.618 0.010 | 13.015 0.010 | – – | – – | 9.110 0.021 | 8.826 0.046 | 8.690 0.021 | 8.708 0.002 | 8.553 0.001 | 8.528 0.003 | 8.328 0.002 | 6.703 0.016 |
| C69-X-E-013 I | 05:36:23.09 | +09:45:15.8 | – – | – – | – – | – – | 6.900 0.024 | 6.468 0.047 | 6.345 0.021 | – – | – – | – – | – – | 6.311 0.009 |
| C69-X-E-014 I | 05:35:51.34 | +09:55:10.9 | 17.505 0.010 | 15.69 0.00 | 14.64 0.00 | 13.45 0.00 | 12.102 0.023 | 11.411 0.022 | 11.156 0.019 | 11.010 0.004 | 10.985 0.005 | 10.895 0.014 | 10.683 0.014 | – – |
| C69-X-E-015 I | 05:36:10.09 | +10:01:58.4 | – – | – – | 21.337 0.015 | 20.606 0.013 | 19.223 0.053 | 18.590 0.072 | 17.896 0.115 | 15.437 0.031 | 15.388 0.055 | 13.126 0.090 | 13.272 0.108 | – – |
| C69-X-E-016 I | 05:36:16.59 | +09:50:48.7 | 16.807 0.010 | 15.314 0.000 | 14.369 0.000 | 13.356 0.000 | 11.991 0.024 | 11.284 0.022 | 11.090 0.023 | 10.804 0.004 | 10.798 0.005 | 10.722 0.012 | 10.636 0.014 | – – |
| C69-X-E-017 I | 05:36:18.85 | +09:51:35.3 | 17.798 0.010 | 16.607 0.000 | 15.453 0.000 | 14.026 0.000 | 12.488 0.024 | 11.872 0.022 | 11.687 0.021 | 11.439 0.005 | 11.417 0.006 | 11.348 0.017 | 11.297 0.021 | – – |
| C69-X-E-018 M | 05:36:47.11 | +10:05:51.8 | – – | 15.738 0.000 | 14.757 0.000 | 13.746 0.000 | 12.454 0.026 | 11.744 0.022 | 11.546 0.026 | 11.360 0.003 | 11.363 0.004 | 11.332 0.013 | 11.280 0.018 | – – |
| C69-X-E-019 M | 05:36:57.50 | +09:53:26.0 | – – | 16.050 0.000 | 15.020 0.000 | 13.910 0.000 | 12.695 0.028 | 11.958 0.023 | 11.767 0.021 | 11.574 0.004 | 11.580 0.005 | 11.551 0.014 | 11.484 0.017 | – – |
| C69-X-E-020 I | 05:36:16.43 | +09:59:25.4 | 14.128 0.010 | 11.785 0.000 | 11.172 0.000 | 10.570 0.000 | 9.729 0.024 | 9.303 0.023 | 9.147 0.019 | 9.154 0.002 | 9.041 0.002 | 9.014 0.004 | 8.993 0.003 | – – |
| C69-X-E-021 c | 05:36:40.04 | +10:04:34.2 | – – | – – | – – | – – | 20.181 0.111 | 19.036 0.107 | 18.478 0.212 | 16.204 0.046 | 15.73 0.057 | 14.53 0.098 | – – | – – |
| ” w | 05:36:39.81 | +10:04:33.7 | – – | – – | – – | – – | 19.944 0.090 | 19.313 0.141 | 19.705 0.620 | 17.067 0.094 | 16.604 0.114 | – – | – – | – – |
| C69-X-E-022 I | 05:36:09.31 | +09:47:03.7 | 18.220 0.010 | 16.46 0.00 | 15.33 0.00 | 13.94 0.00 | 12.410 0.029 | 11.714 0.023 | 11.493 0.021 | 11.252 0.004 | 11.215 0.006 | 11.178 0.016 | 11.080 0.019 | – – |
| C69-X-E-023 I | 05:35:47.55 | +09:45:50.6 | – – | – – | – – | – – | 11.359 0.022 | 10.780 0.023 | 10.548 0.021 | 10.287 0.003 | 10.249 0.004 | 10.185 0.009 | 10.127 0.009 | – – |
| ” o | 05:35:43.26 | +09:59:56.4 | – – | – – | 20.728 0.009 | 19.895 0.010 | 18.920 0.020 | 18.048 0.025 | 17.320 0.016 | 16.024 0.066 | 14.817 0.032 | – – | 13.012 0.065 | – – |
| C69-X-E-025 I | 05:36:26.30 | +09:51:14.3 | 18.037 0.010 | 16.313 0.000 | 15.294 0.000 | 14.189 0.000 | 12.866 0.026 | 12.153 0.022 | 11.931 0.027 | 11.824 0.004 | 11.808 0.005 | 11.737 0.013 | 11.791 0.023 | – – |
| C69-X-E-026 - | 05:36:33.38 | +09:58:02.9 | – – | – – | – – | – – | 19.568 0.069 | 18.219 0.054 | 17.390 0.073 | 15.665 0.037 | 15.275 0.043 | 14.363 0.121 | – – | – – |
| C69-X-E-027 c | 05:36:28.93 | +09:54:27.1 | 18.220 0.010 | 16.573 0.000 | 15.461 0.000 | 14.204 0.000 | 12.893 0.029 | 12.108 0.023 | 11.945 0.024 | 11.771 0.004 | 11.762 0.005 | 11.667 0.016 | 11.697 0.023 | – – |
| ” n | 05:36:28.90 | +09:54:32.4 | – – | – – | – – | 20.650 0.178 | 19.121 0.050 | 18.540 0.071 | 18.141 0.153 | – – | – – | – – | – – | – – |
| C69-X-E-028 c | 05:35:57.65 | +09:47:34.7 | 17.128 0.010 | 15.68 0.00 | 14.65 0.00 | 13.55 0.00 | 12.221 0.027 | 11.471 0.022 | 11.290 0.024 | 11.090 0.004 | 11.114 0.005 | 11.071 0.015 | 10.928 0.018 | – – |
| C69-X-E-029 c | 05:35:34.83 | +10:00:35.3 | – – | 15.873 0.000 | 14.801 0.000 | 13.608 0.000 | 12.455 0.033 | 11.800 0.042 | 11.502 0.027 | 11.146 0.004 | 11.149 0.005 | 11.060 0.015 | 11.020 0.019 | – – |
| C69-X-E-030 I | 05:36:02.93 | +09:42:06.2 | – – | 15.220 0.000 | 14.300 0.000 | 13.390 0.000 | 12.151 0.023 | 11.455 0.022 | 11.250 0.023 | 11.028 0.003 | 11.011 0.003 | 10.924 0.008 | 10.748 0.010 | 8.643 0.077 |
| C69-X-E-031 M | 05:36:52.68 | +09:52:56.3 | – – | 16.690 0.000 | 15.500 0.000 | 14.060 0.000 | 12.512 0.023 | 11.841 0.022 | 11.665 0.024 | 11.407 0.004 | 11.382 0.005 | 11.367 0.012 | 11.382 0.018 | – – |
| C69-X-E-032 - | 05:35:37.90 | +09:44:10.1 | – – | – – | – – | – – | 18.058 0.026 | 17.211 0.022 | 16.320 0.025 | 15.041 0.042 | 14.281 0.030 | 13.774 0.110 | 12.609 0.051 | 8.584 0.080 |
| C69-X-E-033 I | 05:35:59.46 | +09:50:18.6 | – – | – – | 23.114 0.073 | 22.164 0.060 | 19.881 0.037 | 19.564 0.081 | 18.767 0.054 | 17.441 0.119 | 16.425 0.103 | – – | – – | – – |
| C69-X-E-034 c | 05:35:22.21 | +09:52:27.6 | – – | 15.430 0.000 | 14.480 0.000 | 13.610 0.000 | 12.309 0.023 | 11.629 0.026 | 11.459 0.024 | 11.308 0.003 | 11.373 0.004 | 11.313 0.011 | 11.243 0.016 | – – |
| ” w | 05:35:22.02 | +09:52:25.8 | – – | – – | – – | – – | 18.780 0.017 | 18.268 0.028 | 18.219 0.042 | – – | – – | – – | – – | – – |
| C69-X-E-035 c | 05:35:39.49 | +09:50:33.1 | – – | 16.76 0.00 | 15.54 0.00 | 14.05 0.00 | 12.553 0.024 | 11.877 0.022 | 11.594 0.024 | 11.364 0.005 | 11.319 0.006 | 11.231 0.017 | 11.218 0.025 | – – |
| C69-X-E-036 I | 05:35:30.47 | +09:50:34.5 | – – | 17.22 0.00 | 15.87 0.00 | 14.23 0.00 | 12.500 0.024 | 11.856 0.023 | 11.587 0.027 | 11.255 0.004 | 11.187 0.006 | 11.131 0.015 | 11.123 0.021 | – – |
| C69-X-E-037 c | 05:35:51.99 | +09:50:29.8 | 20.124 0.010 | 18.396 0.010 | 16.780 0.010 | 15.340 0.010 | 13.782 0.026 | 13.098 0.025 | 12.846 0.029 | 12.486 0.008 | 12.489 0.011 | 12.378 0.034 | 12.245 0.053 | – – |
| C69-X-E-038 c | 05:35:27.20 | +09:53:10.7 | – – | – – | 20.516 0.088 | 19.738 0.064 | 18.333 0.014 | 17.425 0.014 | 16.621 0.010 | 15.254 0.032 | 14.905 0.039 | 14.349 0.097 | 13.796 0.106 | – – |
| ” w | 05:35:27.06 | +09:53:10.4 | – – | – – | – – | – – | 19.986 0.054 | 19.474 0.084 | 18.714 0.062 | – – | – – | – – | – – | – – |
| C69-X-E-039 - | 05:36:56.41 | +09:53:38.1 | – – | – – | – – | – – | – – | – – | – – | 16.282 0.060 | 15.901 0.068 | – – | – – | – – |
| C69-X-E-040 M | 05:36:50.26 | +09:54:23.8 | 19.039 0.089 | 17.428 0.000 | 16.207 0.000 | 14.756 0.000 | 13.237 0.024 | 12.534 0.022 | 12.304 0.024 | 12.096 0.004 | 12.064 0.005 | 12.009 0.019 | 12.086 0.034 | – – |

Continued on next page…

Table 2.8 – Continued

| Name | RA (J2000) | DEC (J2000) | *B* | *V* | *Rc* | *Ic* | *J* | *H* | *K* | [3.6] | [4.5] | [5.8] | [8.0] | [24] |
|---|---|---|---|---|---|---|---|---|---|---|---|---|---|---|
| C69-X-E-041 M | 05:37:10.18 | +09:55:27.0 | – – | 16.720 0.000 | 15.640 0.000 | 14.300 0.000 | 12.857 0.024 | 12.081 0.022 | 11.768 0.024 | – – | – – | – – | – – | 6.988 0.048 |
| C69-X-E-042 M | 05:36:46.22 | +09:53:14.4 | – – | – – | – – | – – | 7.358 0.019 | 7.130 0.033 | 7.050 0.026 | – – | – – | 6.994 0.002 | 7.002 0.001 | 7.082 0.017 |
| C69-X-E-043 I | 05:35:49.99 | +09:57:52.4 | – – | – – | 22.309 0.028 | 21.606 0.041 | 20.341 0.052 | 19.307 0.069 | 18.702 0.053 | 16.779 0.111 | 16.272 0.110 | – – | – – | – – |
| C69-X-E-044 + | 05:36:26.79 | +09:49:19.0 | – – | – – | – – | – – | – – | – – | – – | 16.749 0.074 | 15.874 0.067 | – – | – – | – – |
| C69-X-E-045 + | 05:35:30.57 | +09:54:29.2 | – – | – – | 22.75 0.000 | 22.75 0.000 | 21.855 0.216 | 20.511 0.207 | 19.410 0.105 | – – | – – | – – | – – | – – |
| C69-X-E-046 g | 05:35:33.40 | +09:51:47.8 | – – | – – | 22.75 0.000 | 22.178 0.058 | 20.503 0.062 | 19.273 0.061 | 18.213 0.035 | 16.476 0.061 | 16.050 0.099 | – – | – – | – – |
| C69-X-E-047 M | 05:36:54.54 | +09:53:26.7 | – – | – – | – – | – – | 14.524 0.032 | 13.928 0.045 | 13.668 0.043 | 13.269 0.008 | 13.177 0.010 | 13.215 0.049 | 13.069 0.059 | – – |
| C69-X-E-048 - | 05:36:50.74 | +09:54:05.3 | – – | – – | – – | – – | 21.00 0.000 | 19.75 0.000 | 18.75 0.000 | – – | – – | – – | – – | – – |
| C69-X-E-049 I | 05:35:48.86 | +09:49:23.9 | – – | – – | 21.801 0.024 | 20.856 0.019 | 20.069 0.045 | 19.398 0.068 | 18.788 0.059 | 17.029 0.104 | 16.594 0.136 | – – | – – | – – |
| C69-X-E-050 I | 05:36:17.46 | +10:01:39.4 | – – | – – | 21.635 0.023 | 20.710 0.015 | 21.00 0.000 | 19.75 0.000 | 18.75 0.000 | – – | – – | – – | – – | – – |
| C69-X-E-051 I | 05:35:57.35 | +09:58:27.1 | – – | – – | 20.688 0.008 | 19.956 0.009 | 19.669 0.029 | 18.867 0.041 | 18.139 0.030 | 15.710 0.036 | 15.560 0.054 | 14.186 0.126 | 13.245 0.087 | – – |
| C69-X-E-052 I | 05:35:20.84 | +09:47:27.2 | – – | 17.904 0.000 | 17.235 0.000 | 16.513 0.000 | 15.105 0.003 | 14.393 0.002 | 14.184 0.004 | 14.137 0.011 | 14.095 0.018 | 14.015 0.067 | – – | – – |
| C69-X-E-053 I | 05:36:13.99 | +09:53:05.5 | – – | – – | 23.627 0.108 | 22.750 0.096 | 21.359 0.128 | 020.75 0.000 | 19.524 0.103 | 17.619 0.129 | 16.788 0.127 | – – | – – | – – |
| C69-X-E-054 I | 05:36:12.15 | +10:00:57.4 | 19.048 0.010 | 17.451 0.010 | 15.910 0.010 | 14.600 0.010 | 13.266 0.024 | 12.559 0.022 | 12.285 0.021 | 12.017 0.006 | 11.995 0.008 | 11.969 0.024 | 11.919 0.035 | – – |
| C69-X-E-055 I | 05:35:52.52 | +09:48:31.7 | 19.348 0.010 | 17.710 0.010 | 16.190 0.010 | 14.730 0.010 | 13.189 0.024 | 12.509 0.022 | 12.271 0.027 | 11.974 0.006 | 11.948 0.009 | 11.805 0.025 | 11.862 0.038 | – – |
| C69-X-E-056 - | 05:36:44.14 | +09:52:05.4 | – – | – – | – – | – – | 21.011 0.315 | 19.800 0.214 | 18.230 0.151 | – – | 15.998 0.135 | – – | – – | – – |
| C69-X-E-057 M | 05:36:49.28 | +09:58:20.0 | 13.300 0.011 | 12.028 0.010 | 11.304 0.000 | 10.712 0.000 | 9.897 0.026 | 9.294 0.022 | 9.191 0.024 | 9.167 0.002 | 9.151 0.002 | 9.098 0.004 | 9.088 0.003 | – – |
| C69-X-E-058 M | 05:36:54.86 | +09:50:25.0 | – – | 15.540 0.000 | 14.570 0.000 | 13.630 0.000 | 12.418 0.024 | 11.717 0.023 | 11.522 0.021 | 11.374 0.003 | 11.421 0.004 | 11.311 0.011 | 11.257 0.018 | – – |
| C69-X-E-059 + | 05:36:14.86 | +09:52:05.6 | – – | – – | 022.75 0.000 | 022.75 0.000 | 021.25 0.000 | 020.75 0.000 | 019.75 0.000 | – – | – – | – – | – – | – – |
| C69-X-E-060 c | 05:36:08.78 | +09:56:21.4 | – – | – – | – – | – – | 12.206 0.026 | 11.572 0.022 | 11.439 0.021 | 11.375 0.004 | 11.388 0.004 | 11.362 0.013 | 11.295 0.016 | – – |
| ” n | 05:36:09.19 | +09:56:22.7 | – – | – – | 20.499 0.017 | 19.679 0.008 | 20.293 0.058 | 20.148 0.152 | 19.048 0.088 | – – | – – | – – | – – | – – |
| C69-X-E-061 I | 05:35:56.70 | +10:01:52.6 | – – | – – | 21.160 0.012 | 20.419 0.014 | 19.995 0.093 | 18.893 0.089 | 18.448 0.194 | 16.113 0.053 | 15.391 0.047 | – – | – – | – – |
| C69-X-E-062 I | 05:36:02.79 | +10:05:39.3 | – – | – – | – – | – – | 11.386 0.024 | 11.018 0.026 | 10.923 0.021 | 10.857 0.003 | 10.887 0.004 | 10.842 0.008 | 10.859 0.013 | – – |
| C69-X-E-063 I | 05:35:54.62 | +10:01:52.1 | – – | – – | 23.006 0.059 | 21.992 0.055 | 20.671 0.176 | 19.917 0.218 | 18.508 0.194 | 16.768 0.095 | 16.062 0.097 | – – | – – | – – |
| C69-X-E-064 I | 05:35:22.18 | +09:53:58.4 | – – | – – | 15.607 0.003 | 14.428 0.001 | 13.083 0.027 | 12.380 0.027 | 12.137 0.024 | 12.021 0.004 | 11.893 0.006 | 11.865 0.016 | 11.853 0.028 | – – |
| C69-X-E-065 M | 05:35:38.12 | +09:53:16.3 | – – | – – | – – | – – | 13.201 0.026 | 12.625 0.027 | 12.499 0.026 | 12.249 0.004 | 12.446 0.007 | 13.342 0.044 | 12.410 0.046 | – – |
| C69-X-E-066 I | 05:35:38.25 | +10:01:03.0 | – – | – – | 20.554 0.103 | 19.866 0.074 | – – | – – | – – | 15.713 0.035 | 14.846 0.032 | 13.828 0.068 | 12.717 0.064 | 8.498 0.075 |
| C69-X-E-067 I | 05:36:08.63 | +09:53:20.2 | 13.754 0.010 | 12.941 0.010 | – – | – – | 11.184 0.026 | 10.943 0.022 | 10.847 0.023 | 10.770 0.002 | 10.770 0.003 | 10.768 0.009 | 10.761 0.011 | – – |
| C69-X-E-068 M | 05:36:20.21 | +09:56:02.8 | 14.758 0.010 | 13.810 0.010 | 13.363 0.000 | 12.915 0.000 | 12.281 0.027 | 12.013 0.023 | 11.910 0.023 | 11.848 0.004 | 11.875 0.005 | 11.523 0.013 | 11.807 0.031 | – – |
| C69-X-E-069 c | 05:35:51.71 | +09:53:34.0 | 16.632 0.010 | 15.499 0.010 | 14.729 0.001 | 14.111 0.001 | 13.268 0.023 | 12.761 0.025 | 12.601 0.029 | 12.573 0.005 | 12.593 0.007 | 12.533 0.024 | 12.54 0.04 | – – |
| C69-X-E-070 + | 05:36:13.50 | +10:01:16.3 | – – | – – | – – | – – | 021.00 0.000 | 019.75 0.000 | 018.75 0.000 | – – | – – | – – | – – | – – |
| C69-X-E-071 c | 05:35:29.21 | +09:46:32.3 | – – | – – | 13.950 0.001 | 13.279 0.001 | 12.313 0.026 | 11.691 0.025 | 11.556 0.026 | 11.448 0.003 | 11.479 0.004 | 11.441 0.013 | 11.352 0.02 | 7.563 0.035 |
| C69-X-E-072 I | 05:36:27.46 | +09:45:25.8 | – – | 17.605 0.000 | 16.443 0.000 | 14.921 0.000 | 13.436 0.032 | 12.763 0.023 | 12.537 0.027 | 12.284 0.004 | 12.274 0.007 | 12.170 0.021 | 12.233 0.034 | – – |
| C69-X-E-073 I | 05:36:11.54 | +09:59:40.5 | 17.109 0.010 | 16.241 0.010 | 15.700 0.002 | 15.144 0.002 | 14.696 0.002 | 14.322 0.002 | 14.217 0.004 | 13.967 0.01 | 13.932 0.017 | 13.8 0.061 | 13.604 0.1 | – – |
| C69-X-E-074 - | 05:36:35.56 | +09:54:23.9 | – – | – – | – – | – – | 18.371 0.028 | 17.257 0.022 | 16.554 0.034 | 15.536 0.040 | 15.577 0.076 | – – | 13.749 0.140 | – – |
| C69-X-E-075 I | 05:35:32.52 | +09:57:55.0 | – – | – – | 22.167 0.033 | 21.416 0.031 | 20.197 0.047 | 19.689 0.091 | 19.118 0.077 | 17.163 0.086 | 16.544 0.114 | – – | – – | – – |
| C69-X-E-076 - | 05:36:46.30 | +09:54:46.8 | – – | – – | – – | – – | 20.068 0.127 | 18.940 0.093 | 18.651 0.239 | – – | – – | – – | – – | – – |
| C69-X-E-077 g | 05:36:01.15 | +09:58:45.6 | 19.569 0.010 | 17.663 0.010 | 16.675 0.000 | 15.737 0.000 | 14.806 0.073 | 13.871 0.096 | 13.490 0.074 | 12.683 0.009 | 12.700 0.012 | 12.588 0.034 | – – | – – |
| C69-X-E-078 I | 05:36:27.06 | +09:51:35.1 | – – | – – | 17.770 0.010 | 16.170 0.010 | 14.515 0.041 | 13.881 0.023 | 13.651 0.051 | 13.226 0.011 | 13.116 0.015 | 12.930 0.047 | 13.126 0.100 | – – |
| C69-X-E-079 I | 05:35:21.43 | +09:49:56.9 | – – | – – | 16.120 0.010 | 14.760 0.010 | 13.184 0.026 | 12.477 0.026 | 12.253 0.026 | 12.044 0.006 | 12.038 0.009 | 12.015 0.029 | 11.902 0.038 | – – |
| C69-X-E-080 - | 05:36:57.65 | +10:03:16.0 | – – | – – | – – | – – | – – | – – | – – | 15.369 0.027 | 14.687 0.026 | 14.340 0.130 | 12.994 0.069 | 8.939 0.103 |
| C69-X-E-081 c | 05:35:55.64 | +09:50:53.7 | 19.069 0.010 | 17.41 0.00 | 16.08 0.00 | 14.41 0.00 | 12.732 0.026 | 12.097 0.031 | 11.827 0.026 | 11.474 0.005 | 11.400 0.006 | 11.303 0.017 | 11.342 0.025 | – – |
| ” e | 05:35:55.79 | +09:50:51.1 | – – | – – | 19.464 0.005 | 18.307 0.003 | – – | – – | – – | – – | – – | – – | – – | – – |
| C69-X-E-082 I | 05:35:57.06 | +09:46:53.0 | 18.315 0.010 | 16.79 0.00 | 15.63 0.00 | 14.18 0.00 | 12.755 0.030 | 12.004 0.023 | 11.775 0.023 | 11.523 0.005 | 11.534 0.007 | 11.434 0.018 | 11.373 0.025 | – – |
| C69-X-E-083 c | 05:36:46.91 | +09:56:22.3 | – – | – – | – – | – – | 19.663 0.075 | 18.949 0.092 | 18.475 0.181 | 17.245 0.091 | 16.526 0.104 | 15.3 0.277 | 13.707 0.105 | – – |
| ” n | 05:36:46.84 | +09:56:25.2 | – – | – – | – – | – – | 19.204 0.050 | 18.541 0.063 | 18.845 0.253 | 17.513 0.127 | – – | – – | – – | – – |
| C69-X-E-084 I | 05:35:35.76 | +09:44:35.4 | – – | 17.230 0.000 | 16.010 0.000 | 14.660 0.000 | 13.230 0.026 | 12.518 0.025 | 12.270 0.026 | 12.083 0.005 | 12.079 0.006 | 12.022 0.023 | 12.120 0.043 | – – |

Continued on next page…

Table 2.8 – Continued

| Name | RA (J2000) | DEC (J2000) | *B* | *V* | *Rc* | *Ic* | *J* | *H* | *K* | [3.6] | [4.5] | [5.8] | [8.0] | [24] |
|---|---|---|---|---|---|---|---|---|---|---|---|---|---|---|
| C69-X-E-085 + | 05:36:13.86 | +09:52:31.0 | – – | – – | – – | – – | 22.373 0.293 | 21.927 0.694 | 21.067 0.409 | – – | – – | – – | – – | – – |
| C69-X-E-086 M | 05:36:53.10 | +09:50:19.4 | 20.109 0.220 | 18.503 0.010 | – – | – – | 13.760 0.024 | 13.099 0.027 | 12.841 0.029 | 12.598 0.005 | 12.542 0.008 | 12.391 0.028 | 12.407 0.042 | – – |
| C69-X-E-087 c | 05:35:49.46 | +10:04:34.5 | – – | – – | 23.026 0.063 | 22.104 0.065 | – – | – – | – – | 16.714 0.054 | 15.746 0.037 | 15.039 0.169 | 13.878 0.108 | – – |
| ” s | 05:35:49.33 | +10:04:32.2 | – – | – – | 23.799 0.138 | 22.583 0.095 | – – | – – | – – | – – | – – | – – | – – | – – |
| C69-X-E-088 n | 05:36:30.11 | +09:43:39.5 | – – | – – | 22.071 0.028 | 21.284 0.026 | – – | – – | – – | 17.48 0.101 | 17.465 0.199 | – – | – – | – – |
| ” s | 05:36:30.59 | +09:43:29.4 | – – | – – | 18.723 0.003 | 17.968 0.002 | – – | – – | – – | 16.17 0.043 | 16.12 0.075 | – – | – – | – – |
| C69-X-E-089 - | 05:36:56.92 | +09:52:53.8 | – – | – – | – – | – – | – – | – – | – – | 16.991 0.107 | 16.448 0.130 | – – | – – | – – |
| C69-X-E-090 g | 05:35:43.89 | +09:56:02.8 | – – | – – | 22.058 0.027 | 21.452 0.043 | 20.083 0.043 | 19.129 0.057 | 18.406 0.039 | 16.646 0.059 | 15.922 0.06 | – – | – – | – – |
| C69-X-E-091 I | 05:36:31.53 | +09:45:01.4 | – – | – – | 18.120 0.010 | 16.400 0.010 | 14.647 0.037 | 13.985 0.045 | 13.682 0.039 | 13.393 0.012 | 13.301 0.016 | 13.284 0.075 | 13.182 0.115 | – – |
| C69-X-E-092 M | 05:37:10.40 | +09:51:27.3 | – – | – – | – – | – – | 13.053 0.024 | 12.482 0.023 | 12.161 0.021 | – – | – – | – – | – – | – – |
| C69-X-E-093 I | 05:35:25.48 | +09:47:41.7 | – – | – – | 20.722 0.008 | 20.171 0.010 | 19.240 0.023 | 18.403 0.028 | 18.036 0.030 | 16.338 0.041 | 15.967 0.055 | 14.656 0.087 | 13.727 0.069 | – – |
| C69-X-E-094 I | 05:35:51.66 | +10:06:35.8 | – – | – – | 21.110 0.013 | 20.071 0.011 | – – | – – | – – | 15.970 0.043 | 15.654 0.067 | – – | – – | – – |
| C69-X-E-095 - | 05:36:55.99 | +09:52:04.9 | – – | – – | – – | – – | – – | – – | – – | 16.334 0.054 | 15.432 0.055 | – – | 13.724 0.135 | – – |
| C69-X-E-096 c | 05:36:10.37 | +10:00:19.2 | 19.906 0.010 | 18.225 0.010 | 16.570 0.010 | 15.060 0.010 | 13.521 0.024 | 12.935 0.022 | 12.643 0.027 | 12.332 0.007 | 12.269 0.010 | 12.172 0.032 | 12.637 0.072 | – – |
| C69-X-E-097 M | 05:37:15.66 | +09:57:50.0 | – – | – – | – – | – – | 16.374 0.130 | 15.676 0.168 | 14.744 0.123 | – – | – – | – – | – – | – – |
| C69-X-E-098 M | 05:36:25.01 | +09:41:31.3 | – – | – – | – – | – – | 15.168 0.054 | 14.439 0.049 | 14.183 0.065 | 13.935 0.010 | 13.862 0.013 | 13.756 0.071 | 13.782 0.127 | – – |
| C69-X-E-099 g | 05:36:14.25 | +09:47:47.6 | – – | – – | 21.943 0.029 | 20.852 0.018 | 19.216 0.022 | 18.164 0.022 | 17.320 0.016 | 15.904 0.040 | 15.405 0.050 | – – | – – | – – |
| C69-X-E-100 - | 05:36:34.86 | +09:58:40.3 | – – | – – | – – | – – | 021.00 0.000 | 019.75 0.000 | 018.75 0.000 | – – | – – | – – | – – | – – |
| C69-X-E-101 - | 05:36:40.15 | +09:48:36.2 | – – | – – | – – | – – | – – | – – | – – | – – | – – | – – | – – | – – |
| C69-X-E-102 c | 05:35:30.57 | +09:56:14.7 | – – | – – | 18.823 0.003 | 18.027 0.002 | 17.069 0.005 | 16.338 0.005 | 16.240 0.007 | 15.529 0.035 | 15.482 0.06 | 15.04 0.216 | 15.103 0.478 | – – |
| ” e | 05:35:30.70 | +09:56:13.9 | – – | – – | 21.055 0.019 | 19.819 0.008 | 18.385 0.012 | 17.670 0.015 | 17.411 0.018 | – – | – – | – – | – – | – – |
| ” s | 05:35:30.68 | +09:56:12.3 | – – | – – | 20.931 0.013 | 20.281 0.012 | 19.339 0.027 | 18.598 0.035 | 18.057 0.032 | 15.364 0.032 | 15.026 0.043 | 14.328 0.116 | 13.556 0.104 | – – |
| C69-X-E-103 c | 05:35:32.60 | +09:56:10.9 | – – | – – | 22.566 0.068 | 21.410 0.031 | 20.170 0.052 | 19.023 0.060 | 18.285 0.046 | 17.444 0.302 | 17.261 0.349 | – – | – – | – – |
| ” s | 05:35:32.61 | +09:56:06.5 | – – | – – | – – | 22.463 0.085 | 20.737 0.079 | 19.816 0.097 | 18.789 0.061 | 16.985 0.116 | 17.053 0.254 | – – | – – | – – |
| ” w | 05:35:32.27 | +09:56:07.6 | – – | – – | 22.246 0.054 | 20.781 0.017 | 19.180 0.021 | 18.156 0.024 | 17.266 0.015 | 15.609 0.038 | 15.702 0.077 | – – | – – | – – |
| C69-X-E-104 c | 05:35:55.57 | +09:52:10.1 | 19.186 0.010 | 17.563 0.010 | 16.179 0.004 | 14.856 0.002 | 13.431 0.001 | 12.732 0.001 | 12.436 0.001 | 12.286 0.005 | 12.255 0.006 | 12.194 0.02 | 12.115 0.033 | – – |
| ” e | 05:35:55.77 | +09:52:08.9 | – – | – – | – – | – – | 19.331 0.032 | 18.951 0.058 | 18.637 0.057 | – – | – – | – – | – – | – – |
| C69-X-E-105 M | 05:36:55.43 | +10:01:10.7 | – – | – – | – – | – – | 14.058 0.028 | 13.439 0.036 | 13.099 0.031 | 12.808 0.007 | 12.787 0.009 | 12.813 0.029 | 12.657 0.050 | – – |
| C69-X-E-106 I | 05:36:00.68 | +09:41:11.6 | – – | – – | – – | – – | 19.958 0.116 | 18.538 0.083 | 17.601 0.086 | 16.353 0.039 | 15.02 0.032 | 13.94 0.062 | 12.979 0.065 | – – |
| C69-X-E-107 I | 05:35:59.37 | +09:53:32.4 | – – | – – | 19.690 0.005 | 18.717 0.004 | 17.646 0.012 | 16.816 0.013 | 16.554 0.035 | 16.248 0.055 | 16.088 0.079 | – – | – – | – – |
| C69-X-E-108 - | 05:36:33.88 | +10:01:08.9 | – – | – – | – – | – – | 021.00 0.000 | 019.75 0.000 | 18.805 0.270 | 17.077 0.141 | 16.129 0.082 | – – | – – | – – |
| C69-X-E-109 c | 05:36:10.87 | +10:00:53.0 | – – | – – | 22.224 0.032 | 21.599 0.033 | 021.00 0.000 | 019.75 0.000 | 18.75 0.000 | 17.082 0.076 | 16.571 0.109 | 15.93 0.287 | – – | – – |
| ” e | 05:36:10.98 | +10:00:53.1 | – – | – – | 22.952 0.095 | 21.346 0.026 | 20.146 0.114 | 19.332 0.141 | 18.551 0.204 | 17.726 0.119 | – – | – – | – – | – – |
| ” w | 05:36:10.65 | +10:00:53.3 | – – | – – | 20.583 0.010 | 19.625 0.006 | 19.018 0.043 | 18.112 0.048 | 18.75 0.000 | 17.191 0.095 | – – | – – | – – | – – |
| C69-X-E-110 - | 05:36:44.54 | +09:59:26.1 | – – | – – | – – | – – | 021.00 0.000 | 019.75 0.000 | 18.75 0.000 | – – | – – | – – | – – | – – |
| C69-X-E-111 I | 05:36:21.32 | +09:53:49.9 | – – | 14.401 0.000 | 14.068 0.000 | 13.720 0.000 | 13.231 0.001 | 13.010 0.001 | 12.932 0.002 | 12.817 0.006 | 12.814 0.008 | 12.996 0.041 | 13.207 0.061 | – – |
| C69-X-E-112 - | 05:37:05.46 | +09:56:09.9 | – – | – – | – – | – – | – – | – – | – – | – – | – – | – – | – – | – – |

**Table 2.9**: Disk properties, physical parameters and membership citeria of the X-ray sources in the Collinder 69 East field.

| Name | $T_{eff}$ | $L_{bol}$ | FluxTot | eFlux | FracF. | IRAC | Disk? | Ha? | DM | ByN | Mem (ByN) | Final |
|---|---|---|---|---|---|---|---|---|---|---|---|---|
| C69-X-E-001 I | 4000 | 0.8184 | 1.641e-10 | 1.886e-12 | 0.519 | III | No | Ha- | 046 | 003 | Y | Y+ |
| C69-X-E-002 I | 4500 | 0.0018 | 3.618e-13 | 4.461e-15 | 0.252 | I | – | – | – | – | - | NM |
| C69-X-E-003 M | 5000 | 2.3562 | 4.725e-10 | 6.502e-12 | 0.580 | III | – | – | – | – | - | Y |
| C69-X-E-004 I | 3750 | 0.6704 | 1.344e-10 | 1.114e-12 | 0.496 | III | No | Ha- | 051 | 008 | Y | Y+ |
| C69-X-E-005 c | 3750 | 0.0006 | 1.238e-13 | 2.656e-15 | 0.518 | II | – | – | – | – | - | NM+ |
| ” w | 3750 | 0.0002 | 5.378e-14 | 2.672e-15 | 0.466 | ?– | – | – | – | – | - | NM+ |
| C69-X-E-006 I | 4000 | 0.4176 | 8.375e-11 | 9.989e-13 | 0.520 | III | No | Ha- | 060 | 017 | Y | Y+ |
| C69-X-E-007 c | 4000 | 0.5081 | 1.019e-10 | 1.346e-12 | 0.519 | III | No | Ha- | 058 | 014 | Y | Y+ |
| C69-X-E-008 I | 4750 | 1.1487 | 2.303e-10 | 2.894e-12 | 0.561 | III | – | – | 057 | – | - | Y+ |
| C69-X-E-009 I | 4750 | 4.2826 | 8.588e-10 | 3.533e-12 | 0.171 | III | T? | – | – | – | - | Y? |
| C69-X-E-010 c | 4750 | 1.6856 | 3.380e-10 | 4.256e-12 | 0.581 | III | – | – | 045 | – | - | Y+ |
| C69-X-E-011 c | 4000 | 0.4452 | 8.928e-11 | 2.174e-12 | 0.519 | III | No | Ha- | 059 | 025 | Y | Y+ |
| ” e | – | – | – | – | 0.000 | ?– | – | – | – | – | - | Y? |
| C69-X-E-012 I | 3750 | 4.3396 | 8.702e-10 | 7.670e-12 | 0.374 | III | T? | – | – | – | - | Y? |
| C69-X-E-013 I | 5500 | 82.106 | 1.646e-08 | 6.517e-11 | 0.132 | ?– | – | – | – | – | - | Y |
| C69-X-E-014 I | 3750 | 0.3874 | 7.770e-11 | 8.367e-13 | 0.499 | III | No | Ha- | 044 | 022 | Y | Y+ |
| C69-X-E-015 I | 4000 | 0.0005 | 1.161e-13 | 2.564e-15 | 0.492 | III | – | – | – | – | - | NM+ |
| C69-X-E-016 I | 3750 | 0.4499 | 9.022e-11 | 1.011e-12 | 0.494 | III | No | Ha- | 056 | 018 | Y | Y+ |
| C69-X-E-017 I | 3700 | 0.2450 | 4.914e-11 | 5.190e-13 | 0.475 | III | No | – | – | 028 | Y | Y+ |
| C69-X-E-018 M | 3750 | 0.3023 | 6.062e-11 | 7.314e-13 | 0.496 | III | – | – | 065 | – | - | Y+ |
| C69-X-E-019 M | 3750 | 0.2448 | 4.909e-11 | 6.220e-13 | 0.498 | III | – | – | 070 | – | - | Y+ |
| C69-X-E-020 I | 5000 | 4.8647 | 9.755e-10 | 1.235e-11 | 0.562 | III | – | – | – | – | - | Y |
| C69-X-E-021 c | 1900 | 0.0002 | 4.776e-14 | 2.218e-15 | 0.368 | ?– | – | – | – | – | - | NM? |
| ” w | 4750 | 0.0004 | 8.149e-14 | 2.187e-15 | 0.168 | ?– | – | – | – | – | - | NM |
| C69-X-E-022 I | 3700 | 0.2765 | 5.545e-11 | 6.656e-13 | 0.471 | III | No | Ha- | 055 | 032 | Y | Y+ |
| C69-X-E-023 I | 4500 | 1.0271 | 2.059e-10 | 8.054e-13 | 0.191 | III | No | – | – | 004 | Y | Y+ |
| ” o | 4000 | 0.0010 | 2.049e-13 | 1.353e-15 | 0.467 | ?– | – | – | – | – | - | NM+ |
| C69-X-E-025 I | 3750 | 0.2030 | 4.071e-11 | 5.046e-13 | 0.530 | III | – | – | 061 | – | - | Y+ |
| C69-X-E-026 - | 1900 | 0.0005 | 1.003e-13 | 2.261e-15 | 0.383 | ?– | – | – | – | – | - | NM? |
| C69-X-E-027 c | 3750 | 0.1887 | 3.785e-11 | 4.979e-13 | 0.504 | III | – | – | 062 | – | - | Y+ |
| ” n | 3300 | 0.0005 | 1.113e-13 | 4.286e-15 | 0.393 | ?– | – | – | – | – | - | NM |
| C69-X-E-028 c | 3750 | 0.3633 | 7.286e-11 | 8.930e-13 | 0.496 | III | No | Ha- | 050 | 023 | Y | Y+ |
| C69-X-E-029 c | 3750 | 0.3027 | 6.071e-11 | 1.141e-12 | 0.499 | III | No | Ha- | 039 | 033 | Y | Y+ |
| C69-X-E-030 I | 4000 | 0.4031 | 8.084e-11 | 9.252e-13 | 0.517 | III | – | – | 053 | – | - | Y+ |
| C69-X-E-031 M | 3600 | 0.2479 | 4.971e-11 | 5.138e-13 | 0.464 | III | – | – | 067 | – | - | Y+ |
| C69-X-E-032 - | 1900 | 0.0015 | 3.119e-13 | 2.489e-15 | 0.358 | I | – | – | – | – | - | NM? |
| C69-X-E-033 I | 3100 | 0.0002 | 4.940e-14 | 1.098e-15 | 0.412 | ?– | – | – | – | – | - | NM |
| C69-X-E-034 c | 4000 | 0.3390 | 6.798e-11 | 8.616e-13 | 0.517 | III | – | – | 035 | – | - | Y+ |
| ” w | 5000 | 0.0012 | 2.541e-13 | 9.269e-16 | 0.156 | ?– | – | – | – | – | - | NM |
| C69-X-E-035 c | 3500 | 0.2490 | 4.994e-11 | 5.114e-13 | 0.455 | III | No | Ha- | 041 | 040 | Y | Y+ |
| C69-X-E-036 I | 3200 | 0.2415 | 4.844e-11 | 5.103e-13 | 0.440 | III | No | Ha- | 038 | 041 | Y | Y+ |
| C69-X-E-037 c | 3400 | 0.0763 | 1.531e-11 | 1.325e-13 | 0.466 | III | Thin | – | – | 064 | Y | Y+ |
| C69-X-E-038 c | 3750 | 0.0016 | 3.283e-13 | 4.909e-15 | 0.436 | II | – | – | – | – | - | NM+ |
| ” w | 2100 | 0.0002 | 4.137e-14 | 9.191e-16 | 0.361 | ?– | – | – | – | – | - | NM? |
| C69-X-E-039 - | – | – | – | – | 0.000 | ?– | – | – | – | – | - | NM? |
| C69-X-E-040 M | 3600 | 0.1304 | 2.614e-11 | 2.726e-13 | 0.463 | III | – | – | – | – | - | Y |
| C69-X-E-041 M | 3700 | 0.2019 | 4.048e-11 | 4.223e-13 | 0.463 | ?– | – | – | 071 | – | - | Y+ |
| C69-X-E-042 M | 7250 | 98.800 | 1.981e-08 | 2.967e-11 | 0.066 | ?– | – | – | – | – | - | Y |
| C69-X-E-043 I | 4000 | 0.0002 | 5.002e-14 | 1.108e-15 | 0.490 | ?– | – | – | – | – | - | NM+ |
| C69-X-E-044 + | – | – | – | – | 0.000 | ?– | – | – | – | – | - | NM? |
| C69-X-E-045 + | 4000 | 0.0001 | 2.038e-14 | 1.944e-15 | 0.509 | ?– | – | – | – | – | - | NM |
| C69-X-E-046 g | 3100 | 0.0002 | 4.994e-14 | 1.140e-15 | 0.452 | ?– | – | – | – | – | - | NM+ |
| C69-X-E-047 M | 4500 | 0.0565 | 1.133e-11 | 7.842e-14 | 0.190 | III | – | – | – | – | - | NM |
| C69-X-E-048 - | – | – | – | – | 0.000 | ?– | – | – | – | – | - | NM? |
| C69-X-E-049 I | 4250 | 0.0003 | 7.081e-14 | 1.135e-15 | 0.465 | ?– | – | – | – | – | - | NM+ |
| C69-X-E-050 I | – | – | – | – | 0.000 | ?– | – | – | – | – | - | NM? |
| C69-X-E-051 I | 4750 | 0.0007 | 1.508e-13 | 1.100e-15 | 0.462 | II | – | – | – | – | - | NM+ |
| C69-X-E-052 I | 3750 | 0.0268 | 5.374e-12 | 1.036e-13 | 0.548 | ?– | – | – | – | – | - | NM |
| C69-X-E-053 I | 3700 | 0.0001 | 2.086e-14 | 6.740e-16 | 0.323 | ?– | – | – | – | – | - | NM+ |
| C69-X-E-054 I | 3500 | 0.1445 | 2.897e-11 | 2.036e-13 | 0.444 | III | No | – | – | 051 | Y | Y+ |
| C69-X-E-055 I | 3300 | 0.1422 | 2.851e-11 | 2.114e-13 | 0.433 | III | No | – | – | 054 | Y | Y+ |
| C69-X-E-056 - | 1900 | 0.0001 | 3.157e-14 | 2.268e-15 | 0.387 | ?– | – | – | – | – | - | NM? |
| C69-X-E-057 M | 4750 | 4.1627 | 8.347e-10 | 1.049e-11 | 0.582 | III | – | – | – | – | - | Y |
| C69-X-E-058 M | 4000 | 0.3147 | 6.311e-11 | 7.483e-13 | 0.519 | III | – | – | 069 | – | - | Y+ |
| C69-X-E-059 + | – | – | – | – | 0.000 | ?– | – | – | – | – | - | NM? |
| C69-X-E-060 c | 4750 | 0.5334 | 1.069e-10 | 4.101e-13 | 0.195 | III | – | – | – | – | - | NM? |
| ” n | 6250 | 0.0009 | 1.922e-13 | 1.518e-15 | 0.350 | ?– | – | – | – | – | - | NM |
| C69-X-E-061 I | 4250 | 0.0005 | 1.109e-13 | 2.478e-15 | 0.448 | ?– | – | – | – | – | - | NM+ |
| C69-X-E-062 I | 5500 | 1.2955 | 2.597e-10 | 7.729e-13 | 0.145 | III | – | – | – | – | - | NM? |

Continued on next page…

Table 2.9 – Continued

| Name | $T_{eff}$ | $L_{bol}$ | FluxTot | eFlux | FracF. | IRAC | Disk? | Ha? | DM | ByN | Mem (ByN) | Final |
|---|---|---|---|---|---|---|---|---|---|---|---|---|
| C69-X-E-063 I | 3750 | 0.0001 | 3.434e-14 | 2.372e-15 | 0.510 | ?– | – | – | – | – | - | NM+ |
| C69-X-E-064 I | 3750 | 0.1598 | 3.204e-11 | 2.231e-13 | 0.485 | III | – | – | – | – | - | Y |
| C69-X-E-065 M | 4750 | 0.2038 | 4.088e-11 | 1.722e-13 | 0.173 | I/I | – | – | – | – | - | NM |
| C69-X-E-066 I | 2800 | 0.0028 | 5.769e-13 | 4.986e-15 | 0.130 | I | – | – | – | – | - | NM? |
| C69-X-E-067 I | 5500 | 1.4050 | 2.817e-10 | 1.143e-12 | 0.258 | III | – | – | – | – | - | NM? |
| C69-X-E-068 M | 5750 | 0.5800 | 1.163e-10 | 1.408e-12 | 0.548 | III | – | – | – | – | - | NM |
| C69-X-E-069 c | 4500 | 0.1842 | 3.694e-11 | 1.925e-13 | 0.562 | III | – | – | – | – | - | NM |
| C69-X-E-070 + | – | – | – | – | 0.000 | ?– | – | – | – | – | - | NM? |
| C69-X-E-071 c | 4500 | 0.4083 | 8.189e-11 | 4.224e-13 | 0.502 | III | – | – | – | – | - | NM? |
| C69-X-E-072 I | 3600 | 0.1070 | 2.145e-11 | 2.805e-13 | 0.467 | III | – | – | – | – | - | Y |
| C69-X-E-073 I | 5500 | 0.0656 | 1.317e-11 | 2.450e-14 | 0.552 | III | – | – | – | – | - | NM |
| C69-X-E-074 - | 1900 | 0.0013 | 2.608e-13 | 2.375e-15 | 0.363 | ?– | – | – | – | – | - | NM? |
| C69-X-E-075 I | 4000 | 0.0002 | 5.130e-14 | 1.112e-15 | 0.461 | ?– | – | – | – | – | - | NM+ |
| C69-X-E-076 - | 3700 | 0.0003 | 6.155e-14 | 2.274e-15 | 0.294 | ?– | – | – | – | – | - | NM |
| C69-X-E-077 g | 4000 | 0.0412 | 8.270e-12 | 3.632e-13 | 0.546 | ?– | – | – | – | – | - | NM+ |
| C69-X-E-078 I | 3400 | 0.0398 | 7.992e-12 | 8.215e-14 | 0.412 | III | No | – | – | 090 | Y | Y+ |
| C69-X-E-079 I | 3700 | 0.1408 | 2.824e-11 | 2.276e-13 | 0.429 | III | No | Ha- | – | 055 | Y | Y+ |
| C69-X-E-080 - | – | – | – | – | 0.000 | I | – | – | – | – | - | NM? |
| C69-X-E-081 c | 3300 | 0.1923 | 3.857e-11 | 4.823e-13 | 0.451 | III | No | Ha- | 047 | 047 | Y | Y+ |
| ” e | – | – | – | – | 0.000 | ?– | – | – | – | – | - | NM? |
| C69-X-E-082 I | 3700 | 0.2106 | 4.224e-11 | 5.246e-13 | 0.472 | III | No | Ha- | 049 | 039 | Y | Y+ |
| C69-X-E-083 c | 2500 | 0.0002 | 5.547e-14 | 2.072e-15 | 0.382 | I | – | – | – | – | - | NM |
| ” n | 4500 | 0.0007 | 1.495e-13 | 2.074e-15 | 0.185 | ?– | – | – | – | – | - | NM |
| C69-X-E-084 I | 3700 | 0.1366 | 2.741e-11 | 3.182e-13 | 0.470 | III | – | – | 040 | – | - | Y+ |
| C69-X-E-085 + | 2100 | 2.2810 | 4.574e-15 | 6.951e-16 | 0.357 | ?– | – | – | – | – | - | NM? |
| C69-X-E-086 M | 3200 | 0.0697 | 1.399e-11 | 1.110e-13 | 0.336 | III | – | – | – | – | - | Y? |
| C69-X-E-087 c | 1600 | 0.0006 | 1.388e-13 | 8.233e-16 | 0.111 | I | – | – | – | – | - | NM? |
| ” s | – | – | – | – | 0.000 | ?– | – | – | – | – | - | NM? |
| C69-X-E-088 n | 4000 | 0.0003 | 6.342e-14 | 1.214e-15 | 0.321 | ?– | – | – | – | – | - | NM |
| ” s | 4000 | 0.0060 | 1.217e-12 | 1.863e-15 | 0.254 | ?– | – | – | – | – | - | NM |
| C69-X-E-089 - | – | – | – | – | 0.000 | ?– | – | – | – | – | - | NM? |
| C69-X-E-090 g | 4000 | 0.0003 | 6.232e-14 | 1.169e-15 | 0.483 | ?– | – | – | – | – | - | NM+ |
| C69-X-E-091 I | 3200 | 0.0350 | 7.037e-12 | 8.351e-14 | 0.407 | III | No | Ha- | – | 098 | Y | Y+ |
| C69-X-E-092 M | 1400 | 0.1090 | 2.186e-11 | 1.771e-13 | 0.382 | ?– | – | – | – | – | - | NM? |
| C69-X-E-093 I | 4250 | 0.0007 | 1.597e-13 | 1.149e-15 | 0.465 | II | – | – | – | – | - | NM+ |
| C69-X-E-094 I | 3750 | 0.0009 | 1.947e-13 | 1.151e-15 | 0.284 | ?– | – | – | – | – | - | NM |
| C69-X-E-095 - | – | – | – | – | 0.000 | ?– | – | – | – | – | - | NM? |
| C69-X-E-096 c | 3300 | 0.0971 | 1.949e-11 | 1.499e-13 | 0.450 | III | No | Ha- | – | 058 | Y | Y+ |
| C69-X-E-097 M | 1900 | 0.0068 | 1.378e-12 | 6.340e-14 | 0.352 | ?– | – | – | – | – | - | NM? |
| C69-X-E-098 M | 4000 | 0.0271 | 5.453e-12 | 6.402e-14 | 0.236 | III | – | – | – | – | - | NM |
| C69-X-E-099 g | 3200 | 0.0007 | 1.405e-13 | 1.166e-15 | 0.432 | ?– | – | – | – | – | - | NM+ |
| C69-X-E-100 - | – | – | – | – | 0.000 | ?– | – | – | – | – | - | NM? |
| C69-X-E-101 - | – | – | – | – | 0.000 | ?– | – | – | – | – | - | NM? |
| C69-X-E-102 c | 4250 | 0.0051 | 1.040e-12 | 1.682e-15 | 0.464 | III | – | – | – | – | - | NM |
| ” e | 3750 | 0.0011 | 2.334e-13 | 1.362e-15 | 0.464 | ?– | – | – | – | – | - | NM |
| ” s | 4250 | 0.0006 | 1.389e-13 | 1.264e-15 | 0.468 | II | – | – | – | – | - | NM+ |
| C69-X-E-103 c | 3700 | 0.0003 | 6.380e-14 | 1.353e-15 | 0.451 | ?– | – | – | – | – | - | NM+ |
| ” s | 3000 | 0.0001 | 3.200e-14 | 9.353e-16 | 0.394 | ?– | – | – | – | – | - | NM+ |
| ” w | 3100 | 0.0007 | 1.434e-13 | 1.278e-15 | 0.424 | ?– | – | – | – | – | - | NM+ |
| C69-X-E-104 c | 3700 | 0.1130 | 2.267e-11 | 1.984e-14 | 0.472 | III | – | – | – | – | - | Y |
| ” e | 1200 | 0.0003 | 6.359e-14 | 9.886e-16 | 0.365 | ?– | – | – | – | – | - | Y |
| C69-X-E-105 M | 3300 | 0.0565 | 1.134e-11 | 1.001e-13 | 0.300 | III | – | – | – | – | - | Y? |
| C69-X-E-106 I | 1900 | 0.0003 | 7.684e-14 | 2.450e-15 | 0.381 | I | – | – | – | – | - | NM? |
| C69-X-E-107 I | 4000 | 0.0028 | 5.726e-13 | 2.733e-15 | 0.470 | ?– | – | – | – | – | - | NM |
| C69-X-E-108 - | 1800 | 0.0001 | – | – | 0.000 | ?– | – | – | – | – | - | h NM? |
| C69-X-E-109 c | 4250 | 0.0002 | 4.830e-14 | 7.989e-16 | 0.363 | ?– | – | – | – | – | - | NM+ |
| ” e | 3700 | 0.0003 | 6.039e-14 | 2.563e-15 | 0.409 | ?– | – | – | – | – | - | NM+ |
| ” w | 4000 | 0.0011 | 2.338e-13 | 2.329e-15 | 0.408 | ?– | – | – | – | – | - | NM+ |
| C69-X-E-110 - | – | – | – | – | 0.000 | ?– | – | – | – | – | - | NM? |
| C69-X-E-111 I | 6250 | 0.3009 | 6.034e-11 | 1.585e-12 | 0.526 | III | – | – | – | – | - | NM |
| C69-X-E-112 - | – | – | – | – | 0.000 | ?– | – | – | – | – | - | NM? |

**Table 2.10**: Optical and infrared photometry for the X-ray sources of Collinder 69 West.

| Name | RA (J2000) | DEC (J2000) | *B* | *V* | *Rc* | *Ic* | *J* | *H* | *K* | [3.6] | [4.5] | [5.8] | [8.0] | [24] |
|---|---|---|---|---|---|---|---|---|---|---|---|---|---|---|
| C69-X-W-001 c | 05:34:06.87 | +10:01:01.6 | – – | 11.929 0.010 | – – | – – | 10.194 0.024 | 9.736 0.027 | 9.589 0.021 | 9.526 0.002 | 9.546 0.002 | 9.506 0.004 | 9.447 0.005 | – – |
| ” n | 05:34:06.61 | +10:01:04.4 | – – | – – | – – | – – | – – | – – | – – | – – | – – | – – | – – | – – |
| C69-X-W-002 c | 05:34:36.20 | +09:53:43.8 | – – | 15.91 0.00 | 14.77 0.00 | 13.53 0.00 | 12.046 0.028 | 11.324 0.024 | 11.092 0.025 | 10.882 0.004 | 10.833 0.005 | 10.811 0.014 | 10.742 0.013 | – – |
| ” n | 05:34:36.48 | +09:53:48.7 | – – | – – | 18.613 0.016 | 17.940 0.014 | 17.008 0.008 | 16.562 0.015 | 16.526 0.029 | – – | – – | – – | – – | – – |
| C69-X-W-003 I | 05:33:56.34 | +09:53:56.6 | – – | 15.69 0.010 | 14.490 0.000 | 13.130 0.000 | 11.656 0.022 | 10.918 0.022 | 10.719 0.023 | 10.511 0.003 | 10.480 0.004 | 10.467 0.011 | 10.344 0.012 | – – |
| C69-X-W-004 I | 05:33:47.18 | +09:55:38.4 | – – | 14.162 0.010 | 13.343 0.003 | 12.514 0.011 | 11.297 0.022 | 10.595 0.022 | 10.426 0.021 | 10.228 0.003 | 10.255 0.004 | 10.214 0.009 | 10.206 0.010 | – – |
| C69-X-W-005 c | 05:34:32.81 | +09:59:31.7 | – – | 14.21 0.00 | 13.46 0.00 | 12.77 0.00 | 11.839 0.027 | 11.227 0.026 | 11.059 0.021 | 10.939 0.003 | 10.964 0.004 | 10.924 0.009 | 10.918 0.013 | – – |
| ” s | 05:34:32.62 | +09:59:26.9 | – – | – – | 16.271 0.004 | 15.722 0.003 | 15.163 0.002 | 14.874 0.004 | 14.749 0.007 | – – | – – | – – | – – | – – |
| ” w | 05:34:32.36 | +09:59:31.0 | – – | – – | 18.057 0.012 | 17.458 0.011 | 16.722 0.006 | 16.370 0.014 | 16.236 0.025 | – – | – – | – – | – – | – – |
| C69-X-W-006 I | 05:34:39.18 | +09:52:55.0 | – – | 15.090 0.000 | 14.170 0.000 | 13.310 0.000 | 12.072 0.027 | 11.360 0.023 | 11.186 0.022 | 11.006 0.003 | 11.039 0.003 | 10.961 0.009 | 10.915 0.013 | – – |
| C69-X-W-007 c | 05:34:28.12 | +09:48:48.1 | – – | 17.419 0.000 | 16.157 0.000 | 14.802 0.000 | 13.319 0.022 | 12.588 0.023 | 12.397 0.027 | 12.218 0.005 | 12.228 0.006 | 12.159 0.016 | 12.279 0.03 | – – |
| ” e | 05:34:28.47 | +09:48:47.9 | – – | – – | – – | – – | 19.300 0.048 | 18.510 0.073 | 17.606 0.070 | 15.815 0.045 | 15.971 0.086 | – – | – – | – – |
| C69-X-W-008 c | 05:33:49.96 | +09:50:37.2 | – – | 16.03 0.00 | 15.05 0.00 | 13.94 0.00 | 12.684 0.030 | 11.954 0.029 | 77.777 0.000 | 11.455 0.005 | 11.320 0.006 | 10.970 0.014 | 9.857 0.008 | 6.211 0.010 |
| ” n | 05:33:49.81 | +09:50:40.5 | – – | – – | 16.522 0.004 | 15.873 0.003 | 14.852 0.002 | 14.319 0.003 | 14.139 0.005 | 13.558 0.011 | 13.584 0.011 | 13.069 0.036 | 11.827 0.024 | – – |
| C69-X-W-009 c | 05:34:04.17 | +10:00:48.3 | – – | 13.056 0.010 | – – | – – | 11.496 0.024 | 11.166 0.027 | 11.120 0.027 | 11.083 0.003 | 11.078 0.004 | 11.057 0.011 | 11.054 0.013 | – – |
| ” s | 05:34:04.43 | +10:00:41.8 | – – | – – | 15.083 0.002 | 14.390 0.001 | 13.364 0.001 | 12.707 0.001 | 12.490 0.001 | 12.72 0.008 | 12.722 0.009 | 12.788 0.037 | 12.678 0.04 | – – |
| C69-X-W-010 c | 05:34:02.01 | +09:58:18.2 | – – | – – | 19.495 0.004 | 18.684 0.004 | 17.602 0.015 | – – | – – | 14.747 0.017 | 14.171 0.02 | 13.548 0.041 | 12.452 0.033 | 8.616 0.072 |
| ” e | 05:34:02.13 | +09:58:16.3 | – – | – – | 20.593 0.009 | 19.800 0.009 | 18.672 0.038 | – – | – – | – – | – – | – – | – – | – – |
| C69-X-W-011 c | 05:34:05.54 | +09:42:46.6 | – – | 12.750 0.000 | 12.160 0.000 | 11.610 0.000 | 10.801 0.023 | 10.262 0.024 | 10.125 0.021 | 10.079 0.002 | 10.11 0.003 | 10.01 0.006 | 10.005 0.007 | – – |
| ” s | 05:34:05.83 | +09:42:41.0 | – – | – – | – – | – – | 17.709 0.020 | 17.021 0.026 | 16.687 0.048 | – – | – – | – – | – – | – – |
| C69-X-W-012 I | 05:34:04.87 | +09:57:06.2 | – – | 16.06 0.00 | 15.05 0.00 | 13.95 0.00 | 12.500 0.022 | 11.727 0.024 | 11.336 0.021 | 10.879 0.002 | 10.598 0.003 | 10.229 0.006 | 9.538 0.005 | 6.926 0.024 |
| C69-X-W-013 c | 05:34:35.58 | +09:59:44.3 | – – | 16.420 0.000 | 15.250 0.000 | 13.930 0.000 | 12.459 0.024 | 11.727 0.026 | 11.492 0.021 | 11.302 0.005 | 11.309 0.006 | 11.198 0.016 | 11.180 0.018 | – – |
| ” n | 05:34:35.65 | +09:59:51.9 | – – | – – | 21.531 0.019 | 20.792 0.024 | 19.498 0.059 | 18.650 0.097 | 18.759 0.225 | – – | – – | – – | – – | – – |
| C69-X-W-014 c | 05:33:50.44 | +10:04:20.9 | – – | 11.883 0.010 | – – | – – | 9.232 0.030 | 9.021 0.030 | 8.894 0.024 | 8.949 0.002 | 8.883 0.002 | 8.854 0.003 | 8.841 0.003 | 7.956 0.050 |
| ” w | 05:33:49.87 | +10:04:21.0 | – – | – – | – – | – – | 14.884 0.308 | 14.401 0.308 | 14.166 0.236 | 13.82 0.059 | 13.835 0.072 | 13.571 0.074 | 13.738 0.166 | – – |
| C69-X-W-015 I | 05:34:08.38 | +09:51:25.0 | – – | 16.826 0.019 | 15.390 0.010 | 14.170 0.010 | 12.924 0.024 | 12.318 0.024 | 12.065 0.023 | 11.837 0.006 | 11.804 0.007 | 11.751 0.023 | 11.674 0.024 | – – |
| C69-X-W-016 - | 05:33:12.95 | +09:49:38.9 | – – | – – | – – | – – | – – | – – | – – | 16.815 0.093 | 16.346 0.117 | – – | – – | – – |
| C69-X-W-017 - | 05:33:36.97 | +09:56:35.7 | – – | – – | – – | – – | – – | – – | – – | 17.259 0.126 | 16.598 0.107 | – – | – – | – – |
| C69-X-W-018 I | 05:34:18.31 | +09:52:38.0 | – – | 15.136 0.010 | 14.306 0.001 | 13.613 0.001 | 12.723 0.022 | 12.207 0.023 | 12.022 0.024 | 11.941 0.004 | 11.933 0.006 | 11.866 0.016 | 11.862 0.028 | – – |
| C69-X-W-019 M | 05:33:42.57 | +10:03:47.8 | – – | 19.404 0.166 | – – | – – | 16.667 0.155 | 15.675 0.149 | 14.770 0.112 | 13.806 0.010 | 13.166 0.011 | 12.573 0.025 | 11.113 0.016 | 8.055 0.052 |
| C69-X-W-020 I | 05:33:51.18 | +09:46:42.4 | – – | – – | – – | – – | 9.479 0.023 | 9.224 0.022 | 9.153 0.023 | 9.242 0.002 | 9.111 0.002 | 9.098 0.004 | 9.079 0.003 | – – |
| C69-X-W-021 - | 05:33:40.58 | +10:02:39.1 | – – | – – | – – | – – | – – | – – | – – | 15.984 0.036 | 15.500 0.047 | – – | 13.845 0.142 | – – |
| C69-X-W-022 - | 05:33:43.13 | +10:10:12.4 | – – | – – | – – | – – | – – | – – | – – | – – | – – | – – | – – | – – |
| C69-X-W-023 I | 05:34:39.25 | +10:01:29.3 | – – | – – | 15.470 0.010 | 13.980 0.010 | 12.576 0.024 | 11.936 0.023 | 11.706 0.021 | 11.395 0.005 | 11.378 0.006 | 11.287 0.018 | 11.260 0.019 | – – |
| C69-X-W-024 c | 05:34:11.77 | +09:57:03.9 | – – | 17.406 0.032 | 15.930 0.010 | 14.630 0.010 | 13.117 0.023 | 12.454 0.024 | 12.192 0.019 | 11.917 0.006 | 11.863 0.008 | 11.764 0.022 | 11.791 0.029 | – – |
| ” s | 05:34:11.85 | +09:56:58.8 | – – | – – | 21.053 0.156 | 20.027 0.085 | 18.543 0.027 | 17.855 0.045 | 17.879 0.105 | 15.873 0.054 | – – | – – | – – | – – |
| C69-X-W-025 c | 05:34:02.41 | +10:07:05.7 | – – | – – | 21.630 0.023 | 20.519 0.015 | 19.291 0.058 | 18.562 0.085 | 18.621 0.205 | 16.898 0.091 | – – | – – | – – | – – |
| ” e | 05:34:02.74 | +10:07:06.7 | – – | – – | 21.767 0.019 | 21.151 0.025 | 19.684 0.082 | 18.729 0.097 | 17.743 0.093 | 16.408 0.047 | 15.637 0.05 | 15.564 0.23 | – – | – – |
| ” w | 05:34:02.25 | +10:07:05.2 | – – | – – | 20.746 0.012 | 19.435 0.006 | 18.087 0.021 | 17.348 0.031 | 16.831 0.040 | 16.602 0.065 | 16.781 0.164 | – – | – – | – – |
| C69-X-W-026 - | 05:33:03.93 | +10:02:06.4 | – – | – – | – – | – – | – – | – – | – – | – – | – – | – – | – – | – – |
| C69-X-W-027 M | 05:33:23.98 | +09:57:07.7 | – – | 16.579 0.014 | 15.965 0.000 | 15.427 0.000 | 14.582 0.035 | 14.134 0.047 | 13.996 0.046 | 13.936 0.011 | – – | 13.860 0.063 | 13.724 0.131 | – – |
| C69-X-W-028 M | 05:33:35.32 | +10:08:26.1 | – – | – – | – – | – – | 16.138 0.101 | 15.389 0.120 | 14.876 0.098 | 14.400 0.015 | 14.219 0.020 | 13.876 0.068 | 13.359 0.082 | – – |
| C69-X-W-029 M | 05:33:15.15 | +09:50:30.2 | – – | 17.505 0.028 | 16.291 0.000 | 14.706 0.000 | 12.949 0.028 | 12.287 0.029 | 11.876 0.028 | 11.446 0.003 | 11.238 0.004 | 11.071 0.010 | 10.608 0.011 | 8.106 0.052 |
| C69-X-W-030 c | 05:34:01.31 | +09:56:35.3 | – – | – – | 19.796 0.005 | 19.123 0.005 | 18.890 0.050 | – – | – – | 15.736 0.034 | 14.598 0.021 | 13.543 0.055 | 12.6 0.052 | – – |
| ” e | 05:34:01.87 | +09:56:33.1 | – – | – – | 20.830 0.010 | 19.729 0.007 | 18.589 0.036 | – – | – – | 17.14 0.099 | – – | – – | – – | – – |
| C69-X-W-031 M | 05:33:26.96 | +10:01:39.5 | – – | – – | – – | – – | 16.826 0.179 | 16.006 0.202 | 15.238 0.135 | 14.381 0.019 | 13.840 0.019 | 13.313 0.055 | 12.306 0.042 | – – |

Continued on next page…

Table 2.10 – Continued

| Name | RA (J2000) | DEC (J2000) | *B* | *V* | *Rc* | *Ic* | *J* | *H* | *K* | [3.6] | [4.5] | [5.8] | [8.0] | [24] |
|---|---|---|---|---|---|---|---|---|---|---|---|---|---|---|
| C69-X-W-032 c | 05:33:48.30 | +10:01:43.5 | – – | 18.410 0.030 | 17.227 0.001 | 16.064 0.001 | 14.471 0.054 | 13.827 0.060 | 13.465 0.063 | 13.084 0.007 | 13.048 0.01 | 13.067 0.042 | 13.35 0.085 | – – |
| ” e | 05:33:48.38 | +10:01:42.1 | – – | – – | 16.802 0.001 | 15.928 0.001 | – – | – – | – – | 13.274 0.008 | 13.184 0.011 | 13.2 0.05 | 13.307 0.085 | – – |
| ” s | 05:33:48.38 | +10:01:36.3 | – – | – – | 23.159 0.103 | 21.993 0.070 | – – | – – | – – | – – | – – | – – | – – | – – |
| ” w | 05:33:47.91 | +10:01:39.6 | – – | – – | 18.710 0.010 | 16.990 0.010 | 15.162 0.048 | 14.576 0.060 | 14.268 0.082 | 13.723 0.017 | 13.579 0.021 | 13.263 0.070 | 12.448 0.054 | – – |
| ” z | 05:33:48.09 | +10:01:36.2 | – – | – – | 99.999 9.999 | 22.532 0.125 | – – | – – | – – | – – | – – | – – | – – | – – |
| C69-X-W-033 + | 05:33:42.71 | +09:58:02.2 | – – | – – | – – | – – | – – | – – | – – | – – | – – | – – | – – | – – |
| C69-X-W-034 M | 05:33:27.83 | +10:04:20.2 | – – | 16.411 0.010 | 15.520 0.000 | 14.718 0.000 | 13.647 0.028 | 12.948 0.032 | 12.752 0.030 | 12.596 0.005 | 12.643 0.008 | 12.649 0.033 | 12.621 0.049 | – – |
| C69-X-W-035 - | 05:33:14.08 | +09:55:45.3 | – – | – – | – – | – – | – – | – – | – – | 17.128 0.128 | – – | – – | – – | – – |
| C69-X-W-036 M | 05:33:40.33 | +09:51:59.3 | – – | 14.596 0.010 | 14.088 0.000 | 13.577 0.030 | 12.799 0.024 | 12.435 0.022 | 12.392 0.027 | 12.205 0.005 | 12.222 0.006 | 12.227 0.021 | 12.325 0.042 | – – |
| C69-X-W-037 M | 05:33:32.98 | +09:57:38.5 | – – | 17.354 0.029 | 16.388 0.000 | 15.228 0.013 | 14.046 0.029 | 13.293 0.036 | 13.070 0.032 | 12.896 0.006 | 12.945 0.009 | 12.880 0.033 | – – | – – |
| C69-X-W-038 c | 05:33:44.65 | +10:01:45.8 | – – | – – | – – | – – | – – | – – | – – | – – | – – | – – | – – | – – |
| ” s | 05:33:44.50 | +10:01:39.1 | – – | – – | 18.415 0.013 | 17.856 0.012 | – – | – – | – – | 15.942 0.034 | 15.684 0.047 | – – | – – | – – |
| C69-X-W-039 c | 05:33:47.85 | +09:52:55.9 | – – | – – | 20.447 0.077 | 19.700 0.009 | – – | – – | – – | 17.57 0.164 | – – | – – | – – | – – |
| ” w | 05:33:47.39 | +09:52:59.6 | – – | 14.620 0.010 | 14.040 0.001 | 13.531 0.001 | 12.972 0.024 | 12.661 0.023 | 12.611 0.032 | 12.997 0.006 | 13.045 0.009 | 13.245 0.043 | 13.068 0.067 | – – |
| C69-X-W-040 M | 05:33:39.20 | +10:00:13.3 | – – | 16.207 0.011 | 15.261 0.000 | 14.343 0.024 | 13.234 0.025 | 12.531 0.031 | 12.352 0.026 | 12.223 0.005 | 12.255 0.006 | 12.149 0.020 | 12.166 0.032 | – – |
| C69-X-W-041 I | 05:33:43.19 | +09:43:40.6 | – – | 17.349 0.097 | 16.336 0.000 | 14.988 0.050 | 13.752 0.029 | 13.129 0.029 | 12.896 0.030 | 12.611 0.006 | 12.603 0.008 | 12.481 0.030 | 12.550 0.051 | – – |
| C69-X-W-042 c | 05:33:51.29 | +09:48:12.3 | – – | – – | 23.161 0.083 | 22.097 0.063 | 20.75 0.000 | 019.75 0.000 | 19.00 0.000 | 17.185 0.106 | 16.944 0.137 | – – | – – | – – |
| ” e | 05:33:51.56 | +09:48:12.3 | – – | – – | 21.017 0.014 | 19.783 0.008 | 18.409 0.028 | 17.659 0.038 | 17.477 0.080 | 16.9 0.097 | – – | – – | – – | – – |
| ” w | 05:33:51.00 | +09:48:16.0 | – – | – – | 23.081 0.074 | 22.243 0.070 | 20.323 0.162 | 20.617 0.625 | 18.833 0.289 | 17.556 0.121 | 16.759 0.119 | – – | – – | – – |
| C69-X-W-043 I | 05:33:52.02 | +09:53:02.7 | – – | 12.353 0.010 | – – | – – | 11.150 0.023 | 10.860 0.023 | 10.798 0.023 | 10.732 0.003 | 10.753 0.003 | 10.722 0.008 | 10.739 0.011 | – – |
| C69-X-W-044 - | 05:33:33.98 | +09:50:23.2 | – – | – – | – – | – – | – – | – – | – – | 16.336 0.067 | 15.781 0.059 | 14.468 0.136 | 13.718 0.138 | – – |
| C69-X-W-045 - | 05:33:12.86 | +09:57:58.0 | – – | – – | – – | – – | – – | – – | – – | 15.661 0.056 | – – | – – | – – | – – |
| C69-X-W-046 M | 05:33:03.79 | +09:58:42.6 | – – | – – | – – | – – | 14.015 0.035 | 13.359 0.033 | 13.053 0.039 | – – | – – | – – | – – | – – |
| C69-X-W-047 M | 05:33:11.61 | +09:59:02.9 | – – | – – | – – | – – | 14.716 0.042 | 14.086 0.049 | 13.815 0.051 | – – | – – | – – | – – | – – |
| C69-X-W-048 I | 05:34:24.67 | +09:56:57.1 | – – | – – | 22.049 0.046 | 20.309 0.015 | 18.595 0.024 | 17.937 0.039 | 17.782 0.083 | 16.767 0.068 | 16.742 0.133 | – – | – – | – – |
| C69-X-W-049 I | 05:34:34.36 | +10:03:19.1 | – – | – – | 22.896 0.060 | 21.827 0.046 | 20.00 0.000 | 19.00 0.000 | 18.25 0.000 | 16.443 0.055 | 15.937 0.059 | – – | – – | – – |
| C69-X-W-050 - | 05:33:28.86 | +09:51:08.6 | – – | – – | – – | – – | – – | – – | – – | – – | – – | – – | – – | – – |
| C69-X-W-051 - | 05:33:39.63 | +09:51:03.7 | – – | – – | – – | – – | – – | – – | – – | – – | – – | – – | – – | – – |
| C69-X-W-052 - | 05:33:23.08 | +09:56:49.3 | – – | – – | – – | – – | – – | – – | – – | – – | – – | – – | – – | – – |

**Table 2.11**: Disk properties, physical parameters and membership citeria of the X-ray sources in the Collinder 69 West field.

| Name | $T_{eff}$ | $L_{bol}$ | FluxTot | eFlux | FracF. | IRAC | Disk? | Ha? | DM | ByN | Mem (ByN) | Final |
|---|---|---|---|---|---|---|---|---|---|---|---|---|
| C69-X-W-001 c | 5000 | 3.4265 | 6.871e-10 | 3.160e-12 | 0.287 | III | – | – | – | – | - | Y? |
| ” n | – | – | – | – | 0.000 | ?– | – | – | – | – | - | bi? |
| C69-X-W-002 c | 3700 | 0.4109 | 8.240e-11 | 9.855e-13 | 0.467 | III | No | Ha- | 012 | 026 | Y | Y+ |
| ” n | 4750 | 0.0055 | 1.105e-12 | 6.729e-15 | 0.452 | ?– | – | – | – | – | - | NM |
| C69-X-W-003 I | 3600 | 0.5802 | 1.163e-10 | 1.135e-12 | 0.465 | III | No | Ha- | 004 | 013 | Y | Y+ |
| C69-X-W-004 I | 4000 | 0.9155 | 1.836e-10 | 1.250e-12 | 0.521 | III | No | Ha- | 001 | 001 | Y | Y+ |
| C69-X-W-005 c | 4500 | 0.6404 | 1.284e-10 | 1.820e-12 | 0.546 | III | – | – | 009 | – | - | Y+ |
| ” s | 5500 | 0.0403 | 8.095e-12 | 1.139e-14 | 0.432 | ?– | – | – | – | – | - | NM |
| ” w | 5000 | 0.0081 | 1.630e-12 | 7.946e-15 | 0.453 | ?– | – | – | – | – | - | NM |
| C69-X-W-006 I | 4000 | 0.4414 | 8.851e-11 | 1.144e-12 | 0.516 | III | – | – | 014 | – | - | Y+ |
| C69-X-W-007 c | 3600 | 0.1249 | 2.506e-11 | 2.769e-13 | 0.463 | III | – | – | – | – | - | Y |
| ” e | 1900 | 0.0004 | 9.588e-14 | 2.042e-15 | 0.359 | ?– | – | – | – | – | - | NM? |
| C69-X-W-008 c | 3750 | 0.2671 | 5.357e-11 | 6.397e-13 | 0.432 | I/I | Thic | Ha+ | 002 | 038 | Y | Y+ |
| ” n | 4500 | 0.0388 | 7.785e-12 | 1.082e-14 | 0.461 | I/I | – | – | – | – | - | NM |
| C69-X-W-009 c | 5750 | 1.1992 | 2.404e-10 | 9.655e-13 | 0.250 | III | – | – | – | – | - | NM |
| ” s | 4500 | 0.1566 | 3.141e-11 | 2.734e-14 | 0.481 | III | – | – | – | – | - | NM |
| C69-X-W-010 c | 4000 | 0.0033 | 6.684e-13 | 2.158e-15 | 0.379 | II | – | – | – | – | - | NM+ |
| ” e | 4000 | 0.0011 | 2.244e-13 | 1.100e-15 | 0.316 | ?– | – | – | – | – | - | NM |
| C69-X-W-011 c | 4750 | 1.8244 | 3.658e-10 | 4.925e-12 | 0.595 | III | – | – | 007 | – | - | Y+ |
| ” s | 3400 | 0.0020 | 4.162e-13 | 3.192e-15 | 0.295 | ?– | – | – | – | – | - | NM |
| C69-X-W-012 I | 3700 | 0.2976 | 5.969e-11 | 6.130e-13 | 0.460 | II | – | – | 006 | – | - | Y+ |
| C69-X-W-013 c | 3700 | 0.2782 | 5.579e-11 | 6.264e-13 | 0.468 | III | No | Ha- | 011 | 037 | Y | Y+ |
| ” n | 4000 | 0.0004 | 9.549e-14 | 2.699e-15 | 0.475 | ?– | – | – | – | – | - | NM |
| C69-X-W-014 c | 4500 | 4.8047 | 9.634e-10 | 6.916e-12 | 0.345 | III | – | – | – | – | - | Y? |
| ” w | 4750 | 0.0423 | 8.496e-12 | 3.957e-13 | 0.171 | III | – | – | – | – | - | NM |
| C69-X-W-015 I | 3750 | 0.1759 | 3.528e-11 | 2.941e-13 | 0.512 | III | No | – | – | 044 | Y | Y+ |
| C69-X-W-016 - | – | – | – | – | 0.000 | ?– | – | – | – | – | - | NM? |
| C69-X-W-017 - | – | – | – | – | 0.000 | ?– | – | – | – | – | - | NM? |
| C69-X-W-018 I | 4500 | 0.2854 | 5.724e-11 | 2.890e-13 | 0.567 | III | – | – | – | – | - | NM? |
| C69-X-W-019 M | 4000 | 0.0088 | 1.766e-12 | 6.872e-14 | 0.296 | I | – | – | – | – | - | NM |
| C69-X-W-020 I | 7000 | 12.483 | 2.503e-09 | 3.885e-12 | 0.081 | III | – | – | – | – | - | Y? |
| C69-X-W-021 - | – | – | – | – | 0.000 | ?– | – | – | – | – | - | NM? |
| C69-X-W-022 - | – | – | – | – | 0.000 | ?– | – | – | – | – | - | NM? |
| C69-X-W-023 I | 3700 | 0.2553 | 5.120e-11 | 3.588e-13 | 0.423 | III | No | – | – | 036 | Y | Y+ |
| C69-X-W-024 c | 3700 | 0.1509 | 3.027e-11 | 2.311e-13 | 0.450 | III | No | – | – | 052 | Y | Y+ |
| ” s | 3750 | 0.0010 | 2.066e-13 | 6.413e-15 | 0.443 | ?– | – | – | – | – | - | NM+ |
| C69-X-W-025 c | 3750 | 0.0005 | 1.129e-13 | 2.742e-15 | 0.449 | ?– | – | – | – | – | - | k NM+ |
| ” e | 4250 | 0.0003 | 7.838e-14 | 2.657e-15 | 0.560 | ?– | – | – | – | – | - | NM+ |
| ” w | 3700 | 0.0018 | 3.666e-13 | 2.975e-15 | 0.413 | ?– | – | – | – | – | - | NM |
| C69-X-W-026 - | – | – | – | – | 0.000 | ?– | – | – | – | – | - | NM? |
| C69-X-W-027 M | 5000 | 0.0555 | 1.113e-11 | 5.284e-13 | 0.574 | ?– | – | – | – | – | - | NM |
| C69-X-W-028 M | 2500 | 0.0073 | 1.467e-12 | 5.583e-14 | 0.382 | II | – | – | – | – | - | Y |
| C69-X-W-029 M | 3200 | 0.1673 | 3.356e-11 | 3.924e-13 | 0.431 | II | – | – | – | – | - | Y |
| C69-X-W-031 M | 1900 | 0.0046 | 9.330e-13 | 5.340e-14 | 0.354 | II | – | – | – | – | - | Y |
| C69-X-W-032 c | 3700 | 0.0450 | 9.030e-12 | 1.342e-13 | 0.438 | III | – | – | – | – | - | NM? |
| ” e | 3750 | 0.0438 | 8.787e-12 | 1.068e-14 | 0.253 | III | – | – | – | – | - | NM? |
| ” s | – | – | – | – | 0.000 | ?– | – | – | – | – | - | NM? |
| ” w | 3100 | 0.0219 | 4.397e-12 | 7.049e-14 | 0.386 | II | Thic | Ha+ | – | 113 | Y | Y+ |
| ” z | – | – | – | – | 0.000 | ?– | – | – | – | – | - | bi? |
| C69-X-W-033 + | – | – | – | – | 0.000 | ?– | – | – | – | – | - | NM? |
| C69-X-W-034 M | 4000 | 0.1161 | 2.328e-11 | 3.326e-13 | 0.510 | III | – | – | – | – | - | NM? |
| C69-X-W-035 - | – | – | – | – | 0.000 | ?– | – | – | – | – | - | NM? |
| C69-X-W-036 M | 5250 | 0.3032 | 6.081e-11 | 7.943e-13 | 0.559 | III | – | – | – | – | - | NM |
| C69-X-W-037 M | 3750 | 0.0727 | 1.459e-11 | 1.896e-13 | 0.490 | ?– | – | – | – | – | - | NM? |
| C69-X-W-038 c | – | – | – | – | 0.000 | ?– | – | – | – | – | - | NM? |
| ” s | 4500 | 0.0062 | 1.261e-12 | 4.634e-15 | 0.291 | ?– | – | – | – | – | - | NM |
| C69-X-W-039 c | 4000 | 0.0012 | 2.465e-13 | 2.991e-15 | 0.253 | ?– | – | – | – | – | - | NM |
| ” w | 6000 | 0.3116 | 6.249e-11 | 2.575e-13 | 0.539 | III | – | – | – | – | - | NM |
| C69-X-W-040 M | 4000 | 0.1550 | 3.110e-11 | 4.028e-13 | 0.526 | III | – | – | – | – | - | NM? |
| C69-X-W-041 I | 3750 | 0.0855 | 1.715e-11 | 3.948e-13 | 0.493 | III | – | – | – | – | - | NM? |
| C69-X-W-042 c | 2700 | 0.0004 | 9.571e-14 | 9.746e-16 | 0.123 | ?– | – | – | – | – | - | NM+ |
| ” e | 3750 | 0.0011 | 2.291e-13 | 2.938e-15 | 0.475 | ?– | – | – | – | – | - | NM |
| ” w | 3750 | 0.0001 | 2.926e-14 | 2.979e-15 | 0.508 | ?– | – | – | – | – | - | NM |
| C69-X-W-043 I | 6250 | 2.0759 | 4.162e-10 | 1.346e-12 | 0.232 | III | – | – | – | – | - | NM |
| C69-X-W-044 - | – | – | – | – | 0.000 | II | – | – | – | – | - | NM? |
| C69-X-W-045 - | – | – | – | – | 0.000 | ?– | – | – | – | – | - | NM? |
| C69-X-W-046 M | 3400 | 0.0604 | 1.211e-11 | 1.160e-13 | 0.297 | ?– | – | – | – | – | - | NM? |
| C69-X-W-047 M | 4250 | 0.0434 | 8.714e-12 | 7.942e-14 | 0.212 | ?– | – | – | – | – | - | NM |
| C69-X-W-048 I | 3400 | 0.0009 | 1.807e-13 | 2.456e-15 | 0.413 | ?– | – | – | – | – | - | NM |

Continued on next page…

Table 2.11 – Continued

| Name | $T_{eff}$ | $L_{bol}$ | FluxTot | eFlux | FracF. | IRAC | Disk? | Ha? | DM | ByN | Mem (ByN) | Final |
|---|---|---|---|---|---|---|---|---|---|---|---|---|
| C69-X-W-049 I | 3000 | 0.0004 | 8.099e-14 | 1.467e-15 | 0.342 | ?– | – | – | – | – | - | NM+ |
| C69-X-W-050 - | – | – | – | – | 0.000 | ?– | – | – | – | – | - | NM? |
| C69-X-W-051 - | – | – | – | – | 0.000 | ?– | – | – | – | – | - | NM? |
| C69-X-W-052 - | – | – | – | – | 0.000 | ?– | – | – | – | – | - | NM? |

## 2.2 Barnard 30 and Barnard 35

Barnard 30 and Barnard 35 are two dark clouds located ∼2.°5 North-West and South-East of the star $\lambda$ Ori, respectively. We have collected optical and mid-IR photometry for these associations (see Figs. 2.4 and 2.5).

- Optical data: On 2005 December 24-26, we conducted an optical photometric survey on the Lambda Orionis Star Forming Region (LOSFR), using the Wide Field Camera (WFC), an optical mosaic camera mounted on the 2.5 m Isaac Newton Telescope at El Roque de los Muchachos Observatory, La Palma. The WFC consists of 4 thinned EEV 2k×4k CCDs. The CCDs have a pixel scale 0.33"/pixel and a field of view of 34′×34′ neglecting the 1′ inter-chip spacing.

  We used the Sloan-gunn r and i filters for this survey and performed 4 different pointings in each region covering the whole stellar associations centered in Barnard 30 and Barnard 35. We collected two different sets of exposures, with short and long exposure times. In the first case, we exposed during 5 s for each filter whereas the long exposure times were 600 and 3×400 for Sloan gunn i and r respectively. In this way we increased the dynamical range and our shallow photometry overlaps with previously published RI cousins data from Dolan & Mathieu (1999). Landolt standards were observed and used for calibrations. Errors in the zero-points are generally less than 1-2%.

  The weather during the run was clear and the mean seeing as measured in the images is 1.5". The reduction and photometry was performed with the CASU INT Wide Field Survey (McMahon et al. 2001) pipeline (Irwin & Lewis 2001). This pipeline uses IRAF for the overall structure, but with supplementary extra stages. Completeness is achieved at $R(complete) \sim 21.5$ mag and $I(complete) \sim 20.5$ mag based on the drop of detected objects for each interval in each filter. Because of the completeness limit in R, the effective completeness is at $I_{(Compl,effect)}$=19.00. Therefore, for an age of 1Myr that would correspond to a mass of 0.025 $M_{\odot}$ and an effective tempereture of 2625 K. For the case of an age of 5 Myr the limit would be at 0.025 $M_{\odot}$ and 2600 K.

- Spitzer data: Our Spitzer data were collected in 2005 October 22 and 26, and 2006 March 25 and 29 with IRAC, and 2006 March 2 and April 3 with MIPS as part of a General Observer cycle 2 program (PID:20339).

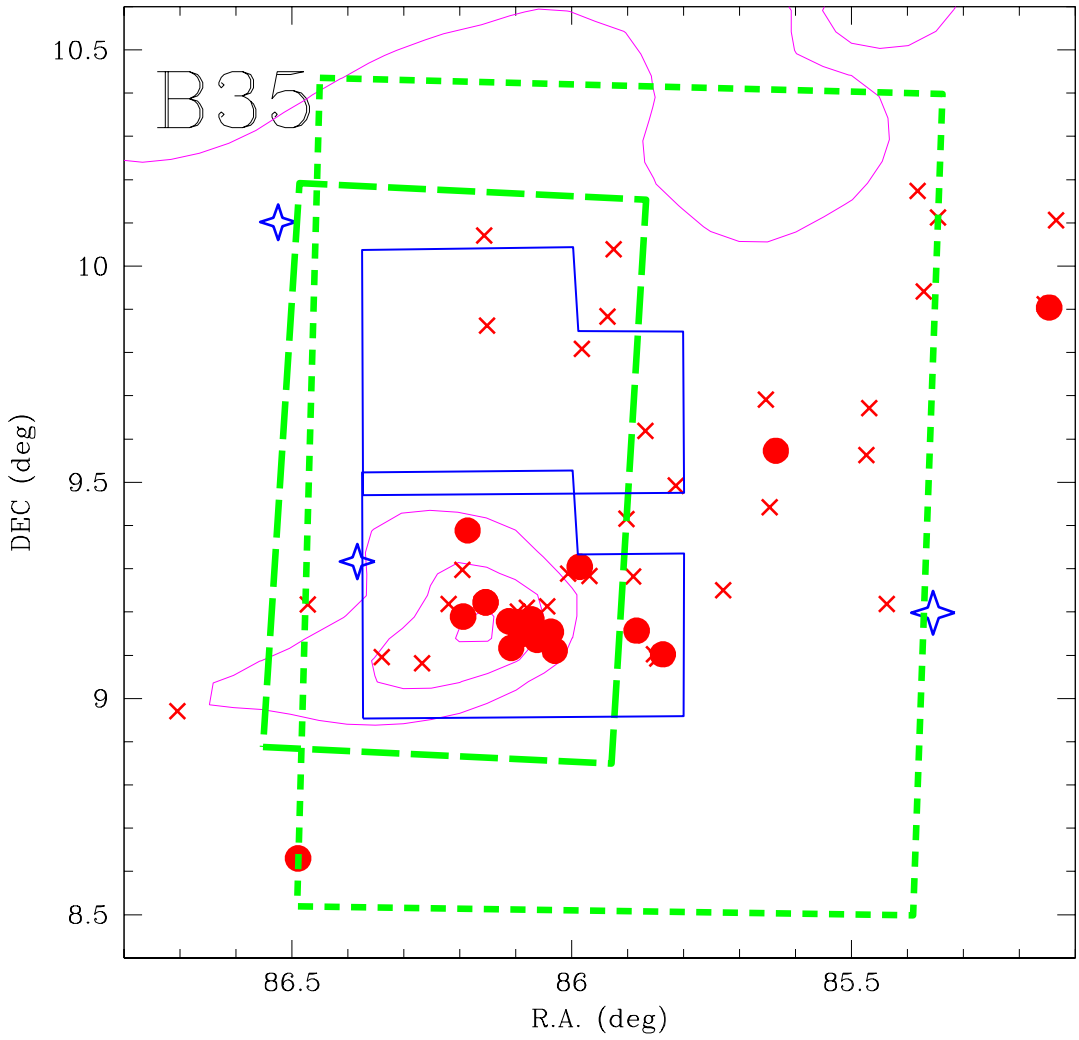


**Figure 2.4**: Layout of observations in the Barnard 35 area. Thick green rectangles represent the Spitzer fields obtained in GO2 (long-dashed: IRAC, and short-dashed: MIPS). Thin blue solid lines define the areas covered by our optical WFC survey. Young stars, identified by Dolan & Mathieu (1999, 2001), appear as crosses (WTTs) and solid circles (CTTs) following the low resolution spectroscopic criterion by Barrado y Navascués & Martín (2003). IRAS contours at 100$\mu$m are displayed in magenta.

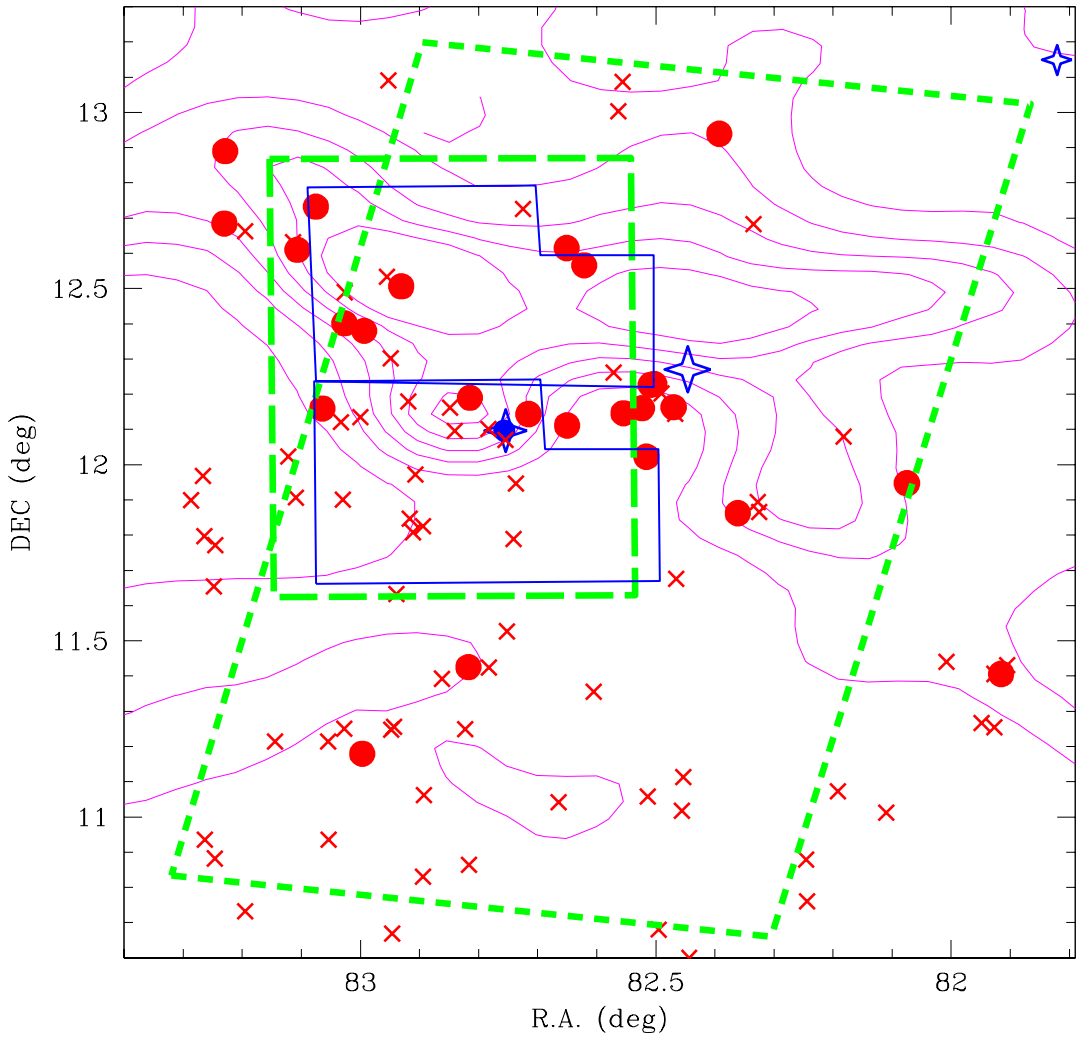


**Figure 2.5**: Layout of observations in the Barnard 30 area. Thick green rectangles represent the Spitzer fields obtained in GO2 (long-dashed: IRAC, and short-dashed: MIPS). Blue solid lines define the areas covered by our optical survey. Young stars, identified by Dolan & Mathieu (1999, 2001), appear as crosses (WTTs) and solid circles (CTTs) following the low resolution spectroscopic criterion (Barrado y Navascués & Martín 2003). IRAS 100 $\mu$m contours are plotted in magenta.

IRAC imaging for each dark cloud was performed in two epochs separated by 7 months. In each epoch, observations were performed in mapping mode with individual exposures of 12 seconds "frame time" (corresponding to 10.4 seconds exposure times) and three dithers at each map step. We used the high dynamic range (HDR) option which provides extra frames, with frame times shorter (0.6 seconds) than our selected frame time. We have used the shorter frames to measure the brightness of the brighter sources and we have combined the longer frames of the two epochs to obtain one single deeper mosaic and thus reach our sensitivity goal. Each of the IRAC images from the Spitzer Science Center pipeline was corrected for instrumental artifacts using the IDL code provided by the Spitzer Science Center and then combined into the mosaics at each of the four bandpasses using the MOPEX package (Makovoz & Khan 2005). The final mosaics cover an area in the sky of $\sim 0.6^\circ \times 1.3^\circ$ and are centered at 05:31:22.77 +12:14:52.35 in Barnard 30, and at 05:44:43.53 +09:30:49.06 in Barnard 35. Note that just half the area observed with the optical WFC survey is observed with IRAC in each of the dark clouds. The mean integration time for the deep mosaics is 62.4 s.

The Multi-band Imaging Photometer for Spitzer (MIPS, Rieke et al. (2004)) was used to map both regions with a fast rate scan mode and 12 legs separated by 302″ in the cross scan direction. The total effective integration time per point on the sky at 24 $\mu$m for most points in the map was 15 seconds, and the mosaics covered an area of $1^\circ \times 1.5^\circ$ centered around 05:30:23.17 +11:55:52.83 for Barnard 30, and 05:43:40.4 +09:26:37.8 for Barnard 35. The overlapping area between IRAC and MIPS in each dark cloud is a region of $\sim 1^\circ \times 0.5^\circ$. Since there were no visible artifacts in the pipeline mosaics for MIPS 24 $\mu$m we used them as our starting point to extract the photometry. Note that since the MIPS surveys of Barnard 30 and Barnard 35 have been done in fast scan mode (3 sec frame time $\times$ 5 frames), they are shallower than that of Collinder 69 which was performed in medium scan mode (4 sec frame time $\times$ 10 frames).

The analysis of the data was done with IRAF.

The new candidate members derived from these surveys can be seen in tables 2.14, 2.15, 2.18 and 2.19.

**Table 2.12**: Photometry for the Dolan and DIL members of Barnard 35.

| Dolan/DIL ID | RA (J2000) | DEC (J2000) | V[2] | R[2] | I[2] | J[3] error | H[3] error | Ks[3] error | [3.6] error | [4.5] error | [5.8] error | [8.0] error | [24] error |
|---|---|---|---|---|---|---|---|---|---|---|---|---|---|
| 217[1] | 05:41:28.91 | +09:56:29.0 | 13.72 | 12.91 | 12.12 | 10.963 0.021 | 10.2 0.023 | 9.777 0.021 | – – | – – | – – | – – | 5.244 0.005 |
| 222[1] | 05:42:32.43 | +09:34:22.8 | 17.03 | 15.81 | 14.25 | 12.648 0.025 | 11.978 0.026 | 11.672 0.026 | – – | – – | – – | – – | 7.856 0.047 |
| 225[1] | 05:42:55.00 | +09:15:01.6 | 15.17 | 14.13 | 13.0 | 11.645 0.023 | 10.887 0.025 | 10.56 0.02 | – – | – – | – – | – – | 6.077 0.01 |
| 227[1] | 05:43:20.92 | +09:06:07.1 | 13.05 | 12.28 | 11.5 | 10.074 0.025 | 9.132 0.02 | 8.411 0.02 | – – | – – | – – | – – | 3.268 0.001 |
| 228[1] | 05:43:23.22 | +09:05:31.7 | 13.37 | 12.57 | 11.78 | 10.342 0.025 | 9.623 0.022 | 9.237 0.02 | – – | – – | – – | – – | 5.562 0.008 |
| 231 | 05:43:32.20 | +09:09:24.0 | 14.71 | 13.75 | 12.76 | 11.293 0.025 | 10.552 0.02 | 10.185 0.022 | 9.409 0.002 | 9.04 0.001 | 8.62 0.003 | 7.901 0.002 | 5.213 0.004 |
| 232 | 05:43:33.50 | +09:16:55.8 | 14.96 | 13.98 | 12.81 | 11.378 0.026 | 10.694 0.023 | 10.464 0.02 | 10.23 0.002 | 10.214 0.003 | 10.136 0.008 | 10.171 0.012 | – – |
| 233 | 05:43:36.60 | +09:24:55.5 | 15.06 | 14.06 | 13.04 | 11.663 0.025 | 10.948 0.023 | 10.762 0.022 | 10.421 0.002 | 10.495 0.002 | 10.443 0.006 | 10.457 0.011 | – – |
| 234 | 05:43:42.09 | +10:02:21.0 | 14.43 | 13.55 | 12.65 | 11.173 0.024 | 10.418 0.022 | 10.01 0.02 | 9.392 0.002 | 8.976 0.001 | 8.652 0.003 | 8.164 0.002 | 6.069 0.011 |
| 235 | 05:43:44.61 | +09:53:01.6 | 13.85 | 12.99 | 12.04 | 10.734 0.026 | 10.067 0.026 | 9.831 0.025 | 9.646 0.002 | 9.635 0.002 | 9.598 0.003 | 9.608 0.003 | – – |
| 236 | 05:43:52.34 | +09:17:00.5 | 17.18 | 15.90 | 14.26 | 12.599 0.027 | 11.932 0.023 | 11.684 0.019 | 11.431 0.002 | 11.373 0.003 | 11.353 0.008 | 11.33 0.012 | – – |
| 237 | 05:43:55.55 | +09:48:30.8 | 15.17 | 14.14 | 13.03 | 11.696 0.022 | 10.946 0.021 | 10.742 0.021 | 10.556 0.002 | 10.584 0.002 | 10.539 0.005 | 10.525 0.006 | – – |
| 238 | 05:43:56.59 | +09:18:16.9 | 17.3 | 16.07 | 14.63 | 12.854 0.026 | 12.036 0.023 | 11.672 0.021 | 11.276 0.002 | 11.091 0.002 | 10.947 0.006 | 10.789 0.007 | 7.024 0.027 |
| 239 | 05:44:01.63 | +09:17:20.8 | 15.64 | 14.64 | 13.59 | 12.335 0.026 | 11.604 0.027 | 11.398 0.024 | 11.143 0.002 | 11.105 0.003 | 11.132 0.007 | 11.113 0.01 | – – |
| 240 | 05:44:07.26 | +09:06:38.1 | 14.65 | 13.74 | 12.91 | 11.656 0.026 | 10.935 0.023 | 10.675 0.021 | 10.438 0.002 | 10.376 0.002 | 10.274 0.005 | 9.978 0.004 | 4.528 0.002 |
| 241 | 05:44:08.99 | +09:09:14.8 | 14.1 | 13.23 | 12.41 | 11.102 0.024 | 10.025 0.022 | 9.252 0.019 | 8.119 0.001 | 7.719 0.001 | 7.439 0.002 | 6.661 0.001 | 3.729 0.002 |
| 242 | 05:44:10.65 | +09:12:45.2 | 14.18 | 13.45 | 12.78 | 11.925 0.024 | 11.32 0.023 | 11.179 0.024 | 11.065 0.002 | 11.103 0.002 | 11.051 0.007 | 11.072 0.009 | – – |
| 243 | 05:44:14.86 | +09:08:08.2 | 17.05 | 15.85 | 14.32 | 12.671 0.024 | 11.967 0.025 | 11.673 0.029 | 11.471 0.002 | 11.333 0.003 | 11.288 0.008 | 11.195 0.011 | 6.296 0.014 |
| 244 | 05:44:17.35 | +09:10:59.2 | 14.07 | 13.13 | 12.21 | 10.793 0.023 | 10.043 0.025 | 9.62 0.023 | 9.109 0.001 | 8.711 0.001 | 8.423 0.002 | 7.676 0.001 | 4.83 0.005 |
| 245 | 05:44:19.21 | +09:12:34.9 | 14.79 | 13.74 | 12.55 | 11.192 0.027 | 10.552 0.038 | 10.223 0.026 | 9.868 0.001 | 9.761 0.002 | 9.614 0.003 | 9.383 0.003 | 7.611 0.051 |
| 246 | 05:44:21.85 | +09:08:52.9 | 15.42 | 14.23 | 12.9 | 11.357 0.032 | 10.672 0.051 | 10.041 0.027 | 9.636 0.002 | 9.343 0.001 | 9.056 0.003 | 8.058 0.002 | 4.706 0.008 |
| 247 | 05:44:22.89 | +09:10:35.3 | 16.09 | 15.01 | 13.82 | 12.452 0.024 | 11.72 0.023 | 11.449 0.027 | 11.108 0.002 | 10.76 0.003 | 10.448 0.005 | 9.697 0.005 | 7.141 0.043 |
| 248 | 05:44:23.21 | +09:12:03.9 | 12.04 | 11.45 | 10.89 | 10.003 0.023 | 9.364 0.025 | 8.952 0.021 | 8.349 0.001 | 8.174 0.001 | 7.939 0.002 | 7.461 0.001 | 4.296 0.004 |
| 249 | 05:44:25.97 | +09:07:00.7 | 14.21 | 13.37 | 12.52 | 11.151 0.023 | 10.35 0.023 | 9.939 0.023 | 9.06 0.001 | 8.649 0.001 | 8.268 0.002 | 7.757 0.001 | 5.876 0.018 |
| 250 | 05:44:26.90 | +09:10:42.4 | 17.08 | 15.92 | 14.59 | 13.238 0.027 | 12.552 0.031 | 12.355 0.033 | 12.076 0.004 | 12.044 0.005 | 11.93 0.015 | 11.923 0.085 | – – |
| 251 | 05:44:36.27 | +09:51:43.9 | 16.81 | 15.69 | 14.37 | 12.863 0.024 | 12.137 0.021 | 11.94 0.021 | 11.797 0.002 | 11.776 0.003 | 11.733 0.01 | 11.726 0.013 | – – |
| 252 | 05:44:37.02 | +09:13:20.0 | 16.94 | 15.65 | 14.02 | 12.329 0.023 | 11.658 0.027 | 11.327 0.019 | 10.843 0.003 | 10.535 0.003 | 10.171 0.006 | 9.554 0.014 | 6.172 0.032 |
| 254 | 05:44:37.61 | +10:04:14.2 | 12.53 | 12.04 | 11.57 | 10.932 0.022 | 10.458 0.021 | 10.391 0.021 | 10.371 0.002 | 10.33 0.002 | 10.397 0.005 | 10.324 0.006 | – – |
| 255 | 05:44:44.64 | +09:23:18.6 | 15.21 | 14.18 | 12.99 | 11.365 0.023 | 10.601 0.026 | 10.139 0.027 | 9.365 0.001 | 8.921 0.001 | 8.603 0.003 | 7.972 0.001 | 5.241 0.005 |
| 256 | 05:44:46.58 | +09:11:21.6 | 16.8 | 15.65 | 14.32 | 12.924 0.024 | 12.212 0.022 | 11.953 0.026 | 11.535 0.002 | 11.183 0.002 | 10.824 0.006 | 10.009 0.005 | 6.558 0.022 |
| 257 | 05:44:47.00 | +09:17:51.9 | 14.9 | 14.08 | 13.26 | 12.206 0.023 | 11.526 0.022 | 11.377 0.025 | 11.235 0.002 | 11.228 0.003 | 11.213 0.01 | 11.246 0.03 | – – |
| 258 | 05:44:52.81 | +09:13:05.3 | 14.6 | 13.76 | 13.0 | 11.754 0.021 | 11.066 0.024 | 10.833 0.025 | 10.267 0.002 | 10.067 0.002 | 9.936 0.004 | 9.885 0.005 | 5.216 0.007 |
| 259 | 05:45:04.10 | +09:04:52.6 | 17.04 | 15.69 | 14.31 | 12.333 0.024 | 11.458 0.022 | 11.13 0.02 | 10.472 0.002 | 9.961 0.002 | 9.481 0.003 | 8.093 0.002 | 3.889 0.002 |
| 260 | 05:45:21.54 | +09:05:45.7 | 16.68 | 15.38 | 13.88 | 12.149 0.022 | 11.316 0.023 | 11.052 0.023 | 10.832 0.002 | 10.802 0.002 | 10.77 0.008 | 10.728 0.009 | – – |
| 261 | 05:45:53.28 | +09:13:01.8 | 14.02 | 13.15 | 12.24 | 11.129 0.021 | 10.437 0.022 | 10.264 0.02 | 10.134 0.002 | 10.182 0.002 | 10.083 0.004 | 10.122 0.004 | – – |
| DIL82 | 05:44:08.70 | +09:19:10.0 | – | – | – | 13.258 0.027 | 12.996 0.023 | 12.939 0.033 | 12.822 0.0040 | 12.83 0.0060 | 12.93 0.024 | 12.857 0.04 | – – |
| DIL85 | 05:44:21.50 | +09:10:04.0 | – | – | – | 14.373 0.029 | 14.028 0.038 | 13.968 0.054 | 13.883 0.0090 | 13.906 0.014 | 13.948 0.072 | 13.876 0.177 | – – |
| DIL86 | 05:44:41.32 | +08:56:59.0 | – | – | – | 11.575 0.023 | 10.976 0.021 | 10.82 0.023 | 10.716 0.0020 | 10.783 0.0030 | 10.71 0.0060 | 10.698 0.0080 | – – |
| DIL88 | 05:45:50.99 | +10:02:28.0 | – | – | – | 11.559 0.024 | 10.786 0.024 | 10.424 0.02 | 9.99 0.0020 | 9.61 0.0020 | 9.141 0.0030 | 7.931 0.0020 | – – |

[1] Out of IRAC FOV.

[2] Magnitudes from Dolan & Mathieu (1999).

[3] 2MASS magnitudes.

**Table 2.13**: Disk properties of the previously known members of Barnard 35.

| Dolan/DIL ID | Mass ($M_\odot$)[1] | Teff (K)[1] | IRAC class[2] | SED slope | Disk Type[3] | $W_\lambda$(H$\alpha$) (Å)[4] | $W_\lambda$(Li) (Å)[4] |
|---|---|---|---|---|---|---|---|
| 217 | 0.72 | 4000 | – | – | - | 3.35 | 0.53 |
| 222 | 0.23 | 3400 | – | – | - | 19.37 | 0.54 |
| 225 | 0.63 | 3900 | – | – | - | 7.82 | 0.60 |
| 227 | 0.72 | 4000 | – | – | - | 52.56 | 0.31 |
| 228 | 0.72 | 4000 | – | – | - | 0.41 | 0.50 |
| 231 | 0.72 | 4000 | II | -1.109 | Thick | 49.93 | 0.49 |
| 232 | 0.47 | 3750 | III | -2.755 | Diskless | 3.07 | 0.60 |
| 233 | 0.47 | 3750 | III | -2.855 | Diskless | 4.83 | 0.66 |
| 234 | 0.72 | 4000 | II | -1.45 | Thick | 4.1 | 0.52 |
| 235 | 0.72 | 4000 | III | -2.789 | Diskless | 2.54 | 0.58 |
| 236 | 0.28 | 3500 | III | -2.73 | Diskless | 5.27 | 0.63 |
| 237 | 0.63 | 3900 | III | -2.789 | Diskless | 2.84 | 0.64 |
| 238 | 0.23 | 3400 | III | -2.286 | Transition | 26.71 | 0.62 |
| 239 | 0.47 | 3750 | III | -2.818 | Diskless | 4.64 | 0.67 |
| 240 | 0.72 | 4000 | III | -2.312 | Transition | 86.96 | 0.54 |
| 241 | 0.63 | 3900 | II | -1.205 | Thick | 27.8 | 0.45 |
| 242 | 1.62 | 5600 | III | -2.828 | Diskless | -0.35 | 0.49 |
| 243 | 0.47 | 3750 | III | -2.54 | Transition | 19.47 | 0.63 |
| 244 | 0.72 | 4000 | II | -1.23 | Thick | 96.46 | 0.44 |
| 245 | 0.63 | 3900 | III | -2.278 | Transition | 5.45 | 0.66 |
| 246 | 0.63 | 3900 | II | -1.057 | Thick | 25.88 | 0.68 |
| 247 | 0.28 | 3500 | II | -1.242 | Thick | 13.73 | 0.62 |
| 248 | 1.10 | 4600 | II | -1.718 | Thick | 3.27 | 0.41 |
| 249 | 0.72 | 4000 | II | -1.351 | Thick | 12.08 | 0.54 |
| 250 | 0.88 | 4200 | III | -2.761 | Diskless | 22.97 | 0.74 |
| 251 | 0.28 | 3500 | III | -2.752 | Diskless | 5.29 | 0.60 |
| 252 | 0.28 | 3500 | II | -1.358 | Thick | 33.09 | 0.50 |
| 254 | 1.57 | 5500 | III | -2.81 | Diskless | -1.57 | 0.24 |
| 255 | 0.19 | 3300 | II | -1.272 | Thick | 21.24 | 0.60 |
| 256 | 0.72 | 4000 | II | -1.103 | Thick | 32.16 | 0.52 |
| 257 | 1.52 | 5400 | III | -2.848 | Diskless | 1.56 | 0.49 |
| 258 | 0.28 | 3500 | III | -2.408 | Transition | -0.22 | 0.41 |
| 259 | 0.35 | 3600 | I/II | -0.149 | Thick | 4.79 | 0.66 |
| 260 | 0.43 | 3700 | III | -2.719 | Diskless | 4.35 | 0.75 |
| 261 | 0.72 | 4000 | III | -2.793 | Diskless | 1.13 | 0.41 |
| DIL82 | 1.84 | 6000 | III | -2.903 | Diskless | – | - |
| DIL85 | 2.30 | 7000 | III | -2.832 | Diskless | – | - |
| DIL86 | 1.18 | 4800 | III | -2.791 | Diskless | – | - |
| DIL88 | – | 2700 | I/II | -1.08 | Thick | – | - |

[1]Effective temperatures are derived from the SED fitting. Masses are estimated based on Teff and a 3 Myr Siess et al. isochrone.

[2]IRAC Class based on the IRAC [3.6]-[4.5] vs. [5.8]-[8.0] color-color diagram (Allen et al. 2004 criteria) and in the SED of each object.

[3]Disk type based on the IRAC slope and SED shape

[4]$W_\lambda$(H$\alpha$) and $W_\lambda$(Li) from Dolan & Mathieu (1999)

**Table 2.14**: Photometry for the new candidate members of Barnard 35 from the Spitzer Survey.

| ID | RA(J2000), DEC(J2000) | R eR | I eI | J eJ | H eH | Ks eKs | [3.6] e[3.6] | [4.5] e[4.5] | [5.8] e[5.8] | [8.0] e[8.0] | [24] e[24] |
|---|---|---|---|---|---|---|---|---|---|---|---|
| 10543 | 05:44:52.79 +09:03:32.0 | 19.459 0.157 | 17.301 0.054 | 14.048 0.036 | 12.393 0.023 | 11.472 0.025 | 10.436 0.002 | 9.923 0.002 | 9.473 0.003 | 8.749 0.002 | 5.821 0.012 |
| 11994 | 05:44:12.78 +09:05:10.5 | 17.398 0.382 | 15.471 0.138 | 13.259 0.027 | 12.594 0.023 | 12.239 0.026 | 11.206 0.002 | 11.102 0.003 | 10.69 0.006 | 10.066 0.004 | 7.324 0.032 |
| 12156 | 05:44:19.36 +09:05:23.3 | 15.366 0.095 | 14.051 0.048 | 12.678 0.024 | 11.933 0.031 | 11.682 0.026 | 11.356 0.002 | 11.195 0.003 | 10.955 0.006 | 10.117 0.005 | 6.717 0.02 |
| 12396[2] | 05:45:42.89 +09:05:33.7 | – – | – – | – – | – – | – – | 13.744 0.008 | 12.871 0.007 | 11.706 0.011 | 10.417 0.006 | 6.612 0.018 |
| 12913 | 05:44:28.66 +09:06:18.6 | 18.923 0.098 | 16.67 0.03 | 14.433 0.033 | 13.813 0.039 | 13.464 0.039 | 12.976 0.005 | 12.689 0.005 | 12.438 0.021 | 11.68 0.037 | 7.652 0.114 |
| 13586 | 05:43:53.49 +09:07:11.7 | 16.512 0.168 | 15.022 0.088 | 13.09 0.027 | 12.227 0.025 | 11.708 0.024 | 10.963 0.003 | 10.508 0.003 | 10.307 0.005 | 9.705 0.003 | 7.116 0.023 |
| 14252 | 05:43:44.51 +09:08:01.1 | 18.051 0.037 | 17.086 0.031 | 14.572 0.041 | 12.624 0.022 | 11.089 0.023 | 9.297 0.001 | 8.542 0.001 | 8.037 0.002 | 7.254 0.001 | 4.099 0.002 |
| 14618 | 05:44:30.86 +09:08:26.1 | – – | – – | 18.392 – | 15.7 0.182 | 12.725 0.035 | 10.6 0.003 | 9.831 0.002 | 9.292 0.003 | 9.06 0.005 | 6.124 0.049 |
| 14785 | 05:44:10.03 +09:08:40.7 | 16.835 0.023 | 15.572 0.021 | 13.846 0.026 | 13.116 0.023 | 12.638 0.029 | 11.502 0.002 | 10.992 0.003 | 10.503 0.005 | 9.924 0.004 | 7.837 0.066 |
| 14804[2] | 05:44:38.39 +09:08:41.8 | – – | – – | 17.257 0.26 | 14.1 0.067 | 12.367 0.023 | 10.602 0.002 | 10.071 0.002 | 9.637 0.004 | 9.15 0.005 | 6.265 0.022 |
| 14943[2] | 05:44:29.28 +09:08:52.8 | – – | – – | – – | – – | – – | 12.313 0.016 | 10.46 0.015 | 9.158 0.007 | 7.783 0.002 | – – |
| 15004[2] | 05:44:30.00 +09:08:56.8 | – – | – – | 18.441[1] – | 15.913 0.214 | 12.4 0.034 | 9.15 0.003 | 8.014 0.003 | 7.033 0.003 | 6.219 0.001 | – – |
| 15017[2] | 05:44:31.64 +09:08:57.9 | – – | – – | 16.521 0.149 | 14.724 0.06 | 13.624 0.051 | 12.515 0.012 | 12.032 0.017 | 11.503 0.03 | 11.068 0.041 | – – |
| 16286 | 05:43:39.59 +09:10:40.9 | 16.386 0.028 | 14.984 0.01 | 13.336 0.033 | 12.656 0.034 | 12.351 0.034 | 11.79 0.003 | 11.448 0.004 | 11.102 0.009 | 10.25 0.005 | 8.002 0.064 |
| 16567 | 05:44:36.62 +09:11:01.1 | – – | – – | 18.196[1] – | 16.237[1] – | 14.596 0.103 | 12.517 0.004 | 11.488 0.004 | 10.711 0.006 | 9.894 0.009 | 5.776 0.013 |
| 17409 | 05:45:07.53 +09:12:10.7 | 16.564 0.303 | 14.929 0.114 | 13.004 0.024 | 12.297 0.022 | 11.924 0.025 | 11.128 0.002 | 10.579 0.002 | 10.122 0.004 | 9.426 0.003 | 7.381 0.045 |
| 17517 | 05:43:50.67 +09:12:25.1 | 16.342 0.391 | 14.801 0.167 | 13.33 0.024 | 12.37 0.022 | 11.821 0.024 | 11.077 0.002 | 10.787 0.002 | 10.667 0.006 | 9.976 0.004 | 6.566 0.015 |
| 17523 | 05:44:30.23 +09:12:23.8 | 18.333 0.056 | 16.338 0.02 | 14.134 0.029 | 13.364 0.033 | 12.914 0.039 | 12.178 0.004 | 11.784 0.004 | 11.44 0.013 | 10.732 0.033 | 6.245 0.083 |
| 17593 | 05:45:05.70 +09:12:28.1 | 18.665 0.075 | 16.257 0.018 | 13.668 0.027 | 13.06 0.022 | 12.674 0.034 | 11.977 0.003 | 11.627 0.003 | 11.247 0.008 | 10.418 0.006 | 7.721 0.064 |
| 18430 | 05:43:51.36 +09:13:40.5 | 19.477 0.152 | 17.208 0.047 | 14.623 0.043 | 13.978 0.035 | 13.736 0.045 | 12.986 0.005 | 12.59 0.005 | 12.164 0.015 | 11.426 0.012 | 8.902 0.138 |
| 20180 | 05:43:52.47 +09:15:59.8 | 17.688 0.062 | 15.806 0.018 | 13.986 0.033 | 13.388 0.035 | 13.008 0.03 | 12.433 0.003 | 12.127 0.004 | 11.837 0.012 | 11.182 0.012 | 8.799 0.13 |
| 20434 | 05:44:19.40 +09:16:19.3 | 16.136 0.231 | 14.664 0.097 | 13.123 0.026 | 12.389 0.023 | 12.032 0.027 | 11.078 0.002 | 10.712 0.002 | 10.319 0.004 | 9.451 0.003 | 6.483 0.015 |
| 20473 | 05:43:56.99 +09:16:23.9 | 15.385 0.092 | 13.955 0.044 | 12.336 0.027 | 11.572 0.022 | 11.173 0.024 | 10.683 0.002 | 10.414 0.002 | 10.285 0.005 | 9.709 0.003 | 6.888 0.023 |
| 23145 | 05:44:16.14 +09:20:00.0 | 16.024 0.19 | 14.463 0.077 | 12.801 0.027 | 12.075 0.025 | 11.757 0.026 | 11.378 0.002 | 11.19 0.003 | 11.1 0.007 | 10.82 0.007 | 7.272 0.028 |
| 23414 | 05:44:52.80 +09:20:18.3 | 13.781 0.005 | 12.713 0.007 | 10.947 0.023 | 10.015 0.024 | 9.698 0.023 | 9.535 0.002 | 9.601 0.002 | 9.532 0.004 | 9.546 0.01 | 7.319 0.101 |
| 24086 | 05:45:10.55 +09:21:09.5 | 19.664 0.147 | 18.13 0.051 | 14.727 0.053 | 14.079 0.074 | 13.694 0.067 | 12.635 0.004 | 12.325 0.005 | 12.073 0.017 | 11.418 0.018 | – – |
| 27556 | 05:44:38.12 +09:25:57.9 | 17.503 0.039 | 15.835 0.014 | 14.078 0.027 | 13.362 0.025 | 13.138 0.034 | 12.632 0.004 | 12.418 0.005 | 12.226 0.016 | 11.781 0.017 | 8.682 0.116 |
| 37817 | 05:43:50.60 +09:40:42.3 | 17.739 0.034 | 16.017 0.015 | 14.08 0.024 | 13.257 0.03 | 12.788 0.026 | 12.102 0.003 | 11.807 0.004 | 11.581 0.01 | 11.16 0.011 | 8.522 0.094 |
| 45299 | 05:43:44.15 +09:50:39.1 | 16.979 0.25 | 15.382 0.118 | 13.358 0.052 | 12.603 0.057 | 12.286 0.044 | 12.033 0.005 | 11.707 0.004 | 11.372 0.01 | 10.935 0.012 | 8.756 0.119 |
| 45860 | 05:44:30.16 +09:51:18.0 | 17.227 0.029 | 15.568 0.018 | 13.788 0.026 | 13.114 0.032 | 12.794 0.027 | 12.227 0.003 | 11.842 0.003 | 11.446 0.009 | 10.698 0.006 | 7.939 0.055 |
| 46311 | 05:44:18.65 +09:51:51.9 | 16.859 0.013 | 15.124 0.0070 | 13.266 0.038 | 12.55 0.042 | 12.213 0.03 | 11.571 0.003 | 11.365 0.004 | 11.129 0.008 | 10.591 0.006 | 8.021 0.06 |
| 47084[2] | 05:43:44.93 +09:52:52.4 | 17.05 0.035 | 15.57 0.029 | 13.978 0.033 | 13.333 0.037 | 12.994 0.038 | 12.292 0.007 | 12.128 0.008 | 11.942 0.015 | 11.286 0.013 | 8.448 0.101 |

[1]Upper limmits

[2]Out of the optical WFC Survey. In the case of 47084 the optical magnitudes were taken from Dolan & Mathieu (2002).

**Table 2.15**: Disk properties of the new candidate members of Barnard 35 selected from the Spitzer survey (i.e. they must have IR excess).

| ID | RA(J2000), DEC(J2000) | Phot. Mem.[1] | Final Mem.[2] | Mass ($M_{\odot}$)[3] | Teff (K)[3] | YSO Class | SED slope | Disk Type |
|---|---|---|---|---|---|---|---|---|
| 10543 | 05:44:52.79 +09:03:32.0 | Y Y Y | Y | 0.006 | 1600 | II | -0.921 | Thick |
| 11994 | 05:44:12.78 +09:05:10.5 | Y Y Y | Y | 0.06 | 2900 | II | -1.483 | Thick |
| 12156 | 05:44:19.36 +09:05:23.3 | Y Y Y | Y | 0.90 | 3800 | II | -1.427 | Thick |
| 12396 | 05:45:42.89 +09:05:33.7 | R - Y | Y? | | – | I | 1.035 | Thick |
| 12913 | 05:44:28.66 +09:06:18.6 | Y Y Y | Y | 0.08 | 3000 | II | -1.377 | Thick |
| 13586 | 05:43:53.49 +09:07:11.7 | Y Y Y | Y | 1.05 | 3900 | II | -1.454 | Thick |
| 14252 | 05:43:44.51 +09:08:01.1 | R Y Y | Y? | | – | I | -0.545 | Thick |
| 14618 | 05:44:30.86 +09:08:26.1 | Y T T | Y | 0.004 | 1200 | II | -1.093 | Thick |
| 14785 | 05:44:10.03 +09:08:40.7 | Y Y Y | Y | 1.05 | 3900 | II | -1.031 | Thick |
| 14804 | 05:44:38.39 +09:08:41.8 | Y Y Y | Y | 0.005 | 1400 | II | -1.188 | Thick |
| 14943 | 05:44:29.28 +09:08:52.8 | R - Y | Y? | | – | I | 2.274 | Thick |
| 15004 | 05:44:30.00 +09:08:56.8 | R Y Y | Y? | | – | I | 0.514 | Thick |
| 15017 | 05:44:31.64 +09:08:57.9 | Y - - | Y | | – | II | -1.162 | Thick |
| 16286 | 05:43:39.59 +09:10:40.9 | Y Y Y | Y | 0.27 | 3300 | II | -1.09 | Thick |
| 16567 | 05:44:36.62 +09:11:01.1 | R Y Y | Y? | | – | I | 0.133 | Thick |
| 17409 | 05:45:07.53 +09:12:10.7 | Y Y Y | Y | 0.14 | 3100 | II | -0.908 | Thick |
| 17517 | 05:43:50.67 +09:12:25.1 | Y Y Y | Y | 0.90 | 3800 | II | -1.628 | Thick |
| 17523 | 05:44:30.23 +09:12:23.8 | Y Y Y | Y | 0.46 | 3500 | II | -1.201 | Thick |
| 17593 | 05:45:05.70 +09:12:28.1 | Y Y Y | Y | 0.02 | 2700 | II | -1.061 | Thick |
| 18430 | 05:43:51.36 +09:13:40.5 | Y Y Y | Y | 0.08 | 3000 | II | -1.053 | Thick |
| 20180 | 05:43:52.47 +09:15:59.8 | Y Y Y | Y | 0.27 | 3300 | II | -1.419 | Thick |
| 20434 | 05:44:19.40 +09:16:19.3 | Y Y Y | Y | 0.46 | 3500 | II | -0.984 | Thick |
| 20473 | 05:43:56.99 +09:16:23.9 | Y Y Y | Y | 0.46 | 3500 | II | -1.763 | Thick |
| 23145 | 05:44:16.14 +09:20:00.0 | Y T T | Y | 0.90 | 3800 | III | -2.223 | Transition |
| 23414 | 05:44:52.80 +09:20:18.3 | F F T | Y | 0.75 | 3700 | III | -2.824 | Transition |
| 24086 | 05:45:10.55 +09:21:09.5 | Y - - | Y? | 0.06 | 2900 | II | -1.467 | Thick |
| 27556 | 05:44:38.12 +09:25:57.9 | Y Y Y | Y | 0.21 | 3200 | II | -1.775 | Thick |
| 37817 | 05:43:50.60 +09:40:42.3 | Y Y Y | Y | 0.08 | 3000 | II | -1.776 | Thick |
| 45299 | 05:43:44.15 +09:50:39.1 | Y Y Y | Y | 0.27 | 3300 | II | -1.579 | Thick |
| 45860 | 05:44:30.16 +09:51:18.0 | Y Y Y | Y | 0.14 | 3100 | II | -1.094 | Thick |
| 46311 | 05:44:18.65 +09:51:51.9 | Y Y Y | Y | 0.14 | 3100 | II | -1.72 | Thick |
| 47084 | 05:43:44.93 +09:52:52.4 | Y Y Y | Y | 1.05 | 3900 | II | -1.699 | Thick |

[1]Membership is [3.6] vs. [3.6]-[8.0], H-Ks vs. Ks-[24], [3.6]-[8.0] vs. [8.0]-[24]. Y: member, R: Very red object in comparison with the theoretical isochrone, Y?: probable member, F: field object; -: Not enough data

[2]Final Membership

[3]The effective temperature is derived from the SED fittings in Figure 3.14 and 3.15. Mass is estimated based on the temperature and a 3 Myr isochrone from Baraffe et al. (1998).For the three objects with the lowest temperatures, the DUSTY models from Chabrier et al. (2000) are used.

**Table 2.16**: Photometry for the DM and DIL members of Barnard 30.

| Dolan/DIL ID | RA (J2000) DEC (J2000) | V[1] | R[1] | I[1] | J[2] error | H[2] error | Ks[3] error | [3.6] error | [4.5] error | [5.8] error | [8.0] error | [24] error |
|---|---|---|---|---|---|---|---|---|---|---|---|---|
| DM90[4] | 05:28:18.00 +11:56:50.6 | 15.382 | 14.232 | 13.05 | 11.651 0.035 | 10.815 0.051 | 10.054 0.033 | – – | – – | – – | – – | 4.55 0.006 |
| DM99[4] | 05:29:26.70 +11:51:44.8 | 15.935 | 14.811 | 13.429 | 11.831 0.023 | 11.055 0.03 | 10.752 0.022 | – – | – – | – – | – – | 5.463 0.011 |
| DM100[4] | 05:29:34.21 +12:56:21.6 | 14.9 | 13.78 | 12.757 | 11.262 0.022 | 10.333 0.021 | 9.895 0.018 | – – | – – | – – | – – | 4.409 0.003 |
| DM106[4] | 05:29:52.77 +12:09:47.5 | 16.125 | 14.934 | 13.541 | 11.918 0.022 | 11.021 0.024 | 10.585 0.021 | – – | – – | – – | – – | 4.577 0.003 |
| DM107[4] | 05:29:57.66 +12:12:07.1 | 14.999 | 13.996 | 13.013 | 11.892 0.02 | 11.034 0.019 | 10.659 0.018 | – – | – – | – – | – – | 6.526 0.016 |
| DM109[4] | 05:30:00.63 +12:13:44.4 | 17.918 | 16.503 | 14.975 | 12.77 0.022 | 11.793 0.021 | 11.11 0.02 | – – | – – | – – | – – | 5.745 0.016 |
| DM110[4] | 05:30:01.89 +12:13:10.0 | 12.737 | 12.024 | 11.398 | 10.637 0.02 | 9.908 0.021 | 9.578 0.018 | – – | – – | – – | – – | 4.876 0.006 |
| DM111[4] | 05:30:02.03 +12:13:35.8 | 13.133 | 12.43 | 11.787 | 10.667 0.023 | 9.721 0.023 | 9.019 0.02 | – – | – – | – – | – – | 3.226 0.002 |
| DM113 | 05:30:03.82 +12:01:21.8 | 15.236 | 14.223 | 13.252 | 11.694 0.022 | 10.89 0.021 | 10.463 0.019 | 9.759 0.002 | 9.35 0.002 | 8.896 0.004 | 8.151 0.002 | 5.418 0.006 |
| DM114 | 05:30:05.65 +12:09:37.2 | 16.863 | 15.539 | 13.937 | 12.273 0.022 | 11.552 0.023 | 11.192 0.02 | 10.843 0.003 | – – | – – | – – | 6.526 0.017 |
| DM115 | 05:30:13.13 +12:08:45.8 | 13.836 | 13.055 | 12.282 | 10.954 0.022 | 10.12 0.023 | 9.557 0.018 | 8.459 0.001 | 7.951 0.001 | 7.251 0.002 | 6.273 0.001 | 3.586 0.001 |
| DM118 | 05:30:17.04 +12:15:41.0 | 16.0 | 14.969 | 13.901 | 12.665 0.024 | 11.921 0.026 | 11.702 0.023 | 11.545 0.003 | 11.584 0.004 | 11.482 0.011 | 11.484 0.017 | – – |
| DM120 | 05:30:29.09 +12:33:56.5 | 16.834 | 15.821 | 14.746 | 13.161 0.023 | 12.412 0.023 | 12.005 0.022 | 11.694 0.002 | 11.303 0.003 | 11.269 0.009 | 10.652 0.008 | 7.104 0.028 |
| DM121 | 05:30:36.08 +12:06:40.6 | 17.18 | 16.0 | 14.71 | 12.91 0.025 | 12.119 0.021 | 11.634 0.018 | 10.602 0.002 | 10.222 0.002 | 10.198 0.004 | 9.997 0.005 | 6.825 0.026 |
| DM123 | 05:30:36.19 +12:36:52.5 | 15.174 | 14.201 | 13.243 | 11.598 0.03 | 10.728 0.029 | 10.163 0.026 | 9.635 0.002 | 9.295 0.003 | 8.988 0.003 | 8.1 0.002 | 4.651 0.004 |
| DM125 | 05:30:51.70 +12:08:36.7 | 14.607 | 13.731 | 12.911 | 11.64 0.023 | 10.867 0.026 | 10.452 0.018 | 9.924 0.002 | 9.62 0.002 | 9.3 0.003 | 8.327 0.003 | 5.749 0.023 |
| DM126 | 05:30:53.97 +12:43:31.6 | 16.848 | 15.77 | 14.713 | 13.159 0.022 | 12.378 0.021 | 12.156 0.022 | 11.989 0.003 | 11.998 0.004 | 11.966 0.013 | 11.972 0.023 | – – |
| DM127 | 05:30:56.91 +11:56:46.9 | 15.092 | 14.046 | 12.923 | 11.607 0.026 | 10.846 0.022 | 10.614 0.02 | 10.384 0.002 | 10.326 0.002 | 10.31 0.004 | 10.317 0.006 | – – |
| DM129 | 05:30:57.86 +11:47:21.4 | 13.41 | 12.729 | 12.043 | 11.056 0.026 | 10.413 0.022 | 10.277 0.021 | 10.17 0.002 | 10.143 0.002 | 10.136 0.004 | 10.076 0.007 | – – |
| DM131 | 05:31:01.01 +12:04:14.3 | 16.534 | 15.372 | 14.086 | 12.752 0.022 | 12.007 0.021 | 11.797 0.021 | 11.615 0.005 | 11.54 0.005 | 11.542 0.016 | 11.578 0.074 | – – |
| DM134[4] | 05:31:07.81 +11:25:26.3 | 16.03 | 14.88 | 13.545 | 12.533 0.042 | 11.817 0.047 | 11.573 0.045 | – – | – – | – – | – – | 6.085 0.01 |
| DM135 | 05:31:08.03 +12:06:06.4 | 15.881 | 14.789 | 13.585 | 12.212 0.022 | 11.469 0.023 | 11.239 0.022 | 10.554 0.002 | 10.271 0.003 | 10.023 0.004 | 9.635 0.005 | 6.7 0.036 |
| DM136 | 05:31:15.51 +12:11:23.7 | 16.364 | 15.145 | 13.863 | 12.097 0.022 | 11.21 0.026 | 10.718 0.018 | 9.988 0.002 | 9.646 0.003 | 9.318 0.003 | 8.769 0.005 | 5.98 0.021 |
| DM138[4] | 05:31:16.15 +11:25:31.3 | 15.308 | 14.372 | 13.41 | 11.744 0.022 | 10.906 0.023 | 10.327 0.025 | – – | – – | – – | – – | 4.453 0.003 |
| DM142 | 05:31:21.65 +12:05:47.8 | 13.76 | 12.809 | 11.842 | 10.946 0.045 | 10.24 0.049 | 10.037 0.049 | 9.754 0.002 | 9.775 0.004 | 9.645 0.005 | – – | – – |
| DM143 | 05:31:23.59 +12:09:43.9 | 12.827 | 12.087 | 11.408 | 10.422 0.02 | 9.623 0.021 | 9.192 0.017 | 8.216 0.001 | 7.732 0.001 | 6.956 0.002 | 6.085 0.002 | 2.73 0.004 |
| DM147 | 05:31:34.59 +11:49:29.8 | 15.025 | 14.045 | 13.007 | 11.684 0.026 | 10.986 0.024 | 10.751 0.022 | 10.659 0.002 | 10.634 0.002 | 10.585 0.005 | 10.555 0.007 | – – |
| DM149 | 05:31:37.61 +11:58:18.3 | 14.644 | 13.938 | 13.239 | 12.192 0.02 | 11.599 0.021 | 11.449 0.019 | 11.359 0.002 | 11.391 0.003 | 11.354 0.008 | 11.321 0.015 | – – |
| DM150 | 05:31:38.60 +11:48:26.4 | 16.082 | 15.013 | 13.883 | 12.61 0.028 | 11.889 0.026 | 11.678 0.027 | 11.477 0.002 | 11.483 0.003 | 11.461 0.009 | 11.498 0.014 | – – |
| DM151 | 05:31:39.93 +11:50:49.6 | 16.369 | 15.497 | 14.356 | 13.154 0.031 | 12.507 0.029 | 12.25 0.034 | 11.96 0.003 | 11.928 0.004 | 11.546 0.009 | 11.087 0.008 | 7.324 0.034 |
| DM152 | 05:31:40.48 +12:10:46.9 | 15.103 | 14.049 | 12.972 | 11.311 0.022 | 10.454 0.023 | 10.184 0.019 | 9.847 0.001 | 9.562 0.002 | 9.052 0.003 | 7.914 0.002 | 5.01 0.005 |
| DM153 | 05:31:43.40 +12:30:22.1 | 13.454 | 12.787 | 12.149 | 11.14 0.022 | 10.532 0.021 | 10.243 0.018 | 10.128 0.002 | 9.818 0.002 | 9.385 0.004 | 8.477 0.004 | 5.641 0.043 |
| DM154 | 05:31:45.43 +11:37:59.3 | 17.272 | 15.914 | 14.229 | 12.981 0.044 | 12.343 0.046 | 12.057 0.049 | 11.694 0.004 | 11.677 0.005 | 11.513 0.016 | – – | – – |
| DM157 | 05:31:47.54 +11:14:51.0 | 17.197 | 15.816 | 14.074 | – – | – – | – – | – – | – – | – – | – – | 7.563 0.043 |
| DM158 | 05:31:47.79 +12:18:08.3 | 13.017 | 12.285 | 11.61 | 10.616 0.022 | 10.002 0.024 | 9.812 0.021 | 9.323 0.003 | 8.989 0.003 | 8.602 0.003 | 7.808 0.008 | 5.209 0.009 |
| DM160 | 05:31:49.15 +12:32:00.8 | 14.548 | 13.524 | 12.465 | 10.991 0.033 | 9.992 0.034 | 9.564 0.032 | 8.376[3] 0.004 | 7.997[3] 0.004 | 7.812[3] 0.012 | 7.163[3] 0.006 | 4.098 0.011 |
| DM161 | 05:31:58.49 +12:22:47.4 | 15.932 | 14.769 | 13.353 | 11.833 0.02 | 11.118 0.024 | 10.85 0.018 | 10.671 0.002 | 10.591 0.002 | 10.641 0.006 | 10.692 0.019 | – – |
| DM164 | 05:31:59.94 +12:08:06.8 | 16.136 | 15.047 | 13.793 | 12.499 0.021 | 11.748 0.021 | 11.525 0.022 | 11.352 0.002 | 11.325 0.003 | 11.304 0.007 | 11.3 0.012 | – – |
| DM165[5] | 05:32:06.41 +12:29:22.2 | 15.228 | 14.227 | 13.166 | 12.02 0.022 | 11.198 0.019 | 10.86 0.019 | 10.29 0.002 | 10.045 0.002 | 9.725 0.005 | 9.128 0.009 | – – |
| DM166 | 05:32:06.51 +12:24:04.5 | 14.793 | 14.003 | 13.331 | 11.931 0.02 | 11.182 0.021 | 10.767 0.019 | 10.252 0.002 | 9.949 0.002 | 9.654 0.003 | 9.108 0.004 | 4.946 0.007 |
| DM168 | 05:32:07.26 +11:54:04.2 | 16.203 | 15.152 | 13.957 | 12.729 0.023 | 11.969 0.024 | 11.754 0.022 | 11.592 0.003 | 11.56 0.003 | 11.506 0.009 | 11.497 0.015 | 6.912 0.021 |
| DM169 | 05:32:07.97 +12:07:14.6 | 13.628 | 12.808 | 12.034 | 10.966 0.021 | 10.33 0.023 | 10.125 0.02 | 9.911 0.001 | 9.912 0.002 | 9.824 0.004 | 9.778 0.004 | 9.431 0.212 |
| DM172 | 05:32:15.46 +12:09:34.3 | 16.375 | 15.399 | 14.172 | 12.7 0.022 | 11.977 0.024 | 11.577 0.023 | 10.561 0.002 | 10.182 0.002 | 9.774 0.004 | 8.883 0.002 | 6.382 0.014 |
| DM173[5] | 05:32:18.11 +12:43:56.3 | 15.317 | 14.24 | 13.169 | 11.822 0.022 | 11.005 0.024 | 10.649 0.02 | 9.819 0.001 | 9.522 0.002 | 9.23 0.003 | 8.694 0.002 | – – |
| DM174[5] | 05:32:25.63 +12:36:35.4 | 14.751 | 13.879 | 13.062 | 11.64 0.022 | 10.827 0.023 | 10.424 0.017 | 9.628 0.001 | 9.34 0.002 | 9.18 0.003 | 8.372 0.003 | – – |
| DM175 | 05:32:26.24 +11:54:24.3 | 15.942 | 14.782 | 13.38 | 11.966 0.021 | 11.243 0.046 | 11.043 0.031 | 10.778 0.002 | 10.765 0.003 | 10.659 0.006 | 10.528 0.007 | – – |

Continued on next page…

Table 2.16 – Continued

| Dolan/DIL ID | RA (J2000) DEC (J2000) | V | R | I | J error | H error | Ks error | [3.6] error | [4.5] error | [5.8] error | [8.0] error | [24] error |
|---|---|---|---|---|---|---|---|---|---|---|---|---|
| DM176[5] | 05:32:27.31 +12:37:54.5 | 13.277 | 12.68 | 12.097 | 11.234 0.022 | 10.63 0.021 | 10.478 0.018 | 10.386 0.002 | 10.379 0.002 | 10.351 0.005 | 10.322 0.008 | – – |
| DM177[5] | 05:32:29.38 +12:01:23.6 | 16.15 | 15.025 | 13.634 | 12.183 0.021 | 11.472 0.021 | 11.26 0.02 | 11.01 0.002 | 10.9 0.003 | 10.924 0.007 | 10.973 0.009 | – – |
| DIL12[4] | 05:29:24.02 +11:51:56.5 | – | – | – | – – | – – | – – | – – | – – | – – | – – | 3.577 0.002 |
| DIL18[4] | 05:30:04.66 +12:13:08.5 | – | – | – | – – | – – | – – | – – | – – | – – | – – | 6.016 0.014 |
| DIL23 | 05:30:42.86 +11:38:18.8 | 14.235 | 13.723 | 13.27 | 12.583 0.024 | 12.117 0.022 | 12.047 0.023 | 12.003 0.004 | 11.983 0.005 | 11.935 0.016 | 12.035 0.029 | – – |
| DIL27 | 05:31:24.75 +12:12:08.7 | 15.576 | 14.4 | 13.204 | 12.049 0.031 | 11.102 0.024 | 10.566 0.018 | 9.538 0.004 | 9.076 0.004 | – – | – – | 4.678 0.007 |
| DIL28[4] | 05:31:26.73 +11:01:22.6 | – | – | – | – – | – – | – – | – – | – – | – – | – – | 7.491 0.038 |
| DIL29 | 05:31:28.19 +12:09:10.5 | 11.544 | 11.106 | 10.638 | 9.408 0.02 | 8.311 0.023 | 7.341 0.031 | 6.317[3] 0.002 | 5.619[3] 0.002 | 4.883[3] 0.003 | 3.652[3] 0.001 | 0.79 0.001 |
| DIL37[5] | 05:32:17.69 +12:23:58.9 | 17.035 | 15.747 | 14.301 | 12.56 0.023 | 11.831 0.027 | 11.428 0.024 | 10.437 0.002 | 10.106 0.002 | 9.735 0.004 | 9.174 0.005 | – – |
| DIL38[5] | 05:32:19.10 +12:24:23.8 | 14.33 | 13.359 | 12.323 | 10.928 0.023 | 10.1 0.026 | 9.656 0.019 | 8.987 0.002 | 8.444 0.002 | 8.071 0.002 | 7.174 0.001 | – – |
| DIL39[5] | 05:32:22.16 +12:18:02.3 | – | – | – | 11.493 0.02 | 10.902 0.023 | 10.642 0.02 | 10.385 0.002 | 10.284 0.002 | 10.295 0.004 | 10.328 0.005 | – – |
| DIL43[4] | 05:32:25.60 +10:29:43.3 | – | – | – | – – | – – | – – | – – | – – | – – | – – | 7.34 0.042 |
| DIL44[4] | 05:32:32.09 +10:44:16.8 | – | – | – | – – | – – | – – | – – | – – | – – | – – | 6.33 0.013 |
| DIL46[5] | 05:32:36.44 +12:26:20.6 | 14.105 | 13.148 | 12.052 | 10.425 0.022 | 9.694 0.023 | 9.291 0.019 | 8.601 0.001 | 8.129 0.001 | 7.823 0.002 | 7.169 0.001 | – – |

[1]Magnitudes from Dolan & Mathieu (1999, 2001, 2002)
[2]2MASS magnitudes
[3]Photometry from the shallow mosaics
[4]Out of IRAC FOV
[5]Out of MIPS FOV

**Table 2.17**: Disk properties of the previously known members of Barnard 30.

| Dolan/DIL ID | Mass ($M_\odot$)[1] | Teff (K)[6] | IRAC class[1] | SED slope | Disk Type[2] | $W_\lambda$(H$\alpha$) (Å)[3] | $W_\lambda$(Li) (Å)[3] |
|---|---|---|---|---|---|---|---|
| DM90[4] | 0.63 | 3900 | II? | – | – | 36.74 | 0.54 |
| DM99[4] | 0.52 | 3800 | ? | – | – | 22.88 | 0.61 |
| DM100[4] | 0.63 | 3900 | ? | – | – | 95.43 | 0.51 |
| DM106[4] | 0.43 | 3700 | ? | – | – | 31.14 | 0.58 |
| DM107[4] | 0.47 | 3750 | ? | – | – | 2.75 | 0.59 |
| DM109[4] | 0.09 | 3000 | II? | – | – | 114.32 | 0.40 |
| DM110[4] | 0.98 | 4400 | ? | – | – | -0.39 | 0.51 |
| DM111[4] | 0.88 | 4200 | II? | – | – | 33.76 | 0.41 |
| DM113 | 0.72 | 4000 | II | -0.994 | Thick | 23.43 | 0.58 |
| DM114 | 0.35 | 3600 | ? | – | - | 39.03 | 0.60 |
| DM115 | 0.72 | 4000 | I/II | -0.303 | Thick | 22.12 | 0.43 |
| DM118 | 0.72 | 4000 | III | -2.739 | Diskless | 6.09 | 0.54 |
| DM120 | 0.52 | 3800 | II | -1.729 | Thick | 171.14 | 0.24 |
| DM121 | 0.47 | 3750 | II | -2.213 | Thin | 244.76 | 0.65 |
| DM123 | 0.47 | 3750 | II | -1.105 | Thick | 127.58 | 0.28 |
| DM125 | 0.28 | 3500 | II | -1.029 | Thick | 42.62 | 0.58 |
| DM126 | 0.12 | 3100 | III | -2.811 | Diskless | -2.63 | 0.22 |
| DM127 | 0.52 | 3800 | III | -2.768 | Diskless | 7.12 | 0.72 |
| DM129 | 0.72 | 4000 | III | -2.737 | Diskless | 0.22 | 0.46 |
| DM131 | 0.28 | 3500 | III | -2.808 | Diskless | 3.55 | 0.66 |
| DM134[4] | 0.63 | 3900 | ? | – | – | 2.36 | 0.53 |
| DM135 | 0.98 | 4400 | II | -1.794 | Thick | 4.76 | 0.64 |
| DM136 | 0.47 | 3750 | II | -1.449 | Thick | 15.05 | 0.50 |
| DM138[4] | 0.63 | 3900 | II? | – | – | 12.18 | 0.53 |
| DM142 | 0.72 | 4000 | III | -2.654 | Diskless | -0.41 | 0.48 |
| DM143 | 0.28 | 3500 | I/II | -0.34 | Thick | 4.74 | 0.45 |
| DM147 | 0.63 | 3900 | III | -2.714 | Diskless | 2.57 | 0.56 |
| DM149 | 0.63 | 3900 | III | -2.783 | Diskless | -14.2 | 0.20 |
| DM150 | 0.98 | 4400 | III | -2.856 | Diskless | 0.83 | 0.62 |
| DM151 | 1.18 | 4800 | II | -1.777 | Thick | -1.03 | 0.27 |
| DM152 | 0.52 | 3800 | II | -0.604 | Thick | 4.32 | 0.51 |
| DM153 | 0.47 | 3750 | II | -0.94 | Thick | 15.04 | 0.43 |
| DM154 | 0.91 | 4250 | III | -2.565 | Diskless | 5.3 | 0.75 |
| DM157 | 0.47 | 3750 | ? | – | – | 7.88 | 0.63 |
| DM158 | 0.47 | 3750 | II | -1.105 | Thick | 1.05 | 0.50 |
| DM160 | 0.72 | 4000 | II | – | Thick | 7.99 | 0.41 |
| DM161 | 2.06 | 6400 | III | -2.886 | Diskless | 16.62 | 0.61 |
| DM164 | 0.23 | 3400 | III | -2.779 | Diskless | 3.17 | 0.67 |
| DM165[5] | 0.35 | 3600 | II | -1.502 | Thick | 3.49 | 0.67 |
| DM166 | 1.39 | 5200 | II | -1.536 | Thick | 88.7 | 0.43 |
| DM168 | 0.98 | 4400 | III | -2.724 | Transition | 8.25 | 0.59 |
| DM169 | 0.72 | 4000 | III | -2.668 | Diskless | 1.1 | 0.60 |
| DM172 | 0.88 | 4200 | II | -0.925 | Thick | 36.51 | 0.63 |
| DM173[5] | 0.91 | 4250 | II | -1.557 | Thick | 30.27 | 0.57 |
| DM174[5] | 0.91 | 4250 | II | -1.446 | Thick | 36.83 | 0.65 |
| DM175 | 0.88 | 4200 | III | -2.536 | Diskless | 5.06 | 0.77 |
| DM176[5] | 1.31 | 5000 | III | -2.762 | Diskless | 0.44 | 0.47 |
| DM177[5] | 0.72 | 4000 | III | -2.819 | Diskless | 4.15 | 0.62 |
| DIL12[4] | 0.88 | 4200 | ? | – | – | – | - |
| DIL18[4] | 0.88 | 4200 | ? | – | – | – | - |
| DIL23 | 0.72 | 4000 | III | -2.864 | Diskless | – | - |
| DIL27 | 1.71 | 5750 | II | -2.180 | Thick | – | - |
| DIL28[4] | 0.72 | 4000 | ? | – | – | – | - |
| DIL29 | 1.57 | 5500 | I/II | -0.324 | Thick | – | - |
| DIL37[5] | 0.88 | 4200 | II | -1.387 | Thick | – | - |
| DIL38[5] | 1.18 | 4800 | II | -0.807 | Thick | – | - |
| DIL39[5] | 0.23 | 3400 | III | -2.792 | Diskless | – | - |
| DIL43[4] | 0.28 | 3500 | ? | – | – | – | - |
| DIL44[4] | 0.19 | 3300 | ? | – | – | – | - |
| DIL46[5] | 0.47 | 3750 | II | -1.236 | Thick | – | - |

Continued on next page…

Table 2.17 – Continued

| Dolan/DIL ID | Mass ($M_\odot$)[1] | Teff (K)[6] | IRAC class[1] | SED slope | Disk Type[2] | $W_\lambda$(H$\alpha$) (Å)[3] | $W_\lambda$(Li) (Å)[3] |
|---|---|---|---|---|---|---|---|

[1]IRAC Class based on the IRAC [3.6]-[4.5] vs. [5.8]-[8.0] color-color diagram and in the SED of each object.

[2]Disk type based on the IRAC slope and SED shape

[3]$W_\lambda$(H$\alpha$) and $W_\lambda$(Li) from Dolan & Mathieu (1999)

[4]Out of IRAC FOV

[5]Out of MIPS FOV

[6]Effective temperatures are derived from the SED fitting perfomed with VOSA. Masses are estimated based on Teff and a 3 Myr Siess et al. isochrone.

**Table 2.18**: Photometry for the new candidate members of Barnard 30 from the Spitzer Survey.

| ID | RA(J2000), DEC(J2000) | R eR | I eI | J eJ | H eH | Ks eKs | [3.6] e[3.6] | [4.5] e[4.5] | [5.8] e[5.8] | [8.0] e[8.0] | [24] e[24] |
|---|---|---|---|---|---|---|---|---|---|---|---|
| 6876 | 05:30:35.19 +11:45:11.5 | 20.404 0.118 | 19.458 0.138 | – – | – – | – – | 13.897 0.007 | 12.823 0.006 | 11.91 0.012 | 10.935 0.01 | 7.91 0.06 |
| 9196 | 05:31:33.36 +11:48:58.3 | 17.826 0.051 | 15.845 0.03 | 14.185 0.035 | 13.458 0.036 | 13.021 0.04 | 12.268 0.003 | 12.099 0.004 | 11.868 0.012 | 11.4 0.012 | – – |
| 10420 | 05:31:39.96 +11:50:49.5 | 16.744 0.077 | 15.046 0.041 | 13.154 0.031 | 12.507 0.029 | 12.25 0.034 | 11.96 0.003 | 11.928 0.004 | 11.546 0.009 | 11.087 0.008 | 7.32 0.034 |
| 12438 | 05:32:07.27 +11:54:04.1 | 15.43 0.037 | 14.148 0.033 | 12.729 0.023 | 11.969 0.024 | 11.754 0.022 | 11.592 0.003 | 11.56 0.003 | 11.506 0.009 | 11.497 0.015 | 6.91 0.021 |
| 12629[2] | 05:32:25.91 +11:54:24.7 | – – | – – | 14.242 0.047 | 13.547 0.057 | 13.128 0.049 | 12.038 0.005 | 11.739 0.005 | 11.151 0.008 | 10.727 0.007 | 8.44 0.099 |
| 13402[2] | 05:32:19.21 +11:55:36.6 | – – | – – | 15.232 0.082 | 14.319 0.075 | 13.895 0.078 | 13.242 0.005 | 13.001 0.007 | 12.904 0.021 | 12.342 0.036 | – – |
| 16599 | 05:30:03.81 +12:01:21.5 | 14.34 0.031 | 13.299 0.031 | 11.694 0.022 | 10.89 0.021 | 10.463 0.019 | 9.759 0.002 | 9.35 0.002 | 8.896 0.004 | 8.151 0.002 | 5.41 0.006 |
| 17792[2] | 05:30:25.93 +12:03:21.4 | – – | – – | 13.65 0.034 | 13.049 0.035 | 12.785 0.036 | 12.276 0.003 | 12.079 0.004 | 11.836 0.012 | 11.191 0.013 | 8.82 0.123 |
| 18115[2] | 05:30:17.88 +12:03:55.6 | – – | – – | 12.574 0.024 | 11.737 0.027 | 11.261 0.027 | 10.419 0.002 | 9.982 0.002 | 9.597 0.003 | 8.794 0.002 | 5.9 0.008 |
| 19172 | 05:31:27.83 +12:05:30.9 | – – | – – | 16.319[1] – | 14.596 0.08 | 12.763 0.04 | 10.976 0.003 | 9.631 0.003 | 8.492 0.003 | 7.12 0.003 | 1.93 0.002 |
| 19198 | 05:31:29.64 +12:05:32.9 | – – | – – | 15.903 0.079 | 14.548 0.054 | 13.838 0.055 | 12.664 0.008 | 11.493 0.004 | 10.358 0.009 | 8.989 0.012 | 4.17 0.016 |
| 19545 | 05:31:08.03 +12:06:06.3 | 15.285 0.037 | 13.97 0.033 | 12.212 0.022 | 11.469 0.023 | 11.239 0.022 | 10.554 0.002 | 10.271 0.003 | 10.023 0.004 | 9.635 0.005 | 6.7 0.036 |
| 19617 | 05:31:23.18 +12:06:11.4 | 20.079 1.931 | 18.84 1.147 | 16.066 0.13 | 15.031 0.097 | 14.62 0.126 | 13.101 0.007 | 12.288 0.005 | 11.559 0.025 | 10.506 0.045 | 5.5 0.038 |
| 19802 | 05:31:34.57 +12:06:31.3 | 20.148 0.112 | 17.533 0.038 | 13.45 0.026 | 11.792 0.024 | 11.027 0.023 | 10.32 0.002 | 10.163 0.002 | 10.0 0.004 | 9.868 0.009 | 7.06 0.056 |
| 19863[2] | 05:30:36.08 +12:06:40.6 | – – | – – | 12.91 0.025 | 12.119 0.021 | 11.634 0.018 | 10.602 0.002 | 10.222 0.002 | 10.198 0.004 | 9.997 0.005 | 6.82 0.026 |
| 20369 | 05:31:24.96 +12:07:30.2 | 20.924 0.211 | 18.357 0.06 | 14.794 0.052 | 13.522 0.046 | 12.658 0.037 | 11.963 0.003 | 11.399 0.004 | 10.978 0.008 | 10.223 0.009 | 7.6 0.078 |
| 20941 | 05:31:27.20 +12:08:28.5 | 19.526 1.147 | 17.308 0.284 | 13.452 0.024 | 12.278 0.023 | 11.604 0.019 | 10.799 0.002 | 10.389 0.002 | 10.028 0.005 | 9.249 0.011 | 5.33 0.032 |
| 20993 | 05:30:51.70 +12:08:36.7 | 13.718 0.03 | 12.892 0.03 | 11.64 0.023 | 10.867 0.026 | 10.452 0.018 | 9.924 0.002 | 9.62 0.002 | 9.3 0.003 | 8.327 0.003 | 5.74 0.023 |
| 21068[2] | 05:30:13.12 +12:08:45.7 | – – | – – | 10.954 0.022 | 10.12 0.023 | 9.557 0.018 | 8.459 0.001 | 7.951 0.001 | 7.251 0.002 | 6.273 0.001 | 3.58 0.001 |
| 21232 | 05:31:19.54 +12:08:58.4 | 21.548 0.37 | 19.536 0.163 | 16.645 0.132 | 14.735 0.059 | 13.135 0.036 | 11.886 0.004 | 11.492 0.004 | 11.086 0.013 | 10.656 0.028 | 5.67 0.027 |
| 21424 | 05:31:19.48 +12:09:15.4 | 16.116 0.055 | 14.584 0.038 | 11.987 0.022 | 10.776 0.023 | 10.091 0.018 | 9.085 0.001 | 8.52 0.002 | 8.099 0.002 | 7.295 0.001 | 4.3 0.011 |
| 21495 | 05:31:22.26 +12:09:21.4 | 19.913 0.094 | 17.228 0.035 | 15.687 0.063 | 13.787 0.041 | 12.2 0.024 | 9.98 0.002 | 9.411 0.002 | 8.81 0.003 | 8.035 0.003 | 4.64 0.012 |
| 21677 | 05:32:15.47 +12:09:34.3 | 15.513 0.04 | 14.296 0.035 | 12.7 0.022 | 11.977 0.024 | 11.577 0.023 | 10.561 0.002 | 10.182 0.002 | 9.774 0.004 | 8.883 0.002 | 6.38 0.014 |
| 21725 | 05:31:23.61 +12:09:43.9 | 12.828 0.03 | 11.927 0.03 | 10.422 0.02 | 9.623 0.021 | 9.192 0.017 | 8.216 0.001 | 7.732 0.001 | 6.956 0.002 | 6.085 0.002 | 2.73 0.004 |
| 21900 | 05:32:12.32 +12:09:55.5 | 15.679 0.043 | 15.179 0.05 | 14.217 0.03 | 13.427 0.031 | 12.653 0.028 | 11.568 0.003 | 11.274 0.004 | 10.564 0.005 | 9.296 0.003 | 4.83 0.004 |
| 22102 | 05:31:26.97 +12:10:20.6 | 17.023 0.113 | 14.61 0.039 | 11.956 0.022 | 11.249 0.02 | 10.887 0.018 | 10.378 0.002 | 10.223 0.002 | 10.031 0.007 | 9.802 0.038 | 7.05 0.21 |
| 22233 | 05:31:23.14 +12:10:33.8 | 18.35 0.38 | 15.912 0.084 | 13.165 0.022 | 12.462 0.023 | 12.021 0.019 | 11.49 0.003 | 11.255 0.004 | 10.949 0.011 | 10.492 0.026 | 6.67 0.217 |
| 22362 | 05:31:40.50 +12:10:46.8 | 14.177 0.031 | 13.109 0.031 | 11.311 0.022 | 10.454 0.023 | 10.184 0.019 | 9.847 0.001 | 9.562 0.002 | 9.052 0.003 | 7.914 0.002 | 5.01 0.005 |
| 22691 | 05:31:15.52 +12:11:23.6 | 15.606 0.042 | 14.131 0.034 | 12.097 0.022 | 11.21 0.026 | 10.718 0.018 | 9.988 0.002 | 9.646 0.003 | 9.318 0.003 | 8.769 0.005 | 5.98 0.021 |
| 22786 | 05:31:26.06 +12:11:33.5 | 20.332 0.128 | 17.885 0.044 | 14.4 0.029 | 12.875 0.023 | 12.056 0.023 | 11.211 0.002 | 10.769 0.003 | 10.388 0.005 | 9.729 0.005 | 4.65 0.011 |
| 22957 | 05:31:28.10 +12:11:51.1 | 17.748 0.051 | 15.84 0.03 | 12.98 0.023 | 12.001 0.021 | 11.49 0.019 | 10.903 0.002 | 10.552 0.002 | 10.118 0.004 | 9.358 0.003 | 6.19 0.041 |
| 23445 | 05:31:28.42 +12:12:35.3 | 16.975 0.108 | 15.04 0.047 | 13.019 0.022 | 12.344 0.021 | 12.066 0.021 | 11.593 0.002 | 11.34 0.003 | 11.091 0.007 | 10.449 0.009 | 7.79 0.103 |
| 23598 | 05:31:25.68 +12:12:51.4 | 18.309 0.053 | 16.183 0.031 | 12.703 0.022 | 11.752 0.021 | 11.271 0.018 | 10.557 0.002 | 10.191 0.002 | 9.79 0.004 | 9.077 0.003 | 6.09 0.017 |
| 25472 | 05:31:51.31 +12:16:20.8 | 16.577 0.07 | 15.071 0.043 | 12.742 0.022 | 11.715 0.024 | 11.043 0.023 | 10.229 0.002 | 9.753 0.002 | 9.454 0.003 | 9.005 0.003 | 6.98 0.059 |
| 26565 | 05:31:47.81 +12:18:08.2 | 12.417 0.03 | 11.578 0.03 | 10.616 0.022 | 10.002 0.024 | 9.812 0.021 | 9.323 0.003 | 8.989 0.003 | 8.602 0.003 | 7.808 0.008 | 5.2 0.009 |
| 28513 | 05:30:50.45 +12:21:28.0 | 9.405 0.03 | 8.693 0.03 | 8.061 0.019 | 7.913 0.02 | 7.914 0.024 | 7.834 0.001 | 8.026 0.001 | 7.849 0.002 | 7.866 0.002 | 6.23 0.058 |
| 29908[2,3] | 05:32:17.75 +12:23:58.7 | – – | – – | 12.56 0.023 | 11.831 0.027 | 11.428 0.024 | 10.437 0.002 | 10.106 0.002 | 9.735 0.004 | 9.174 0.005 | – – |
| 29957[2] | 05:32:06.52 +12:24:04.4 | – – | – – | 11.931 0.02 | 11.182 0.021 | 10.767 0.019 | 10.252 0.002 | 9.949 0.002 | 9.654 0.003 | 9.108 0.004 | 4.94 0.007 |
| 30116[3] | 05:32:19.07 +12:24:22.4 | 13.718 0.03 | 12.487 0.03 | 10.928 0.023 | 10.1 0.026 | 9.656 0.019 | 8.987 0.002 | 8.444 0.002 | 8.071 0.002 | 7.174 0.001 | – – |
| 30172[3] | 05:32:14.51 +12:24:29.0 | 19.248 0.801 | 17.12 0.226 | 14.564 0.032 | 13.78 0.03 | 13.338 0.037 | 12.167 0.003 | 11.668 0.004 | 11.164 0.007 | 10.416 0.009 | – – |
| 30256 | 05:31:56.36 +12:24:41.4 | 13.34 0.03 | 12.287 0.03 | 10.899 0.022 | 10.199 0.019 | 10.009 0.019 | 9.863 0.001 | 9.896 0.002 | 9.864 0.004 | 9.833 0.004 | 7.5 0.065 |
| 30354[3] | 05:32:13.06 +12:24:52.4 | 16.404 0.063 | 15.612 0.064 | 14.218 0.026 | 13.196 0.03 | 12.532 0.026 | 11.575 0.003 | 10.891 0.003 | 10.23 0.005 | 8.815 0.006 | – – |
| 31202[2,3] | 05:32:36.42 +12:26:19.4 | – – | – – | 10.425 0.022 | 9.694 0.023 | 9.291 0.019 | 8.601 0.001 | 8.129 0.001 | 7.823 0.002 | 7.169 0.001 | – – |
| 31833 | 05:30:14.76 +12:27:36.5 | 19.105 0.619 | 16.405 0.099 | 13.758 0.024 | 12.865 0.024 | 12.48 0.024 | 11.883 0.003 | 11.584 0.004 | 11.419 0.011 | 10.962 0.021 | 7.71 0.113 |
| 31902[2,3] | 05:32:34.32 +12:27:32.3 | – – | – – | 11.761 0.023 | 10.935 0.024 | 10.581 0.019 | 9.459 0.002 | 9.174 0.003 | 8.957 0.003 | 8.394 0.003 | – – |

Continued on next page…

Table 2.18 – Continued

| ID | RA(J2000), DEC(J2000) | R eR | I eI | J eJ | H eH | Ks eKs | [3.6] e[3.6] | [4.5] e[4.5] | [5.8] e[5.8] | [8.0] e[8.0] | [24] e[24] |
|---|---|---|---|---|---|---|---|---|---|---|---|
| 32037[2,3] | 05:32:36.58 +12:27:48.3 | – – | – – | 13.87 0.024 | 12.651 0.026 | 11.73 0.021 | 10.044 0.002 | 9.398 0.002 | 8.988 0.003 | 8.401 0.002 | – – |
| 32340[3] | 05:32:06.23 +12:28:24.1 | 19.607 1.123 | 16.943 0.193 | 14.08 0.026 | 13.27 0.026 | 12.779 0.024 | 11.997 0.003 | 11.458 0.003 | 11.104 0.008 | 10.448 0.016 | 99.9 9.999 |
| 32951[3] | 05:32:06.43 +12:29:22.2 | 14.362 0.031 | 13.171 0.031 | 12.02 0.022 | 11.198 0.019 | 10.86 0.019 | 10.29 0.002 | 10.045 0.002 | 9.725 0.005 | 9.128 0.009 | – – |
| 33125[3] | 05:32:11.94 +12:29:41.9 | – – | – – | 16.801[1] – | 15.381 0.1 | 13.856 0.058 | 12.852 0.006 | 11.876 0.004 | 11.259 0.011 | 10.063 0.012 | – – |
| 33419 | 05:30:35.04 +12:30:17.0 | 13.282 0.03 | 12.617 0.03 | 11.966 0.022 | 11.433 0.021 | 11.295 0.017 | 11.246 0.003 | 11.293 0.003 | 11.25 0.01 | 11.165 0.027 | 6.98 0.049 |
| 33525 | 05:31:43.43 +12:30:22.0 | 12.995 0.03 | 12.222 0.03 | 11.14 0.022 | 10.532 0.021 | 10.243 0.018 | 10.128 0.002 | 9.818 0.002 | 9.385 0.004 | 8.477 0.004 | 5.64 0.043 |
| 33661[3] | 05:32:08.06 +12:30:34.8 | – – | – – | 16.745[1] – | 14.562 0.052 | 12.634 0.036 | 10.152 0.002 | 9.075 0.002 | 8.327 0.003 | 7.738 0.002 | – – |
| 33936 | 05:32:02.89 +12:31:05.8 | – – | – – | 15.559 0.062 | 12.159 0.026 | 10.184 0.021 | 8.434 0.001 | 7.802 0.001 | 7.327 0.002 | 6.825 0.001 | 3.44 0.003 |
| 34050 | 05:32:02.58 +12:31:17.4 | – – | – – | 16.767 0.17 | 13.826 0.043 | 12.288 0.028 | 11.069 0.006 | 10.481 0.006 | 10.141 0.012 | 9.405 0.015 | 3.65 0.004 |
| 34119 | 05:31:50.23 +12:31:26.0 | 17.039 0.105 | 15.112 0.047 | 12.205 0.023 | 10.89 0.023 | 10.393 0.02 | 10.076 0.002 | 10.043 0.002 | 9.968 0.006 | 9.958 0.024 | 6.63 0.056 |
| 35518 | 05:30:29.09 +12:33:56.5 | 16.041 0.046 | 14.775 0.037 | 13.161 0.023 | 12.412 0.023 | 12.005 0.022 | 11.694 0.002 | 11.303 0.003 | 11.269 0.009 | 10.652 0.008 | 7.1 0.028 |
| 35582 | 05:30:34.17 +12:34:03.4 | 20.194 1.728 | 18.88 0.91 | 16.635 0.131 | 15.463 0.092 | 14.465 0.083 | 12.668 0.004 | 12.082 0.004 | 11.239 0.008 | 10.329 0.006 | 6.68 0.024 |
| 35766 | 05:32:00.56 +12:34:15.1 | 17.322 0.134 | 15.325 0.053 | 13.48 0.024 | 12.841 0.024 | 12.553 0.026 | 12.165 0.004 | 11.92 0.005 | 11.734 0.014 | 11.067 0.027 | 8.58 0.318 |
| 37215[2,3] | 05:32:25.65 +12:36:35.3 | – – | – – | 11.64 0.022 | 10.827 0.023 | 10.424 0.017 | 9.628 0.001 | 9.34 0.002 | 9.18 0.003 | 8.372 0.003 | – – |
| 37312[2] | 05:30:36.19 +12:36:52.5 | – – | – – | 11.598 0.03 | 10.728 0.029 | 10.163 0.026 | 9.635 0.002 | 9.295 0.003 | 8.988 0.003 | 8.1 0.002 | 4.65 0.004 |
| 39428 | 05:31:41.23 +12:40:15.7 | 16.598 0.082 | 14.757 0.043 | 12.499 0.023 | 11.419 0.021 | 10.933 0.018 | 10.05 0.001 | 9.575 0.001 | 8.977 0.003 | 8.247 0.002 | 4.39 0.003 |
| 40421[2] | 05:30:27.08 +12:42:02.9 | – – | – – | 14.987 0.039 | 14.234 0.031 | 14.078 0.057 | 13.736 0.008 | 13.53 0.01 | 13.145 0.035 | 12.364 0.041 | – – |
| 41615[3] | 05:32:18.12 +12:43:56.3 | 14.341 0.031 | 13.122 0.031 | 11.822 0.022 | 11.005 0.024 | 10.649 0.02 | 9.819 0.001 | 9.522 0.002 | 9.23 0.003 | 8.694 0.002 | – – |
| 41741[2] | 05:30:40.96 +12:44:16.1 | – – | – – | 12.866 0.023 | 11.832 0.021 | 11.349 0.021 | 10.702 0.002 | 10.212 0.002 | 10.056 0.005 | 9.638 0.003 | 6.71 0.021 |
| 45191[2] | 05:31:39.75 +12:50:02.8 | – – | – – | 17.015 0.185 | 16.235 0.207 | 14.875 0.11 | 12.467 0.004 | 11.637 0.004 | 10.826 0.007 | 9.949 0.005 | 6.58 0.019 |
| 45371[2] | 05:30:31.60 +12:50:27.1 | – – | – – | 13.258 0.023 | 12.377 0.021 | 11.891 0.021 | 11.066 0.002 | 10.594 0.003 | 10.207 0.005 | 8.96 0.003 | 5.72 0.01 |

[1]Upper limmits
[2]Out of the optical WFC Survey.
[3]Out of the MIPS 24 $\mu$m survey.

**Table 2.19**: Disk properties of the 66 new candidate members of Barnard 30 selected from the Spitzer data.

| ID | Phot. Mem.[2] | Final Mem.[3] | Mass ($M_\odot$)[1] | Teff (K)[1] | YSO Class | SED slope | Disk Type |
|---|---|---|---|---|---|---|---|
| 6876 | R - Y | Y | 0.002 | 1300 | I | 0.538 | Thick |
| 9196 | Y - - | Y? | 0.276 | 3300 | II | -1.84 | Thin |
| 10420 | Y Y Y | Y | 0.467 | 3500 | II | -1.777 | Thick |
| 12438 | ? T T | Y | 0.754 | 3700 | III | -2.724 | Transition |
| 12629 | Y Y Y | Y | 0.029 | 2700 | II | -1.272 | Thick |
| 13402 | Y - - | Y? | 2.968 | 5600 | II | -1.85 | Thin |
| 16599 | Y Y Y | Y | 1.052 | 3900 | II | -0.994 | Thick |
| 17792 | Y Y Y | Y | 0.041 | 2800 | II | -1.601 | Thick |
| 18115 | Y Y Y | Y | 0.004 | 1800 | II | -0.997 | Thick |
| 19172 | R Y Y | Y | 0.002 | 1400 | I | 1.551 | Thick |
| 19198 | R Y Y | Y | 0.003 | 1700 | I | 1.373 | Thick |
| 19545 | Y T T | Y | 1.115 | 4000 | II | -1.794 | Thick |
| 19617 | R Y Y | Y | 0.029 | 2700 | I | 0.117 | Thick |
| 19802 | ? T T | Y | 0.003 | 1700 | III | -2.316 | Thin |
| 19863 | Y T T | Y | 0.063 | 2900 | II | -2.213 | Thin |
| 20369 | Y Y Y | Y | 0.004 | 1800 | II | -0.877 | Thick |
| 20941 | Y Y Y | Y | 0.004 | 2200 | II | -1.083 | Thick |
| 20993 | Y Y Y | Y | 1.115 | 4000 | II | -1.029 | Thick |
| 21068 | R Y Y | Y | 0.006 | 2000 | I/II | -0.303 | Thick |
| 21232 | Y Y Y | Y | 0.004 | 1500 | II | -1.423 | Thick |
| 21424 | Y Y Y | Y | 0.029 | 2700 | II | -0.822 | Thick |
| 21495 | Y Y Y | Y | 0.276 | 3300 | I | -0.603 | Thick |
| 21677 | Y Y Y | Y | 0.213 | 3200 | II | -0.925 | Thick |
| 21725 | R Y Y | Y | 1.340 | 4200 | I/II | -0.34 | Thick |
| 21900 | R Y Y | Y | 0.004 | 1800 | I/II | -0.178 | Thick |
| 22102 | Y T T | Y | 0.063 | 2900 | III | -2.171 | Transition |
| 22233 | Y Y Y | Y | 0.063 | 2900 | II | -1.685 | Thick |
| 22362 | Y Y Y | Y | 0.355 | 3400 | II | -0.604 | Thick |
| 22691 | Y Y Y | Y | 0.604 | 3600 | II | -1.449 | Thick |
| 22786 | Y Y Y | Y | 0.004 | 1700 | II | -1.157 | Thick |
| 22957 | Y Y Y | Y | 0.029 | 2700 | II | -1.062 | Thick |
| 23445 | Y Y Y | Y | 0.213 | 3200 | II | -1.541 | Thick |
| 23598 | Y Y Y | Y | 0.019 | 2500 | II | -1.144 | Thick |
| 25472 | Y Y Y | Y | 0.063 | 2900 | II | -1.468 | Thick |
| 26565 | Y Y Y | Y | 0.213 | 3200 | II | -1.105 | Thick |
| 28513 | ? ? T | Y |  | 8600 | III | -2.803 | Transition |
| 29908 | Y - - | Y? | 0.213 | 3200 | II | -1.387 | Thick |
| 29957 | Y Y Y | Y | 0.088 | 3000 | II | -1.536 | Thick |
| 30116 | Y - - | Y? | 0.903 | 3800 | I/II | -0.807 | Thick |
| 30172 | Y - - | Y? | 0.041 | 2800 | I/II | -0.835 | Thick |
| 30256 | ? ? T | Y | 1.052 | 3900 | III | -2.793 | Transition |
| 30354 | R - - | Y? | 0.004 | 1800 | I | 0.298 | Thick |
| 31202 | Y - - | Y? | 0.008 | 2100 | II | -1.236 | Thick |
| 31833 | Y Y Y | Y | 0.019 | 2500 | II | -1.816 | Thick |
| 31902 | Y - - | Y? | 0.604 | 3600 | II | -1.641 | Thick |
| 32037 | Y - - | Y? | 0.004 | 1700 | I | -0.998 | Thick |
| 32340 | Y - - | Y? | 0.006 | 2000 | II | -1.103 | Thick |
| 32951 | Y - - | Y? | 0.213 | 3200 | II | -1.502 | Thick |
| 33125 | R - - | Y? | 0.004 | 1600 | I | 0.281 | Thick |

Continued on next page...

Table 2.19 – Continued

| ID | Phot. Mem.[2] | Final Mem.[3] | Mass ($M_\odot$)[1] | Teff (K)[1] | YSO Class | SED slope | Disk Type |
|---|---|---|---|---|---|---|---|
| 33419 | ? T T | Y | | 7800 | III | -2.732 | Transition |
| 33525 | Y Y Y | Y | | 6000 | II | -0.94 | Thick |
| 33661 | R - - | Y? | 0.002 | 1300 | I | -0.111 | Thick |
| 33936 | Y Y Y | Y | 0.002 | 1400 | I | -1.016 | Thick |
| 34050 | Y Y Y | Y | 0.003 | 1500 | I/II | -0.986 | Thick |
| 34119 | ? T T | Y | 0.029 | 2700 | III | -2.693 | Transition |
| 35518 | Y Y Y | Y | 0.355 | 3400 | II | -1.729 | Thick |
| 35582 | R Y Y | Y | 0.003 | 1500 | I | -0.106 | Thick |
| 35766 | Y - Y | Y | 0.355 | 3400 | II | -1.608 | Thick |
| 37215 | Y - - | Y? | 0.006 | 1900 | II | -1.446 | Thick |
| 37312 | Y Y Y | Y | 0.007 | 2100 | II | -1.105 | Thick |
| 39428 | Y Y Y | Y | 0.144 | 3100 | I/II | -0.749 | Thick |
| 40421 | Y - - | Y? | 0.355 | 3400 | II | -1.247 | Thick |
| 41615 | Y - - | Y? | 1.340 | 4200 | II | -1.557 | Thick |
| 41741 | Y Y Y | Y | 0.006 | 2000 | II | -1.685 | Thick |
| 45191 | R Y Y | Y | 0.002 | 1300 | I | 0.052 | Thick |
| 45371 | R Y Y | Y | 0.009 | 2300 | I/II | -0.47 | Thick |

[1]Teff is derived from the SED fittings shown in Figures from 4.13 to 4.17. Mass estimate based on Teff and a 3Myr isochrone from the Lyon group or from Siess et al. (2000) depending on the object.

[2]Membership is [3.6] vs. [3.6]-[8.0], H-Ks vs. Ks-[24], [3.6]-[8.0] vs. [8.0]-[24]. Y: member, R: Very red object, Y?: probable member, F: field object; -: Not enough data

[3]Final Membership

# Chapter 3

# Collinder 69: the Central Cluster

Collinder 69 is one of the richest young clusters near the Sun in the age range when young stars lose their circunstellar disks and stop accretion (1 – 10 Myr, Hartmann 1999 and references there in). It is the central cluster of the Lambda Orionis Star Forming Region and it is associated to the eponymous $\lambda$ Ori star. Dolan & Mathieu (1999, 2001, 2002) derived a distance of 450±50 pc, larger than both the distance derived by Murdin & Penston (1977) and the value derived by Hipparcos (Perryman et al. 1997) for the five stars in the central area, 380±30 pc. According to Dolan & Mathieu (2002), the turn-off age for the massive stars is ∼6 Myr (see also Murdin & Penston 1977 for another age determination based on the massive stars, 4 Myr).

In this chapter we describe how we have confirmed and rejected candidate members to the Collinder 69 open cluster; the different methodologies used to derived stellar parameters for these members (analysis of high, medium and low resolution optical and near-infrared spectroscopy and comparison of the Spectral Energy Distributions with models) and how these estimations compare with each other.

The candidate members were selected based on a variety of photometric surveys and a X-rays campaign (as described in the previous chapter). This chapter is organized as follows: in Section 3.1 we focus on the Collinder 69 candidate members from our CFHT survey to present a new tool (VOSA) developed to analyze Spectral Energy Distributions of large lists of objects in an automatic manner. We compare the results that we obtain with those derived with classical methodologies. In Section 3.2 we describe the spectroscopic surveys that have already been performed and published by other authors. In Section 3.3 we provide the analysis and the results obtained from the optical spectra gathered by our group. In Section 3.4 we describe the analysis and results from our infrared spectroscopic surveys. Finally, in Section 3.8 we present the conclusions achieved from this work.

**Table 3.1**: Example of the photometric data for our sources.

| Name | R[a] | I[a] | J[b] | H[b] | Ks[b] | [3.6][c] | [4.5][c] | [5.8][c] | [8.0][c] | [24][d] |
|---|---|---|---|---|---|---|---|---|---|---|
| ... | ... | ... | ... | ... | ... | ... | ... | ... | ... | ... |
| LOri029 | 14.89±0.00 | 13.69±0.00 | 12.210±0.026 | 11.460±0.027 | 11.071±0.019 | 10.259±0.003 | 9.830±0.003 | 9.321±0.006 | 8.416±0.003 | 5.684±0.007 |
| LOri034 | 15.10±0.00 | 13.97±0.00 | 12.442±0.026 | 11.639±0.026 | 11.184±0.023 | 10.068±0.003 | 9.734±0.003 | 9.314±0.007 | 8.325±0.003 | 5.738±0.007 |
| ... | ... | ... | ... | ... | ... | ... | ... | ... | ... | ... |

Filters corresponding to the telescope/instrument configuration described below:

[a]CFHT

[b]2MASS, Skrutskie et al. (2006)

[c]Spitzer/IRAC, Fazio et al. (2004)

[d]Spitzer/MIPS, Rieke et al. (2004)

## 3.1 A test for the VOSA methodology. Spectral Energy Distribution analysis of the candidate members from the CFHT1999 survey

During this Thesis we developed (in collaboration with the SVO team members located at LAEFF) VOSA (which stands for Virtual Observatory SED analyzer), a VO-Tool designed to perform SED fitting and isochrones interpolation (see Appendix C for detailed explanations on the technical issues). As it can be inferred so far, our group has been involved in a very exhaustive study of the LOSFR. One of the caveats of doing this kind of observational studies is the fact that the amount of data to be processed and analyzed is not negligible. Although in the analysis of astronomical data there are important tasks that have to be performed in a one by one basis, there are others that not only can be automatized but also benefit from the methodologies brought up by the Virtual Observatory.

The Virtual Observatory (IVOA[1]) is an international, community-based initiative to provide seamless access to the data available from astronomical archives and services as well as state-of-the-art tools for the efficient analysis of this huge amount of information. The works by Padovani et al. (2004) and Tsalmantza et al. (2006) are good examples of the efficiency of such tools in helping astronomers to produce scientific results.

In the SED fitting process of the candidate members we made use of multi-wavelength data; optical to mid-infrared photometry. The data were taken from Barrado y Navascués et al. (2007b) and complemented with VO photometric services (see Section C for details). None of our sources had Tycho or Hauck/Strömgren counterparts, but some of them did have 2MASS counterparts (we have used 2MASS photometry for those sources for which we did not have near IR photometry either from CAHA/Omega2000 or WHT/INGRID, see Barrado y Navascués et al. 2007b for details). Ten photometric points per object, covering from 0.6 up to 24 $\mu$m were typically used in the analysis (see the example in Table 3.1).

[1]http://www.ivoa.net

### 3.1.1 General Results

Following the work-flow explained in Section C.2 we were able to build Spectral Energy Distributions and estimate effective temperatures, gravities and bolometric luminosities for 167 candidate members of Collinder 69, and even infer ages and masses for 145 of these sources in an **automatic manner**.

Examples of the estimations made through synthetic photometry fittings are shown in Figs. C.6, C.7, C.8 and C.9 and the results achieved for each source are shown in Table 3.2.

Regarding the comparison with theoretical isochrones and evolutionary tracks in the Hertzsprung-Russell diagram, VOSA does not provide estimations of either age or mass for 20 sources (~12% of the total) due to the peculiar location of these sources in the diagram (see the VOSA Help menu for further details on the cases where the interpolation process cannot be completed and no estimation of age and/or mass can be provided).

Besides the case of two special sources, there are two main causes for this peculiar location in the HR diagram: either the source might harbour a close to edge-on disk that reprocess the light emitted from the photosphere of the source (and therefore both the effective temperature and the bolometric luminosity are underestimated) or the source does not belong to cluster. See Fig. 3.5 for details on the specific location of the peculiar sources and Subsection 3.1.3 for the discussion on each particular case.

### 3.1.2 Comparison with other methodologies.

In order to test the results provided by VOSA, we have compared some of the parameters and properties discussed in this work with those derived using other methodologies (mainly based on colours and classical bolometric corrections).

#### 3.1.2.1 Infrared excesses.

Barrado y Navascués et al. (2007b) studied in detail the Spitzer/IRAC data of the candidates, and based on the criteria developed by Allen et al. (2004) and Hartmann et al. (2005) derived a fraction of members with disks of 25% and 40% for the stellar and substellar population of C69, respectively.

VOSA detects infrared excesses by calculating iteratively the $\alpha$ parameter (a measurement of the slope of the SED at infrared wavelengths) from Lada et al. (2006). This method provides us with excess fractions of 32% for candidates with stellar masses (from 0.72 M$\odot$ to 1.15 M$\odot$ ), and 44% for sources with estimated masses $\leq$ 0.72 M$\odot$. The differences, which are not significant, can be explained by the presence of optically thin disks that mimic the location

of single photospheres in the Spitzer/IRAC colour-colour diagrams and are therefore classified as Class III sources.

#### 3.1.2.2 Effective temperature estimation.

In order to compare our estimations with other classical photometric methodologies, we derived the effective temperature of our candidates using two different colours ([R-I] and [I-Ks]) and temperature-colour relationships (Bessell 1991 and Leggett 1992). In Fig. 3.1 we have plotted the relationships mentioned before and overplotted as solid and open circles (diskless and disk harbouring sources) the results obtained with VOSA.
There is a good agreement between the different relationships (especially with the one proposed by Bessell 1991) with offsets of -150K and +100K for the two colours, [R-I] and [I-Ks], respectively. These offsets have already been reported in the literature when comparing temperatures obtained with models and those obtained with colour and temperature scales (see for example Barrado y Navascués et al. 2004a, Barrado y Navascués 2006 and Mohanty et al. 2007).
We have selected one specific case, LOri055, where the differences between the temperatures derived from the colors and the one estimated by VOSA are much higher than the mentioned offset. For this case we have forced VOSA to find the best multiplicative factor to fit the SED of this object with NextGen models at temperatures in the range between the lowest (3200 K from the [I-Ks] colour and the Leggett 1992 temperature scale) and the highest (3600 K from VOSA) derived for the source.
In Fig 3.2 we show the fits obtained when forcing the different temperatures. An inspection of the behaviour of the $\chi^2$ of the fits concludes that the temperature proposed by VOSA improves by one and a half orders of magnitude the goodness of the fit obtained with the lowest temperature (the one derived with the [I-Ks] colour).

#### 3.1.2.3 Bolometric luminosity estimation.

In the case of the computation of the bolometric luminosity, we have applied different bolometric corrections to several photometric bands (I band by Kenyon & Hartmann 1995, J band by Lawson et al. 1996 and Ks band by Tinney et al. 1993) and as can be seen in Fig. 3.3, there are no systematic differences among the various methods. In our case we use the whole observed SED (except for the wavelength range where some excess is detected) to infer the total emitted flux, and therefore, the better the accuracy of the observations, the better the estimation.

### 3.1.3 Individual sources in C69

As mentioned previously, the location in a $T_{eff}$ vs $L_{bol}$ diagram of 20 of our sources made it impossible for VOSA to estimate their ages and masses. Besides, the ages estimated with our methodology for three other sources were much higher than the average age estimated in the

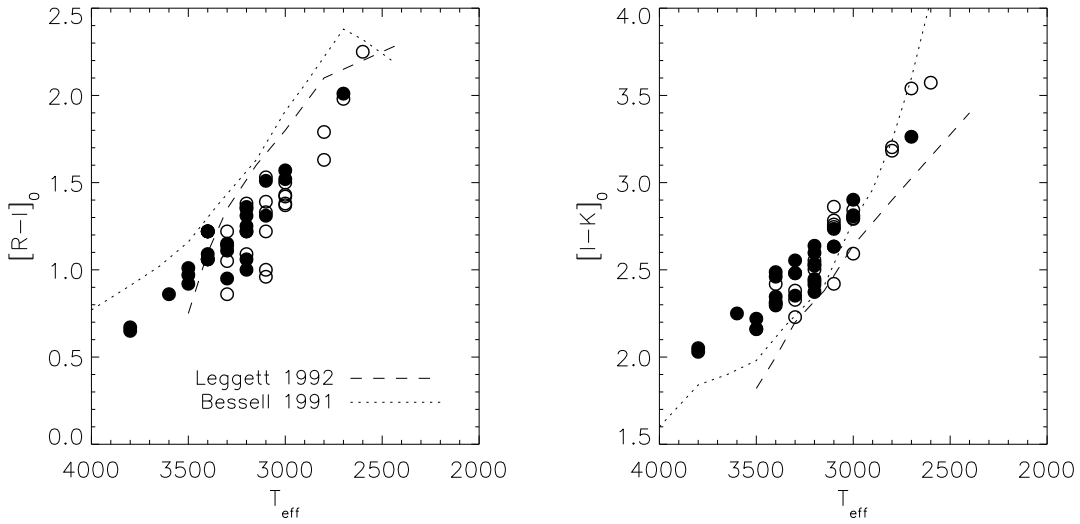


**Figure 3.1**: Dereddened colours CFHT [R-I] and CFHT–2MASS [I-K] vs. $T_{eff}$ (obtained with VOSA) for the candidate members of C69. The dotted line represents the relationship derived by Bessell (1991) and the dashed line the one derived by Leggett (1992). Open circles highlight sources harbouring disks.

literature for Collinder 69. We have divided these 23 "peculiar sources" into four groups according to the cause that might explain their location in the HR diagram (we have used the same number code as in Table 3.2).

1. Sources with infrared excess caused by the presence of a disk. The dust belonging to the disk reprocesses the light emitted by the central object, and in the cases where the angle of the disk and/or the amount of flaring is high enough, the light from the star can be blocked (see examples of very low mass stars and brown dwarfs surrounded by edge-on disks and the effects on the light from the central object in Fernández & Comerón 2001; Barrado y Navascués et al. 2004a; Pontoppidan et al. 2005; Luhman et al. 2007, and Huelamo et al. 2009, submitted).

   Whenever this is the case, our methodology will underestimate both the effective temperature and the bolometric luminosity of the central object. We propose this hypothesis as the cause for the peculiar location in the HR diagram of LOri029, LOri034, LOri146, LOri147 and LOri156.

   We do not see this effect in any of the remaining 24 sources that show infrared excess. See as an example, in Fig 3.4, the comparison between the best fit obtained for one of the sources classified as "peculiar", LOri034, and the one achieved for LOri062; in the latter case, the derived parameters, mainly the age, are consistent with the hypothesis that the source belongs to C69. Thus we consider that 18% of sources harbouring disks with inclinations

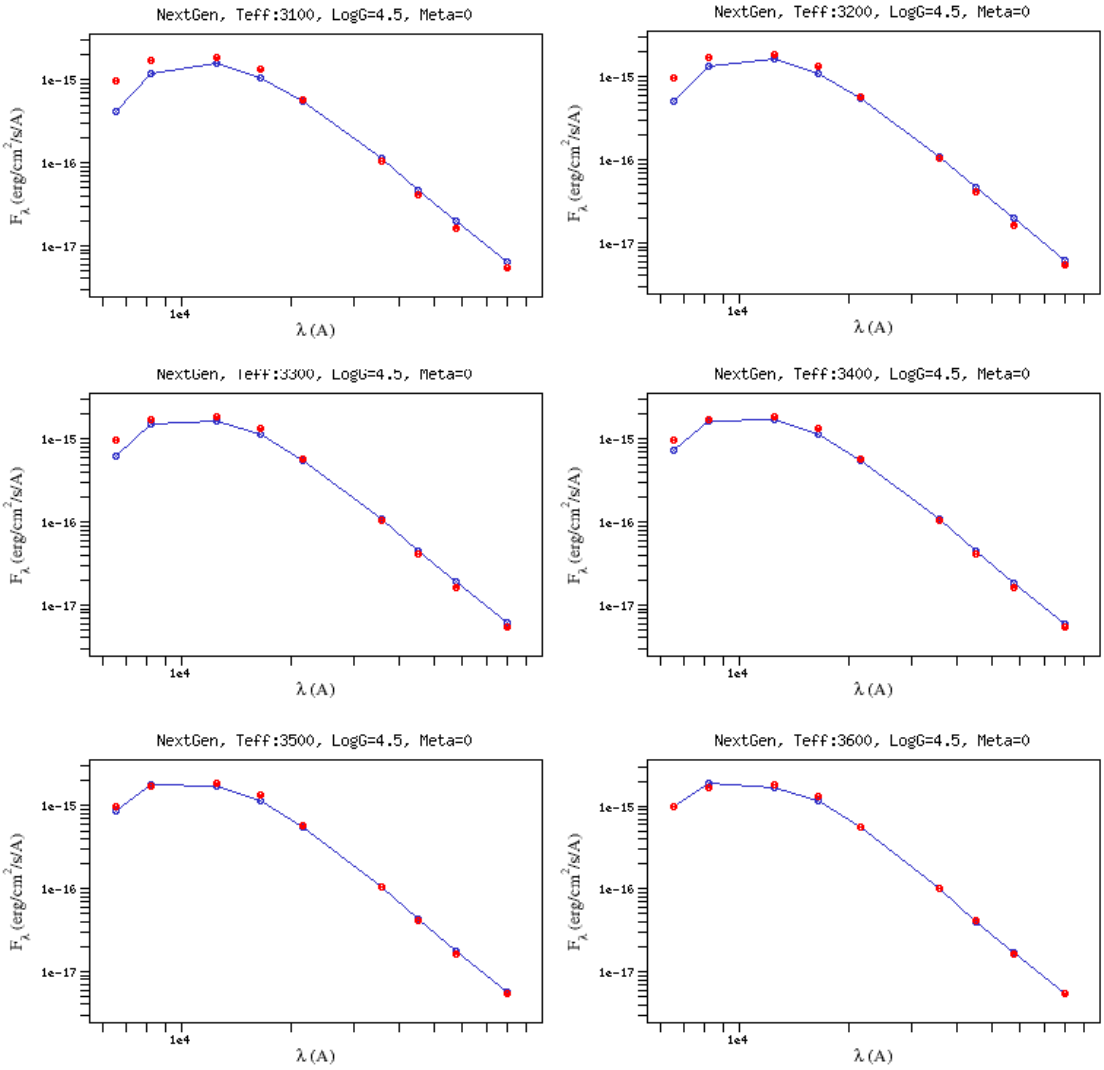


**Figure 3.2**: Forced fits to the SED of LOri055 for the range of effective temperatures estimated according to the different methods. According to our calculations, the $\chi^2$ improves by one and a half orders of magnitude when comparing the 3100 K and the 3600 K fits.

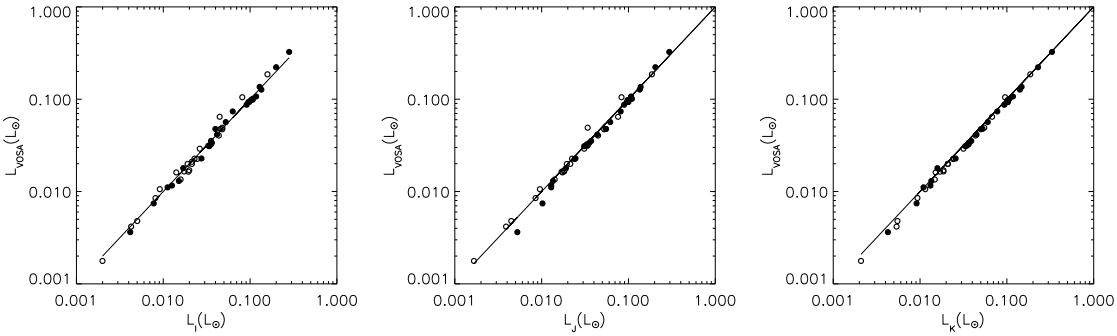


**Figure 3.3**: Comparison between the bolometric luminosities estimated with different bolometric corrections applied to various photometrical bands and those obtained with VOSA. Open circles highlight sources harbouring disks.

or disk structures that block part of the stellar light is a reasonable percentage.

2. Sources previously flagged as possible non-members. Barrado y Navascués et al. (2007b) studied the photometric properties of the sample, and flagged 16 sources as probable non-members according to these properties. With our methodology, we independently confirm this classification for all 16 sources (see Table 3.2 for the corresponding IDs); 13 of the cases were very clear, since the location of those sources in the HR diagram fell outside the parameter space confined by the isochrones and evolutionary tracks, in the other three cases (LOri101, LOri141 and LOri165), the derived ages (32, 37 and 85 Myr, respectively) were inconsistent with the upper-limit age derived for the whole cluster (12.3–16 Myr, see Subsection 3.1.4 for details).

3. Degeneracy of the fitting process. In the case of LOri169 no conclusion can be assessed, since the number of points making up the SED is as low as five (one of them, the R-band magnitude has a very large error), whilst we try to fit four independent parameters.

4. New non-member candidate. Even thought the best fit achieved for LOri162 seems to reproduce quite well the observational data (see Fig 3.6), the estimated luminosity is not compatible at all with the hypothesis that this object belongs to C69. Its luminosity is much higher than the one expected for a cluster member with the derived effective temperature of 1600 K. This luminosity would imply a radius of the star of ~0.5 $R_\odot$ (assuming a distance of 400 pc and the relationship $M_d = (R/D)^2$), whilst according to the isochrones from Baraffe et al. (2003), assuming an age of ~10 Myr, the radius of this object should be ~0.15 $R_\odot$.

   The effective temperature of LOri162 suggests that it might be a field L dwarf that, due to its very low temperature, mimics the colours of the less massive members of Collinder 69. Using the $M_d$ factor and assuming a typical radius for 1-5 Gyr dwarfs with the given temperature of 1600 K (according to isochrones from Baraffe et al. 2003), we estimate a

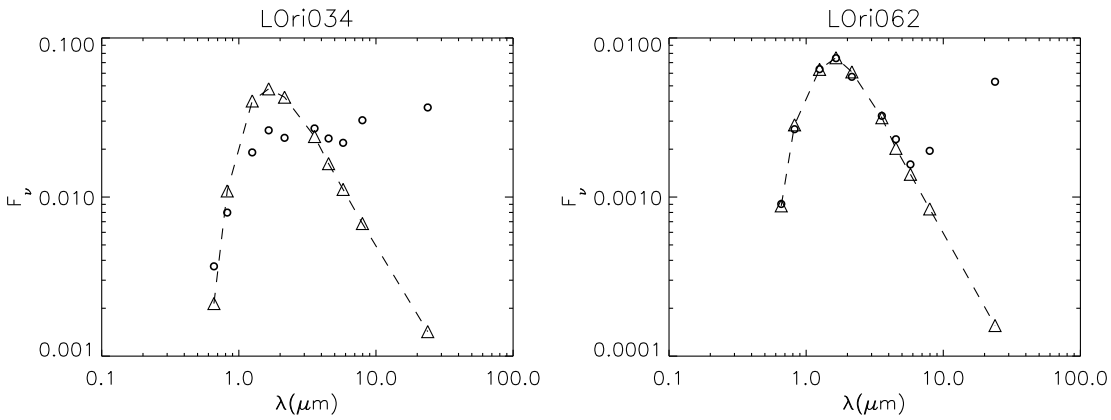


**Figure 3.4**: Comparison of the best fits achieved for two sources showing infrared excess (open circles for the observed photometry and open triangles joined with a dashed line for the synthetic set). On the left side, LOri034, a source whose estimated location in the HR diagram does not allow VOSA to infer either its mass or its age. On the right hand side, LOri062, another source harbouring a disk but for which all the parameters can be estimated by VOSA and with an inferred age of 12.3 Myr, consistent with the range of ages estimated previously in the literature for C69.

distance to this object of between 61 and 69 parsecs and a spectral type of L6-L7 according to the $T_{eff}$ scale by Basri et al. (2000).

### 3.1.4 The CFHT1999 survey as a whole.

Dolan & Mathieu (1999) studied the $\lambda$ Orionis Star Forming Region (which includes the central cluster Collinder 69 and several younger, dark clouds), and, based on the presence of the Li I $\lambda$6708 absorption (in mid-resolution optical spectra) and different theoretical isochrone sets, they concluded that the star formation in this region (high- and low-mass) began 5–7 Myr ago with a dramatic change in the low-mass star formation happening 1–2 Myr ago: either an abrupt cessation (through removal of the gas supply), or a burst (caused by star birth via cloud compression).

Dolan & Mathieu (2001) derived a turnoff age of 6–7 Myr based on Strömgren photometry for the massive stars of the cluster.

Barrado y Navascués et al. (2007b) studied Collinder 69, the older central cluster, in detail, and proposed an upper-limit for the age of 20 Myr based on colour-magnitude (optical/near-infrared) diagrams and isochrones by Baraffe et al. (1998), with an optimal age of 5 Myr for the isochrones (Baraffe et al. 2002) corresponding to the DUSTY models. The methodology presented in this work provides us with an estimation of the age of the association through the analysis of the statistics of the ages inferred for each individual member of the cluster. We have selected a subsample of 120 sources (out of the total of 167 candidates) that makes up the “least-possible biased” set in the sense that we do not include either sources flagged as possible non-member

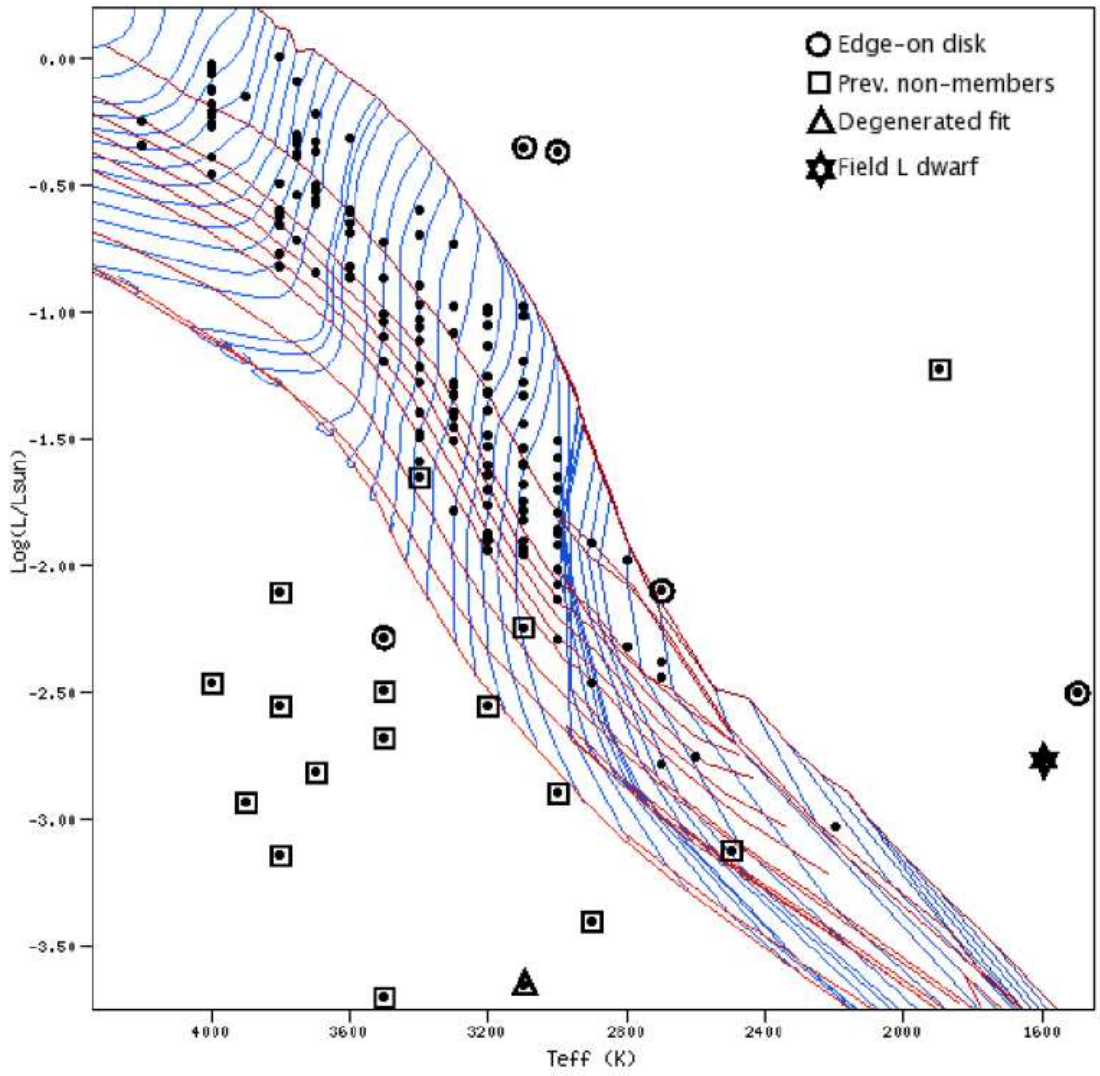


**Figure 3.5**: Location in the HR diagram of the "peculiar sources" analyzed in Section 3.1.3. Squares surround non-members candidates from Barrado y Navascués et al. (2007b); circles around sources showing infrared excess, and a triangle and a star highlight LOri169 and LOri162, respectively. See text for details.

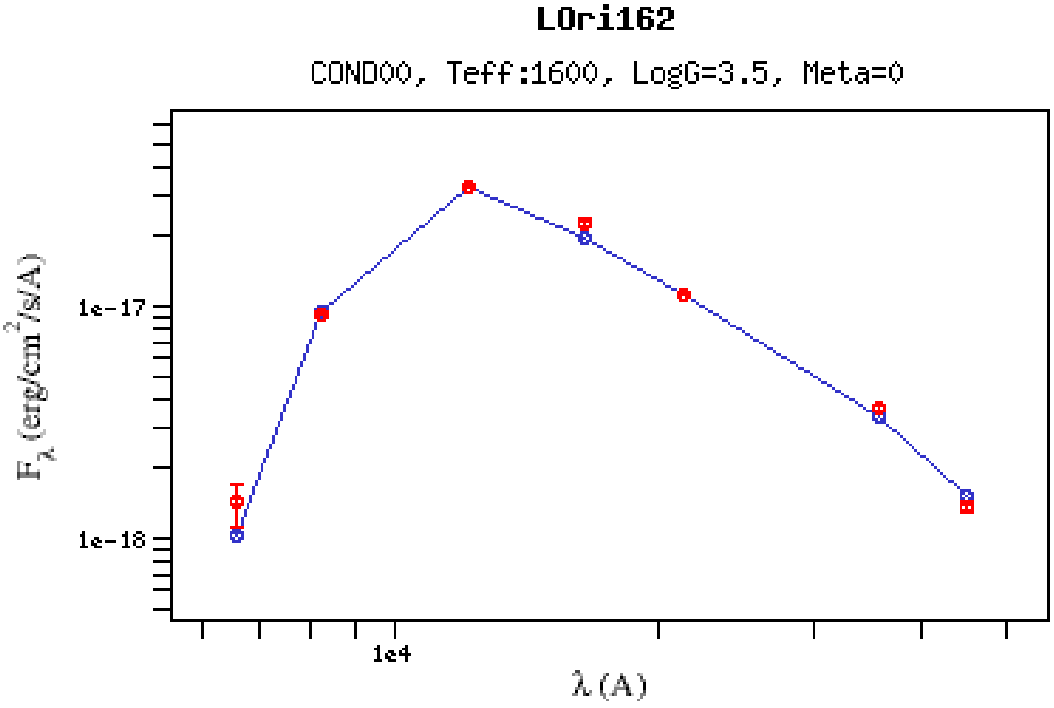


**Figure 3.6**: Best fit achieved for LOri162, a possible L field dwarf. The SED fitting process is quite insensitive to the surface gravity of the source; also, at the beginning of the process, we constrained the values of $\log g$ to be between 3.5 and 4.5. Thus, the value of $\log g$ 3.5 shown in the caption should not be taken into account; instead, as a reference, the radius assumed when estimating the distance to this source (61-69 parsecs) corresponds to a $\log g$ range of 5.2-5.5

or sources with infrared excesses whose age estimation might be affected by the effect of the disk on the apparent luminosity of the central object. This set of sources can be considered as a representative sample of the Class III population of Collinder 69 in the 0.014–1.15$M_{\odot}$ range of masses. From the 120 sources, the SEDs of three of them are best reproduced with models from the DUSTY collection (with temperatures below 2300 K), while for the remaining 117 the best fitting model always corresponds to either the NextGen or the Kurucz collection. Since different sets of isochrones and evolutionary tracks have to be applied when using the DUSTY models or the NextGen and Kurucz models, we will split our sample in two sets:

- For the three sources where the DUSTY models reproduce the best observed SEDs, we derive an upper-limit age of 5 Myr
- Among the remaining 117 sources, we find that while 90% of them are younger than 16 Myr, the 3rd quartile is located at 12.3 Myr; therefore we infer an upper-limit age for Collinder

69 of 12.3-16 Myr.

This final upper-limit of 12.3-16 Myr is consistent with the estimated ages for the cluster by other authors; for example the previously mentioned 5 Myr optimal age derived by Barrado y Navascués et al. (2007b) and the turn-off age for massive stars of 6–7 Myr from Dolan & Mathieu (2001).

A limitation of our methodology is that, since we are performing a fit with four free parameters, a minimum of six data-points in the observed SED is desirable (to avoid degeneracy). Another issue to take into account is that our results (mainly the derivation of the effective temperatures) are quite discrete, since the minimum step in temperature in the grid of models is 100K.

On the other hand, a great advantage is that the process followed is completely automatic; therefore, if a new (denser) grid of models is published, new observational data become available or new candidate members are detected, our determination of the age can be easily and quickly re-computed.

**Table 3.2**: Parameters derived for each individual source of the sample. For some of the sources, we have not been able to interpolate between the isochrones and evolutionary tracks (to infer ages and masses), because of their peculiar location in the HR diagram; we have grouped these sources in four possible categories according to the probable cause for this peculiar location (last column of the table, see footnotes for more details)

| ID | Model | $T_{eff}$ | logg | $F_{obs}/F_{Tot}$ | $L(L_\odot)$ | $\Delta L(L_\odot)$ | Age(Myr) | $M(M_\odot)$ | Note |
|---|---|---|---|---|---|---|---|---|---|
| LOri001 | Kurucz | 4000 | 3.5 | 0.48 | 9.52e-1 | 2.80e-3 | 3.0 | 1.1265 | - |
| LOri002 | NextGen | 3800 | 4.5 | 0.48 | 1.02e+0 | 3.18e-3 | 1.6 | 0.9508 | - |
| LOri003 | Kurucz | 4000 | 3.5 | 0.47 | 8.78e-1 | 2.55e-3 | 3.2 | 1.105 | - |
| LOri004 | Kurucz | 3750 | 4.0 | 0.48 | 8.23e-1 | 2.45e-3 | 1.7 | 0.8613 | - |
| LOri005 | NextGen | 4000 | 4.0 | 0.48 | 9.10e-1 | 2.73e-3 | 3.2 | 1.113 | - |
| LOri006 | Kurucz | 4000 | 3.5 | 0.47 | 7.66e-1 | 2.45e-3 | 4.0 | 1.0983 | - |
| LOri007 | Kurucz | 4000 | 4.5 | 0.48 | 6.61e-1 | 2.17e-3 | 5.0 | 1.0471 | - |
| LOri008 | Kurucz | 4000 | 3.5 | 0.48 | 7.44e-1 | 2.45e-3 | 4.0 | 1.0962 | - |
| LOri009 | NextGen | 4000 | 3.5 | 0.49 | 5.96e-1 | 1.88e-3 | 5.8 | 1.0505 | - |
| LOri010 | NextGen | 4200 | 4.0 | 0.48 | 5.73e-1 | 1.84e-3 | 10.0 | 1.1466 | - |
| LOri011 | NextGen | 3900 | 4.5 | 0.47 | 7.06e-1 | 2.33e-3 | 3.7 | 1.037 | - |
| LOri012 | NextGen | 4000 | 4.5 | 0.48 | 6.22e-1 | 2.00e-3 | 5.2 | 1.0544 | - |
| LOri013 | NextGen | 3700 | 4.5 | 0.49 | 6.12e-1 | 1.93e-3 | 2.3 | 0.7737 | - |
| LOri014 | Kurucz | 4000 | 4.5 | 0.49 | 5.37e-1 | 1.74e-3 | 6.4 | 1.0473 | - |
| LOri015 | Kurucz | 4000 | 3.5 | 0.49 | 5.60e-1 | 1.77e-3 | 6.3 | 1.0495 | - |
| LOri016 | Kurucz | 3750 | 4.5 | 0.47 | 5.06e-1 | 1.65e-3 | 3.4 | 0.8185 | - |
| LOri017 | NextGen | 4200 | 4.0 | 0.48 | 4.52e-1 | 1.36e-3 | 13.7 | 1.0499 | - |
| LOri018 | Kurucz | 3750 | 3.5 | 0.47 | 4.91e-1 | 1.51e-3 | 3.7 | 0.8153 | - |
| LOri019 | Kurucz | 3750 | 3.5 | 0.48 | 4.65e-1 | 1.52e-3 | 4.0 | 0.8102 | - |
| LOri020 | NextGen | 3600 | 4.5 | 0.48 | 4.86e-1 | 1.75e-3 | 2.0 | 0.624 | - |
| LOri021 | Kurucz | 4000 | 3.5 | 0.47 | 4.10e-1 | 1.33e-3 | 9.9 | 0.9998 | - |
| LOri022 | Kurucz | 3750 | 4.0 | 0.48 | 4.26e-1 | 1.29e-3 | 4.5 | 0.8043 | - |
| LOri023 | NextGen | 4000 | 4.5 | 0.47 | 4.08e-1 | 1.30e-3 | 10.0 | 0.9996 | - |
| LOri024 | Kurucz | 3750 | 3.5 | 0.48 | 4.11e-1 | 1.50e-3 | 4.9 | 0.8024 | - |
| LOri025 | NextGen | 3700 | 4.5 | 0.44 | 4.71e-1 | 2.25e-3 | 3.2 | 0.7504 | - |
| LOri026 | NextGen | 3700 | 4.5 | 0.48 | 4.30e-1 | 1.51e-3 | 3.7 | 0.75 | - |
| LOri027 | NextGen | 4000 | 4.5 | 0.48 | 3.51e-1 | 1.11e-3 | 12.5 | 0.9586 | - |
| LOri028 | Kurucz | 3750 | 4.0 | 0.49 | 2.93e-1 | 9.22e-4 | 7.4 | 0.7584 | - |
| LOri029 | NextGen | 3100 | 4.5 | 0.4 | 4.49e-1 | 1.27e-3 | | | [1] |
| LOri030 | NextGen | 3700 | 4.5 | 0.48 | 3.19e-1 | 1.11e-3 | 5.3 | 0.7237 | - |
| LOri031 | NextGen | 3800 | 4.5 | 0.47 | 3.25e-1 | 1.12e-3 | 7.7 | 0.8366 | - |
| LOri032 | NextGen | 3700 | 4.5 | 0.48 | 3.04e-1 | 1.05e-3 | 5.9 | 0.7128 | - |
| LOri033 | NextGen | 3700 | 4.5 | 0.46 | 3.17e-1 | 1.34e-3 | 5.3 | 0.7231 | - |
| LOri034 | NextGen | 3000 | 4.0 | 0.36 | 4.32e-1 | 1.08e-3 | | | [1] |

Continued on next page…

Table 3.2 – Continued

| ID | Model | $T_{eff}$ | logg | $F_{obs}/F_{Tot}$ | $L(L_\odot)$ | $\Delta L(L_\odot)$ | Age(Myr) | $M(M_\odot)$ | Note |
|---|---|---|---|---|---|---|---|---|---|
| LOri035 | NextGen | 3700 | 4.5 | 0.48 | 2.67e-1 | 9.09e-4 | 6.6 | 0.7005 | - |
| LOri036 | NextGen | 3600 | 4.5 | 0.49 | 2.49e-1 | 8.21e-4 | 5.0 | 0.5883 | - |
| LOri037 | NextGen | 3700 | 4.5 | 0.48 | 2.82e-1 | 9.78e-4 | 6.3 | 0.7033 | - |
| LOri038 | NextGen | 3800 | 4.5 | 0.4 | 2.55e-1 | 7.92e-4 | 10.1 | 0.8002 | - |
| LOri039 | NextGen | 3800 | 4.5 | 0.47 | 2.41e-1 | 8.26e-4 | 11.1 | 0.7997 | - |
| LOri040 | NextGen | 3600 | 4.5 | 0.48 | 2.56e-1 | 8.55e-4 | 5.0 | 0.5922 | - |
| LOri041 | NextGen | 3400 | 4.5 | 0.49 | 2.54e-1 | 8.89e-4 | 2.0 | 0.3932 | - |
| LOri042 | NextGen | 3800 | 4.5 | 0.47 | 2.22e-1 | 7.69e-4 | 12.6 | 0.7929 | - |
| LOri043 | NextGen | 3600 | 4.5 | 0.49 | 2.25e-1 | 7.95e-4 | 5.6 | 0.5744 | - |
| LOri044 | Kurucz | 3750 | 3.5 | 0.48 | 1.94e-1 | 6.37e-4 | 12.6 | 0.7261 | - |
| LOri045 | NextGen | 3600 | 4.5 | 0.49 | 2.07e-1 | 7.30e-4 | 6.3 | 0.5703 | - |
| LOri046 | NextGen | 3800 | 4.5 | 0.47 | 1.71e-1 | 5.72e-4 | 18.0 | 0.7508 | - |
| LOri047 | NextGen | 3400 | 4.5 | 0.47 | 2.03e-1 | 7.80e-4 | 2.5 | 0.3614 | - |
| LOri048 | NextGen | 3500 | 4.5 | 0.47 | 1.90e-1 | 7.20e-4 | 4.3 | 0.4516 | - |
| LOri049 | NextGen | 3800 | 4.5 | 0.47 | 1.52e-1 | 5.52e-4 | 20.4 | 0.7471 | - |
| LOri050 | NextGen | 3300 | 4.5 | 0.44 | 1.86e-1 | 6.76e-4 | 1.9 | 0.2996 | - |
| LOri051 | NextGen | 3700 | 4.5 | 0.48 | 1.44e-1 | 4.64e-4 | 15.8 | 0.6508 | - |
| LOri052 | NextGen | 3600 | 4.5 | 0.48 | 1.52e-1 | 5.03e-4 | 9.5 | 0.5604 | - |
| LOri053 | NextGen | 3600 | 4.5 | 0.48 | 1.40e-1 | 5.42e-4 | 10.0 | 0.5588 | - |
| LOri054 | NextGen | 3500 | 4.5 | 0.48 | 1.38e-1 | 4.66e-4 | 6.5 | 0.45 | - |
| LOri055 | NextGen | 3600 | 4.5 | 0.49 | 1.36e-1 | 5.28e-4 | 10.4 | 0.5584 | - |
| LOri056 | NextGen | 3400 | 4.5 | 0.47 | 1.27e-1 | 4.93e-4 | 4.6 | 0.35 | - |
| LOri057 | NextGen | 3400 | 4.5 | 0.46 | 1.07e-1 | 3.76e-4 | 5.9 | 0.35 | - |
| LOri058 | NextGen | 3500 | 4.5 | 0.49 | 9.87e-2 | 3.55e-4 | 10.5 | 0.4498 | - |
| LOri059 | NextGen | 3500 | 4.5 | 0.48 | 9.79e-2 | 3.84e-4 | 10.7 | 0.4498 | - |
| LOri060 | NextGen | 3500 | 4.5 | 0.49 | 9.28e-2 | 4.03e-4 | 12.2 | 0.4498 | - |
| LOri061 | NextGen | 3300 | 4.5 | 0.44 | 1.06e-1 | 3.54e-4 | 3.7 | 0.2753 | - |
| LOri062 | NextGen | 3500 | 4.5 | 0.46 | 9.20e-2 | 3.54e-4 | 12.3 | 0.4498 | - |
| LOri063 | NextGen | 3100 | 4.0 | 0.39 | 1.05e-1 | 3.37e-4 | 1.5 | 0.157 | - |
| LOri064 | NextGen | 3500 | 4.5 | 0.48 | 8.10e-2 | 3.05e-4 | 14.9 | 0.4496 | - |
| LOri065 | NextGen | 3400 | 4.5 | 0.49 | 7.76e-2 | 3.10e-4 | 9.6 | 0.3503 | - |
| LOri066 | NextGen | 3200 | 4.5 | 0.5 | 8.87e-2 | 3.66e-4 | 2.9 | 0.2098 | - |
| LOri067 | NextGen | 3500 | 4.5 | 0.49 | 6.44e-2 | 2.94e-4 | 19.9 | 0.4469 | - |
| LOri068 | NextGen | 3400 | 4.5 | 0.47 | 9.32e-2 | 3.52e-4 | 7.1 | 0.3501 | - |
| LOri069 | NextGen | 3200 | 4.5 | 0.5 | 1.04e-1 | 4.29e-4 | 2.4 | 0.2151 | - |
| LOri070 | NextGen | 3400 | 4.5 | 0.49 | 6.13e-2 | 2.78e-4 | 12.7 | 0.35 | - |
| LOri071 | NextGen | 3200 | 4.5 | 0.48 | 7.37e-2 | 2.98e-4 | 3.4 | 0.2028 | - |
| LOri072 | NextGen | 3100 | 4.5 | 0.43 | 9.69e-2 | 3.61e-4 | 1.6 | 0.1614 | - |
| LOri073 | NextGen | 3400 | 4.5 | 0.46 | 8.71e-2 | 3.15e-4 | 7.9 | 0.3502 | - |
| LOri074 | NextGen | 3300 | 4.5 | 0.49 | 8.33e-2 | 3.18e-4 | 4.9 | 0.2619 | - |
| LOri075 | NextGen | 3200 | 4.5 | 0.46 | 1.01e-1 | 3.72e-4 | 2.5 | 0.2144 | - |
| LOri076 | NextGen | 3400 | 4.5 | 0.48 | 5.31e-2 | 2.13e-4 | 15.8 | 0.3485 | - |
| LOri077 | NextGen | 3200 | 4.5 | 0.5 | 5.65e-2 | 2.57e-4 | 4.3 | 0.1965 | - |
| LOri078 | NextGen | 3300 | 4.5 | 0.48 | 5.28e-2 | 3.26e-4 | 8.1 | 0.2502 | - |
| LOri079 | NextGen | 3300 | 4.5 | 0.5 | 4.84e-2 | 2.43e-4 | 9.5 | 0.25 | - |
| LOri080 | NextGen | 3100 | 4.0 | 0.49 | 6.45e-2 | 2.56e-4 | 2.5 | 0.1519 | - |
| LOri081 | NextGen | 3200 | 4.5 | 0.42 | 4.91e-2 | 1.96e-4 | 5.0 | 0.1783 | - |
| LOri082 | NextGen | 3300 | 4.5 | 0.5 | 4.77e-2 | 2.34e-4 | 9.7 | 0.25 | - |
| LOri083 | NextGen | 3300 | 4.5 | 0.49 | 4.69e-2 | 2.41e-4 | 9.8 | 0.25 | - |
| LOri084 | NextGen | 3300 | 4.5 | 0.51 | 5.18e-2 | 2.36e-4 | 8.3 | 0.2501 | - |
| LOri085 | NextGen | 3100 | 4.5 | 0.43 | 5.32e-2 | 2.12e-4 | 3.1 | 0.1497 | - |
| LOri086 | NextGen | 3400 | 4.5 | 0.49 | 4.06e-2 | 2.04e-4 | 20.1 | 0.315 | - |
| LOri087 | NextGen | 3300 | 4.5 | 0.5 | 4.76e-2 | 2.49e-4 | 9.7 | 0.25 | - |
| LOri088 | NextGen | 3200 | 4.5 | 0.51 | 4.80e-2 | 2.64e-4 | 5.0 | 0.1762 | - |
| LOri089 | NextGen | 3300 | 4.5 | 0.5 | 4.04e-2 | 2.15e-4 | 11.7 | 0.2482 | - |
| LOri090 | NextGen | 3300 | 4.5 | 0.46 | 3.89e-2 | 1.83e-4 | 12.4 | 0.2471 | - |
| LOri091 | NextGen | 3100 | 4.0 | 0.49 | 4.72e-2 | 2.32e-4 | 3.2 | 0.1432 | - |
| LOri092 | NextGen | 3300 | 4.5 | 0.47 | 3.94e-2 | 1.92e-4 | 12.2 | 0.2475 | - |
| LOri093 | NextGen | 3300 | 4.5 | 0.49 | 3.91e-2 | 2.24e-4 | 12.3 | 0.2473 | - |
| LOri094 | NextGen | 3200 | 4.0 | 0.48 | 4.14e-2 | 2.10e-4 | 5.8 | 0.1743 | - |
| LOri095 | NextGen | 3300 | 4.5 | 0.5 | 3.53e-2 | 1.95e-4 | 12.8 | 0.243 | - |
| LOri096 | NextGen | 3100 | 4.5 | 0.44 | 3.66e-2 | 1.89e-4 | 4.0 | 0.1295 | - |
| LOri098 | NextGen | 3400 | 4.0 | 0.49 | 3.37e-2 | 2.09e-4 | 25.0 | 0.3 | - |
| LOri099 | NextGen | 3400 | 4.0 | 0.47 | 3.25e-2 | 1.64e-4 | 25.1 | 0.2998 | - |
| LOri100 | NextGen | 3300 | 4.5 | 0.46 | 3.10e-2 | 1.80e-4 | 15.7 | 0.2337 | - |
| LOri101 | NextGen | 3400 | 4.5 | 0.45 | 2.60e-2 | 1.49e-4 | 31.7 | 0.2989 | - |
| LOri102 | NextGen | 3200 | 4.0 | 0.48 | 3.27e-2 | 2.34e-4 | 7.6 | 0.1653 | - |
| LOri103 | NextGen | 3200 | 4.5 | 0.49 | 2.99e-2 | 1.50e-4 | 8.0 | 0.162 | - |
| LOri104 | NextGen | 3000 | 4.0 | 0.45 | 3.10e-2 | 1.54e-4 | 3.1 | 0.0899 | - |
| LOri105 | NextGen | 3200 | 4.0 | 0.49 | 2.51e-2 | 1.82e-4 | 10.0 | 0.1565 | - |
| LOri106 | NextGen | 3100 | 4.0 | 0.45 | 2.91e-2 | 1.92e-4 | 4.9 | 0.116 | - |

Continued on next page…

Table 3.2 – Continued

| ID | Model | $T_{eff}$ | logg | $F_{obs}/F_{Tot}$ | $L(L_{\odot})$ | $\Delta L(L_{\odot})$ | Age(Myr) | $M(M_{\odot})$ | Note |
|---|---|---|---|---|---|---|---|---|---|
| LOri107 | NextGen | 3000 | 3.5 | 0.49 | 3.14e-2 | 2.08e-4 | 3.1 | 0.0899 | - |
| LOri108 | NextGen | 3100 | 4.5 | 0.5 | 2.56e-2 | 1.75e-4 | 5.1 | 0.1103 | - |
| LOri109 | NextGen | 3200 | 4.5 | 0.52 | 2.28e-2 | 5.08e-5 | 11.2 | 0.1544 | - |
| LOri110 | NextGen | 3400 | 4.0 | 0.48 | 2.25e-2 | 1.74e-4 | 39.8 | 0.2947 | - |
| LOri111 | NextGen | 3000 | 4.0 | 0.5 | 2.66e-2 | 1.86e-4 | 3.4 | 0.0882 | - |
| LOri112 | NextGen | 3100 | 4.0 | 0.48 | 2.49e-2 | 1.77e-4 | 5.2 | 0.1101 | - |
| LOri113 | NextGen | 3200 | 4.5 | 0.49 | 1.99e-2 | 4.14e-5 | 12.7 | 0.1513 | - |
| LOri114 | NextGen | 3000 | 4.0 | 0.48 | 2.27e-2 | 1.73e-4 | 4.0 | 0.0822 | - |
| LOri115 | NextGen | 3300 | 4.5 | 0.48 | 1.64e-2 | 1.48e-4 | 31.4 | 0.2 | - |
| LOri116 | NextGen | 3200 | 4.0 | 0.47 | 1.75e-2 | 1.46e-4 | 15.6 | 0.1501 | - |
| LOri117 | NextGen | 3100 | 3.5 | 0.5 | 2.10e-2 | 4.51e-5 | 6.3 | 0.1096 | - |
| LOri118 | NextGen | 3000 | 4.0 | 0.43 | 1.99e-2 | 1.36e-4 | 4.3 | 0.08 | - |
| LOri119 | NextGen | 3100 | 4.0 | 0.54 | 1.79e-2 | 5.97e-5 | 7.8 | 0.1084 | - |
| LOri120 | NextGen | 3100 | 4.0 | 0.46 | 1.65e-2 | 1.38e-4 | 8.1 | 0.1072 | - |
| LOri121 | NextGen | 3200 | 4.5 | 0.48 | 1.34e-2 | 1.35e-4 | 20.0 | 0.1476 | - |
| LOri122 | NextGen | 3100 | 4.0 | 0.46 | 1.52e-2 | 1.37e-4 | 9.5 | 0.1057 | - |
| LOri124 | NextGen | 3200 | 4.0 | 0.45 | 1.30e-2 | 1.36e-4 | 20.4 | 0.1464 | - |
| LOri125 | NextGen | 3200 | 4.0 | 0.46 | 1.26e-2 | 1.40e-4 | 21.3 | 0.1452 | - |
| LOri126 | NextGen | 3000 | 4.5 | 0.5 | 1.35e-2 | 2.80e-5 | 6.2 | 0.0736 | - |
| LOri127 | DUSTY00 | 1900 | 4.5 | 0.74 | 6.04e-2 | 4.21e-4 | | | [2] |
| LOri128 | NextGen | 3100 | 4.0 | 0.49 | 1.26e-2 | 1.67e-4 | 11.9 | 0.1022 | - |
| LOri129 | NextGen | 3000 | 3.5 | 0.44 | 1.61e-2 | 1.48e-4 | 5.0 | 0.075 | - |
| LOri130 | NextGen | 3200 | 4.0 | 0.47 | 1.16e-2 | 1.23e-4 | 24.9 | 0.1439 | - |
| LOri131 | NextGen | 3000 | 3.5 | 0.5 | 1.39e-2 | 1.44e-4 | 6.1 | 0.0742 | - |
| LOri132 | NextGen | 3000 | 3.5 | 0.49 | 1.21e-2 | 1.53e-4 | 6.6 | 0.0723 | - |
| LOri133 | NextGen | 3800 | 3.5 | 0.43 | 7.85e-3 | 1.24e-4 | | | [2] |
| LOri134 | NextGen | 3100 | 3.5 | 0.49 | 1.17e-2 | 1.32e-4 | 12.6 | 0.1017 | - |
| LOri135 | NextGen | 3100 | 3.5 | 0.46 | 1.11e-2 | 1.38e-4 | 12.9 | 0.1015 | - |
| LOri136 | NextGen | 2900 | 3.5 | 0.5 | 1.24e-2 | 1.80e-4 | 5.0 | 0.0602 | - |
| LOri137 | NextGen | 4000 | 4.0 | 0.31 | 3.50e-3 | 3.94e-5 | | | [2] |
| LOri138 | NextGen | 3000 | 4.0 | 0.49 | 9.78e-3 | 1.28e-4 | 8.8 | 0.0738 | - |
| LOri139 | NextGen | 3000 | 4.0 | 0.49 | 8.50e-3 | 1.84e-5 | 10.1 | 0.0745 | - |
| LOri140 | NextGen | 2800 | 3.5 | 0.43 | 1.06e-2 | 1.23e-4 | 4.0 | 0.0405 | - |
| LOri141 | NextGen | 3100 | 4.0 | 0.5 | 5.69e-3 | 1.67e-5 | 36.8 | 0.1088 | - |
| LOri142 | NextGen | 3000 | 4.0 | 0.51 | 7.33e-3 | 1.92e-5 | 12.6 | 0.0749 | - |
| LOri143 | NextGen | 3000 | 4.0 | 0.53 | 7.43e-3 | 2.29e-5 | 12.6 | 0.0749 | - |
| LOri144 | NextGen | 3800 | 4.5 | 0.54 | 2.85e-3 | 4.29e-5 | | | [2] |
| LOri146 | NextGen | 2700 | 3.5 | 0.44 | 8.00e-3 | 1.32e-4 | | | [1] |
| LOri147 | NextGen | 3500 | 3.5 | 0.51 | 5.24e-3 | 2.00e-5 | | | [1] |
| LOri148 | NextGen | 3000 | 4.5 | 0.54 | 5.19e-3 | 1.63e-5 | 20.4 | 0.0756 | - |
| LOri149 | Kurucz | 3500 | 3.5 | 0.24 | 2.12e-3 | 4.22e-6 | | | [2] |
| LOri150 | NextGen | 2800 | 3.5 | 0.48 | 4.79e-3 | 1.31e-4 | 9.8 | 0.0472 | - |
| LOri151 | NextGen | 3200 | 4.5 | 0.51 | 2.81e-3 | 1.48e-5 | | | [2] |
| LOri152 | NextGen | 3500 | 3.5 | 0.5 | 3.26e-3 | 1.17e-4 | | | [2] |
| LOri153 | NextGen | 2900 | 4.5 | 0.52 | 3.49e-3 | 1.38e-5 | 25.1 | 0.0659 | - |
| LOri154 | NextGen | 2700 | 3.5 | 0.48 | 4.17e-3 | 1.20e-4 | 7.9 | 0.0315 | - |
| LOri155 | NextGen | 2700 | 4.5 | 0.53 | 3.63e-3 | 1.11e-5 | 9.4 | 0.0336 | - |
| LOri156 | COND00 | 1500 | 3.5 | 0.54 | 3.20e-3 | 1.43e-5 | | | [1] |
| LOri157 | NextGen | 3700 | 3.5 | 0.47 | 1.54e-3 | 9.04e-6 | | | [2] |
| LOri158 | NextGen | 3900 | 3.5 | 0.45 | 1.18e-3 | 8.72e-6 | | | [2] |
| LOri159 | NextGen | 3000 | 4.5 | 0.49 | 1.28e-3 | 1.17e-5 | | | [2] |
| LOri160 | NextGen | 2700 | 3.5 | 0.5 | 1.65e-3 | 1.02e-5 | 31.6 | 0.0467 | - |
| LOri161 | NextGen | 2600 | 4.5 | 0.52 | 1.77e-3 | 1.37e-5 | 16.0 | 0.0308 | - |
| LOri162 | COND00 | 1600 | 3.5 | 0.6 | 1.71e-3 | 2.37e-5 | | | [4] |
| LOri163 | DUSTY00 | 2000 | 4.0 | 0.55 | 1.65e-3 | 2.13e-5 | 1.0 | 0.006 | - |
| LOri164 | NextGen | 3800 | 3.5 | 0.45 | 7.29e-4 | 5.92e-6 | | | [2] |
| LOri165 | DUSTY00 | 2500 | 3.5 | 0.51 | 7.50e-4 | 1.50e-5 | 85.3 | 0.048 | [2] |
| LOri166 | DUSTY00 | 2200 | 4.5 | 0.43 | 9.35e-4 | 6.94e-6 | 4.7 | 0.0136 | - |
| LOri167 | DUSTY00 | 2000 | 3.5 | 0.51 | 1.35e-3 | 1.85e-5 | 1.0 | 0.006 | [*] |
| LOri168 | NextGen | 2900 | 4.0 | 0.45 | 3.99e-4 | 7.44e-6 | | | [2] |
| LOri169 | NextGen | 3100 | 4.5 | 0.45 | 2.21e-4 | 6.63e-6 | | | [3] |
| LOri170 | NextGen | 3500 | 3.5 | 0.45 | 1.99e-4 | 8.21e-6 | | | [2] |

Continued on next page…

Table 3.2 – Continued

| ID | Model | $T_{eff}$ | logg | $F_{obs}/F_{Tot}$ | $L(L_\odot)$ | $\Delta L(L_\odot)$ | Age(Myr) | $M(M_\odot)$ | Note |
|---|---|---|---|---|---|---|---|---|---|

This whole section has been included to illustrate the advantages of using this methodology to analyze large lists of candidate members to star forming regions. VOSA turns out to be specially useful when the wavelength coverage of the candidate members is inhomogeneus (not the same photometric bands are available for all the candidates).

One of the caveats on the other hand can arise from the nature of the datasets themselves; for example, in our case, where Strömgrem photometry is not available for any of our candidates (candidates from the surveys described in the previous Chapter); VOSA fits are quite insensitive to the logg parameter. In order to be consistent during this thesis we have repeated the VOSA fits of the CFHT sample forcing for logg a value of 4.0 dex (as can be seen in the $T_{eff}$ and $L_{bol}$ listed on Table 3.25 the differences are no dramatic at all). The same constrain is applied to every candidate member to derive the values of $T_{eff}$ and $L_{bol}$ listed on Table 3.25.

## 3.2 Previous Spectroscopic Surveys

As mentioned in the Introduction, several spectroscopic surveys have been carried out targeting the LOSFR, and in particular its central cluster Collinder 69. Here we summarize the most relevant results obtained so far:

Combining previous H$\alpha$ objective prism observations of the LOSFR with their own 100 square degree survey(50% completeness at 17.0 mag in the V band), Duerr et al. (1982) tabulated ~100 stars detected to have H$\alpha$ emission in one or more of these observations (for every case in which a star was bright enough for study, it had also been found in the literature to be variable photometrically, see Duerr et al. 1982 for details).

In the last eight years deeper but spatially limited H$\alpha$ surveys have been performed. Dolan & Mathieu (2001) found 23 new stars with H$\alpha$ equivalent widths greater than 10 Å; all but two are associated with the B30 and B35 clouds. On the other hand, strong H$\alpha$ emission has also been detected from candidate substellar members (in this case to C69) in the very deep survey for young stars of Barrado y Navascués et al. (2004b). They suggest that three such stars have such large EW(H$\alpha$), 73 Å to 123 Å, as to be candidates for active accretion disks.

[1] Source with disk.

[2] Previous "non-member" candidates according to the photometric properties (see Barrado y Navascués et al. 2007b for further details).

[3] Degenerated fit due the small number of points to be fitted vs number of free parameters.

[4] Possible foreground cool source.

(see Section 3.1.3 for details on each individual case).

[*] For a more detailed analysis in LOri167 see Barrado y Navascués et al. (2007a).

Regarding diagnosis on youth and kinematics; Dolan & Mathieu (2001) surveyed 11 $1^o$-diameter fields located radially across the SFR, with an emphasis on the regions in which H$\alpha$ emission stars were found by Duerr et al. (1982). The observations were done with the WIYN Hydra Multi-Object Spectrograph achieving ~90% completeness in all but two fields. They obtained 4177 spectra of 3618 stars. Each spectrum was centered at 6640 Å, and thus included the Li I $\lambda$6707 Å and H$\alpha$ lines, and a rich array of metal lines near 6450 Å for precise radial velocity measurements. With a resolution R~20000 and a typical SNR per pixel of 25-40, lithium absorption could be detected to a minimum equivalent width of 0.1 Å with 5$\sigma$ confidence, and the radial-velocity precision was 0.5 km/s.

Lithium absorption was detected in ~650 stars, of which, less than half showed strong lithium absorption indicative of youth (defined as EW(Li) $\geq$ 0.2 Å). As mentioned before, one of their main result states that those stars with strong Li I absorption are kinematically associated, and their mean velocity of 24.5 km/s is typical of the Orion association.

Finally, during the last year, Sacco et al. (2008) and Maxted et al. (2008) published their results on the comparative analysis of high resolution spectra of two samples of low-mass young stars. One sample was composed by candidate members to C69 and the other one by candidate members to the $\sigma$ Ori cluster (with estimated ages 1–8 Myrs). While their main results have already been described in the Introduction, in this section we will focus on the redundancy of those surveys with our own survey (coincident sources are shown in Table 3.3 and Table 3.4 along with the measurements and parameters provided by Maxted et al. 2008 and Sacco et al. 2008, respectively).

Maxted et al. (2008) obtained several spectra (from three to seven) with SNR better than five for 73 candidate members from those proposed by Barrado y Navascués et al. (2004b). The observations were performed with the FLAMES multi-object spectrograph (Pasquini et al. 2002) with a resolution of R~16000 and a wavelength coverage from 8073 to 8632 Å. They studied binarity and membership to C69 based on radial velocity determinations and analysis of the Na I $\lambda$8200 lines and TiO band strength. Comparison with our results will be provided in Section 3.3.

On the other hand, Sacco et al. (2008), observed 49 sources in the $\lambda$ Ori cluster: five candidate members from Dolan & Mathieu (1999), 34 from Barrado y Navascués et al. (2004b), and ten candidates listed in both studies. From the 44 sources in common with Barrado y Navascués et al. (2004b) 31 were also observed by Maxted et al. (2008) (see last column of Table 3.3). These authors based their study on observations that were as well performed with FLAMES but with a different set-up. They observed the C69 candidates with two different gratings, achieving resolutions of R~17000 and R~16200 for the spectral ranges 6470–6790 Å and 8480–9000 Å, respectively. Radial velocities, Li absorption and H$\alpha$ emission were used to establish membership, and H$\alpha$ and other optical emission lines to study the accretion properties of the members. Comparison with our sample and results will be provided in the following sections.

**Table 3.3**: Physical properties derived by Maxted et al. (2008) for a sample of the Colinder 69 candidate members from Barrado y Navascués et al. (2004b). Sources also observed by Sacco et al. (2008) are marked in the last column.

| Name | MJO2008 | <RV> | eRV | EW(NaI) | eEW(NaI) | TiO(8442) | eTiO | SB Type | S08 |
|---|---|---|---|---|---|---|---|---|---|
| LOri039 | J053557.0+094652 | 28.7 | 0.37 | 2.34 | 0.01 | 0.677 | 0.0010 | | |
| LOri040 | J053539.4+095032 | 27.44 | 0.38 | 2.34 | 0.02 | 0.667 | 0.0020 | | x |
| LOri041 | J053530.4+095034 | 28.98 | 0.44 | 2.33 | 0.01 | 0.668 | 0.0010 | | x |
| LOri043 | J053502.7+095647 | 30.06 | 1.01 | 2.33 | 0.02 | 0.663 | 0.0010 | SB2 | |
| LOri044 | J053408.3+095125 | 6.52 | 0.34 | 2.61 | 0.02 | 0.637 | 0.0010 | | |
| LOri046 | J053426.0+095149 | -0.65 | 0.34 | 2.85 | 0.01 | 0.657 | 0.0010 | | x |
| LOri047 | J053555.6+095053 | 27.26 | 0.39 | 2.53 | 0.02 | 0.682 | 0.0020 | | |
| LOri048 | J053512.5+095311 | 27.71 | 0.56 | 2.21 | 0.02 | 0.663 | 0.0010 | | x |
| LOri049 | J053500.9+094936 | 23.47 | 0.34 | 2.87 | 0.02 | 0.642 | 0.0020 | | x |
| LOri050 | J053456.3+095504 | 26.2 | 2.32 | 2.21 | 0.01 | 0.656 | 0.0010 | SB1 | x |
| LOri051 | J053612.1+100056 | 28.66 | 2.68 | 2.23 | 0.1 | 0.666 | 0.0080 | SB1 | |
| LOri052 | J053411.7+095703 | 36.31 | 0.73 | 2.6 | 0.02 | 0.645 | 0.0020 | | |
| LOri053 | J053436.7+095258 | 27.49 | 0.35 | 2.27 | 0.02 | 0.661 | 0.0020 | | x |
| LOri054 | J053552.5+094831 | 29.46 | 0.38 | 2.52 | 0.02 | 0.685 | 0.0020 | | |
| LOri055 | J053521.4+094956 | 26.66 | 0.26 | 2.53 | 0.02 | 0.658 | 0.0010 | | x |
| LOri056 | J053458.3+095347 | 26.64 | 0.35 | 2.35 | 0.02 | 0.689 | 0.0020 | | x |
| LOri058 | J053610.3+100018 | 30.06 | 0.57 | 2.78 | 0.09 | 0.688 | 0.0090 | | |
| LOri059 | J053423.5+094343 | 29.8 | 0.36 | 2.68 | 0.03 | 0.683 | 0.0020 | | |
| LOri060 | J053520.0+094906 | 27.24 | 0.26 | 2.2 | 0.02 | 0.654 | 0.0020 | | x |
| LOri061 | J053518.1+095224 | 26.88 | 0.42 | 2.22 | 0.02 | 0.659 | 0.0020 | | x |
| LOri062 | J053515.3+094837 | 26.87 | 0.27 | 2.23 | 0.02 | 0.674 | 0.0020 | | x |
| LOri063 | J053519.1+095442 | 26.42 | 0.44 | 2.0 | 0.07 | 0.61 | 0.0060 | | x |
| LOri064 | J053552.0+095029 | 28.07 | 0.38 | 2.78 | 0.03 | 0.672 | 0.0020 | | |
| LOri065 | J053517.9+095657 | 27.15 | 0.29 | 2.39 | 0.02 | 0.683 | 0.0020 | | |
| LOri066 | J053506.7+095727 | 28.9 | 0.35 | 2.84 | 0.02 | 0.73 | 0.0030 | | |
| LOri067 | J053626.3+094546 | 27.44 | 0.4 | 2.37 | 0.03 | 0.681 | 0.0040 | | |
| LOri068 | J053448.0+094326 | 30.35 | 0.35 | 2.84 | 0.02 | 0.688 | 0.0020 | | x |
| LOri069 | J053443.9+094835 | 22.56 | 3.48 | 2.66 | 0.02 | 0.732 | 0.0020 | SB2 | x |
| LOri073 | J053446.8+095037 | 27.57 | 0.35 | 2.5 | 0.02 | 0.69 | 0.0020 | | |
| LOri074 | J053600.5+094238 | 27.63 | 0.38 | 2.64 | 0.03 | 0.719 | 0.0030 | | |
| LOri075 | J053455.2+100034 | 27.92 | 2.2 | 2.37 | 0.02 | 0.71 | 0.0020 | SB1 | x |
| LOri076 | J053510.9+095743 | 28.53 | 0.38 | 2.38 | 0.04 | 0.718 | 0.0030 | | x |
| LOri077 | J053441.7+094242 | 29.93 | 0.46 | 2.97 | 0.03 | 0.707 | 0.0030 | | |
| LOri078 | J053616.4+095015 | 27.76 | 0.39 | 2.43 | 0.04 | 0.686 | 0.0040 | | |
| LOri079 | J053448.2+095953 | 27.38 | 0.36 | 2.53 | 0.03 | 0.695 | 0.0030 | | x |
| LOri080 | J053530.0+095925 | 29.44 | 1.36 | 2.73 | 0.15 | 0.739 | 0.017 | | x |
| LOri082 | J053600.8+095257 | 27.4 | 0.66 | 2.78 | 0.04 | 0.702 | 0.0040 | | |
| LOri083 | J053543.4+095426 | 25.94 | 0.42 | 2.46 | 0.04 | 0.701 | 0.0040 | | x |
| LOri085 | J053521.5+095329 | 27.35 | 0.29 | 2.64 | 0.03 | 0.706 | 0.0030 | | |
| LOri086 | J053411.5+094914 | 30.01 | 0.44 | 2.53 | 0.04 | 0.689 | 0.0040 | | |
| LOri087 | J053433.7+095534 | 27.07 | 0.36 | 2.52 | 0.03 | 0.687 | 0.0030 | | x |
| LOri088 | J053449.5+095846 | 27.44 | 0.36 | 2.86 | 0.04 | 0.73 | 0.0040 | | x |
| LOri090 | J053627.0+095134 | 26.75 | 0.43 | 2.77 | 0.07 | 0.725 | 0.0080 | | |
| LOri091 | J053435.8+095426 | 28.32 | 0.39 | 2.92 | 0.03 | 0.761 | 0.0040 | | |
| LOri092 | J053550.9+095103 | 27.55 | 0.4 | 2.5 | 0.04 | 0.711 | 0.0040 | | x |
| LOri093 | J053441.1+095016 | 27.8 | 0.36 | 2.74 | 0.04 | 0.69 | 0.0040 | | x |
| LOri094 | J053443.1+100159 | 30.51 | 0.8 | 2.68 | 0.04 | 0.728 | 0.0050 | | x |
| LOri095 | J053524.1+095515 | 27.36 | 0.46 | 2.4 | 0.08 | 0.707 | 0.0080 | | x |
| LOri096 | J053511.1+095719 | 27.98 | 0.38 | 2.39 | 0.04 | 0.701 | 0.0040 | | x |
| LOri098 | J053631.4+094501 | 28.17 | 0.41 | 2.95 | 0.06 | 0.739 | 0.0070 | | |
| LOri100 | J053500.0+094614 | 29.51 | 0.37 | 2.85 | 0.05 | 0.718 | 0.0050 | | x |
| LOri102 | J053522.0+095252 | 28.62 | 0.29 | 2.79 | 0.04 | 0.719 | 0.0040 | | x |
| LOri103 | J053522.5+094501 | 28.04 | 0.36 | 2.67 | 0.04 | 0.749 | 0.0050 | | |
| LOri104 | J053507.0+095401 | 27.87 | 0.38 | 2.69 | 0.05 | 0.737 | 0.0060 | | |
| LOri105 | J053417.5+095229 | 27.08 | 0.4 | 2.9 | 0.05 | 0.728 | 0.0060 | | x |
| LOri106 | J053528.7+095410 | 27.15 | 0.3 | 2.61 | 0.05 | 0.785 | 0.0060 | | x |
| LOri107 | J053555.1+095219 | 28.64 | 0.46 | 2.5 | 0.06 | 0.868 | 0.0090 | | |
| LOri109 | J053408.5+095043 | 28.1 | 0.44 | 2.71 | 0.06 | 0.741 | 0.0070 | | |
| LOri110 | J053532.6+095248 | 13.44 | 0.5 | 3.59 | 0.04 | 0.699 | 0.0040 | | |
| LOri114 | J053618.1+095225 | 27.15 | 0.47 | 2.72 | 0.08 | 0.776 | 0.011 | | |
| LOri116 | J053512.0+100104 | 27.02 | 0.5 | 3.12 | 0.08 | 0.764 | 0.01 | | |
| LOri118 | J053524.3+095351 | 27.55 | 0.37 | 2.58 | 0.06 | 0.773 | 0.0080 | | |
| LOri120 | J053446.2+095537 | 27.85 | 0.42 | 2.77 | 0.07 | 0.805 | 0.0090 | | |
| LOri122 | J053435.4+095118 | 29.97 | 0.68 | 3.08 | 0.07 | 0.744 | 0.0080 | | |
| LOri125 | J053414.2+094826 | 30.76 | 0.57 | 3.26 | 0.08 | 0.732 | 0.0090 | | |
| LOri126 | J053539.8+095324 | 27.02 | 0.65 | 2.56 | 0.11 | 0.776 | 0.013 | | |
| LOri129 | J053609.8+094237 | 27.11 | 0.48 | 2.72 | 0.09 | 0.8 | 0.012 | | |
| LOri130 | J053456.5+094233 | 30.09 | 0.47 | 3.33 | 0.1 | 0.722 | 0.01 | | |
| LOri131 | J053606.9+095251 | 28.28 | 0.5 | 3.32 | 0.09 | 0.895 | 0.015 | | |

Continued on next page…

Table 3.3 – Continued

| Name | MJO2008 | <RV> | eRV | EW(NaI) | eEW(NaI) | TiO(8442) | eTiO | SB Type | S08 |
|---|---|---|---|---|---|---|---|---|---|
| LOri135 | J053509.3+095244 | 27.81 | 0.42 | 3.35 | 0.09 | 0.816 | 0.013 | | |
| LOri140 | J053419.2+094827 | 27.36 | 0.51 | 2.59 | 0.12 | 0.85 | 0.021 | | |
| LOri143 | J053500.9+095820 | 26.06 | 0.66 | 2.55 | 0.16 | 0.84 | 0.023 | | |
| LOri146 | J053500.1+095240 | 28.53 | 0.66 | 3.08 | 0.17 | 0.824 | 0.028 | | |

**Table 3.4**: Sacco et al. (2008) measurements derived for 49 of the Barrado y Navascués et al. (2004b) candidate members.

| Name | SpT | <RV> eRV | vsini+E-e | EW(Li) | Bin. | EW(H$\alpha$) | $FW_{10\%}$ | log($M_{acc}$) | EW(NII) | EW(HeI) | EW(SII[1]) | EW(SII[2]) | ID |
|---|---|---|---|---|---|---|---|---|---|---|---|---|---|
| LOri003 | K8.5 | | | 520±32 | SB | -1.13 ±0.15 | | | <0.04 | <0.04 | <0.04 | <0.04 | L01 |
| LOri016 | K8.0 | | | 531±33 | SB | -1.58 ±0.13 | | | <0.03 | <0.03 | <0.03 | <0.03 | L03 |
| LOri020 | M2.0 | 21.43±0.53 | | 18 ±29 | | | | | | | | | L05 |
| LOri022 | M1.5 | 28.4 ±0.38 | <17.0 | 516±33 | | -6.96 ±0.69 | 219±43 | | <0.03 | 0.12 | <0.03 | <0.03 | L06 |
| LOri024 | M0.0 | 27.28±0.29 | <17.0 | 554±21 | | -2.0 ±0.12 | 137±20 | | <0.05 | <0.05 | <0.05 | <0.05 | L07 |
| LOri026 | K9.5 | 27.29±0.43 | 26.0+6.0-1.0 | 581±43 | | -5.3 ±0.3 | 198±18 | | <0.03 | <0.03 | <0.03 | <0.03 | L08 |
| LOri030 | M1.5 | | | | SB2 | | | | | | | | L10 |
| LOri034 | M1.0 | 24.36±0.3 | <17.0 | 541±35 | | -8.47 ±0.47 | 215±25 | -10.8±0.4 | <0.06 | <0.06 | <0.06 | <0.06 | L11 |
| LOri035 | M2.5 | 21.36±0.72 | 30.2+10.0-6.2 | 572±21 | | -3.32 ±0.35 | 146±34 | | <0.06 | <0.06 | <0.06 | <0.06 | L12 |
| LOri036 | M3.0 | 24.63±0.38 | | 56 ±22 | | | | | | | | | L13 |
| LOri037 | M2.0 | 27.13±0.33 | <17.0 | 566±57 | | -3.67 ±0.34 | 148±29 | | <0.06 | <0.06 | <0.06 | <0.06 | L14 |
| LOri040 | M3.0 | 26.95±0.46 | <21.3 | 561±45 | | -5.15 ±0.62 | 141±18 | | <0.08 | <0.08 | <0.08 | <0.08 | L15 |
| LOri041 | M3.5 | 27.05±0.71 | 61.9+11.8-5.7 | 485±40 | | -7.05 ±0.86 | 306±52 | | <0.06 | <0.06 | <0.06 | <0.06 | L16 |
| LOri045 | M2.0 | 26.89±0.42 | <17.0 | 554±23 | | -3.04 ±0.33 | 123±27 | | <0.08 | <0.08 | <0.08 | <0.08 | L18 |
| LOri046 | M2.0 | -0.28±0.43 | | 148±64 | | | | | | | | | L19 |
| LOri048 | M2.5 | 27.04±0.44 | <17.0 | 545±12 | | -3.34 ±0.44 | 159±36 | <-11.0 | <0.08 | <0.08 | <0.08 | <0.08 | L20 |
| LOri049 | M2.0 | 24.06±0.36 | | 64 ±13 | | | | | | | | | L21 |
| LOri050 | M2.5 | | | 596±58 | SB | -11.14±0.96 | ± | | <0.09 | <0.15 | <0.09 | <0.09 | L22 |
| LOri053 | M2.5 | 27.0 ±0.42 | <18.3 | 561±30 | | -2.93 ±0.2 | 130±22 | | <0.09 | <0.09 | <0.09 | <0.09 | L24 |
| LOri055 | M2.5 | 26.7 ±0.39 | <17.0 | 602±33 | | -6.53 ±0.49 | 118±13 | | <0.09 | <0.09 | <0.09 | <0.09 | L25 |
| LOri056 | M3.0 | 26.84±0.56 | <19.3 | 576±23 | | -5.57 ±0.81 | 130±13 | | <0.1 | 0.15 | <0.1 | <0.1 | L26 |
| LOri057 | M3.5 | 26.99±0.49 | <17.0 | 677±19 | | -5.2 ±0.52 | 107±11 | | <0.1 | 0.2 | <0.1 | <0.1 | L27 |
| LOri060 | M2.5 | 27.22±0.45 | <18.5 | 599±28 | | -4.18 ±0.48 | 121±18 | | <0.08 | <0.08 | <0.08 | <0.08 | L28 |
| LOri061 | M2.5 | 26.8 ±0.47 | 17.9+1.4-1.8 | 591±30 | | -13.97±1.38 | 274±15 | -10.2±0.3 | <0.1 | 0.18 | <0.1 | <0.1 | L29 |
| LOri062 | M3.0 | 26.8 ±0.47 | <17.0 | 648±48 | | -4.41 ±0.3 | 123±22 | <-11.0 | <0.1 | <0.1 | <0.1 | <0.1 | L30 |
| LOri068 | M3.0 | 29.37±0.47 | <17.0 | 698±25 | | -7.9 ±1.26 | 116±16 | | <0.1 | <0.15 | <0.1 | <0.1 | L31 |
| LOri069 | M3.5 | | | 516±57 | SB | -7.39 ±1.46 | ± | | <0.1 | <0.1 | <0.1 | <0.1 | L32 |
| LOri075 | M5.0* | 26.02±0.82 | 61.3+11.5-4.9 | 455±44 | | -10.71±0.98 | 326±9 | | <0.1 | <0.1 | <0.1 | <0.1 | L33 |
| LOri063 | M3.0 | 27.19±0.47 | <18.2 | 505±52 | | -19.14±2.53 | 230±4 | -10.7±0.3 | 3.6 | 0.8 | 0.26 | 0.31 | L34 |
| LOri076 | M3.0 | 27.52±0.5 | <17.0 | 608±19 | | -4.92 ±0.6 | 121±20 | | <0.1 | <0.1 | <0.1 | <0.1 | L35 |
| LOri079 | M3.0 | 27.03±0.51 | <17.0 | 607±59 | | -5.06 ±0.53 | 127±25 | <-11.0 | <0.1 | <0.2 | <0.1 | <0.1 | L36 |
| LOri080 | M3.0 | 25.74±0.81 | 60.2+21.3-5.9 | 523±20 | | -14.47±1.25 | 287±41 | -10.1±0.5 | 0.1 | <0.1 | <0.1 | <0.1 | L37 |
| LOri083 | M3.0 | 26.32±0.57 | 19.1+7.9-2.6 | 585±77 | | -5.32 ±0.68 | 134±16 | | <0.1 | 0.1 | <0.1 | <0.1 | L38 |
| LOri087 | M4.5* | 27.25±0.57 | 18.4+6.0-1.7 | 609±42 | | -5.56 ±0.7 | 125±18 | <-11.0 | <0.1 | <0.2 | <0.1 | <0.1 | L39 |
| LOri088 | M3.5 | 26.75±0.53 | <17.0 | 660±42 | | -9.44 ±1.12 | 107±13 | | <0.1 | 0.17 | <0.1 | <0.1 | L40 |
| LOri092 | M3.5 | 26.66±0.57 | 19.8+2.8-2.6 | 661±51 | | -2.9 ±0.34 | 107±29 | | 0.14 | <0.1 | <0.1 | <0.1 | L41 |
| LOri093 | M3.5 | 27.0 ±0.56 | <18.3 | 623±61 | | -6.25 ±0.94 | 137±29 | | <0.1 | 0.15 | <0.1 | <0.1 | L42 |
| LOri094 | M4.0 | 26.36±0.8 | 54.8+5.5-8.2 | 538±204 | | -15.53±2.23 | 228±18 | | <0.2 | <0.2 | <0.2 | <0.2 | L43 |
| LOri095 | M6.0* | 27.31±0.55 | <19.7 | 559±30 | | -4.96 ±0.62 | 105±9 | | <0.25 | <0.25 | <0.25 | <0.25 | L44 |
| LOri096 | M3.5 | 26.92±0.55 | <19.1 | 553±48 | | -6.97 ±1.1 | 114±20 | <-11.0 | 0.22 | <0.2 | <0.2 | <0.2 | L45 |
| LOri100 | M3.5 | 28.04±0.46 | <17.0 | 717±43 | | -8.18 ±1.4 | 98 ±6 | | 0.6 | <0.25 | 0.59 | <0.25 | L46 |
| LOri102 | M4.0 | 28.1 ±0.53 | <17.0 | 584±62 | | -5.94 ±0.96 | 93 ±4 | | 0.25 | <0.1 | 0.25 | 0.16 | L47 |
| LOri105 | M4.0 | 26.45±0.7 | <20.0 | | | | | | | | | | L48 |
| LOri106 | M4.0 | 26.83±0.54 | <17.0 | 636±132 | | -26.16±2.4 | 107±4 | <-11.0 | 0.7 | 0.4 | 0.4 | 0.3 | L49 |

Li I equivalent width in mÅ; the remaining EWs are given in Å, mean $v_r$ and $FW_{10\%}$(H$\alpha$) in km/s and accretion rates in $M_\odot$/yr.

[1] [SII] at 6716Å

[2] [SII] at 67131Å

[*] Spectral type spectroscopically derived by Barrado y Navascués et al. (2004b). The remainig spectral types have been photometrically determined by Sacco et al. (2008).

**Table 3.5**: Collinder 69 optical spectroscopic campaigns.

| Date | Observatory/Telescope/Instrument | Resolution | Wavelength coverage | Number of sources observed | Original photometric survey |
|---|---|---|---|---|---|
| November 2-5, 2002 | Mauna Kea / Keck I / LRIS | ~2650 | 6425–7692Å | 12 | CFHT1999 |
| November 2-5, 2002 | Mauna Kea / Keck I / LRIS | ~ 950 | 6250–9600Å | 29 | CFHT1999 |
| December 11-14, 2002 | Las Campanas / Magellan Baade / MIKE | ~11250 | 4430–7250Å | 14 | CFHT1999 |
| March 9-11, 2003 | Las Campanas / Magellan II / B&C | ~2600 | 6200–7825Å | 2 | CFHT1999 |
| March 9-11, 2003 | Las Campanas / Magellan II / B&C | ~800 | 5000–10200Å | 3 | CFHT1999 |
| November 22-25, 2005 | CAHA / 3.5m / TWIN | ~1100 | 5600–10425Å | 5 | CFHT1999 |
| November 20-23, 2006 | CAHA / 3.5m / TWIN | ~1100 | 5700–9900Å | 8 | CFHT1999 & $1^o \times 1^o$ Spitzer |
| Nov. 30 - Dec. 11, 2007 | CAHA / 2.5m /CAFOS | ~600 | 6200–10350Å | 37 | CFHT1999 & $1^o \times 1^o$ Spitzer & *XMM-Newton* survey |
| January 5, 2008 | Paranal / UT2/FLAMES | ~8600 | 6438–7184Å | 40 | CFHT1999 & $1^o \times 1^o$ Spitzer |

## 3.3 Our optical spectroscopic surveys

During the last seven years, our group has been granted with time in different observatories to perform spectroscopic observations of our photometrically-selected candidate members to the different associations within the Lambda Orionis Star Forming Region. These observations comprise a wide range of resolutions and wavelength coverages.

The highest resolution spectra were obtained in order to study the H$\alpha$ emission of the sources (and its relation with accretion processes), other emission lines such as He I and some forbidden lines (commonly used as tracers of mass loss), and the presence of Li I absorption (confirming the youth of the sources). On the other hand, lower resolution optical spectra were obtained for fainter sources to derive spectral types and study their surface gravity. As a byproduct we have been able to study the biases introduced when measuring line profiles (such as H$\alpha$) at different resolutions.

In Appendix A we provide details on the data reduction procedures carried out for each specific technical set-up; while, in Table 3.5, some of the most relevant specifications characterizing the observations are summarized.

In the following subsections we will describe the different kinds of analyses that we have been able to perform depending on the characteristics of the observational data. Most of these analyses are based on the measurement of parameters of the lines such as their equivalent width, full width half maximum and full width at 10% of the maximum. In order to ease this process we have developed a code that, given the approximate center of the line, the resolution of the spectra and the uncertainty in the wavelength calibration, provides the user with the mean of three measurements of each the previously mentioned EW, FWHM and $FW_{10\%}$ (as well as a $\sigma$ for the derived values) in an automatic manner (see Appendix B for details on the process).

### 3.3.1 Spectral type determination based on molecular bands.

We have followed two different approaches to determine the spectral types of our candidate members. For the hotter part of the sample (a fraction of the XMM candidates), we have compared our optical (low resolution, CAFOS) spectra with those obtained (with the same con-

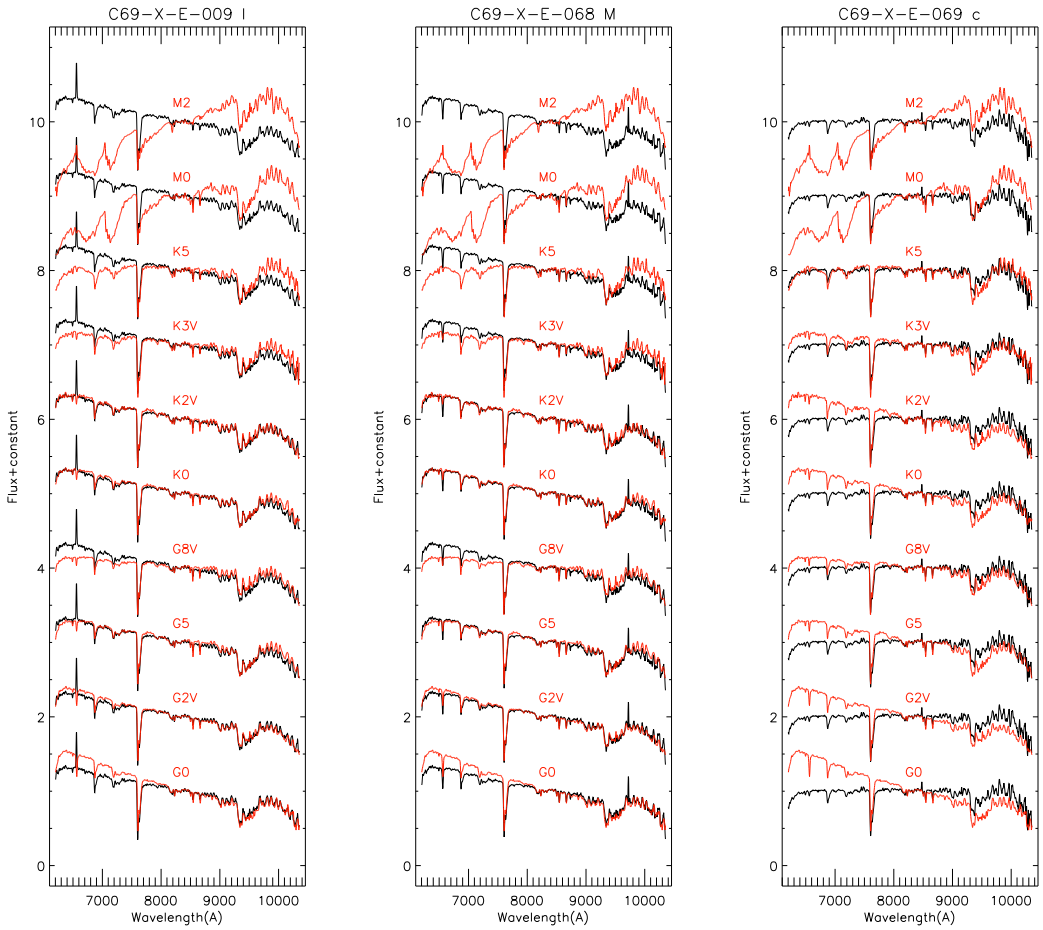


**Figure 3.7**: Spectral type determination for three candidate members by comparison with templates obtained with the same instrumental set-up. The "science spectra" is displayed in black and the templates (labelled according to the spectral type) in red.

figuration during the same campaigns) as templates from Taurus members and also field dwarfs within a spectral type range of G0 to M0. Since the extinction is quite low and homogeneous in Collinder 69, the comparison with the templates is very direct. In Fig 3.7 we show as examples of these comparisons three K-type stars candidate members.

On the other hand, for the majority of our candidates (in principle with $T_{eff}$ derived from their SEDs consistent with being M type stars) we have inferred their spectral types studying their molecular bands. Several spectral ratios or indices (quantifying different band strengths) have been proposed in the literature to derive spectral types both, from optical and infrared spectra. From those oriented to classify for late-type stars, some are based on the relative depths of the mentioned molecular bands that present dramatic variations tied to changes in effective temperature (see for example Reid et al. 1995; Cruz & Reid 2002 and references therein); others are based on measuring the slope of the pseudocontinuum (since the overall optical-NIR spectrum of very cool stars is

**Table 3.6**: Regions that define the Spectral Indices used to classify the C69 candidate members (and the empirical relations between those indices and the Spectral Types).

| Index | Numerator (Å) | Denominator (Å) | Ref | Relation with SpT |
|---|---|---|---|---|
| TiO 1 | 7000–7040 | 7060–7100 | 3 | *SpT = 2.433 × (TiO1 + TiO2) + 58.345 |
| TiO 2 | 7058–7061 | 7043–7046 | 1 | *SpT = 1.989 × (TiO1 + TiO2)$^2$ - 13.759 × (TiO1 + TiO2) + 92.645 |
| TiO 5 | 7126–7135 | 7042–7046 | 1 | SpT = -10.775×(TiO 5) + 8.200, for (TiO 5) ≤ 0.75 |
| | | | 1 | SpT = 5.673×(TiO 5) + 6.221, for (TiO 5) ≥ 0.3 |
| VO-a | Sum of 7350–7370 and 7550-7570 | 7430–7470 | 2 | SpT = 10.511(VO-a) - 16.272 |
| | | | 2 | SpT = -7.037(VO-a) + 26.737 |
| PC3 | 8230–8270 | 7540–7580 | 4 | SpT = -8.009 + 14.080 × PC3 - 2.810 × PC3$^2$ |

(1) Kirkpatrick et al. (1999)

(2) Reid et al. (1995)

(3) Martin et al. (1996)

(4) Martín et al. (1999)

* These relationships have been derived in this work with data from Martín et al. (1999) and assuming a linear behaviour of the (TiO 1+ TiO 2) index for spectral types earlier than M9, and a cuadratic one for cooler spectral types.

largely depressed by molecular opacity, the true stellar continuum is never seen, but at a few regions the molecules are a little more transparent and one can reach deeper in the photosphere), using indices that increase monotonically when the effective temperature decreases (for example PC3 and PC6 from Martin et al. 1996 and Martín et al. 1999).

As we mentioned previously in the Introduction, M-dwarfs stars are characterized spectroscopically by the presence of molecular bands of titanium and vanadium oxide (TiO, VO). These bands, being very prominent up to M7 spectral type are also known to become weaker when moving on to cooler temperatures (due to the condensation of Ti and V dust). We will therefore use not only more than one band but also ratios between bands that show opposite tendencies to avoid ambiguity in the spectral type determination (see Table 3.6 for a list of the indices used and their relations with spectral types). This combination of indices should provide us with a spectral classification with ∼0.5 subclass accuracy.

Due to the restrictions of the wavelength coverage and resolution of each instrumental setup, we have not been able to calculate every index for all the sources. As an example, while in the case of the MIKE observations we have used TiO 5 and the ratio of TiO 1 over TiO 2; for the LRS and FLAMES samples we have been able to compare the results obtained with PC3 and the combination of TiO 5 and VO-a.

In Fig. 3.9 we show several spectral sequences obtained for the different campaigns combining the use of spectral indices with template comparison (note the large diferences in resolution

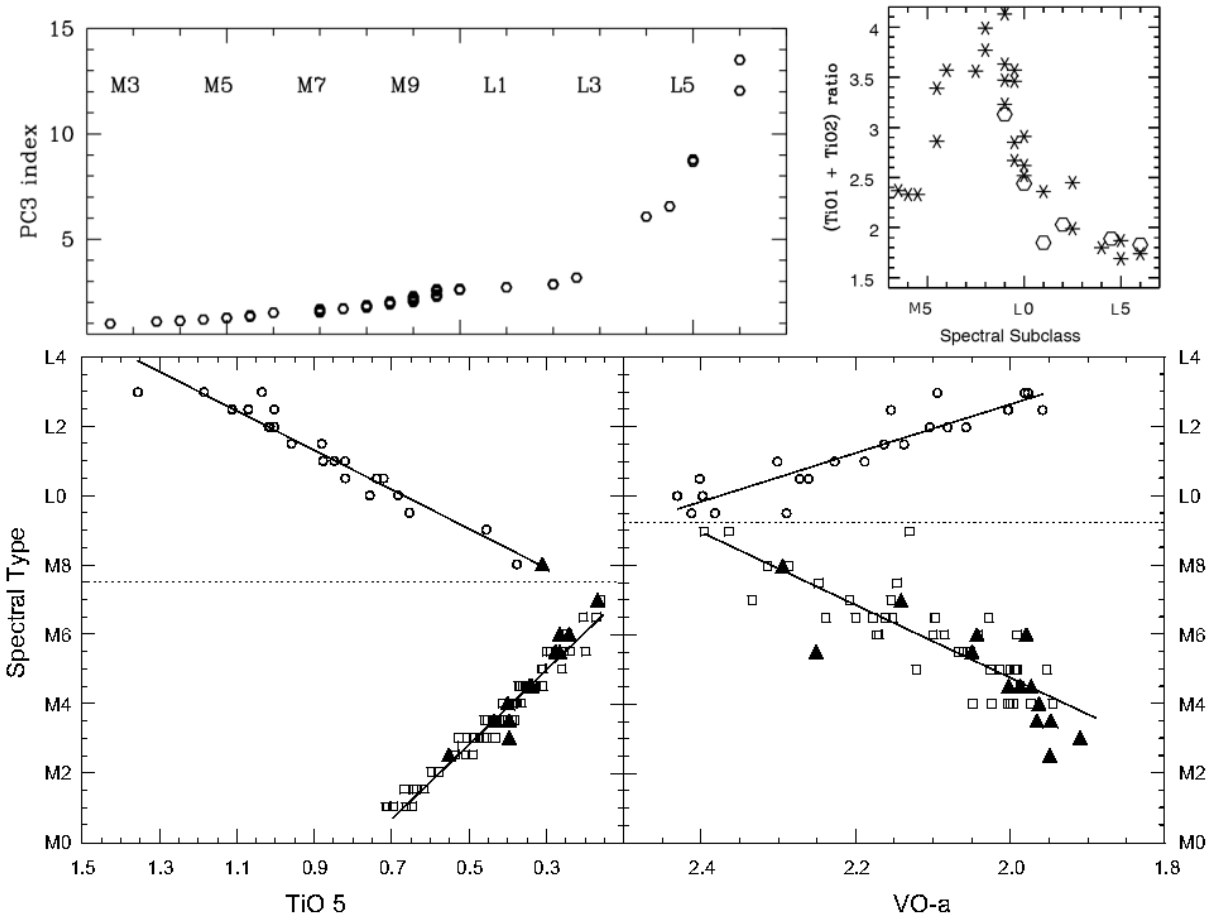


**Figure 3.8**: Examples of different indices used to determine the spectral types of our sources. **Top-Left:** Pseudo continuum PC3 index from Martin et al. (1996). **Top-Right:** TiO 1 over TiO 2 ratio from Martín et al. (1999). **Bottom-Pannel:** Dependence of the TiO 5 and VO-a indices with the spectral type (from Cruz & Reid 2002).

and wavelenth coverage between the different campaigns). As can be seen in the reddest parts of the spectra, TiO and VO absorptions, as stated before, clearly represent the dominant feature for this spectral range.

Once we had derived the spectral type for each source (either with templates or molecular indices), we compared them with the effective temperatures derived from their SEDs, and we derived the temperature scale showed in Table 3.13 (with a regresion coefficient of 0.86). This scale shows an offset of ~+400 K with respect to that of Leggett et al. (1996, 2000) and ~+200 K compared with the one from Luhman (1999); this effect has already been discussed in Section 3.1; to preserve self-consistency we will use our derived scale in the following Sections.

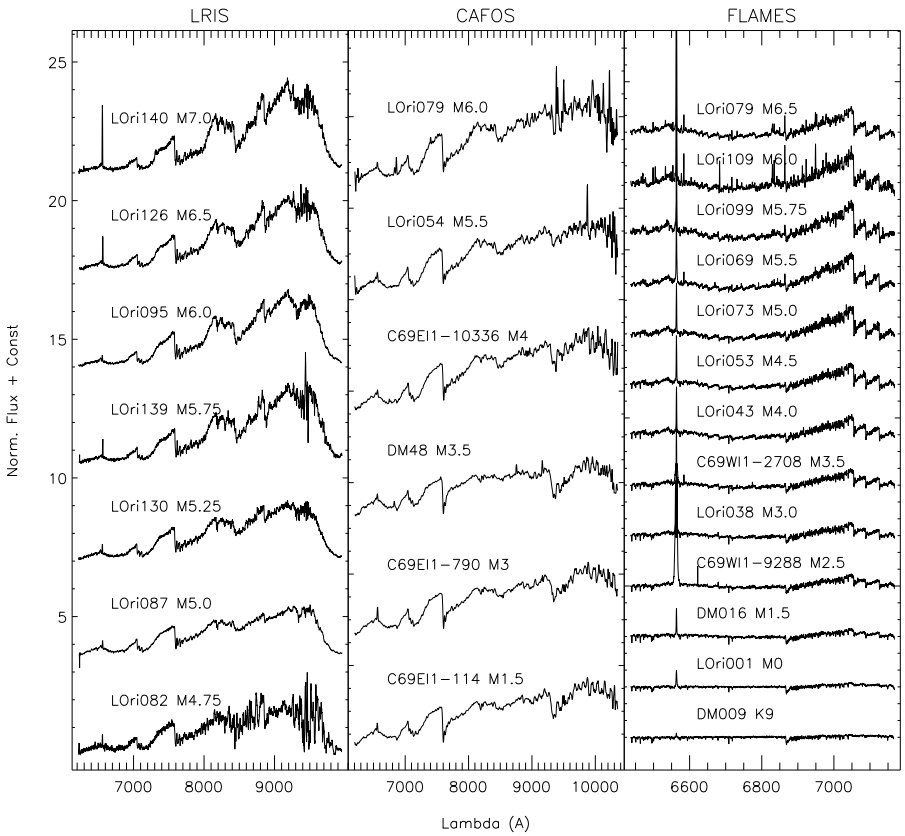


**Figure 3.9**: Spectral sequence determined for the sources observed during three different campaigns.

**Table 3.7**: Parameters derived from for the MIKE sample.

| Source | Model collection | $T_{eff}$ | logg | Spectral Type | vsin($i$) (km/s) | EW(H$\alpha$)crit[1] | log($\dot{M}_{acc}$)($M_\odot$/yr) | Binary[3] |
|---|---|---|---|---|---|---|---|---|
| LOri017* | Kurucz | 4250 | 4.0 | — | 70 | — | | |
| LOri031 | Kurucz | 3750 | 4.0 | M3.5 | 40 | ✗ | | |
| LOri042 | Kurucz | 3750 | 4.0 | M4.0 | 30 | ✗ | | |
| LOri050 | NextGen | 3700 | 4.0 | M4.0 | 60 | ✓ | -10.878±0.05 | M08, S08 |
| LOri055 | NextGen | 3700 | 4.0 | M4.0 | <20 | ✗ | | |
| LOri056 | NextGen | 3700 | 4.0 | M4.0 | — | ✗ | | |
| LOri057 | NextGen | 3700 | 4.0 | M5.5 | <20 | ✗ | | |
| LOri058 | NextGen | 3500 | 4.0 | M3.5 | — | ✗ | | |
| LOri059 | NextGen | 3500 | 4.0 | M4.0 | — | ✗ | | |
| LOri060 | NextGen | 3500 | 4.0 | M4.0 | 60 | ✗ | | |
| LOri063 | NextGen | 3700 | 4.0 | M4.0 | — | ✗ | | |
| LOri068 | NextGen | 3700 | 4.0 | M5.0 | — | ✗ | | |
| LOri073 | NextGen | 3700 | 4.0 | M5.5 | — | ✗ | | |
| LOri075 | NextGen | 3400 | 4.0 | M5.0 | 65[2] | ✗ | | M08, B09 |

*There were problems on the extraction of several orders. We have used the $T_{eff}$ corresponding to the SED fit shown in Sect. 3.1

[1] ✓ indicates that the object fulfills the accretion criterion by Barrado y Navascués & Martín (2003) (those marked with ✗ do not).

[2] From Maxted et al. (2008).

[3] Binary system according to Maxted et al. (2008) (M08), Sacco et al. (2008) (S08) or this work (B09).

**Table 3.8**: Parameters derived for the LRIS (low resolution spectra) sample.

| Object | Spectral Type | EW(H$\alpha$)crit[1] | log($\dot{M}_{acc}$)(M$_\odot$/yr) | Na I Mem[2] | Object | Spectral Type | EW(H$\alpha$)crit[1] | log($\dot{M}_{acc}$)(M$_\odot$/yr) | Na I Mem[2] |
|---|---|---|---|---|---|---|---|---|---|
| LOri075 | M5.0 | ✗ | | Mem | LOri133 | M4.75 | ✗ | | NM |
| LOri081 | M5.25 | ✗ | | Mem | LOri134 | M5.0 | ✗ | | Mem |
| LOri082 | M4.75 | ✗ | | Mem | LOri135 | M6.5 | ✗ | | Mem |
| LOri087 | M5.0 | ✗ | | Mem | LOri139 | M5.75 | ✗ | | Mem |
| LOri095 | M6.0 | ✗ | | Mem | LOri140 | M7.0 | ✓ | -8.875±0.14 | Mem |
| LOri098 | M5.0 | ✗ | | Mem | LOri141 | M4.0 | ✗ | | NM |
| LOri107 | M6.0 | ✗ | | Mem | LOri147 | M5.5 | ✗ | | NM |
| LOri110 | M5.25 | ✗ | | NM | LOri150 | M7.0 | ✗ | | Mem |
| LOri114 | M6.0 | ✗ | | Mem | LOri151 | M5.5 | ✗ | | NM |
| LOri115 | M5.0 | ✗ | | NM | LOri154 | M8.0 | ✗ | | NM |
| LOri116 | M5.5 | ✗ | | Mem | LOri155 | M8.0 | ✗ | | Mem |
| LOri118 | M5.5 | ✗ | | Mem | LOri156 | M8.0 | ✓ | -8.022±0.10 | Mem |
| LOri124 | M5.5 | ✗ | | Mem | LOri161 | M8.0 | ✓ | -9.967±0.42 | Mem |
| LOri126 | M6.5 | ✓ | -8.781±0.10 | Mem | LOri165 | M7.5 | – | | Mem |
| LOri130 | M5.25 | ✗ | | Mem | | | | | |

[1] ✓ indicates that the object fulfills the accretion criterion by Barrado y Navascués & Martín (2003) (those marked with ✗ do not).
[2] Membership based on the measured Na I EW.

**Table 3.9**: Parameters derived for the LRIS (medum resolution spectra) sample.

| Object | Spectral Type | EW(H$\alpha$)crit[1] | log($\dot{M}_{acc}$)(M$_\odot$/yr) | LC[2] | Object | Spectral Type | EW(H$\alpha$)crit[1] | log($\dot{M}_{acc}$)(M$_\odot$/yr) | LC[2] |
|---|---|---|---|---|---|---|---|---|---|
| LOri068 | M4.5 | ✗ | | IV | LOri099 | M5.25 | ✗ | | IV |
| LOri071 | M5.0 | ✗ | | IV | LOri106 | M5.5 | ✓ | -10.917±0.01 | IV |
| LOri077 | M5.0 | ✗ | | IV | LOri109 | M5.5 | ✗ | | IV |
| LOri089 | M5.0 | ✗ | | IV | LOri113 | M5.5 | ✓ | -10.574±0.03 | IV |
| LOri091 | M5.5 | ✗ | | IV | LOri119 | M5.5 | ✗ | | V |
| LOri094 | M5.5 | ✗ | | IV | LOri129 | M6.0 | ✗ | | IV |

[1] ✓ indicates that the object fulfills the accretion criterion by Barrado y Navascués & Martín (2003) (those marked with ✗ do not).
[2] Based on comparison of the KI bluer component of the $\lambda$7700 doublet with standards of luminosity class III, IV and V and similar spectral type (one half subclass maximuum difference).

**Table 3.10**: Parameters derived for the TWIN sample.

| Object | Spectral Type | EW(H$\alpha$)crit[1] | log($\dot{M}_{acc}$)(M$_\odot$/yr) | Alkali Mem[2] | Object | Spectral Type | EW(H$\alpha$)crit[1] | log($\dot{M}_{acc}$)(M$_\odot$/yr) | Alkali Mem[2] |
|---|---|---|---|---|---|---|---|---|---|
| DM48 | M1.5 | ✗ | | Mem | LOri061 | M2.0 | ✓ | -7.647±0.05 | Mem |
| LOri007 | M1.0 | –* | | Mem? | LOri062 | M3.0 | ✗ | | Mem |
| LOri036 | M3.5 | ✗ | | NM | LOri080 | M5.5 | ✓ | -7.061±0.05 | Mem |
| LOri044 | M4.5 | ✗ | | NM | LOri091 | M4.5 | ✓ | -9.177±0.19 | Mem |
| LOri045 | M2.0 | ✗ | | Mem | LOri092 | M4.5 | ✗ | | Mem |
| LOri048 | M3.0 | ✗ | | Mem | LOri105 | M6.0 | ✗ | | Mem |
| LOri052 | M5.0 | ✗ | | NM | | | | | |

[1] ✓ indicates that the object fulfills the accretion criterion by Barrado y Navascués & Martín (2003) (those marked with ✗ do not).
[2] Membership based on the measured Na I and K I doublets equivalent widths.
* See Section 3.3.5

**Table 3.11**: Parameters derived for the CAFOS sample.

| Object | Spectral Type | EW(H$\alpha$)crit[1] | log($\dot{M}_{acc}$)(M$_\odot$/yr) | Alkali Mem[2] | Object | Spectral Type | EW(H$\alpha$)crit[1] | log($\dot{M}_{acc}$)(M$_\odot$/yr) | Alkali Mem[2] |
|---|---|---|---|---|---|---|---|---|---|
| C69-X-E-009 I | K2 | ✓ | -7.555±0.35 | Mem | C69-X-E-068 M | K2 | ✗ | – | NM |
| C69-X-E-010 sX | K3 | ✗ | – | NM | C69-X-E-069 c | K5 | ✗ | – | NM |
| C69-X-E-027 n | M4.0 | ✗ | – | Mem | C69-X-E-071 c | K7 | ✗ | – | NM |
| C69-X-E-040 M | M3.5 | ✗ | – | Mem | C69-X-E-072 I | M3 | ✗ | – | NM |
| C69-X-E-060 n | K6 | ✗ | – | NM | C69-X-E-073 I | K4 | ✗ | – | NM |
| C69-X-E-064 I | M4.0 | ✗ | – | Mem | C69-X-E-104 c | M3.5 | ✗ | – | Mem |
| C69EI1-10336 | M4 | ✗ | – | Mem | LOri046 | M4.0 | ✗ | – | NM |
| C69EI1-114 | M1.5 | ✗ | – | Mem | LOri049 | M5.0 | ✗ | – | NM |
| C69EI1-13542 | K3 | ✗ | – | NM | LOri053 | M5.5 | ✗ | – | Mem |
| C69EI1-14424 | M3.5 | ✗ | – | Mem | LOri054 | M5.5 | ✗ | – | Mem |
| C69EI1-14609 | M3 | ✓ | -5.559±0.25 | Mem | LOri064 | M5.5 | ✗ | – | Mem? |
| C69EI1-790 | M3 | ✗ | – | Mem | LOri069 | – | ✗ | – | –* |
| C69WI1-3226 | K7-M0 | ✗ | – | NM | LOri070 | M5.5 | ✗ | – | Mem |
| C69WI1-4897 | F9 | ✗ | – | NM | LOri072 | M6.0 | ✗ | – | Mem |
| C69_1d03367 | M3.5 | ✗ | – | Mem | LOri078 | M3.5 | ✗ | – | Mem |
| DM065 | M3.5 | ✗ | – | Mem | LOri079 | M6.0 | ✗ | – | Mem |
| DM070 | M3.5 | ✗ | – | Mem | LOri083 | – | ✗ | – | –* |
| DM48 | M3.5 | ✗ | – | Mem | LOri084 | M6.0 | ✗ | – | Mem |

[1] ✓ indicates that the object fulfills the accretion criterion by Barrado y Navascués & Martín (2003) (those marked with ✗ do not).
[2] Membership based on the measured Na I and K I doublets equivalent widths. * See Section 3.3.5

**Table 3.12**: Parameters derived for the FLAMES sample.

| Object | Spectral Type | EW(H$\alpha$)crit[1] | log($\dot{M}_{acc}$)(M$_\odot$/yr) | Li I Mem[2] | Object | Spectral Type | EW(H$\alpha$)crit[1] | log($\dot{M}_{acc}$)(M$_\odot$/yr) | Li I Mem[2] |
|---|---|---|---|---|---|---|---|---|---|
| C69WI1-2708 | M3.5 | ✗ | – | ✓ | LOri053 | M4.5 | ✗ | – | ✓ |
| C69WI1-9288 | M2.5 | ✓ | -7.049±0.024 | ✓ | LOri056 | M5.0 | ✗ | – | ✓ |
| DM009 | K9 | ✗ | – | ✓ | LOri059 | M5.0 | ✗ | – | ✓ |
| DM016 | M1.5 | ✗ | – | ✓ | LOri069 | M5.5 | ✗ | – | ✓ |
| LOri001 | M0 | ✗ | – | ✓ | LOri073 | M5.0 | ✗ | – | ✓ |
| LOri007 | M1.5 | ✗ | – | ✗ | LOri075 | M5.5 | ✗ | – | ✓ |
| LOri011 | K9 | ✗ | – | ✗ | LOri079 | M6.5 | ✗ | – | ✓ |
| LOri012 | K8 | ✗ | – | ✗ | LOri086 | M5.0 | ✗ | – | ✓ |
| LOri013 | M3.5 | ✗ | – | ✓ | LOri087 | M5.0 | ✗ | – | ✓ |
| LOri024 | M1.5 | ✗ | – | ✓ | LOri088 | M5.5 | ✗ | – | ✓ |
| LOri026 | M2.5 | ✗ | – | ✓ | LOri091 | M5.5 | ✗ | – | ✓ |
| LOri037 | M3.5 | ✗ | – | ✓ | LOri093 | M5.5 | ✗ | – | ✓ |
| LOri038 | M3.0 | ✓ | -10.904±0.030 | ✓ | LOri094 | M5.5 | ✗ | – | ✓ |
| LOri043 | M4.0 | ✗ | – | ✓ | LOri096 | M5.0 | ✗ | – | ✓ |
| LOri044 | M3.5 | ✗ | – | ✗ | LOri099 | M5.75 | ✗ | – | ✓ |
| LOri045 | M4.0 | ✗ | – | ✓ | LOri105 | M6.0 | ✗ | – | ✓? |
| LOri046 | M4.0 | ✗ | – | ✗ | LOri109 | M6.0 | ✗ | – | ✓ |
| LOri049 | M4.0 | ✗ | – | ✗ | LOri112 | M6.5 | ✗ | – | ✓ |
| LOri050 | M4.0 | ✗ | – | ✓ | LOri115 | M5.0 | ✗ | – | ✓ |
| LOri052 | M4.0 | ✗ | – | ✗? | LOri120 | M5.5 | ✗ | – | ✓ |

[1] ✓ indicates that the object fulfills the accretion criterion by Barrado y Navascués & Martín (2003) (those marked with ✗ do not).
[2] Membership based on the measured Li I equivalent width.

**Table 3.13**: Temperature scale derived from our spectroscopic data of Collinder 69.

| Spectral Type | Effective Temperature |
|---|---|
| K3 | 5000 K |
| K4 | 4850 K |
| K5 | 4700 K |
| K6 | 4600 K |
| K7 | 4450 K |
| K8 | 4325 K |
| K9 | 4200 K |
| M0 | 4050 K |
| M1 | 3900 K |
| M2 | 3775 K |
| M3 | 3625 K |
| M4 | 3500 K |
| M5 | 3350 K |
| M6 | 3225 K |
| M7 | 3050 K |
| M8 | 2950 K |
| M9 | 2800 K |
| L0 | 2650 K |

### 3.3.2 Rotational velocities estimation.

For the sample of sources observed with the highest resolution (those observed with MIKE, Table 3.7) we tried to measure the rotational velocity by comparing with Kurucz model synthetized for different velocities. Since there is a known dispersion between effective temperature based on spectral types and $T_{eff}$ scales and those derived using models (and we are going to use the latter in our $v \sin(i)$ estimation), we performed synthetic spectra fit to our observational data. We built a grid of synthetic spectra using different colections: Kurucz, NextGen and Dusty covering effective temperatures in the range 5000-2000 K, asuming solar metallicities, and a range of log g between 3.5 and 5.0. We lowered the resolution of our spectra to R~200, which is the resolution provided in the public servers by the Lyon group in order to perform a direct fitting process. Table 3.7 shows the best fitting parameter for each case.

According to the effective temperatures derived, we computed high resolution Kurucz synthetic spectra in the wavelength range 6090–6130 Åwith log g of 4.0 dex and different vsin($i$) values. We chose that precise wavelength range because the SNR of our spectra is not very high in all the cases, and, according to the Kurukz models, two of the most prominent photospheric absorption lines (from Ca I) are located within this region. We have performed a model fit to those lines in order to estimate the rotational velocities of our sources. Prior to this comparison, we included the instrumental response measured on the MIKE lamp arc. The mean full-widh half

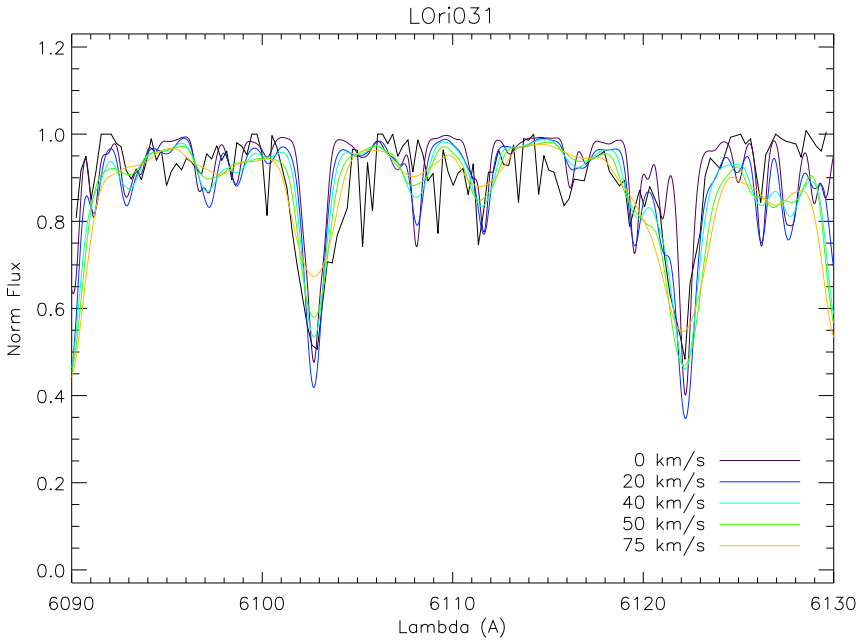


**Figure 3.10**: Rotational velocity.

maximum value measured on the lamp spectra was 0.4914 Å, corresponding to a velocity of ~20 km/s (the lower limit we can provide for several cases). The estimates rotational velocities are provided in Table 3.7 and are in the same range of values of those derived by Sacco et al. (2008) for other members with similar spectral types. In particular there are three sources for which Sacco et al. (2008) and us have estimated vsin(*i*). In two of these cases, LOri055 and LOri057, both estimations are in very good agreement, but in the case of LOri060 we provide a value 40 km/s higher than the one obtained by Sacco et al. (2008). Since our determination is based only on a doublet and theirs on the cross-correlation of their whole spectra we must take their upper-limit of ~ 20 km/s as a more robust measurement.

### 3.3.3 The effect of the resolution on the measurement of the lines.

As has been stated at the begining of this section, we have obtained data from many different telescopes using various instrumental configurations; this way, as a logical consequence, our dataset comprises a varity of resolutions. In order to assure that we do not incur in any formal mistake when mixing the measured properties of the lines (in particular EW, FHWM and $FW_{10\%}$) of spectra taken at different resolutions, we have performed the following exercise:

We have degraded one of our FLAMES spectra (from LOri038, a M3, accreting, Class II, confirmed member) to different resolutions (including those listed in Table 3.5). We have then

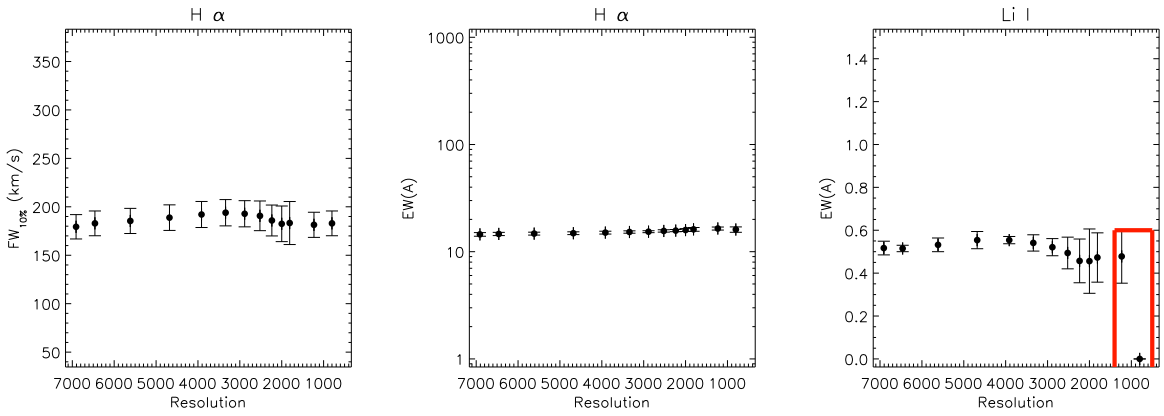


**Figure 3.11**: Relationship between different measurements of the H$\alpha$ and Li I line profiles and the resolution os the spectra where the measurement has been performed.

(on those degraded spectra) measured FHWM, EW and $FW_{10\%}$ for the H$\alpha$ (emission) and Li $\lambda$6708 Å lines (absorption) with the automatic procedure explained in Appendix B. In Fig. 3.11 we provide those values (EW and $FW_{10\%}$ for H$\alpha$ and EW for Li I $\lambda$6708 Å) as a function of the resolution of the spectra. The length of the y-axes has been fixed by purpose for each plot: in the first panel (from left to right), it represents the variation of the instrumental response (the FHWM measured on the respective arc adapted for each value of the resolution) among the resolutions considered. In the cases of the middle and right-side pannels, the length of this axes provides an idea of the variation within members of Collinder 69 for the corresponding equivalent width. Note that in the case of H$\alpha$ there is clearly no significant dependence on the measurements made at different resolutions (the variations lie within the error bars). For the case of the Lithium, due to the intrinsic weakness of the line, the accuracy of the measurement (meaning the errorbars) lowers with the spectral resolution, but still it seems perfectly reasonable to compare meaurements at R $\sim$ 2000 and R $\sim$ 8000. In the same figure we have highlighted te range of resolutions where Li is not detectable anymore. A detailed view of the "degeneration" of the lines for this example is provided in fig. 3.12

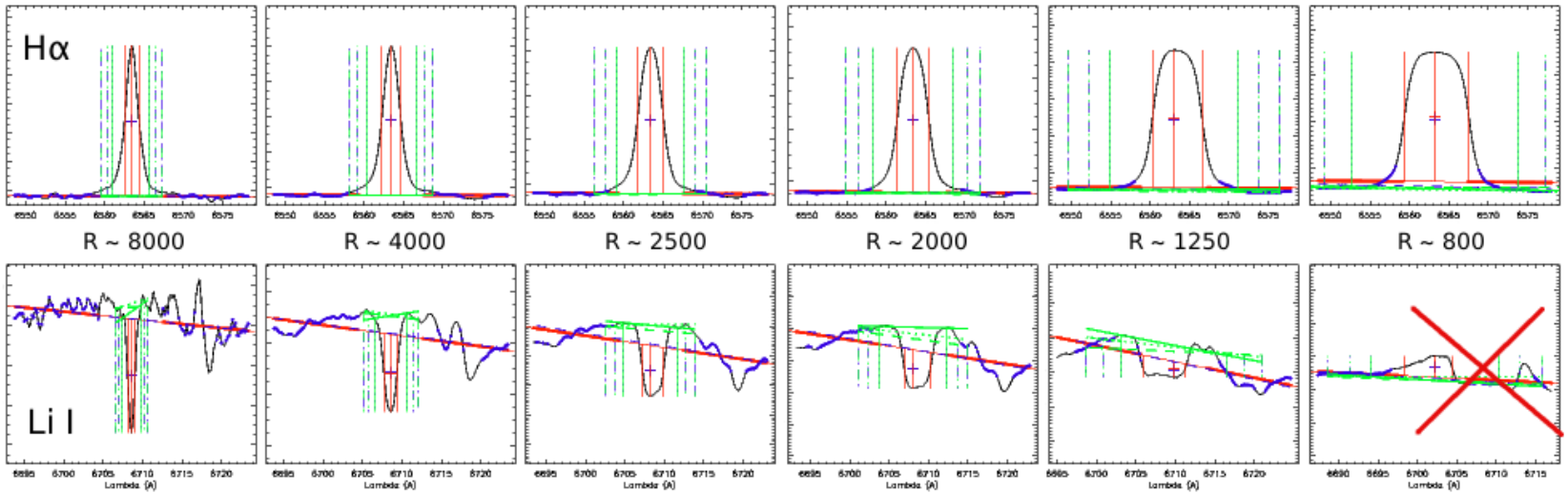


**Figure 3.12**: Sequence composed by a detailed view of the evolution of the profiles of the H$\alpha$ (emission) and Li I (absorption) lines with the variation of the spectral resolution. The first panel (from left to right) corresponds to the original resolution of our FLAMES spectrum of LOri038, a M3 member of C69 (R ~8000). In the last panel we have degraded the FLAMES spectra to a resolution similar to that of our low-resolution campaign (R ~800 obtained with the B&C spectrograph). As can be seen in this figure and in Fig. 3.11 the lithium's equivalent width can be measured down to resolutions of the order of 1250 (for a good signal to noise ratio as it is the case of our spectrum of LOri038). The linestyles and color code are those explained on Appendix B.

### 3.3.4 Activity, accretion and youth indicators.

Several features were detected in our spectra; features such as H$\alpha$ and H$\beta$ emission, some forbidden lines in emission (OI, II, SII), He I also in emission, Lithium absorption and several alkali absorption lines (mainly Na I and K1).

**Activity and accretion:**

The forbidden emission lines of [OI], [SII] and [NII] have been attributed in the literature to low density regions such as winds, and are therefore a tracer of the mass loss process (see Shu et al. 1994; Hartmann et al. 1994 and Hartmann 1999). In the same context, both the He I $\lambda$6678 Åand H$\alpha$ emissions are characteristic of classical T Tauri stars and their substellar analogs (Martín et al. 2001; Natta & Testi 2001; Natta et al. 2002; Testi et al. 2002; Mohanty et al. 2003; Jayawardhana et al. 2002b,a, 2003a,b; Barrado y Navascués et al. 2002, 2003; White & Basri 2003).

We have detected forbidden emission lines in some of our higher resolution spectra (see tables 3.15, 3.16, 3.17 and 3.21), but since most of these detections are quite marginal we cannot assure whether we are receiving signal from the source itself or nebular emission. Regarding the He I $\lambda$6678 and H$\alpha$ emissions, ~55% of the sources showing H$\alpha$ large enough to suggest that the source is undergoing accretion (see the following paragraphs) also show He I in emission. In two of the cases (FLAMES spectra) the line could be contaminated by the nebular emission, the remaining cases correspond to long-slit spectra, and therefore, if our reduction process has been performed properly, this effect should not be present. There is a clear trend among both equivalent widths; the stronger the H$\alpha$ emission, the strongest the He I one; but our sample is not statistically significant to derive a quantitative relationship.

As has been mentioned before, even though H$\alpha$ emission is commonly used as a proxy for active accretion, some considerations have to be taken into account when studying this fenomena in cool objects since part of that emission can be chromospheric and has nothing to do with accretion processes. Barrado y Navascués & Martín (2003) proposed an empirical criterion, based on the saturation limit of chromospheric activity, to determine whether a star or brown dwarf is accretting matter from a disk or not.

This criterion is translated into a relationship between the spectral type and the EW(H$\alpha$) of the source. We have applied the temperature scale provided in Table 3.13 to convert the spectral types in $T_{eff}$ compatibles with those derived for our sources from their SEDs (see Section 3.1), and applying this relation, we have estimated which from our candidates are active accretors. In Fig 3.13 we display the diagram relating this two parameters for all the confirmed members of Collinder 69 (members confirmed by Dolan & Mathieu 1999, 2001; Maxted et al. 2008; Sacco et al. 2008 or this work). Our measurements are displayed as solid dots (while Dolan & Mathieu 1999, 2001 members are represented with squares, and Sacco et al. 2008 members with diamonds). We have also included the information regarding the infrared class (as a proxy for the presence of disk, from Barrado y Navascués et al. 2007b) with larger circumferences sourrounding Class

II sources. There are two brown dwarfs classified as active accretors that are not classified as Class II according to their IRAC data. One of them is LOri156; although it is classified as Class III according to the criteria from Allen et al. (2004), the large $\alpha$ parameter ($\alpha = -1.54$) suggests that indeed, the source harbours a thick disk. The other brown dwarf, LOri161, was not detected on the 5.8 and 8.0 micron channels of IRAC, and therefore no IR Class has been assigned to it. The strong H$\alpha$ emission could be explained either as a result of active accretion from a thin disk that has not been detected due to lack of sensitivity (the third and fourth channels of the IRAC camera are less sensitive than the first two); or as a flare. We would need another spectra to be able to decide between the two options; in any case, the signal-to-noise ratio of the average of the spectra taken was not too high yielding a large uncertainty in the measurement of the EW(H$\alpha$) (74.51±33.07 Å).

On the other hand, there is one source, LOri091 showing a very large H$\alpha$ emission in one of our spectra (it has been observed three times by us); we have not classified it as an accreting source since we are quite confident that the spectra from which we measured this strong emission was taking during a flare of this very low mass star (see Section 3.3.5 for more details).

When studying the H$\alpha$ emission of our sources, we were also forced to take into account the environment where the sources are located. In cases like Collinder 69, where a non-negligiable nebular H$\alpha$ component can be observed along the whole cluster (see Fig. 1.7), one has to be very careful make sure that the nebular component is subtracted properly from the spectrum of each science target. This is not an issue for instance when dealing with long-slit spectroscopy (like most of our campaigns), since the parts of the slit where the science object is not located will allow us to estimate this "contamination". On the other hand, when observing with fiber spectrographs the location of the "sky fibers" is crucial in order not to introduce a bias on the measurements.

In Fig. 3.14 we show an H$\alpha$ image (from Finkbeiner 2003, with very low spatial resolution) of the LOSFR where we have masked the location of the sources observed with FLAMES in 2008 and also the location of the sky fibers used to correct our measurements. At a first sight, some structure can be inferred in the nebular emission surrounded by our science targets; we studied the variations of the H$\alpha$ nebular emission with the sky fibers; we measured a mean full width at 10% of ∼41 km/s with a standard deviation of ∼3 km/s. We computed a median sky fiber and corrected the science spectra with that median; therefore the dispersion measured in those fibers translated into an added ∼7% uncertainty in our measurements.

In Tables 3.15, 3.18, 3.16, 3.17, 3.19, 3.20 and 3.21 we present the measured EW (also FWHM and $FW_{10\%}$ for H$\alpha$) for all the previously mentioned lines (when consistent with the wavelength coverage of the particular instrumental set-up). For those sources fulfilling the Barrado y Navascués & Martín (2003) criteria on the H$\alpha$ equivalent width, we have estimated the mass accretion rate using the measured $FW_{10\%}$(H$\alpha$) and the following relationship derived by Natta et al. (2004):

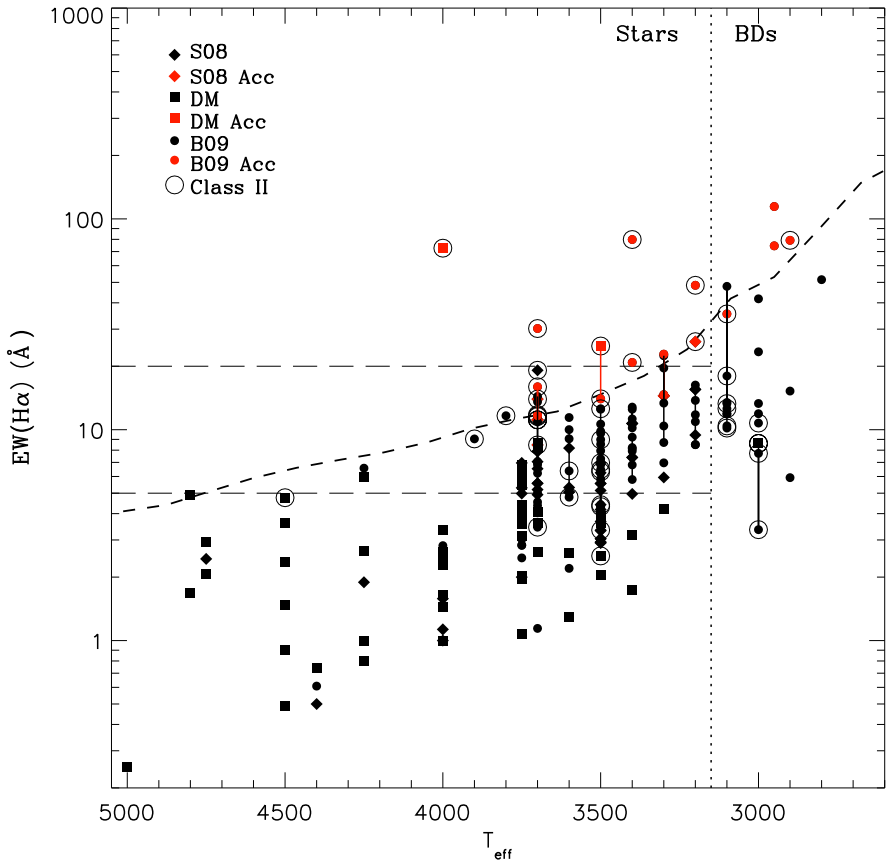


**Figure 3.13**: H$\alpha$ equivalent width versus the effective temperature for confirmed members of Collinder 69. We display data from Dolan & Mathieu (1999, 2001), with filled squares and from Sacco et al. (2008) with filled diamonds. Our data are displayed with solid dots; in every sample red symbols are used for those sources with measured equivalent width above the saturation criteria. Overlapping large circles denote Class II objects (IR Class from Spitzer/IRAC data). For some sources we had more than one epoch of data (either our own data or those from Dolan & Mathieu 1999, 2001; Sacco et al. 2008); the different measurements for each of this sources appear joint with a solid line. The short-dashed line corresponds to the saturation criteria defined by Barrado y Navascués & Martín (2003), whereas the two long-dashed lines are other criteria which have been used to discriminate between Classical and Weak line TTauri stars. A vertical dotted line highlights the substellar frontier for an estimated age of 5 Myr according to the isochrones form the Lyon group (Baraffe et al. 2002).

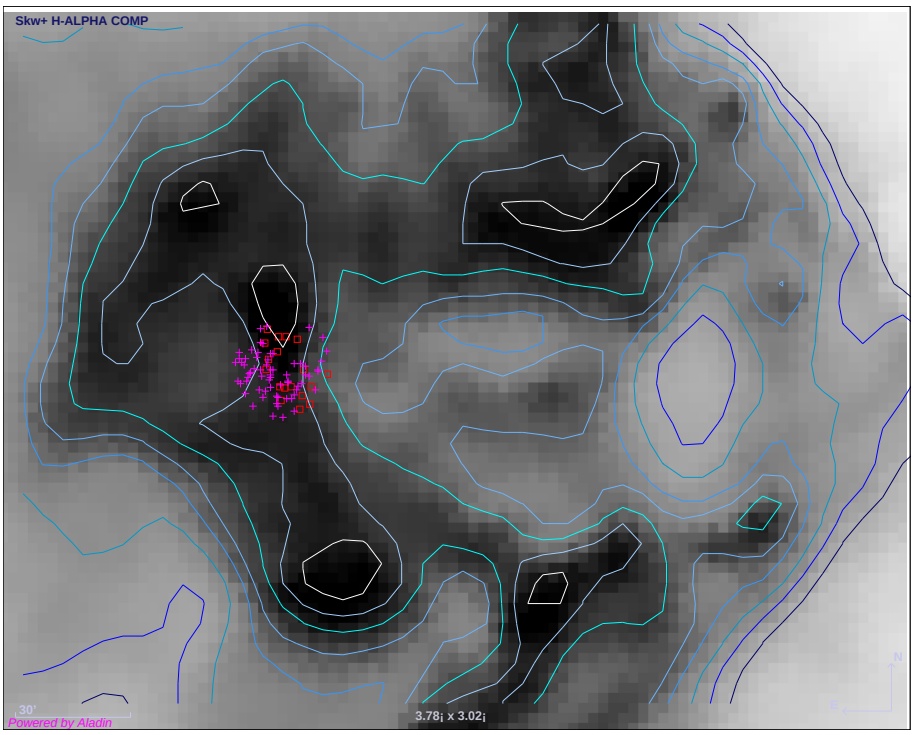


**Figure 3.14**: Same image as in Fig. 1.7 but with contour levels overplotted. On top of it we have marked with pink crosses the positions of the candidates observed with FLAMES, and with red squares the locus of the sky fibers used to correct our observations.

$$\log(\dot{M}_{acc}) = -12.89(\pm 0.3) + 9.7(\pm 0.7) \times 10^{-3} \mathrm{FW}_{10\%}(H\alpha) \quad (3.1)$$

These accretion rates are listed on Tables 3.7, 3.8, 3.9, 3.10, 3.11 and 3.12 (as well as other physical parameters derived in the forthcoming sections). Individual sources are analyzed in detail in Section 3.3.5. In Fig. 3.15 we show an accretion rate versus mass diagram where we compare the values estimated in this work with those derived in the literature for different young stellar and substellar sources (Calvet et al. (2004); Muzerolle et al. (2005); Mohanty et al. (2005) and Natta et al. (2006)) and even higher mass YSOs (Mendigutia et al. 2009, priv. comm.). Our data follow the $\dot{M}_{acc} \propto \mathrm{M}_*^2$ trend with similar scatter than the rest of studies published so far.

We have also tried to relate the H$\alpha$ emission with the properties of the disks. The theoretical disk models used to interpret the IRAC colour-colour diagram by Allen et al. (2004) suggest that the accretion rates increase from the bottom-left to the top-right of the Class II region on the [5.8]-[8.0] vs [3.6]-[4.5] space due to the increase of both, the disk emission and the wall emission. In Fig. 3.16 we show the mentioned IRAC colour-colour diagram for the members of Collinder 69 (spectroscopically confirmed members, and highly reliable photometric candidates). We have included information regarding the presence of disk (large red circles) and the intensity

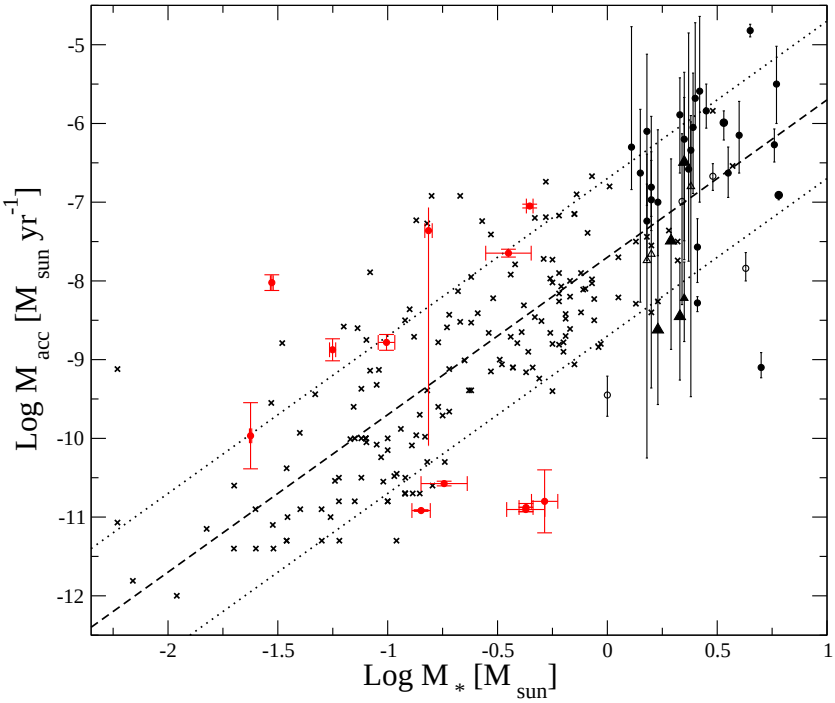


**Figure 3.15**: Mass accretion rates for a wide range of stellar masses. Red filled dots from this work. Crosses are from Calvet et al. (2004); Muzerolle et al. (2005); Mohanty et al. (2005) and Natta et al. (2006). Filled and open black symbols from Mendigutia et al 2009 (private communication), corresponding to the objects with EW(H$\alpha$) > 10 Å and < 10 Å, respectively. Triangles represent lower limits. The vertical bars (without top nor bottom dash) over these symbols (the black ones from the literature and also LOri080 from this work) represent variability measured in time scales of hours – months, not uncertainty in the measurements. The mass that we show in this figure is the average between the one derived from the $L_{bol}$ and the one derived from the $T_{eff}$ (with the error bars displaying the differences among them). The dashed line follows $\dot{M}_{acc} \propto M_*^2$, and the dotted lines ± 1 dex.

of the emission of H$\alpha$. Apart from LOri143 (the black dot surrounded only by a big blue square), a source that shows large variability in H$\alpha$ and probably the large EW measured corresponds with a flare event; the tendency shown by the remaining sources seems to agree with the hypothesis just explained. A similar behaviour is observed in Fig. 3.17 where we use the same symbols to represent the effective temperature vs the $\alpha$ parameter introduced by Lada et al. (2006) to represent the IRAC slope of the sources. It is quite eye-catching the fact that the largest values of the $\alpha$ parameter (the thicker disks) are concentrated around an specific range of temperatures. Since our method to derive the effective temperature does not account for possible effects of the disk on the "photospheric" part of the SED, this might simply be a bias introduced by our methodology.

**Youth indicators:**

Regarding youth indicators, above ~0.065 $M_\odot$ (less massive objects cannot develop the necessary temperature in their cores), lithium acts as an age scale because the length of time it

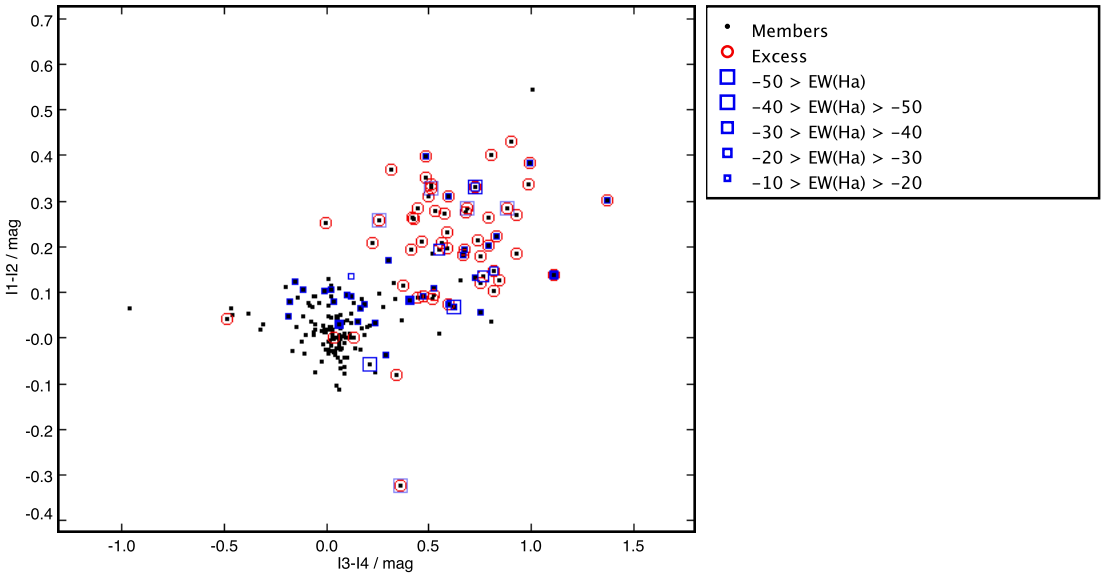


**Figure 3.16**: IRAC color-color diagram including information about the nature of the disk and the H$\alpha$ emission of the sources. Sources showing infrared excess have been surrounded by a red circumference. A blue square with a size proportional to the intensity of the H$\alpha$ emission of the sources is also shown in the figure.

takes for the core to reach $3.0\times10^6$ K is a sensitive function of mass (Basri 1997). Because these stars are fully convective, once the core temperature exceeds the necessary limit, the entire lithium content of the star should be exhausted rapidly and thus be reflected in an observable change in the photospheric lithium abundance.Theoretical models make specific predictions about the time evolution of this lithium depletion boundary. For example, Ventura et al. (1998) predict that at ages 30, 70, and 140 Myr, the lithium depletion edge should occur at 0.17, 0.09, and 0.07 $M_{\odot}$, respectively. Other models by Chabrier & Baraffe (1997) and Burrows et al. (1997) make similar predictions of the variation of this lithium depletion boundary with age. Indeed, Bildsten et al. (1997) and others have argued that the age for an open cluster derived in this manner should be more accurate than those found by any other method.

Due to the intrinsic weakness of the lithium line we have only been able to use it as a youth indicator for the sources observed with a high signal-to-noise ratio (specially in the lower resolution campaigns) and down to a certain spectral resolution (see Section 3.3.3). In Table 3.12, for example, we have included a membership column based on the presence or absence of Li I in the spectra (see Fig 3.18 for an example of two sets of objects clearly showing Li I in absorption in spectra taken with two different instrumental set-ups).

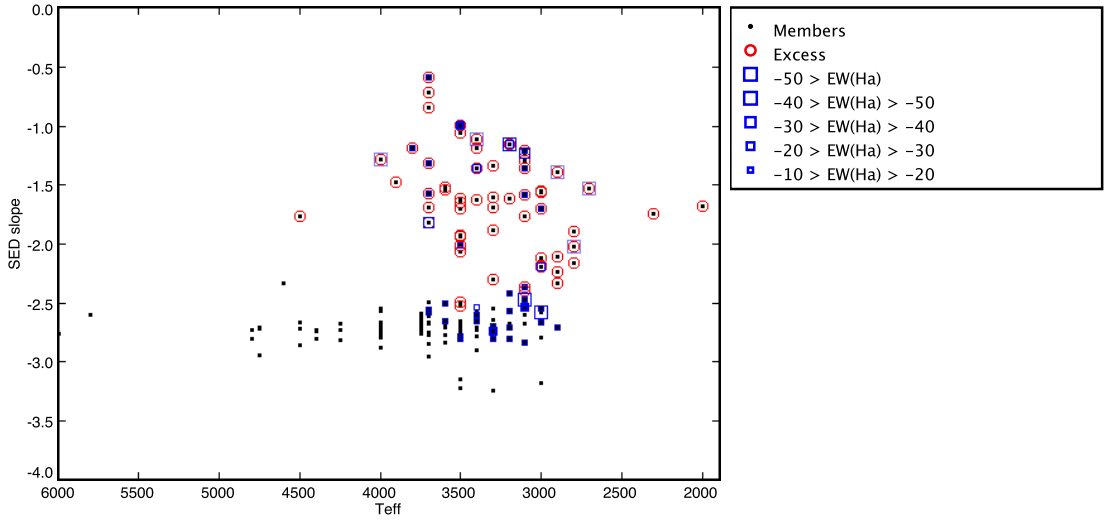


**Figure 3.17**: Effective temperature vs. IRAC SED slope of the confirmed and candidate members to Collinder 69 including information about the nature of the disk and the H$\alpha$ emission of the sources. Same symbols and colors as in Fig 3.16

Figure 3.19 shows the measured lithium equivalent width versus the spectral type of the candidate members to Collinder 69. We have included the data from Dolan & Mathieu (1999, 2001) and the measurements from this work. For comparison we have also displayed data corresponding to a similar age cluster, $\sigma$ Orionis, as well as an older one, IC2391. We have also overploted the theoretical equivalent widths from Zapatero Osorio et al. (2002) considering $\log g = 4.0$ and $\log g = 4.5$ and initial cosmic abundance (A(Li) = 3.1). Note that a significant fraction of our sources lie on top or above of the theoretical curves, implying that lithium is still preserved at the age of Collinder 69.

The scatter of the Li I equivalent widths is considerable for all spectral types included in the figure, getting even larger for temperatures cooler than M4. This is a well-known open problem (see Barrado y Navascués et al. 2001, Zapatero Osorio et al. 2002 and references therein). The dispersion could be ascribed to a variability in the Li I line as a consequence of stellar activity, different mixing processes, presence or absence of circumstellar disks, binarity, or different rotation rates from star to star. We have overplotted red dots over the sources in our sample classified as accretors. It turns out to be quite clear that all of them but LOri080 (the lowest red dot discussed in Section 3.3.5) follow a trend showing average equivalent widths.

In addition to the discussed dispersion in the Lithium equivalent width measured on sources with different temperatures, we have observed some variability in this line when compar-

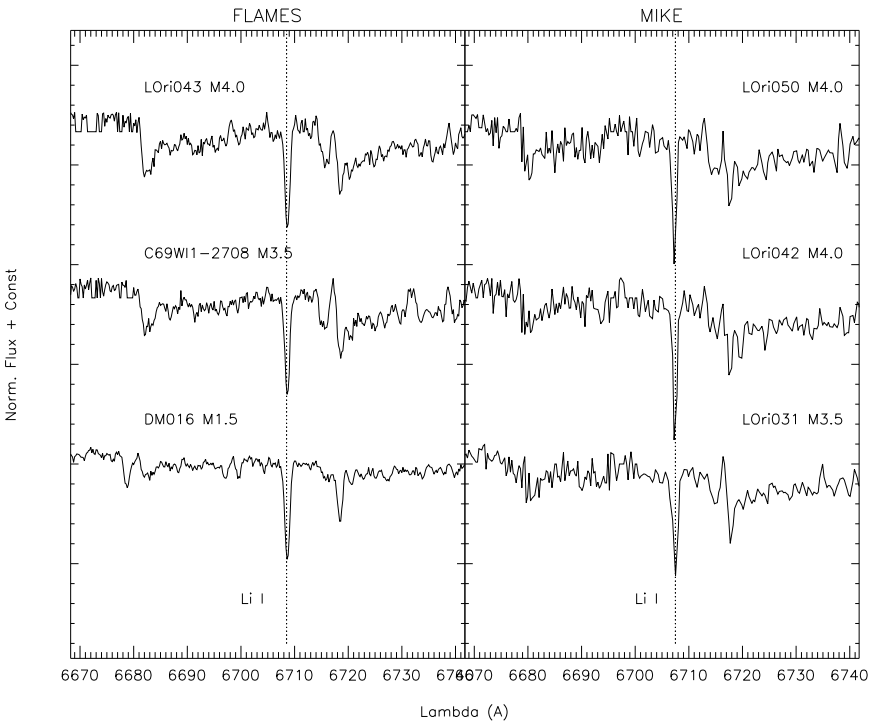


**Figure 3.18**: Detail around Li I $\lambda$6708Å for eight confirmed members with different spectral types. The two panels correspond to two different campaigns: Magellan/MIKE echelle spectra (only the order corresponding to this line), and FLAMES multi-fiber spectra.

ing our data with the values measured by Sacco et al. (2008) for some of the sources. We display our measurements against theirs in Fig. 3.20. It looks like most of our measured values are lower than those from Sacco et al. (2008), but we are dealing with too low numbers to perform any statistics. In any case, this behaviour is not systematic (we provide measurements that are higher than the ones that they provide), and from the exercise that we performed in Section 3.3.3 we are quite confident that what we are showing is not an instrumental bias. In Table 3.14 we provide the properties of the sources showing this variability in the Li absorption. Most of the sources show features typical of active stars (such as X-ray emission or H$\alpha$ variability). Neuhaeuser et al. (1998) monitored the young star Par 1724 finding a variable Lithium equivalent width consistent with rotational modulation. In any case we only have two measurements per source, and the sample is too small to arrive to any conclusion.

Finally, several alkali lines are known to be gravity sensitive in M-type stars. For example the K I doublet at 7665 & 7700 Å and the Na I doublet at 8184 & 8195.5 (see Martin et al. 1996; Schiavon et al. 1997). The surface gravity of members of Collinder 69 is expected to be $\log(g) = 3 - 4$ (Maxted et al. 2008), whereas a typical M-type giant will have $\log(g) \sim 2$. Thus, the equivalent width of both doublets, EW(K I) & EW(Na I), can be used to identify background giants in our sample. We have used the most suitable of these lines depending on the resolution

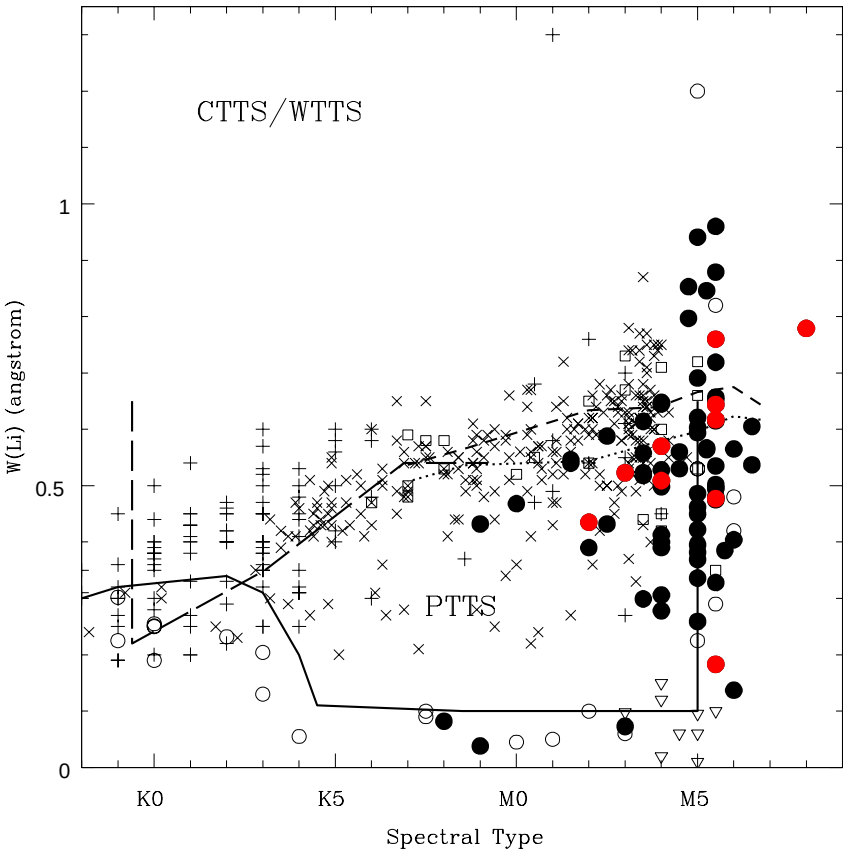


**Figure 3.19**: Lithium equivalent width versus the spectral type. We display data from Dolan & Mathieu (1999, 2001) as crosses, whereas our new data appear as solid circles. Values for Sigma Orionis low mass stars are displayed as open squares Zapatero Osorio et al. (2002). The Weak-line TTauri stars belonging to Taurus and the Sco-Cen complex are included as plus symbols, whereas the open circles correspond to members of the IC2391 open cluster. The solid line corresponds to the upper envelope of the values measured in young open clusters such as IC2391, IC2602, the Pleiades and M35. The long-dashed line delimits the areas for weak-line and post-TTauri stars (adapted from Martin 1997 and Martín & Magazzù 1999. Short-dashed and dotted lines correspond to the cosmic abundances – A(Li) = 3.1 – from gravities of log g = 4.5 and 4.0, respectively (curves of growth from Zapatero Osorio et al. 2002).

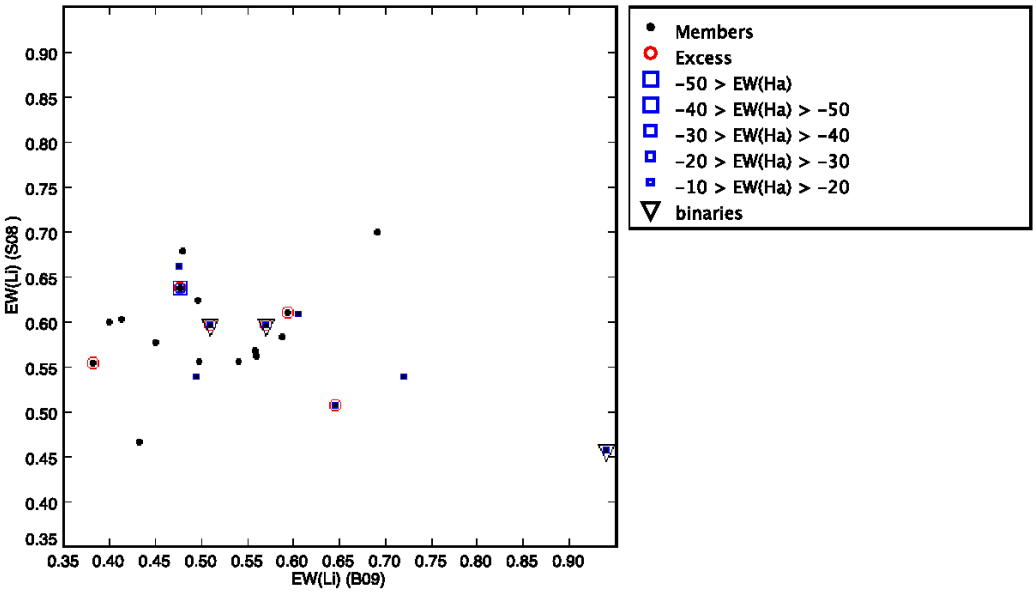


**Figure 3.20**: Lithium equivalent width provided in Sacco et al. (2008) versus the values measured in this work. We have used the same symbols and color as in Figs. 3.16 and 3.17 adding the information about binarity provided by Sacco et al. (2008); Maxted et al. (2008)

**Table 3.14**: Properties of the sources showing Li variability (Sacco et al. (2008) values compared to the values derived in this work). Note that there is no bias concerning the resolution of the spectra (as was also proved with the exercise of Sec. 3.3.3). The instrument code is the same as in 3.25

| Object | SpT | INS | Binarity[1] | IR Class | $T_{eff}$[2] | vsini[3] | H$\alpha$ Vble[4] | X-ray[5] |
|---|---|---|---|---|---|---|---|---|
| LOri050 | M4.0 | (8) (3) | SB1(M08 S08) | II | 3700.0 | | N | Y |
| LOri055 | M4.0 | (3) | | III | 3700.0 | <17.0 | N | N |
| LOri056 | M4.0 M5.0 | (3) (8) | | III | 3700.0 | <19.3 | Y | N |
| LOri057 | M5.5 | (3) | | III | 3700.0 | <17.0 | N | N |
| LOri060 | M4.0 | (3) | | III | 3500.0 | <18.5 | N | N |
| LOri063 | M4.0 | (3) | | II | 3700.0 | <18.2 | Y | N |
| LOri068 | M4.5 M5.0 | (1) (3) | | III | 3700.0 | <17.0 | Y | N |
| LOri069 | M5.5 | (8) | SB2(M08 S08) | III | 3400.0 | | Y | N |
| LOri075 | M5.0 M5.5 | (2) (8) (3) | SB1 (M08) | III | 3400.0 | 61.3+11.5-4.9 | Y | N |
| LOri088 | M5.5 | (8) | | III | 3200.0 | <17.0 | Y | N |
| LOri093 | M5.5 | (8) | | III | 3500.0 | <18.3 | Y | N |
| LOri094 | M5.5 | (8) (1) | | III | 3200.0 | 54.8+5.5-8.2 | Y | N |
| LOri096 | M5.0 | (8) | | II | 3500.0 | <19.1 | Y[6] | N |
| LOri106 | M5.5 | (1) | | II | 3200.0 | <17.0 | Y | N |

[1] According to Sacco et al. (2008) (S08) or Maxted et al. (2008) (M08).
[2] Derived with VOSA.
[3] From Sacco et al. (2008).
[4] Comparing the measurements of this work (in the case of LOri056 the variation in the H$\alpha$ emission is also clear between the two spectra taken in different campaigns) with those of Sacco et al. (2008).
[5] Sources detected in our *XMM-Newton* survey (see previous Chapter).
[6] Although no H$\alpha$ measurement is provided for LOri096 from our FLAMES spectra, the raw spectra, no "sky substraction performed", shows an EW(H$\alpha$) lower than the one measured by Sacco et al. (2008).

and the wavelength coverage of each campaign; as an example, for the medium resolution LRIS sample, we have only been able to compare the bluest component of the previously mentioned K I doublet with templates of different luminosity class, since the wavelength range covered with our instrumental configuration did not cover the other component (see Fig. 3.21 for an example of this comparison). We must note anyway that the EW of this component measured on the templates has a very strong dependency on the luminosity class, and therefore we think that our estimated values listed in Table 3.9 are reliable.

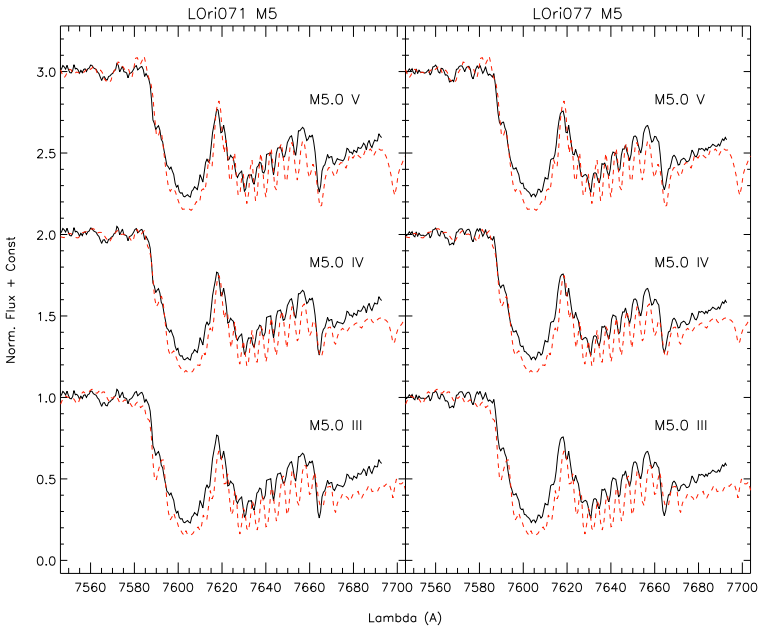


**Figure 3.21**: Determination of the gravity by comparison of the bluest component of the K I doublet on two M5.0 candidate members (LOri071 and LOri077) with respect to several templates with different luminosity class.

In Fig. 3.22 we plot the effective temperature of members and rejected candidates to Collinder 69 against their measured Na I. We have also included the measurements from Maxted et al. (2008) and highlighted those sources classified as Weak-line TTauri (showing X-ray emission) and as active accretors (green and red solid dots respectively). As we did with the Li I measurements, we have compared the values measured by us with those from Maxted et al. (2008) for the sources in common. We find that ~35% of the common sources show Na I variability (differences not compatible within the error bars for both measurements). More than half of these sources are either Classical TTauris or X-ray emitters.

Considering mean values in the variable sources, we have checked the following trend: while there is a mix between the two populations (Classical and Weak-line TTauris) in the stellar-mass domain, for the substellar one (the boundary is located at $T_{eff}$~3150 K for 5 Myr according to the SIESS + COND isochrone), we find lower Na I EWs on the active accretors than in the rest

of the sample.

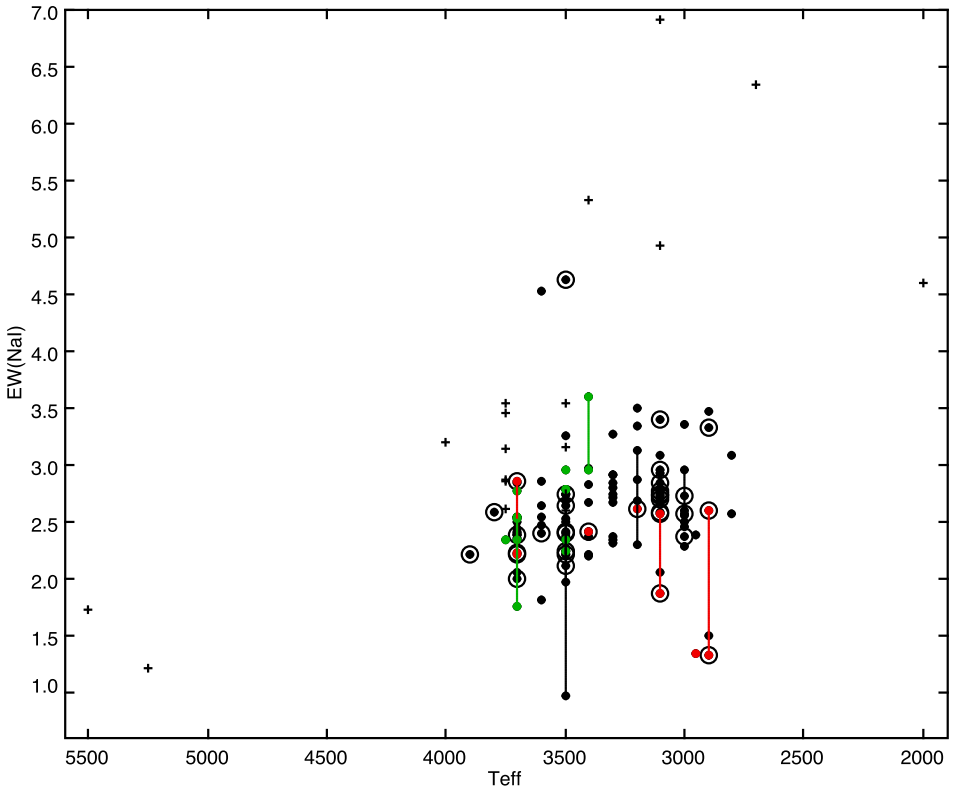


**Figure 3.22**: $T_{eff}$ vs EW(NaI) for members and non-members of Collinder 69. Rejected candidates are displayed as plus signs, confirmed members as solid dots, where: red ones highlight sources classified as active accretors and green ones Weak-line TTauri stars detected on our X-rays survey. For those sources showing large variability in the measured Na I equivalent widths (measurements from Maxted et al. 2008 and this work) we have included vertical bars (with the same color code described before) connecting those measurements. Large black circunferences surround Class II sources. The only solid red dot not classified as Class II corresponds to LOri156; a brown dwarf harbouring a thick disk already discussed in the Activity and accretion section.

**Table 3.15**: Equivalent width of the main lines observed in the spectra obtained with MIKE. For the case of the H$\alpha$ emission the values of FWHM and $FW_{10\%}$ have also been included. The symbol "–" indicates that the line is not detectable. We note that for most of the sources we took three exposures. In this table we provide the value measured on the averaged spectra (no significant variability was detected in such a short time scale).

| Object | H$\beta$ | [OI] | [OI] | [OI] | [NII] | [NII] | H$\alpha$ | | | HeI | LiI | [SII] | [SII] |
|---|---|---|---|---|---|---|---|---|---|---|---|---|---|
| | 4861 | 5577 | 6300 | 6364 | 6548 | 6581 | 6563 | | | 6678 | 6708 | 6717 | 6731 |
| | EW(Å) eEW | EW(Å) eEW | EW(Å) eEW | EW(Å) eEW | EW(Å) eEW | EW(Å) eEW | EW(Å) eEW | $FW_{10\%}$(km/s) eFW10 | FWHM(km/s) eFWHM | EW(Å) eEW | EW(Å) eEW | EW(Å) eEW | EW(Å) eEW |
| LOri017 | – | – | – | – | – | – | -6.572±2.307 | 19.033± 0.891 | 6.360±0.379 | – | – | – | – |
| LOri031 | – | – | – | – | – | – | -2.838±0.139 | 133.886± 0.100 | 57.470±0.100 | – | 0.614±0.045 | – | – |
| LOri042 | – | – | – | – | – | – | -3.024±0.156 | 130.237± 0.100 | 52.283±0.100 | – | 0.648±0.078 | – | – |
| LOri050 | -9.412±1.637 | -0.531±0.041 | -0.584±0.034 | – | – | – | -15.979±1.578 | 204.190± 5.078 | 80.844±0.583 | -0.437±0.070 | 0.570±0.016 | – | – |
| LOri055 | -5.112±0.295 | – | – | – | – | – | -7.054±0.132 | 105.422± 0.100 | 54.690±0.100 | – | 0.413±0.079 | – | – |
| LOri056 | -5.158±0.784 | – | – | – | – | – | -4.367±0.446 | 118.967± 0.100 | 29.772±0.100 | – | 0.306±0.047 | – | – |
| LOri057 | – | – | – | – | – | – | -4.999±0.307 | 133.405± 0.100 | 42.783±0.100 | – | 0.480±0.083 | – | – |
| LOri058 | – | – | – | – | – | – | -7.280±0.398 | 177.662± 0.100 | 65.785±0.100 | – | 0.299±0.056 | – | – |
| LOri059 | – | – | – | – | – | – | -6.874±0.288 | 123.839± 0.100 | 44.380±0.100 | – | 0.390±0.042 | – | – |
| LOri060 | -4.133±0.473 | – | -1.141±0.416 | 0.914±0.095 | – | – | -4.032±0.214 | 128.601± 12.311 | 42.838±0.132 | – | 0.400±0.069 | – | – |
| LOri063 | – | – | – | – | 0.732±0.045 | -2.508±0.385 | -11.547±0.692 | 103.513± 0.100 | 34.225±0.100 | – | 0.645±0.088 | -0.929±0.218 | -0.784±0.065 |
| LOri068 | -5.488±0.619 | – | – | – | – | – | -6.815±0.516 | 144.819± 0.751 | 52.574±0.379 | – | 0.691±0.090 | – | – |
| LOri073 | – | – | – | – | – | – | -10.906±1.041 | 308.589± 0.100 | 35.491±0.100 | – | 0.615±0.055 | – | – |
| LOri075 | – | -5.466±1.529 | -1.756±0.504 | – | – | – | -12.806±0.861 | 280.897± 0.100 | 63.352±0.100 | – | 0.941±0.052 | – | – |

**Table 3.16**: Equivalent width of the main lines observed in the spectra obtained with LRIS in the lowest resolution mode used. For the case of the H$\alpha$ emission the values of FWHM and $FW_{10\%}$ have also been included. The symbol "–" indicates that the line is not detectable. In the case of the Na I doublet at ~8200 Åthe value given is the addition of the EW measured for each component of the doublet. We do not list values for LOri165 since the poor S/N of its spectra does not allow us to provide reliable measurements.

| Object | [OI] 6300 | [OI] 6364 | [NII] 6548 | [NII] 6581 | H$\alpha$ 6563 | | | HeI 6678 | [SII] 6731 | Na I 8200 |
|---|---|---|---|---|---|---|---|---|---|---|
| | EW(Å) eEW | EW(Å) eEW | EW(Å) eEW | EW(Å) eEW | EW(Å) eEW | $FW_{10\%}$(km/s) eFW10 | FWHM(km/s) eFWHM | EW(Å) eEW | EW(Å) eEW | EW(Å) eEW |
| LOri075 | – | – | – | – | -10.203±0.885 | 508.674±28.187 | 329.813± 2.818 | – | – | 2.815± 0.378 |
| LOri081 | – | – | – | – | -3.450±0.071 | 507.292±10.104 | 79.108± 1.236 | – | – | 2.379± 0.190 |
| LOri082 | – | – | – | – | -10.631±2.094 | 365.138±32.646 | 243.652± 8.528 | – | – | 1.968± 0.100 |
| LOri087 | – | – | – | – | -6.995±0.393 | 524.099±16.692 | 319.621± 2.182 | – | – | 3.257± 0.405 |
| LOri095 | – | – | – | – | -8.231±1.177 | 472.947±41.735 | 268.336± 7.519 | – | – | 2.199± 0.345 |
| LOri098 | – | – | – | – | -12.508±0.904 | 192.404±14.548 | 163.184± 2.570 | -2.243±0.578 | – | 3.598± 0.513 |
| LOri107 | – | -0.682±0.130 | – | – | -11.915±1.018 | 192.824±10.091 | 101.558± 2.808 | – | – | 2.947± 0.063 |
| LOri110 | – | – | – | – | -5.731±2.728 | 315.067±28.476 | 280.498± 27.434 | – | – | 5.319± 0.690 |
| LOri114 | -2.392±0.859 | – | – | – | -12.589±1.734 | 443.986±52.475 | 244.657± 5.723 | – | – | 2.955± 0.207 |
| LOri115 | -0.950±0.030 | – | – | – | -8.974±0.879 | 488.641±43.944 | 228.659± 3.564 | – | – | 4.625± 1.472 |
| LOri116 | – | – | – | – | -11.779±1.543 | 550.587±47.371 | 231.602± 6.291 | – | – | 2.291± 0.063 |
| LOri118 | – | – | – | – | -10.429±0.205 | 385.889±3.739 | 200.330± 1.367 | – | – | 2.836± 0.665 |
| LOri124 | – | – | – | – | -6.965±1.776 | 275.810±30.964 | 236.637± 8.759 | – | – | 2.901± 0.776 |
| LOri126 | – | – | – | – | -35.424±3.504 | 423.619±10.226 | 275.512± 2.163 | – | – | 1.858± 0.300 |
| LOri130 | – | – | – | – | -8.505±0.629 | 380.821±11.137 | 231.322± 2.643 | – | – | 3.498± 0.778 |
| LOri133 | – | – | – | – | -2.200±0.402 | 383.101±11.900 | 83.850± 11.900 | – | – | 4.519± 0.617 |
| LOri134 | – | – | – | – | -5.925±0.307 | 414.258±13.816 | 251.489± 2.375 | – | – | 3.471± 0.381 |
| LOri135 | – | – | – | – | -13.320±3.533 | 387.911±89.677 | 272.093± 11.159 | – | – | 2.447± 0.936 |
| LOri139 | -2.760±0.278 | – | – | – | -17.986±1.019 | 318.437±3.694 | 236.181± 1.902 | -0.884±0.181 | -1.134±0.300 | 2.742± 0.398 |
| LOri140 | -11.817±3.639 | – | – | – | -79.143±9.439 | 413.949±14.091 | 286.552± 2.040 | -4.242±0.171 | – | 2.328± 0.223 |
| LOri141 | – | – | – | – | -3.060±0.768 | 383.389±27.805 | 344.335± 9.999 | – | – | 4.918± 1.376 |
| LOri147 | – | – | – | – | -9.804±1.373 | 474.165±24.845 | 241.861± 6.880 | – | – | 6.908± 0.417 |
| LOri150 | – | – | – | – | -15.254±2.046 | 294.012±9.445 | 275.049± 3.071 | – | – | 1.496± 0.575 |
| LOri151 | – | – | – | – | -9.567±2.024 | 383.255±72.881 | 264.943± 5.638 | – | – | 7.022± 1.360 |
| LOri154 | – | – | – | – | -17.465±3.030 | 306.366±6.798 | 255.896± 8.450 | -4.429±1.202 | -4.092±1.439 | 6.331± 1.235 |
| LOri155 | – | – | -4.276±0.821 | -4.418±0.549 | -51.493±18.697 | 786.706±292.685 | 308.948± 8.489 | -2.809±0.644 | – | 2.565± 0.434 |
| LOri156 | – | – | – | – | -114.455±1.812 | 501.896±10.670 | 316.907± 8.456 | – | – | 1.332± 0.270 |
| LOri161 | – | – | – | – | -74.510±33.069 | 301.382±42.955 | 227.491± 11.467 | – | – | 2.383± 0.379 |

**Table 3.17**: Equivalent width of the main lines observed in the spectra obtained with LRIS in medium resolution. For the case of the H$\alpha$ emission the values of FWHM and $FW_{10\%}$ have also been included. The symbol "–" indicates that the line is not detectable. In the case of the K I doublet at ∼7700 Å only the component at 7665 Å has been measured.

| Object | [NII] 6548 EW(Å) eEW | [NII] 6581 EW(Å) eEW | H$\alpha$ 6563 EW(Å) eEW | $FW_{10\%}$(km/s) eFW10 | FWHM(km/s) eFWHM | HeI 6678 EW(Å) eEW | LiI 6708 EW(Å) eEW | [SII] 6717 EW(Å) eEW | [SII] 6731 EW(Å) eEW | K1 I 7665 EW(Å) eEW |
|---|---|---|---|---|---|---|---|---|---|---|
| LOri068 | – | – | -14.388± 0.742 | 314.426± 3.189 | 135.978± 0.379 | -1.424± 0.244 | 0.530± 0.045 | -0.757± 0.378 | -0.406± 0.180 | 1.492± 0.247 |
| LOri071 | -0.490±0.109 | -1.127± 0.594 | -6.812± 0.232 | 229.188± 5.875 | 118.052± 0.549 | – | 0.395± 0.071 | – | -0.070± 0.008 | 1.645± 0.061 |
| LOri077 | -0.721±0.245 | – | -7.923± 0.231 | 233.149± 2.097 | 119.660± 0.407 | – | 0.486± 0.098 | -1.142± 0.519 | – | 1.900± 0.212 |
| LOri089 | -0.422±0.113 | – | -3.896± 0.225 | 368.666± 8.329 | 115.970± 1.517 | – | 0.603± 0.218 | -0.824± 0.377 | – | 1.545± 0.135 |
| LOri091 | – | -0.109± 0.002 | -11.932± 1.123 | 266.885± 33.657 | 114.534± 1.133 | -0.945± 0.305 | 0.644± 0.074 | -0.950± 0.693 | -0.341± 0.099 | 2.168± 0.463 |
| LOri094 | – | – | -8.488± 0.095 | 321.999± 0.786 | 141.460± 0.132 | -1.870± 0.386 | 0.719± 0.082 | – | -1.211± 0.821 | 2.087± 0.518 |
| LOri099 | -0.575±0.117 | – | -5.806± 0.638 | 307.278± 19.619 | 136.007± 4.172 | – | 0.567± 0.158 | – | – | 1.866± 0.069 |
| LOri106 | -0.576±0.186 | – | -48.423± 1.850 | 203.433± 0.821 | 109.098± 0.098 | -1.005± 0.248 | 0.477± 0.033 | -0.192± 0.018 | -0.255± 0.040 | 3.071± 0.887 |
| LOri109 | – | – | -8.696± 0.447 | 228.950± 2.223 | 113.744± 0.365 | -1.139± 0.219 | 0.502± 0.148 | – | -0.153± 0.038 | 2.623± 0.568 |
| LOri113 | – | -0.167± 0.054 | -20.853± 0.914 | 238.784± 2.710 | 129.651± 0.332 | -1.102± 0.139 | 0.617± 0.139 | -1.734± 0.420 | – | 2.678± 0.625 |
| LOri119 | -4.156±1.031 | – | -11.876± 0.409 | 227.861± 2.631 | 112.936± 0.339 | -0.578± 0.187 | 0.879± 0.184 | -0.252± 0.083 | – | 3.421± 0.668 |
| LOri129 | – | – | -10.757± 0.936 | 221.341± 4.472 | 100.069± 0.871 | -0.675± 0.150 | 0.404± 0.092 | – | – | 3.117± 0.769 |

**Table 3.18**: Equivalent width of the main lines observed in the spectra obtained with B&C in low and medium resolution. For the case of the H$\alpha$ emission the values of FWHM and $FW_{10\%}$ have also been included. The symbol "–" indicates that the line is not detectable. We also include the parameters derived for these objects. Note that, whenever possible, the Na I doublet is preferred over the K I to estimate the gravity of our sources since the measurement of the latter can be affected by the absorption band on top of which it is located.

| Object | H$\alpha$ | | | KI | KI | NaI | | EW(H$\alpha$)crit[1] | Alkali g |
|---|---|---|---|---|---|---|---|---|---|
| | 6563 | | | 7665 | 7700 | 8200 | SpT | | |
| | EW(Å) eEW | $FW_{10\%}$(km/s) eFW10 | FWHM(km/s) eFWHM | EW(Å) eEW | EW(Å) eEW | EW(Å) eEW | | | |
| LOri117 | 23.421±1.442 | 351.588± 13.503 | 137.967± 2.905 | | | 2.278±0.176 | M6.0 | ✗ | Mem |
| LOri120 | 10.182±1.967 | 271.625±733.136 | 112.917±15.762 | | | 3.388±0.361 | M5.5 | ✗ | Mem |
| LOri143 | 41.783±4.663 | 289.273± 4.808 | 238.369± 3.072 | | | 2.590±0.276 | M7.0 | ✗ | Mem |
| LOri080 | 14.671±1.001 | 259.417± 24.445 | 125.030± 1.767 | 1.662± 0.886 | 1.205± 0.253 | | M5.5 | ✗ | Mem |
| LOri100 | 11.425±1.839 | 205.041± 24.653 | 130.484± 3.571 | 2.063± 0.217 | 1.241± 0.063 | | M5.5 | ✗ | Mem |

[1] ✓ indicates that the object fulfills the accretion criterion by Barrado y Navascués & Martín (2003) (those marked with ✗ do not).

### 3.3.5 Particular sources:

#### 3.3.5.1 Accretion:

**LOri050:** Class II source according to its IRAC photometry (see Chapter 2) and active accretor based to the measured H$\alpha$ equivalent width (Table 3.15), its derived spectral type (Table 3.7) and its H$\alpha$ full width at 10% of the flux (Table 3.15). Via SED fitting we have determined a mass of ∼0.3 $M_\odot$ for this source (see Section 3.1), and we have estimated an accretion rate of $9.11\times10^{-11}$ $M_\odot$/yr. As can be seen in Fig. 3.15, this accretion rate is slightly lower than the one expected according to the mass of the source, but this is not surprising since according to Sacco et al. 2008 and Maxted et al. 2008 LOri050 is a spectroscopic binary. Therefore we are observing a very interesting system with a total stellar mass of ∼0.3 $M_\odot$ and a circumbinary disk actively accreting.

**LOri061, LOri126, LOri140, LOri156, LOri161:** All of them but LOri161 are classified as harbouring a thick disk (see Chapter 2) based on the IRAC slope (Lada et al. 2006). LOri161 in fact has not been classified according to its IRAC photometry since it was only detected in the two first channels. On the other hand, all of them are active accretors according to Barrado y Navascués & Martín (2003) criterion. As in the case of LOri050, we have estimated the accretion rate based in the measured H$\alpha$ full width at 10% of the flux (Table 3.16) and the mass of the source based on the SED fitting. We have obtained quite high accretion rates as can be seen in Fig. 3.15. We must note that the mass of one of the sources with the highest rate (LOri156) was not derived from the SED fit (since, due to the infrared excess shown by this target, the number of useful data-points to be reproduced with a synthetic photosphere was not enough to perform the fitting process, see Appendix C for further details); it was inferred from other members with no disk and similar spectral type.

With such high accretion rates some veiling (due to excess emission from the accretion shock) could be expected on these sources (as it is the case for LS-RCrA 1, Barrado y Navascués

**Table 3.19**: Equivalent width of the main lines observed in the spectra obtained with TWIN during 2005 and 2006 campaigns (medium resolution). For the case of the H$\alpha$ emission the values of FWHM and $FW_{10\%}$ have also been included. The symbol "–" indicates that the line is not detectable. Note that, whenever possible, the Na I doublet is preferred over the K I to estimate the gravity of our sources since the measurement of the latter can be affected by the absorption band on top of which it is located.

| Object | H$\alpha$ | | | HeI | LiI | KI | KI | NaI |
|---|---|---|---|---|---|---|---|---|
| | 6563 | | | 6678 | 6708 | 7665 | 7700 | 8200 |
| | EW(Å) eEW | $FW_{10\%}$(km/s) eFW10 | FWHM(km/s) eFWHM | EW(Å) eEW | EW(Å) eEW | EW(Å) eEW | EW(Å) eEW | EW(Å) eEW |
| DM48 | 7.724±0.190 | 587.785±10.910 | 328.313± 1.868 | – | – | 0.494 ±0.211 | 0.667 ±0.127 | 2.361±0.178 |
| LOri007 | – | – | – | – | – | 0.470 ±0.213 | 0.693 ±0.110 | 3.195±0.306 |
| LOri036 | 4.797±0.224 | 478.437± 7.954 | 287.713± 2.940 | – | – | 1.435 ±0.140 | 1.109 ±0.105 | 3.532±0.194 |
| LOri044 | 1.571±0.200 | 600.775±85.749 | 337.349± 9.449 | – | – | 1.124 ±0.107 | 0.997 ±0.041 | 3.450±0.157 |
| LOri045 | 6.849±0.105 | 626.681± 6.209 | 331.207± 1.516 | – | 0.390± 0.933 | 0.626 ±0.200 | 0.584 ±0.044 | 2.775±0.611 |
| LOri048 | 4.319±0.193 | 546.682±14.598 | 315.965± 3.477 | – | – | 0.628 ±0.106 | 0.583 ±0.079 | 2.740±0.255 |
| LOri052 | 6.796±0.440 | 487.216± 0.061 | 271.568± 0.014 | – | – | 1.420 ±0.120 | 0.930 ±0.099 | 3.151±0.032 |
| LOri061 | 11.776±0.165 | 540.469± 5.459 | 309.810± 0.962 | – | 0.435± 0.272 | 0.983 ±0.374 | 0.542 ±0.052 | 2.851±0.146 |
| LOri062 | 6.480±0.732 | 447.922±251.407 | 315.481± 8.221 | – | 0.073± 0.126 | 0.959 ±0.230 | 0.569 ±0.118 | 2.411±0.667 |
| LOri080 | 22.822±0.616 | 600.883± 4.756 | 336.845± 1.268 | – | 0.183± 0.080 | 1.772 ±0.330 | 0.629 ±0.184 | 2.340±0.455 |
| LOri091 | 47.870±8.314 | 382.777±19.556 | 228.429± 4.020 | 0.450 ±0.087 | – | – | – | 2.053±0.700 |
| LOri092 | 12.512±1.367 | 585.237±16.524 | 385.393± 7.298 | – | – | 0.704 ±0.070 | 0.746 ±0.120 | 2.732±0.430 |
| LOri105 | 13.376±2.603 | 581.478±39.131 | 362.935±11.431 | – | – | 2.131 ±0.904 | 1.331 ±0.540 | 2.367±0.647 |

et al. 2004a). In order to study this possibility, for each of our accretors, we selected a non-accreting Class III source with very similar spectral type (one half subclass) and we compared the strength of several TiO molecular bands on both spectra. As can be seen in Fig 3.23 no significant differences are found on the continuum level of any pair of sources. In fact, we have estimated that veiling, defined as $r_\lambda = F(\lambda)_{\rm excess}/F(\lambda)_{\rm photosphere}$ is negligeable in all of our cases: whilst for LS-RCrA 1, Barrado y Navascués et al. (2004a) found that $r_\lambda$ varies from ∼1 to ∼0.25 for the wavelength range 6200–6750 Å we find a horizontal slope in this interval. The only cases where a linear horizontal $r_\lambda$ does not work are located on the very edges of the detector, and therefore we can conclude that no veiling is present on our spectra.

**LOri106, LOri113:** These sources were classified as Class II based on their position in the IRAC colour-colour diagram. They harbour thick disks according to the mid-infrared slope of the SED and are active accretors following Barrado y Navascués & Martín (2003). We derived accretion rates which follow $\dot{M}_{acc} \propto {\rm M}_*^2 \pm 1$ dex (see Fig. 3.15 and Table 3.17).

**LOri080, LOri091:** This set of sources represent and interesting puzzle since both of them show variable H$\alpha$ emission (see following sections); according to the maximum measured EW of this line, both were classified as active accretors but none of them show infrared excess (see Barrado y Navascués et al. 2007b). Since no signpost of disk has been observed, the variation in H$\alpha$ might arise from chromospheric activity of these sources. We have analyzed the possible wavelength dependence of changes in the spectra of both sources from one observation to the other one. In the case of LOri091 no significant changes are observed apart from the difference in the H$\alpha$ profile. For LOri080, on the other hand, some wavelength dependent wavelength structure has been detected. In Fig. 3.24 we show this structure. To make this comparison we have used both, the spectra of LOri080 observed with the B&C spectrograph and the TWIN spectra of LOri105

**Table 3.20**: Equivalent width of the main lines observed in the spectra obtained with CAFOS. For the case of the H$\alpha$ emission the values of FWHM and $FW_{10\%}$ have also been included. The symbol "–" indicates that the line is not detectable. No measurements are provided for LOri069 and LOri083 since some problems with the identification of the right counterpart of the sources have been found (see 3.3.5).

| Object | H$\alpha$ | | | Ca II (IRT) | KI | KI | NaI |
|---|---|---|---|---|---|---|---|
| | 6563 | | | 8498, 8542,8662 | 7665 | 7700 | 8200 |
| | EW(Å) eEW | $FW_{10\%}$(km/s) eFW10 | FWHM(km/s) eFWHM | EW(Å) eEW | EW(Å) eEW | EW(Å) eEW | EW(Å) eEW |
| C69EI1-10336 | -6.312±0.579 | 520.180±15.077 | 386.596± 9.207 | – | 1.249 ±0.211 | 0.732 ±0.127 | 2.110±0.178 |
| C69EI1-114 | -4.788±0.160 | 425.320±15.108 | 217.719± 4.857 | – | 1.027 ±0.213 | 0.863 ±0.110 | 2.396±0.306 |
| C69EI1-13542 | – | – | – – | – | – | – | 1.210±0.194 |
| C69EI1-14424 | -11.652±0.249 | 536.653±10.869 | 349.084± 1.113 | – | 0.412 ±0.107 | 0.633 ±0.041 | 2.574±0.157 |
| C69EI1-14609 | -79.824±5.012 | 779.540±25.366 | 377.713± 6.584 | -5.361,-5.599,-4.245 | 1.310 ±0.870 | 0.398 ±0.044 | 2.402±0.611 |
| C69EI1-790 | -9.047±0.478 | 439.634±62.832 | 266.683±10.416 | – | 0.973 ±0.106 | 0.714 ±0.079 | 2.208±0.255 |
| C69WI1-3226 | – | – | – – | – | 4.844 ±0.120 | 3.819 ±0.099 | 4.59 ±0.032 |
| C69WI1-4897 | – | – | – – | – | – | – | 1.718±0.146 |
| C69_1d03367 | -6.869±0.350 | 736.586±77.050 | 374.092±10.892 | – | 0.374 ±0.230 | 0.328 ±0.118 | 2.259±0.667 |
| DM065 | -3.473 ± 0.115 | 465.345 ± 30.345 | 201.279 ± 4.954 | – | – | – | 1.727 ± 0.566 |
| DM070 | -1.560 ± 0.120 | 412.223 ± 29.733 | 249.214 ± 17.378 | – | – | – | 2.099 ± 0.635 |
| C69-X-E-009 I | -5.861 ± 0.282 | 565.053 ± 60.339 | 366.346 ± 12.633 | – | – | – | 1.022 ± 0.305 |
| C69-X-E-010 sX | -0.130 ± 0.038 | 661.376 ± 25.935 | 407.115 ± 114.145 | – | – | – | 0.712 ± 0.264 |
| C69-X-E-027 n | -5.580 ± 0.155 | 497.237 ± 75.874 | 255.838 ± 2.736 | – | – | – | 2.156 ± 0.568 |
| C69-X-E-040 M | -4.909 ± 0.577 | 929.244 ± 40.856 | 705.234 ± 15.234 | – | – | – | 1.828 ± 0.544 |
| C69-X-E-060 n | 1.494 ± 0.065 | 875.720 ± 60.309 | 503.664 ± 15.852 | – | – | – | 0.919 ± 0.273 |
| C69-X-E-064 I | -7.571 ± 0.340 | 480.504 ± 84.239 | 257.710 ± 8.095 | – | 0.215 ± 0.188 | 0.214 ± 0.186 | 2.095 ± 0.592 |
| C69-X-E-068 M | 4.165 ± 0.198 | 1310.578 ± 97.850 | 619.490 ± 17.607 | – | – | – | 0.460 ± 0.227 |
| C69-X-E-069 c | 1.443 ± 0.106 | 1485.519 ± 165.080 | 765.851 ± 21.626 | – | – | – | 0.935 ± 0.241 |
| C69-X-E-071 c | 1.491 ± 0.052 | 943.769 ± 20.335 | 579.984 ± 5.637 | – | – | – | 0.548 ± 0.269 |
| C69-X-E-072 I | -4.643 ± 1.096 | 784.025 ± 149.766 | 356.684 ± 41.958 | – | – | – | 0.646 ± 0.373 |
| C69-X-E-073 I | 4.209 ± 0.579 | 1691.144 ± 393.990 | 842.876 ± 38.903 | – | – | – | 0.476 ± 0.114 |
| C69-X-E-104 c | -2.618 ± 0.196 | 793.690 ± 8.992 | 444.372 ± 11.133 | – | – | – | 1.719 ± 0.463 |
| DM48 | -3.357±0.111 | 361.042±58.248 | 207.629±34.510 | – | 0.291 ±0.070 | 0.229 ±0.120 | 2.566±0.430 |
| LOri046 | – | – | – | – | 1.007 ±0.904 | 1.576 ±0.540 | 3.539±0.647 |
| LOri049 | – | – | – | – | 0.922 ±0.070 | 0.462 ±0.050 | 3.142±0.194 |
| LOri053 | -5.833±0.216 | 682.681± 30.222 | 444.106±17.941 | – | 0.807 ±0.211 | 0.554 ±0.271 | 1.965±0.157 |
| LOri054 | -8.346±0.476 | 679.312± 35.771 | 436.269±12.554 | – | 1.125 ±0.213 | 0.726 ±0.233 | 1.752±0.611 |
| LOri064 | -9.617±0.563 | 775.658±196.878 | 689.032±17.970 | – | 1.393 ±0.207 | 1.461 ±0.107 | 2.954±0.255 |
| LOri069 | – | – | – | – | – | – | – |
| LOri070 | -13.555±3.256 | 857.564± 62.661 | 657.945±46.892 | – | 1.139 ±0.107 | – | 2.412±0.146 |
| LOri072 | -11.258±0.508 | 424.469± 85.548 | 301.016±26.867 | – | 1.868 ±0.870 | 1.383 ±0.370 | 2.202±0.667 |
| LOri078 | -1.142±0.186 | 502.345± 42.514 | 367.513±35.751 | – | 0.420 ±0.106 | 0.557 ±0.106 | 2.050±0.455 |
| LOri079 | -9.061±3.351 | 702.366± 76.618 | 495.637±81.053 | – | 0.708 ±0.120 | 0.583 ±0.120 | 1.806±0.700 |
| LOri083 | – | – | – | – | – | – | – |
| LOri084 | -10.419±3.180 | 681.666±105.135 | 414.736±62.763 | – | 1.538 ±0.904 | 1.145 ±0.904 | 2.311±0.255 |

(a non accretting member to C69 with no sign of accretion) as standards to compare the overall shape of the spectra. We find a very faint component on top of the photospheric one using both standards. Once this excess is corrected from the TWIN spectra we measure a marginal detection of Li I with a EW of 0.183±0.081 Å.

**C69EI1-14609:** Accretor according to Barrado y Navascués & Martín (2003) criterion. For this particular object we have been able to obtain a different estimation for the accretion rate based on the equivalent width measurement of the components of the CaII triplet (at 8498 Å, 8542 Å and 8662 Å). This emission could be a sign of chromospheric activity, but the equivalent widths measured are too large, placing our measurements in the broad-line component of the unresolved line structures, that is generally related to accretion (see Comerón et al. 2003; Mohanty et al. 2005). We also note that as in Comerón et al. (2003) the CaII triplet line ratios are very close to 1:1:1 (quite different from the 1:9:5 expected ratio for optically thin emission). As in Comerón

**Table 3.21**: Equivalent width of the main lines observed in the spectra obtained with FLAMES. For the case of the H$\alpha$ emission the values of FWHM and $FW_{10\%}$ have also been included (and the aditional 7% uncertainty due to the nebulosity component has been taken into account). The symbol "–" indicates that the line is not detectable.

| Object | [NII] 6581 EW(Å) | H$\alpha$ 6563 EW(Å) | $FW_{10\%}$(km/s) | FWHM(km/s) | HeI 6678 EW(Å) | LiI 6708 EW(Å) | [SII] 6717 EW(Å) | [SII] 6731 EW(Å) |
|---|---|---|---|---|---|---|---|---|
| C69WI1-2708 | -0.691±0.060 | -6.377±0.128 | 552.227±39.125 | 183.578±12.945 | – | 0.518±0.014 | -0.388±0.128 | -0.307±0.051 |
| C69WI1-9288 | – | -30.202±1.140 | 602.118±44.632 | 183.86±13.029 | -0.482±0.148 | 0.432±0.040 | – | -0.198±0.037 |
| DM009 | – | -0.608±0.039 | 205.370±14.376 | 75.593±5.291 | – | 0.432±0.029 | – | – |
| DM016 | – | -2.828±0.101 | 153.631±10.754 | 66.407±4.648 | – | 0.546±0.010 | – | – |
| LOri001 | – | -2.819±0.159 | 251.751±17.623 | 97.268±6.809 | – | 0.468±0.015 | – | – |
| LOri007 | – | – | – | – | – | – | – | – |
| LOri011 | – | – | – | – | – | – | – | – |
| LOri012 | – | – | – | – | – | – | – | – |
| LOri013 | – | -4.308±0.207 | 190.175±13.312 | 75.889±5.312 | – | 0.523±0.037 | – | – |
| LOri024 | – | -2.466±0.107 | 163.825±11.468 | 66.436±4.651 | – | 0.540±0.017 | – | – |
| LOri026 | – | -5.537±0.298 | 236.544±16.558 | 83.764±5.863 | – | 0.588±0.046 | – | – |
| LOri037 | – | -4.401±0.233 | 171.951±12.037 | 70.046±4.903 | – | 0.558±0.037 | – | – |
| LOri038 | – | -14.012±0.513 | 204.755±14.333 | 90.727±6.351 | -0.454±0.133 | 0.523±0.035 | – | – |
| LOri043 | – | -3.920±0.123 | 125.701±8.799 | 60.390±4.227 | – | 0.528±0.070 | -0.261±0.071 | – |
| LOri044 | – | -1.615±0.098 | 123.614±8.653 | 52.944±3.706 | – | – | – | – |
| LOri045 | -0.402±0.044 | -6.220±0.337 | 165.632±11.594 | 59.234±4.146 | -0.343±0.068 | 0.498±0.044 | – | – |
| LOri046 | – | -0.369±0.014 | – | 13.254±1.255 | – | – | – | – |
| LOri049 | – | – | – | – | – | – | -0.205±0.037 | – |
| LOri050 | -0.452±0.059 | -11.646±1.290 | 226.620±23.719 | 84.980±6.760 | -0.627±0.242 | 0.509±0.036 | – | – |
| LOri052 | – | -7.262±0.423 | 234.239±16.397 | 85.283±5.970 | – | 0.278±0.103 | – | – |
| LOri053 | – | -4.298±0.148 | 128.460±9.293 | 64.825±4.554 | – | 0.560±0.041 | -0.254±0.032 | – |
| LOri056 | – | -6.219±0.221 | 143.572±10.191 | 66.654±4.688 | – | 0.450±0.023 | – | – |
| LOri059 | -0.624±0.129 | -9.833±0.301 | 121.439±8.501 | 52.399±3.668 | -0.313±0.053 | 0.369±0.063 | -0.679±0.128 | -0.362±0.083 |
| LOri069 | -0.756±0.134 | -8.123±0.466 | 185.720±13.000 | 61.282±4.290 | – | 0.328±0.041 | -0.459±0.113 | -0.503±0.104 |
| LOri073 | -0.374±0.086 | -4.542±0.186 | 131.898±10.403 | 61.659±4.432 | -0.215±0.031 | 0.462±0.092 | – | – |
| LOri075 | -0.731±0.171 | -10.729±0.726 | 270.528±20.109 | 101.942±8.074 | – | 0.960±0.202 | – | – |
| LOri079 | -1.430±0.072 | -10.010±0.243 | 92.566±6.480 | 39.784±2.785 | -0.403±0.058 | 0.605±0.090 | – | -0.665±0.035 |
| LOri086 | -1.121±0.132 | -6.978±0.205 | 103.888±7.272 | 48.805±3.416 | -0.338±0.047 | 0.621±0.086 | – | – |
| LOri087 | -0.575±0.131 | -7.947±0.231 | 126.534±8.857 | 54.013±3.781 | -0.506±0.032 | 0.594±0.078 | -0.901±0.054 | -0.406±0.076 |
| LOri088 | -1.639±0.134 | -16.288±0.483 | 97.336±6.991 | 48.506±3.426 | -0.506±0.094 | 0.475±0.111 | -1.593±0.365 | -0.719±0.183 |
| LOri091 | -0.440±0.055 | -13.473±1.112 | 152.509±13.524 | 67.343±4.999 | – | 0.760±0.060 | -0.813±0.355 | – |
| LOri093 | -1.002±0.061 | -8.536±0.219 | 119.687±8.378 | 59.589±4.171 | -0.238±0.029 | 0.496±0.083 | – | – |
| LOri094 | -1.705±0.210 | -13.775±0.728 | 164.273±11.499 | 46.247±3.237 | -0.412±0.065 | 0.495±0.024 | – | -0.983±0.190 |
| LOri096* | – | – | – | – | – | 0.382±0.156 | – | – |
| LOri099 | – | -9.221±0.667 | 121.811±8.527 | 33.522±2.347 | – | 0.385±0.115 | – | – |
| LOri105 | -2.675±0.519 | -22.429±0.449 | 85.105±5.957 | 35.092±2.456 | – | 0.137±0.026 | – | -0.719±0.194 |
| LOri109 | -2.636±0.436 | -19.615±0.516 | 94.108±6.588 | 36.735±2.571 | – | 0.565±0.113 | -1.421±0.165 | -1.039±0.129 |
| LOri112 | -1.756±0.197 | -10.927±1.683 | 132.260±21.057 | 90.340±6.824 | – | 0.537±0.195 | -2.070±0.249 | – |
| LOri115 | – | -12.575±0.592 | 81.994±5.740 | 20.491±1.434 | -0.831±0.082 | 0.336±0.090 | -0.983±0.285 | – |
| LOri120 | -3.310±0.165 | -13.304±1.000 | 80.596±7.327 | 37.101±2.721 | – | 0.657±0.084 | -4.725±0.554 | 1.341±0.122 |

*No measurements for the emission lines are provided since the substraction of the nebulosity for this particular source was not satisfactory.

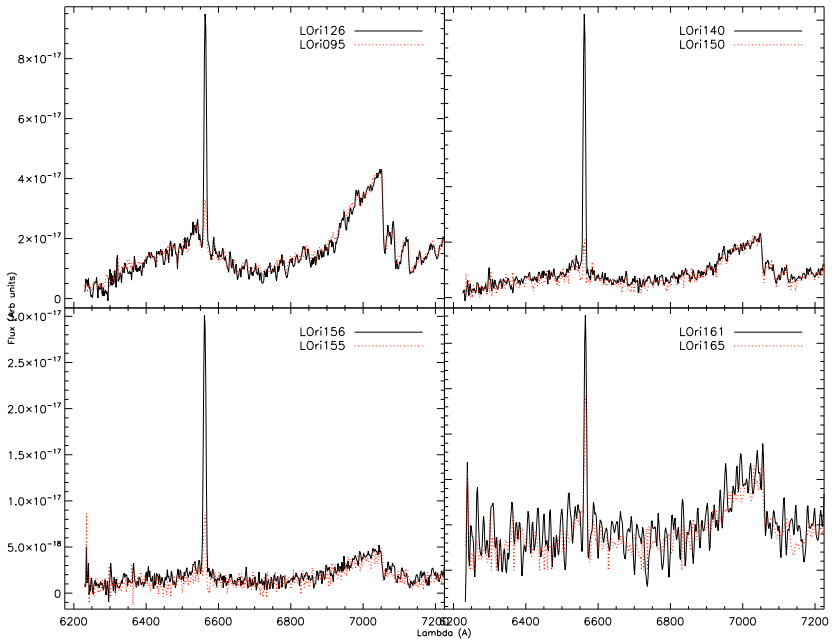


**Figure 3.23**: Comparison of accreting (black solid line) and non accreting (red dotted line) sources of the LRIS low resolution sample of objects. Note the absence of a super-imposed continuum.

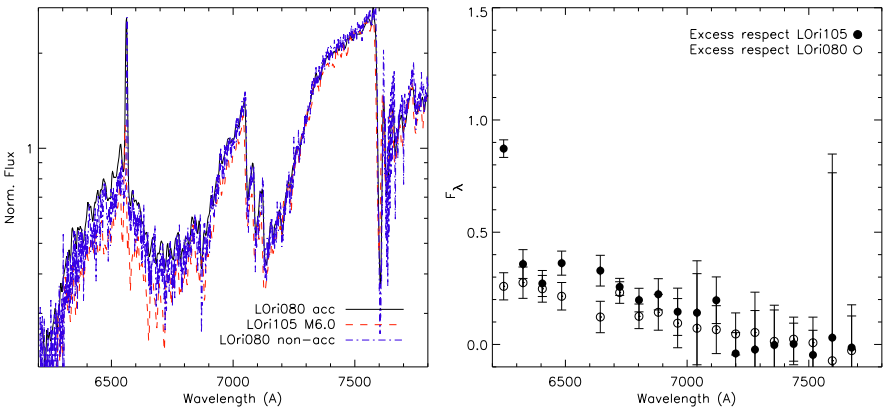


**Figure 3.24**: **Left:** Comparison of the spectra of LOri080 taken in two different campaigns and the spectra of a non-accreting member with a very similar spectral type. LOri080 spectra showing the largest H$\alpha$ emission has been plotted with a solid black line, the spectra of the comparison member is plotted with a red dashed line; and the LOri080 spectra with much lower H$\alpha$ emission is displayed in blue (dot-dashed line). **Right:** Veiling emission ($r_\lambda$) estimated as function of the wavelength for LOri080 with large H$\alpha$ emission. We have used LOri80 itself and LOri105 as comparison templates. Note that the region around the H$\alpha$ emission has been omitted.

et al. (2003) we used the following equations to estimate the accretion rate of this source (these equations were derived from the accretion line profile study by Muzerolle et al. 1998):

$$\log(\dot{M}_{acc}) = -34.15 + 0.89\log(F_{\mathrm{CaII}(\lambda 8542)}) \tag{3.2}$$

$$F_{\mathrm{CaII}(\lambda 8542)} = 4.72 \times 10^{33} EW(\mathrm{CaII}(\lambda 8542)) \times 10^{-0.4(m_\lambda - 0.54 A_V)} \tag{3.3}$$

where $F_{\mathrm{CaII}(\lambda 8542)}$ is the flux in the line, $m_\lambda$ is the magnitude of the star at $\lambda$8542, and $A_V$ is the visual extinction translated to the wavelength of the line of study using Fitzpatrick (1999) relations. Since the bluest photometric point that we had for this object is the 2MASS J magnitude, we used the best fitting model to the SED of the source as a scaling factor to estimate $m_\lambda$. On the other hand, according to the intrinsic colors by Leggett (1992) and our determination of the spectral type (M3), we find a very low $A_V$ value of 0.03 mag. Finally we obtained an accretion rate value of $2.95\times10^{-7}$ $M_\odot$/yr; almost an order of magnitude lower than the one obtained based on H$\alpha$. We have also checked for this object the presence of veiling comparing its spectrum with the one of C69EI1-790 (another confirmed member with the same spectral type). In this case no blue excess has been found in the source (further than a marginal excess right in the blue edge of the spectra that we think corresponds to an instrumental signature rather than a real excess).

**C69WI1-9288, C69WI1-2708:** Both sources are classified as Class II based on their IRAC photometry, and they show double-peaked structure on the H$\alpha$ emission as can be see in Fig 3.25. Whilst the sky subtraction for C69WI1-9288 worked very well, some residual could remain in the case of C69WI1-2708 (although we do not see any structure on other, very narrow, "sky lines"). The accretion rate calculated for C69WI1-9288 is shown in Table 3.21 since this source fulfills the Barrado y Navascués & Martín (2003) criterion. On the other hand the measured H$\alpha$ equivalent width of C69WI1-2708 lies well below the saturation criteria, but its wide $FW_{10\%}$ velocity would translate in an accretion rate of $\sim 2.93 \times 10^{-08}$ $M_\odot$/yr. As in previous cases we have compared the spectra of these two sources with non-accreting targets of the same spectral type (LOri026 and LOri037, respectively) and no veiling has been detected.

#### 3.3.5.2 Binarity

**LOri075:** This source has been classified as SB1 by Maxted et al. (2008) (but no binarity signpost has been reported in Sacco et al. 2008). According to Maxted et al. (2008), the spectral lines for this star show rotational broadening; they compared them to those of a narrow-lined star of similar spectral type and estimated a projected rotational velocity of vsin($i$) $\sim$ 65 km/s. They classified the source as SB1, but they also noted that there is an asymmetry in the cross-correlation function (CCF) in the form of a blue-wing, particularly when the measured RV corresponds to a red-shift. Therefore they suggested that the fainter component in this binary was detected but unresolved in their spectra.

We have detected a double peaked structure in H$\alpha$ and Li I in our MIKE spectra which made us believed that we had spectroscopically resolved the source. Further research on the struc-

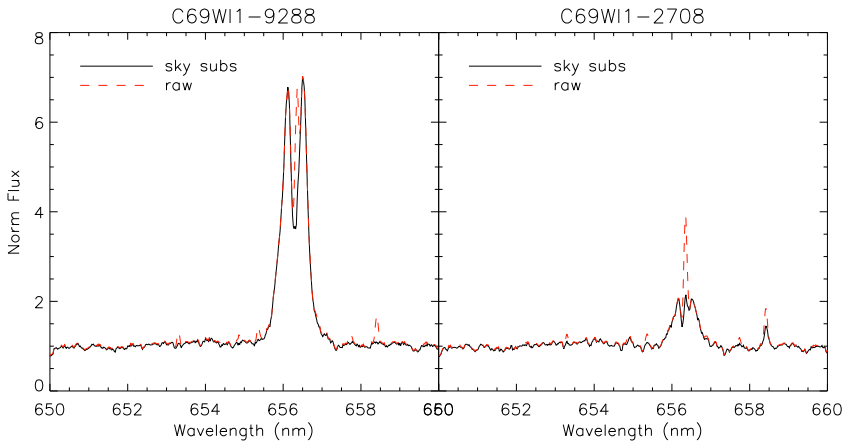


**Figure 3.25**: Double peaked structure in the H$\alpha$ emission of C69WI1-9288 and C69WI1-2708.

ture of some photospheric lines marginally suggests that we might have resolved the binary. In Fig 3.26 we show the double peaked structure found in some of the most prominent photospheric lines for this object (given the low temperature of the source these "most prominent lines" are still very weak). We have measured a mean relative velocity of ~45 km/s ($\sigma$ ~8.7 km/s). We have synthesized a 3500 K (log($g$) = 4.) Kurucz spectra (an effective temperature ~200 K hotter than the one estimated for our source, but the coolest temperature for the Kurucz collection) in the region of the Ba $\lambda$5535Å line with the same resolution and a rotational velocity close to the one derived by Maxted et al. (2008) (~50 km/s). We have checked that the closest line in the synthetic spectra has a relative velocity of ~110 km/s, much higher than those measured by us. We show on the right-hand side panel that the relative velocity derived for the photospheric lines does not agree with the one that would be measured on the H$\alpha$ profile. This fact and the weakness of the lines measured force us to consider the resolution of the binary as tentative. We must note anyway that the environmental H$\alpha$ component (see Fig 1.7) of the region can change the relative velocity of the peaks of this emission line.

#### 3.3.5.3 Membership

**LOri044, LOri046, LOri049, LOri052:** All these sources (but LOri052) have been classified as non-members based on the absence or very marginal detection of Li I. In the cases of LOri044, LOri046, LOri049, LOri052, either Maxted et al. (2008) or Sacco et al. (2008) also classify them as non-members based on their radial velocities. On our FLAMES spectra of LOri052 a marginal detection of Li I in absorption with EW of ~0.28 Å was measured; this value is too low compared to other members with similar spectral type; therefore, together with Maxted et al. (2008) radial velocity determination and our alkali lines study, we classify this source as possible non-member.

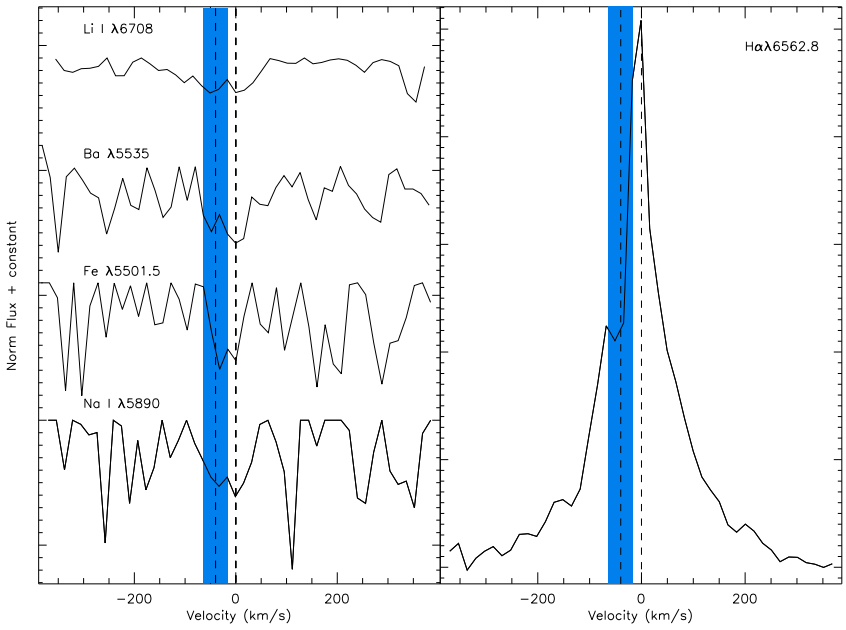


**Figure 3.26**: **Left:** Double peaked structure found in photospheric lines for LOri075. Rest frame velocity and mean relative velocity of the second peak are indicated with dashed lines. The blue rectangle shows the $\pm 3\sigma$ area of the second peak location. **Right:** H$\alpha$ profile of the same source. Note how the secondary peak dashed line location (calculated from the photospheric lines) does not agree with the position of the peak (see text for details).

**LOri110, LOri115, LOri133, LOri141, LOri147, LOri151, LOri154**: All these sources show surface gravities (based on the measured EW(NaI), see Table 3.16 and 3.19) too large compared with other cluster members. For the particular case of LOri110, no Li I was detected on our LRIS spectra, and Maxted et al. (2008) also measured Na I EWs inconsistent with membership and confirmed that the radial velocities derived ruled out membership too. Regarding LOri133 and LOri151, Barrado y Navascués et al. (2004b) already classified these objects as doubtful candidate members based on their photometric properties. To enforce our classification as non-members for these sources we have compared the strength of their Na I doublet with field dwarf of the same spectral types and with objects having an EW value consistent with membership. We show this comparison in Fig. 3.27. Even though LOri115 shows very deep Na I absorption (as shown in the previously mentioned figure), it shows an EW(Li) (measured on or FLAMES spectra) compatible with a young source. The variability in H$\alpha$ found between our two spectra, suggests that this depth of the Na I doublet could be related to stellar activity.LOri165 was also classify as possible non-member by Barrado y Navascués et al. (2004b) and even though our LRIS low resolution spectra has a very poor signal-to-noise ratio to be able to provide reliable measurements of the Na I doublet, the rough profile of the doublet suggests that it does not correspond to a young source.

**LOri007:** No significant H$\alpha$ emission was measured on the spectra of this source (ob-

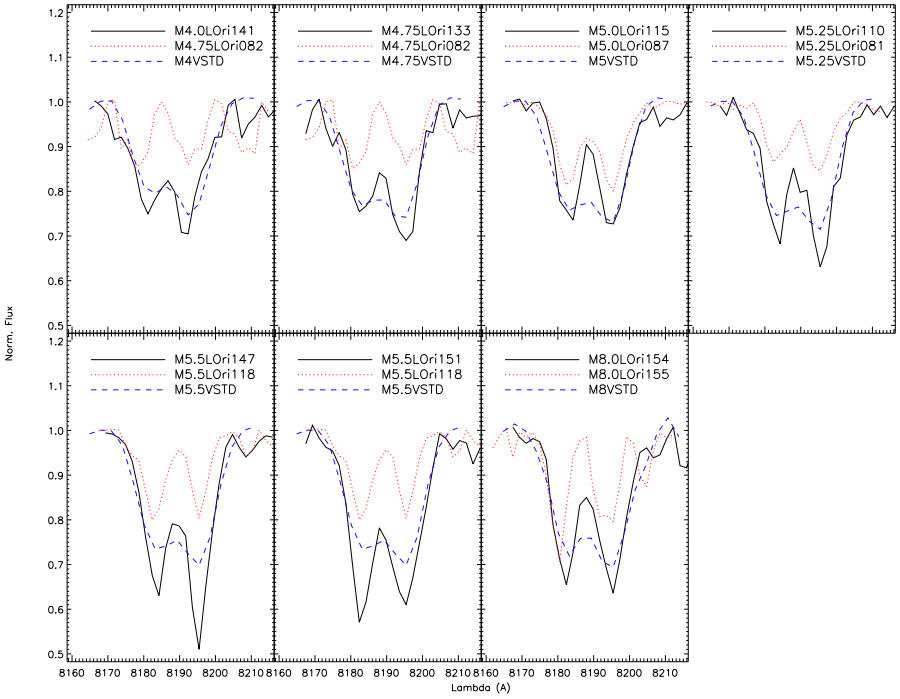


**Figure 3.27**: Candidates discarded as members based on the Na I $\lambda$8200 doublet. For each case we have over-plotted in red a candidate member with a EW value consistent with membership and the same spectral type. In blue we have plotted the same region for spectra of field dwarfs obtained in the same campaign with the same spectral type (for spectral types M4.75 and M5.25 we have averaged spectra of field dwarfs with spectral types M4.5 and M5.0; M5.0 and M5.5, respectively). Note how the depth of the absorption resembles the spectra corresponding to the dwarfs more than those from the candidate members.

served with TWIN and with FLAMES), and although the equivalent widths values of the alkali lines are consistent with membership (see Table 3.10), no Li I in absorption has been detected (see Table 3.12). Therefore we provide a classification of non-member.

**LOri036, LOri044:** Both sources show faint H$\alpha$ emission, but the alkali lines suggest that both objects are older than the cluster members. Besides Sacco et al. (2008) found a RV value not fully compatible with membership for LOri036, and (Maxted et al. 2008) estimated a RV that clearly rules out membership for LOri044.

**C69EI1-13542, C69WI1-3226, C69WI1-4897, LOri046, LOri049:** None of these sources show H$\alpha$ emission. In fact, several of them show this feature in absorption along with very low gravity according to the alkali absorptions strengths; therefore we classify them as non-members. In particular, LOri046 and LOri049 have also been classified as non-members by Sacco et al. (2008) due to their measured radial velocity.

**LOri069, LOri083:** Both sources are members according to Sacco et al. (2008) and Maxted et al. (2008). The spectra that we obtained with CAFOS do not correspond to a M star at

all; after some checking, we arrived to the conclusion that in both cases we made a mistake when positioning the slit and the spectra of a background source was obtained. A year later we observed again LOri069 with FLAMES. In this case we are sure that the observed source is indeed LOri069 and we confirmed its membership by the presence of Li I absorption in the spectra.

#### 3.3.5.4 Variability

**LOri068, LOri075, LOri080, LOri091, LOri109, LOri115:** All these sources have been observed with two different instrumental set-ups. All of them show variations in the measured H$\alpha$ profile. We have checked for each case whether this variations could be related to the different resolutions the spectra were obtained with or they are signpost of real variability of the source. In Table 3.22, we resume the different values measured for these sources that we have used to distinguish between instrumental bias or real variability.

LOri068 and LOri109 have been classified as non-accreting sources with the data from both campaigns; we have measured EW values of the Li I absorption compatible (within the errors) in both runs while the variation in H$\alpha$ is much larger. Therefore we consider that those variations in the H$\alpha$ emission are not an instrumental bias, but reflects chromospheric variable activity.

LOri115 also shows variable H$\alpha$ emission; it has been classified as Class II with a thin disk according to the IRAC data, but none of the measured H$\alpha$ equivalent widths suggest that the disk might be accreting onto the star. As in the previous case we think that this variability has its origins on the chromospheric activity and not in the interaction with it disk.

The case of the SB LOri075 is more difficult to analyze since (due to the very different resolution and wavelength coverage of the spectra) we have not been able to measure common lines to perform the same comparison as with LOri068. In any case, since LOri075 is an unresolved (or marginally resolved) double system, variability in the measured H$\alpha$ is not surprising.

LOri080 and LOri091 as stated before in this section, represent very interesting cases; due to the similar resolution (in both cases but specially in the latter one comparing the TWIN and B&C measurements) and compatible KI measured EWs (for LOri080), the large variations in H$\alpha$ emission should not arise from any instrumental effect. These sources change from being under the H$\alpha$ saturation criteria (Barrado y Navascués & Martín 2003) to be well above. The estimated accretion rates would change in one order of magnitude for LOri091 up to three orders of magnitude for LOri080. As shown in Fig. 3.15 this large variable accretion has been detected on higher masses sources. In the case of LOri091 a flare is more likely to explain such variations in H$\alpha$ than the variable accretion scenario since no infrared excess has been detected. On the other hand LOri080 remains a puzzle; some infrared excess has been detected on IRAC bands but the slope of its SED at these wavelengths (from 3.6 to 8.0 micron) classify this object as harbouring a thin disk, for which the calculated accretion rate variability seems to be too high.

There are other sources like LOri050, LOri059, LOri073, LOri094, LOri099 and LOri105 that show some variation in the measured EW, but these variations are very close to the estimated

**Table 3.22**: Parameters measured and calculated for those sources observed with different instrumental set-ups. The symbol "–" indicates that the parameter was not estimated for this particular source.

| Name | EW(H$\alpha$) | Ins. Res | log($\dot{M}_{acc}$)(M$_\odot$/yr) | LiI | KI | NaI |
|---|---|---|---|---|---|---|
| LOri068 | 6.82±0.52 | MIKE R~10000 | – | 0.69±0.09 | – | – |
| LOri068 | 14.39±0.74 | LRIS R~3500 | – | 0.53±0.05 | – | – |
| LOri075 | 12.81±0.86 | MIKE R~10000 | – | 0.94±0.05 | – | – |
| LOri075 | 10.20±0.89 | LRIS R~1100 | – | – | – | 2.82±0.38 |
| LOri080 | 14.67±1.00 | BC R~2600 | -10.374±0.24 | – | 1.66±0.89 | – |
| LOri080 | 22.82±0.62 | TWIN R~3500 | -7.061±0.05 | – | 1.77±0.33 | 2.34±0.46 |
| LOri091 | 11.93±1.12 | LRIS R~3500 | -10.301±0.33 | 0.23±0.07 | 2.17±0.46 | – |
| LOri091 | 47.87±8.3 | TWIN R~3500 | -9.177±0.19 | – | – | 2.05±0.70 |
| LOri091 | 13.47±1.11 | FLAMES R~8600 | -11.411±0.03 | 0.76±0.06 | – | – |
| LOri109 | 19.62±0.52 | FLAMES R~8600 | – | 0.57±0.11 | – | – |
| LOri109 | 8.70±0.45 | LRIS R~3500 | – | 0.50±0.15 | 2.62±0.57 | – |
| LOri115 | 12.58±0.59 | FLAMES R~8600 | – | 0.34±0.09 | – | – |
| LOri115 | 8.97±0.88 | LRIS R~1100 | – | – | – | 4.63±1.47 |

**Table 3.23**: Collinder 69 near infrared spectroscopic campaigns.

| Date | Observatory/Telescope/Instrument | Resolution | Wavelength coverage | Number of sources observed observed | Original photometric survey |
|---|---|---|---|---|---|
| December 22-23, 2004 | Mauna Kea / Keck II / NIRSPEC | ~2000 | 1.143–1.375$\mu$m | 4* | CFHT1999 |
| December 9, 2005 | Mauna Kea / Keck II / NIRSPEC | ~2000 | 1.143–1.375$\mu$m | 9* | CFHT1999 |
| January 9-11, 2007 | La Silla / NTT / SOFI | ~950 | 0.950–2.500$\mu$m | 2 | CFHT1999 |
| November 10, 2008 | Mauna Kea / SUBARU /IRCS | ~200 | 1.400–2.500$\mu$m | 8* | Subaru2006 |

* For some of the sources the obtained S/N ratio was too poor to perform the analysis and therefore are not listed on the tables with the results from these analyses.

errors or has also been measured on the Lithium line and the probability that they only reflect biases due to the different resolution of the spectra seems to be quite high.

## 3.4 Low resolution near-infrared spectroscopy

In order to be able to characterize the colder–redder candidate members to Collinder 69 we requested time in different observatories to perform infrared spectroscopy. We were granted with four campaigns (details about the campaigns themselves are provided in Table 3.4 and the reduction procedures followed are described in Appendix A). Two of the runs were focused on confirming the candidates by studying their surface gravity (with alkali lines as in the optical). The aim of the other two campaigns was to derive infrared spectral types analyzing the water vapour bands. In the following sections we provide a description of the methodologies used and the results achieved.

### 3.4.1 Estimating infrared spectral types: Water vapour indices and templates.

We have derived infrared spectral types for the sources observed with SOFI and SUBARU using spectral indices and templates. We did not make this analysis for the NIRSPEC sources due to the short wavelength coverage of the observations.

At this low spectral resolution, there are no absorption lines present in our spectra that can be reliably used to derive spectral types in the infrared domain. However, as has already

been mentioned in the Introduction, the depths of the broad water vapour absorption bands are extremely sensitive to spectral type for M and L dwarfs.

Comerón et al. (2000) defined a reddening independent index, $I_{H_2O}$, to perform a spectral type classification measuring the depth of the wings of the water band of late M dwarfs centered near 1.9 $\mu$m. This index is defined as:

$$I_{H_2O} = \frac{f_1}{f_2}\left(\frac{f_4}{f_3}\right)^{0.76} \tag{3.4}$$

where $f_1$, $f_2$, $f_3$ and $f_4$ are the density fluxes in four narrow bands, 0.05 $\mu$m wide, centered at 1.675 $\mu$m, 1.75 $\mu$m, 2.075 $\mu$m and 2.250 $\mu$m, respectively.

Gómez & Persi (2002) tested this method by comparing the estimated spectral types with the $Q$ index defined by Wilking et al. (1999) obtaining excellent agreements (see Fig.8 in their paper). This $Q$ index is reddening independent too and was defined in order to characterize the strength of the 1.7-2.1 $\mu$m and $\geq$ 2.4 $\mu$m water absorption bands. It has the following expression:

$$Q = \frac{F_1}{F_2}\left(\frac{F_3}{F_2}\right)^{1.22} \tag{3.5}$$

where $F_1$, $F_2$ and $F_3$ are the relative flux densities calculated in the three narrow bands: [2.070 – 2.130$\mu$m], [2.267 – 2.285$\mu$m] and [2.400 – 2.500$\mu$m], respectively.

We have not been able to calculate the $Q$ index accurately for our targets, because the bands considered (in particular F3), are located too close to the edge of the detector (in both campaigns) and affected by our reduction. However, we can still use the $I_{H_2O}$ index and the comparison with spectral templates (obtained during the same night) to estimate the infrared spectral type of our candidates.

Examples of these comparisons with spectral templates for the four L brown dwarfs confirmed in this work are displayed in Fig 3.28.

We show the derived spectral types in Table 3.4.2. Whenever the source had a derived optical spectral type we present both estimations. In both cases the infrared spectral type turns out to be slightly colder than the optical but within the half subclass domain as previously reported (Luhman et al. 2003).

### 3.4.2 Estimating surface gravities

In order to estimate the surface gravity of our sources, we compared the strength of the gravity sensitive doublets of K I (at 1.169 & 1.177 $\mu$m and 1.244 & 1.253 $\mu$m) with a grid of models by Allard et al. (2003). For each source we made this comparison for different values of log($g$) and a value of the effective temperature obtained applying Leggett (1992) temperature scale to the optical spectral types derived in this work. For the case of LOri146 where no optical spectra has been collected by our group, we assumed the effective temperature derived from the SED fitting (see Section 3.1).

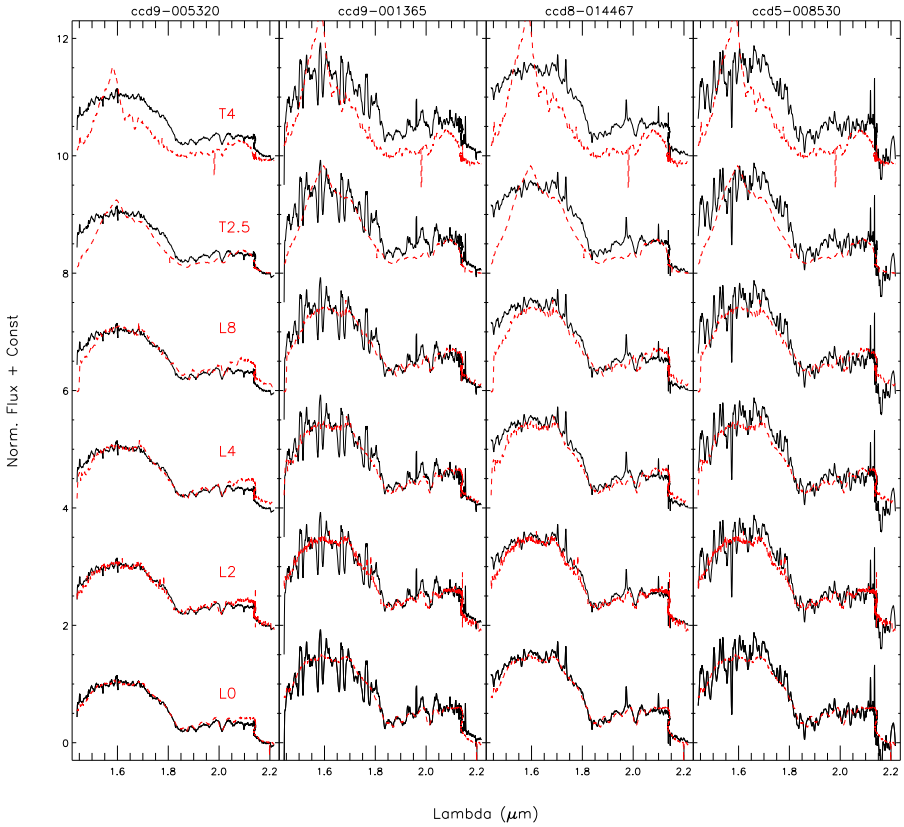


**Figure 3.28**: Infra-red spectral type determination by comparison with field L dwarfs. Spectra coming from the Subaru campaign.

In Fig 3.29 we show an example of this comparison for two sources, LOri135 and LOri146, where, even though the signal to noise ratio was not too high, it is very clear that these sources must have a value of log($g$) lower then 4.0; what confirm them as young sources. The values derived for all the sources are listed in Table 3.4.2.

## 3.5 The spatial distribution of the members.

In Table 3.25 we have included a column with the final membership assigned to each source. We consider members those labeled as Y? (fulfilling most of the photometric criteria, see

**Table 3.24**: Parameters derived from the near-infrared spectroscopy.

| Object | Opt SpT | IR SpT | log($g$) | Object | Opt SpT | IR SpT | log($g$) |
|---|---|---|---|---|---|---|---|
| LOri135 | M6.5 | | <4.0 | LOri091 | M5.5 | M6 | 4.0 |
| LOri146 | | | <4.0 | ccd9-007028 | | M8 | |
| LOri107 | M6 | | 4.0-4.5 | ccd9-005320 | | L0-L2 | |
| LOri109 | M5.5 | | 4.0 | ccd9-001365 | | L0-L2 | |
| LOri139 | M5.75 | | 4.0-4.5 | ccd8-014467 | | L0-L2 | |
| LOri140 | M7 | | <4.0 | ccd5-008530 | | L0-L2 | |
| LOri089 | M5 | M6 | 4.0 | ccd9-006362 | | L0-L2 | |

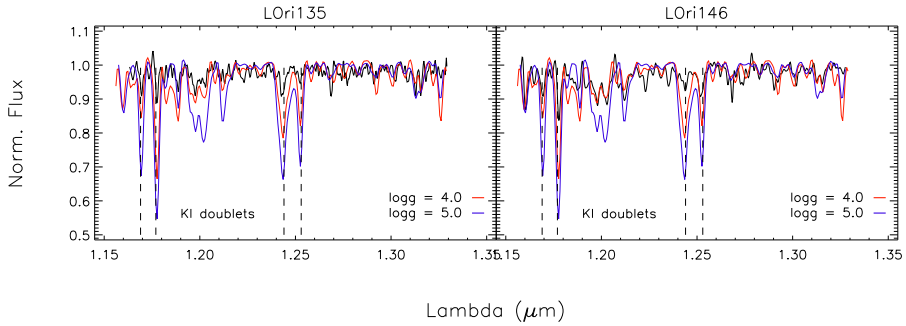


**Figure 3.29**: Example of the surface gravity determination in the NIRSPEC spectra by comparison with theoretical models.

previous chapter), Y (highly reliable photometric candidates, see previous chapter for more details) and Y+ (spectroscopically confirmed members; in this case we have included the reference of the work were the spectroscopic confirmation was provided). There are ∼240 members from which 225 have been labeled as Y or Y+.

In order to better understand the accretion and disk evolution of the confirmed members of Collinder 69, we have estimated the correlation in spatial distribution of different sets of data: Class II vs. Class III candidates, objects with any kind of disk (thin, thick and transition) vs. diskless objects. We have also tried to distinguish between the stellar and substellar populations.

In Fig. 3.30 we show this spatial distribution (members confirmed either by Dolan & Mathieu 1999, 2001; Sacco et al. 2008; Maxted et al. 2008 or this work) including information about the presence of disk and whether the disk is accreting or not. As can be seen in the figure, the sources with disk show a higher concentration towards the center of the cluster with respect to the diskless population (contrary to what one would expect according to the supernove scenario). In fact, if we assume that actively accreting systems are younger than those which do not show any sign of accretion, the youngest population of Collinder 69 seems to be clustered either around the central star $\lambda$ Ori or to the South-West.

We have computed the two-sided Kuiper statistic (invariant Kolmogorov-Smirnov), and its associated probability that any of the previously mentioned populations were drawn from the same distribution. The tests reveal that the cumulative distribution function of Class II candidates is very different from that of Class III, with a 99.9% probability that both populations have been drawn from different distributions.

We have performed a similar analysis comparing the distribution of substellar and stellar sources. We have used different isochrones (1, 3, 5 and 8 Myrs) to build different sets of masses for our confirmed members and study therefore the relation of the age on the probability that stellar and substellar sources follow the same spatial distribution. In this case, the test points out a trend revealing that the larger the age assumed, the lower the probability that this two populations share a common distribution. This tendency might be degenerated though, since for the larger ages, the

set of substellar objects is quite reduced in number; and therefore this result should be only taken account as tentative.

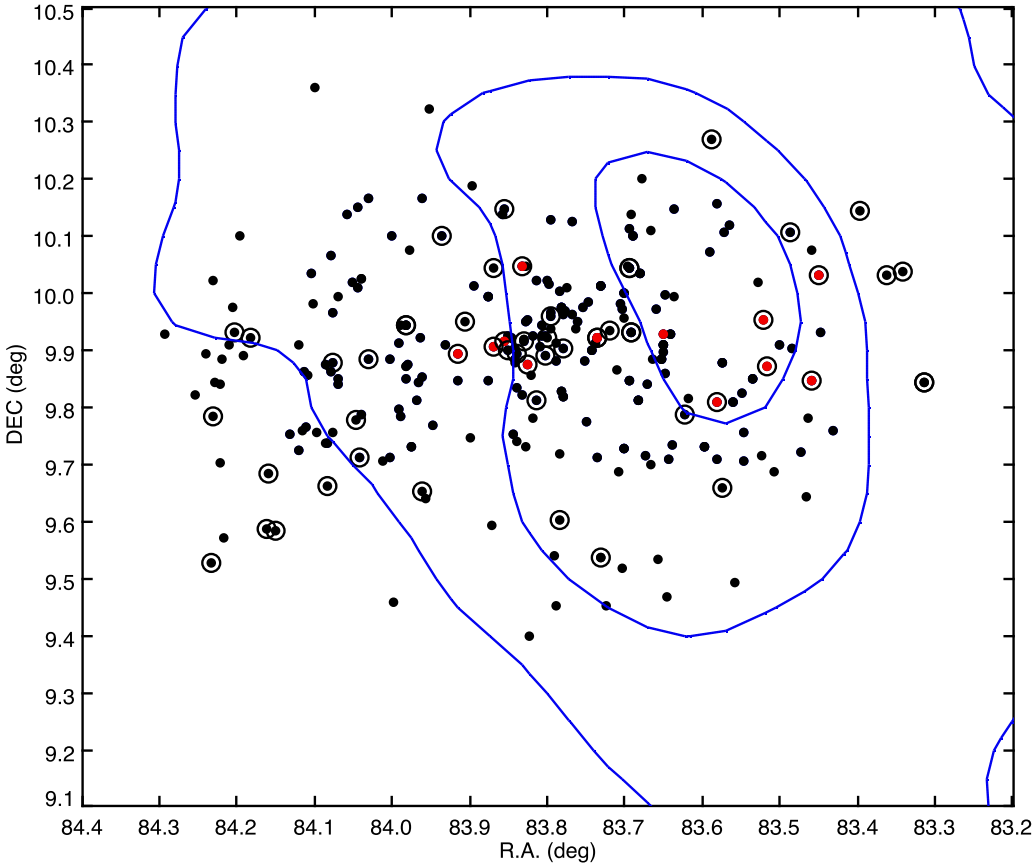


**Figure 3.30**: Spatial distribution of the members of Collinder 69 (spectroscopically confirmed and photometric candidates). Active accretors according to the saturation criterion are highlighted in red. We have also included the information regarding the near infrared excess (as a proxy for the presence of disk, from Barrado y Navascués et al. 2007b) with larger circumferences sourounding the Class II sources. Note that LOri156 is not sourounded by a large circle even though its IRAC slope suggests that harbours a thick disk (see details on Secion 3.3.5)

Finally, in Fig. 3.31 we show the spatial distribution of weak line TTauri and that of classical TTauri highlighting the spectroscopically confirmed members. As can be seen in the figure, our spatial coverage is quite homogeneous, and so our uncertainties when constructing the different cumulative distributions. Therefore the results of our statistical tests are robust against uncertainties on the membership of the candidates.

At a simple sight it could look like the sources showing infrared excess but no accretion

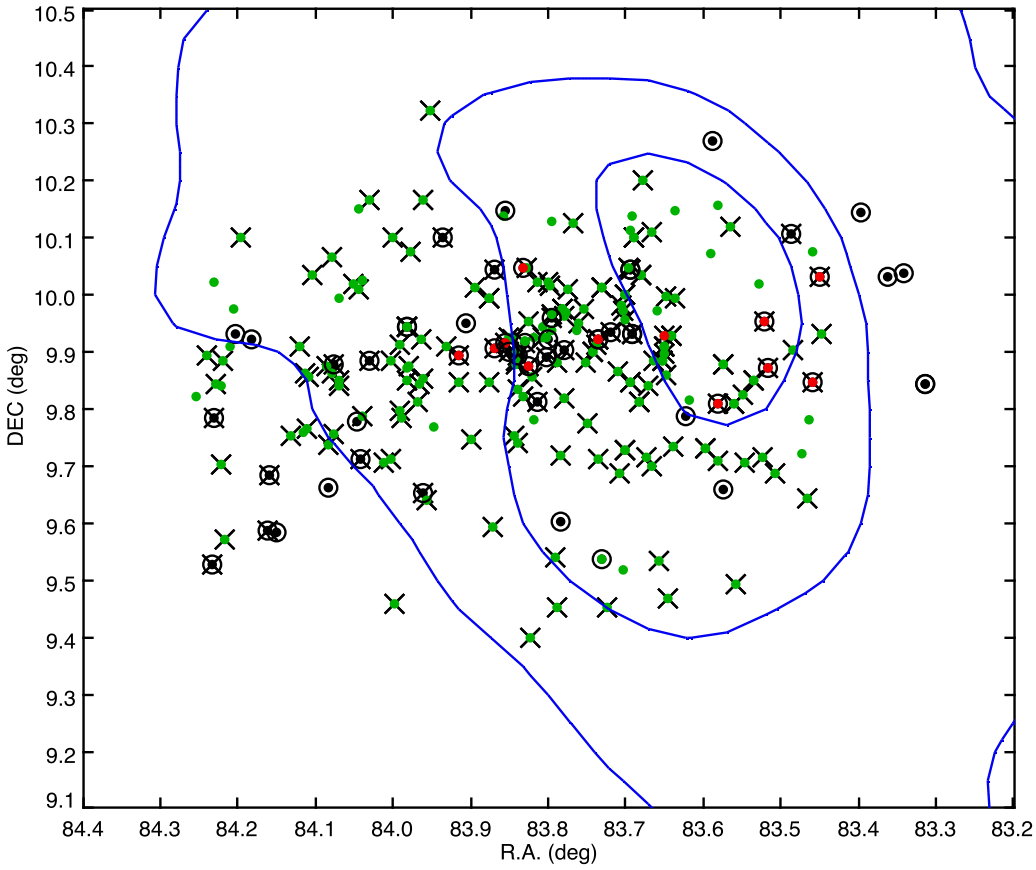


**Figure 3.31**: Spatial distribution of weak line and classical TTauri stars and substellar analogs. Green solid dots for weak line TTauri (and substellar analogs), considered as those not showing any IR excess on the IRAC bands; and red solid dots for classical TTauri (and substellar analogs). Note the different spatial distribution of both samples. Candidate members for which no IR class has been inferred are not shown in this figure. Class II sources are highlighted with large black circumferences as in the previous figure, and large black crosses mark those sources whose membership has been confirmed spectroscopically by Dolan & Mathieu (1999, 2001); Sacco et al. (2008); Maxted et al. (2008) or this work.

are distributed in a more similar manner than the weak-line TTauri population, being the accretors the population that introduces the differences in spatial distribution. We have checked this hypothesis performing again a two-sided Kuiper statistic analysis obtaining a slightly larger correlation between the distribution of both populations, but still with a very high probability (99%) that they are not drawn from the same distribution.

## 3.6 The Hertzsprung–Russell diagram of Collinder 69.

In Fig. 3.32, we show the Hertzsprung–Russell diagram of Collinder 69 including all the (spectroscopically) confirmed members and the reliable (photometric) candidate members. We have overplotted three sets of isochrones composed (to achieve a complete mass range coverage) joining the collections by Siess et al. (2000) and COND by Baraffe et al. (2003) for three different ages: 1, 5 and 50 Myr. Taking into account the error bars in the determination of $L_{bol}$ and $T_{eff}$ (not displayed in the figure for cosmetic reasons) only one source, LOri169, lies below the 50 Myr isochrone. This source has been assigned the Y? membership code, meaning it is a probable photometric candidate. Its location in the HR diagram may suggest that it is not a real member, but we kept the Y? membership flag since the SED is not very well populated, and therefore the estimated effective temperature and luminosities hold large uncertainties.

On the other hand it seems remarkable that Class II sources tend to concentrate between effective temperatures of 1900–4000 K. This difference in distribution must be taken into account with caution anyways since the criteria from Allen et al. (2004) to assign infrared class to the YSOs according to their IRAC colors are biased towards low mass stars.

In any case, as can be inferred from this diagram, the previously derived optimal age of 5 Myr for Collinder 69 derived by Barrado y Navascués et al. (2007b) agrees very well with our results (including a larger range in mass). Besides, $\sim$ 90% of our sources lie above the 20 Myr isochrone (composed in the same manner as those shown in the figure); we therefore propose an upper-limit age of 20 Myr for the Collinder 69 open cluster.

## 3.7 The Initial Mass Function of Collinder 69.

As has been already mentioned along this chapter; we have used the estimated $T_{eff}$ and $L_{bol}$ from the SED fit along with a composite 5 Myr isochrone (Siess et al. 2000 + COND from Baraffe et al. 2003) to derive the mass of our confirmed and candidate members. These two estimations are provided in Table 3.25. As can be seen in Fig. 3.33 there is a quite large dispersion when comparing both estimations. If we separate our members according to the ratio between the two estimated masses into large dispersion (those where one of the masses is larger than 1.5 times the other one) and “acceptable” dispersion (the ratio between the largest and the lowest mass lower than 1.5); we find that $\sim$30% of the so-called “large dispersion” sources have been classified as

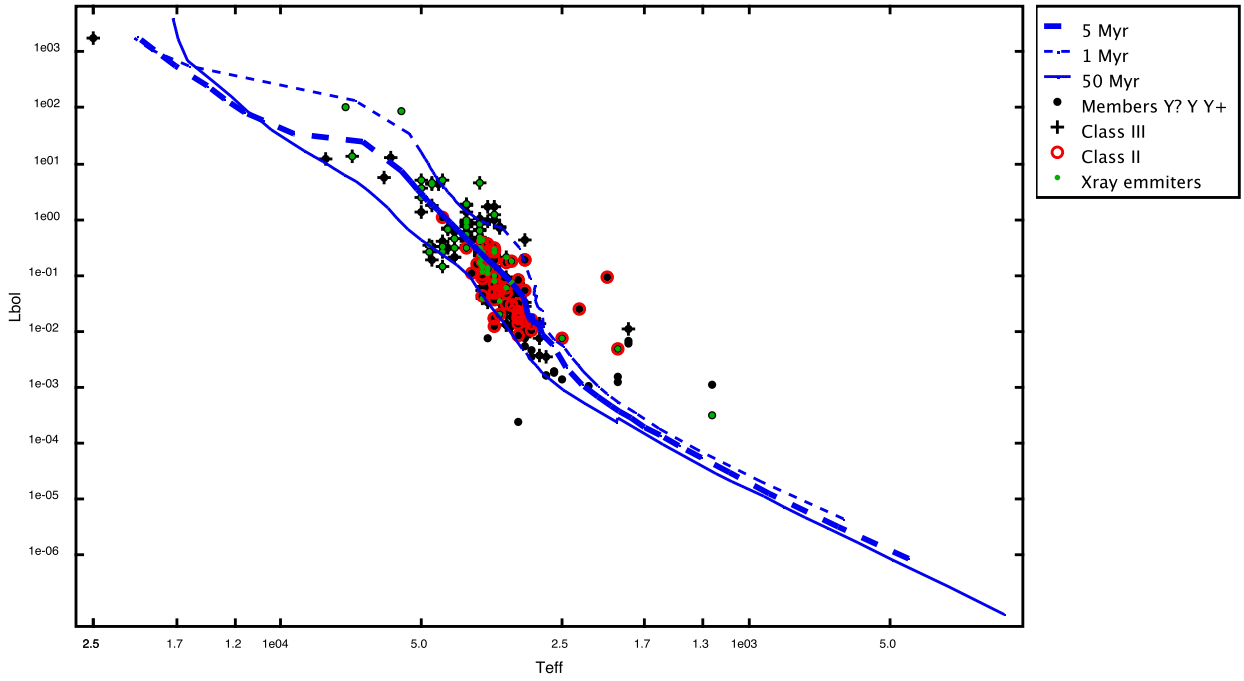


**Figure 3.32**: HR diagram of the confirmed (spectroscopically) and highly reliable (photometric) candidate members.

Class II according to their IRAC colours, while the same class in the acceptable dispersion sample lowers down to 15% (this is not a question of scale since both samples have a similar amount of sources). In fact, ~65% of the sources undergoing active accretion fall into the large dispersion sample. Therefore, our estimations of masses are quite sensitive to the presence of disks (a caveat that do not surprise us as has already been discussed in Section 3.1). To take into account this uncertainty, in this section we will present all the calculations for both estimations of the mass of the members and for an averaged mass.

In Figs. 3.34, 3.35 and 3.36 we present the derived Initial Mass Functions (according to the different procedures followed to derive the masses of the sources) for Collinder 69. We have considered all confirmed (Y+) and candidate members (Y? and Y) confined in the intersection of the CFHT, Spitzer and XMM fields of view. We emphasize that this intersection leaves the central part of the cluster (where $\lambda$ Ori itself is located) aside. In order to take this effect into account, in Fig. 3.37 we show another IMF for Collinder 69 but this time we focus on the CFHT field of view not including the XMM candidates and estimating the masses of our sources based on the I band magnitude and the same isochrone as in the previous cases. For comparison, in that figure

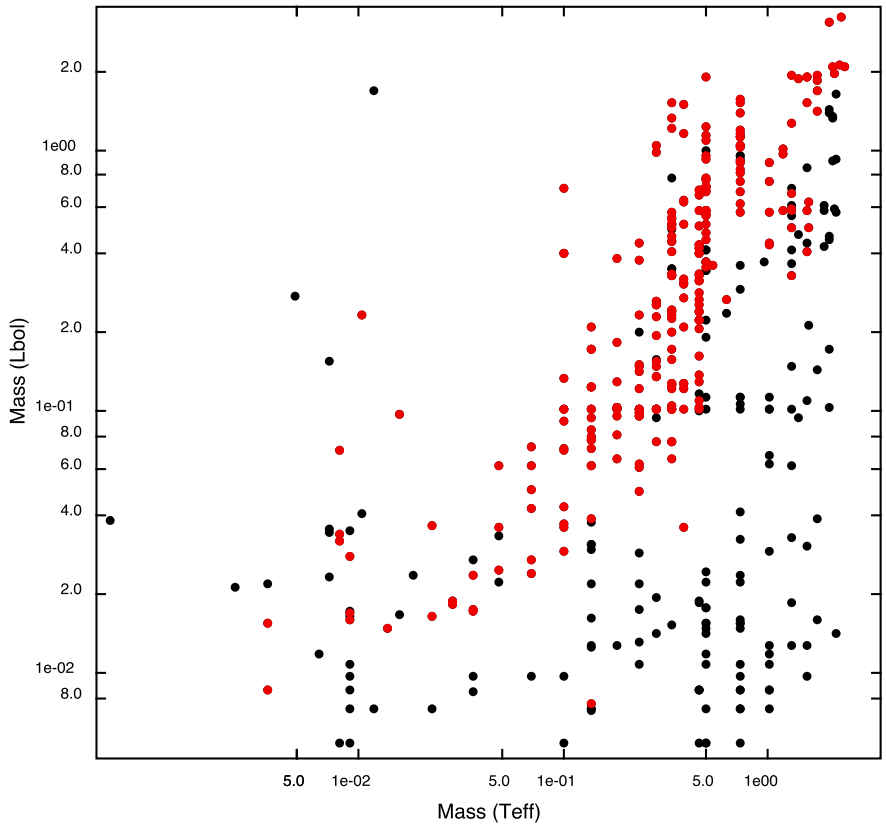


**Figure 3.33**: Relationship between the masses derived from $T_{eff}$ and $L_{bol}$. Members (confirmed or photometric Y and Y?) are displayed as solid red dots while the discarded candidates are shown as solid black dots. Note that although there is a large dispersion among the members between both estimations, the dispersion is much larger in the non-member sample with the masses estimated form the $L_{bol}$ being systematically lower than those derived from the $T_{eff}$. Note the logarithmic scale on both axes.

we present the IMF derived in a similar manner for the $\sigma$ Orionis cluster (with data from Béjar et al. 2001).

In all the cases, to enlarge the mass range coverage of our calculated IMF, we have included data from Murdin & Penston (1977) (scaling to the respective areas). The last point at the massive end correspond to a possible SN (open triangle). The figure indicates that the SN hypothesis is compatible with the IMF of the cluster.

Regardless of the parameter used to infer the mass of our confirmed and candidate members, for masses above 1 $M_{\odot}$, the power law index of the IMF can be assimilated to Salpeter's value, being much smaller for lower masses. In particular, the fitted slopes in the mass range 25–0.70 $M_{\odot}$ vary from 2.11 to 2.27; and those for the low and very low mass range, 0.70-0.01 $M_{\odot}$, correspond to much lower values; from 0.55 to 0.60.

As we have mentioned before, the two areas for which we have derived the IMFs (the CFHT survey coverage and the intersection of CFHT, Spitzer and XMM) comprise populations that show distinct trends in terms of spatial distribution (the XMM pointings leave a side a relatively large population of Class II sources). Surprisingly, this fact does not seem to affect the shape of the IMF; the slopes shown in Figs. 3.34, 3.35 and 3.36 agree among themselves in the same manner as those from Fig. 3.37 do.

Our estimated slopes are consistent with those derived in the same manner (as that of our Figure 3.37) for several open clusters: SOri, data from Béjar et al. (2001) – $\alpha$=0.8; APer, data fom Barrado y Navascués et al. (2001, 2002) – $\alpha$=0.6; M35, data fom Barrado y Navascués et al. (2001, 2002) – $\alpha$=0.81 from 0.8 to 0.2 $M_{\odot}$ and $\alpha$=-0.88 $M_{\odot}$ for lower masses; and the Pleiades, data from Bouvier et al. (1998) – $\alpha$=0.6. For the low mass stars/substellar domain, the slope is very similar, regardless the total mass, the environments and the age of each association, except in the case of M35 –which corresponds to the core of the cluster–, a very rich association, about 150 Myr old, where an important dynamical evolution might have taken place.

## 3.8 Conclusions

We have analyzed ~170 optical and near infrared spectra with a wide range of resolutions of candidate members to the Collinder 69 cluster. Based on different criteria regarding molecular bands absorptions we have provided spectral types for all the sources. Using alkali lines as youth indicators we have confirmed 90 members (and 9 possible members). For those sources of our survey overlapping with radial velocities surveys (by Sacco et al. 2008; Maxted et al. 2008) we obtain very similar results regarding membership.

A summary of the sources analyzed in this work can be found in Table 3.25.

For those sources showing large H$\alpha$ equivalent widths (larger than the one expected to arise from chromospheric activity) we have derived accretion rates using mainly the full width at 10% of the flux of the H$\alpha$ emission line (but also the Ca II IRT) obtaining values compatible with

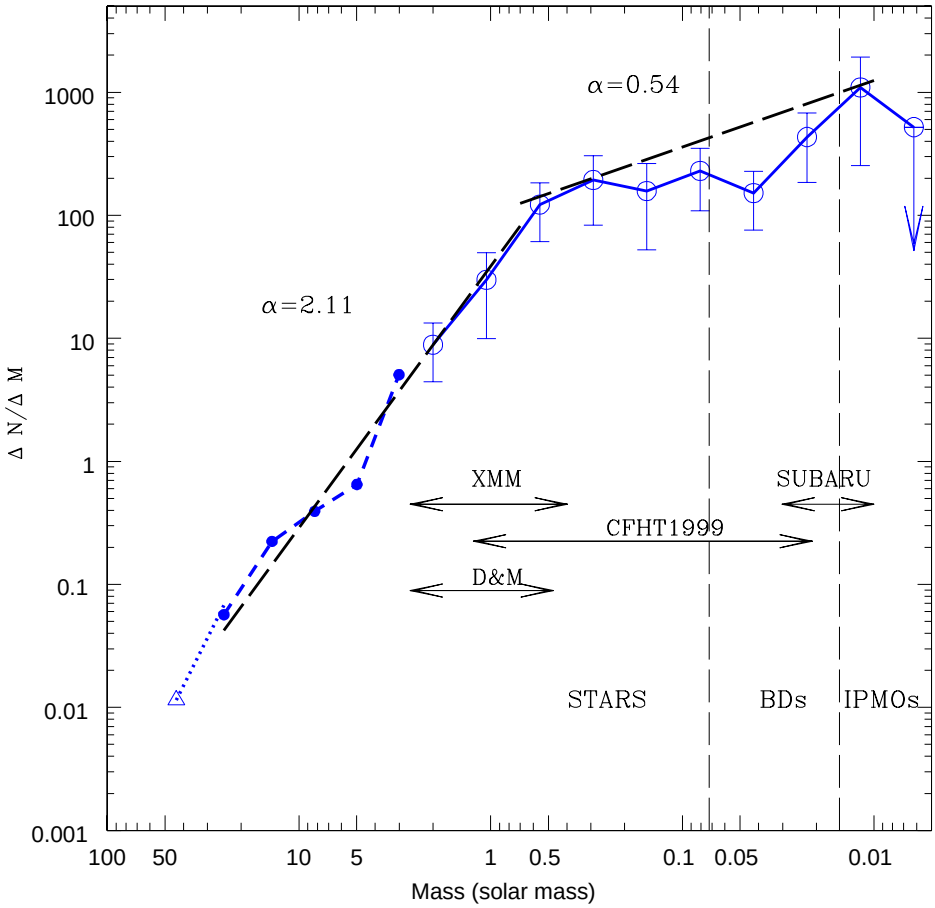


**Figure 3.34**: IMF derived for Collinder 69 (I). Masses derived combining the estimated $T_{eff}$ and the composite 5 Myr isochrone (SIESS + COND).

those previously reported in the literature for objects of similar mass and age (Mohanty et al. 2005; Natta et al. 2006).

We have studied the accretion and disk properties of the confirmed members of Collinder 69. In Fig. 3.30 we show the spatial distribution of the confirmed members (either by Dolan & Mathieu 1999, 2001; Sacco et al. 2008; Maxted et al. 2008 or this work) including information about the presence of disk and whether the disk is accreting or not. As can be seen in the figure, the sources with disk show a higher concentration towards the center of the cluster with respect to the diskless population (contrary to what one would expect according to the supernove scenario). In fact, if we assume that actively accreting systems are younger than those which do not show sign of accretion, the youngest population of Collinder 69 is clearly concentrated around the central O population.

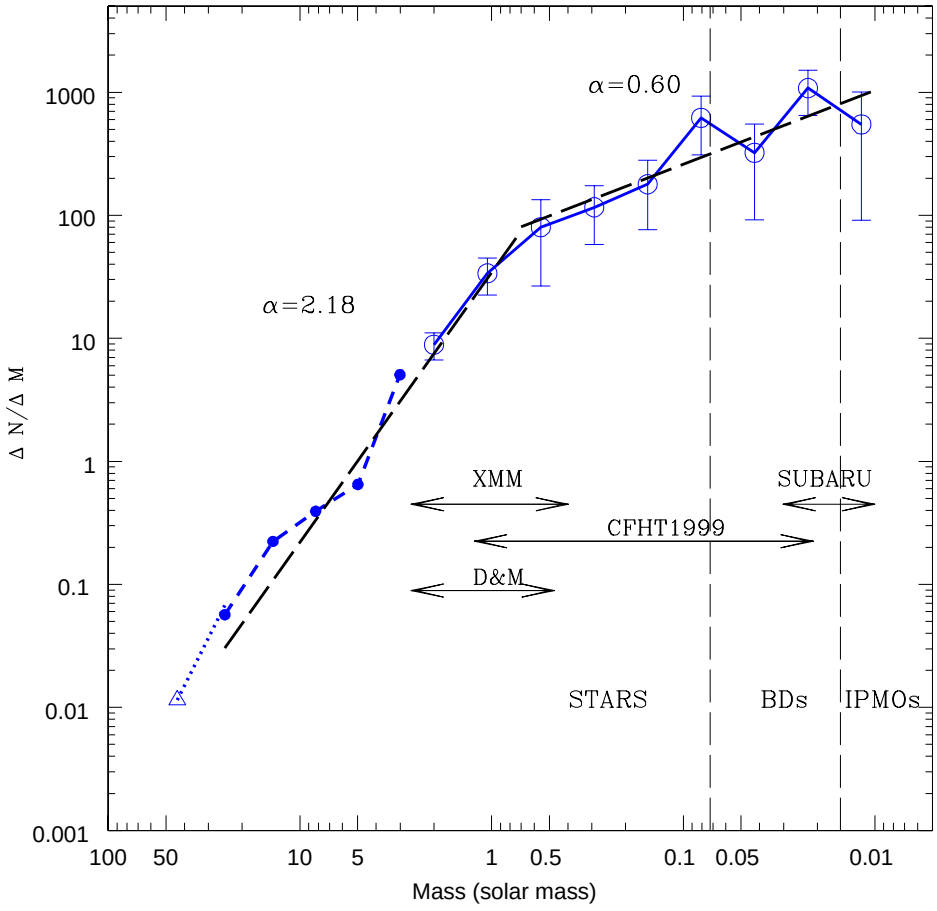


**Figure 3.35**: IMF derived for Collinder 69 (II). Masses derived combining the estimated $L_{bol}$ and the composite 5 Myr isochrone (SIESS + COND).

With the data from our SUBARU campaign we have confirmed the cool nature of the **the lowest mass candidate members to Collinder 69** reported so far. With derived spectral types L0-L2 corresponding to effective temperatures of ~ 2000 K (according to the spectroscopic temperature scales derived by Basri et al. 2000), if members, they have estimated masses, following the 5 Myr DUSTY isochrone by Chabrier et al. 2000, as low as 0.012 $M_{\odot}$ (~12.6 $M_{Jupiter}$).

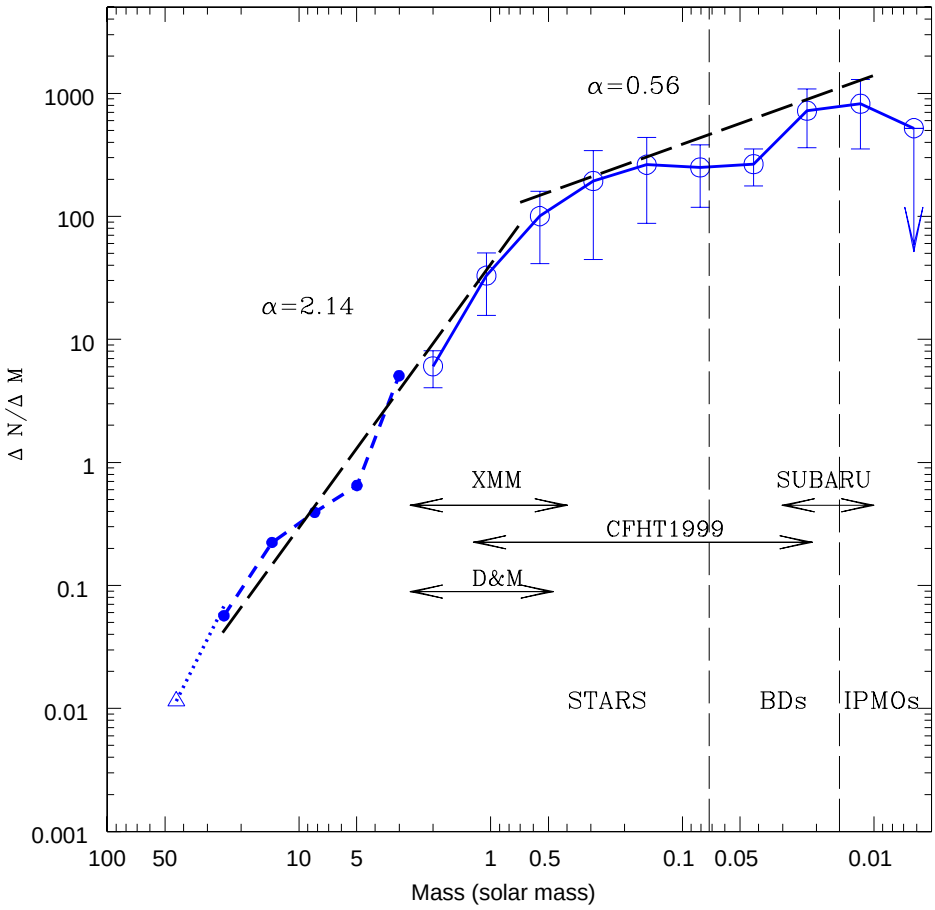


**Figure 3.36**: IMF derived for Collinder 69 (I). Mases derived averaging the masses from the previous two figures2.

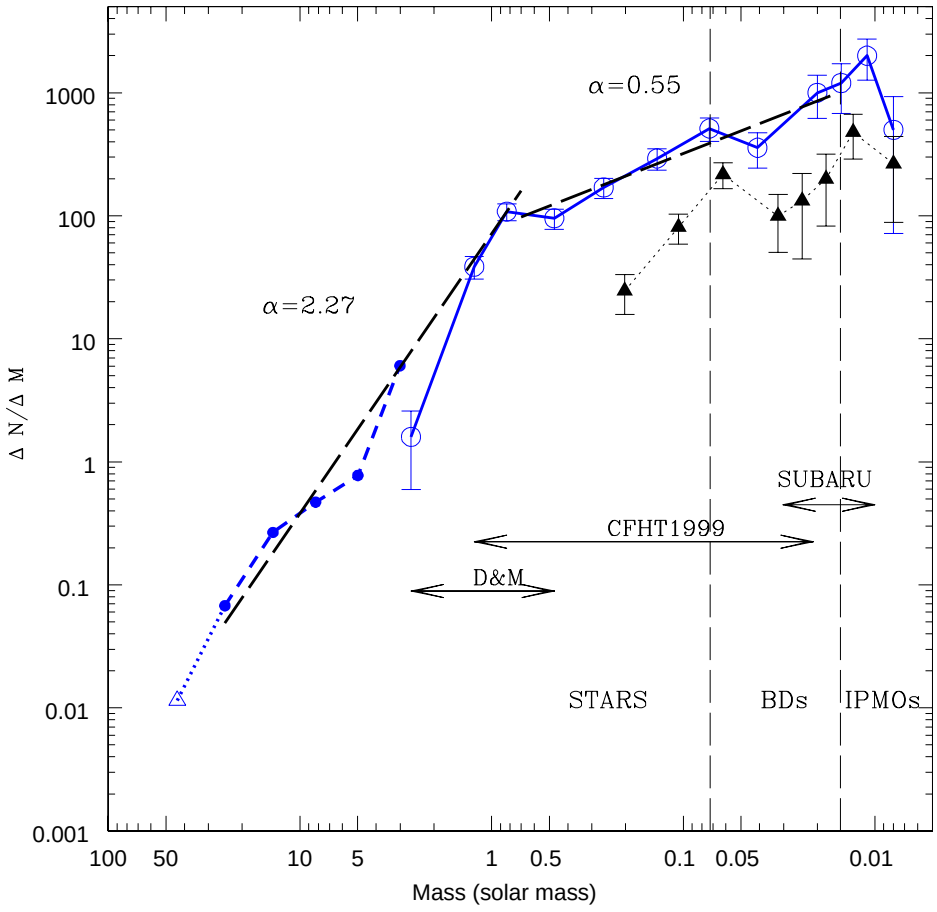


**Figure 3.37**: IMF derived for Collinder 69. Comparison with the $\sigma$ Ori cluster.

**Table 3.25**: Summary of the parameters derived in this work for Collinder 69 candidate members and comparison with previous studies.

| Object | Alt ID | DM ID | SpT | INS[3] | Accret. | Membership[5] | $\log(\dot{M}_{acc})(M_\odot/yr)$[4] | Bin | Class[6] | EW(H$\alpha$)[4] | EW(Li)[4] | $T_{eff}$ | $L_{bol}$ | $Mass_{Teff}$ | $Mass_{Lbol}$ |
|---|---|---|---|---|---|---|---|---|---|---|---|---|---|---|---|
| ccd9-007028 | | | M8[1] | (11) | | NM? | | | – | | | 1200 | 0.0027 | 0.0036 | 0.0217 |
| ccd9-005320 | | | L0-L2[1] | (11) | | Y (B09) | | | III | | | 1800 | 0.0107 | 0.0081 | 0.0704 |
| ccd9-001365 | | | L0-L2[1] | (11) | | Y (B09) | | | – | | | 1800 | 0.0065 | 0.0081 | 0.0333 |
| ccd8-021927 | | | | | | NM? | | | – | | | 1000 | 0.0025 | 0.0025 | 0.0211 |
| ccd8-014467 | | | L0-L2[1] | (11) | | Y? (B09) | | | – | | | 1800 | 0.0059 | 0.0081 | 0.0314 |
| ccd8-005864 | | | | | | Y | | | – | | | 1200 | 0.0011 | 0.0036 | 0.0152 |
| ccd5-008530 | | | L0-L2[1] | (11) | | Y? (B09) | | | – | | | 1900 | 0.0012 | 0.0092 | 0.0157 |
| ccd5-002230 | | | | | | NM? | | | – | | | 2700 | 3.0E-4 | 0.0361 | 0.0084 |
| ccd4-005127 | | | | | | Y | | | – | | | 1900 | 0.0015 | 0.0092 | 0.0168 |
| ccd3-007031 | | | | | | NM? | | | – | | | 2300 | 0.0014 | 0.016 | 0.0165 |
| ccd3-006362 | | | L0-L2[1] | (11) | | Y? (B09) | | | – | | | 2600 | 0.0017 | 0.029 | 0.0179 |
| ccd3-005774 | | | | | | NM? | | | – | | | 500 | 0.0079 | 6.0E-4 | 0.0379 |
| ccd2-024918 | | | | | | NM? | | | – | | | 2400 | 0.0033 | 0.0186 | 0.0233 |
| ccd2-009766 | | | | | | NM? | | | – | | | 3300 | 0.0048 | 0.2342 | 0.0281 |
| ccd1-016078 | | | | | | NM? | | | – | | | | | | |
| LOri170 | | | | | | NM? | | | – | | | 3100 | 2.0E-4 | 0.1365 | 0.0070 |
| LOri169 | | | | | | Y? | | | – | | | 3100 | 2.0E-4 | 0.1365 | 0.0075 |
| LOri168 | | | | | | NM? | | | – | | | 2900 | 4.0E-4 | 0.0701 | 0.0095 |
| LOri167 | | | | | | Y | | | – | | | 2500 | 0.0013 | 0.0229 | 0.0162 |
| LOri166 | | | | | | Y? | | | – | | | 2200 | 0.0010 | 0.0138 | 0.0145 |
| LOri165 | | | | | | NM? | | | – | | | 3100 | 7.0E-4 | 0.1365 | 0.0124 |
| LOri164 | | | | | | NM | | | – | | | 3300 | 8.0E-4 | 0.2342 | 0.0129 |
| LOri163 | | | | | | Y | | | – | | | 2700 | 0.0015 | 0.0361 | 0.0171 |
| LOri162 | | | | | | Y | | | – | | | 2600 | 0.0018 | 0.029 | 0.0183 |
| LOri161 | | | M8.0 | (2) | Y | Y+ (B09) | -9.967±0.42[4)] | | – | -74.51±33.069[4)] | | 2600 | 0.0018 | 0.029 | 0.0185 |
| LOri160 | | | | | | Y | | | – | | | 2700 | 0.0016 | 0.0361 | 0.0173 |
| LOri159 | | | | | | NM? | | | – | | | 3100 | 0.0013 | 0.1365 | 0.016 |
| LOri158 | | | | | | NM? | | | – | | | 3500 | 0.0011 | 0.3382 | 0.0151 |
| LOri157 | | | | | | NM | | | – | | | 3300 | 0.0016 | 0.2342 | 0.0172 |
| LOri156 | | | M8.0 | (2) | Y | Y+ (B09) | -8.022±0.10[4)] | | III | -114.455±1.812[4)] | | 2700 | 0.0033 | 0.0361 | 0.0233 |
| LOri155 | | | M8.0 | (2) | N | Y+ (B09) | | | III | -51.493±18.697[4)] | | 2800 | 0.0036 | 0.0488 | 0.0244 |
| LOri154 | | | M8.0 | (2) | N | NM+ (B09) | | | – | -17.465±3.03[4)] | | 2700 | 0.0044 | 0.0361 | 0.0267 |
| LOri153 | | | | | | Y | | | – | | | 2900 | 0.0034 | 0.0701 | 0.0237 |
| LOri152 | | | | | | NM? | | | – | | | 3100 | 0.0027 | 0.1365 | 0.0217 |
| LOri151 | | | M5.5 | (2) | N | NM+ (B09) | | | – | -9.567±2.024[4)] | | 3300 | 0.0027 | 0.2342 | 0.0216 |
| LOri150 | | | M7.0 | (2) | N | Y+ (B09) | | | – | -15.254±2.046[4)] | | 2900 | 0.0043 | 0.0701 | 0.0266 |
| LOri149 | | | | | | NM | | | – | | | 3700 | 0.0018 | 0.4582 | 0.0184 |
| LOri148 | | | | | | Y? | | | – | | | 3000 | 0.0051 | 0.1 | 0.0289 |
| LOri147 | | | M5.5 | (2) | N | NM+ (B09) | | | – | -9.804±1.373[4)] | | 3100 | 0.0052 | 0.1365 | 0.0291 |
| LOri146 | | | | (9) | | Y+ (M08, B09) | | | III | | | 2800 | 0.0071 | 0.0488 | 0.0353 |
| LOri144 | | | | | | NM? | | | – | | | 3750 | 0.0028 | 0.4936 | 0.022 |
| LOri143 | | | M7.0 | (4) | N | Y+ (M08, B09) | | | III | -41.783±4.663[4)] | | 3000 | 0.0076 | 0.1 | 0.0368 |
| LOri142 | | | | | | Y | | | – | | | 3000 | 0.0072 | 0.1 | 0.0357 |
| LOri141 | | | M4.0 | (2) | N | NM+ (B09) | | | – | -3.06±0.768[4)] | | 3100 | 0.0056 | 0.1365 | 0.0305 |
| LOri140 | | | M7.0 | (2) (9) | Y | Y+ (M08, B09) | -8.875±0.14[4)] | | II | -79.143±9.439[4)] | | 2900 | 0.0098 | 0.0701 | 0.0421 |

Continued on next page…

Table 3.25 – Continued

| Object | Alt ID | DM ID | SpT | INS[3] | Accret. | Membership[5] | log($\dot{M}_{acc}$)($M_\odot$/yr)[4] | Bin | Class[6] | EW(H$\alpha$)[4] | EW(Li)[4] | $T_{eff}$ | $L_{bol}$ | $Mass_{Teff}$ | $Mass_{Lbol}$ |
|---|---|---|---|---|---|---|---|---|---|---|---|---|---|---|---|
| LOri139 | | | M5.75 | (2) (9) | N | Y+ (B09) | | | II | -17.986±1.019[4)] | | 3100 | 0.0080 | 0.1365 | 0.0383 |
| LOri138 | | | | | | Y | | | – | | | 3000 | 0.0098 | 0.1 | 0.0422 |
| LOri137 | | | | | | NM | | | – | | | 3750 | 0.0035 | 0.4936 | 0.0239 |
| LOri136 | | | | | | Y | | | III | | | 2800 | 0.0129 | 0.0488 | 0.0607 |
| LOri135 | | | M6.5 | (2) (9) | N | Y+ (M08, B09) | | | III | -13.32±3.533[4)] | | 3000 | 0.0108 | 0.1 | 0.07 |
| LOri134 | | | M5.0 | (2) | N | Y+ (N09) | | | III | -5.925±0.307[4)] | | 2900 | 0.0138 | 0.0701 | 0.0492 |
| LOri133 | | | M4.75 | (2) | N | Y+ (B09) | | | – | -2.2±0.402[4)] | | 3600 | 0.0071 | 0.3906 | 0.0353 |
| LOri132 | | | | | | Y | | | II | | | 2900 | 0.013 | 0.0701 | 0.0611 |
| LOri131 | | | | | | Y+ (M08) | | | II | | | 2900 | 0.0154 | 0.0701 | 0.0721 |
| LOri130 | | | M5.25 | (2) | N | Y+ (M08, B09) | | | III | -8.505±0.629[4)] | | 3200 | 0.0117 | 0.1839 | 0.0649 |
| LOri129 | | | M6.0 | (1) | N | Y+ (M08, B09) | | | II | -10.757±0.936[4)] | 0.404±0.092[4)] | 3000 | 0.015 | 0.1 | 0.0707 |
| LOri128 | | | | | | Y | | | III | | | 3100 | 0.0124 | 0.1365 | 0.0606 |
| LOri127 | | | | | | NM | | | III | | | 1700 | 0.0593 | 0.0073 | 0.153 |
| LOri126 | | | M6.5 | (2) | Y | Y+ (M08, B09) | -8.781±0.10[4)] | | II | -35.424±3.504[4)] | | 3100 | 0.013 | 0.1365 | 0.061 |
| LOri125 | | | | | | Y+ (M08) | | | III | | | 3300 | 0.0122 | 0.2342 | 0.0619 |
| LOri124 | | | M5.5 | (2) | N | Y+ (B09) | | | III | -6.965±1.776[4)] | | 3300 | 0.0126 | 0.2342 | 0.0602 |
| LOri122 | | | | | | Y+ (M08) | | | III | | | 3100 | 0.0152 | 0.1365 | 0.0713 |
| LOri121 | | | | | | Y | | | | | | 3300 | 0.0135 | 0.2342 | 0.0486 |
| LOri120 | | | M5.5 | (4) (8) | N | Y+ (M08, B09) | | | II | -13.304±1.0[4)] | 0.657±0.084[4)] | 3100 | 0.0165 | 0.1365 | 0.0765 |
| ” | | | M5.5 | (4) (8) | N | Y+ (M08, B09) | | | II | -10.182±1.967[4)] | | 3100 | 0.0165 | 0.1365 | 0.0765 |
| LOri119 | | | M5.5 | (1) | N | Y+ (B09) | | | III | -11.876±0.409[4)] | 0.879±0.184[4)] | 3100 | 0.0172 | 0.1365 | 0.0791 |
| LOri118 | | | M5.5 | (2) | N | Y+ (M08, B09) | | | II | -10.429±0.205[4)] | | 3100 | 0.0183 | 0.1365 | 0.0833 |
| LOri117 | | | M6.0 | (4) | N | Y+ (B09) | | | – | -23.421±1.442[4)] | | 3000 | 0.0202 | 0.1 | 0.0901 |
| LOri116 | | | M5.5 | (2) | N | Y+ (M08, B09) | | | III | -11.779±1.543[4)] | | 3200 | 0.0174 | 0.1839 | 0.0801 |
| LOri115 | | | M5.0 | (8) (2) | N | Y+ (B09) | | | II | -12.575±0.592[4)] | 0.336±0.09[4)] | 3500 | 0.0162 | 0.3382 | 0.0753 |
| LOri115 | | | M5.0 | (8) (2) | N | Y+ (B09) | | | II | -8.974±0.879[4)] | | 3500 | 0.0162 | 0.3382 | 0.0753 |
| LOri114 | | | M6.0 | (2) | N | Y+ (M08, B09) | | | II | -12.589±1.734[4)] | | 3100 | 0.0217 | 0.1365 | 0.0925 |
| LOri113 | C69-X-W-032 w | | M5.5 | (1) | Y | Y+ (B09) | -10.574±0.03[4)] | | II | -20.853±0.914[4)] | 0.617±0.139[4)] | 3400 | 0.0196 | 0.286 | 0.0755 |
| LOri112 | | | M6.5 | (8) | N | Y+ (B09) | | | III | -10.927±1.683[4)] | 0.537±0.195[4)] | 3200 | 0.023 | 0.1839 | 0.0948 |
| LOri111 | | | | | | Y | | | III | | | 3000 | 0.0271 | 0.1 | 0.1 |
| LOri110 | | | M5.25 | (2) | N | NM+ (M08, B09) | | | III | -5.731±2.728[4)] | | 3400 | 0.0223 | 0.286 | 0.0936 |
| LOri109 | | | M6.0 M5.5 | (8) (9) (1) | N | Y+ (M08, B09) | | | III | -19.615±0.516[4)] | 0.565±0.113[4)] | 3300 | 0.0228 | 0.2342 | 0.0944 |
| ” | | | M6.0 M5.5 | (8) (9) (1) | N | Y+ (M08, B09) | | | III | -8.696±0.447[4)] | 0.502±0.148[4)] | 3300 | 0.0228 | 0.2342 | 0.0944 |
| LOri108 | | | | | | Y | | | III | | | 3100 | 0.0262 | 0.1365 | 0.1 |
| LOri107 | | | M6.0 | (2) (9) | N | Y+ (M08, B09) | | | III | -11.915±1.018[4)] | | 3000 | 0.0308 | 0.1 | 0.1 |
| LOri106 | | | M5.5 | (1) | Y | Y+ (S08, M08, B09) | ¡ -11.0[2)]; -10.917±0.01[4)] | | II | -26.16±2.4[2)]; -48.423±1.85[4)] | 0.636±0.0132[2)]; 0.477±0.033[4)] | 3200 | 0.0283 | 0.1839 | 0.1 |
| LOri105 | | | M6.0 | (6) (8) | N | Y+ (S08, M08, B09) | | | III | -22.429±0.449[4)] | 0.137±0.026[4)] | 3300 | 0.0248 | 0.2342 | 0.0976 |
| ” | | | M6.0 | (6) (8) | N | Y+ (S08, M08, B09) | | | III | -13.376±2.603[4)] | | 3300 | 0.0248 | 0.2342 | 0.0976 |
| LOri104 | | | | | | Y+ (M08) | | | II | | | 3100 | 0.029 | 0.1365 | 0.1 |
| LOri103 | | | | | | Y+ (M08) | | | III | | | 3300 | 0.0307 | 0.2342 | 0.1 |
| LOri102 | | | M4.0[2] | | N | Y+ (S08, M08) | | | III | -5.94±0.96[2)]; | 0.584±0.062[2)] | 3300 | 0.0313 | 0.2342 | 0.1 |
| LOri101 | | | | | | NM | | | III | | | 3700 | 0.0252 | 0.4582 | 0.0983 |
| LOri100 | | | M5.5 | (4) | N | Y+ (S08, M08, B09) | | | III | -8.18±1.4[2)]; -11.425±1.84[4)] | 0.717±0.043[2)] | 3600 | 0.0308 | 0.3906 | 0.1 |
| LOri099 | | | M5.25 M5.75 | (1) (8) | N | Y+ (B09) | | | III | -9.221±0.667[4)] | 0.385±0.115[4)] | 3400 | 0.0321 | 0.286 | 0.1 |
| ” | | | M5.25 M5.75 | (1) (8) | N | Y+ (B09) | | | III | -5.806±0.638[4)] | 0.567±0.158[4)] | 3400 | 0.0321 | 0.286 | 0.1 |
| LOri098 | C69-X-E-091 I | | M5.0 | (2) | N | Y+ (M08, B09) | | | III | -12.508±0.904[4)] | | 3400 | 0.0334 | 0.286 | 0.1 |
| LOri096 | | | M5.0 | (8) | N | Y+ (S08, M08, B09) | <-11.0[2)] | | II | -6.97±1.1[2)] | 0.553±0.048[2)]; 0.382±0.156[4)] | 3500 | 0.0344 | 0.3382 | 0.1 |

Continued on next page…

Table 3.25 – Continued

| Object | Alt ID | DM ID | SpT | INS[3] | Accret. | Membership[5] | log($\dot{M}_{acc}$)($M_\odot$/yr)[4] | Bin | Class[6] | EW(H$\alpha$)[4] | EW(Li)[4] | $T_{eff}$ | $L_{bol}$ | $Mass_{Teff}$ | $Mass_{Lbol}$ |
|---|---|---|---|---|---|---|---|---|---|---|---|---|---|---|---|
| LOri095 | | | M6.0 | (2) | N | Y+ (S08, M08, B09) | | | III | -4.96±0.62[2]; -8.231±1.177[4] | 0.559±0.030[2] | 3400 | 0.0361 | 0.286 | 0.1 |
| LOri094 | | | M5.5 | (8) (1) | N | Y+ (S08, M08, B09) | | | III | -15.53±2.23[2]; -13.775±0.73[4] | 0.538±0.0204[2]; 0.495±0.024[4] | 3200 | 0.0403 | 0.1839 | 0.1026 |
| ” | | | M5.5 | (8) (1) | N | Y+ (S08, M08, B09) | | | III | -15.53±2.23[2]; -8.488±0.095[4] | 0.538±0.0204[2]; 0.719±0.082[4] | 3200 | 0.0403 | 0.1839 | 0.1026 |
| LOri093 | | | M5.5 | (8) | N | Y+ (S08, M08, B09) | | | III | -6.25±0.94[2]; -8.536±0.219[4] | 0.623±0.061[2]; 0.496±0.083[4] | 3500 | 0.0392 | 0.3382 | 0.1 |
| LOri092 | | | M4.5 | (6) | N | Y+ (S08, M08, B09) | | | III | -2.9±0.34[2]; -12.512±1.367[4] | 0.661±0.051[2] | 3500 | 0.0396 | 0.3382 | 0.1007 |
| LOri091 | | | M4.0 M5.5 M6.0[1] | (1) (10) (8) (6) | N | Y+ (M08, B09) | | | III | -13.473±1.112[4] | 0.76±0.06[4] | 3100 | 0.0473 | 0.1365 | 0.1212 |
| ” | | | M4.0 M5.5 M6.0[1] | (1) (10) (8) (6) | N | Y+ (M08, B09) | | | III | -47.87±8.314[4] | | 3100 | 0.0473 | 0.1365 | 0.1212 |
| ” | | | M4.0 M5.5 M6.0[1] | (1) (10) (8) (6) | N | Y+ (M08, B09) | | | III | -11.932±1.123[4] | 0.644±0.074[4] | 3100 | 0.0473 | 0.1365 | 0.1212 |
| LOri090 | C69-X-E-078 I | | | | | Y+ (M08) | | | III | | | 3700 | 0.0374 | 0.4582 | 0.1 |
| LOri089 | | | M5.0 M6.0[1] | (1) (10) | N | Y+ (B09) | | | III | -3.896±0.225[4] | 0.603±0.218[4] | 3500 | 0.0407 | 0.3382 | 0.1036 |
| LOri088 | | | M5.5 | (8) | N | Y+ (S08, M08, B09) | | | III | -9.44±1.12[2]; -16.288±0.483[4] | 0.660±0.042[2]; 0.475±0.111[4] | 3200 | 0.05 | 0.1839 | 0.1284 |
| LOri087 | | | M5.0 | (2) (8) | N | Y+ (S08, M08, B09) | <-11.0[2] | | III | -5.56±0.7[2]; -7.947±0.231[4] | 0.609±0.042[2]; 0.594±0.078[4] | 3500 | 0.0481 | 0.3382 | 0.1233 |
| ” | | | M5.0 | (2) (8) | N | Y+ (S08, M08, B09) | <-11.0[2] | | III | -5.56±0.7[2]; -6.995±0.393[4] | 0.609±0.042[2] | 3500 | 0.0481 | 0.3382 | 0.1233 |
| LOri086 | | | M5.0 | (8) | N | Y+ (S08, B09) | | | III | -6.978±0.205[4] | 0.621±0.086[4] | 3700 | 0.0402 | 0.4582 | 0.1023 |
| LOri085 | | | | | | Y+ (M08) | | | II | | | 3500 | 0.0488 | 0.3382 | 0.1251 |
| LOri084 | | | M6.0 | (7) | N | Y+ (B09) | | | III | -10.419±3.18[4] | | 3300 | 0.0541 | 0.2342 | 0.1393 |
| LOri083 | | | M3.0[2] | | N | Y+ (S08, M08) | | | III | -5.32±0.68[2] | 0.585±0.077[2] | 3600 | 0.0468 | 0.3906 | 0.1199 |
| LOri082 | | | M4.75 | (2) | N | Y+ (M08, B09) | | | III | -10.631±2.094[4] | | 3500 | 0.049 | 0.3382 | 0.1257 |
| LOri081 | | | M5.25 | (2) | N | Y+ (B09) | | | II | -3.45±0.071[4] | | 3700 | 0.0423 | 0.4582 | 0.1079 |
| LOri080 | | | M5.5 | (4) (6) | Y | Y+ (S08, M08, B09) | -10.1±0.5[2]; -7.061±0.05[4] | | III | -14.47±1.25[2]; -22.82±0.62[4] | 0.523±0.020[2] | 3100 | 0.0658 | 0.1365 | 0.1703 |
| ” | | | M5.5 | (4) (6) | Y | Y+ (S08, M08, B09) | -10.1±0.5[2]; -7.061±0.05[4] | | III | -14.47±1.25[2]; -14.67±1.00[4] | 0.523±0.020[2] | 3100 | 0.0658 | 0.1365 | 0.1703 |
| LOri079 | | | M6.5 M6.0 | (8) (7) | N | Y+ (S08, M08, B09) | <-11.0[2] | | III | -5.06±0.53[2]; -9.06±3.35[4] | 0.607±0.059[2] | 3600 | 0.0491 | 0.3906 | 0.1259 |
| ” | | | M6.5 M6.0 | (8) (7) | N | Y+ (S08, M08, B09) | <-11.0[2] | | III | -5.06±0.53[2]; -10.0±0.24[4] | 0.607±0.059[2]; 0.605±0.09[4] | 3600 | 0.0491 | 0.3906 | 0.1259 |
| LOri078 | | | M3.5 | (7) | N | Y+ (M08, B09) | | | III | -1.142±0.186[4] | | 3700 | 0.0501 | 0.4582 | 0.1287 |
| LOri077 | | | M5.0 | (1) | N | Y+ (M08, B09) | | | III | -7.923±0.231[4] | 0.486±0.098[4] | 3400 | 0.0571 | 0.286 | 0.1473 |
| LOri076 | | | M3.0[2] | | N | Y+ (S08, M08) | | | III | -4.92±0.6[2] | 0.608±0.019[2] | 3700 | 0.0527 | 0.4582 | 0.1354 |
| LOri075 | | | M5.0 M5.5 | (2) (8) (3) | N | Y+ (S08, M08, B09) | | SB1 (M08) | III | -10.71±0.98[2]; -12.81±0.86[4] | 0.455±0.044[2]; 0.941±0.052[4] | 3400 | 0.0999 | 0.286 | 0.2516 |
| ” | | | M5.0 M5.5 | (2) (8) (3) | N | Y+ (S08, M08, B09) | | SB1 (M08) | III | -10.71±0.98[2]; -10.73±0.73[4] | 0.455±0.044[2]; 0.96±0.202[4] | 3400 | 0.0999 | 0.286 | 0.2516 |
| ” | | | M5.0 M5.5 | (2) (8) (3) | N | Y+ (S08, M08, B09) | | SB1 (M08) | III | -10.71±0.98[2]; -10.20±0.89[4] | 0.455±0.044[2] | 3400 | 0.0999 | 0.286 | 0.2516 |
| LOri074 | | | | | | Y+ (M08) | | | III | | | 3600 | 0.0807 | 0.3906 | 0.2085 |
| LOri073 | | | M5.5 M5.0 | (3) (8) | N | Y+ (M08, B09) | | | III | -10.906±1.041[4] | 0.615±0.055[4] | 3700 | 0.0865 | 0.4582 | 0.2215 |
| ” | | | M5.5 M5.0 | (3) (8) | N | Y+ (M08, B09) | | | III | -4.542±0.186[4] | 0.462±0.092[4] | 3700 | 0.0865 | 0.4582 | 0.2215 |
| LOri072 | | | M6.0 | (7) | N | Y+ (B09) | | | III | -11.258±0.508[4] | | 3400 | 0.0892 | 0.286 | 0.2275 |
| LOri071 | | | M5.0 | (1) | N | Y+ (B09) | | | III | -6.812±0.232[4] | 0.395±0.071[4] | 3400 | 0.0736 | 0.286 | 0.1911 |
| LOri070 | | | M5.5 | (7) | N | Y+ (B09) | | | III | -13.555±3.256[4] | | 3700 | 0.0621 | 0.4582 | 0.1606 |
| LOri069 | | | M5.5 | (8) | N | Y+ (S08, M08, B09) | | SB2(M08 S08) | III | -7.39±1.46[2] | 0.516±0.057[2] | 3400 | 0.1043 | 0.286 | 0.2613 |
| ” | | | M5.5 | (8) | N | Y+ (S08, M08, B09) | | SB2(M08 S08) | III | -7.39±1.46[2]; -8.123±0.466[4] | 0.516±0.057[2]; 0.328±0.041[4] | 3400 | 0.1043 | 0.286 | 0.2613 |
| LOri068 | | | M4.5 M5.0 | (1) (3) | N | Y+ (S08, M08, B09) | | | III | -7.9±1.26[2]; -6.815±0.516[4] | 0.698±0.025[2]; 0.691±0.09[4] | 3700 | 0.094 | 0.4582 | 0.2383 |
| ” | | | M4.5 M5.0 | (1) (3) | N | Y+ (S08, M08, B09) | | | III | -7.9±1.26[2]; -14.388±0.742[4] | 0.698±0.025[2]; 0.53±0.045[4] | 3700 | 0.094 | 0.4582 | 0.2383 |
| LOri067 | | | | | | Y+ (M08) | | | III | | | 3500 | 0.0602 | 0.3382 | 0.1555 |
| LOri066 | | | | | | Y+ (M08) | | | III | | | 3300 | 0.0904 | 0.2342 | 0.2301 |
| LOri065 | | | | | | Y+ (M08) | | | III | | | 3700 | 0.0791 | 0.4582 | 0.2048 |
| LOri064 | C69-X-E-037 c | | M5.5 | (7) | N | Y+ (M08, B09) | | | III | -9.617±0.563[4] | | 3500 | 0.0757 | 0.3382 | 0.1967 |
| LOri063 | | | M4.0 | (3) | N | Y+ (S08, M08, B09) | -10.7±0.3[2] | | II | -19.14±2.53[2]; -11.55±0.69[4] | 0.505±0.052[2]; 0.645±0.088[4] | 3700 | 0.0853 | 0.4582 | 0.2186 |
| LOri062 | | | M3.0 | (6) | N | Y+ (S08, M08, B09) | <-11.0[2] | | II | -4.41±0.3[2]; -6.48±0.732[4] | 0.648±0.048[2] | 3500 | 0.0879 | 0.3382 | 0.2245 |
| LOri061 | | | M2.0 | (6) | Y | Y+ (S08, M08, B09) | -10.2±0.3[2]; -7.647±0.05[4] | | II | -13.97±1.38[2]; -11.78±0.17[4] | 0.591±0.030[2] | 3700 | 0.0997 | 0.4582 | 0.251 |
| LOri060 | | | M4.0 | (3) | N | Y+ (S08, M08, B09) | | | III | -4.18 ±0.48[2]; -4.03±0.21[4] | 0.599±0.028[2]; 0.4±0.069[4] | 3500 | 0.091 | 0.3382 | 0.2316 |

Continued on next page…

Table 3.25 – Continued

| Object | Alt ID | DM ID | SpT | INS[3] | Accret. | Membership[5] | log($\dot{M}_{acc}$)($M_\odot$/yr)[4] | Bin | Class[6] | EW(H$\alpha$)[4] | EW(Li)[4] | $T_{eff}$ | $L_{bol}$ | $Mass_{Teff}$ | $Mass_{Lbol}$ |
|---|---|---|---|---|---|---|---|---|---|---|---|---|---|---|---|
| LOri059 | | | M4.0 M5.0 | (3) (8) | N | Y+ (M08, B09) | | | III | -6.874±0.288[4)] | 0.39±0.042[4)] | 3500 | 0.0938 | 0.3382 | 0.2379 |
| ” | | | M4.0 M5.0 | (3) (8) | N | Y+ (M08, B09) | | | III | -9.833±0.301[4)] | 0.369±0.063[4)] | 3500 | 0.0938 | 0.3382 | 0.2379 |
| LOri058 | C69-X-E-096 c | | M3.5 | (3) | N | Y+ (M08, B09) | | | III | -7.28±0.398[4)] | 0.299±0.056[4)] | 3500 | 0.0951 | 0.3382 | 0.2407 |
| LOri057 | | | M5.5 | (3) | N | Y+ (S08, B09) | | | III | -5.2±0.52[2)]; -4.999±0.307[4)] | 0.677±0.019[2)]; 0.48±0.083[4)] | 3700 | 0.106 | 0.4582 | 0.2653 |
| LOri056 | | | M4.0 M5.0 | (3) (8) | N | Y+ (S08, M08, B09) | | | III | -5.57±0.81[2)]; -4.367±0.446[4)] | 0.576±0.023[2)]; 0.306±0.047[4)] | 3700 | 0.127 | 0.4582 | 0.3096 |
| ” | | | M4.0 M5.0 | (3) (8) | N | Y+ (S08, M08, B09) | | | III | -5.57±0.81[2)]; -6.219±0.221[4)] | 0.576±0.023[2)]; 0.45±0.023[4)] | 3700 | 0.127 | 0.4582 | 0.3096 |
| LOri055 | C69-X-E-079 I | | M4.0 | (3) | N | Y+ (S08, M08, B09) | | | III | -6.53±0.49[2)]; -7.054±0.132[4)] | 0.602±0.033[2)]; 0.413±0.079[4)] | 3700 | 0.1382 | 0.4582 | 0.3292 |
| LOri054 | C69-X-E-055 I | | M5.5 | (7) | N | Y+ (M08, B09) | | | III | -8.346±0.476[4)] | | 3700 | 0.1363 | 0.4582 | 0.3258 |
| LOri053 | | | M4.5 M5.5 | (8) (7) | N | Y+ (S08, M08, B09) | | | III | -2.93±0.2[2)]; -5.833±0.216[4)] | 0.561±0.030[2)] | 3500 | 0.136 | 0.3382 | 0.3253 |
| ” | | | M4.5 M5.5 | (8) (7) | N | Y+ (S08, M08, B09) | | | III | -2.93±0.2[2)]; -4.298±0.148[4)] | 0.561±0.030[2)]; 0.56±0.041[4)] | 3500 | 0.136 | 0.3382 | 0.3253 |
| LOri052 | C69-X-W-024 c | | M5.0 M4.0 | (6) (8) | N | NM?+ (M08, B09) | | | III | -7.262±0.423[4)] | 0.278±0.103[4)] | 3500 | 0.1466 | 0.3382 | 0.3438 |
| ” | C69-X-W-024 c | | M5.0 M4.0 | (6) (8) | N | NM?+ (M08, B09) | | | III | -6.796±0.44[4)] | | 3500 | 0.1466 | 0.3382 | 0.3438 |
| LOri051 | C69-X-E-054 I | | | | | Y+ (M08) | | SB1 (M08) | III | | | 3500 | 0.1377 | 0.3382 | 0.3283 |
| LOri050 | | | M4.0 | (8) (3) | Y | Y+ (S08, M08, B09) | -10.878±0.05[4)] | SB1(M08 S08) | II | -11.14±0.96[2)]; -15.98±1.58[4)] | 0.596±0.058[2)]; 0.57±0.016[4)] | 3700 | 0.1756 | 0.4582 | 0.3944 |
| ” | | | M4.0 | (8) (3) | Y | Y+ (S08, M08, B09) | -10.878±0.05[4)] | SB1(M08 S08) | II | -11.14±0.96[2)]; -11.646±1.29[4)] | 0.596±0.058[2)]; 0.509±0.036[4)] | 3700 | 0.1756 | 0.4582 | 0.3944 |
| LOri049 | | | M5.0 M4.0 | (7) (8) | N | NM+ (S08, B09) | | | III | | 0.64 ±0.013[2)] | 3750 | 0.1439 | 0.4936 | 0.339 |
| ” | | | M5.0 M4.0 | (7) (8) | N | NM+ (S08, B09) | | | III | | 0.64 ±0.013[2)] | 3750 | 0.1439 | 0.4936 | 0.339 |
| LOri048 | | | M3.0 | (6) | N | Y+ (S08, M08, B09) | <-11.0[2)] | | II | -3.34±0.44[2)]; -4.319±0.193[4)] | 0.545±0.012[2)] | 3500 | 0.1804 | 0.3382 | 0.4023 |
| LOri047 | C69-X-E-081 c | DM047 | | | N | Y+ (M08) | | | III | -8.65[1)] | 0.57[1)] | 3700 | 0.1977 | 0.4582 | 0.4277 |
| LOri046 | | | M4.0 | (7) (8) | N | NM+ (S08, M08, B09) | | | III | | 0.148±0.064[2)] | 3750 | 0.1588 | 0.4936 | 0.3652 |
| ” | | | M4.0 | (7) (8) | N | NM+ (S08, M08, B09) | | | III | -0.369±0.014[4)] | 0.148±0.064[2)] | 3750 | 0.1588 | 0.4936 | 0.3652 |
| LOri045 | | | M4.0 M2.0 | (8) (6) | N | Y+ (S08, B09) | | | III | -3.04±0.33[2)]; -6.22±0.337[4)] | 0.554±0.023[2)]; 0.498±0.044[4)] | 3500 | 0.2045 | 0.3382 | 0.4375 |
| ” | | | M4.0 M2.0 | (8) (6) | N | Y+ (S08, B09) | | | III | -3.04±0.33[2)]; -6.849±0.105[4)] | 0.554±0.023[2)] | 3500 | 0.2045 | 0.3382 | 0.4375 |
| LOri044 | C69-X-W-015 I | | M4.5 M3.5 | (6) (8) | N | NM + (M08, B09) | | | III | -1.615±0.098[4)] | | 3750 | 0.1863 | 0.4936 | 0.4109 |
| ” | C69-X-W-015 I | | M4.5 M3.5 | (6) (8) | N | NM+ (M08, B09) | | | III | -1.571±0.2[4)] | | 3750 | 0.1863 | 0.4936 | 0.4109 |
| LOri043 | | | M4.0 | (8) | N | Y+ (M08, B09) | | SB2 (M08) | III | -3.92±0.123[4)] | 0.528±0.07[4)] | 3500 | 0.2198 | 0.3382 | 0.4598 |
| LOri042 | | | M4.0 | (3) | N | Y+ (B09) | | | III | -3.024±0.156[4)] | 0.648±0.078[4)] | 3750 | 0.2101 | 0.4936 | 0.4457 |
| LOri041 | C69-X-E-036 I | DM038 | M3.5[2] | | N | Y+ (S08, M08) | | | III | -8.2[1)]; -7.05±0.86[2)] | 0.74[1)]; 0.485±0.040[2)] | 3700 | 0.2506 | 0.4582 | 0.5044 |
| LOri040 | C69-X-E-035 c | DM041 | M3.0[2] | | N | Y+ (S08, M08) | | | III | -3.9[1)]; -5.15±0.62[2)] | 0.64[1)]; 0.561±0.045[2)] | 3500 | 0.2472 | 0.3382 | 0.4998 |
| LOri039 | C69-X-E-082 I | DM049 | | | N | Y+ (DM, M08) | | | III | -3.59[1)] | 0.55[1)] | 3750 | 0.2278 | 0.4936 | 0.4715 |
| LOri038 | C69-X-W-008 c | DM002 | M3.0 | (8) | Y | Y+ (B09) | -10.904±0.030[4)] | | II | -24.95[1)]; -14.012±0.513[4)] | 0.47[1)]; 0.523±0.035[4)] | 3500 | 0.2563 | 0.3382 | 0.5119 |
| LOri037 | C69-X-W-013 c | DM011 | M3.5 | (8) | N | Y+ (S08, B09) | | | III | -3.63[1)]; -3.67±0.34[2)]; -4.40±0.23[4)] | 0.63[1)]; 0.566±0.057[2)]; 0.558±0.037[4)] | 3500 | 0.2756 | 0.3382 | 0.5374 |
| LOri036 | C69-X-W-023 I | | M3.5 | (6) | N | NM+ (S08, B09) | | | III | -4.797±0.224[4)] | 0.56 ±0.022[2)] | 3500 | 0.2414 | 0.3382 | 0.4914 |
| LOri035 | | | M2.5[2] | | N | Y+ (S08) | | | III | -3.32±0.35[2)] | 0.572±0.021[2)] | 3500 | 0.2587 | 0.3382 | 0.5151 |
| LOri034 | | | M1.0[2] | | Y | Y?+ (S08) | -10.8±0.4[2)]; -10.80±0.40[4)] | | II | -8.47±0.47[2)] | 0.541±0.035[2)] | 3700 | 0.3063 | 0.4582 | 0.578 |
| LOri033 | C69-X-E-029 c | DM039 | | | N | Y+ (DM) | | | III | -3.14[1)] | 0.36[1)] | 3750 | 0.2932 | 0.4936 | 0.5607 |
| LOri032 | C69-X-E-022 I | DM055 | | | N | Y+ (DM) | | | III | -6.83[1)] | 0.62[1)] | 3750 | 0.2925 | 0.4936 | 0.5598 |
| LOri031 | | | M3.5 | (3) | N | Y+ (B09) | | | III | -2.838±0.139[4)] | 0.614±0.045[4)] | 3750 | 0.3067 | 0.4936 | 0.5785 |
| LOri030 | | | M1.5[2] | | | Y?+ (S08) | | SB2 (S08) | III | | | 3750 | 0.3037 | 0.4936 | 0.5746 |
| LOri029 | | | | | | Y | | | II | | | 3700 | 0.3704 | 0.4582 | 0.6582 |
| LOri028 | C69-X-E-017 I | | | | | Y+ | | | III | | | 3750 | 0.2837 | 0.4936 | 0.5481 |
| LOri027 | | | | | | Y | | | III | | | 4000 | 0.3366 | 0.7341 | 0.6168 |
| LOri026 | C69-X-W-002 c | DM012 | M2.5 | (8) | N | Y+ (DM, S08, B09) | | | III | -6.07[1)]; -5.3±0.3[2)]; -5.537±0.298[4)] | 0.66[1)]; 0.581±0.043[2)]; 0.588±0.046[4)] | 3750 | 0.4153 | 0.4936 | 0.7124 |
| LOri025 | C69-X-E-011 c | DM059 | | | N | Y+ (DM) | | | III | -3.95[1)]; | 0.53[1)] | 3750 | 0.4139 | 0.4936 | 0.7109 |
| LOri024 | | | M1.5 | (8) | N | Y+ (S08, B09) | | | III | -2.0±0.12[2)]; -2.466±0.107[4)] | 0.554±0.021[2)]; 0.54±0.017[4)] | 3750 | 0.3979 | 0.4936 | 0.6919 |
| LOri023 | C69-X-E-028 c | DM050 | | | N | Y+ (DM) | | | III | -1.95[1)] | 0.47[1)] | 3750 | 0.3859 | 0.4936 | 0.6772 |
| LOri022 | C69-X-E-014 I | DM044 | M1.5[2] | | N | Y+ (DM, S08) | | | III | -4.39[1)]; -6.96±0.69[2)] | 0.54[1)] 0.516±0.033[2)] | 3750 | 0.4163 | 0.4936 | 0.7135 |

Continued on next page…

Table 3.25 – Continued

| Object | Alt ID | DM ID | SpT | INS[3] | Accret. | Membership[5] | log($\dot{M}_{acc}$)($M_\odot$/yr)[4] | Bin | Class[6] | EW(H$\alpha$)[4] | EW(Li)[4] | $T_{eff}$ | $L_{bol}$ | $Mass_{Teff}$ | $Mass_{Lbol}$ |
|---|---|---|---|---|---|---|---|---|---|---|---|---|---|---|---|
| LOri021 | | | | | | Y | | | III | | | 4000 | 0.392 | 0.7341 | 0.6847 |
| LOri020 | | | M2.0[2] | | | NM+ (S08) | | | III | | 0.18 ±0.029[2)] | 3500 | 0.4655 | 0.3382 | 0.7703 |
| LOri019 | | | | | | Y | | | III | | | 3750 | 0.4495 | 0.4936 | 0.7519 |
| LOri018 | C69-X-E-016 I | DM056 | | | N | Y+ (DM) | | | III | -2.02[1)] | 0.59[1)] | 3750 | 0.4647 | 0.4936 | 0.7694 |
| LOri017 | C69-X-E-006 I | DM060 | | (3) | N | Y+ (DM, B09) | | | III | -0.8[1)]; -6.572±2.307[4)] | 0.49[1)] | 4250 | 0.4449 | 1.0094 | 0.7465 |
| LOri016 | | | K8.0[2] | | | Y+ (S08) | | SB (S08) | III | -1.58±0.13[2)] | 0.531±0.033[2)] | 4000 | 0.4903 | 0.7341 | 0.7989 |
| LOri015 | | | | | | Y | | | III | | | 4000 | 0.5631 | 0.7341 | 0.8754 |
| LOri014 | C69-X-E-007 c | DM058 | | | N | Y+ (DM) | | | III | -1.45[1)] | 0.55[1)] | 4000 | 0.522 | 0.7341 | 0.8323 |
| LOri013 | C69-X-W-003 I | DM004 | M3.5 | (8) | N | Y+ (DM, B09) | | | III | -4.41[1)]; -4.308±0.207[4)] | 0.33[1)]; 0.523±0.037[4)] | 3750 | 0.5978 | 0.4936 | 0.9104 |
| LOri012 | | | K8 | (8) | N | NM+ (B09) | | | III | | 0.082±0.017[4)] | 4000 | 0.6017 | 0.7341 | 0.914 |
| LOri011 | | | K9 | (8) | N | NM+ (B09) | | | III | | 0.038±0.0040[4)] | 3750 | 0.6729 | 0.4936 | 0.9796 |
| LOri010 | | | | | | Y | | | III | | | 4250 | 0.5716 | 1.0094 | 0.8843 |
| LOri009 | | | | | | Y | | | III | | | 4000 | 0.5789 | 0.7341 | 0.892 |
| LOri008 | C69-X-E-004 I | DM051 | | | N | Y+ (DM) | | | III | -1.65[1)] | 0.55[1)] | 4000 | 0.7191 | 0.7341 | 1.0195 |
| LOri007 | | | M1.5 M1.0 | (8) (6) | N | NM+ (B09) | | | III | | | 4000 | 0.6272 | 0.7341 | 0.9375 |
| ” | | | M1.5 M1.0 | (8) (6) | N | NM+ (B09) | | | III | | | 4000 | 0.6272 | 0.7341 | 0.9375 |
| LOri006 | | | | | | Y | | | III | | | 4000 | 0.7323 | 0.7341 | 1.0303 |
| LOri005 | | | | | | Y | | | III | | | 4000 | 0.8772 | 0.7341 | 1.1403 |
| LOri004 | C69-X-E-023 I | | | | | Y | | | III | | | 3750 | 0.7806 | 0.4936 | 1.0697 |
| LOri003 | C69-X-E-001 I | DM046 | K8.5[2] | | N | Y+ (S08) | | SB (S08) | III | -3.35[1)]; -1.13±0.15[2)] | 0.55[1)]; 0.520±0.032[2)] | 4000 | 0.8231 | 0.7341 | 1.1036 |
| LOri002 | | | | | | Y | | | III | | | 3750 | 0.984 | 0.4936 | 1.2104 |
| LOri001 | C69-X-W-004 I | DM001 | M0 | (8) | N | Y+ (B09) | | | III | -2.51[1)]; -2.819±0.159[4)] | 0.56[1)]; 0.468±0.015[4)] | 4000 | 0.928 | 0.7341 | 1.1748 |
| DM071 | C69-X-E-041 M | DM071 | | | | Y+ (DM) | | | – | | 0.52[1)] | 3700 | | | |
| DM070 | C69-X-E-019 M | DM070 | | | | Y+ (DM) | | | III | -0.9[1)] | 0.58[1)] | 4500 | 0.244 | 1.2911 | 0.4952 |
| DM069 | C69-X-E-058 M | DM069 | | | | Y+ (DM) | | | III | -0.49[1)] | 0.51[1)] | 4500 | 0.315 | 1.2911 | 0.5896 |
| DM068 | | DM068 | | | | Y+ (DM) | | | III | 0.04[1)] | 0.44[1)] | 3750 | 0.844 | 0.4936 | 1.1178 |
| DM067 | C69-X-E-031 M | DM067 | | | | Y+ (DM) | | | III | -4.88[1)] | 0.66[1)] | 4800 | 0.247 | 1.5748 | 0.4996 |
| DM066 | | DM066 | | | | Y+ (DM) | | | III | -1.0[1)] | 0.55[1)] | 4000 | 1.655 | 0.7341 | 1.5 |
| DM065 | C69-X-E-018 M | DM065 | | | | Y+ (DM) | | | III | -2.67[1)] | 0.58[1)] | 4250 | 0.302 | 1.0094 | 0.5724 |
| DM064 | | DM064 | | | | Y+ (DM) | | | II | -2.52[1)] | 0.45[1)] | 3500 | 0.3 | 0.3382 | 0.5697 |
| DM063 | | DM063 | | | | Y+ (DM) | | | II | -4.76[1)] | 0.54[1)] | 4500 | 1.032 | 1.2911 | 1.2368 |
| DM062 | C69-X-E-027 c | DM062 | | | | Y+ (DM) | | | III | -4.05[1)] | 0.61[1)] | 3700 | 0.188 | 0.4582 | 0.4134 |
| DM061 | C69-X-E-025 I | DM061 | | | | Y+ (DM) | | | III | -4.23[1)] | 0.56[1)] | 3300 | 0.203 | 0.2342 | 0.4353 |
| DM057 | C69-X-E-008 I | DM057 | | | | Y+ (DM) | | | III | 0.15[1)] | 0.39[1)] | 3500 | 1.148 | 0.3382 | 1.3004 |
| DM053 | C69-X-E-030 I | DM053 | | | | Y+ (DM) | | | III | -3.62[1)] | 0.52[1)] | 3700 | 0.402 | 0.4582 | 0.6969 |
| DM052 | | DM052 | | | | Y+ (DM) | | | III | 0.36[1)] | 0.25[1)] | 3750 | 0.625 | 0.4936 | 0.9355 |
| DM048 | | DM048 | M3.5 M1.5 | (7) (6) | N | Y+ (DM, B09) | | | II | -8.61[1)]; -3.357±0.111[4)] | 0.58[1)] | 3000 | 0.178 | 0.1 | 0.3986 |
| ” | | DM048 | M3.5 M1.5 | (7) (6) | N | Y+ (DM, B09) | | | II | -8.61[1)]; -7.724±0.19[4)] | | 3000 | 0.178 | 0.1 | 0.3986 |
| DM045 | C69-X-E-010 c | DM045 | | | | Y+ (DM) | | | III | 0.12[1)] | 0.46[1)] | 4750 | 1.658 | 1.5313 | 1.5008 |
| DM043 | | DM043 | | | | Y+ (DM) | | | III | -2.6[1)] | 0.57[1)] | 3600 | 0.255 | 0.3906 | 0.5102 |
| DM042 | | DM042 | | | | Y+ (DM) | | | III | -2.94[1)] | 0.58[1)] | 4750 | 0.18 | 1.5313 | 0.4018 |
| DM040 | C69-X-E-084 I | DM040 | | | | Y+ (DM) | | | III | -3.63[1)] | 0.55[1)] | 4500 | 0.136 | 1.2911 | 0.3253 |
| DM037 | | DM037 | | | | Y+ (DM) | | | III | -0.08[1)] | 0.43[1)] | 3000 | 0.405 | 0.1 | 0.7006 |
| DM035 | C69-X-E-034 c | DM035 | | | | Y+ (DM) | | | III | -1.68[1)] | 0.55[1)] | 4800 | 0.338 | 1.5748 | 0.6185 |
| DM034 | | DM034 | | | | Y+ (DM) | | | III | -2.64[1)] | 0.49[1)] | 3700 | 0.188 | 0.4582 | 0.4134 |
| DM032 | | DM032 | | | | Y+ (DM, S08) | <-11.0[2)] | | III | -5.5[1)]; -4.98±0.49[2)] | 0.42[1)]; 0.589±0.016[2)] | 3750 | 0.151 | 0.4936 | 0.3515 |
| DM031 | | DM031 | | | | Y+ (DM) | | | III | 0.01[1)] | 0.42[1)] | 3600 | 0.875 | 0.3906 | 1.1388 |

Continued on next page…

Table 3.25 – Continued

| Object | Alt ID | DM ID | SpT | INS[3] | Accret. | Membership[5] | log($\dot{M}_{acc}$)($M_\odot$/yr)[4] | Bin | Class[6] | EW(H$\alpha$)[4] | EW(Li)[4] | $T_{eff}$ | $L_{bol}$ | $Mass_{Teff}$ | $Mass_{Lbol}$ |
|---|---|---|---|---|---|---|---|---|---|---|---|---|---|---|---|
| DM030 | | DM030 | | | | Y+ (DM, S08) | <-11.0[2)] | | III | -1.0[1)]; -1.89±0.15[2)] | 0.61[1)]; 0.571±0.034[2)] | 4250 | 0.204 | 1.0094 | 0.4368 |
| DM028 | | DM028 | | | | Y+ (DM) | | | III | 0.35[1)] | 0.47[1)] | 4000 | 0.697 | 0.7341 | 1.0015 |
| DM027 | | DM027 | | | | Y+ (DM) | | | III | -3.64[1)] | 0.59[1)] | 3500 | 0.282 | 0.3382 | 0.5459 |
| DM026 | | DM026 | | | | Y+ (DM) | | | III | 0.39[1)] | 0.35[1)] | 3600 | 1.591 | 0.3906 | 1.4775 |
| DM025 | | DM025 | | | | Y+ (DM) | | | III | -1.47[1)] | 0.54[1)] | 4500 | 0.381 | 1.2911 | 0.6712 |
| DM024 | | DM024 | | | | Y+ (DM) | | | III | 1.07[1)] | 0.3[1)] | 3500 | 1.616 | 0.3382 | 1.4863 |
| DM023 | | DM023 | | | | Y+ (DM) | | | III | -2.04[1)] | 0.53[1)] | 3500 | 0.259 | 0.3382 | 0.5155 |
| DM022 | | DM022 | | | | Y+ (DM) | | | III | -2.37[1)] | 0.54[1)] | 4500 | 0.308 | 1.2911 | 0.5803 |
| DM021 | | DM021 | | | | Y+ (DM) | | | III | -1.73[1)] | 0.5[1)] | 3400 | 0.657 | 0.286 | 0.9649 |
| DM019 | | DM019 | | | | Y+ (DM, S08) | <-11.0[2)] | | III | -2.07[1)]; -2.44±0.23[2)] | 0.56[1)]; 0.571±0.027[2)] | 4750 | 0.304 | 1.5313 | 0.575 |
| DM018 | | DM018 | | | | Y+ (DM) | | | III | -2.64[1)] | 0.52[1)] | 4000 | 0.824 | 0.7341 | 1.1042 |
| DM017 | | DM017 | | | | Y+ (DM) | | | III | -0.25[1)] | 0.47[1)] | 5000 | 1.314 | 1.7371 | 1.3749 |
| DM016 | | DM016 | M1.5 | (8) | N | Y+ (DM, B09) | | | III | -5.45[1)]; -2.828±0.101[4)] | 0.61[1)]; 0.546±0.01[4)] | 3750 | 0.308 | 0.4936 | 0.5803 |
| DM015 | | DM015 | | | | Y+ (DM) | | | III | -1.07[1)] | 0.49[1)] | 3750 | 0.257 | 0.4936 | 0.5128 |
| DM014 | C69-X-W-006 I | DM014 | | | | Y+ (DM, S08) | <-11.0[2)] | | III | -2.28[1)]; -1.00±0.08[2)] | 0.57[1)]; 0.523±0.026[2)] | 4000 | 0.441 | 0.7341 | 0.7421 |
| DM013 | | DM013 | | | | Y+ (DM) | | | III | -1.29[1)] | 0.53[1)] | 3600 | 0.348 | 0.3906 | 0.6308 |
| DM010 | | DM010 | | | | Y+ (DM) | | | III | -5.97[1)] | 0.51[1)] | 4250 | 0.198 | 1.0094 | 0.428 |
| DM009 | C69-X-W-005 c | DM009 | K9 | (8) | N | Y+ (DM, S08, B09) | <-11.0[2)] | | III | -0.74[1)]; -0.5±0.03[2)]; -0.608±0.039[4)] | 0.4[1)]; 0.464±0.023[2)]; 0.432±0.029[4)] | 4400 | 0.639 | 1.1901 | 0.9483 |
| DM008 | | DM008 | | | | Y+ (DM) | | | III | 0.09[1)] | 0.41[1)] | 3500 | 0.945 | 0.3382 | 1.1864 |
| DM007 | C69-X-W-011 c | DM007 | | | | Y+ (DM) | | | III | 0.12[1)] | 0.42[1)] | 4000 | 1.841 | 0.7341 | 1.5496 |
| DM006 | C69-X-W-012 I | DM006 | | | | Y+ (DM) | | | II | -72.64[1)] | 0.43[1)] | 4000 | 0.297 | 0.7341 | 0.5657 |
| DM005 | | DM005 | | | | Y+ (DM) | | | III | -0.06[1)] | 0.46[1)] | 4000 | 1.286 | 0.7341 | 1.3623 |
| DM003 | | DM003 | | | | Y+ (DM) | | | III | -3.18[1)] | 0.44[1)] | 3400 | 0.724 | 0.286 | 1.0236 |
| C69WI1-9847 | C69WI1-9847 | | | | | NM | | | – | | | 4200 | 0.1605 | 0.9517 | 0.368 |
| C69WI1-9696 | C69WI1-9696 | | | | | NM | | | II | | | 1700 | 0.0032 | 0.0073 | 0.023 |
| C69WI1-9288 | C69WI1-9288 | | M2.5 | (8) | Y | Y+ (B09) | -7.049±0.024[4)] | | II | -30.202±1.14[4)] | 0.432±0.04[4)] | 3700 | 0.198 | 0.4582 | 0.428 |
| C69WI1-7809 | C69WI1-7809 | | | | | Y | | | II | | | 2300 | 0.0234 | 0.016 | 0.0955 |
| C69WI1-718 | C69WI1-718 | | | | | NM | | | – | | | 4500 | 0.013 | 1.2911 | 0.0611 |
| C69WI1-7152 | C69WI1-7152 | | | | | Y | | | II | | | 3300 | 0.0579 | 0.2342 | 0.1492 |
| C69WI1-6820 | C69WI1-6820 | | | | | NM | | | III | | | 5250 | 0.3267 | 1.8909 | 0.6047 |
| C69WI1-6412 | C69WI1-6412 | | | | | NM | | | I | | | 0 | 0.0 | 0.0 | 0.0 |
| C69WI1-6018 | C69WI1-6018 | | | | | NM | | | – | | | 4250 | 0.0114 | 1.0094 | 0.0668 |
| C69WI1-4897 | C69WI1-4897 | | F9 | (7) | N | NM+ (B09) | | | – | | | 5500 | 0.2213 | 1.9992 | 0.4621 |
| C69WI1-4614 | C69WI1-4614 | | | | | NM | | | – | | | 3100 | 0.0077 | 0.1365 | 0.0373 |
| C69WI1-4232 | C69WI1-4232 | | | | | Y | | | III | | | 4400 | 0.6839 | 1.1901 | 0.9897 |
| C69WI1-3226 | C69WI1-3226 | | K7-M0 | (7) | N | NM | | | II | | | 2000 | 0.0087 | 0.0105 | 0.0402 |
| C69WI1-306 | C69WI1-306 | | | | | NM | | | III | | | 4600 | 0.2239 | 1.3929 | 0.4659 |
| C69WI1-2708 | C69WI1-2708 | | M3.5 | (8) | N | Y+ (B09) | | | II | -6.377±0.128[4)] | 0.518±0.014[4)] | 3600 | 0.1228 | 0.3906 | 0.3023 |
| C69WI1-2303 | C69WI1-2303 | | | | | NM | | | III | | | 3900 | 0.0914 | 0.631 | 0.2324 |
| C69WI1-2261 | C69WI1-2261 | | | | | NM | | | III | | | 5500 | 0.2131 | 1.9992 | 0.4501 |
| C69WI1-15496 | C69WI1-15496 | | | | | NM | | | I | | | 0 | 0.0 | 0.0 | 0.0 |
| C69WI1-15404 | C69WI1-15404 | | | | | NM | | | III | | | 4250 | 0.037 | 1.0094 | 0.1 |
| C69WI1-15377 | C69WI1-15377 | | | | | Y | | | II | | | 3300 | 0.1642 | 0.2342 | 0.3744 |
| C69WI1-15281 | C69WI1-15281 | | | | | NM | | | – | | | 4600 | 0.0219 | 1.3929 | 0.0929 |
| C69WI1-14892 | C69WI1-14892 | | | | | Y | | | II | | | 3400 | 0.052 | 0.286 | 0.1336 |
| C69WI1-1388 | C69WI1-1388 | | | | | Y | | | III | | | 4400 | 0.3031 | 1.1901 | 0.5738 |
| C69WI1-1322 | C69WI1-1322 | | | | | Y | | | II | | | 3300 | 0.0291 | 0.2342 | 0.1 |

Continued on next page…

Table 3.25 – Continued

| Object | Alt ID | DM ID | SpT | INS[3] | Accret. | Membership[5] | log($\dot{M}_{acc}$)($M_\odot$/yr)[4] | Bin | Class[6] | EW(H$\alpha$)[4] | EW(Li)[4] | $T_{eff}$ | $L_{bol}$ | $Mass_{Teff}$ | $Mass_{Lbol}$ |
|---|---|---|---|---|---|---|---|---|---|---|---|---|---|---|---|
| C69WI1-12378 | C69WI1-12378 | | | | | NM | | | I | | | 1700 | 0.0070 | 0.0073 | 0.0351 |
| C69WI1-10971 | C69WI1-10971 | | | | | NM | | | III | | | 6250 | 0.5895 | 2.1305 | 0.9028 |
| C69SWI1-937 | C69SWI1-937 | | | | | Y? | | | III | | | 8000 | 11.7952 | 2.3494 | 2.0585 |
| C69SWI1-496 | C69SWI1-496 | | | | | Y | | | III | | | 6000 | 5.2983 | 2.0869 | 1.9277 |
| C69SEI1-4263 | C69SEI1-4263 | | | | | Y? | | | III | | | 25000 | 1634.483 | 0.0 | 0.0 |
| C69SEI1-4253 | C69SEI1-4253 | | | | | Y | | | III | | | 4600 | 3.9697 | 1.3929 | 1.8527 |
| C69SEI1-2889 | C69SEI1-2889 | | | | | Y | | | III | | | 5800 | 11.8429 | 2.052 | 2.0591 |
| C69EI1-790 | C69EI1-790 | | M3 | (7) | N | Y+ (B09) | | | II | -9.047±0.478[4)] | | 3900 | 0.1054 | 0.631 | 0.2639 |
| C69EI1-7620 | C69EI1-7620 | | | | | Y | | | II | | | 2000 | 0.0902 | 0.0105 | 0.2297 |
| C69EI1-7312 | C69EI1-7312 | | | | | NM | | | I | | | 0 | 0.0 | 0.0 | 0.0 |
| C69EI1-7070 | C69EI1-7070 | | | | | NM | | | I | | | 3100 | 0.0057 | 0.1365 | 0.0307 |
| C69EI1-7021 | C69EI1-7021 | | | | | Y? | | | I | | | 0 | 0.0 | 0.0 | 0.0 |
| C69EI1-6539 | C69EI1-6539 | | | | | NM | | | I | | | 0 | 0.0 | 0.0 | 0.0 |
| C69EI1-6036 | C69EI1-6036 | | | | | Y | | | II | | | 3500 | 0.0467 | 0.3382 | 0.1195 |
| C69EI1-4761 | C69EI1-4761 | | | | | NM? | | | III | | | 5750 | 1.1663 | 2.0433 | 1.3086 |
| C69EI1-3574 | C69EI1-3574 | | | | | NM | | | I | | | 0 | 0.0 | 0.0 | 0.0 |
| C69EI1-3465 | C69EI1-3465 | | | | | Y | | | II | | | 3200 | 0.0275 | 0.1839 | 0.1 |
| C69EI1-3154 | C69EI1-3154 | | | | | NM | | | – | | | 1700 | 0.0067 | 0.0073 | 0.0341 |
| C69EI1-3042 | C69EI1-3042 | | | | | Y | | | II | | | 3500 | 0.0117 | 0.3382 | 0.0645 |
| C69EI1-2229 | C69EI1-2229 | | | | | Y | | | II | | | 3400 | 0.0518 | 0.286 | 0.1332 |
| C69EI1-16821 | C69EI1-16821 | | | | | NM | | | I | | | 0 | 0.0 | 0.0 | 0.0 |
| C69EI1-16578 | C69EI1-16578 | | | | | Y | | | II | | | 3000 | 0.0516 | 0.1 | 0.1325 |
| C69EI1-16472 | C69EI1-16472 | | | | | Y | | | II | | | 3300 | 0.047 | 0.2342 | 0.1202 |
| C69EI1-16121 | C69EI1-16121 | | | | | NM | | | – | | | 4250 | 0.0133 | 1.0094 | 0.0617 |
| C69EI1-15980 | C69EI1-15980 | | | | | NM | | | – | | | 2800 | 0.0063 | 0.0488 | 0.0327 |
| C69EI1-14609 | C69EI1-14609 | | M3 | (7) | Y | Y+ (B09) | -5.559±0.25[4)] | | II | -79.824±5.012[4)] | | 3400 | 0.059 | 0.286 | 0.1524 |
| C69EI1-14424 | C69EI1-14424 | | M3.5 | (7) | N | Y+ (B09) | | | II | -11.652±0.249[4)] | | 3800 | 0.1532 | 0.5373 | 0.3553 |
| C69EI1-13824 | C69EI1-13824 | | | | | Y? | | | I | | | 0 | 0.0 | 0.0 | 0.0 |
| C69EI1-13667 | C69EI1-13667 | | | | | NM | | | III | | | 4500 | 0.328 | 1.2911 | 0.6062 |
| C69EI1-13542 | C69EI1-13542 | | K3 | (7) | N | NM+ (B09) | | | II | | | 5250 | 0.192 | 1.8909 | 0.4193 |
| C69EI1-13002 | C69EI1-13002 | | | | | Y | | | II | | | 3100 | 0.0804 | 0.1365 | 0.2078 |
| C69EI1-12787 | C69EI1-12787 | | | | | NM | | | – | | | 4000 | 0.0437 | 0.7341 | 0.1116 |
| C69EI1-12304 | C69EI1-12304 | | | | | NM | | | – | | | 4800 | 0.0817 | 1.5748 | 0.2107 |
| C69EI1-11637 | C69EI1-11637 | | | | | NM | | | II | | | 3750 | 0.0016 | 0.4936 | 0.0175 |
| C69EI1-11541 | C69EI1-11541 | | | | | NM? | | | II | | | 3300 | 0.0763 | 0.2342 | 0.1983 |
| C69EI1-11529 | C69EI1-11529 | | | | | NM | | | III | | | 4250 | 0.0263 | 1.0094 | 0.1 |
| C69EI1-114 | C69EI1-114 | | M1.5 | (7) | N | Y+ (B09) | | | II | -4.788±0.16[4)] | | 3600 | 0.3387 | 0.3906 | 0.6193 |
| C69EI1-10963 | C69EI1-10963 | | | | | NM | | | II | | | 4000 | 0.0436 | 0.7341 | 0.1113 |
| C69EI1-10336 | C69EI1-10336 | | M4 | (7) | N | Y+ (B09) | | | II | -6.312±0.579[4)] | | 3500 | 0.066 | 0.3382 | 0.1708 |
| C69-X-W-052 - | | | | | | NM? | | | – | | | | | | |
| C69-X-W-051 - | | | | | | NM? | | | – | | | | | | |
| C69-X-W-050 - | | | | | | NM? | | | – | | | | | | |
| C69-X-W-049 I | | | | | | NM | | | – | | | 3000 | 4.0E-4 | 0.1 | 0.0096 |
| C69-X-W-048 I | | | | | | NM | | | – | | | 3400 | 9.0E-4 | 0.286 | 0.0139 |
| C69-X-W-047 M | | | | | | NM | | | – | | | 4250 | 0.0434 | 1.0094 | 0.1108 |
| C69-X-W-046 M | | | | | | NM? | | | – | | | 3400 | 0.0604 | 0.286 | 0.156 |
| C69-X-W-045 - | | | | | | NM? | | | – | | | | | | |

Continued on next page…

Table 3.25 – Continued

| Object | Alt ID | DM ID | SpT | INS[3] | Accret. | Membership[5] | $\log(\dot{M}_{acc})(M_\odot/yr)$[4] | Bin | Class[6] | EW(H$\alpha$)[4] | EW(Li)[4] | $T_{eff}$ | $L_{bol}$ | $Mass_{Teff}$ | $Mass_{Lbol}$ |
|---|---|---|---|---|---|---|---|---|---|---|---|---|---|---|---|
| C69-X-W-044 | - | | | | | NM? | | | II | | | | | | |
| C69-X-W-043 | I | | | | | NM | | | III | | | 6250 | 2.0759 | 2.1305 | 1.609 |
| C69-X-W-042 | w | | | | | NM | | | – | | | 3750 | 1.0E-4 | 0.4936 | 0.0053 |
| C69-X-W-042 | e | | | | | NM | | | – | | | 3750 | 0.0011 | 0.4936 | 0.0152 |
| C69-X-W-042 | c | | | | | NM | | | – | | | 2700 | 4.0E-4 | 0.0361 | 0.0096 |
| C69-X-W-041 | I | | | | | NM? | | | III | | | 3750 | 0.0855 | 0.4936 | 0.2192 |
| C69-X-W-040 | M | | | | | NM? | | | III | | | 4000 | 0.155 | 0.7341 | 0.3585 |
| C69-X-W-039 | w | | | | | NM | | | III | | | 6000 | 0.3116 | 2.0869 | 0.5851 |
| C69-X-W-039 | c | | | | | NM | | | – | | | 4000 | 0.0012 | 0.7341 | 0.0157 |
| C69-X-W-038 | s | | | | | NM | | | – | | | 4500 | 0.0062 | 1.2911 | 0.0324 |
| C69-X-W-038 | c | | | | | NM? | | | – | | | | | | |
| C69-X-W-037 | M | | | | | NM? | | | – | | | 3750 | 0.0727 | 0.4936 | 0.1887 |
| C69-X-W-036 | M | | | | | NM | | | III | | | 5250 | 0.3032 | 1.8909 | 0.5739 |
| C69-X-W-035 | - | | | | | NM? | | | – | | | | | | |
| C69-X-W-034 | M | | | | | NM? | | | III | | | 4000 | 0.1161 | 0.7341 | 0.2879 |
| C69-X-W-033 | + | | | | | NM? | | | – | | | | | | |
| C69-X-W-032 | z | | | | | NM? | | | – | | | | | | |
| C69-X-W-032 | s | | | | | NM? | | | – | | | | | | |
| C69-X-W-032 | e | | | | | NM? | | | III | | | 3750 | 0.0438 | 0.4936 | 0.1118 |
| C69-X-W-032 | c | | | | | NM? | | | III | | | 3700 | 0.045 | 0.4582 | 0.115 |
| C69-X-W-031 | M | | | | | Y | | | II | | | 1900 | 0.0046 | 0.0092 | 0.0274 |
| C69-X-W-030 | e | | | | | NM? | | | – | | | | | | |
| C69-X-W-030 | c | | | | | NM? | | | I | | | | | | |
| C69-X-W-029 | M | | | | | Y | | | II | | | 3200 | 0.1673 | 0.1839 | 0.3799 |
| C69-X-W-028 | M | | | | | Y | | | II | | | 2500 | 0.0073 | 0.0229 | 0.0359 |
| C69-X-W-027 | M | | | | | NM | | | – | | | 5000 | 0.0555 | 1.7371 | 0.1429 |
| C69-X-W-026 | - | | | | | NM | | | – | | | | | | |
| C69-X-W-025 | w | | | | | NM | | | – | | | 3700 | 0.0018 | 0.4582 | 0.0183 |
| C69-X-W-025 | e | | | | | NM | | | – | | | 4250 | 3.0E-4 | 1.0094 | 0.0084 |
| C69-X-W-025 | c | | | | | NM | | | – | | | 3750 | 5.0E-4 | 0.4936 | 0.0106 |
| C69-X-W-024 | s | | | | | NM | | | – | | | 3750 | 0.0010 | 0.4936 | 0.0147 |
| C69-X-W-022 | - | | | | | NM | | | – | | | | | | |
| C69-X-W-021 | - | | | | | NM? | | | – | | | | | | |
| C69-X-W-020 | I | | | | | Y? | | | III | | | 7000 | 12.483 | 2.2389 | 2.0673 |
| C69-X-W-019 | M | | | | | NM | | | I | | | 4000 | 0.0088 | 0.7341 | 0.0404 |
| C69-X-W-018 | I | | | | | NM? | | | III | | | 4500 | 0.2854 | 1.2911 | 0.5504 |
| C69-X-W-017 | - | | | | | NM? | | | – | | | | | | |
| C69-X-W-016 | - | | | | | NM? | | | – | | | | | | |
| C69-X-W-014 | w | | | | | NM | | | III | | | 4750 | 0.0423 | 1.5313 | 0.1078 |
| C69-X-W-014 | c | | | | | Y? | | | III | | | 4500 | 4.8047 | 1.2911 | 1.909 |
| C69-X-W-013 | n | | | | | NM | | | – | | | 4000 | 4.0E-4 | 0.7341 | 0.0096 |
| C69-X-W-011 | s | | | | | NM | | | – | | | 3400 | 0.0020 | 0.286 | 0.0192 |
| C69-X-W-010 | e | | | | | NM | | | – | | | 4000 | 0.0011 | 0.7341 | 0.0152 |
| C69-X-W-010 | c | | | | | NM | | | II | | | 4000 | 0.0033 | 0.7341 | 0.0234 |
| C69-X-W-009 | s | | | | | NM | | | III | | | 4500 | 0.1566 | 1.2911 | 0.3613 |
| C69-X-W-009 | n | | | | | NM | | | – | | | | | | |
| C69-X-W-009 | c | | | | | NM | | | III | | | 5750 | 1.1992 | 2.0433 | 1.3234 |

Continued on next page…

Table 3.25 – Continued

| Object | Alt ID | DM ID | SpT | INS[3] | Accret. | Membership[5] | log($\dot{M}_{acc}$)($M_\odot$/yr)[4] | Bin | Class[6] | EW(H$\alpha$)[4] | EW(Li)[4] | $T_{eff}$ | $L_{bol}$ | $Mass_{Teff}$ | $Mass_{Lbol}$ |
|---|---|---|---|---|---|---|---|---|---|---|---|---|---|---|---|
| C69-X-W-008 n | | | | | | NM | | | – | | | 4500 | 0.0388 | 1.2911 | 0.1 |
| C69-X-W-007 e | | | | | | NM? | | | – | | | 1900 | 4.0E-4 | 0.0092 | 0.0096 |
| C69-X-W-007 c | | | | | | Y | | | III | | | 3600 | 0.1249 | 0.3906 | 0.3059 |
| C69-X-W-005 w | | | | | | NM | | | – | | | 5000 | 0.0081 | 1.7371 | 0.0385 |
| C69-X-W-005 s | | | | | | NM | | | – | | | 5500 | 0.0403 | 1.9992 | 0.1025 |
| C69-X-W-002 n | | | | | | NM | | | – | | | 4750 | 0.0055 | 1.5313 | 0.0301 |
| C69-X-W-001 n | | | | | | NM? | | | – | | | | | | |
| C69-X-W-001 c | | | | | | Y? | | | III | | | 5000 | 3.4265 | 1.7371 | 1.8097 |
| C69-X-E-112 - | | | | | | NM? | | | – | | | | | | |
| C69-X-E-111 I | | | | | | NM | | | III | | | 6250 | 0.3009 | 2.1305 | 0.5709 |
| C69-X-E-110 - | | | | | | NM? | | | – | | | | | | |
| C69-X-E-109 w | | | | | | NM | | | – | | | 4000 | 0.0011 | 0.7341 | 0.0152 |
| C69-X-E-109 e | | | | | | NM | | | – | | | 3700 | 3.0E-4 | 0.4582 | 0.0084 |
| C69-X-E-109 c | | | | | | NM | | | – | | | 4250 | 2.0E-4 | 1.0094 | 0.0072 |
| C69-X-E-108 - | | | | | | NM? | | | – | | | 1800 | 1.0E-4 | 0.0081 | 0.0053 |
| C69-X-E-107 I | | | | | | NM | | | – | | | 4000 | 0.0028 | 0.7341 | 0.0219 |
| C69-X-E-106 I | | | | | | NM? | | | I | | | 1900 | 3.0E-4 | 0.0092 | 0.0084 |
| C69-X-E-105 M | | | | | | Y? | | | III | | | 3300 | 0.0565 | 0.2342 | 0.1456 |
| C69-X-E-104 e | | | | | | Y | | | – | | | 1200 | 3.0E-4 | 0.0036 | 0.0084 |
| C69-X-E-104 c | | | | | | Y | | | III | | | 3700 | 0.113 | 0.4582 | 0.2809 |
| C69-X-E-103 w | | | | | | NM | | | – | | | 3100 | 7.0E-4 | 0.1365 | 0.0124 |
| C69-X-E-103 s | | | | | | NM | | | – | | | 3000 | 1.0E-4 | 0.1 | 0.0053 |
| C69-X-E-103 c | | | | | | NM | | | – | | | 3700 | 3.0E-4 | 0.4582 | 0.0084 |
| C69-X-E-102 s | | | | | | NM | | | II | | | 4250 | 6.0E-4 | 1.0094 | 0.0116 |
| C69-X-E-102 e | | | | | | NM | | | – | | | 3750 | 0.0011 | 0.4936 | 0.0152 |
| C69-X-E-102 c | | | | | | NM | | | III | | | 4250 | 0.0051 | 1.0094 | 0.0289 |
| C69-X-E-101 - | | | | | | NM? | | | – | | | | | | |
| C69-X-E-100 - | | | | | | NM? | | | – | | | | | | |
| C69-X-E-099 g | | | | | | NM | | | – | | | 3200 | 7.0E-4 | 0.1839 | 0.0124 |
| C69-X-E-098 M | | | | | | NM | | | III | | | 4000 | 0.0271 | 0.7341 | 0.1 |
| C69-X-E-097 M | | | | | | NM? | | | – | | | 1900 | 0.0068 | 0.0092 | 0.0343 |
| C69-X-E-096 n | | | | | | NM | | | – | | | | | | |
| C69-X-E-095 - | | | | | | NM? | | | – | | | | | | |
| C69-X-E-094 I | | | | | | NM | | | – | | | 3750 | 9.0E-4 | 0.4936 | 0.0139 |
| C69-X-E-093 I | | | | | | NM | | | II | | | 4250 | 7.0E-4 | 1.0094 | 0.0124 |
| C69-X-E-092 M | | | | | | NM? | | | – | | | 1400 | 0.109 | 0.0049 | 0.2719 |
| C69-X-E-090 g | | | | | | NM | | | – | | | 4000 | 3.0E-4 | 0.7341 | 0.0084 |
| C69-X-E-089 - | | | | | | NM? | | | – | | | | | | |
| C69-X-E-088 s | | | | | | NM | | | – | | | 4000 | 0.0060 | 0.7341 | 0.0317 |
| C69-X-E-088 n | | | | | | NM | | | – | | | 4000 | 3.0E-4 | 0.7341 | 0.0084 |
| C69-X-E-088 c | | | | | | NM | | | – | | | | | | |
| C69-X-E-087 s | | | | | | NM? | | | – | | | | | | |
| C69-X-E-087 c | | | | | | NM? | | | I | | | 1600 | 6.0E-4 | 0.0065 | 0.0116 |
| C69-X-E-086 M | | | | | | Y? | | | III | | | 3200 | 0.0697 | 0.1839 | 0.1807 |
| C69-X-E-085 + | | | | | | NM? | | | – | | | 2100 | 2.281 | 0.012 | 1.6492 |
| C69-X-E-083 n | | | | | | NM | | | – | | | 4500 | 7.0E-4 | 1.2911 | 0.0124 |
| C69-X-E-083 c | | | | | | NM | | | I | | | 2500 | 2.0E-4 | 0.0229 | 0.0072 |

Continued on next page…

Table 3.25 – Continued

| Object | Alt ID | DM ID | SpT | INS[3] | Accret. | Membership[5] | $\log(\dot{M}_{acc})(M_\odot/yr)$[4] | Bin | Class[6] | EW(H$\alpha$)[4] | EW(Li)[4] | $T_{eff}$ | $L_{bol}$ | $Mass_{Teff}$ | $Mass_{Lbol}$ |
|---|---|---|---|---|---|---|---|---|---|---|---|---|---|---|---|
| C69-X-E-081 | e | | | | | NM? | | | – | | | | | | |
| C69-X-E-080 | - | | | | | NM? | | | I | | | | | | |
| C69-X-E-077 | g | | | | | NM | | | – | | | 4000 | 0.0412 | 0.7341 | 0.1049 |
| C69-X-E-076 | - | | | | | NM | | | – | | | 3700 | 3.0E-4 | 0.4582 | 0.0084 |
| C69-X-E-075 | I | | | | | NM | | | – | | | 4000 | 2.0E-4 | 0.7341 | 0.0072 |
| C69-X-E-074 | - | | | | | NM? | | | – | | | 1900 | 0.0013 | 0.0092 | 0.0161 |
| C69-X-E-073 | I | | | | | NM | | | III | | | 5500 | 0.0656 | 1.9992 | 0.1698 |
| C69-X-E-072 | I | | | | | Y | | | III | | | 3600 | 0.107 | 0.3906 | 0.2674 |
| C69-X-E-071 | e | | | | | NM | | | – | | | | | | |
| C69-X-E-071 | c | | | | | NM? | | | III | | | 4500 | 0.4083 | 1.2911 | 0.7044 |
| C69-X-E-070 | + | | | | | NM? | | | – | | | | | | |
| C69-X-E-069 | s | | | | | NM | | | – | | | | | | |
| C69-X-E-069 | c | | | | | NM | | | III | | | 4500 | 0.1842 | 1.2911 | 0.4079 |
| C69-X-E-068 | M | | | | | NM | | | III | | | 5750 | 0.58 | 2.0433 | 0.8932 |
| C69-X-E-067 | I | | | | | NM? | | | III | | | 5500 | 1.405 | 1.9992 | 1.4123 |
| C69-X-E-066 | I | | | | | NM? | | | I | | | 2800 | 0.0028 | 0.0488 | 0.0219 |
| C69-X-E-065 | M | | | | | NM | | | – | | | 4750 | 0.2038 | 1.5313 | 0.4365 |
| C69-X-E-064 | I | | | | | Y | | | III | | | 3750 | 0.1598 | 0.4936 | 0.3668 |
| C69-X-E-063 | I | | | | | NM | | | – | | | 3750 | 1.0E-4 | 0.4936 | 0.0053 |
| C69-X-E-062 | I | | | | | NM? | | | III | | | 5500 | 1.2955 | 1.9992 | 1.3666 |
| C69-X-E-061 | I | | | | | NM | | | – | | | 4250 | 5.0E-4 | 1.0094 | 0.0106 |
| C69-X-E-060 | n | | | | | NM | | | – | | | 6250 | 9.0E-4 | 2.1305 | 0.0139 |
| C69-X-E-060 | c | | | | | NM? | | | III | | | 4750 | 0.5334 | 1.5313 | 0.8442 |
| C69-X-E-059 | + | | | | | NM? | | | – | | | | | | |
| C69-X-E-057 | M | | | | | Y | | | III | | | 4750 | 4.1627 | 1.5313 | 1.8679 |
| C69-X-E-056 | - | | | | | NM? | | | – | | | 1900 | 1.0E-4 | 0.0092 | 0.0053 |
| C69-X-E-053 | I | | | | | NM | | | – | | | 3700 | 1.0E-4 | 0.4582 | 0.0053 |
| C69-X-E-052 | I | | | | | NM | | | – | | | 3750 | 0.0268 | 0.4936 | 0.1 |
| C69-X-E-051 | I | | | | | NM | | | II | | | 4750 | 7.0E-4 | 1.5313 | 0.0124 |
| C69-X-E-050 | I | | | | | NM? | | | – | | | | | | |
| C69-X-E-049 | I | | | | | NM | | | – | | | 4250 | 3.0E-4 | 1.0094 | 0.0084 |
| C69-X-E-048 | - | | | | | NM? | | | – | | | | | | |
| C69-X-E-047 | M | | | | | NM | | | III | | | 4500 | 0.0565 | 1.2911 | 0.1456 |
| C69-X-E-046 | g | | | | | NM | | | – | | | 3100 | 2.0E-4 | 0.1365 | 0.0072 |
| C69-X-E-045 | + | | | | | NM | | | – | | | 4000 | 1.0E-4 | 0.7341 | 0.0053 |
| C69-X-E-044 | + | | | | | NM? | | | – | | | | | | |
| C69-X-E-043 | I | | | | | NM | | | – | | | 4000 | 2.0E-4 | 0.7341 | 0.0072 |
| C69-X-E-042 | M | | | | | Y | | | – | | | 7250 | 98.8 | 2.2665 | 3.1783 |
| C69-X-E-040 | M | | | | | Y | | | III | | | 3600 | 0.1304 | 0.3906 | 0.3155 |
| C69-X-E-039 | - | | | | | NM? | | | – | | | | | | |
| C69-X-E-038 | w | | | | | NM? | | | – | | | 2100 | 2.0E-4 | 0.012 | 0.0072 |
| C69-X-E-038 | c | | | | | NM | | | II | | | 3750 | 0.0016 | 0.4936 | 0.0174 |
| C69-X-E-037 | nX | | | | | NM | | | – | | | | | | |
| C69-X-E-035 | n | | | | | NM | | | – | | | | | | |
| C69-X-E-034 | w | | | | | NM | | | – | | | 5000 | 0.0012 | 1.7371 | 0.0157 |
| C69-X-E-033 | I | | | | | NM | | | – | | | 3100 | 2.0E-4 | 0.1365 | 0.0072 |
| C69-X-E-032 | - | | | | | NM? | | | I | | | 1900 | 0.0015 | 0.0092 | 0.017 |

Continued on next page…

Table 3.25 – Continued

| Object | Alt ID | DM ID | SpT | INS[3] | Accret. | Membership[5] | log($\dot{M}_{acc}$)($M_\odot$/yr)[4] | Bin | Class[6] | EW(H$\alpha$)[4] | EW(Li)[4] | $T_{eff}$ | $L_{bol}$ | $Mass_{Teff}$ | $Mass_{Lbol}$ |
|---|---|---|---|---|---|---|---|---|---|---|---|---|---|---|---|
| C69-X-E-029 | n | | | | | NM | | | – | | | | | | |
| C69-X-E-028 | w | | | | | NM | | | – | | | | | | |
| C69-X-E-027 | n | | | | | NM | | | – | | | 3300 | 5.0E-4 | 0.2342 | 0.0106 |
| C69-X-E-026 | - | | | | | NM? | | | – | | | 1900 | 5.0E-4 | 0.0092 | 0.0106 |
| C69-X-E-023 | o | | | | | NM | | | – | | | 4000 | 0.0010 | 0.7341 | 0.0147 |
| C69-X-E-021 | w | | | | | NM | | | – | | | 4750 | 4.0E-4 | 1.5313 | 0.0096 |
| C69-X-E-021 | c | | | | | NM? | | | – | | | 1900 | 2.0E-4 | 0.0092 | 0.0072 |
| C69-X-E-020 | I | | | | | Y | | | III | | | 5000 | 4.8647 | 1.7371 | 1.9113 |
| C69-X-E-015 | I | | | | | NM | | | III | | | 4000 | 5.0E-4 | 0.7341 | 0.0106 |
| C69-X-E-013 | I | | | | | Y | | | – | | | 5500 | 82.106 | 1.9992 | 3.0417 |
| C69-X-E-012 | I | | | | | Y? | | | III | | | 3750 | 4.3396 | 0.4936 | 1.8819 |
| C69-X-E-011 | e | | | | | Y? | | | – | | | | | | |
| C69-X-E-010 | sX | | | | | NM | | | – | | | | | | |
| C69-X-E-009 | I | | | | | Y? | | | III | | | 4750 | 4.2826 | 1.5313 | 1.8774 |
| C69-X-E-007 | sX | | | | | NM | | | – | | | | | | |
| C69-X-E-005 | w | | | | | NM | | | – | | | 3750 | 2.0E-4 | 0.4936 | 0.0072 |
| C69-X-E-005 | c | | | | | NM | | | II | | | 3750 | 6.0E-4 | 0.4936 | 0.0116 |
| C69-X-E-003 | M | | | | | Y | | | III | | | 5000 | 2.3562 | 1.7371 | 1.664 |
| C69-X-E-002 | I | | | | | NM | | | I | | | 4500 | 0.0018 | 1.2911 | 0.0183 |

[1] Infrared spectral type (see Section 3.4.1).

[2] Spectral type photometrically determined by Sacco et al. (2008) (all the remainig spectral types were obtained spectroscopically in this work).

[3] Instrumental configuration as follows:
(1) LRIS R~2650
(2) LRIS R~950
(3) MIKE R~11250
(4) B&C R~2600
(5) B&C R~800
(6) TWIN R~1100
(7) CAFOS R~600
(8) FLAMES R~8600
(9) NIRSPEC R~2000
(10) SOFI R~950
(11) IRCS R~200

[4] Measurement from; [5] Membership confirmed by:
1); DM - Dolan & Mathieu (1999, 2001)
2); S08 - Sacco et al. (2008)
3); M08 - Maxted et al. (2008)
4); B09 - This work

[6] Infrared Class derived with the IRAC data in Barrado y Navascués et al. (2007b) or Chapter 2 ("–" indicates that the sources has not been detected in the four IRAC bands).

# Chapter 4

# The dark cloud Barnard 35

Barnard 35 is a dark cloud located ∼2.5$^{o}$ in the SE direction from the $\lambda$ Ori star. Duerr et al. (1982) first identified a clustering of stars centered around it and it was later confirmed from a statistical point of view by Gomez & Lada (1998). Barnard 35 is located halfway between the CO and dust ring that surrounds the whole star forming region and the star $\lambda$ Ori itself, it represents quite a different environment than that of Collinder 69. In this chapter we will study the Barnard 35 association, confirming new members and deriving their properties.

This chapter is structured in three parts: Section 4.1 summarizes the spectroscopic surveys already published in the literature for this dark cloud; Section 4.2 deals with the analysis of optical spectra of previously known members and new candidate groups proposed by Morales-Calderón (2008) (based on Spitzer observations). Finally, in Section 4.5 we provide the conclusions of this work.

## 4.1 Previous Surveys

As stated in Section 3.2, Dolan & Mathieu (1999, 2001) have previously surveyed the whole Lambda Orionis star forming region using, initially, a photometric survey based on H$\alpha$ emission with confirmation of 266 pre-main sequence stars a posteriori using the presence of Li $\lambda$6708 Å in absorption and the radial velocity distribution. Thirty out of these 266 pre-main sequence stars identified by Dolan & Mathieu (1999, 2001) fall within our Spitzer field of view within the B35 area. We consider the 30 objects as bona-fide members of Barnard 35 and will be hereafter called DM members. The faintest member has I = 15 which corresponds to ∼0.3 $M_{\odot}$ (assuming an age of 3 Myr).

Duerr et al. (1982) surveyed a region of ∼100 square degrees around the star $\lambda$ Ori identifying nearly 100 H$\alpha$ emission objects. Seven of the Duerr et al. members (3 out of them are in common with the Dolan members) fall within the field of view of our Spitzer images. We consider these 4 objects (more massive than the DM members) as bona-fide members of Barnard 35 and will be hereafter called the DIL members.

**Table 4.1**: Barnard 35 optical spectroscopic campaigns.

| Date | Observatory/Telescope/Instrument | Resolution | Wavelength coverage | Number of sources observed observed | Original photometric survey |
|---|---|---|---|---|---|
| Nov. 30 - Dec. 11, 2006 | CAHA / 2.5m /CAFOS | ~600 | 6200–10350Å | 18 | DM & Morales-Calderón (2008) |
| December 5-7, 2006 | LICK / 3m Shane / Hamilton | ~50000 | 3800–9750Å | 2 | DM |
| Nov. 30 - Dec. 11, 2007 | CAHA / 2.5m /CAFOS | ~600 | 6200–10350Å | 41 | DM & Morales-Calderón (2008) |

We present the study of the optical spectra of a sample of DM members to Barnard 35 as well as Morales-Calderón (2008) candidate members in Section 4.2.

## 4.2 Spectroscopy for the Barnard 35 sample

With the Spitzer detections in Morales-Calderón (2008) as the starting point we selected a sample of sources in the effective temperature range from 1500 – 10500 K (as determined by SED fitting, see Appendix C) to obtain optical spectra at different resolutions and study membership/youth, activity and accretion.

As in the previous chapter, the kind of analysis performed over the data depends on the characteristics of the data themselves (mainly resolution) and those of the science targets (for example, the spectral type determination of M stars and brown dwarfs was performed in a different manner than that of hotter stars) and will be explained in the forthcomming sections.

### 4.2.1 Spectral type determination

As stated before, the sample of candidate members studied for the Barnard 35 dark cloud covers a larger range in temperature (as estimated with the SED of the candidates) than the one selected for Collinder 69. The confirmed M stars and brown dwarfs of the sample were classified following the same scheme described in Section 3.3.1. For the "next step" in temperature, stars up to ~G0 spectral type, we used the templates obtained with CAFOS already mentioned also in Section 3.3.1 (see Fig. 4.1 for several examples).

On the other hand, for the sources showing bluer spectra (four sources in total), corresponding to even hotter effective temperatures, a spectral type was assigned according to the strength of their Ca II triplet and H$\alpha$ over Fe I $\lambda$6495 Å ratio; and the luminosity class was inferred from the O I $\lambda$ 7776 Å absorption (when measureable) following Danks & Dennefeld (1994). Figure 4.2 shows the relation between the equivalent width of the third component of the Ca II infrared triplet and the spectral type. The same figure highlights the goodness of the equivalent width of the mentioned O I line as a diagnosis of the luminosity class. We are aware that this methodology could present some problems with active or accreting stars, but none of the sources present any emission line and the H$\alpha$ line is clearly in absorption with no visible structure.

As can be inferred from the figure, the Ca II triplet is present in dwarfs but never reaches the strength exhibited in the supergiants. Regarding the behaviour with temperature; in dwarfs,

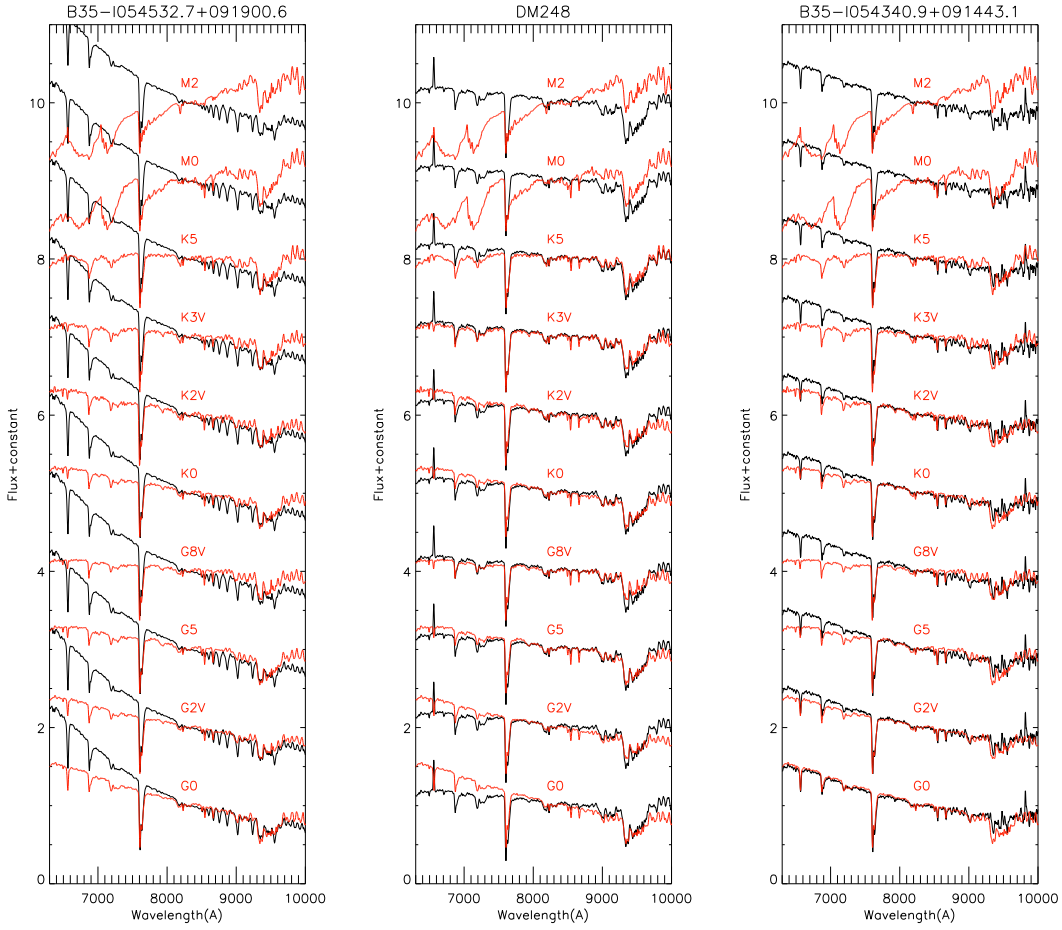


**Figure 4.1**: Spectral type determination for three candidate members by comparison with templates obtained with the same instrumental set-up. The "science spectra" are displayed in black and the templates (labelled according to the spectral type) in red. The first pannel (from left to right) shows a source with an effective temperature too high for our spectral templates; to determine its spectral type we used the Ca II triplet and the H$\alpha$ over Fe I (6495 Å) ratio explained in this section.

it starts to be evident at A2, growing in strength up to M0. Regarding supergiants; the triplet is evident at A0, peaking in strength at K3 and remaining quite evident at M2.

In Figure 4.3 we display a spectral sequence obtained applying the criteria explained previously in this section and in Section 3.3.1 to the data obtained in the CAFOS campaign of November 2006. In Table 4.3 we show the estimated spectral types for all the Barnard 35 candidate members observed by us using CAFOS.

### 4.2.2 Rotational velocities estimation.

As in the previous chapter, we have studied the projected rotational velocity of the sources observed with sufficient resolution to perform this kind of analysis.

In this case, only two sources were observed at high resolution. We followed similar steps as in Section 3.3.2 and we determined that DM248 has a projected rotational velocity of ~40 km/s. The case of DM248 has to be analyzed more carfully. This source, as it will be discussed in the forthcoming Sections, shows a very strong variability in its H$\alpha$ emission. The three values of EW(H$\alpha$) measured by us (this source has been observed in the three campaigns) as well as the value provided in Dolan & Mathieu (2001) place DM244 well above the saturation criteria of Barrado y Navascués & Martín (2003). Although our high resolution spectra was taken at an apparent minimum of accretion rate (see next Sections for more details), we have tried to estimate the amount of veiling that might be affecting our measurement of the Ca I doublet, and therefore our estimation of the rotational velocity.

In figures 4.4 and 4.5 we show the blue excess detected (when comparing with a source of similar spectral type) in DM244 in 2006 and 2007 on the spectra taken with CAFOS. If we define $r_\lambda$ as the ratio of excess emission over phosopheric emission and we extrapolate the tendency observed in figure 4.5 (where the CAFOS measured H$\alpha$ emission was similar to the high resolution one) we estimate a value of $r_\lambda$~0.45. We used this value to correct the measured EW on the Ca I doublet in order to compare this value with the one of the synthesized spectra. The correction was performed according to:

$$r_\lambda = \frac{W_{int}}{W_{veiled}} - 1 \tag{4.1}$$

The comparison of the theoretical spectra with our corrected measurments provided us with an estimation of the rotational velocity of DM244 of ~30 Km/s.

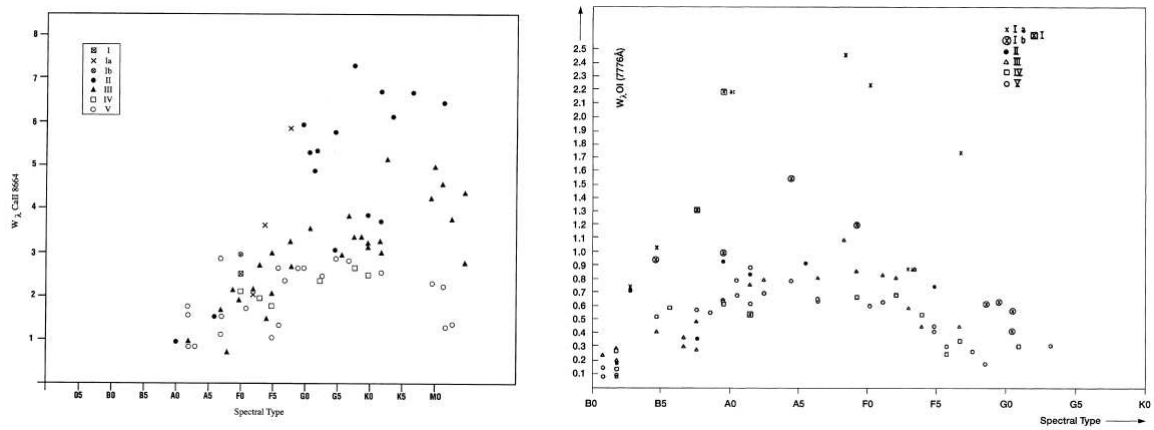


**Figure 4.2**: Absorption lines used for the spectral classification of the hottest sources of our sample. **Left-pannel:** Equivalent width in Å of the Ca II $\lambda$8662 Å component of the IRT versus spectral type (from Danks & Dennefeld 1994). **Right-pannel:** Equivalent width in Å of the O I $\lambda$7776 Å line versus spectral type (from Danks & Dennefeld 1994).

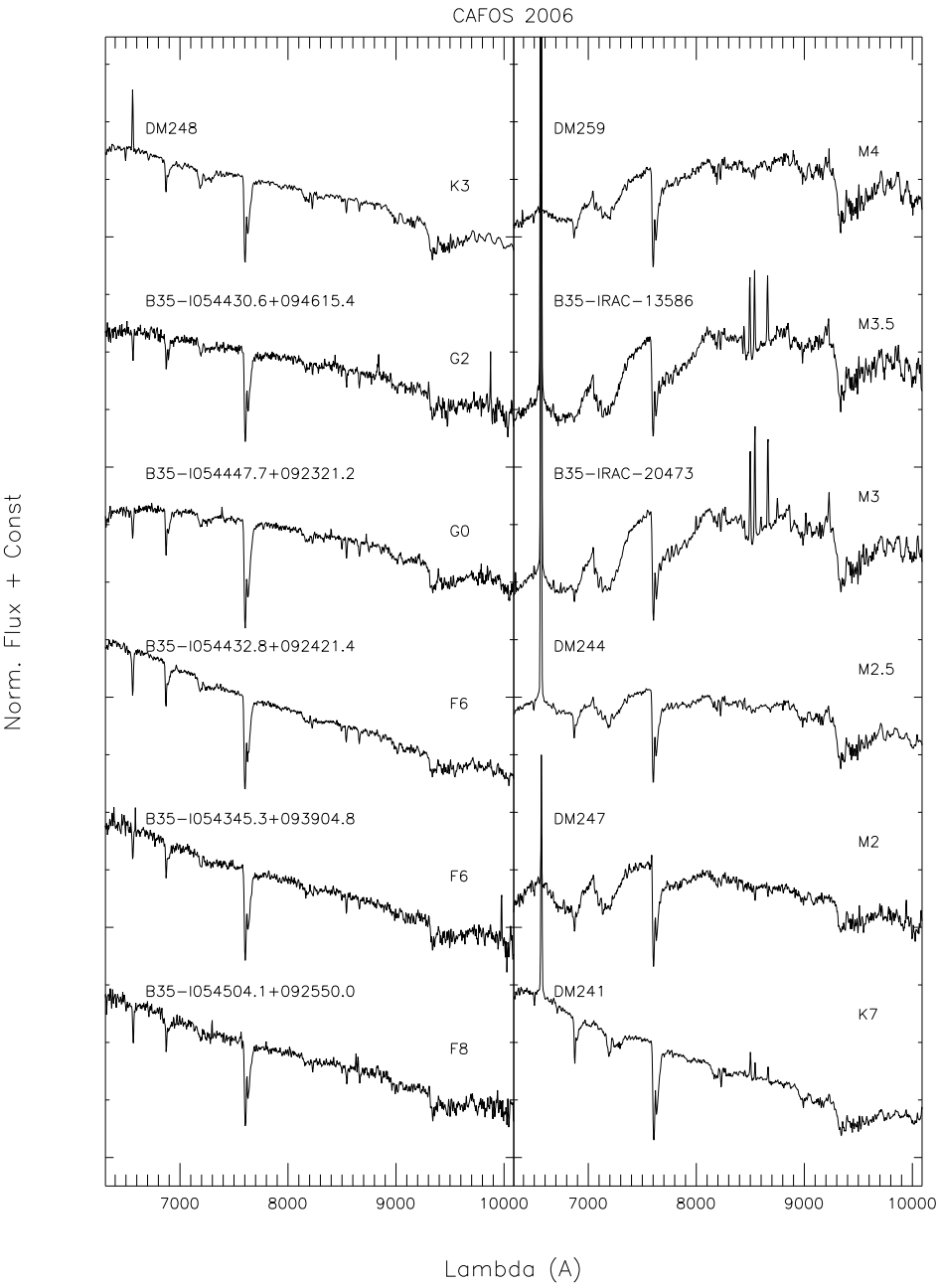


**Figure 4.3**: Spectral sequence of Barnard 35 candidate members. From the 2006 campaign with CAFOS.

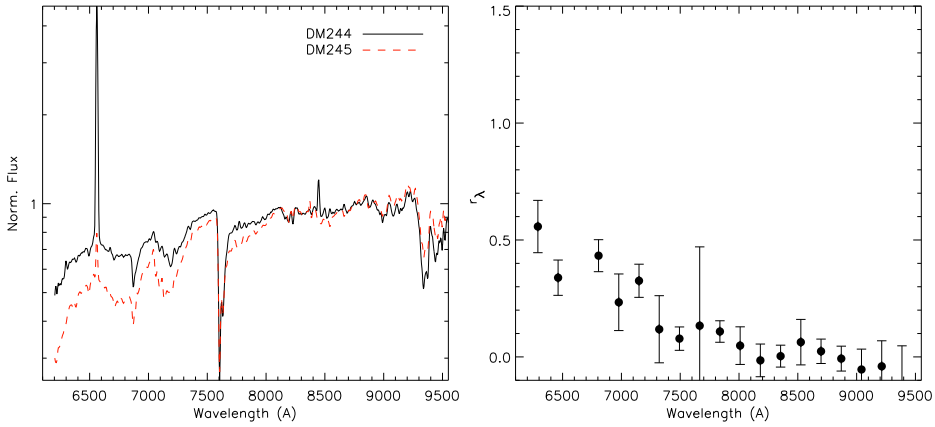


**Figure 4.4**: Comparison between the spectra obtained in 2007 of DM244 (at the strongest measured H$\alpha$ emission) and the one of DM245 (with similar spectral type and classified as non-accreting source).

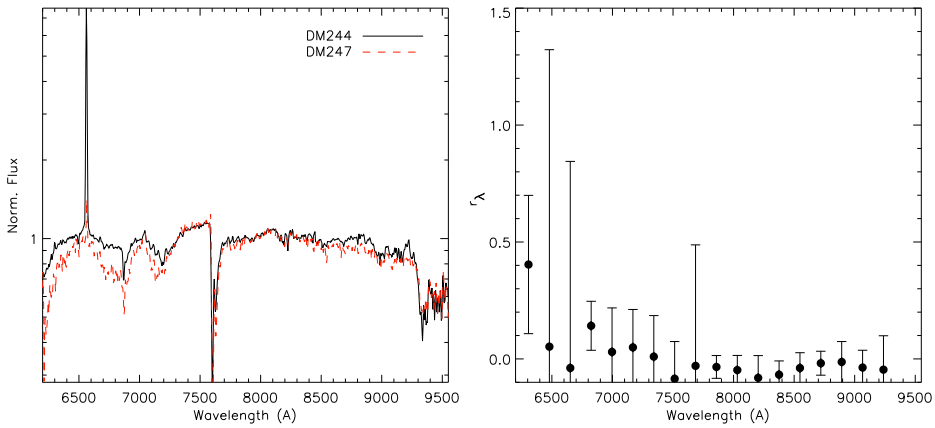


**Figure 4.5**: Comparison between the spectra obtained in 2006 of DM244 (when a much lower H$\alpha$ emission was detected with respec to the previous figure) and the one of DM247 (with similar spectral type and classified as non-accreting source).

**Table 4.2**: Equivalent width of the main lines observed in the spectra obtained with CAFOS in both campaigns. The symbol "–" indicates that the line is not detectable.

| Object | H$\alpha$ 6563 EW(Å) | $FW_{10\%}$(km/s) | FWHM(km/s) | HeI 6678 EW(Å) | OI 7776 EW(Å) | NaI 8200 EW(Å) | CaII 8498 EW(Å) | 8542 EW(Å) | 8662 EW(Å) | Campaign |
|---|---|---|---|---|---|---|---|---|---|---|
| B35-I054532.7+091900.6 | 7.271 ± 0.463 | 1428.461 ± 125.337 | 709.925 ± 20.478 | – | 0.169±0.051 | 0.294±0.166 | – | – | – | 2007 |
| B35-I054504.1+092550.0 | 3.331 ± 0.246 | ≤ 200.0 | ≤ 110.0 | -0.151±0.073 | – | 0.301±0.174 | 0.530±0.037 | 2.440±0.277 | 1.437±0.796 | 2006 |
| DM248 | -4.288 ± 0.259 | ≤ 200.0 | ≤ 110.0 | -0.292±0.183 | – | 1.446±0.555 | 0.424±0.023 | 1.854±0.052 | 1.799±0.316 | 2006 |
| DM248 | -5.945 ± 0.171 | ≤ 200.0 | ≤ 110.0 | -0.789±0.306 | – | 1.028±0.369 | – | – | – | 2007 |
| B35-I054345.3+093904.8 | 3.491 ± 1.576 | 237.3130 ± 85.118 | 130.177 ± 16.983 | – | – | 0.906±0.451 | 0.971±0.219 | 2.152±0.173 | 1.828±0.341 | 2006 |
| B35-I054430.6+094615.4 | 2.399 ± 0.127 | ≤ 200.0 | ≤ 110.0 | – | – | 1.489±0.859 | 0.859±0.252 | 2.084±0.301 | 2.425±0.419 | 2006 |
| B35-I054430.6+094615.1 | 3.177 ± 0.286 | ≤ 200.0 | ≤ 110.0 | -0.103±0.043 | 0.463±0.046 | 0.404±0.138 | 0.889±0.161 | 2.217±0.129 | 1.891±0.469 | 2007 |
| B35-I054340.9+091443.1 | 3.813 ± 0.254 | 812.2777 ± 107.801 | 297.547 ± 12.814 | -0.036±0.013 | 0.434±0.043 | 0.264±0.093 | – | – | – | 2007 |
| B35-I054432.8+092421.4 | 4.284 ± 0.105 | 336.2998 ± 40.118 | 184.476 ± 9.453 | – | 0.282±0.077 | 0.862±0.287 | 0.742±0.147 | 2.261±0.075 | 2.579±0.376 | 2006 |
| B35-I054439.1+091807.8 | 4.372 ± 0.252 | 720.3364 ± 80.118 | 395.137 ± 15.222 | – | 0.060±0.023 | 0.918±0.251 | 1.625±0.917 | 3.281±0.597 | 2.729±0.306 | 2007 |
| B35-I054449.0+091306.9 | 3.841 ± 0.237 | 735.0700 ± 91.532 | 403.219 ± 13.645 | -0.214±0.070 | 0.186±0.025 | 0.662±0.298 | 1.138±0.162 | 2.536±0.293 | 3.179±0.316 | 2007 |
| B35-I054447.7+092321.2 | 3.114 ± 0.215 | ≤ 200.0 | ≤ 110.0 | – | 0.723±0.086 | 0.759±0.380 | 1.107±0.042 | 2.321±0.381 | 2.921±0.411 | 2006 |
| B35-I054502.6+090350.0 | 1.767 ± 0.036 | ≤ 200.0 | ≤ 110.0 | – | – | 1.500±0.670 | 1.117±0.099 | 2.931±0.085 | 3.357±0.447 | 2007 |
| DM241 | -17.886 ± 0.251 | ≤ 200.0 | ≤ 110.0 | -1.431±0.501 | – | 1.596±0.760 | -3.391±0.374 | -1.767±0.073 | -1.909±0.034 | 2006 |
| DM241 | -25.963 ± 1.201 | ≤ 200.0 | ≤ 110.0 | -1.298±0.406 | – | 0.938±0.317 | -3.658±0.189 | -2.496±0.092 | -2.630±0.062 | 2007 |
| B35-I054515.8+094741.0 | 1.668 ± 0.242 | ≤ 200.0 | ≤ 110.0 | – | – | 1.341±0.716 | 1.982±0.707 | 3.228±1.170 | 2.623±1.173 | 2006 |
| B35-IRAC-14252 | -93.662 ± 13.366 | 246.3576 ± 40.145 | 135.138 ± 12.453 | -0.546±0.427 | 0.456±0.218 | 0.252±0.083 | -0.683±0.184 | -2.237±0.617 | -0.943±0.469 | 2007 |
| DM247 | -4.473 ± 0.205 | ≤ 200.0 | ≤ 110.0 | -0.982±0.038 | 0.399±0.115 | 1.606±0.827 | – | – | – | 2006 |
| DM247 | -2.995 ± 0.314 | ≤ 200.0 | ≤ 110.0 | – | – | 2.349±0.737 | 0.200±0.037 | 2.045±0.326 | 0.689±0.192 | 2007 |
| B35-IRAC-45299 | -16.987 ± 1.279 | 897.7811 ± 40.361 | 492.474 ± 7.144 | – | – | 1.143±0.348 | – | – | – | 2007 |
| B35-IRAC-20434 | -66.169 ± 2.223 | ≤ 200.0 | ≤ 110.0 | – | – | 2.184±0.765 | – | – | – | 2007 |
| B35-IRAC-20434 | -46.755 ± 1.917 | ≤ 200.0 | ≤ 110.0 | – | 2.154±1.212 | 2.214±0.879 | – | – | – | 2006 |
| DM234 | -5.170 ± 0.199 | 560.9170 ± 70.354 | 307.689 ± 15.234 | -0.699±0.412 | – | 0.787±0.320 | 0.424±0.087 | 1.632±0.226 | 1.464±0.202 | 2007 |
| DM240 | -115.809 ± 9.768 | ≤ 200.0 | ≤ 110.0 | -1.566±0.501 | – | 1.357±0.496 | 0.253±0.175 | 1.157±0.311 | 0.465±0.064 | 2007 |
| DM244 | -68.563 ± 0.603 | ≤ 200.0 | ≤ 110.0 | -1.136±0.605 | 0.538±0.352 | 1.809±0.659 | 0.247±0.000 | 0.478±0.013 | 0.081±0.028 | 2006 |
| DM244 | -90.313 ± 5.524 | 47.96292 ± 15.785 | 26.3098 ± 9.847 | -1.382±0.458 | – | 1.192±0.454 | -1.022±0.346 | -0.910±0.144 | -1.060±0.170 | 2007 |
| DM249 | -2.882 ± 0.091 | ≤ 200.0 | ≤ 110.0 | -0.074±0.030 | – | 1.665±0.769 | 0.288±0.050 | 1.985±0.203 | 1.685±0.289 | 2006 |
| DM249 | -3.081 ± 0.186 | ≤ 200.0 | ≤ 110.0 | – | – | 1.351±0.437 | – | – | – | 2007 |
| DM258 | 0.695 ± 0.066 | ≤ 200.0 | ≤ 110.0 | -0.731±0.255 | – | 1.203±0.444 | 0.483±0.034 | 2.184±0.150 | 1.975±0.166 | 2007 |
| B35-I054436.7+091321.6 | 2.207 ± 0.343 | ≤ 200.0 | ≤ 110.0 | -0.420±0.115 | – | – | 0.907±0.025 | 2.078±0.297 | 2.614±0.692 | 2007 |
| B35-I054444.0+091014.5 | 4.051 ± 0.108 | 548.3428 ± 67.734 | 300.791 ± 16.982 | – | 0.353±0.176 | 0.578±0.302 | 1.087±0.171 | 2.388±0.037 | 4.612±1.435 | 2007 |
| B35-IRAC-20473 | -144.823 ± 3.997 | ≤ 200.0 | ≤ 110.0 | -2.357±0.515 | – | 1.749±0.771 | -10.496±1.445 | -12.869±1.160 | -9.571±0.169 | 2006 |
| B35-IRAC-23145 | -16.306 ± 0.962 | 631.7487 ± 40.256 | 346.543 ± 3.826 | – | – | 1.218±0.476 | – | – | – | 2007 |
| B35-IRAC-23414 | 1.538 ± 0.277 | 979.9151 ± 60.741 | 537.528 ± 49.315 | – | – | – | 3.232±0.594 | 3.247±0.124 | 3.468±0.184 | 2007 |
| B35-IRAC-46311 | -12.199 ± 1.018 | ≤ 200.0 | ≤ 110.0 | – | 1.743±1.020 | 2.210±0.845 | 0.792±1.041 | 1.057±0.285 | 0.264±0.281 | 2007 |
| DM231 | -30.560 ± 0.852 | ≤ 200.0 | ≤ 110.0 | -2.007±0.660 | 1.013±0.258 | 1.530±0.463 | 0.824±0.430 | 0.873±0.208 | 0.592±0.203 | 2007 |
| DM255 | -20.252 ± 0.238 | ≤ 200.0 | ≤ 110.0 | -0.971±0.200 | – | 1.993±1.069 | 1.298±0.716 | 0.783±0.373 | 0.315±0.065 | 2006 |
| DM255 | -20.717 ± 0.680 | ≤ 200.0 | ≤ 110.0 | – | 0.626±0.315 | 1.647±0.514 | – | – | – | 2007 |
| DM252 | -50.226 ± 2.744 | ≤ 200.0 | ≤ 110.0 | – | – | 1.041±0.406 | -2.121±0.072 | -2.373±0.595 | -0.291±0.130 | 2007 |
| DM252 | -43.006 ± 1.366 | ≤ 200.0 | ≤ 110.0 | – | – | 1.362±0.640 | -3.181±0.676 | -1.864±0.467 | -0.997±0.159 | 2006 |
| DM256 | -29.114 ± 0.839 | ≤ 200.0 | ≤ 110.0 | -1.132±0.981 | – | – | – | – | – | 2007 |
| B35-I054357.0+091631.7 | -166.291 ± 2.928 | ≤ 200.0 | ≤ 110.0 | -3.610±1.224 | – | 1.313±0.674 | -5.762±0.420 | -6.706±1.356 | -5.388±0.587 | 2006 |
| B35-I054428.7+091109.9 | 2.013 ± 0.117 | 970.1769 ± 58.109 | 532.187 ± 16.644 | -0.077±0.019 | – | – | 2.854±0.461 | 3.291±0.253 | 2.691±0.391 | 2007 |

Continued on next page…

Table 4.2 – Continued

| Object | H$\alpha$ | | | HeI | OI | NaI | CaII | | | Campaign |
|---|---|---|---|---|---|---|---|---|---|---|
| | 6563 | | | 6678 | 7776 | 8200 | 8498 | 8542 | 8662 | |
| | EW(Å) | $FW_{10\%}$(km/s) | FWHM(km/s) | EW(Å) | EW(Å) | EW(Å) | EW(Å) | EW(Å) | EW(Å) | |
| B35-I054516.9+090718.3 | 1.681 ± 0.259 | ≤ 200.0 | ≤ 110.0 | – | – | – | 1.202±0.128 | 3.321±0.208 | 3.486±0.496 | 2007 |
| B35-IRAC-13586 | -187.987 ± 2.243 | ≤ 200.0 | ≤ 110.0 | -2.666±0.803 | 2.445±0.921 | 2.540±0.969 | -7.568±0.953 | -7.557±0.949 | -6.615±0.308 | 2006 |
| B35-IRAC-13586 | -216.341 ± 37.843 | 128.4579 ± 35.356 | 70.4651 ± 20.345 | -2.771±0.232 | – | 1.474±0.465 | -11.458±2.236 | -12.660±0.868 | -10.762±0.241 | 2007 |
| DM245 | -6.869 ± 0.398 | ≤ 200.0 | ≤ 110.0 | – | 0.658±0.421 | 1.282±0.468 | – | – | – | 2007 |
| DM259 | -5.130 ± 0.190 | ≤ 200.0 | ≤ 110.0 | -0.277±0.128 | 0.252±0.077 | 1.149±0.332 | 1.274±0.870 | 1.708±0.394 | 1.069±0.105 | 2007 |
| DM259 | -4.465 ± 0.135 | ≤ 200.0 | ≤ 110.0 | – | 0.414±0.202 | 2.320±0.767 | 1.148±0.135 | 1.048±0.251 | 1.184±0.446 | 2006 |
| DM246 | -11.349 ± 0.324 | 238.0892 ± 64.983 | 130.602 ± 13.847 | -1.304±0.604 | 1.022±0.726 | 1.084±0.395 | – | – | – | 2007 |
| B35-IRAC-12156 | -2.135 ± 0.242 | 670.8591 ± 40.36 | 367.997 ± 6.488 | -0.640±0.560 | – | 0.932±0.334 | 0.314±0.044 | 1.570±0.041 | 1.334±0.231 | 2007 |
| B35-IRAC-14785 | -67.526 ± 3.047 | ≤ 200.0 | ≤ 110.0 | -1.396±0.349 | 1.227±0.200 | 0.884±0.369 | -27.541±4.698 | -28.994±4.396 | -27.364±0.471 | 2007 |
| B35-IRAC-17517 | -31.732 ± 1.201 | ≤ 200.0 | ≤ 110.0 | -1.392±0.466 | – | 1.290±0.504 | -1.661±0.313 | -1.350±0.523 | -0.689±0.205 | 2007 |
| DM238 | -21.918 ± 1.110 | ≤ 200.0 | ≤ 110.0 | – | – | 1.671±0.460 | – | – | – | 2007 |
| DM243 | -45.429 ± 1.337 | ≤ 200.0 | ≤ 110.0 | – | – | 1.793±0.667 | – | – | – | 2007 |
| B35-IRAC-11994 | -82.168 ± 6.860 | ≤ 200.0 | ≤ 110.0 | – | 2.828±1.005 | 1.649±0.619 | – | – | – | 2007 |
| B35-IRAC-20473 | -141.203 ± 9.209 | ≤ 200.0 | ≤ 110.0 | – | – | 1.249±0.486 | -7.001±0.695 | -7.836±1.724 | -6.739±0.448 | 2007 |
| B35-IRAC-17409 | -68.470 ± 1.865 | ≤ 200.0 | ≤ 110.0 | – | – | 0.130±0.057 | – | – | – | 2007 |
| B35-IRAC-16286 | -17.395 ± 0.622 | 650.5694 ± 90.444 | 356.867 ± 1.822 | -5.960±0.521 | 0.549±0.289 | 1.380±0.346 | – | – | – | 2007 |

**Table 4.3**: Parameters derived for the CAFOS sample.

| Object | SpT | EW(H$\alpha$)crit[1] | LC[2] | Alkali Mem[3] | log($\dot{M}_{acc}$) | Campaign | Object | SpT | EW(H$\alpha$)crit[1] | LC[2] | Alkali Mem[3] | log($\dot{M}_{acc}$) | Campaign |
|---|---|---|---|---|---|---|---|---|---|---|---|---|---|
| B35-I054532.7+091900.6 | B9 | N | V | – | | 2007 | B35-I054444.0+091014.5 | M3 | N | – | NM | | 2007 |
| B35-I054504.1+092550.0 | F8 | N | – | – | | 2006 | B35-IRAC-20473 | M3 | Y | – | Mem | ≤-10.95 | 2006 |
| DM248 | K3 | Y | IV-V | – | ≤ -10.95 | 2006 | B35-IRAC-23145 | M3 | Y | – | Mem | -6.762±0.390 | 2007 |
| DM248 | K4 | Y | IV-V | – | ≤ -10.95 | 2007 | B35-IRAC-23414 | M3 | N | – | NM | | 2007 |
| B35-I054345.3+093904.8 | F6 | N | – | – | | 2006 | B35-IRAC-46311 | M3 | N | – | Mem | | 2007 |
| B35-I054430.6+094615.4 | G2 | N | III | – | | 2006 | DM231 | M3 | Y | – | Mem | ≤-10.95 | 2007 |
| B35-I054430.6+094615.1 | G5 | N | I | – | | 2007 | DM255 | M3 | Y | – | Mem | ≤-10.95 | 2006 |
| B35-I054340.9+091443.1 | G0 | N | I | – | | 2007 | DM255 | M3.5 | Y | – | Mem | ≤-10.95 | 2007 |
| B35-I054432.8+092421.4 | F6 | N | IV | – | | 2006 | DM252 | M3.25 | Y | – | Mem | ≤ -10.95 | 2007 |
| B35-I054439.1+091807.8 | K5 | N | – | – | | 2007 | DM252 | M3.5 | Y | – | Mem | ≤ -10.95 | 2006 |
| B35-I054449.0+091306.9 | K0 | N | – | NM | | 2007 | DM256 | M3.25 | Y | – | Mem | ≤ -10.95 | 2007 |
| B35-I054447.7+092321.2 | G0 | N | – | NM | | 2006 | B35-I054357.0+091631.7 | M3.5 | Y | – | Mem | ≤ -10.95 | 2006 |
| B35-I054502.6+090350.0 | K3 | N | – | Mem | | 2007 | B35-I054428.7+091109.9 | M3.5 | N | – | NM | | 2007 |
| DM241 | K7 | Y | – | Mem | ≤ -10.95 | 2006 | B35-I054516.9+090718.3 | M3.5 | N | – | NM | | 2007 |
| DM241 | K8 | Y | – | Mem | ≤ -10.95 | 2007 | B35-IRAC-13586 | M3.5 | Y | – | Mem | ≤ -10.95 | 2006 |
| B35-I054515.8+094741.0 | M1.5 | N | – | Mem | | 2006 | B35-IRAC-13586 | M4 | Y | – | Mem | -11.643±0.342 | 2007 |
| B35-IRAC-14252 | M2 | Y | – | Mem | -10.500±0.389 | 2007 | DM245 | M3.5 | N | – | Mem | | 2007 |
| DM247 | M2 | N | – | Mem | | 2006 | DM259 | M3.5 | N | – | Mem | | 2007 |
| DM247 | M3 | N | – | Mem | | 2007 | DM259 | M4 | N | – | Mem | | 2006 |
| B35-IRAC-45299 | M2.25 | Y | – | Mem | -4.182±0.392 | 2007 | DM246 | M3.75 | N | – | Mem | | 2007 |
| B35-IRAC-20434 | M2.5 | Y | – | Mem | ≤ -10.95 | 2007 | B35-IRAC-12156 | M4 | N | – | NM | | 2007 |
| B35-IRAC-20434 | M3.0 | Y | – | Mem | ≤ -10.95 | 2006 | B35-IRAC-14785 | M4 | Y | – | Mem | ≤ -10.95 | 2007 |
| DM234 | M2.5 | N | – | Mem | | 2007 | B35-IRAC-17517 | M4 | Y | – | Mem | ≤ -10.95 | 2007 |
| DM240 | M2.5 | Y | – | Mem | ≤ -10.95 | 2007 | DM238 | M4 | Y | – | Mem | ≤ -10.95 | 2007 |
| DM244 | M2.5 | Y | – | Mem | ≤ -10.95 | 2006 | DM243 | M4 | Y | – | Mem | ≤ -10.95 | 2007 |
| DM244 | M3 | Y | – | Mem | -12.425±0.153 | 2007 | B35-IRAC-11994 | M4.5 | Y | – | Mem | ≤ -10.95 | 2007 |
| DM249 | M2.5 | N | – | Mem | | 2006 | B35-IRAC-20473 | M4.5 | Y | – | Mem | ≤ -10.95 | 2007 |
| DM249 | M3 | N | – | Mem | | 2007 | B35-IRAC-17409 | M5.5 | Y | – | Mem | ≤ -10.95 | 2007 |
| DM258 | M2.5 | N | – | Mem | | 2007 | B35-IRAC-16286 | M6 | N | – | Mem | | 2007 |
| B35-I054436.7+091321.6 | M3 | N | – | NM | | 2007 | | | | | | | |

[1] Accretion criterion by Barrado y Navascués & Martín (2003).
[2] Luminosity Class based on the O I line.
[3] Membership based on the measured Na I doublet equivalent widths.

### 4.2.3 H$\alpha$ and other emission lines: accretion, activity and outflows

As in the previous Chapter, we have used our measured H$\alpha$ equivalent widths and those given in Dolan & Mathieu (1999, 2001) along with the derived spectral types as a diagnosis for accretion. In figure 4.6, a $T_{eff}$ versus EW(H$\alpha$) diagram is shown. Unlike the case of Collinder 69 where the extinction is quite homogeneous, plenty of dust structure is present in Barnard 35. We have derived an extinction map based on an adaptive star count method; similar to that of Cambresy et al. (1997) for the Chamaleon I dark cloud but adapted to the 2MASS J band and the Barnard 35 galactic latitude. The $A_V$ derived values are shown in Table 4.4 and have been used to deredden the SED of the candidate members prior to the perform the fit. In the figure, we display the derived spectral types transformed into temperatures (according to the temperature scale derived in the previous chapter) for those sources observed by us and the effective temperature derived from the SED fit for the confirmed members by Dolan & Mathieu not observed by us.

There are several sources, namely DM238, DM240, DM243, B35-IRAC-23145 and B35-I054357.0+091631.7 that show very large values of the equivalent width of H$\alpha$ but were classified as Class III according to the IRAC colour-colour diagram (Morales-Calderón 2008). On the other hand, all the sources show large excess at 24 $\mu$m and are therefore classified as transition disks (disks with inner holes). Our H$\alpha$ measurements in two cases are slightly larger but compatible with those from Dolan & Mathieu (2001). Thus these sources might harbour transition actively accreting disks. All the accretion rates measured for these sources but one are upper limits (see Fig. 4.7); the source showing a much larger rate has a value $\log \dot{M}_{acc} \sim -6.8$, compatible with other sources showing transitions disks such as LkH$\alpha$329 ($\log \dot{M}_{acc} \sim -6.1$, Merin et al. 2009, private communication).

On the other hand, the source observed by us showing the largest infrared excess, the Class I source B35-IRAC-14252, is also part of the sample of sources with strongest H$\alpha$ emission (and highest estimated accretion rates).

In this $T_{eff}$ vs. EW(H$\alpha$) diagram we have highlighted the Class II population overplotting large black circumferences around them. Appart from the five sources classified as transition disks, there are other two sources (DM239 and DM250) for which the EWs provided in Dolan & Mathieu (1999, 2001) locate them among the accretors but for which no infrared excess has been detected at all on our IRAC data. We believe that the spectra obtained by Dolan & Mathieu must have been taking during a flare in both cases.

In general terms, when comparing this diagram with its analog in Collinder 69 (Fig. 3.13) a clear difference shows up; whilst there is a significant fraction of Class II sources that were not classified as active accretors in Collinder 69; every Barnard 35 Class II source observed by our team shows H$\alpha$ equivalent widths too high to only have a chromospheric activity origin. Therefore Barnard 35 seems to be significantly younger than Collinder 69 (as has already been suggested in the literature).

In order to study the variability of the accretion rate in young stellar objects, we observed

ten of the sources during both campaigns (i.e., with a difference of one year). Eight of these sources were Dolan & Mathieu candidates and the remaining two are candidate members proposed by Morales-Calderón (2008). In most of the cases we only obtained upper limits for the accretion rates, but the dramatic changes in the measured H$\alpha$ equivalent widths (see for example DM244) suggest that low mass stars show variable accretion periods as higher mass stars do (see, in Fig. 4.7 the solid black dots with vertical bars from Mendigutia et al 2009, private communication).

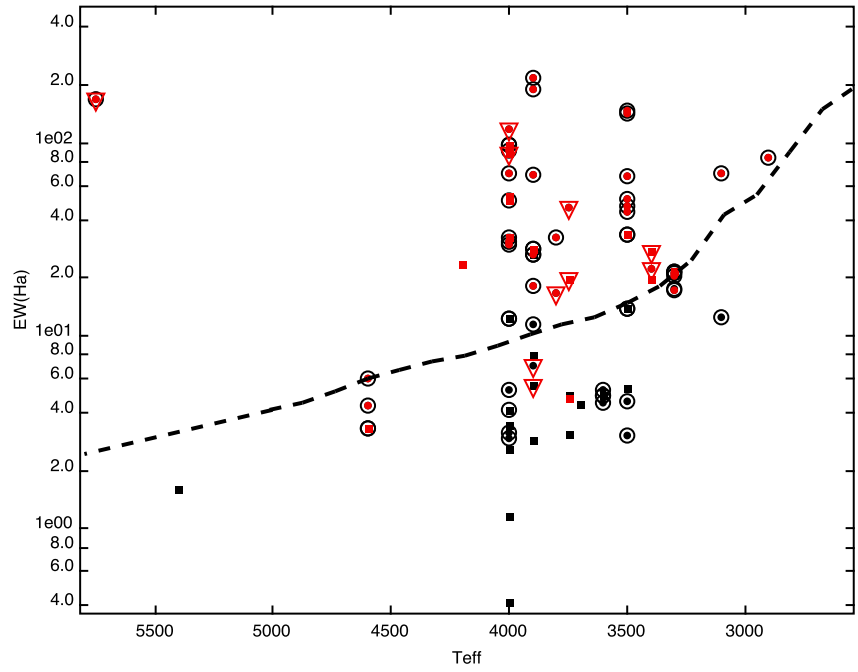


**Figure 4.6**: H$\alpha$ equivalent width versus the effective temperature for confirmed members of Barnard 35. We display data from Dolan & Mathieu (1999, 2001), with filled squares (red ones for those fulfilling the saturation criteria). Our data are displayed with solid dots; red for those above the saturation criteria. Overlapping large circles denote objects with near infrared excess from Spitzer/IRAC data (and open red triangles transition disks). The dotted lines correspondsto the saturation criteria defined by Barrado y Navascués & Martín (2003)

As in the previous chapter we have also tried to relate the H$\alpha$ emission with the properties of the disks. In Fig. 4.8 we show an IRAC colour-colour diagram for the members of Barnard 35 (spectroscopically confirmed members, and highly reliable photometric candidates). We have included information regarding the presence of transition disks (large red triangles) and the intensity of the emission of H$\alpha$ (blue open squares with sizes proportional to the equivalent width measured). Although the sources showing the largest H$\alpha$ emission seem to be located to the upper-right part of the diagram (as expected according to the theoretical disk models used to interpret the

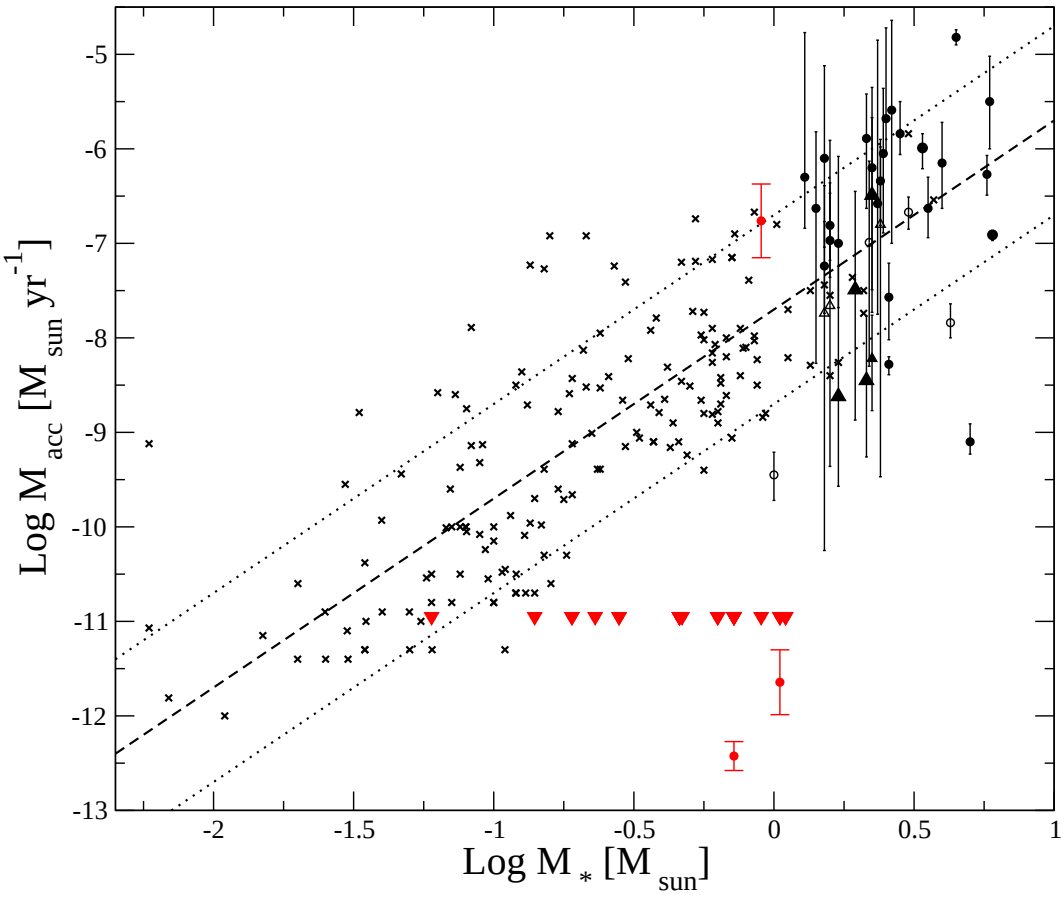


**Figure 4.7**: Mass accretion rates for a wide range of stellar masses. Red filled dots from this work. Crosses are from Calvet et al. (2004); Muzerolle et al. (2005); Mohanty et al. (2005) and Natta et al. (2006). Filled and open black symbols from Mendigutia et al 2009 (private communication), corresponding to the objects with EW(H$\alpha$) > 10 Å and < 10 Å, respectively. Triangles represent lower limits. The vertical bars over these symbols represent variability measured in time scales of hours – months (not uncertainty in the measurements as is the case for the vertical bars over the points calculated in this work). The dashed line follows $\dot{M}_{acc} \propto M_*^2$, and the dotted lines ± 1 dex.

IRAC colour-colour diagram by Allen et al. 2004), we must note that two of the transition disks (located much closer to the Class III population) show very intense H$\alpha$ emissions.

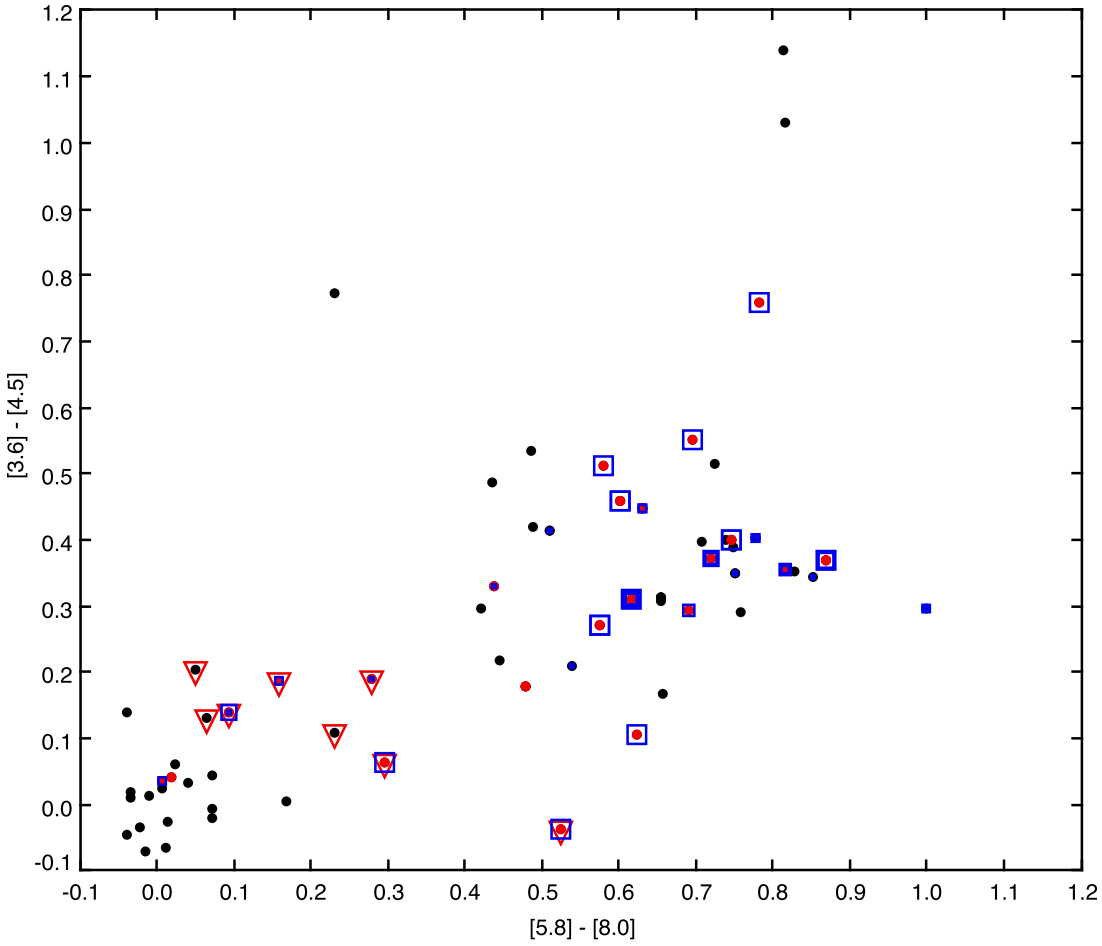


**Figure 4.8**: IRAC color-color diagram including information about the nature of the disk and the H$\alpha$ emission of the sources. Sources showing a transition disk have been surrounded by a red triangle. A blue square with a size proportional to the intensity of the H$\alpha$ emission of the sources is also shown in the figure.

### 4.2.4 Youth indicators using Alkali: Li $\lambda$6708 Å and NaI $\lambda$8200 Å

In order to estimate the youth of our candidates we have followed different approaches according to the resolution of the data or the nature of the source (its spectral type).

For the two sources observed with high resolution, DM244 and DM248, we have de-

tected Li I absorption which confirms their youth and therefore membership to the dark cloud (see Fig. 4.9). We measure values for these two objects of 0.491±0.091 and 0.436±0.067 Å respectively. These values are in good agreement with those measured by Dolan & Mathieu (2001) (0.44 and 0.41 Å respectively). DM244, nevertheless, as stated before, is classified as an accreting source and the effect of the veiling should be taken into account. Once this correction is performed, the actual Lithium I equivalent width for DM244 is 0.540 Å.

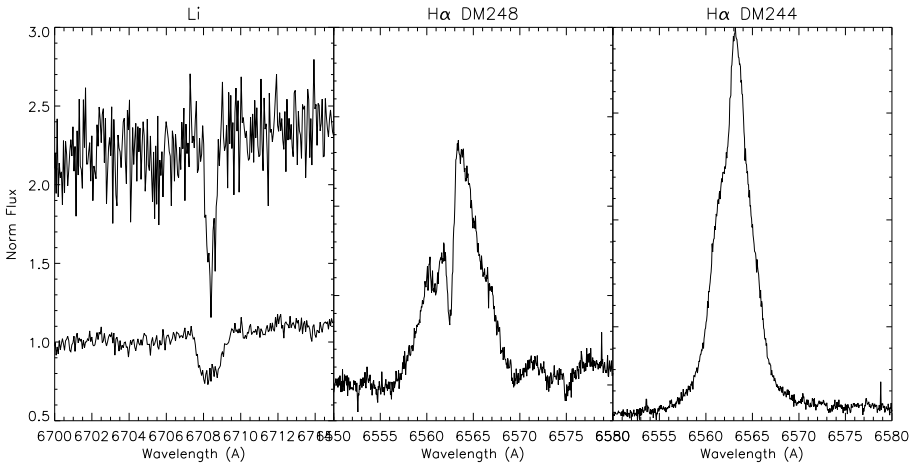


**Figure 4.9**: Detail on the Li I absorption line and H$\alpha$ emission for DM248 and DM244, the two sources observed in high resolution at LICK. Note the double peaked H$\alpha$ emission detected on DM248 and the asymmetric profile of the same emission line on DM244.

In Fig. 4.10 we show the lithium equivalent width measured by Dolan & Mathieu (2001) versus the effective temperatures derived in this work for the confirmed members of Barnard 35. We also show the theoretical equivalent widths from Zapatero Osorio et al. (2002) considering $\log g = 4.0$ and $\log g = 4.5$ and an initial cosmic abundance (A(Li) = 3.1). Note that a significant fraction of our sources lie on top of the theoretical curves, implying that lithium is still preserved at the age of Barnard 35. We also note that, though the Barnard 35 sample is not too large, the mean Li equivalent width measured in Collinder 69 is somewhat larger than the measured in Barnard 35; this could be an effect of the veiling, since, at a first sight, the red solid dots (active accretors according to their H$\alpha$ emission) follow a trend of lower values than the solid black ones. In fact, the source showing the lowest value is DM227, an active accretor studied in the previous Section. In any case, this remains as a suggestion, since, as mentioned before, the statistic is not large enough to arrive to any conclussion.

Regarding the sources with spectral type hotter than K, as stated before, we used the measured equivalent width of the O I $\lambda$7776 Å absorption line as a proxy of the luminosity class (Danks & Dennefeld 1994) to estimate the possible contamination of giants in our sample. From the eight sources observed (two sources were observed in the two campaigns), in three of them

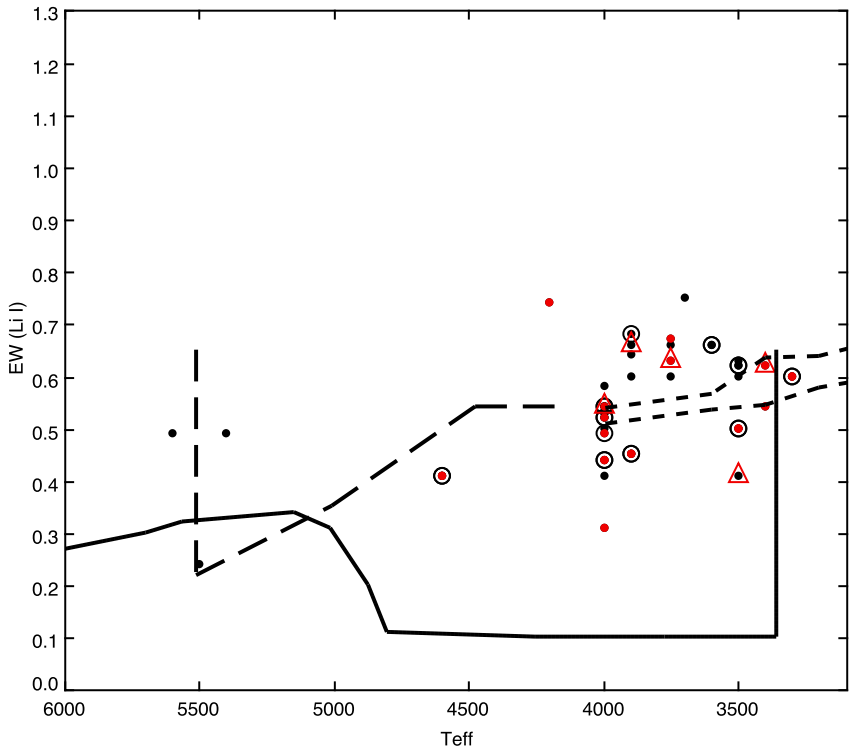


**Figure 4.10**: Lithium equivalent width versus effective temperature. Confirmed members are displayed as solid dots, where: red ones highlight sources classified as active accretors. Large black circunferences surround Class II sources and open red triangles transition disks.The solid line corresponds to the upper envelope of the values measured in young open clusters such as IC2391, IC2602, the Pleiades and M35. The long-dashed line delimits the areas for weak-line and post-TTauri stars (adapted from Martin 1997 and Martín & Magazzù 1999. Short-dashed and dotted lines correspond to the cosmic abundances – A(Li) = 3.1 – from gravities of Logg=4.5 and 4.0, respectively (curves of growth from Zapatero Osorio et al. 2002).

the signal to noise ratio of the spectra did not allow us to measure the profile of this line. From the remaining seven, two of them show equivalent widths quite high for their spectral type (G1); compatible with them being supergiants (although B35-I054430.6+094615.4 shows some variability and could also be classiffied a giant). The hottest star (B35-I054532.7+091900.6) shows a value typical of a dwarf, whilst B35-I054432.8+092421.4 was classified as subgiant. The other two sources show values compatible with class IV and class V sources.

Finally, as in the previous chapter, for the cooler sources of the sample (K and M spectral types), we have used the Na I doublet at ~8200 Å as a proxy for youth. As a reference, we have used our own data from Collinder 69 and the data gathered by Maxted et al. (2008) for $\sigma$ Orionis (with a similar age than Barnard 35, ~3 Myr).

This last criterion had to be applied carefully to the sources that are actively accreting, since the veiling provokes some weakening in the strength of the absorption lines, and members could be wrongly classified as lower luminosity class contaminants. Whenever this could have been the case, we studied the contribution of the veiling and corrected our measurements prior to classifying our sources as members or not.

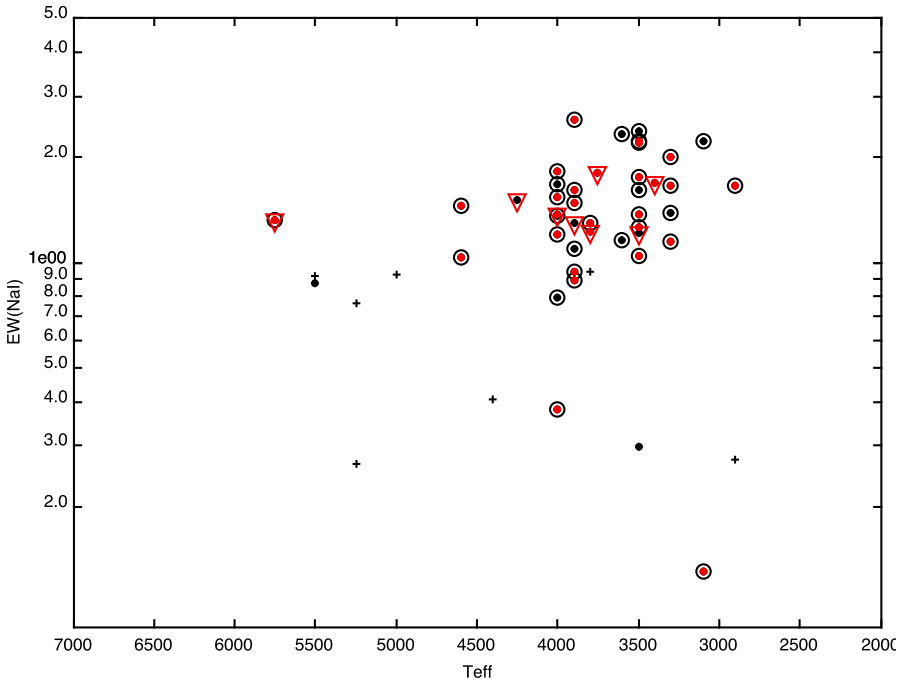


**Figure 4.11**: $T_{eff}$ vs EW(NaI) for members and non-members of Barnard 35. Rejected candidates are displayed as plus signs, confirmed members as solid dots, where: red ones highlight sources classified as active accretors. Large black circunferences surround Class II sources and open red triangles transition disks.

In Fig. 4.11 we plot the effective temperature of members and rejected candidates to Barnard 35 against their measured Na I. As we have previously mentioned, some accreting sources show much lower equivalent widht that those measured for similar-temperature members. Although there is a large dispersion, as in the case of Collinder 69 some correlation can be inferred between both quantities.

As can be seen in Table 4.2, there are sources (like in the case of Collinder 69) that show large variations in the measured Na I equivalent width, and others, like DM244 and DM248 for which de differences among the measurements are within the error-bars (like the differences between the Li I measurements by Dolan & Mathieu 2001 and ours).

## 4.3 The spatial distribution of the members.

In Table 4.4 we have included a column with the final membership assigned to each source. As in the previous chapter, we consider members those labeled as Y? (fulfilling most of the photometric criteria, see previous chapter), Y (highly reliable photometric candidates, see previous chapter for more details) and Y+ (spectroscopically confirmed members; in this case we have included the reference of the work were the spectroscopic confirmation was provided). There are ~75 members from which 67 have been labeled as Y or Y+.

The sample of sources that we have in this case is not populated enough to compute the Kuiper statistics and look for correlation in the spatial distribution of disk and diskless sources. Besides, this test would not be very relevant since our candidate selection criteria are completely biased towards the low mass Class II population. In any case, from a cualitative point of view, the confirmed members show a clustered distribution towards the dustier areas (IRAS 100 micron contours are overplotted in blue in the figure).

Finally, it is quite eye-catching the fact the all the “so-called” transition disks (highlighted with open red triangles in Fig. 4.12) are located along the previously mentiones IRAS contours.

## 4.4 The Hertzsprung-Russell diagram of Barnard 35.

In Fig. 4.13, we show the Hertzsprung–Russell diagram of Barnard 35 including all the (spectroscopically) confirmed members and the reliable (photometric) candidate members. We have overplotted two sets of composed isochrones (to achieve a complete mass range coverage) joining the collections by Siess et al. (2000) and COND by Baraffe et al. (2003) for two ages: 1 and 5 Myr. Taking into account the error bars in the determination of $L_{bol}$ and $T_{eff}$, there are several sources that lie well below the 5 Myr isochrone; some of them show infrared excesses, and therefore our determinations of these two parameters might be affected (as has been explained before, see Section 3.1).

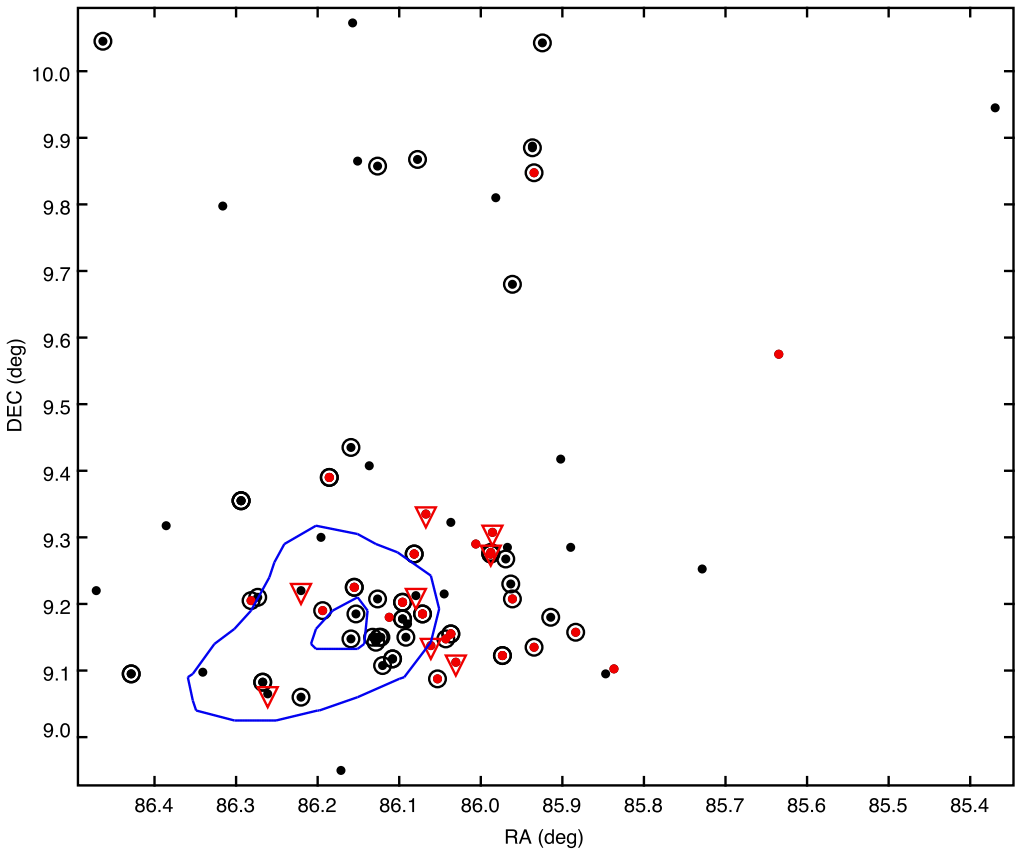


**Figure 4.12**: Spatial distribution of the members of Barnard 35 (spectroscopically confirmed and photometric candidates). Active accretors according to the saturation criterion are highlighted in red. We have also included the information regarding the near infrared excess with larger circumferences sourounding the Class II sources and open red triangles sourounding the transition disks.

On the other hand, if we focus on the three sources that do not show infrared excess (but still lie well below the 5 Myr isochrone curve); two of them are “DIL-members”. Since the selection criteria applyied by Duerr et al. (1982) consisted only in the detection of H$\alpha$ emission, active late F or G field dwarfs could mimic the emission of a YSO. The remaining object has been observed by us and it was classiffied as a tentative member since its youth was inferred studying its O I $\lambda$ 7776 Å absorption; a method that can have caveats when dealing with active sources.

In this case, unlike what happens with Collinder 69, all our sources show an homogeneous distribution in the diagram, regardless whether the source shows infrared excess or it is accreting. We must note in any case that our study (due to the selection criteria applyied to produce the candidate lists) is biased towards the Class II population of Barnard 35 and therefore we are not sensitive to inhomogenities with the Class III population.

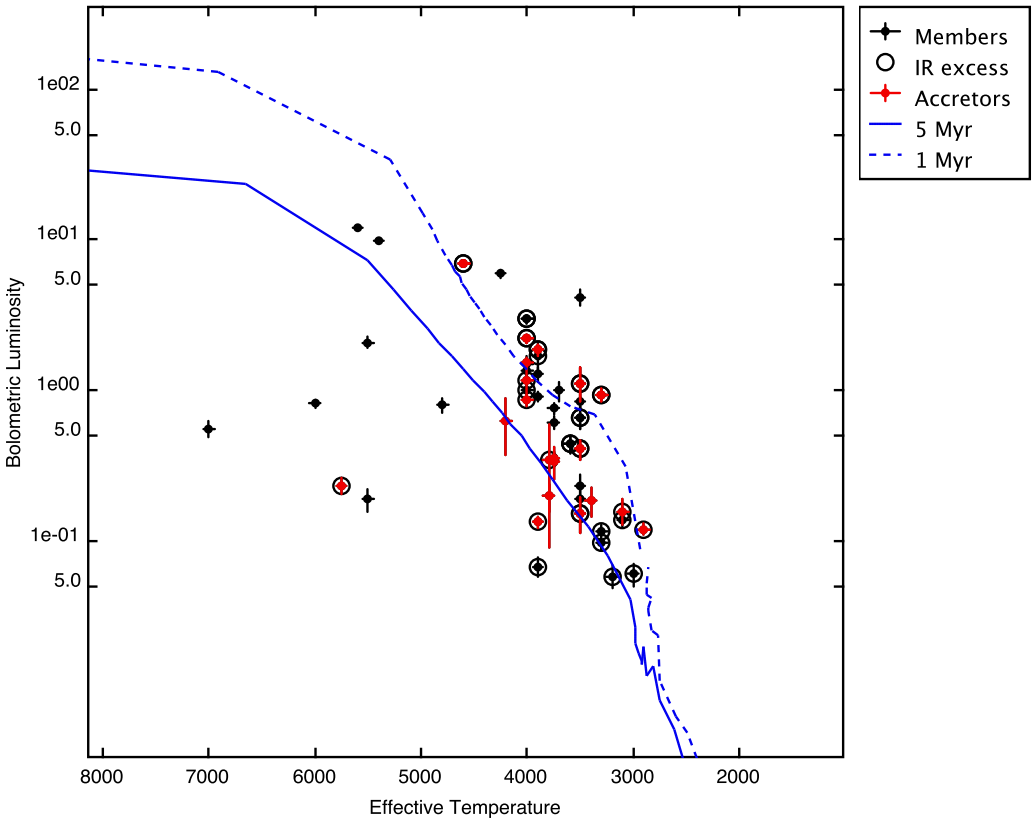


**Figure 4.13**: HR diagram of the confirmed (spectroscopically) and highly reliable (photometric) candidate members of Barnard 35.

## 4.5 Conclusions

We have analyzed ~60 optical spectra from known members and candidate members to the dark cloud Barnard 35. With different criteria based on line and molecular bands strengths, we have derived spectral types for all of them.

By studying youth indicators we have confirmed as new members 18 (plus two possible members) sources and discarded 12. We have also observed and analyzed ~20 members already observed by Dolan & Mathieu (1999, 2001).

We have analyzed the variability of the accretion rate of a subset of our sample of sources finding a large amplitude in the variations that do not appear to be correlated with the mass of the central star.

We have derived accretion rates for three sources harbouring so-called transition disks that agree with the few measurements of such disks that have been reported so far.

We have compared the evolutionary status of the disks around sources in Barnard 35 and those of Collinder 69 finding a very significant behaviour; being the latter diks much less active than those studied around members belonging to Barnard 35.

In Table 4.4 we provide a summary of all the parameters derived for the sources studied in this chapter.

**Table 4.4**: Summary of the parameters derived in this work for Barnard 35 candidate members and comparison with previous studies.

| Object | SpT | Accret. | Membership[5] | $\log(\dot{M}_{acc})(M_\odot/yr)$[4] | Class[6] | EW(H$\alpha$)[4] | EW(Li)[4] | $\alpha$ Slope | Disk Type | $T_{eff}$ | $L_{bol}$ | $Mass_{Teff}$ | $A_V$ |
|---|---|---|---|---|---|---|---|---|---|---|---|---|---|
| B35-I054340.9+091443.1 | G0 | N | NM+ (B09) | | I/II | 3.813±0.254[4)] | | 1.333 | Thick | 5250 | 0.049± 0.0010 | | 1.404 |
| B35-I054345.3+093904.8 | F6 | N | | | III | 3.491±1.576[4)] | | | | 5500 | 0.074± 0.0020 | | 0.362 |
| B35-I054357.0+091631.7 | M3.5 | Y | Y+ (B09) | ≤-10.95 | II/III | -166.291±2.928[4)] | | -2.563 | Transition | 5750 | 0.228± 0.0030 | | 0.861 |
| B35-I054428.7+091109.9 | M3.5 | N | NM+ (B09) | | III | 2.013±0.117[4)] | | -2.588 | Diskless | 3300 | 1.867± 0.031 | | 3.456 |
| B35-I054430.6+094615.1 | G5 | N | NM+ (B09) | | II | 3.177±0.286[4)] | | -1.253 | Thick | 4400 | 0.03± 0.0 | | 0.062 |
| B35-I054430.6+094615.4 | G2 | N | NM+ (B09) | | – | 2.399±0.127[4)] | | | | | | | |
| B35-I054432.8+092421.4 | F6 | N | Y?+ (B09) | | III | 4.284±0.105[4)] | | -2.913 | Diskless | 5500 | 0.184± 0.0030 | | 0.362 |
| B35-I054436.7+091321.6 | M3 | N | NM+ (B09) | | – | 2.207±0.343[4)] | | | | | | | 3.385 |
| B35-I054439.1+091807.8 | K5 | N | NM?+ (B09) | | I/II | 4.372±0.252[4)] | | | | 5000 | 0.042± 0.0010 | | 1.425 |
| B35-I054444.0+091014.5 | M3 | N | NM+ (B09) | | III | 4.051±0.108[4)] | | -2.262 | Diskless | | | | 7.392 |
| B35-I054447.7+092321.2 | G0 | N | NM+ (B09) | | III | 3.114±0.215[4)] | | -2.892 | Diskless | 5250 | 0.163± 0.0030 | | 0.362 |
| B35-I054449.0+091306.9 | K0 | N | NM+ (B09) | | III | 3.841±0.237[4)] | | -2.739 | Diskless | | | | 1.912 |
| B35-I054502.6+090350.0 | K3 | N | Y+ (B09) | | III | 1.767±0.036[4)] | | -2.568 | Transition | 4250 | 5.827± 0.038 | 1.023 | 1.391 |
| B35-I054504.1+092550.0 | F8 | N | | | – | 3.331±0.246[4)] | | | | | | | |
| B35-I054515.8+094741.0 | M1.5 | N | Y+ (B09) | | – | 1.668±0.242[4)] | | | | | | | |
| B35-I054516.9+090718.3 | M3.5 | N | NM+ (B09) | | III | 1.681±0.259[4)] | | -2.548 | Diskless | 2900 | 3.098± 0.032 | | 2.471 |
| B35-I054532.7+091900.6 | B9 | N | Y? (B09) | | III | 7.271±0.463[4)] | | -2.805 | Diskless | 3500 | 4.065± 0.046 | | 0.381 |
| B35-IRAC-10543 | | | Y | | II | | | -0.921 | Thick | 1600 | | 0.006 | 1.106 |
| B35-IRAC-11994 | M4.5 | Y | Y+ (B09) | ≤-10.95 | II | -82.168± 6.86[4)] | | -1.483 | Thick | 2900 | 0.117± 0.001 | 0.06 | 0.296 |
| B35-IRAC-12156 | M4 | N | NM+ (B09) | | II | -2.135± 0.242[4)] | | -1.427 | Thick | 3800 | 0.333± 0.006 | 0.9 | 1.403 |
| B35-IRAC-12396 | | | Y? | | I | | | 1.035 | Thick | | | | 1.392 |
| ” | | | Y? | | I | | | 1.035 | Thick | | | | 1.42 |
| B35-IRAC-12913 | | | Y | | II | | | -1.377 | Thick | 3000 | | 0.08 | 3.073 |
| B35-IRAC-13586 | M3.5 | Y | Y+ (B09) | ≤-10.95 | II | -187.987± 2.243[4)] | | -1.454 | Thick | 3900 | | 1.05 | 0.362 |
| ” | M4 | Y | Y+ (B09) | -11.644±0.343 | II | -216.341± 37.843[4)] | | -1.454 | Thick | 3900 | | 1.05 | 0.362 |
| B35-IRAC-14252 | M2 | Y | Y+ (B09) | -10.5± 0.389 | I | -93.662± 13.366[4)] | | -0.545 | Thick | | 0.115± 0.001 | | 0.084 |
| B35-IRAC-14618 | | | Y | | II | | | -1.093 | Thick | 1200 | | 0.004 | 5.4 |
| B35-IRAC-14785 | M4 | Y | Y+ (B09) | ≤-10.95 | II | -67.526± 3.047[4)] | | -1.031 | Thick | 3900 | 0.13± 0.001 | 1.05 | 2.031 |
| B35-IRAC-14804 | | | Y | | II | | | -1.188 | Thick | 1400 | | 0.005 | 8.346 |
| B35-IRAC-14943 | | | Y? | | I | | | 2.274 | Thick | | | | 5.314 |
| B35-IRAC-15004 | | | Y? | | I | | | 0.514 | Thick | | | | 5.736 |
| B35-IRAC-15017 | | | Y | | II | | | -1.162 | Thick | | | | 6.524 |
| B35-IRAC-16286 | M6 | N | Y+ (B09) | | II | -17.39±5 0.622[4)] | | -1.09 | Thick | 3300 | 0.114± 0.001 | 0.27 | 0.362 |
| B35-IRAC-16567 | | | Y? | | I | | | 0.133 | Thick | | | | 7.756 |
| B35-IRAC-17409 | M5.5 | Y | Y+ (B09) | ≤-10.95 | II | -68.47± 1.865[4)] | | -0.908 | Thick | 3100 | 0.154± 0.003 | 0.14 | 0.362 |
| B35-IRAC-17517 | M4 | Y | Y+ (B09) | ≤-10.95 | II | -31.732± 1.201[4)] | | -1.628 | Thick | 3800 | 0.338± 0.025 | 0.9 | 3.203 |
| B35-IRAC-17523 | | | Y | | II | | | -1.201 | Thick | 3500 | | 0.46 | 0.362 |
| B35-IRAC-17593 | | | Y | | II | | | -1.061 | Thick | 2700 | | 0.02 | 0.362 |
| B35-IRAC-18430 | | | Y | | II | | | -1.053 | Thick | 3000 | | 0.08 | 2.642 |
| B35-IRAC-20180 | | | Y | | II | | | -1.419 | Thick | 3300 | 0.094± 0.001 | 0.27 | 1.915 |
| B35-IRAC-20434 | M2.5 | Y | Y+ (B09) | ≤-10.95 | II | -66.169± 2.223[4)] | | -0.984 | Thick | 3500 | 0.149± 0.004 | 0.46 | 0.362 |
| ” | M3.0 | Y | Y+ (B09) | ≤-10.95 | II | -46.755± 1.917[4)] | | -0.984 | Thick | 3500 | 0.149± 0.004 | 0.46 | 0.362 |
| B35-IRAC-20473 | M3 | Y | Y+ (B09) | ≤-10.95 | II | -144.823± 3.997[4)] | | -1.763 | Thick | 3500 | 0.396± 0.006 | 0.46 | 1.082 |
| ” | M4.5 | Y | Y+ (B09) | ≤-10.95 | II | -141.203± 9.209[4)] | | -1.763 | Thick | 3500 | 0.396± 0.006 | 0.46 | 1.082 |
| B35-IRAC-23145 | M3 | Y | Y+ (B09) | -6.762± 0.39 | III | -16.306± 0.962[4)] | | -2.223 | Transition | 3800 | 0.194± 0.004 | 0.9 | 0.362 |

Continued on next page…

Table 4.4 – Continued

| Object | SpT | Accret. | Membership[5] | log($\dot{M}_{acc}$)($M_\odot$/yr)[4] | Class[6] | EW(H$\alpha$)[4] | EW(Li)[4] | $\alpha$ Slope | Disk Type | $T_{eff}$ | $L_{bol}$ | $Mass_{Teff}$ | $A_V$ |
|---|---|---|---|---|---|---|---|---|---|---|---|---|---|
| B35-IRAC-23414 | M3 | N | NM+ (B09) | | III | 1.538± 0.277[4)] | | -2.824 | Transition | 3700 | 1.188± 0.012 | 0.75 | 0.436 |
| B35-IRAC-24086 | | | Y? | | II | | | -1.467 | Thick | 2900 | | 0.06 | 1.148 |
| ” | | | Y? | | II | | | -1.467 | Thick | 2900 | | 0.06 | 1.152 |
| ” | | | Y? | | II | | | -1.467 | Thick | 2900 | | 0.06 | 1.149 |
| B35-IRAC-27556 | | | Y | | II | | | -1.775 | Thick | 3200 | 0.057± 0.001 | 0.21 | 0.362 |
| B35-IRAC-37817 | | | Y | | II | | | -1.776 | Thick | 3000 | 0.059± 0.001 | 0.08 | 0.362 |
| B35-IRAC-45299 | M2.25 | Y | Y+ (B09) | -4.182± 0.392 | II | -16.987± 1.279[4)] | | -1.579 | Thick | 3300 | | 0.27 | 0.362 |
| B35-IRAC-45860 | | | Y | | II | | | -1.094 | Thick | 3100 | 0.133± 0.001 | 0.14 | 2.226 |
| B35-IRAC-46311 | M3 | N | Y+ (B09) | | II | -12.199± 1.018[4)] | | -1.72 | Thick | 3100 | | 0.14 | 0.362 |
| B35-IRAC-47084 | | | Y | | II | | | -1.699 | Thick | 3900 | 0.066± 0.001 | 1.05 | 0.362 |
| DIL82 | | | Y (DIL) | | III | | | -2.903 | Diskless | 6000 | 0.803± 0.005 | 1.84 | 1.501 |
| DIL85 | | | Y (DIL) | | III | | | -2.832 | Diskless | 7000 | 0.544± 0.007 | 2.3 | 2.217 |
| DIL86 | | | Y (DIL) | | III | | | -2.791 | Diskless | 4800 | 0.779± 0.008 | 1.18 | 0.362 |
| DIL88 | | | Y (DIL) | | I/II | | | -1.08 | Thick | 2700 | | | |
| DM217 | | N | Y+ (DM) | | – | -3.35[1)] | 0.53 | | | 4000 | | 0.72 | |
| DM222 | | Y | Y+ (DM) | | – | -19.37[1)] | 0.54 | | | 3400 | | 0.23 | |
| DM225 | | N | Y+ (DM) | | – | -7.82[1)] | 0.6 | | | 3900 | | 0.63 | |
| DM227 | | Y | Y+ (DM) | | – | -52.56[1)] | 0.31 | | | 4000 | | 0.72 | |
| DM228 | | N | Y+ (DM) | | – | -0.41[1)] | 0.5 | | | 4000 | | 0.72 | |
| DM231 | M3 | Y | Y+ (DM, B09) | ≤-10.95 | II | -49.93[1)]; -30.56± 0.852[4)] | 0.49 | -1.109 | Thick | 4000 | 0.838± 0.007 | 0.72 | 0.385 |
| DM232 | | N | Y+ (DM) | | III | -3.07[1)] | 0.6 | -2.755 | Diskless | 3750 | 0.738± 0.006 | 0.47 | 0.362 |
| DM233 | | N | Y+ (DM) | | III | -4.83[1)] | 0.66 | -2.855 | Diskless | 3750 | 0.601± 0.006 | 0.47 | 0.362 |
| DM234 | M2.5 | N | Y+ (DM, B09) | | II | -4.1[1)]; -5.17± 0.199[4)] | 0.52 | -1.45 | Thick | 4000 | 0.974± 0.01 | 0.72 | 0.362 |
| DM235 | | N | Y+ (DM) | | III | -2.54[1)] | 0.58 | -2.789 | Diskless | 4000 | 1.472± 0.016 | 0.72 | 0.362 |
| DM236 | | N | Y+ (DM) | | III | -5.27[1)] | 0.63 | -2.73 | Diskless | 3500 | 0.229± 0.004 | 0.28 | 0.362 |
| DM237 | | N | Y+ (DM) | | III | -2.84[1)] | 0.64 | -2.789 | Diskless | 3900 | 0.895± 0.007 | 0.63 | 1.435 |
| DM238 | M4 | Y | Y+ (DM, B09) | ≤-10.95 | III | -26.71[1)]; -21.918± 1.11[4)] | 0.62 | -2.286 | Transition | 3400 | 0.181± 0.004 | 0.23 | 0.362 |
| DM239 | | Y | Y+ (DM) | | III | -4.64[1)] | 0.67 | -2.818 | Diskless | 3750 | 0.345± 0.004 | 0.47 | 0.362 |
| DM240 | M2.5 | Y | Y+ (DM, B09) | ≤-10.95 | III | -86.96[1)]; -115.809± 9.768[4)] | 0.54 | -2.312 | Transition | 4000 | 1.505± 0.011 | 0.72 | 2.165 |
| DM241 | K7 | Y | Y+ (DM, B09) | ≤-10.95 | II | -27.8[1)]; -17.886± 0.251[4)] | 0.45 | -1.205 | Thick | 3900 | 1.814± 0.017 | 0.63 | 1.276 |
| ” | K8 | Y | Y+ (DM, B09) | ≤-10.95 | II | -27.8[1)]; -25.963± 1.201[4)] | 0.45 | -1.205 | Thick | 3900 | 1.814± 0.017 | 0.63 | 1.276 |
| DM242 | | N | Y+ (DM) | | III | 0.35[1)] | 0.49 | -2.828 | Diskless | 5600 | 11.877± 0.02 | 1.62 | 3.404 |
| DM243 | M4 | Y | Y+ (DM, B09) | ≤-10.95 | III | -19.47[1)]; -45.429± 1.337[4)] | 0.63 | -2.54 | Transition | 3750 | 0.332± 0.008 | 0.47 | 1.991 |
| DM244 | M2.5 | Y | Y+ (DM, B09) | ≤-10.95 | II | -96.46[1)]; -68.563± 0.603[4)] | 0.44 | -1.23 | Thick | 4000 | 2.145± 0.015 | 0.72 | 1.516 |
| ” | M3 | Y | Y+ (DM, B09) | -12.425±0.153 | II | -96.46[1)]; -90.313± 5.524[4)] | 0.44 | -1.23 | Thick | 4000 | 2.145± 0.015 | 0.72 | 1.516 |
| DM245 | M3.5 | N | Y+ (DM, B09) | | III | -5.45[1)]; -6.869± 0.398[4)] | 0.66 | -2.278 | Transition | 3900 | 1.247± 0.013 | 0.63 | 1.191 |
| DM246 | M3.75 | N | Y+ (DM, B09) | | II | -25.88[1)]; -11.349± 0.324[4)] | 0.68 | -1.057 | Thick | 3900 | 1.664± 0.033 | 0.63 | 2.47 |
| DM247 | M2 | N | Y+ (DM, B09) | | II | -13.73[1)]; -4.473± 0.205[4)] | 0.62 | -1.242 | Thick | 3500 | 0.646± 0.011 | 0.28 | 2.359 |
| ” | M3 | N | Y+ (DM, B09) | | II | -13.73[1)]; -2.995± 0.314[4)] | 0.62 | -1.242 | Thick | 3500 | 0.646± 0.011 | 0.28 | 2.359 |
| DM248 | K3 | Y | Y+ (DM, B09) | ≤-10.95 | II | -3.27[1)]; -4.288± 0.259[4)] | 0.41 | -1.718 | Thick | 4600 | 6.875± 0.024 | 1.1 | 1.394 |
| ” | K4 | Y | Y+ (DM, B09) | ≤-10.95 | II | -3.27[1)]; -5.945± 0.171[4)] | 0.41 | -1.718 | Thick | 4600 | 6.875± 0.024 | 1.1 | 1.394 |
| DM249 | M2.5 | N | Y+ (DM, B09) | | II | -12.08[1)]; -2.882± 0.091[4)] | 0.54 | -1.351 | Thick | 4000 | 2.916± 0.017 | 0.72 | 2.688 |
| ” | M3 | N | Y+ (DM, B09) | | II | -12.08[1)]; -3.081± 0.186[4)] | 0.54 | -1.351 | Thick | 4000 | 2.916± 0.017 | 0.72 | 2.688 |
| DM250 | | Y | Y+ (DM) | | III | -22.97[1)] | 0.74 | -2.761 | Diskless | 4200 | 0.615± 0.025 | 0.88 | 3.552 |
| DM251 | | N | Y+ (DM) | | III | -5.29[1)] | 0.6 | -2.752 | Diskless | 3500 | 0.186± 0.003 | 0.28 | 0.362 |
| DM252 | M3.25 | Y | Y+ (DM, B09) | ≤-10.95 | II | -33.09[1)]; -50.226± 2.744[4)] | 0.5 | -1.358 | Thick | 3500 | 1.094± 0.028 | 0.28 | 3.524 |
| ” | M3.5 | Y | Y+ (DM, B09) | ≤-10.95 | II | -33.09[1)]; -43.006± 1.366[4)] | 0.5 | -1.358 | Thick | 3500 | 1.094± 0.028 | 0.28 | 3.524 |

Continued on next page…

Table 4.4 – Continued

| Object | SpT | Accret. | Membership[5] | $\log(\dot{M}_{acc})(M_{\odot}/yr)$[4] | Class[6] | EW(H$\alpha$)[4] | EW(Li)[4] | $\alpha$ Slope | Disk Type | $T_{eff}$ | $L_{bol}$ | $Mass_{Teff}$ | $A_V$ |
|---|---|---|---|---|---|---|---|---|---|---|---|---|---|
| DM254 | | N | Y+ (DM) | | III | 1.57[1)] | 0.24 | -2.81 | Diskless | 5500 | 2.034± 0.017 | 1.57 | 0.376 |
| DM255 | M3 | Y | Y+ (DM, B09) | ≤-10.95 | II | -21.24[1)]; -20.252± 0.238[4)] | 0.6 | -1.272 | Thick | 3300 | 0.915± 0.01 | 0.19 | 0.878 |
| ” | M3.5 | Y | Y+ (DM, B09) | ≤-10.95 | II | -21.24[1)]; -20.717± 0.68[4)] | 0.6 | -1.272 | Thick | 3300 | 0.915± 0.01 | 0.19 | 0.878 |
| DM256 | M3.25 | Y | Y+ (DM, B09) | ≤-10.95 | II | -32.16[1)]; -29.114± 0.839[4)] | 0.52 | -1.103 | Thick | 4000 | 1.145± 0.029 | 0.72 | 4.1 |
| DM257 | | N | Y+ (DM) | | III | -1.56[1)] | 0.49 | -2.848 | Diskless | 5400 | 9.584± 0.027 | 1.52 | 3.97 |
| DM258 | M2.5 | N | Y+ (DM, B09) | | III | 0.22[1)]; 0.695± 0.066[4)] | 0.41 | -2.408 | Transition | 3500 | 0.816± 0.008 | 0.28 | 1.106 |
| DM259 | M3.5 | N | Y+ (DM, B09) | | I/II | -4.79[1)]; -5.13± 0.19[4)] | 0.66 | -0.149 | Thick | 3600 | 0.432± 0.006 | 0.35 | 1.58 |
| ” | M4 | N | Y+ (DM, B09) | | I/II | -4.79[1)]; -4.465± 0.135[4)] | 0.66 | -0.149 | Thick | 3600 | 0.432± 0.006 | 0.35 | 1.58 |
| DM260 | | N | Y+ (DM) | | III | -4.35[1)] | 0.75 | -2.719 | Diskless | 3700 | 0.97± 0.015 | 0.43 | 2.915 |
| DM261 | | N | Y+ (DM) | | III | -1.13[1)] | 0.41 | -2.793 | Diskless | 4000 | 1.317± 0.013 | 0.72 | 0.908 |

[4] Measurement from; [5] Membership confirmed by:
[1)]; DM - Dolan & Mathieu (1999, 2001)
[4)]; B09 - This work
DIL - Duerr et al. (1982)

[6] Infrared Class derived with the IRAC data in Barrado y Navascués et al. (2007b) or Chapter 2 (“–” indicates that the sources has not been detected in the four IRAC bands).

# Chapter 5

# The dark cloud Barnard 30

Barnard 30 is a dark cloud located ~2.5$^o$ NW of the star $\lambda$ Ori. Duerr et al. (1982) first identified a stellar cluster centered around it and it was later confirmed from a statistical point of view by Gomez & Lada (1998). Because Barnard 30 is embedded in the CO and dust ring that surrounds the whole Lambda Orionis complex, it represents a quite different environment than that of Collinder 69 and Barnard 35. In this chapter we will study the Barnard 30 association following the same scheme as for Barnard 35.

This chapter is structured in three parts: Section 5.1 shortly summarizes the spectroscopic surveys performed over Barnard 30 that have already been published by other groups; Section 5.2 deals with the analysis of optical spectra of previously known members and new candidate groups proposed by Morales-Calderón (2008) . Finally, in Section 5.5 we provide the conclusions of this work.

## 5.1 Previous Surveys

The Barnard 30 association, as part of the Lambda Orionis Star Forming Region, has also been studied by Dolan & Mathieu (1999, 2001, 2002)) – See Section 3.2 for a summary of their observations. 62 out of the 266 pre-main sequence stars found by those authors fall within the area studied by Morales-Calderón (2008) in B30. We consider those objects bona fide members of the Barnard 30 association and will be called hereafter the DM members. In addition, 15 of the Duerr et al. members not in common with the DM members fall within the Spitzer field of view. We consider these 15 objects as bona-fide members of Barnard 30 (hereafter DIL members).

## 5.2 Spectroscopy for the Barnard 30 sample

For our spectroscopic campaigns we selected a sample of candidate members to Barnard 30 from those proposed by Morales-Calderón (2008) to confirm their membership to the dark

**Table 5.1**: Barnard 30 optical spectroscopic campaigns.

| Date | Observatory/Telescope/Instrument | Resolution | Wavelength coverage | Number of sources observed observed | Original photometric survey |
|---|---|---|---|---|---|
| November 20-23, 2006 | CAHA / 3.5m / TWIN | ~1100 | 5700–9900Å | 29 | DM & DIL & Morales-Calderón (2008) |
| December 5-7, 2006 | Lick / 3m Shane / Hamilton | ~50000 | 3800–9750Å | 7 | DM & DIL & Morales-Calderón (2008) |
| Nov. 30 - Dec. 11, 2006 | CAHA / 2.5m /CAFOS | ~600 | 6200–10350Å | 8 | DM & Morales-Calderón (2008) |
| Nov. 30 - Dec. 11, 2007 | CAHA / 2.5m /CAFOS | ~600 | 6200–10350Å | 4 | DM & Morales-Calderón (2008) |
| January 17-18, 2008 | Lick / 3m Shane / KAST | ~5000 | 5650–7050Å | 16 | DM & Morales-Calderón (2008) |

cloud and study their properties. And, also, as in the case of Barnard 35 we added to our sample some confirmed members from DM and DIL to study their variability.

In this case, as happened with Collinder 69, we have observations covering a wide range of resolutions, and therefore different analysis techniques were applied depending on the characteristics of the data gathered by us.

### 5.2.1 Spectral type determination

Like in the previous chapters; to perform the spectral classification of the M candidates we used the spectral indices described in Section 3.3.1 based on depth of some molecular bands (TiO and VO; see Fig. 5.1 for an example of a spectral sequence determined for the TWIN campaign). Nevertheless, the wavelength coverage of the instrumental set-up used during the Lick/KAST campaign was too short in the red domain to apply the mentioned indexes. For this particular dataset we used a different index based on the CaH feature at 6975 Å described in Kirkpatrick et al. (1991). Figure 5.2, extracted from Kirkpatrick et al. (1991) shows the clear correlation between this index and the spectral type of late K and M dwarfs. For the warmest part of the sample, observed with TWIN and expected to be K-type stars based on their estimated $T_{eff}$, we took spectra of the same set of templates obtained with CAFOS (described in the previous chapter) to use them as comparison (see Fig. 5.3 for an example of a possible contaminant galaxy and a K5 dwarf).

### 5.2.2 Rotational velocities estimation.

As in the previous chapters, for those sources observed in high resolution (those from the Lick/Hamilton campaign of 2006), we have studied their rotational velocity by comparing the depth of photospheric lines with theoretical spectra synthesized to match the effective temperature of each source and different rotational velocities.

From the 2006-LICK sample, one of the sources did not show Li I in absorption, being classified as non-member we did not study its rotational velocity. Regarding the remaining six sources; all but one are classified as active accretors, and, as explained in the previous chapter, veiling can introduce large uncertainties in the method we are using to determine the rotational velocity of the sources.

DM158, on the other hand shows a very subtle H$\alpha$ emission (see Table 5.2) that can

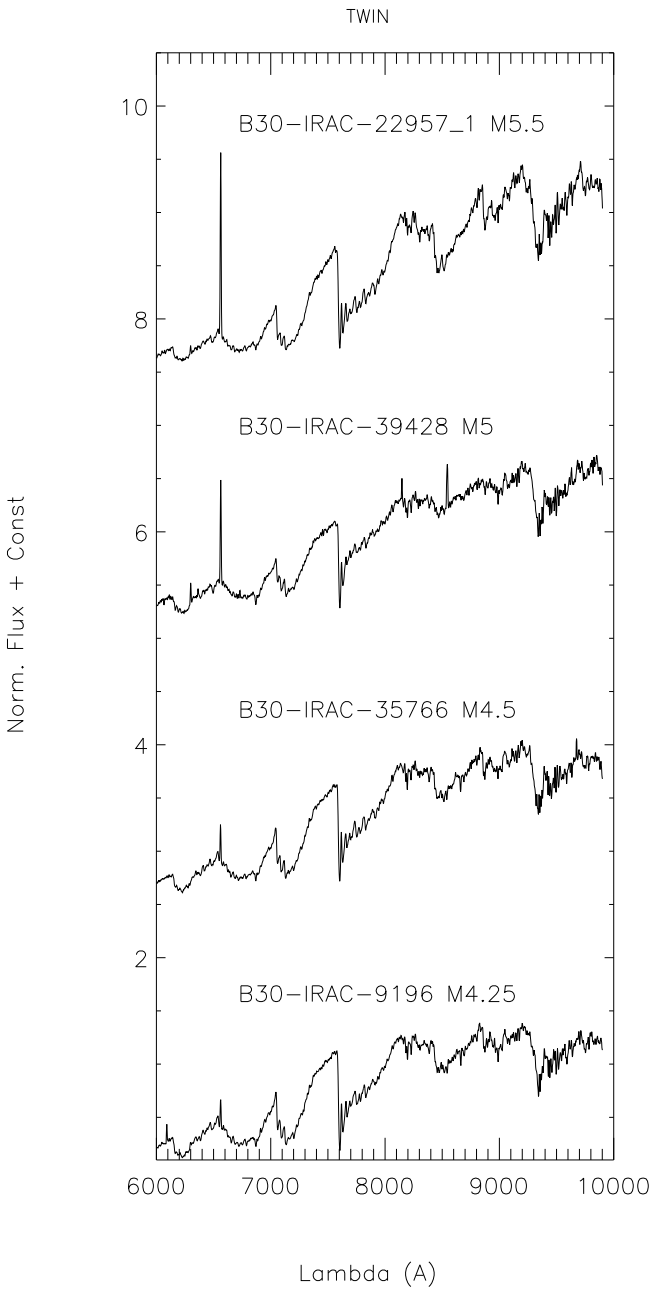


**Figure 5.1**: Spectral sequence for members of Barnard 30 observed with CAFOS.

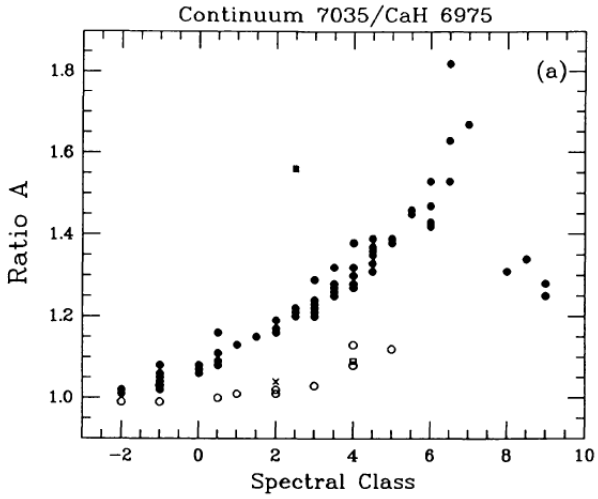


**Figure 5.2**: CaH index versus spectral type for late K and M dwarfs (from Kirkpatrick et al. 1991). Super-giants are marked by crosses, giants by open circles and dwarfs by filled circles.

be attributed merely to chromospheric activity. We show the comparison with theoretical models for this source in the top-right panel of Fig. 5.8. From this comparison, we derive a value for the projected rotational velocity of this source of 75 Km/s. In the top-left panel of Fig. 5.8 we show the same source, DM158, but this time compared to other two members with the same estimated effective temperature but very different intensities of both lines.

This effective temperature was estimated via SED fitting; in the lower panels of the same figure, we show the SEDs of the three sources. Note the similarities among them (especially between DM153 and DM158) but a first sight of the SED of DM153 already reveals some blue excess caused by the veiling. We have not been able to estimate precisely the veiling affecting DM123 and DM153. We provide the rotational velocity estimated for DM158 as possible upper-limits for the other two sources. The extremely high rotational velocities that would be derive not taking the veiling into account do not fit the commonly observed picture of young sources remaining slow rotator due disk locking (see Fig. 5.9 for an example of the comparison of the measured rotational velocities of young sources, -members of the ∼1 Myr Chamaleon I dark cloud harbouring disks-, and older, field dwarfs).

For the cases of DIL38, DM143 and DM166; the three sources were classified as active accretors, and we did not have same temperature-non-accreting template to try to infer the veiling affecting the Ca I doublet region. Therefore we were not able to provide an estimation of the rotational velocities of these sources.

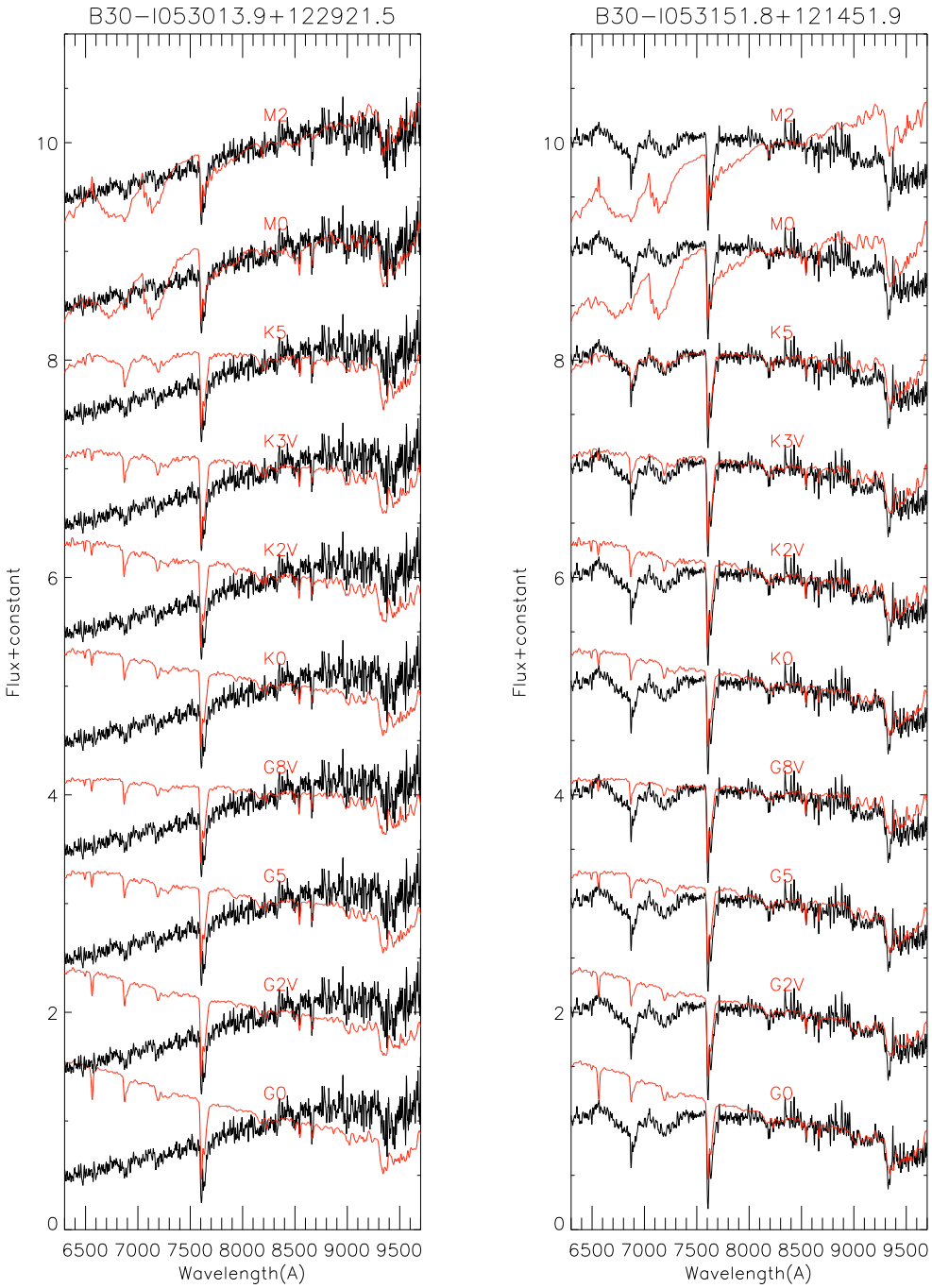


**Figure 5.3**: Spectral type determination for two candidate members by comparison with templates obtained with the same instrumental set-up. The "science spectra" are displayed in black and the templates (labeled according to the spectral type) in red. The first panel (from left to right) shows a possible galaxy contaminant; even though the slope of the spectrum is compatible with an early M star, the absence of the typical molecular bands lead us to consider it as contaminant. On the second panel we show a K5 V.

**Table 5.2**: Equivalent width of the main lines observed in the spectra obtained with Lick/Hamilton.

| Object | H$\beta$ 4861 EW(Å) | [OI] 5577 EW(Å) | [OI] 6300 EW(Å) | [OI] 6364 EW(Å) | [NII] 6581 EW(Å) | H$\alpha$ 6563 EW(Å) | $FW_{10\%}$(km/s) | FWHM(km/s) | HeI 6678 EW(Å) | LiI 6708 EW(Å) | [SII] 6717 EW(Å) | [SII] 6731 EW(Å) | CaII 8498 EW(Å) | CaII 8542 EW(Å) | CaII 8662 EW(Å) |
|---|---|---|---|---|---|---|---|---|---|---|---|---|---|---|---|
| B30-I053* | – | -5.396±0.327 | -0.425±0.056 | – | -0.372±0.038 | -2.357±1.594 | 36.944±4.592 | 16.998±1.947 | -0.117±0.000 | – | -0.368±0.050 | -0.214±0.004 | – | – | – |
| DIL38 | -4.013±0.400 | -1.774±0.412 | -0.581±0.089 | – | -0.222±0.016 | -21.442±0.998 | 314.295±3.30 | 106.778±0.000 | -0.062±0.022 | 0.302±0.019 | -0.150±0.040 | -0.236±0.035 | -0.157±0.079 | -0.447±0.108 | -0.393±0.074 |
| DM123 | -0.897±0.172 | -1.953±0.421 | -0.239±0.056 | -2.044±1.552 | -0.052±0.011 | -41.343±2.280 | 372.750±0.862 | 153.331±0.654 | -0.523±0.082 | 0.042±0.010 | -0.032±0.003 | -0.135±0.013 | – | – | – |
| DM143 | – | -1.961±0.160 | -0.178±0.027 | – | -0.391±0.042 | -4.934±0.719 | 312.598±2.500 | 78.163±0.000 | -0.625±0.174 | 0.299±0.056 | – | -0.082±0.015 | – | – | – |
| DM153 | – | -1.028±0.175 | -0.103±0.004 | -0.081±0.011 | – | -16.644±0.987 | 493.070±3.760 | 343.070±3.560 | – | 0.306±0.060 | -0.533±0.197 | -0.100±0.025 | -0.059±0.037 | -0.035±0.008 | -0.154±0.023 |
| DM158 | -0.158±0.029 | -0.651±0.064 | -0.034±0.009 | – | -0.107±0.036 | -0.975±0.087 | 170.573±0.980 | 52.590±0.500 | -0.137±0.018 | 0.479±0.058 | – | -0.158±0.034 | – | – | – |
| DM166 | -4.232±0.483 | -3.171±0.154 | -0.369±0.046 | – | -0.360±0.040 | -37.180±0.989 | 613.768±1.600 | 374.221±1.500 | -0.157±0.002 | 0.209±0.011 | -0.185±0.045 | -0.288±0.067 | – | – | – |

* B30-I053021.8+120025.4

**Table 5.3**: Equivalent width of the main lines observed in the spectra obtained with CAHA/TWIN.

| Object | H$\alpha$ 6563 EW(Å) | $FW_{10\%}$(km/s) | FWHM(km/s) | HeI 6678 EW(Å) | LiI 6708 EW(Å) | KI 7665 EW(Å) | KI 7700 EW(Å) | NaI 8200 EW(Å) | CaII 8498 EW(Å) | CaII 8542 EW(Å) | CaII 8662 EW(Å) |
|---|---|---|---|---|---|---|---|---|---|---|---|
| B30-I053013.9+122921.5 | 0.948±0.426 | 221.840 ± 18.373 | ≤85.0 | – | – | – | – | 2.144±1.073 | 1.248±0.458 | 1.850±0.610 | 5.771±1.753 |
| B30-I053014.4+121211.5 | -5.360±0.237 | 142.639 ± 42.422 | 27.626 ± 4.923 | – | – | 1.563±0.112 | 1.606±0.163 | 4.357±0.288 | 0.466±0.112 | 0.313±0.116 | 1.003±0.278 |
| B30-I053022.9+122347.1 | 2.460±0.502 | 845.736 ±267.872 | 606.819 ±27.302 | – | 1.007±0.135 | – | – | 1.677±0.218 | 0.596±0.032 | 2.706±0.687 | 2.270±0.189 |
| B30-I053023.8+121854.9 | 2.835±0.241 | 1340.270 ± 65.651 | 294.795 ± 8.703 | – | – | – | – | 1.359±0.251 | 0.701±0.203 | 2.299±0.486 | 1.720±0.238 |
| B30-I053055.3+122428.4 | 2.981±0.306 | 470.516 ± 38.107 | 87.979 ±10.174 | – | – | – | – | 0.443±0.085 | 1.140±0.395 | 3.253±0.211 | 2.967±0.154 |
| B30-I053131.1+120731.3 | -7.320±0.050 | ≤150.0 | ≤85.0 | – | – | 2.182±0.243 | 2.100±0.183 | 4.641±0.214 | 0.071±0.009 | 1.193±0.175 | 0.613±0.215 |
| B30-I053151.8+121451.9 | -0.728±0.311 | 1250.293 ± 29.496 | 391.952 ±16.726 | -0.415±0.240 | – | – | – | 2.906±0.553 | – | – | – |
| B30-I053156.8+122025.0 | -2.365±0.963 | 888.778 ±231.223 | 373.238 ±37.970 | -0.407±0.190 | 1.086±0.600 | – | – | 1.895±0.138 | – | – | – |
| B30-I053158.5+121238.9 | 4.919±0.033 | ≤150.0 | ≤85.0 | – | 0.786±0.287 | – | – | 1.520±0.153 | 0.632±0.071 | 2.068±1.172 | 1.972±0.125 |
| B30-I053158.7+122730.3 | 2.783±0.314 | 1461.646 ± 41.319 | 440.915 ±21.597 | -1.133±0.169 | 0.693±0.315 | – | – | 0.971±0.112 | 0.988±0.069 | 3.589±0.835 | 2.866±0.198 |
| B30-IRAC-18115 | -28.085±0.859 | 293.380 ± 6.501 | 157.161 ± 1.630 | -1.860±0.105 | – | – | – | 1.803±0.213 | -1.551±0.680 | -0.536±0.179 | -0.269±0.083 |
| B30-IRAC-21424 | -11.285±0.136 | 378.379 ± 0.184 | 157.336 ± 0.022 | -0.346±0.172 | 0.968±0.361 | – | – | 1.024±0.246 | -1.136±0.089 | -0.550±0.103 | -0.445±0.249 |
| B30-IRAC-22957_1* | -50.626±1.226 | 58.779 ± 4.713 | ≤85.0 | – | – | 1.334±1.035 | 1.349±0.749 | 0.833±0.250 | – | – | – |
| B30-IRAC-22957_2 | -62.734±1.541 | 486.997 ± 0.000 | 218.396 ± 0.000 | -1.164±0.089 | – | – | – | 0.955±0.484 | -5.073±0.482 | -4.314±0.091 | -4.724±0.337 |
| B30-IRAC-22957_3 | -27.494±0.217 | ≤150.0 | ≤85.0 | – | – | – | – | 0.919±0.322 | – | – | – |
| B30-IRAC-23445 | -12.387±0.783 | ≤150.0 | 89.735 ± 5.620 | – | 0.250±0.048 | – | – | 2.053±0.270 | – | – | – |
| B30-IRAC-23598 | -11.206±0.512 | 172.245 ± 16.088 | 181.981 ± 3.622 | – | – | – | – | 1.167±0.304 | 0.621±0.098 | 0.685±0.218 | 0.420±0.022 |
| B30-IRAC-30354 | -77.103±1.664 | 175.246 ± 0.000 | 26.299 ± 0.000 | – | 0.108±0.065 | – | – | 1.958±0.518 | -5.704±0.437 | -4.086±0.869 | -4.035±0.430 |
| B30-IRAC-35766 | -8.199±0.479 | ≤150.0 | ≤85.0 | – | – | – | – | 2.439±0.244 | 0.166±0.082 | 0.833±0.090 | 1.225±0.077 |
| B30-IRAC-39428 | -17.980±0.245 | ≤150.0 | ≤85.0 | – | 0.529±0.151 | – | – | 2.054±0.181 | – | – | – |
| B30-IRAC-9196 | -5.693±0.536 | ≤150.0 | ≤85.0 | – | – | – | – | 2.263±0.235 | – | – | – |
| DIL37 | -153.608±3.517 | 503.634 ± 1.568 | 219.943 ± 0.350 | -1.757±0.202 | 0.218±0.197 | – | – | 1.645±0.169 | -1.774±0.423 | -2.382±0.660 | -1.465±0.404 |
| DIL38 | -29.794±0.213 | ≤150.0 | ≤85.0 | -0.914±0.480 | 0.815±0.305 | – | – | 1.832±0.218 | – | – | – |
| DM123 | -110.442±0.941 | 223.536 ± 0.000 | 83.974 ± 0.000 | -2.267±0.836 | 1.139±0.581 | – | – | 2.185±0.294 | -3.635±0.197 | -3.966±0.624 | -2.649±0.110 |
| DM125 | -10.963±0.148 | 301.381 ± 2.297 | 59.857 ± 0.470 | – | 1.374±0.150 | – | – | 1.413±0.133 | 1.186±0.343 | 1.566±0.429 | 1.453±0.384 |
| DM135 | -3.299±0.127 | ≤150.0 | ≤85.0 | – | 0.518±0.081 | – | – | 2.256±0.224 | 1.165±0.043 | 1.343±0.090 | 1.349±0.147 |
| DM143 | -10.322±0.101 | 311.349 ± 4.202 | 138.892 ± 1.069 | -0.745±0.309 | 0.773±0.130 | – | – | 0.944±0.090 | -1.469±0.128 | -0.578±0.103 | -0.506±0.156 |
| DM172 | -88.416±0.804 | 304.499 ± 0.000 | 153.100 ± 0.000 | -2.851±0.398 | 0.699±0.240 | – | – | 1.484±0.165 | -1.970±0.329 | -1.240±0.255 | -1.917±0.778 |
| DM173 | -13.466±0.177 | ≤150.0 | 57.115 ± 0.217 | – | 0.360±0.096 | – | – | 2.081±0.291 | – | – | – |

* Three sources were aligned in the slit. The three of them are actively accreting and show other features characteristic of young sources (either LiI, KI or NaI), compatible with membership.

**Table 5.4**: Equivalent width of the main lines observed in the spectra obtained with CAHA/CAFOS during both campaigns.

| Campaign | Object | H$\alpha$ 6563 EW(Å) | $FW_{10\%}$(km/s) | FWHM(km/s) | HeI 6678 EW(Å) | KI 7665 EW(Å) | OI 7776 EW(Å) | NaI 8200 EW(Å) | CaII 8498 EW(Å) | CaII 8542 EW(Å) | CaII 8662 EW(Å) |
|---|---|---|---|---|---|---|---|---|---|---|---|
| 2006 | B30-I053014.4+121211.5 | -3.703±0.499 | ≤200.0 | ≤110.0 | – | 1.680±0.525 | 0.471±0.188 | 4.824±1.762 | 0.318±0.027 | 1.293±0.504 | 1.081±0.275 |
| 2006 | B30-I053131.1+120731.3 | -4.824±0.125 | 2123.886± 24.969 | 167.312± 6.582 | – | 1.885±0.153 | – | 4.763±2.090 | – | – | – |
| 2006 | B30-IRAC-18115 | -41.550±1.294 | ≤200.0 | ≤110.0 | -1.232±0.402 | 1.589±0.324 | – | 1.687±0.725 | -2.974±0.445 | -2.696±0.606 | -1.121±0.071 |
| 2006 | B30-IRAC-21424 | -9.262±0.335 | ≤200.0 | ≤110.0 | – | – | – | 2.107±0.975 | – | – | – |
| 2006 | DM125 | -16.157±0.199 | 120.726± 10.830 | 451.563± 2.255 | – | – | – | 2.375±1.205 | 1.591±0.556 | 1.900±0.214 | 1.616±0.321 |
| 2006 | DM135 | -6.804±0.121 | ≤200.0 | ≤110.0 | – | – | – | 2.758±1.343 | 0.735±0.447 | 1.745±0.279 | 0.774±0.113 |
| 2006 | DM136 | -18.334±0.978 | ≤200.0 | ≤110.0 | -0.896±0.441 | – | – | 1.783±0.590 | – | – | – |
| 2006 | DM143 | -7.959±0.484 | ≤200.0 | ≤110.0 | -1.709±0.033 | – | 0.315±0.124 | 1.456±0.336 | 0.208±0.010 | 0.412±0.084 | 0.702±0.170 |
| 2007 | B30-I053052.4+120544.1 | 4.529±0.528 | 1305.333±259.940 | 563.497±37.828 | – | – | 0.175±0.073 | 0.102±0.059 | 0.870±0.093 | 2.087±0.510 | 1.780±0.102 |
| 2007 | DM153 | -16.892±0.544 | 626.601± 38.561 | 381.370± 5.955 | – | – | – | 0.523±0.266 | 0.626±0.037 | 1.508±0.200 | 2.157±0.470 |
| 2007 | DM158 | -0.581±0.065 | 2510.041± 94.654 | 305.698±34.019 | – | – | – | 1.342±0.476 | 0.463±0.083 | 1.720±0.048 | 2.152±0.445 |
| 2007 | DM165 | -1.824±0.043 | 369.630± 66.309 | 353.333±12.820 | – | – | 0.558±0.246 | 1.536±0.545 | – | – | – |

**Table 5.5**: Equivalent width of the main lines observed in the spectra obtained with Lick/KAST and parameters derived.

| Object | Hα 6563 EW(Å) | $FW_{10\%}$(km/s) | FWHM(km/s) | HeI 6678 EW(Å) | LiI 6708 EW(Å) | SpT | EW(Hα)crit[1] | log($\dot{M}_{acc}$)($M_\odot$/yr) | Li[2] |
|---|---|---|---|---|---|---|---|---|---|
| B30-I053021.8+120025.4 | 1.934±0.149 | 156.407± 0.000 | 28.620± 0.000 | – | – | K7 | N | | N |
| B30-I053035.4+124735.9 | 3.931±0.391 | 967.801± 0.000 | 280.716± 0.000 | -0.274±0.021 | – | M0.5 | N | | N |
| B30-I053052.4+122512.3 | 2.031±0.248 | 683.165± 5.547 | 163.160± 1.194 | – | – | K7 | N | | N |
| B30-I053159.1+115110.9 | 0.368±0.104 | 200.266± 6.337 | < 125[3] | – | – | K7 | N | | N |
| B30-I053159.2+121440.5 | 1.213±0.213 | 972.037± 0.000 | 123.439± 0.000 | – | – | M0 | N | | N |
| B30-I053206.1+121826.2 | 1.111±0.114 | 686.728± 83.196 | < 125 | -0.204±0.028 | – | K6 | N | | N |
| B30-I053213.2+120655.3 | -7.376±0.473 | 138.192± 9.878 | 74.300± 2.098 | – | – | –[4] | Y | | N |
| B30-I053218.9+123106.5 | 1.142±0.184 | 438.738± 0.000 | 26.934± 0.000 | – | – | K7 | N | | N |
| B30-I053221.5+121000.2 | 0.776±0.365 | 238.918± 9.563 | < 125 | – | – | K7 | N | | N |
| B30-I053230.4+115722.8 | 3.129±0.332 | 982.014± 0.000 | 196.722± 0.000 | -0.078±0.017 | – | M0 | N | | N |
| DM120 | -83.750±2.759 | 343.595± 0.000 | 162.268± 0.000 | – | 0.389±0.119 | M1.5 | Y | -9.557±0.234 | Y |
| DM153 | -14.133±1.818 | 542.314± 0.000 | 141.186± 0.000 | – | 0.527±0.059 | M1 | Y | -7.630±0.436 | Y |
| DM158 | -1.495±0.284 | 340.988± 74.783 | 85.482± 11.548 | – | 0.533±0.074 | M0 | N | | Y |
| DM165 | -2.845±0.080 | 215.136± 11.935 | 93.078± 3.056 | – | 0.560±0.093 | M2 | N | | Y |
| DM166 | -111.729±1.163 | 630.850± 0.536 | 426.453± 0.053 | -0.426±0.183 | 0.411±0.051 | M0 | Y | -6.771±0.519 | Y |
| DM174 | -16.079±0.675 | 487.965± 7.649 | 315.874± 1.232 | -0.324±0.131 | 0.508±0.016 | M0 | Y | -8.157±0.741 | Y |

[1] Accretion criterion by Barrado y Navascués & Martín (2003).
[2] Membership based on the Lithium absorption.
[3] FHWM measured in the instrumental respones limit.
[4] Visual inspection of the spectra confirms it as a galaxy.

### 5.2.3 Hα and other emission lines: accretion, activity and outflows

We have observed an interesting variety of Hα profiles among the sources of our sample (some of them are displayed in Fig. 5.6). Assymetries and double peaked structures frequently seen in T Tauri stars.

Following the same scheme as in the previous chapters, we used our measured Hα equivalent widths and the derive spectral types as a diagnosis for accretion. In figure 5.5 a EW(Hα) versus spectral type diagram is shown with the saturation criterion by Barrado y Navascués & Martín (2003) displayed as a dotted line.

This diagram resembles the Barnard 35 case much more than the Collinder 69 one. We found an unexpected feature though; a larger ratio of non accreting vs. accreting Class II sources than in Barnard 35. On the other hand the estimated accretion rates are in general much larger than those derived for Barnard 35.

Regarding variability; from the 16 sources for which we have more than one measurement of the equivalent width of Hα (either in different runs from our team or the measurement by Dolan & Mathieu 2001), most of them show variable emission. Only three sources show differences in the measured equivalent width within the error bars. On the other hand there are sources that show differences of ∼70 Å (as is the case of DM123) in Hα equivalent width which translates in more than 2.5 orders of magnitude variation in the estimated accretion rate. In Fig. 5.4 we display, as we did for the cases of Collinder 69 and Barnard 35, a Mass accretion rate versus stellar mass diagram. We have only been able to estimate accretion rates for the sources observed by us. The variation of the six sources with different estimated accretion rates depending on the Hα

**Table 5.6**: Parameters derived from for the Lick/Hamilton sample.

| Object | Li Mem[1] | $T_{eff}$[2] | vsin($i$)(km/s) | EW(H$\alpha$)crit[3] | log($\dot{M}_{acc}$) | Mass($M_\odot$)[4] | IR Class[5] |
|---|---|---|---|---|---|---|---|
| B30-I053021.8+120025.4 | N | – | – | N | – | – | III |
| DIL38 | Y | 4800 | – | Y | -9.841±0.654 | 1.18 | II |
| DM123 | Y | 3750 | <75 | Y | -9.274±0.836 | 0.47 | II |
| DM143 | Y | 3500 | – | Y | -9.858±0.987 | 0.28 | I/II |
| DM153 | Y | 3750 | <75 | Y | -8.107±0.364 | 0.47 | II |
| DM158 | Y | 3750 | 75 | N | – | 0.47 | II |
| DM166 | Y | 5200 | – | Y | -6.936±0.155 | 1.39 | II |

[1] Memebership based on the measured WE(Li).
[2] Derive fitting synthetic spectra to the SED.
[3] Accretion criterion by Barrado y Navascués & Martín (2003).
[4] Mass derived from the SED fitting and isochrones Baraffe et al. (1998) assuming an age of 1 Myr.
[5] Infrared class derived from the IRAC photometry.

**Table 5.7**: Parameters derived for the CAHA/TWIN sample.

| Object | SpT | EW(H$\alpha$)crit[1] | log($\dot{M}_{acc}$)($M_\odot$/yr) | Alkali[2] | Li[3] | Object | SpT | EW(H$\alpha$)crit[1] | log($\dot{M}_{acc}$)($M_\odot$/yr) | Alkali[2] | Li[3] |
|---|---|---|---|---|---|---|---|---|---|---|---|
| B30-I053013.9+122921.5 | –[4] | N | | Y | N | B30-IRAC-23445 | M4.5 | N | | Y | Y |
| B30-I053014.4+121211.5 | M3.75 | N | | N | N | B30-IRAC-23598 | M4.5 | N | | Y | Y |
| B30-I053022.9+122347.1 | K6 | N | | Y | Y | B30-IRAC-30354 | M3.5 | Y | -11.190±0.187 | Y | Y |
| B30-I053023.8+121854.9 | K5 | N | | Y | N | B30-IRAC-35766 | M4.5 | N | | Y | Y? |
| B30-I053055.3+122428.4 | K4 | N | | Y | N | B30-IRAC-39428 | M5 | N | | Y | Y |
| B30-I053131.1+120731.3 | M4.25 | N | | N | N | B30-IRAC-9196 | M4.25 | N | | Y | N |
| B30-I053151.8+121451.9 | K5 | N | | N | N | DIL37 | M4 | Y | -8.004±0.015 | Y | Y? |
| B30-I053156.8+122025.0 | K5 | N | | Y | Y | DIL38 | M3.5 | Y | ≤-11.43 | Y | Y |
| B30-I053158.5+121238.9 | K7 | N | | Y | Y | DM123 | M4 | Y | -10.721±0.098 | Y | Y |
| B30-I053158.7+122730.3 | K6 | N | | Y | Y | DM125 | M3.5 | N | | Y | Y |
| B30-IRAC-18115 | M5 | Y | -10.044±0.063 | Y | Y | DM135 | M3.5 | N | | Y | Y |
| B30-IRAC-21424 | M4 | N | | Y | Y | DM143 | M0 | Y | -9.869±0.040 | Y | Y |
| B30-IRAC-22957_1 | M5.5 | Y | -12.319±0.046 | Y | Y | DM172 | M3 | Y | -9.936±0.387 | Y | Y |
| B30-IRAC-22957_2 | M4 | Y | -8.166±0.055 | Y | N | DM173 | M3.75 | Y | ≤-11.43 | Y | Y |
| B30-IRAC-22957_3 | M5.5 | Y | ≤-11.43 | Y | N | | | | | | |

[1] Accretion criterion by Barrado y Navascués & Martín (2003).
[2] Membership based on the measured Na I and K I doublets equivalent widths.
[3] Membership based on the presence of Li I in absorption.
[4] Possible galaxy (see Fig. 5.3).

**Table 5.8**: Parameters derived for the CAHA/CAFOS sample.

| Run | Object | SpT | EW(H$\alpha$)crit[1] | log($\dot{M}_{acc}$)($M_\odot$/yr) | Alkali[2] | Run | Object | SpT | EW(H$\alpha$)crit[1] | log($\dot{M}_{acc}$)($M_\odot$/yr) | Alkali[2] |
|---|---|---|---|---|---|---|---|---|---|---|---|
| 2006 | B30-I053014.4+121211.5 | M3 | N | | N | 2006 | DM136 | M2.5 | Y | ≤-10.95 | Y |
| 2006 | B30-I053131.1+120731.3 | M3.25 | N | | N | 2006 | DM143 | M5 | N | | Y |
| 2006 | B30-IRAC-18115 | M3.75 | Y | ≤-10.95 | Y | 2007 | B30-I053052.4+120544.1 | M2.5 | N | | N |
| 2006 | B30-IRAC-21424 | M4 | N | | Y | 2007 | DM153 | K9 | Y | -6.836±0.374 | Y |
| 2006 | DM125 | K9 | Y | -11.72±0.105 | Y | 2007 | DM158 | M0 | N | | Y |
| 2006 | DM135 | M2 | N | | Y | 2007 | DM165 | M3 | N | | Y |

[1] Accretion criterion by Barrado y Navascués & Martín (2003).
[2] Membership based on the measured Na I and K I doublets equivalent widths.

emission is highlighted in Fig. 5.4 with a vertical red line line (the remaining variable sources for which we had more than one spectra are not active accretors according to the saturation criterion by Barrado y Navascués & Martín 2003). Again, as in the case of Barnard 35 no mass dependence can be inferred for the variations in the accretion rate, although our sample might be to small to try to infer any kind of conclusion to this respect.

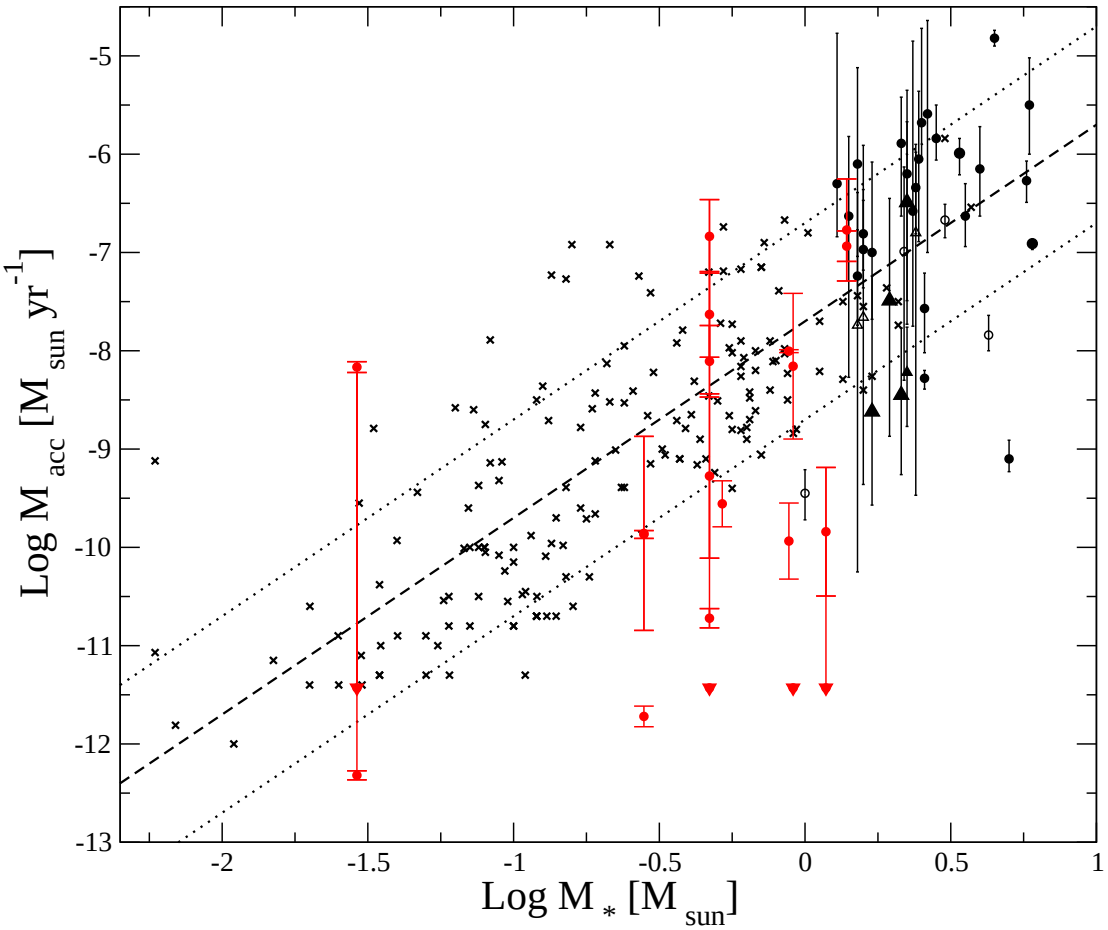


**Figure 5.4**: Mass accretion rates for a wide range of stellar masses. Red filled dots from this work. Crosses are from Calvet et al. (2004); Muzerolle et al. (2005); Mohanty et al. (2005) and Natta et al. (2006). Filled and open black symbols from Mendigutia et al 2009 (private communication), corresponding to the objects with EW(H$\alpha$) > 10 Å and < 10 Å, respectively. Triangles represent lower limits. The vertical bars over these symbols represent variability measured in time scales of hours – months (not uncertainty in the measurements as is the case for the vertical bars over the points calculated in this work). The dashed line follows $\dot{M}_{acc} \propto M_*^2$, and the dotted lines ± 1 dex.

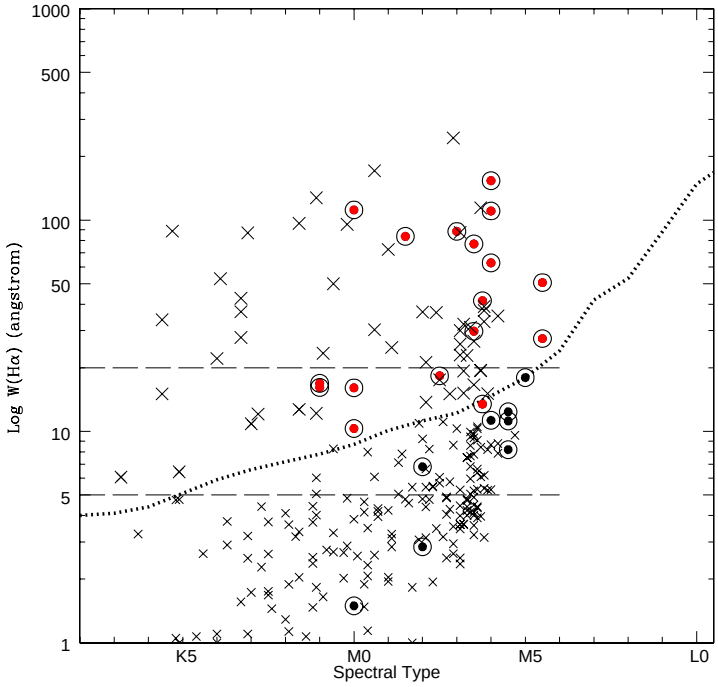


**Figure 5.5**: H$\alpha$ equivalent width versus the spectral type for confirmed members of Barnard 30. We display data from Dolan & Mathieu (1999, 2001), with crosses (larger ones for those fulfilling the saturation criteria). Our data are displayed with solid dots; red for those above the saturation criteria. Overlapping large circles denote objects with near infrared excess from Spitzer/IRAC data. The dotted lines correspondsto the saturation criteria defined by Barrado y Navascués & Martín (2003), whereas the two dashed lines are other criteria which have been used to define Classical TTauri stars.

### 5.2.4 Youth indicators using Alkali: Li $\lambda$6708 Å, KI $\lambda$7700 Å and NaI $\lambda$8200 Å

As in the previous Chapters we have used different indicators of youth to study the membership to the dark cloud of our candidates. In Fig 5.6 we show the Lithium I absorption present in three confirmed members of the DM sample.

We have confirmed 14 members with these alkali criteria (10 by their measured Lithium absorption, and the remaining four based on the Na I and K I lines). The Li I measurements in common with Dolan & Mathieu (2001) agree within the error bars when taking into account the differences measured in H$\alpha$; as a general rule whenever a larger H$\alpha$ emission is measured either by Dolan & Mathieu (2001) or us, a lower equivalent width is given for the Lithium line; what agrees with the veiling "hiding" part of the line. This applies for every source but for DM123, on which we measured a much lower value than the one provided by Dolan & Mathieu (2001). The spectra taken with Hamilton had the lower signal to noise ration from our sample, and therefore our measurement could not be reliable.

In Figure 5.6 we show as an example, a detail of the Lithium absorption observed for three sources during the Hamilton campaign.

In Fig. 5.7 we show the lithium equivalent width (measured on the higher resolution spectra) versus the spectral types derived in Section 5.2.1 for the newly confirmed members of Barnard 30 and previously known members from Dolan & Mathieu (2001). We have also included the sources from Dolan & Mathieu (1999, 2001) that have not been analyzed by us. For comparison, as in the previous chapters, we display data corresponding to a similar age cluster, $\sigma$ Orionis, as well as an older one, IC2391. We also show the theoretical equivalent widths from Zapatero Osorio et al. (2002) considering $\log g = 4.0$ and $\log g = 4.5$ and initial cosmic abundance (A(Li) = 3.1). Note that a significant fraction of our sources lie on top of the theoretical curves, implying that lithium is still preserved at the age of Barnard 30. We also note that, though the statistics are quite poor, there is a larger scatter on this diagram than on the Barnard 35 analog (Fig. 4.10). Once again the effect of the veiling is quite obvious in this diagram, since the smaller equivalent widths measured among the confirmed members correspond to active accreting sources (solid red dots).

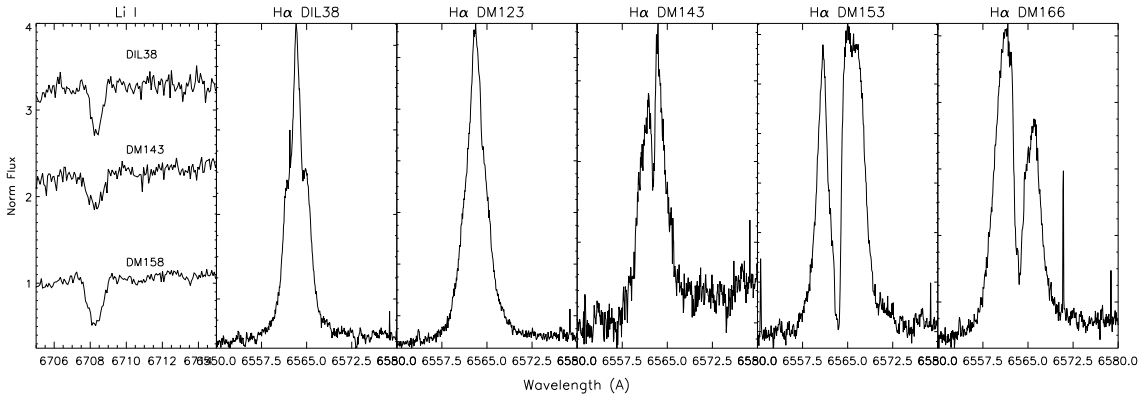


**Figure 5.6**: Detail on the Li I absorption line and H$\alpha$ emission for several sources observed with Hamilton. Note the variety of profiles shown by the sources.

## 5.3 The spatial distribution of the members

In Table 5.9 we have included a column with the final membership assigned to each source. We consider members those labeled as Y (highly reliable photometric candidates, see previous chapter for more details) and Y+ (spectroscopically confirmed members; in this case we have included the reference of the work were the spectroscopic confirmation was provided). There are ~136 members labeled as Y or Y+.

We have computed the Kuiper statistics to look for correlation in the spatial distribution of disk and diskless sources. As in the case of Collinder 69 we have derived a probability of 99.9% that both populations have not been drawn from the same distribution. In Fig. 5.10 we

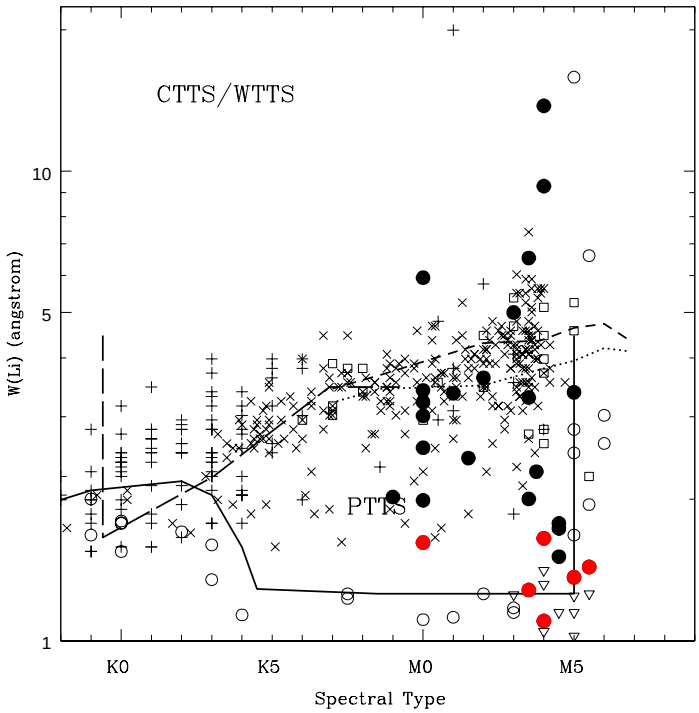


**Figure 5.7**: Lithium equivalent width versus the spectral type. We display data from Dolan & Mathieu (1999, 2001) as crosses, whereas our measurements appear as solid circles. Values for Sigma Orionis low mass stars are displayed as open squares Zapatero Osorio et al. (2002). The Weak-line TTauri stars belonging to Taurus and the Sco-Cen complex are included as plus symbols, whereas the open circles correspond to members of the IC2391 open cluster. The solid line corresponds to the upper envelope of the values measured in young open clusters such as IC2391, IC2602, the Pleiades and M35. The long-dashed line delimits the areas for weak-line and post-TTauri stars (adapted from Martin 1997 and Martín & Magazzù 1999. Short-dashed and dotted lines correspond to the cosmic abundances – A(Li) = 3.1 – from gravities of Logg=4.5 and 4.0, respectively (curves of growth from Zapatero Osorio et al. 2002).

see how the sources harbouring disks seem to be clustered around four specific locations while the Weak-line TTauri population is distributed homogeneously. As in the case of Barnard 35, this clustering phenomenon correlates quite well with the dust emission as inferred from the 100 $\mu$m IRAS contours.

In this figure we can also clearly see how most (all but two) of the sources with high H$\alpha$ emission but have not been clasified as Class II are located outside our IRAC coverage, and therefore no mid-infrared photometry is available for them. The remaining two sources do not show mid-infrared excesses (not even at 24 micron) and the strong H$\alpha$ emission could be attributed to a flare.

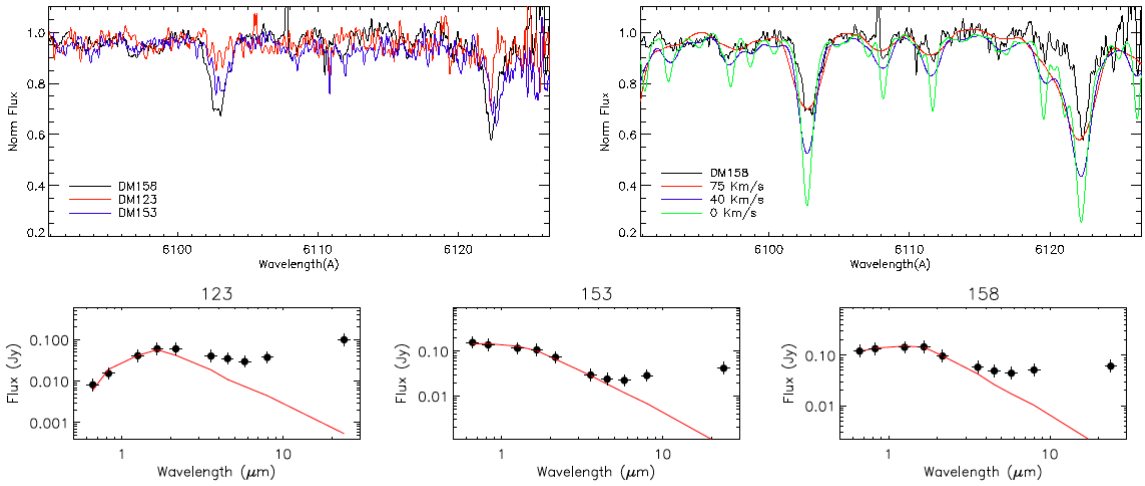


**Figure 5.8**: **Top-left:** Three Barnard 30 members with the same determined effective temperature and disk class but showing very different depth of the absorption lines used to study the rotational velocity. **Top-right:** Rotatioinal velocity determination for the only non-accreting source. **Bottom:** SED of the three sources shown on the top-left pannel with the best fitting photospheric model overplotted (Kurucz model of 3750 K).

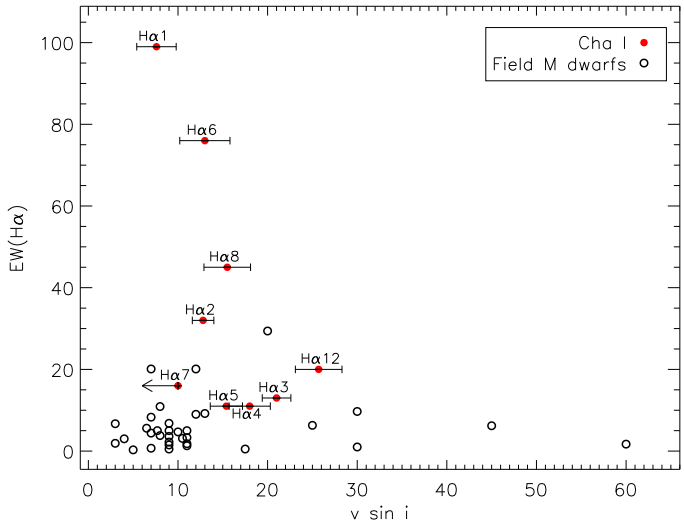


**Figure 5.9**: Projected rotational velocites versus H$\alpha$ equivalent width for some Chamaeleon I members with M spectral types (red dots) and a sample of M6–M9 field dwarfs (black dots) from Mohanty & Basri (2003). The projected rotational velocites of the objects of Cha I are from Joergens & Guenther (2001) and the H$\alpha$ equivalent widths from Comerón et al. (2000)

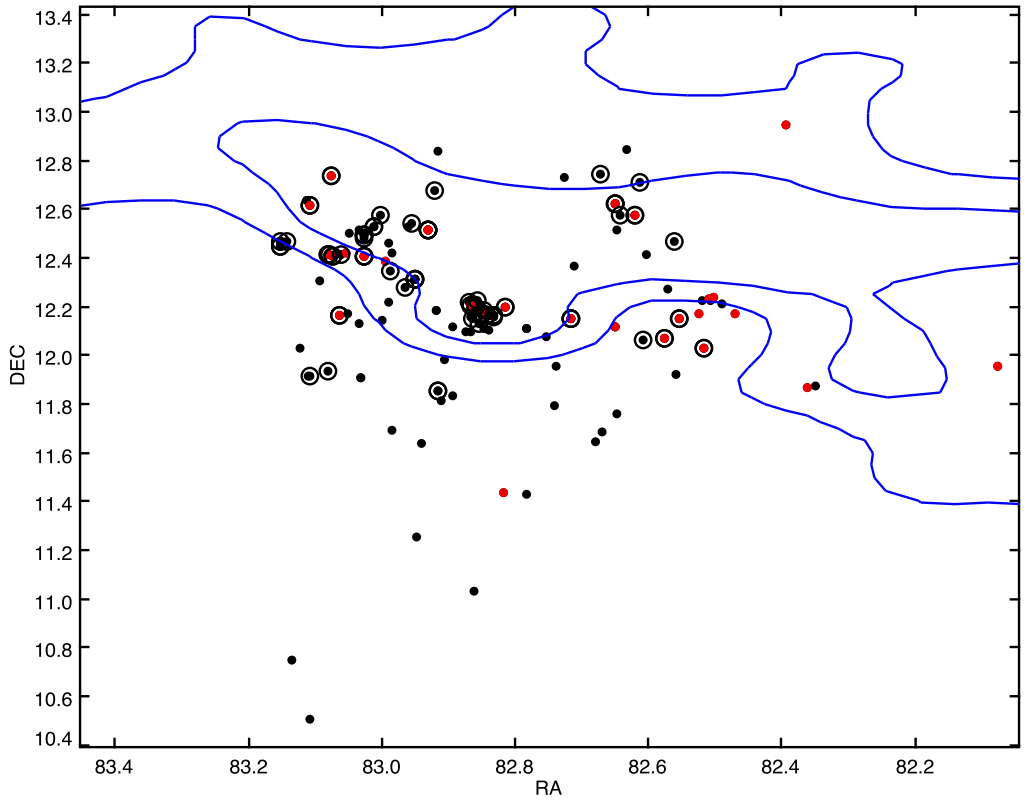


**Figure 5.10**: Spatial distribution of the members of Barnard 30 (spectroscopically confirmed and photometric candidates). Active accretors according to the saturation criterion are highlighted in red. We have also included the information regarding the near infrared excess with larger circumferences sourounding the Class II sources and open red triangles sourounding the transition disks.

## 5.4 The Hertzsprung-Russell diagram of Barnard 30.

In Fig. 5.11, we show the Hertzsprung–Russell diagram of Barnard 30 including all the (spectroscopically) confirmed members and the reliable (photometric) candidate members. We have overplotted two sets of isochrones composed (to achieve a complete mass range coverage) joining the collections by Siess et al. (2000) and COND by Baraffe et al. (2003) for two ages: 1 and 5 Myr.

This is the HR diagram showing the largest dispersion from those derived for this thesis; since only half of the photometric-candidates sample has been spectroscopically confirmed, it would reasonable to attribute this dispersion to contamination in our sample. We have checked that this dispersion is also shown among the sources spectroscopically confirmed by us and by Dolan & Mathieu (1999, 2001); Duerr et al. (1982). We think that this dispersion arises from our determination of the extinction and the effect that this parameter has on our determinations of the $T_{eff}$ and $L_{bol}$ of the sources. In any case, we must note that there is a quite large population showing positions in the HR diagram compatible with younger than 1 Myr, confirming B30 as a good candidate to be the youngest associations from those studied in this work.

## 5.5 Conclusions

We have analyzed 64 optical spectra at different resolutions corresponding to 45 sources: 13 known members to Barnard 30 (from Dolan & Mathieu 2001) and 32 candidate members from Morales-Calderón (2008). The previously known members were observed in order to study their variability (especially the accretion rate) and try to place these variations in context with the age and mass of the sources. The sample of candidate members was observed in order to confirm their membership to the dark cloud and study their properties.

Fourteen from these candidates were confirmed as new members based on the intensities of several alkali lines.

Regarding the variability; most of both, accreting and non-accreting sources would be classified variable according to the comparison of our own measurements of the H$\alpha$ emission and those from Dolan & Mathieu (2001). In fact, accreting sources seem to show larger amplitudes that translate in very large differences in the estimated accretion rates (the largest difference measured arrives to 2.5 orders of magnitude). These large differences have already been reported in the literature on more massive sources. We do not see any dependence of these variations with the stellar mass, although our sample is not significatively large enough to arrive to any definite conclusion.

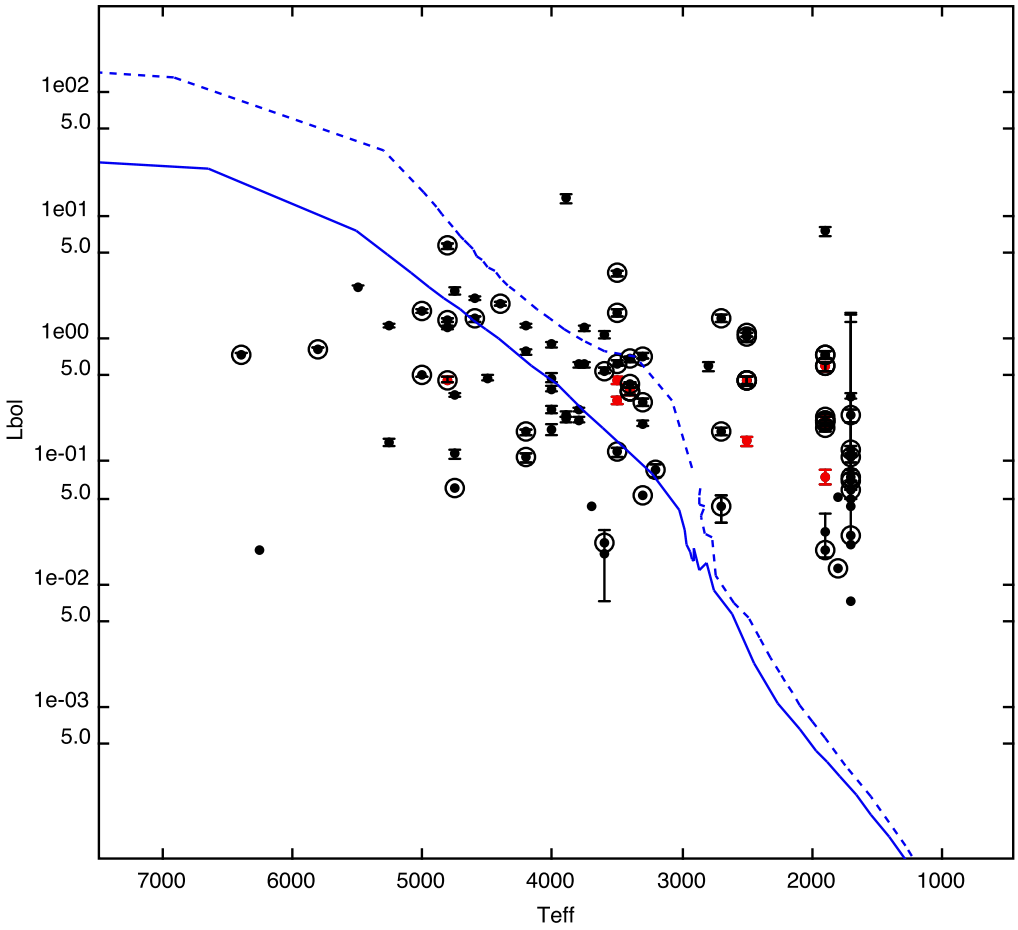


**Figure 5.11**: HR diagram of the confirmed (spectroscopically) and highly reliable (photometric) candidate members of Barnard 30. As in the previous figures, the members of Barnard 30 are displayed as solid dots, those active accretors are highlighted in red and Class II sources are surrounded by large black circumferences. The 1 Myr isochrone is plotted as a short-dashed blue curve and the 5 Myr one as a solid blue line.

**Table 5.9**: Summary of the parameters derived in this work for Barnard 30 candidate members and comparison with previous studies.

| Object | SpT | Accret. | Membership | $\log(\dot{M}_{acc})(M_\odot/yr)$[4] | | Class[6] | EW(H$\alpha$)[1] | EW(H$\alpha$)[2] | EW(Li)[1] | EW(Li)[2] | $\alpha$ Slope | Disk Type | $T_{eff}$ | $L_{bol}$ | | $Mass_{Teff}$ | $A_V$ |
|---|---|---|---|---|---|---|---|---|---|---|---|---|---|---|---|---|---|
| B30-I053013.9+122921.5 | | N | NM+ (B09) | | | | | 0.948 | 0.426 | | | | 3600.0 | 0.046 | 0.0 | 0.029 | 0.356 |
| B30-I053014.4+121211.5 | M3.75 | N | NM+ (B09) | | | | | -5.36 | 0.237 | | | | 4200.0 | 0.066 | 0.0 | 0.467 | 0.116 |
| B30-I053014.4+121211.5 | M3 | N | NM+ (B09) | | | | | -3.703 | 0.499 | | | | 4200.0 | 0.066 | 0.0 | 0.467 | 0.116 |
| B30-I053021.8+120025.4 | | N | NM+ (B09) | | | | | -2.357 | 1.594 | | | | 5250.0 | 0.25 | 0.49 | 1.115 | 0.84 |
| B30-I053021.8+120025.4 | K7 | N | NM+ (B09) | | | | | 1.934 | 0.149 | | | | 5250.0 | 0.25 | 0.49 | 1.115 | 0.84 |
| B30-I053021.8+120025.4 | | N | NM+ (B09) | | | | | -2.357 | 1.594 | | | | | | | | 2.38 |
| B30-I053021.8+120025.4 | K7 | N | NM+ (B09) | | | | | 1.934 | 0.149 | | | | | | | | 2.38 |
| B30-I053022.9+122347.1 | K6 | N | Y+ (B09) | | | | | 2.46 | 0.502 | 1.007 | 0.135 | | 5250.0 | 0.139 | 0.0010 | 1.115 | 2.444 |
| B30-I053023.8+121854.9 | K5 | N | NM+ (B09) | | | | | 2.835 | 0.241 | | | | 5500.0 | 0.111 | 0.0 | 0.72 | 1.863 |
| B30-I053035.4+124735.9 | M0.5 | N | NM+ (B09) | | | | | 3.931 | 0.391 | | | | 6500.0 | 0.483 | 0.0010 | | 2.794 |
| B30-I053052.4+122512.3 | K7 | N | NM+ (B09) | | | | | 2.031 | 0.248 | | | | 4600.0 | 0.269 | 0.0010 | 0.355 | 0.669 |
| B30-I053055.3+122428.4 | K4 | N | NM+ (B09) | | | | | 2.981 | 0.306 | | | | 5250.0 | 0.18 | 0.0010 | 1.115 | 1.538 |
| B30-I053131.1+120731.3 | M4.25 | N | NM+ (B09) | | | | | -7.32 | 0.05 | | | | 5600.0 | 0.385 | 0.0010 | 1.18 | 3.379 |
| B30-I053131.1+120731.3 | M3.25 | N | NM+ (B09) | | | | | -4.824 | 0.125 | | | | 5600.0 | 0.385 | 0.0010 | 1.18 | 3.379 |
| B30-I053151.8+121451.9 | K5 | N | NM+ (B09) | | | | | -0.728 | 0.311 | | | | 4200.0 | 0.06 | 0.0 | 0.467 | 1.008 |
| B30-I053156.8+122025.0 | K5 | N | Y+ (B09) | | | | | -2.365 | 0.963 | 1.086 | 0.6 | | 3600.0 | 0.021 | 0.0 | 0.35 | 0.116 |
| B30-I053158.5+121238.9 | K7 | N | Y+ (B09) | | | | | 4.919 | 0.033 | 0.786 | 0.287 | | 3700.0 | 0.041 | 0.0 | 0.43 | 0.116 |
| B30-I053158.7+122730.3 | K6 | N | Y+ (B09) | | | | | 2.783 | 0.314 | 0.693 | 0.315 | | 4750.0 | 0.11 | 0.0010 | 0.355 | 1.216 |
| B30-I053159.1+115110.9 | K7 | N | NM+ (B09) | | | | | 0.368 | 0.104 | | | | 5000.0 | 0.05 | 0.0 | 0.213 | 0.116 |
| B30-I053159.2+121440.5 | M0 | N | NM+ (B09) | | | | | 1.213 | 0.213 | | | | 5600.0 | 0.21 | 0.0010 | 1.18 | 1.309 |
| B30-I053206.1+121826.2 | K6 | N | NM+ (B09) | | | | | 1.111 | 0.114 | | | | 4500.0 | 0.099 | 0.0 | 0.63 | 0.116 |
| B30-I053213.2+120655.3 | | N | NM+ (B09) | | | | | -7.376 | 0.473 | | | | 5250.0 | 0.173 | 0.0010 | 1.115 | 0.116 |
| B30-I053218.9+123106.5 | K7 | N | NM+ (B09) | | | | | 1.142 | 0.184 | | | | | | | | 3.541 |
| B30-I053221.5+121000.2 | K7 | N | NM+ (B09) | | | | | 0.776 | 0.365 | | | | 5750.0 | 0.042 | 0.0 | 1.18 | 0.116 |
| B30-I053230.4+115722.8 | M0 | N | NM+ (B09) | | | | | 3.129 | 0.332 | | | | 5600.0 | 0.189 | 0.0010 | 1.18 | 0.116 |
| B30-IRAC-10420 | | | Y | | | II | | | | | -1.777 | Thick | 4200.0 | 0.166 | 0.0010 | 0.467 | 0.116 |
| B30-IRAC-1053 | | | Y | | | | | | | | | | | | | | 1.092 |
| B30-IRAC-11448 | | | Y | | | | | | | | | | | | | | |
| B30-IRAC-12438 | | | Y | | | III | | | | | -2.724 | Transition | 3800.0 | 0.208 | 0.0010 | 0.754 | 0.116 |
| B30-IRAC-12629 | | | Y | | | II | | | | | -1.272 | Thick | 2700.0 | 0.041 | 0.0010 | 0.029 | 0.116 |
| B30-IRAC-13304 | | | Y | | | | | | | | | | 6250.0 | 0.018 | 0.0 | | 0.204 |
| B30-IRAC-13402 | | | Y | | | II | | | | | -1.85 | Thin | 1900.0 | 0.018 | 0.0 | 2.968 | 0.116 |
| B30-IRAC-1371 | | | Y | | | | | | | | | | | | | | 2.313 |
| B30-IRAC-16599 | | | Y | | | II | | | | | -0.994 | Thick | 3400.0 | 0.65 | 0.0040 | 1.052 | 0.965 |
| B30-IRAC-17792 | | | Y | | | II | | | | | -1.601 | Thick | 4200.0 | 0.103 | 0.0010 | 0.041 | 0.116 |
| B30-IRAC-18115 | M5 | Y | Y+ (B09) | -10.044 | 0.063 | II | | -28.085 | 0.859 | | -0.997 | Thick | 1900.0 | 0.205 | 0.0020 | 0.0040 | 0.116 |
| B30-IRAC-18115 | M3.75 | Y | Y+ (B09) | -10.95 | | II | | -41.55 | 1.294 | | -0.997 | Thick | 1900.0 | 0.205 | 0.0020 | 0.0040 | 0.116 |
| B30-IRAC-19172 | | | Y | | | I | | | | | 1.551 | Thick | 1700.0 | 0.041 | 0.152 | 0.0020 | 2.866 |
| B30-IRAC-19198 | | | Y | | | I | | | | | 1.373 | Thick | 1900.0 | 0.026 | 0.0010 | 0.0030 | 3.383 |
| B30-IRAC-19545 | | | Y | | | II | | | | | -1.794 | Thick | 5250.0 | 1.242 | 0.0040 | 1.115 | 3.201 |
| B30-IRAC-19617 | | | Y | | | I | | | | | 0.117 | Thick | 3600.0 | 0.017 | 0.0010 | 0.029 | 2.134 |
| B30-IRAC-19802 | | | Y | | | III | | | | | -2.316 | Thin | 1700.0 | 0.327 | 0.0020 | 0.0030 | 3.025 |
| B30-IRAC-19863 | | | Y | | | II | | | | | -2.213 | Thin | 2900.0 | | | 0.063 | |
| B30-IRAC-20369 | | | Y | | | II | | | | | -0.877 | Thick | 1700.0 | 0.066 | 0.0010 | 0.0040 | 2.286 |
| B30-IRAC-20941 | | | Y | | | II | | | | | -1.083 | Thick | 1900.0 | 0.178 | 0.0010 | 0.0040 | 2.235 |

Continued on next page…

Table 5.9 – Continued

| Object | SpT | Accret. | Membership | log($\dot{M}_{acc}$)($M_\odot$/yr)[4] | | Class[6] | EW(H$\alpha$)[1] | EW(H$\alpha$)[2] | | EW(Li)[1] | EW(Li)[2] | | $\alpha$ Slope | Disk Type | $T_{eff}$ | $L_{bol}$ | | $Mass_{Teff}$ | $A_V$ |
|---|---|---|---|---|---|---|---|---|---|---|---|---|---|---|---|---|---|---|---|
| B30-IRAC-20993 | | | Y | | | II | | | | | | | -1.029 | Thick | 4000.0 | | | 1.115 | |
| B30-IRAC-21068 | | | Y | | | I/II | | | | | | | -0.303 | Thick | 2500.0 | 1.061 | 0.0080 | 0.0060 | 1.065 |
| B30-IRAC-21232 | | | Y | | | II | | | | | | | -1.423 | Thick | 1700.0 | 0.024 | 0.0 | 0.0040 | 1.795 |
| B30-IRAC-21424 | M4 | N | Y+ (B09) | | | II | | -11.285 | 0.136 | | 0.968 | 0.361 | -0.822 | Thick | 1900.0 | 0.711 | 0.0050 | 0.029 | 2.298 |
| B30-IRAC-21424 | M4 | N | Y+ (B09) | | | II | | -9.262 | 0.335 | | | | -0.822 | Thick | 1900.0 | 0.711 | 0.0050 | 0.029 | 2.298 |
| B30-IRAC-21495 | | | Y | | | I | | | | | | | -0.603 | Thick | 1700.0 | 0.057 | 0.0010 | 0.276 | 2.133 |
| B30-IRAC-21677 | | | Y | | | II | | | | | | | -0.925 | Thick | 2700.0 | 0.17 | 0.0010 | 0.213 | 0.116 |
| B30-IRAC-21725 | | | Y | | | I/II | | | | | | | -0.34 | Thick | 3500.0 | 3.283 | 0.016 | 1.34 | 2.742 |
| B30-IRAC-21900 | | | Y | | | I/II | | | | | | | -0.178 | Thick | 1800.0 | 0.049 | 0.0 | 0.0040 | 0.116 |
| B30-IRAC-22102 | | | Y | | | III | | | | | | | -2.171 | Transition | 4800.0 | 1.167 | 0.0040 | 0.063 | 2.607 |
| B30-IRAC-22233 | | | Y | | | II | | | | | | | -1.685 | Thick | 5000.0 | 0.481 | 0.0010 | 0.063 | 3.186 |
| B30-IRAC-22362 | | | Y | | | II | | | | | | | -0.604 | Thick | 4600.0 | 2.05 | 0.0080 | 0.355 | 2.608 |
| B30-IRAC-22691 | | | Y | | | II | | | | | | | -1.449 | Thick | 3300.0 | 0.69 | 0.0040 | 0.604 | 2.954 |
| B30-IRAC-22786 | | | Y | | | II | | | | | | | -1.157 | Thick | 1700.0 | 0.119 | 0.0010 | 0.0040 | 2.641 |
| B30-IRAC-22957 | M5.5$^1$ | Y | Y+ (B09) | -12.319 | 0.046 | II | | -50.626 | 1.226 | | | | -1.062 | Thick | 3400.0 | 0.359 | 0.0020 | 0.029 | 3.389 |
| B30-IRAC-22957 | M4$^2$ | Y | Y+ (B09) | -8.166 | 0.055 | II | | -62.734 | 1.541 | | | | -1.062 | Thick | 3400.0 | 0.359 | 0.0020 | 0.029 | 3.389 |
| B30-IRAC-22957 | M5.5$^3$ | Y | Y+ (B09) | -11.43 | | II | | -27.494 | 0.217 | | | | -1.062 | Thick | 3400.0 | 0.359 | 0.0020 | 0.029 | 3.389 |
| B30-IRAC-23445 | M4.5 | N | Y+ (B09) | | | II | | -12.387 | 0.783 | | 0.25 | 0.048 | -1.541 | Thick | 5800.0 | 0.796 | 0.0020 | 0.213 | 3.613 |
| B30-IRAC-23598 | M4.5 | N | Y+ (B09) | | | II | | -11.206 | 0.512 | | | | -1.144 | Thick | 3400.0 | 0.409 | 0.0020 | 0.019 | 2.858 |
| B30-IRAC-25472 | | | Y | | | II | | | | | | | -1.468 | Thick | 1900.0 | 0.219 | 0.0020 | 0.063 | 0.41 |
| B30-IRAC-26565 | | | Y | | | II | | | | | | | -1.105 | Thick | 4400.0 | 1.846 | 0.0080 | 0.213 | 0.116 |
| B30-IRAC-28513 | | | Y | | | III | | | | | | | -2.803 | Transition | 3900.0 | 13.279 | 0.126 | 0.72 | 3.743 |
| B30-IRAC-29908 | | | Y | | | II | | | | | | | -1.387 | Thick | 3300.0 | 0.288 | 0.0020 | 0.213 | 1.224 |
| B30-IRAC-29957 | | | Y | | | II | | | | | | | -1.536 | Thick | 4800.0 | 1.34 | 0.0040 | 0.088 | 2.992 |
| B30-IRAC-30116 | | | Y | | | I/II | | | | | | | -0.807 | Thick | 2500.0 | 0.985 | 0.0080 | 0.903 | 0.78 |
| B30-IRAC-30172 | | | Y | | | I/II | | | | | | | -0.835 | Thick | 3300.0 | 0.051 | 0.0 | 0.041 | 1.598 |
| B30-IRAC-30256 | | | Y | | | III | | | | | | | -2.793 | Transition | 3750.0 | 1.18 | 0.0060 | 1.052 | 0.116 |
| B30-IRAC-30354 | M3.5 | Y | Y+ (B09) | -11.19 | 0.187 | I | | -77.103 | 1.664 | | 0.108 | 0.065 | 0.298 | Thick | 1900.0 | 0.072 | 0.0010 | 0.0040 | 1.672 |
| B30-IRAC-31202 | | | Y | | | II | | | | | | | -1.236 | Thick | 2700.0 | 1.389 | 0.01 | 0.0080 | 0.116 |
| B30-IRAC-31833 | | | Y | | | II | | | | | | | -1.816 | Thick | 3500.0 | 0.115 | 0.0010 | 0.019 | 1.586 |
| B30-IRAC-31902 | | | Y | | | II | | | | | | | -1.641 | Thick | 3600.0 | 0.525 | 0.0030 | 0.604 | 0.116 |
| B30-IRAC-32037 | | | Y | | | I | | | | | | | -0.998 | Thick | 1700.0 | 0.103 | 0.0010 | 0.0040 | 0.116 |
| B30-IRAC-32340 | | | Y | | | II | | | | | | | -1.103 | Thick | 3200.0 | 0.082 | 0.0010 | 0.0060 | 1.72 |
| B30-IRAC-32951 | | | Y | | | II | | | | | | | -1.502 | Thick | 5000.0 | 1.602 | 0.0050 | 0.213 | 3.753 |
| B30-IRAC-33125 | | | Y | | | I | | | | | | | 0.281 | Thick | 1700.0 | 0.02 | 0.127 | 0.0040 | 3.813 |
| B30-IRAC-33419 | | | Y | | | III | | | | | | | -2.732 | Transition | | | | | 4.07 |
| B30-IRAC-33525 | | | Y | | | II | | | | | | | -0.94 | Thick | 3500.0 | 1.571 | 0.012 | 0.019 | 4.805 |
| B30-IRAC-33661 | | | Y | | | I | | | | | | | -0.111 | Thick | 1700.0 | 0.048 | 0.143 | 0.0020 | 4.054 |
| B30-IRAC-33936 | | | Y | | | I | | | | | | | -1.016 | Thick | 1700.0 | 0.228 | 0.0030 | 0.0020 | 4.287 |
| B30-IRAC-34050 | | | Y | | | I/II | | | | | | | -0.986 | Thick | 1700.0 | 0.071 | 0.0010 | 0.0030 | 4.213 |
| B30-IRAC-34119 | | | Y | | | III | | | | | | | -2.693 | Transition | 3600.0 | 1.027 | 0.0060 | 0.029 | 3.97 |
| B30-IRAC-35518 | | | Y | | | II | | | | | | | -1.729 | Thick | 3400.0 | | | 0.355 | |
| B30-IRAC-35582 | | | Y | | | I | | | | | | | -0.106 | Thick | 1800.0 | 0.013 | 0.0 | 0.0030 | 3.389 |
| B30-IRAC-35766 | M4.5 | N | Y+ (B09) | | | II | | -8.199 | 0.479 | | | | -1.608 | Thick | 6400.0 | 0.717 | 0.0010 | 0.355 | 4.081 |
| B30-IRAC-37215 | | | Y | | | II | | | | | | | -1.446 | Thick | 2500.0 | 0.441 | 0.0030 | 0.0060 | 0.116 |
| B30-IRAC-37312 | | | Y | | | II | | | | | | | -1.105 | Thick | 2100.0 | | | 0.0070 | |
| B30-IRAC-39428 | M5 | N | Y+ (B09) | | | I/II | | -17.98 | 0.245 | | 0.529 | 0.151 | -0.749 | Thick | 3500.0 | 0.604 | 0.0030 | 0.144 | 3.451 |

Continued on next page…

Table 5.9 – Continued

| Object | SpT | Accret. | Membership | log($\dot{M}_{acc}$)($M_\odot$/yr)[4] | | Class[6] | EW(H$\alpha$)[1] | EW(H$\alpha$)[2] | | EW(Li)[1] | EW(Li)[2] | | $\alpha$ Slope | Disk Type | $T_{eff}$ | $L_{bol}$ | | $Mass_{Teff}$ | $A_V$ |
|---|---|---|---|---|---|---|---|---|---|---|---|---|---|---|---|---|---|---|---|
| B30-IRAC-40421 | | | Y | | | II | | | | | | | -1.247 | Thick | 4750.0 | 0.059 | 0.0 | 0.355 | 1.772 |
| B30-IRAC-41615 | | | Y | | | II | | | | | | | -1.557 | Thick | 4600.0 | 1.382 | 0.0050 | 1.34 | 2.987 |
| B30-IRAC-41741 | | | Y | | | II | | | | | | | -1.685 | Thick | 1900.0 | 0.2 | 0.0010 | 0.0060 | 0.779 |
| B30-IRAC-45191 | | | Y | | | I | | | | | | | 0.052 | Thick | 1700.0 | 0.0070 | 0.0 | 0.0020 | 1.723 |
| B30-IRAC-45371 | | | Y | | | I/II | | | | | | | -0.47 | Thick | 3300.0 | 0.194 | 0.0010 | 0.0090 | 1.926 |
| B30-IRAC-6876 | | | Y | | | I | | | | | | | 0.538 | Thick | | | | 0.0020 | 0.116 |
| B30-IRAC-9196 | M4.25 | N | NM+ (B09) | | | II | | -5.693 | 0.536 | | | | -1.84 | Thin | 2500.0 | 0.041 | 0.0010 | 0.276 | 0.116 |
| DIL12 | | | Y+ (DIL) | | | ? | | | | | | | | – | 4200.0 | | | 0.88 | |
| DIL18 | | | Y+ (DIL) | | | ? | | | | | | | | – | 4200.0 | | | 0.88 | |
| DIL23 | | | Y+ (DIL) | | | III | | | | | | | -2.864 | Diskless | 4000.0 | | | 0.72 | |
| DIL27 | | | Y+ (DIL) | | | II | | | | | | | -2.18 | Thick | 2800.0 | 0.57 | 0.0050 | 1.71 | 2.168 |
| DIL28 | | | Y+ (DIL) | | | ? | | | | | | | | – | 4000.0 | | | 0.72 | |
| DIL29 | | | Y+ (DIL) | | | I/II | | | | | | | -0.324 | Thick | 1900.0 | 7.202 | 0.06 | 1.57 | 2.031 |
| DIL37 | M4 | Y | Y+ (DIL, B09) | -8.004 | 0.015 | II | | -153.608 | 3.517 | | 0.218 | 0.197 | -1.387 | Thick | 4200.0 | | | 0.88 | |
| DIL38 | M3.5 | Y | Y+ (DIL, B09) | -11.43 | | II | | -29.794 | 0.213 | | 0.815 | 0.305 | -0.807 | Thick | 4800.0 | | | 1.18 | |
| DIL38 | | Y | Y+ (DIL, B09) | -9.841 | 0.654 | II | | -21.442 | 0.998 | | 0.302 | 0.019 | -0.807 | Thick | 4800.0 | | | 1.18 | |
| DIL39 | | | Y+ (DIL) | | | III | | | | | | | -2.792 | Diskless | 4200.0 | 0.747 | 0.0030 | 0.23 | 0.116 |
| DIL43 | | | Y+ (DIL) | | | ? | | | | | | | | – | 3500.0 | | | 0.28 | |
| DIL44 | | | Y+ (DIL) | | | ? | | | | | | | | – | 3300.0 | | | 0.19 | |
| DIL46 | | | Y+ (DIL) | | | II | | | | | | | -1.236 | Thick | 3750.0 | | | 0.47 | |
| DM100 | | Y | Y+ (DM) | | | ? | -95.43 | | | 0.51 | | | | – | 3900.0 | | | 0.63 | |
| DM106 | | Y | Y+ (DM) | | | ? | -31.14 | | | 0.58 | | | | – | 3700.0 | | | 0.43 | |
| DM107 | | N | Y+ (DM) | | | ? | -2.75 | | | 0.59 | | | | – | 3750.0 | | | 0.47 | |
| DM109 | | Y | Y+ (DM) | | | II? | -114.32 | | | 0.4 | | | | – | 3000.0 | | | 0.09 | |
| DM110 | | N | Y+ (DM) | | | ? | 0.39 | | | 0.51 | | | | – | 4400.0 | | | 0.98 | |
| DM111 | | Y | Y+ (DM) | | | II? | -33.76 | | | 0.41 | | | | – | 4200.0 | | | 0.88 | |
| DM113 | | Y | Y+ (DM) | | | II | -23.43 | | | 0.58 | | | -0.994 | Thick | 4000.0 | | | 0.72 | |
| DM114 | | Y | Y+ (DM) | | | ? | -39.03 | | | 0.6 | | | | - | 3500.0 | 0.304 | 0.0020 | 0.35 | 0.116 |
| DM115 | | Y | Y+ (DM) | | | I/II | -22.12 | | | 0.43 | | | -0.303 | Thick | 4000.0 | | | 0.72 | |
| DM118 | | N | Y+ (DM) | | | III | -6.09 | | | 0.54 | | | -2.739 | Diskless | 3900.0 | 0.233 | 0.0010 | 0.72 | 0.23 |
| DM120 | M1.5 | Y | Y+ (DM, B09) | -9.557 | 0.234 | II | -171.14 | -83.75 | 2.759 | 0.24 | 0.389 | 0.119 | -1.729 | Thick | 4800.0 | 0.445 | 0.0020 | 0.52 | 3.174 |
| DM121 | | Y | Y+ (DM) | | | II | -244.76 | | | 0.65 | | | -2.213 | Thin | 2500.0 | 0.14 | 0.0010 | 0.47 | 0.116 |
| DM123 | M4 | Y | Y+ (DM, B09) | -10.721 | 0.098 | II | -127.58 | -110.442 | 0.941 | 0.28 | 1.139 | 0.581 | -1.105 | Thick | 1900.0 | 0.576 | 0.0050 | 0.47 | 0.608 |
| DM123 | | Y | Y+ (DM, B09) | -9.274 | 0.836 | II | -127.58 | -41.343 | 2.28 | 0.28 | 0.042 | 0.01 | -1.105 | Thick | 1900.0 | 0.576 | 0.0050 | 0.47 | 0.608 |
| DM125 | M3.5 | N | Y+ (DM, B09) | | | II | -42.62 | -10.963 | 0.148 | 0.58 | 1.374 | 0.15 | -1.029 | Thick | 2500.0 | 0.432 | 0.0040 | 0.28 | 0.116 |
| DM125 | K9 | Y | Y+ (DM, B09) | -11.72 | 0.105 | II | -42.62 | -16.157 | 0.199 | 0.58 | | | -1.029 | Thick | 2500.0 | 0.432 | 0.0040 | 0.28 | 0.116 |
| DM126 | | N | Y+ (DM) | | | III | 2.63 | | | 0.22 | | | -2.811 | Diskless | 4750.0 | 0.331 | 0.0010 | 0.12 | 1.909 |
| DM127 | | N | Y+ (DM) | | | III | -7.12 | | | 0.72 | | | -2.768 | Diskless | 3800.0 | 0.588 | 0.0030 | 0.52 | 0.116 |
| DM129 | | N | Y+ (DM) | | | III | -0.22 | | | 0.46 | | | -2.737 | Diskless | 5500.0 | 2.548 | 0.0070 | 0.72 | 0.995 |
| DM131 | | N | Y+ (DM) | | | III | -3.55 | | | 0.66 | | | -2.808 | Diskless | 3900.0 | 0.211 | 0.0010 | 0.28 | 0.145 |
| DM134 | | N | Y+ (DM) | | | ? | -2.36 | | | 0.53 | | | | – | 3900.0 | | | 0.63 | |
| DM135 | M3.5 | N | Y+ (DM, B09) | | | II | -4.76 | -3.299 | 0.127 | 0.64 | 0.518 | 0.081 | -1.794 | Thick | 4400.0 | | | 0.98 | |
| DM135 | M2 | N | Y+ (DM, B09) | | | II | -4.76 | -6.804 | 0.121 | 0.64 | | | -1.794 | Thick | 4400.0 | | | 0.98 | |
| DM136 | M2.5 | Y | Y+ (DM, B09) | -10.95 | | II | -15.05 | -18.334 | 0.978 | 0.5 | | | -1.449 | Thick | 3750.0 | | | 0.47 | |
| DM138 | | Y | Y+ (DM) | | | II? | -12.18 | | | 0.53 | | | | – | 3900.0 | | | 0.63 | |
| DM142 | | N | Y+ (DM) | | | III | 0.41 | | | 0.48 | | | -2.654 | Diskless | 4750.0 | 2.364 | 0.018 | 0.72 | 1.786 |
| DM143 | M0 | Y | Y+ (DM, B09) | -9.869 | 0.04 | I/II | -4.74 | -10.322 | 0.101 | 0.45 | 0.773 | 0.13 | -0.34 | Thick | 3500.0 | | | 0.28 | |

Continued on next page…

Table 5.9 – Continued

| Object | SpT | Accret. | Membership | log($\dot{M}_{acc}$)($M_\odot$/yr)[4] | | Class[6] | EW(H$\alpha$)[1] | EW(H$\alpha$)[2] | | EW(Li)[1] | EW(Li)[2] | | $\alpha$ Slope | Disk Type | $T_{eff}$ | $L_{bol}$ | | $Mass_{Teff}$ | $A_V$ |
|---|---|---|---|---|---|---|---|---|---|---|---|---|---|---|---|---|---|---|---|
| DM143 | | Y | Y+ (DM, B09) | -9.858 | 0.987 | I/II | -4.74 | -4.934 | 0.719 | 0.45 | 0.299 | 0.056 | -0.34 | Thick | 3500.0 | | | 0.28 | |
| DM143 | M5 | N | Y+ (DM, B09) | | | I/II | -4.74 | -7.959 | 0.484 | 0.45 | | | -0.34 | Thick | 3500.0 | | | 0.28 | |
| DM147 | | N | Y+ (DM) | | | III | -2.57 | | | 0.56 | | | -2.714 | Diskless | 3750.0 | 0.592 | 0.0030 | 0.63 | 0.116 |
| DM149 | | N | Y+ (DM) | | | III | 14.2 | | | 0.2 | | | -2.783 | Diskless | 4500.0 | 0.461 | 0.0020 | 0.63 | 0.285 |
| DM150 | | N | Y+ (DM) | | | III | -0.83 | | | 0.62 | | | -2.856 | Diskless | 4000.0 | 0.255 | 0.0020 | 0.98 | 0.116 |
| DM151 | | N | Y+ (DM) | | | II | 1.03 | | | 0.27 | | | -1.777 | Thick | 4800.0 | | | 1.18 | |
| DM152 | | N | Y+ (DM) | | | II | -4.32 | | | 0.51 | | | -0.604 | Thick | 3800.0 | | | 0.52 | |
| DM153 | | Y | Y+ (DM, B09) | -8.107 | 0.364 | II | -15.04 | -16.644 | 0.987 | 0.43 | 0.306 | 0.06 | -0.94 | Thick | 3750.0 | | | 0.47 | |
| DM153 | M1 | Y | Y+ (DM, B09) | -7.63 | 0.436 | II | -15.04 | -14.133 | 1.818 | 0.43 | 0.527 | 0.059 | -0.94 | Thick | 3750.0 | | | 0.47 | |
| DM153 | K9 | Y | Y+ (DM, B09) | -6.836 | 0.374 | II | -15.04 | -16.892 | 0.544 | 0.43 | | | -0.94 | Thick | 3750.0 | | | 0.47 | |
| DM154 | | N | Y+ (DM) | | | III | -5.3 | | | 0.75 | | | -2.565 | Diskless | 4000.0 | 0.176 | 0.0020 | 0.91 | 0.116 |
| DM157 | | N | Y+ (DM) | | | ? | -7.88 | | | 0.63 | | | | – | 3750.0 | | | 0.47 | |
| DM158 | | N | Y+ (DM, B09) | | | II | -1.05 | -0.975 | 0.087 | 0.5 | 0.479 | 0.058 | -1.105 | Thick | 3750.0 | | | 0.47 | |
| DM158 | M0 | N | Y+ (DM, B09) | | | II | -1.05 | -1.495 | 0.284 | 0.5 | 0.533 | 0.074 | -1.105 | Thick | 3750.0 | | | 0.47 | |
| DM158 | M0 | N | Y+ (DM, B09) | | | II | -1.05 | -0.581 | 0.065 | 0.5 | | | -1.105 | Thick | 3750.0 | | | 0.47 | |
| DM160 | | N | Y+ (DM) | | | II | -7.99 | | | 0.41 | | | | Thick | 4800.0 | 5.416 | 0.028 | 0.72 | 4.95 |
| DM161 | | Y | Y+ (DM) | | | III | -16.62 | | | 0.61 | | | -2.886 | Diskless | 3500.0 | 0.442 | 0.0030 | 2.06 | 0.116 |
| DM164 | | N | Y+ (DM) | | | III | -3.17 | | | 0.67 | | | -2.779 | Diskless | 3800.0 | 0.256 | 0.0010 | 0.23 | 0.116 |
| DM165 | M2 | N | Y+ (DM, B09) | | | II | -3.49 | -2.845 | 0.08 | 0.67 | 0.56 | 0.093 | -1.502 | Thick | 3600.0 | | | 0.35 | |
| DM165 | M3 | N | Y+ (DM, B09) | | | II | -3.49 | -1.824 | 0.043 | 0.67 | | | -1.502 | Thick | 3600.0 | | | 0.35 | |
| DM166 | | Y | Y+ (DM, B09) | -6.936 | 0.155 | II | -88.7 | -37.18 | 0.989 | 0.43 | 0.209 | 0.011 | -1.536 | Thick | 5200.0 | | | 1.39 | |
| DM166 | M0 | Y | Y+ (DM, B09) | -6.771 | 0.519 | II | -88.7 | -111.729 | 1.163 | 0.43 | 0.411 | 0.051 | -1.536 | Thick | 5200.0 | | | 1.39 | |
| DM168 | | N | Y+ (DM) | | | III | -8.25 | | | 0.59 | | | -2.724 | Transition | 4400.0 | | | 0.98 | |
| DM169 | | N | Y+ (DM) | | | III | -1.1 | | | 0.6 | | | -2.668 | Diskless | 4200.0 | 1.227 | 0.0050 | 0.72 | 0.116 |
| DM172 | M3 | Y | Y+ (DM, B09) | -9.936 | 0.387 | II | -36.51 | -88.416 | 0.804 | 0.63 | 0.699 | 0.24 | -0.925 | Thick | 4200.0 | | | 0.88 | |
| DM173 | M3.75 | Y | Y+ (DM, B09) | -11.43 | | II | -30.27 | -13.466 | 0.177 | 0.57 | 0.36 | 0.096 | -1.557 | Thick | 4250.0 | | | 0.91 | |
| DM174 | M0 | Y | Y+ (DM, B09) | -8.157 | 0.741 | II | -36.83 | -16.079 | 0.675 | 0.65 | 0.508 | 0.016 | -1.446 | Thick | 4250.0 | | | 0.91 | |
| DM175 | | N | Y+ (DM) | | | III | -5.06 | | | 0.77 | | | -2.536 | Diskless | 4000.0 | 0.461 | 0.0040 | 0.88 | 0.116 |
| DM176 | | N | Y+ (DM) | | | III | -0.44 | | | 0.47 | | | -2.762 | Diskless | 4000.0 | 0.864 | 0.0040 | 1.31 | 0.116 |
| DM177 | | N | Y+ (DM) | | | III | -4.15 | | | 0.62 | | | -2.819 | Diskless | 4000.0 | 0.376 | 0.0020 | 0.72 | 0.116 |
| DM90 | | Y | Y+ (DM) | | | II? | -36.74 | | | 0.54 | | | | – | 3900.0 | | | 0.63 | |
| DM99 | | Y | Y+ (DM) | | | ? | -22.88 | | | 0.61 | | | | – | 3800.0 | | | 0.52 | |

[1] Measurement from Dolan & Mathieu (1999, 2001)

[2] Measurement from this work.

# Chapter 6

# Conclusions

## 6.1 Collinder 69

We have analyzed ~160 optical and near infrared spectra with a wide range of resolutions of candidate members to the Collinder 69 cluster. Based on different criteria regarding molecular bands absorptions we have provided spectral types for all the sources. Using alkali lines as youth indicators we have confirmed 90 members (and 9 possible members). For those sources of our survey overlaping with radial velocities surveys (by Sacco et al. 2008; Maxted et al. 2008) we obtain very similar results regarding membership.

A summary of the sources analyzed in this cluster can be found in Table 3.25.

For those sources showing large H$\alpha$ equivalent widths (larger than the one expected to arise from chromospheric activity) we have derived accretion rates using mainly the full width at 10% of the flux of the H$\alpha$ emission line (but also the Ca II IRT) obtaining values compatible with those previously reported in the literature for objects of similar mass and age (Mohanty et al. 2005; Natta et al. 2006).

We have studied the accretion and disk evolution of the confirmed members of Collinder 69. In Fig. 3.30 we show the spatial distribution of the confirmed members (either by Dolan & Mathieu 1999, 2001; Sacco et al. 2008; Maxted et al. 2008 or this work) including information about the presence of disk and whether the disk is accreting or not. As can be seen in the figure, the sources with disk show a higher concentration towards the center of the cluster with respect to the diskless population (contrary to what one would expect according to the supernove scenario). In fact, if we assume that actively accreting systems are younger than those which do not show sign of accretion, the youngest population of Collinder 69 is clearly concentrated around the central O population.

With the data from our SUBARU campaign we have confirmed the cool nature of the **the lowest mass candidate members to Collinder 69** reported so far. With derived spectral types L0-L2 corresponding to effective tempetartures of ~ 2000 K (according to the spectroscopic temperature scales derived by Basri et al. 2000), if members, they have estimated masses, following

the 5 Myr DUSTY isochrone by Chabrier et al. 2000, as low as 0.012 $M_{\odot}$ (~12.6 $M_{Jupiter}$).

## 6.2 Barnard 35

We have analyzed ~60 optical spectra from known members and candidate members to the dark cloud Barnard 35. With different criteria based on line and molecular bands strengths, we have derived spectral types for all of them. By studying youth indicators we have confirmed as new members 18 sources and discarded eight.

We have analyzed the variability of the accretion rate of a subset of our sample of sources finding a large amplitude in the variations that do not appear to be correlated with the mass of the central star.

We have derived accretion rates for three sources harbouring so-called transition disks that agree with the few measurements of such disks that have been reported so far.

We have compared the evolutionary status of the disks around sources in Barnard 35 and those of Collinder 69 finding a very significant behaviour; being the latter diks much less active than those studied around members belonging to Barnard 35.

## 6.3 Barnard 30

We have analyzed 64 optical spectra at different resolutions corresponding to 45 sources: 13 known members to Barnard 30 (from Dolan & Mathieu 2001) and 32 candidate members from Morales-Calderón (2008). The previously known members were observed in order to study their variability (especially the accretion rate) and try to place these variations in context with the age and mass of the sources. The sample of candidate members was observed in order to confirm their membership to the dark cloud and study their properties. Fourteen from these candidates were confirmed as new members based on the intensities of several alkali lines.

The analysis of the presence of accretion in confirmed members known to harbour disks (based on their mid-infrared excesses) led to the preliminar idea that Barnard 30 might not be younger than Barnard 35 (as suggested in the literature). The sample of studied members should be enlarged and some bias should be removed for this suggestion to be confirmed.

Regarding the variability; most of both, accreting and non-accreting sources would be classified variable according to the comparison of our own measurements of the H$\alpha$ emission and those from Dolan & Mathieu (2001). In fact, accreting sources seem to show larger amplitudes that translate in very large differences in the estimated accretion rates (the largest difference measured arrives to 2.5 orders of magnitude). These large differences have already been reported in the literature on more massive sources. We do not see any dependence of these variations with the stellar mass, although our sample is not significatively large enough to arrive to any definite conclusion. The same behaviour has been observed among the Barnard 35 sample.

# Chapter 7

# Conclusiones

## 7.1 Collinder 69

Hemos analizado alrededor de 160 espectros de candidatos a miembros de Collinde 69 en los rangos del óptico y el infrarrojo cercano con una amplia diversidad de resoluciones. Basándonos en diversos criterios que conciernen el estudio de bandas moleculares, hemos estimado los tipoes espectrales de estas fuentes. Usando líneas de alcalinos como indicadores de juventud, hemos confirmado 90 miembros y 9 posibles miembros de este cluster. Para aquellas fuentes de nuetro estudio que han sido analizadas también en trabajos basados en el cálculo de velocidades radiales (por Sacco et al. 2008; Maxted et al. 2008) obtenemos resultados muy similares de pertenencia al cúmulo.

Para aquellas fuentes que mostraban grandes anchuras equivalentes de H$\alpha$ (mayor de la que se esperaría poder atribuir a la actividad cromosférica), hemos derivado tasas de acrecimiento usando principalmente la anchura al 10% del flujo de la l'ınea de emisión de H$\alpha$ (pero también el triplete infrarrojo del calcio), obteniendo valores compatibles con otros previamente publicados en la literatura para objetos de edad y masa similares (Mohanty et al. 2005; Natta et al. 2006).

Hemos estudiado el acrecimiento y la evolución de los discos en los miembros confirmados de Collinder 69. En la Figura 3.30 mostramos la distribución espacial de los miembros confirmados (bien por Dolan & Mathieu 1999, 2001; Sacco et al. 2008; Maxted et al. 2008 o por este trabajo) incluyendo información sobre la presencia de disco y si éste se encuentra cativamente acretando o no. Como se puede ver en la figure, las fuentes con disco muestran una mayor concentración en torno al centro del cluster con respecto a la población sin disco (contrariamente a lo qeu cabría esperar según la hipoótesis de la explosión de supernova). De hecho, si asumimos que los sistemas que están acretando son en general más jóvenes que aquellos que no muestran signos de acrecimiento, la población más joven de Collinder 69 estaría claramente concentrada alrededor de la población central O.

Con datos de nuestra campaña en SUBARU hemos confirmado la naturaleza extremadamente fría de **los candidatos de masa más baja** propuestos a formar parte de Collinder 69. Con

tipos espectrales derivados entre L0 y L2, les corresponden temperaturas efectivas ~ 2000 K (usando en esta estimación la escala de tempertauras derivada por Basri et al. 2000). Si se confirmaran como miembros, tendrían masas (según la isocrona de cinco millones de años de Chabrier et al. 2000) tan bajas como 0.012 $M_{\odot}$ (~12.6 $M_{Jupiter}$).

## 7.2 Barnard 35

Hemos analizado ~60 espectros ópticos, principalmente de resolución baja–intermedia de candidatos a miembros de la nube obscura Barnard 35. Siguiendo distintos criterios basados en cocientes de líneas y fuerza de bandas moleculares, hemos derivado tipos espectrales para todos ellos. Estudiando indicadores de juventud hemos confirmado como nuevos miembros 18 de estos candidatos y hemos descartado ocho como contamiantes.

Hemos analizado la variabilidad en la tasa de acrecimiento de un subconjunto de nuestros candidatos, encontrando una gran amplitud en estas variaciones que no parece estar correlacionada con la masa del objeto central.

Hemos derivado tasas de acrecimietno para tres fuentes que albergan discos de transición. Las tasas derivadas som compatibles con las pocas medidas que se han porporcionado hasta ahora para este tipo de objetos.

Hemos comparado el estado evolutivo de los discos entorno a fuentes de Barnard 35 y aquellas de Collinder 69 encontrando una tendencia muy marcada; los discos que rodean a objetos de Collinder 69 parecen ser en término general mucho menos activos que aquellos que rodean a miembros de Barnard 35.

## 7.3 Barnard 30

Hemos analizado 64 espectros ópticos con distintas resoluciones correspondientes a 45 fuentes: 13 son miembros conocidos de Barnard 30 (de Dolan & Mathieu 2001) y 32 son nuevos candidatos propuestos por Morales-Calderón (2008). Los miembros conocidos preciamente fueron observados para estudiar su variabilidad (especialmente en lo que refiere a la tasa de acrecimiento) y tratar de poner estas variaciones en contexto junto con la edad y la masa de las fuentes. Por otro lado, el conjunto formado por los candidatos propuestos por Morales-Calderón (2008) fueron observados para confirmar la pertenencia a Barnard 30 y estudiar sus propiedades. Catorce de estos candidatos han sido confirmados en base a las intensidades de determinadas líneas de alcalinos.

El analisis sobre la presencia de acrecimiento en miembros ya conocidos que sabemos están rodeados por discos (basándonos en el exceso infrarrojo que presentan estas fuentes) nos condujo a una teoría muy preliminar que sugiere que Barnard 30 no parece ser más joven que Barnard 35 (como se ha sugerido previamente en la lieteratura). El conjunto de miembros estudia-

dos debería de crecer y algunos sesgos referentes a la selección de candidatos deberían de tenerse en cuenta antes de que esta sugerencia pueda ser confirmada.

En cuanto a la variabilidad; la mayor parte de objetos, ya sean acretores activos o no, han sido clasificados como variables según la comparación de nuestras propias medidas de la emisión de H$\alpha$ y aquellas de Dolan & Mathieu (2001). De hecho, Las fuentes que están acretando, parecen mostrar mayores amplitudes en estas variaciones que se traducen en inmensas variaciones en las tasas de acrecimiento estimadas (la mayor diferencia medida en nuestro conjunto llega a los 2.5 órdenes de magnitud). Estas diferencias tan grandes ya han sido anunciadas en la literatura en objetos de mayor masa. De acuerdo con nuestros datos, no se infiere ninguna dependencia de estas variaciones con la masa del objeto central, aunque nuestra muestra parece ser demasiado pequeña como para poder llegar a una conclusión definitiva. La misma falta de dependencia con la masa del objeto central se observa en la muestra de objetos de Barnard 35.

**200**

# List of publications

The work done during this thesis has given rise to the following publications in international refereed journals:

Papers in refereed journals

1. *The young, wide and very low mass visual binary Lambda Orionis 167*. D. Barrado Y Navascués, **A. Bayo**, M. Morales-Calderón, N. Huélamo, J. R. Stauffer, and H. Bouy. A&A, 468:L5–L8, June 2007.

2. *Spitzer: Accretion in Low-Mass Stars and Brown Dwarfs in the $\lambda$ Orionis Cluster*. D. Barrado y Navascués, J. R. Stauffer, M. Morales-Calderón, **A. Bayo**, G. Fazzio, T. Megeath, L. Allen, L. W. Hartmann, and N. Calvet. ApJ, 664:481–500, July 2007.

3. *VOSA: virtual observatory SED analyzer. An application to the Collinder 69 open cluster*. **A. Bayo**, C. Rodrigo, D. Barrado Y Navascués, E. Solano, R. Gutiérrez, M. Morales-Calderón, and F. Allard. A&A, 492:277–287, Dec. 2008.

4. *Structural and compositional properties of brown dwarf disks: the case of 2MASS J04442713+2512164*. H. Bouy, N. Huélamo, C. Pinte, J. Olofsson, D. Barrado y Navascués, E. L. Martín, E. Pantin, J.-L. Monin, G. Basri, J.-C. Augereau, F. Ménard, G. Duvert, G. Duchêne, F. Marchis, **A. Bayo**, S. Bottinelli, B. Lefort, and S. Guieu. A&A, 486:877–890, Aug. 2008.

5. *A deep look into the core of young clusters. II. lambda-Orionis*. H. Bouy, N. Huélamo, D. Barrado y Navascués, E. L. Martín, M. G. Petr-Gotzens, J. Kolb, E. Marchetti, M. Morales-Calderón, **A. Bayo**, E. Artigau, M. Hartung, F. Marchis, M. Tamura, M. Sterzik, R. Koehler, V. D. Ivanov, D. Nuernberger. A&A, Accepted, Jul. 2009.

6. *A proto brown dwarf candidate in Taurus*. D. Barrado y Navascués, M. Morales-Calderón, A. Palau, **A. Bayo**, I. de Gregorio, C. Eiroa N. Huélamo, H. Bouy, O. Morata. A&A, Accepted, Sept. 2009.

# Appendix A

# Observations and data reduction

During this thesis we have performed optical and near-infrared observations with the following configurations:

## A.1 Medium and high-resolution optical spectroscopy

1. **LRIS, Low Resolution Imaging Spectrometer,** at Keck I telescope in November 2-5, 2002. We made use of the LRIS spectrograph with the 1200 lines/mm grating., covering the spectral range 6425–7692 Å, with a scale of 0.63 Å/pixel and a resolution of about 2 Å, as measured in a NeHe comparison lamp (about R∼3500 at $\lambda$=7000 Å). Individual exposure time ranges from 120 to 1200 seconds. We took three of these exposures and combine them in order to improve the signal-to-noise and to remove cosmic rays. Note that during the same run we colected low-resolution spectra, which will be described below.

2. **MIKE, Magellan Inamori Kyocera Echelle,** at the Magellan Baade 6.5m telescope in December 11–14, 2002. With our set-up, the spectral coverage in its red arm was 4430–7250 Å. In order to improve the final S/N, we degraded the resolution by rebinning the original data during the readout to 2 and 8 pixels in the spatial and spectral directions, respectively, achieving a resolution of 0.55 Å. To reconstruct the spectra we have used the *getchelle* routine by Carlos Allende `ttp://`ebe.as.utexas.edu/stools/

3. **B&C, Boller & Chivens spectrograph,** at the Magellan II telescope (Las Campanas, Chile) in March 9–11, 2003. We made use of the B&C spectrograph with the 1200 l/mm grating . The spectral coverage was 6200-7825 Å, with a scale of 0.79 Å/pixel, and a resolution of 2.5 Åas measured in a HeNeAr comparison lamp (R∼2600)

4. **FLAMES, Fibre Large Array Multi Element Spectrograph,** at VLT/UT2 in January 5, 2008. The data reduction was performed using the GIRAFFE gir–BLDRS pipeline vers.

1.12, following the standard steps which include bias subtraction, division by a normalized flat-field, correction for the differences in the fiber transmission, and wavelength calibration using a dispersion solution from a Thorium-Argon arc lamp. The spectra processed by the pipeline are not corrected for instrumental response and sky background, but all measurements were performed after subtracting a sky background spectrum (see Section 3.3.4 for further details on the implications inour measurements of the sky substraction).

5. **Hamilton Spectrograph,** at the 3m Shane telescope at the Lick Observatory in December 5–7, 2006. The data reduction was performed using the Hamilton starndard pipeline on site. This pipeline follows the standard steps which include bias subtraction, division by a normalized flat-field, sky substraction, and wavelength calibration using a dispersion solution from a Thorium-Argon arc lamp.

## A.2 Low resolution Optical spectrocopy

1. **LRIS, Low Resolution Imaging Spectrometer,** during the previiosly mentioned run in November 2-5, 2002. We made use of the 400 l/mm grating with a one arcsec slit. Typical integration times were 300–900 seconds. The wavelength calibration is better than 0.4 Å, the spectral coverage is 6250–9600 Åand the resolution is R∼1100 (6.0 Åaround H$\alpha$), as measured in a NeAr lamp. The data were processed within the IRAF environment in a standard way.

2. **B&C, Boller & Chivens spectrograph,** also during the run in March 9–11, 2003 at the Magellan II telescope. We used the 300 l/mm grating; this way, the Magellan spectra have slightly worse resolution and larger spectral range (R∼800, 5000–10200 Å). Relative flux calibration for the spectra was derived using observations obtained of several spectrophotometric standards. The reduction was carried out in a similar way as in the case of the Keck sample.

3. **CAFOS, Calar Alto Faint Object Spectrograph,** we had several runs at Calar Alto using the CAFOS spectrograph during 2006 and 2007 (see Tables 3.5, 4.2 and 5.2 for details on the specific dates). The data were processed within the IRAF environment in a standard way.

4. **TWIN,** we had several runs at Calar Alto using the TWIN spectrograph during 2006 and 2007 (see Tables 3.5, 4.2 and 5.2 for details on the specific dates). In every run we used the T-13 grating and only the data coming from the red arm were processed. The data reduction was performed within the IRAF environment in a standard way.

5. **Kast Spectrograph,** at the 3m Shane telescope at the Lick Observatory in January 17-18, 2008. We used the grating number 4 providing a reolution of ∼5000 at 6000 Å. The data

reduction was performed within the IRAF environment in a standard way.

## A.3 Low resolution Near Infrared spectrocopy

1. **SOFI, Son of ISAAC,** at NTT (La Silla, Chile) in April 25–27 2006. We used two low-resolution grisms (red and blue) to roughly cover the *JHK* bands on a Hawaii HgCdTe 1024×1024 detector with a plate scale of 0.292″/pix. The blue grism covers 0.95–1.63 $\mu$m and the red grism the region between 1.53–2.52 $\mu$m. The corresponding spectral resolutions were 930 and 980 respectively.

   The integration time and the number of exposures per target were chosen according to the brightness of the individual sources . In most cases we obtained a total of two blue spectra of the same integration time, and four red spectra. Typical individual integration times were 60–180 s for the blue grism and 60–240 s for the red one for the brightest sources of the sample and up to 3600 s (for each grism) for the faintest. The telescope was nodded 30″ along the slit between consecutive positions following the usual ABBA pattern.

   In addition to the program sources we observed several A0V objects (taken with airmasses similar to those of the science objects). These spectra were used (combined with a high-resolution model of Vega) to remove telluric water absorption bands as described by Vacca et al. (2003), and to estimate the instrumental response.

   We obtained multiple flat-field images, with both grisms, illuminating a dome screen, using incandescent lamps on and off. A xenon lamp provided the wavelength calibration for our data (consistent with the OH airglow calibration) with an accuracy of 1.2 Å for the blue grism, and 2 Å for the red one (corresponding to 1/5 of the size of the pixel).

   To reduce the data we used IRAF. We subtracted one image from another (using pairs of nodded observations) to eliminate the background and sky contribution in a first approximation. This subtraction automatically took care of the dark current and bias level. We flat-fielded our data dividing by the appropriate normalized flat-field for each of the grisms, and bad pixels were replaced by linear interpolation from neighbouring pixels.

   We aligned individual exposures and combined the corresponding frames into one blue and one red image per object. Then we shifted all the data, corresponding to each target and grism, to a common position and co-added them.

   We used the *twodspec* task APALL to trace and extract the spectra. A further sky subtraction was done by fitting a polynomial to the regions on both sides of the aperture. A non-linear low-order fit to the lines of the xenon lamp was used to calibrate the spectra in wavelength. We verified our wavelength solution using the positions of well known OH sky lines (Oliva & Origlia 1992) finding differences lower than 0.5 Å.

We finally combined the blue and the red grism spectra for each object and eliminated regions of deep atmospheric absorptions from our analysis as not satisfactory corrections were obtained in these regions. The useful spectral ranges are: 9300–11000 Å, 11600–13300 Å, 14900–17800 Å, and 20500–25000 Å, with some edge effects at the very beginning and very end of the first an last intervals, respectively. To test the flux calibration, we have computed synthetic magnitudes applying the normalized relative spectral response (from Cohen et al. 2003) to the calibrated spectra; and we have compared them to the magnitudes given in the 2MASS catalogue. We have obtained differences of less than 10% in flux, which are equivalent to $\sim 0.1$ mag. In Fig. A.1 we can see our calibrated spectra (black solid lines), the photometry from 2MASS (red circles) and the synthetic calculated photometry (blue triangles). The deep atmospheric absorptions regions have been removed from the spectra and are shown as shadowed grey rectangles in the figures.

2. **NIRSPEC, the Near InfRared echelle SPECtrograph,** at Keck II (Mauna Kea observatory) in December 22–23 2004 and December 9 2005. In both campaigns we used the same filter: Nirspec-3, a J band filter covering the wavelength region 1.143-1.375 $\mu$m. The corresponding spectral resolution is ∼2000. Again, classical ABBA pattern was followed to perform the observations, and standard A0V were observed at simmilar air masses to correct the terrestrial atmospheric signatures. In this case, the data reduction process was carried out using the IDL based software REDSPEC.

   This software performs all the previously described procedures in an pseudo-automatic (some interactivity with the user is required) manner. In this case we did not scale our spectra using sinthetic photometry since our analysis was focussed on the study of the alkali lines, and therefore the spectra were normalized.

3. **IRCS, the InfraRed Camera and Spectrograph,** at SUBARU (NAOJ, Mauna Kea observatory) in November 10 2008. We used the "Grism HK" covering a wavelength range of 1.4–2.5 $\mu$m at a very low resolution of ∼200. The spectra of the science targets, spectral templates and A0V "standards" were obtained following an ABBA pattern. The reduction of the data was performed using IRAF and following the steps described in detail for the NTT campaign.

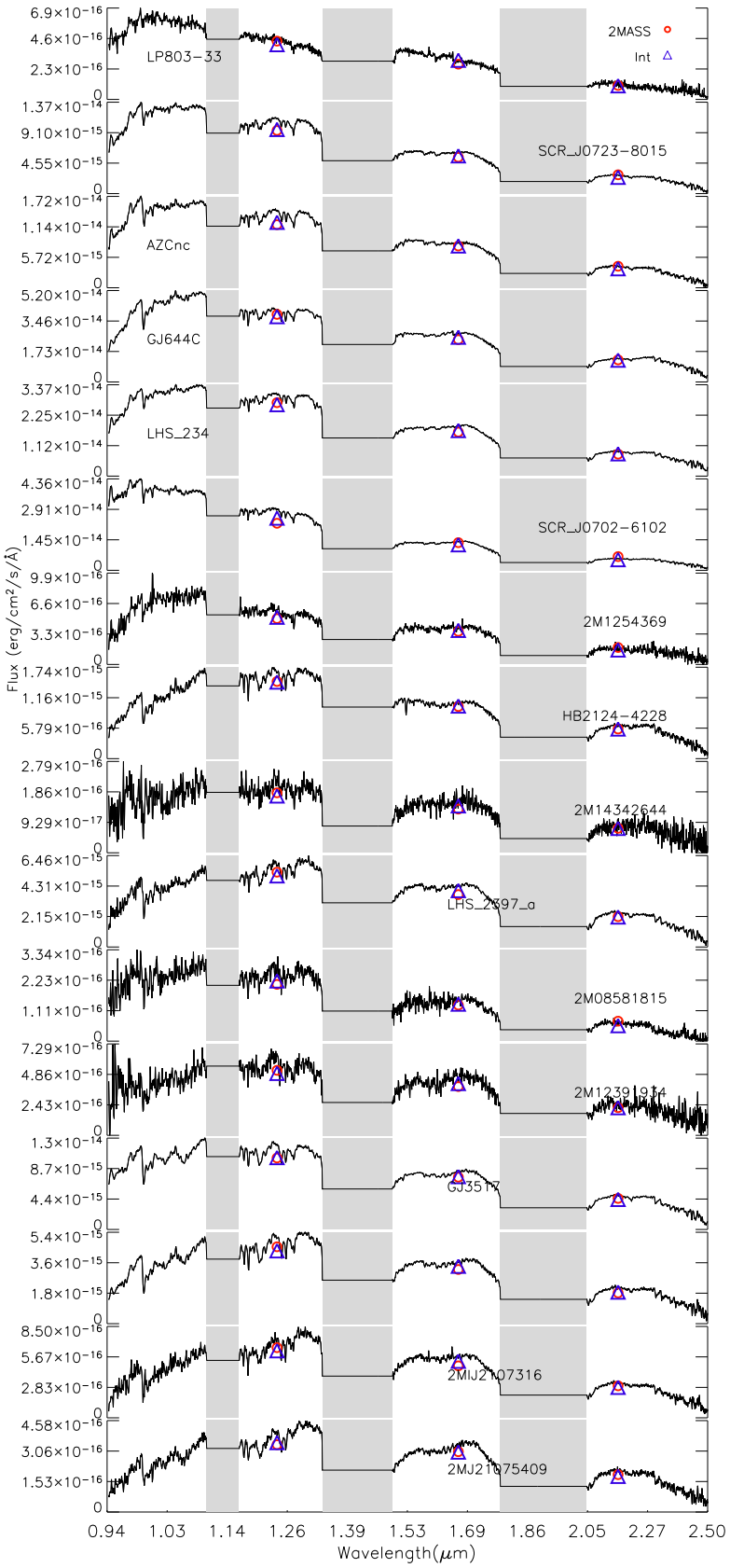


**Figure A.1**: Spectrophotometry of the sample of field targets. The sequence is ordered in terms of the spectral type assigned in the literature (see Table **??**).

# Appendix B

# Automating the measurement of line properties.

In short; one of the most difficult steps to automate when measuring line properties is the determination of the continuum on top of which the line lies. Even when this task is performed manually, different astronomers might select different points as the bases of the continum when, for example, facing a noisy spectrum or a line embeded in a molecular band. The code that we have developed tries to solve this problem proceeding in an iterative way.

First of all it locates where the actual peak of the line is; in this step the wavelength calibration accuracy is taken into account providing limits in the wavelength coverage where the search for the peak of the line is carried out. Once this task is accomplished, two regions are defined: one to the right and another to the left of the estimated central wavelength; the width of the regions is fixed to 100 points to be statistically significant (and therefore the width in wavelength units would depend on the resolution of the spectra). A linear fit using those regions is performed (red dotted line in Fig B.1). With this attempt to define a continiuum (the linear fit), the code calculates a first guess of the FWHM (red cross in Fig B.1).

For the second iteration, the code considers that the line is a gaussian, and, therefore, FWHM $= 2 \times \sqrt{2 \times \log(2)} \times \sigma$. Assuming that at a distance of $\pm 10\sigma$ one should be outside the line, two new regions on the spectra are selected: starting at $\pm 10\sigma$ from the wavelength of the peack and ending at the same limits as before. These two regions are close to the edges of the line unless the line has a very wide double peaked structure.

At this point the code will perform two linear fits in a sequential way; a second continuum is derived with a linear fit to these new regions of the spectra close to the edges of the line, and the third one with another lineal fitting, but this time considering only those data-points that differ from the second continuum less than once the dispersion of the difference between the actual spectra and this second continuum (the blue dots in Fig B.1 represent those data-points considered to define a third continuum and the blue dashed line is the resulting one).

Once the third guess on the locus of the continuum is estimated, the code calculates a second iteration of the FWHM (blue cross in Fig B.1). Assuming one more time that the line can be described with a gaussian (and calculating the associated $\sigma$), it considers three pairs of lambdas in the spectra to make the final measurements (pairs located at $\pm 3\sigma$, $\pm 4\sigma$ and $\pm 5\sigma$ from the lambda of the peak). As a final refinement, for each selected pair of wavelengths; for example $\lambda_1$ and $\lambda_2$ corresponding to $\lambda_{peak} \pm 3\sigma$ the code checks whether the linear continuum defined by ($\lambda_1$,F($\lambda_1$)), ($\lambda_2$,F($\lambda_2$)) intersects the wings of the line; when this is the case (for example the upper-left pannel of Fig B.1), the code will use the third continuum to perform the measurements.

Prior to provide these measururements, the code substracts the instrumental profile from the values estimated for the FWHM and $FW_{10\%}$ considering that the FWHM of the convolution ($G_{measured}$) of two gussians ($G_{instr}$, $G_{line}$) follows:

$$FWHM(G_{measured}) = \sqrt{FWHM(G_{instr})^2 + FWHM(G_{line})^2} \tag{B.1}$$

and that FWHM and $FW_{10\%}$ relate accordig to: $FW_{10\%} = \sqrt{\frac{\log(2)}{\log(10)}} \times FWHM$.

The final product is the mean of the three measurements for each parameter (FWHM, $FW_{10\%}$ and EW) and their corresponding standard deviation $\sigma$.

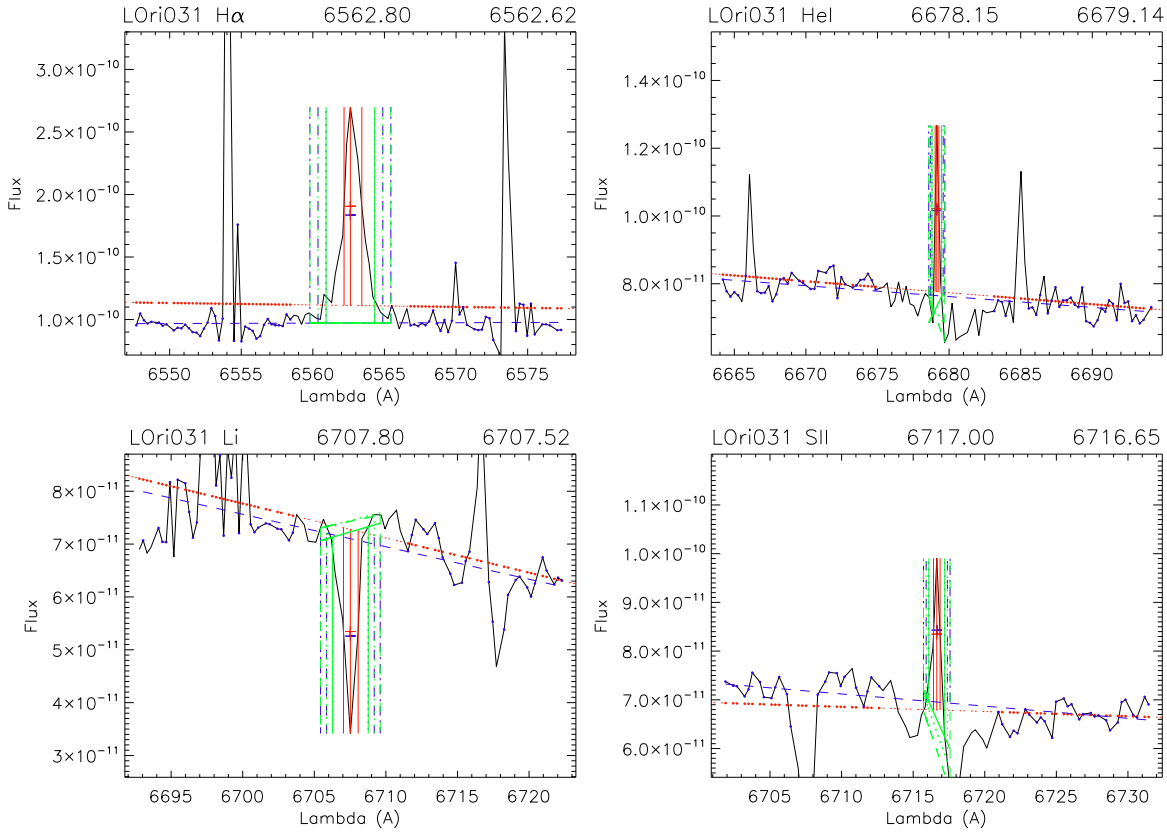


**Figure B.1**: Example of the output of the code designed to measure EW, FWHM and $FW_{10\%}$ of the different lines detected on the spectra in an automatic manner. In this case we show four of the measured lines on the averaged MIKE spectra obtained for LOri031: H$\alpha$ at 6562.80Å, He I at 6678.15Å, Li I at 6707.8Åand S II at 6717.0Å. For each case the canonical wavelength for the measured line and the actual wavelength where the line has been found in our spectra are displayed o the title of the plot (all of them within the errors on wavelength calibration). The iterative process in the continiuum determination is diplayed using different colours: red for the first iteration (including the first guess for the half maximum flux value, red cross), blue for the second one (filled blue dots on the datapoints used to refine the first continiuum, blue cross showin the second half maximum estimation) and the three green lines (filled, dotted and dashed) representing the final determined continuum.

# Appendix C

# Virtual Observatory SED Analyser

Studying the physical parameters of a large population of sources belonging to the same cluster is advantageous, since properties can be infered not only for individual sources but also for the association as a whole, a clear example is the age, since we can assume that all objects in that particular cluster are coeval.

Whenever an astronomer wants to derive physical parameters and properties by comparing observed SEDs with theoretical data, a first mandatory step is to compile all the photometric/spectral information available for each source in order to be able to decide which model best reproduces the observed data. On the other hand, there are different collections of models (consisting of thousands of individual models) that we might want to compare to the observations.

Trying to compile all this information for each object one by one with classical methodologies and then compare the built SED with all the available models can be very tedious and time consuming. VOSA (VO Sed Analyzer) is a tool designed to ease this processes by performing the following tasks in an automatic manner:

- Read user photometry-tables. The input file can be either an ASCII table or a VOTable but with a specific format consisting of eight columns/fields as follows:

  **Source identifier**: this will be used, for instance, as the title of the plots of the fittings.

  **Coordinates of the source**: Right ascension and declination (in J2000) will be used to look for counterparts in various catalogs.

  **Distance to the source in parsecs**: this datum is mandatory in order to estimate the bolometric luminosity of the source. Should this parameter be unknown then a value of "– – –" should be used and a generic distance of 10 parsecs will be assumed.

  **Visual extincion** ($A_V$ in magnitudes) affecting the source: this value is used to deredden each SED (the Indebetouw et al. 2005 extinction law is applied).

**Filter name**: a list of the already available filters can be found in the Help menu; new filters can be included upon user request.

**Observed flux/magnitude** (flux in units of erg/cm$^2$/s/Å).

**Flux/magnitude error** (same units as in the previous field). For an example of the data input interface see Fig. C.2 in Appendix B. A more detailed description of the file format, available filters, fluxes for zero magnitude, etc. can be accessed from the VOSA Help menu.

- Query several photometrical catalogs accessible through VO services in order to increase the wavelength coverage of the data to be analysed. Currently the user can query the 2MASS All-Sky Point Source Catalog (Skrutskie et al. 2006), the Tycho-2 Catalog (Høg et al. 2000), and the Strömgren uvby-beta Catalog (Hauck & Mermilliod 1998) using different radii according to the astrometic precision of each catalog.

- Query VO-compliant theoretical models (spectra) for a given range of physical parameters.

  The user can choose among the different available collections of models (in a future implementation of the tool, it will offer the possibility of accessing any VO-compliant theoretical model collection). These models are accessible in a VO environment from the SVO theoretical data server at `http://laeff.inta.es/svo/theory/db2vo/`

- Calculate the synthetic photometry of the theoretical spectra (within the range of physical parameters required by the user) for the set of filters used to obtain the observed data (including the dataset coming from the VO photometrical services).

  The synthetic photometry is calculated by convolving the filter response curve with the synthetic spectra. Prior to this, both the response curve and the synthetic spectra are interpolated to match the spectral resolution; the area of the response curve is normalised to unity to provide the user with a flux density that can be directly compared with the observed one (see Section C.1 for a formal description of the process).

- Perform a statistical test to determine which model reproduces best the observed data. The provided "best" fitting model is the one that minimises the value of the reduced $\chi^2$ defined as:

$$\chi^2_r \;=\; \frac{1}{N-n_p}\;\sum_{i=1}^{N}\left\{\frac{1}{\sigma^2_{o,i}}(Y_{o,i}-M_d\;Y_{m,i})^2\right\}$$

  where $Y_0$ is the observed flux, $\sigma_0$ the observational error in the flux, $N$ the number of photometric points, $n_P$ the number of parameters being fitted, $Y_{\rm m}$ the theoretical flux predicted by the model and $M_d$ the multiplicative dilution factor, defined as $(R/D)^2$, $R$ being the radius of the source and $D$ the distance to the object.

  During the fitting process, the tool detects possible infrared excesses (in our scientific case some of the sources might be surrounded by disks). Thus, since the theoretical spectra

correspond to stellar atmospheres, for the calculation of the $\chi^2$ the tool only considers those data points of the SED corresponding to bluer wavelengths than the one where the excess has been flagged.

The excesses are detected by iteratively calculating (adding a new data point from the SED at a time), in the mid-infrared (wavelengths redder than 2.5$\mu$m), the $\alpha$ parameter as defined in Lada et al. (2006) (which becomes larger than -2.56 when the source presents an infrared excess). The last wavelength considered in the fitting process together with the ratio between the total number of points belonging to the SED to those really used are displayed in the result tables.

Once the fitting process is completed, the tool allows the user to check whether any other of the five "best" fits per collection of models (meaning 20 best fits when using the four collections of models available on the server), is more convincing than the one that minimises the $\chi^2$ and choose that one as the best model to include in the final results table. For instance, the user might have a more accurate estimation of the gravity, which is important since changes in the surface gravity of stellar and sub-stellar sources do not produce dramatic differences in the shape of their SEDs (whenever those SEDs have been constructed using photometry from wide filters).

- Use the best-fit model as the source of a bolometric correction.

  The best fitting model is used to infer the total observed flux for each source of the sample; this process is performed by integrating the total observed flux (where no excess has been detected), and using the best fitting model to infer that flux in the wavelength range where no observational data is available or some infrared excess has been detected (see Appendix A for a formal description of the procedure). We note that if the model reproduces the data correctly, this estimation is much more accurate than the one obtained using a bolometric correction derived only from a single colour.

  Regarding the estimation of the error in the calculated "total observed flux", VOSA uses the model to infer the total flux emitted by the source in the wavelength range where no observational data is provided or some infrared excess has been detected; since we cannot provide any uncertainties for the model itself we have extrapolated the errors of the observed photometry to the whole wavelength range, and therefore we provide an error for the total flux parameter dependent on the accuracy of the provided measurements.

- Provide the estimated bolometric luminosity for each source.

  The tool scales the total observed flux to the distance given by the user and therefore estimates the bolometric luminosity of each source in the sample. In those cases where the user has not provided a value of the distance, a generic value of 10 parsecs is assumed:

$$L(L_{\odot}) = 4\pi D^2 \, F_{obs} \tag{C.1}$$

- Generate a Hertzsprung-Russel diagram with the estimated parameters.

  The tool provides the user with the possibility of selecting and overplotting in this diagram different sets of isochrones and evolutionary tracks with masses and ages within the selected range.

- Provide an estimation of the mass and age of each source

  VOSA interpolates among the previously mentioned collections of isochrones and evolutionary tracks to estimate the mass and age of each source from the input sample (see the Help menu from VOSA for details on the interpolation processes and possible warning flags).

In order to use VOSA, the user only has to register at the service and start working. The system is based on sessions that can be saved, so that the user can recover the files and results obtained in a previous session (without redoing the fit) and compare those results with new approaches (models, parameters, etc.). These sessions will remain in the system unless there is no activity for seven days (in which case the session will be erased).

## C.1 Synthetic photometry.

- Starting point: observed magnitudes (in filters $G_i$) that are translated with the zero point $ZP$ into Jy. Thus, we have a flux density per unit of frequency, that is $F_{\nu,G_i}$. We can also use $ZP$ for $F_\lambda$ and then have another flux density (in this case $F_{\lambda,G_i}$). For each case, the flux is assigned to an effective wavelength/frequency:

$$\lambda_{\rm eff} = \frac{\int \lambda\, T(\lambda)\, d\lambda}{\int T(\lambda)\, d\lambda} \tag{C.2}$$

- The models are functions $F(\lambda)$ with values in erg/cm$^2$/s/Å, the filters are functions $G_1(\lambda)$ without physical units, but when we normalize the response curves:

$$N_1(\lambda) = G_1(\lambda) / \int_\lambda G_1(\lambda')d\lambda', \tag{C.3}$$

  this new function $N_1(\lambda)$ is no longer dimensionless, it has physical units of $\lambda^{-1}$. This is the function that we multiply by the model to obtain a synthetic flux density. So,

$$F_{\rm syn,N} = \int_\lambda F_{{\rm mod},\lambda}(\lambda) \times N_1(\lambda)d\lambda, \tag{C.4}$$

with units of erg/cm$^2$/s/Å.

- Our observational data-point corresponds to a **weighted** average of the flux observed through a filter. The process is:

  - The light ($F_*$) passes through the filter (a function with values between 0 and 1): $F_* \times G_1(\lambda)$
  - This "total amount of light" is translated into a density by dividing by the area enclosed by the filter: $\int_\lambda G_1(\lambda) d\lambda$

- To recover the total flux that was observed through the filter $G_1$, we multiply the "observed flux density" by the integral of the flux:

  $F_{\mathrm{total,G_1}} = F_{G_1} \times \int_\lambda G_1(\lambda) d\lambda.$

  This $F_{\mathrm{total,G_1}}$ has the required physical units of a flux: erg/cm$^2$/s.

- If we want to compute the bolometric correction using the model, we integrate it:

  $F_M = \int_\lambda F(\lambda) d\lambda,$

  subtract the density fluxes corresponding to each filter multiplied by the areas of the filters:

  $F_M - \sum_i (F_{syn,N_i} \times \int_\lambda G_i(\lambda) d\lambda)),$

  and add the $F_{\mathrm{total,G_i}}$ calculated in the previous step.

  This takes into the account the model in correcting for possible intersections among the filter wavelength coverage.

## C.2 Workflow.

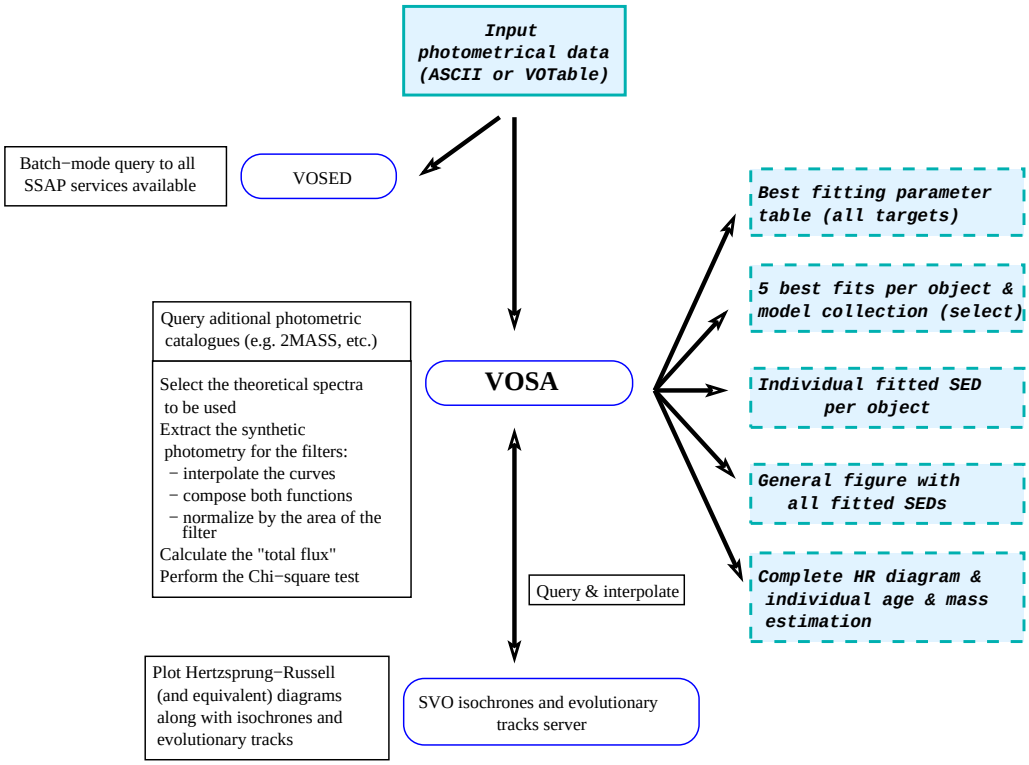


**Figure C.1**: Work-flow scheme. The shaded squares represent the input data (top) and the products obtained when the workflow has been completed (bottom-right corner, dashed box). The names of the applications used are written in rounded boxes, and the tasks performed by these applications are listed in rectangular boxes on the left hand side.

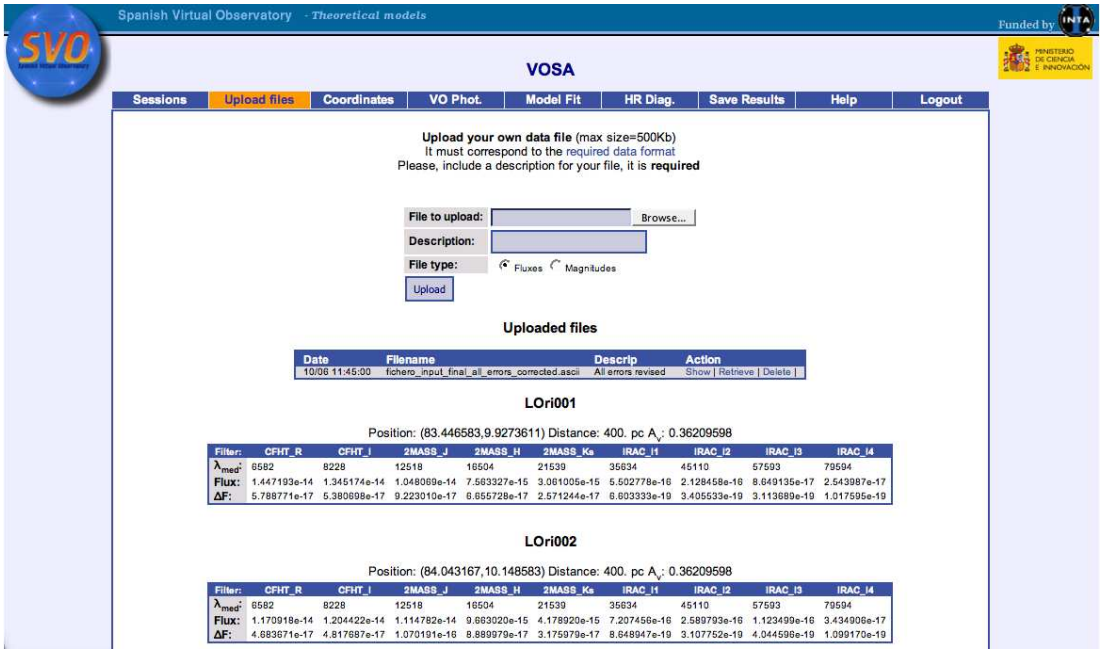


**Figure C.2**: Part of the input data in the web interface of the SVO SED fitting tool.

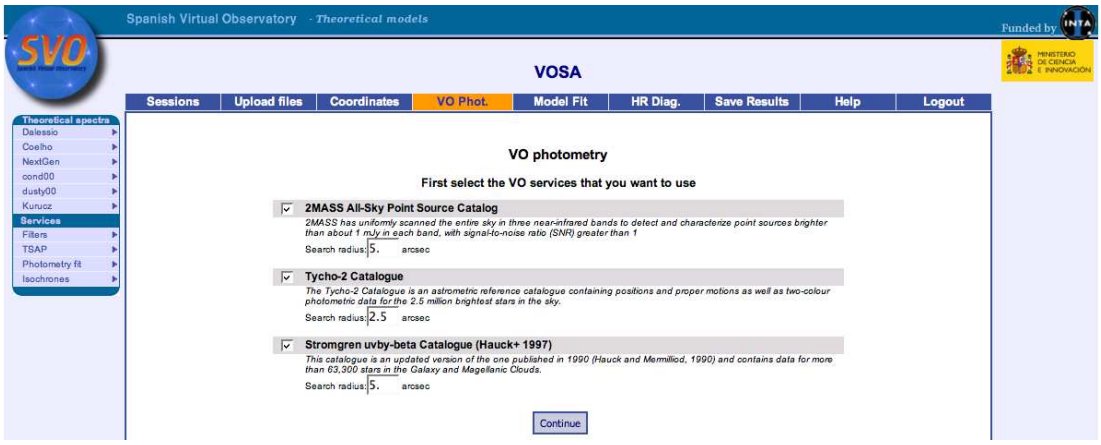


**Figure C.3**: Photometrical catalogs to be queried with the respective search radii.

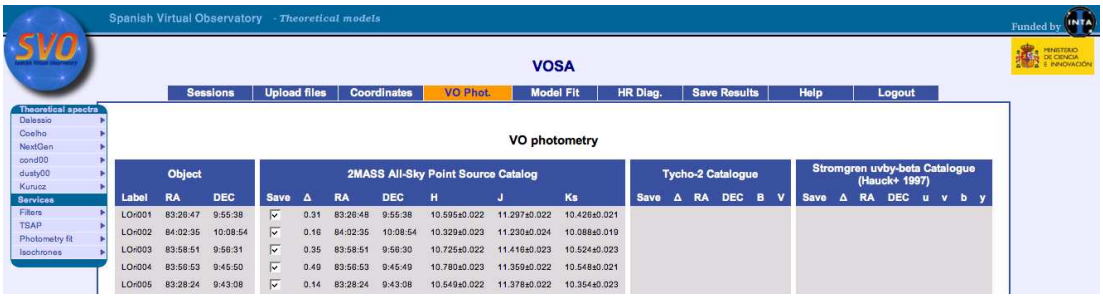


**Figure C.4**: 2MASS photometry found. We will use these JHKs measurements in those objects for which we do not have our own photometrical data.

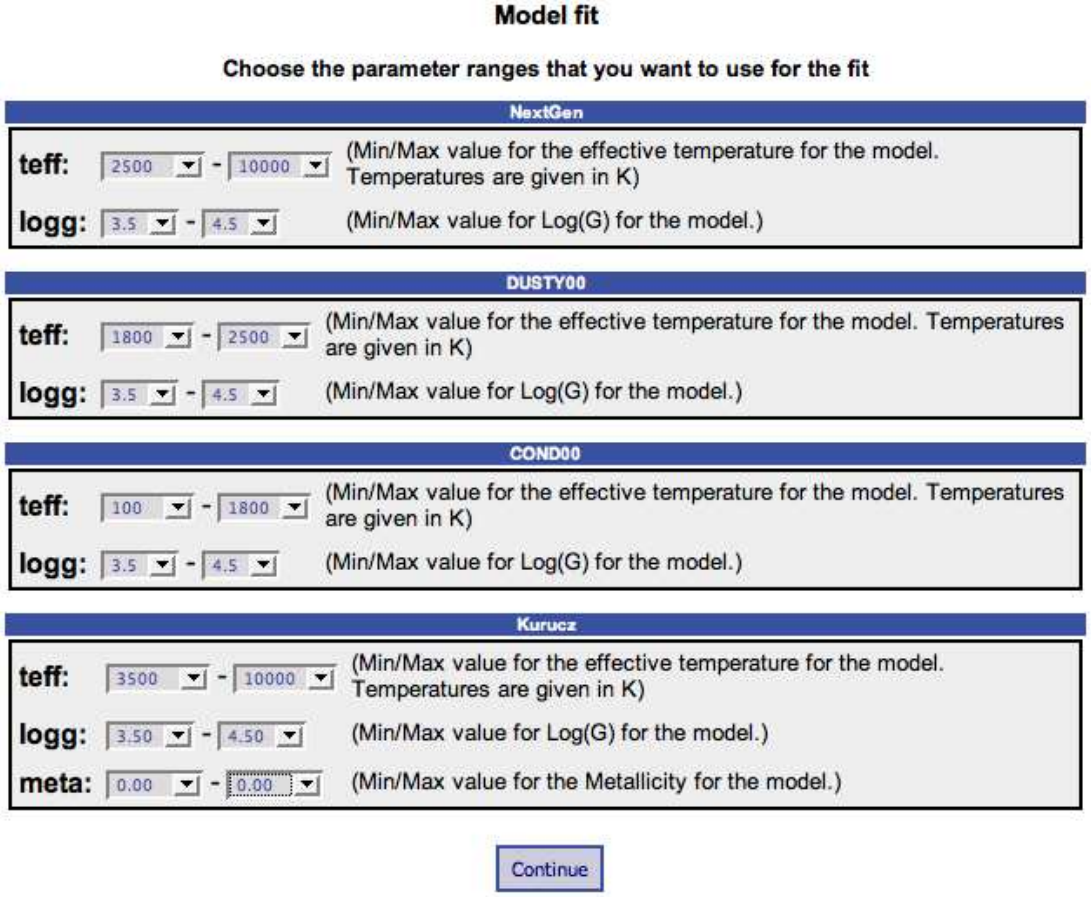


**Figure C.5**: Range of parameters queried for each collection of synthetic spectra.

**Model fit**

Hide Graphs

| Object | Model | $T_{eff}$ | LogG | Metallicity | $\chi^2$ | $M_d$ | $F_{tot}$ | $\Delta F_{tot}$ | $F_{obs}/F_{tot}$ | D (pc) | $L_{bol}/L_{sun}$ | $\Delta L_{bol}/L_{sun}$ | $\lambda_{last}$ | $N_{fit}/N_{tot}$ | Data VOtables |
|---|---|---|---|---|---|---|---|---|---|---|---|---|---|---|---|
| LOri001 | Kurucz | 4000 | 3.50 | 0.00 | 1.71e+2 | 4.02e-1 | 1.91e-10 | 5.61e-13 | 0.48 | 4.00e+2 | 9.52e-1 | 2.80e-3 | 79594 | 9/9 | Photometry \| Synth.Spectrum |
| LOri002 | NextGen | 3800 | 4.5 | 0 | 1.44e+3 | 1.75e-20 | 2.04e-10 | 6.37e-13 | 0.48 | 4.00e+2 | 1.02e+0 | 3.18e-3 | 79594 | 9/9 | Photometry \| Synth.Spectrum |
| LOri003 | Kurucz | 4000 | 3.50 | 0.00 | 5.05e+2 | 3.82e-1 | 1.76e-10 | 5.12e-13 | 0.47 | 4.00e+2 | 8.78e-1 | 2.55e-3 | 79594 | 9/9 | Photometry \| Synth.Spectrum |
| LOri004 | Kurucz | 3750 | 4.00 | 0.00 | 2.82e+2 | 4.57e-1 | 1.65e-10 | 4.91e-13 | 0.48 | 4.00e+2 | 8.23e-1 | 2.45e-3 | 79594 | 9/9 | Photometry \| Synth.Spectrum |
| LOri005 | NextGen | 4000 | 4.0 | 0 | 8.26e+2 | 1.28e-20 | 1.82e-10 | 5.47e-13 | 0.48 | 4.00e+2 | 9.10e-1 | 2.73e-3 | 79594 | 9/9 | Photometry \| Synth.Spectrum |
| LOri006 | Kurucz | 4000 | 3.50 | 0.00 | 3.36e+2 | 3.28e-1 | 1.54e-10 | 4.91e-13 | 0.47 | 4.00e+2 | 7.66e-1 | 2.45e-3 | 79594 | 9/9 | Photometry \| Synth.Spectrum |
| LOri007 | Kurucz | 4000 | 4.50 | 0.00 | 2.49e+2 | 2.81e-1 | 1.33e-10 | 4.34e-13 | 0.48 | 4.00e+2 | 6.61e-1 | 2.17e-3 | 79594 | 9/9 | Photometry \| Synth.Spectrum |
| LOri008 | Kurucz | 4000 | 3.50 | 0.00 | 4.43e+2 | 3.16e-1 | 1.49e-10 | 4.91e-13 | 0.48 | 4.00e+2 | 7.44e-1 | 2.45e-3 | 79594 | 9/9 | Photometry \| Synth.Spectrum |
| LOri009 | NextGen | 4000 | 3.5 | 0 | 6.22e+1 | 8.30e-21 | 1.19e-10 | 3.77e-13 | 0.49 | 4.00e+2 | 5.96e-1 | 1.88e-3 | 79594 | 9/9 | Photometry \| Synth.Spectrum |
| LOri010 | NextGen | 4200 | 4.0 | 0 | 1.87e+2 | 6.50e-21 | 1.15e-10 | 3.69e-13 | 0.48 | 4.00e+2 | 5.73e-1 | 1.84e-3 | 45110 | 7/9 | Photometry \| Synth.Spectrum |
| LOri011 | NextGen | 3900 | 4.5 | 0 | 1.20e+3 | 1.11e-20 | 1.41e-10 | 4.67e-13 | 0.47 | 4.00e+2 | 7.06e-1 | 2.33e-3 | 79594 | 9/9 | Photometry \| Synth.Spectrum |
| LOri012 | NextGen | 4000 | 4.5 | 0 | 6.56e+2 | 8.75e-21 | 1.25e-10 | 4.02e-13 | 0.48 | 4.00e+2 | 6.22e-1 | 2.00e-3 | 79594 | 9/9 | Photometry \| Synth.Spectrum |
| LOri013 | NextGen | 3700 | 4.5 | 0 | 3.50e+2 | 1.15e-20 | 1.23e-10 | 3.88e-13 | 0.49 | 4.00e+2 | 6.12e-1 | 1.93e-3 | 79594 | 9/9 | Photometry \| Synth.Spectrum |
| LOri014 | Kurucz | 4000 | 4.50 | 0.00 | 4.70e+1 | 2.25e-1 | 1.08e-10 | 3.48e-13 | 0.49 | 4.00e+2 | 5.37e-1 | 1.74e-3 | 79594 | 9/9 | Photometry \| Synth.Spectrum |
| LOri015 | Kurucz | 4000 | 3.50 | 0.00 | 8.73e+1 | 2.32e-1 | 1.12e-10 | 3.55e-13 | 0.49 | 4.00e+2 | 5.60e-1 | 1.77e-3 | 79594 | 9/9 | Photometry \| Synth.Spectrum |
| LOri016 | Kurucz | 3750 | 4.50 | 0.00 | 5.53e+2 | 2.78e-1 | 1.01e-10 | 3.30e-13 | 0.47 | 4.00e+2 | 5.06e-1 | 1.65e-3 | 45110 | 7/9 | Photometry \| Synth.Spectrum |
| LOri017 | NextGen | 4200 | 4.0 | 0 | 7.56e+1 | 5.16e-21 | 9.06e-11 | 2.74e-13 | 0.48 | 4.00e+2 | 4.52e-1 | 1.36e-3 | 79594 | 9/9 | Photometry \| Synth.Spectrum |
| LOri018 | Kurucz | 3750 | 3.50 | 0.00 | 4.31e+2 | 2.74e-1 | 9.86e-11 | 3.02e-13 | 0.47 | 4.00e+2 | 4.91e-1 | 1.51e-3 | 79594 | 9/9 | Photometry \| Synth.Spectrum |
| LOri019 | Kurucz | 3750 | 3.50 | 0.00 | 1.90e+2 | 2.56e-1 | 9.33e-11 | 3.04e-13 | 0.48 | 4.00e+2 | 4.65e-1 | 1.52e-3 | 79594 | 9/9 | Photometry \| Synth.Spectrum |
| LOri020 | NextGen | 3600 | 4.5 | 0 | 2.96e+2 | 1.04e-20 | 9.75e-11 | 3.52e-13 | 0.48 | 4.00e+2 | 4.86e-1 | 1.75e-3 | 79594 | 9/9 | Photometry \| Synth.Spectrum |
| LOri021 | Kurucz | 4000 | 3.50 | 0.00 | 3.08e+2 | 1.76e-1 | 8.23e-11 | 2.66e-13 | 0.47 | 4.00e+2 | 4.10e-1 | 1.33e-3 | 79594 | 9/9 | Photometry \| Synth.Spectrum |
| LOri022 | Kurucz | 3750 | 4.00 | 0.00 | 1.76e+2 | 2.33e-1 | 8.54e-11 | 2.59e-13 | 0.48 | 4.00e+2 | 4.26e-1 | 1.29e-3 | 57593 | 8/9 | Photometry \| Synth.Spectrum |
| LOri023 | NextGen | 4000 | 4.5 | 0 | 2.35e+2 | 5.80e-21 | 8.18e-11 | 2.61e-13 | 0.47 | 4.00e+2 | 4.08e-1 | 1.30e-3 | 79594 | 9/9 | Photometry \| Synth.Spectrum |
| LOri024 | Kurucz | 3750 | 3.50 | 0.00 | 2.22e+2 | 2.25e-1 | 8.23e-11 | 3.00e-13 | 0.48 | 4.00e+2 | 4.11e-1 | 1.50e-3 | 79594 | 9/9 | Photometry \| Synth.Spectrum |
| LOri025 | NextGen | 3700 | 4.5 | 0 | 1.37e+3 | 9.61e-21 | 9.45e-11 | 4.50e-13 | 0.44 | 4.00e+2 | 4.71e-1 | 2.25e-3 | 79594 | 9/9 | Photometry \| Synth.Spectrum |
| LOri026 | NextGen | 3700 | 4.5 | 0 | 4.81e+2 | 8.16e-21 | 8.63e-11 | 3.03e-13 | 0.48 | 4.00e+2 | 4.30e-1 | 1.51e-3 | 79594 | 9/9 | Photometry \| Synth.Spectrum |
| LOri027 | NextGen | 4000 | 4.5 | 0 | 2.35e+2 | 4.90e-21 | 7.03e-11 | 2.22e-13 | 0.48 | 4.00e+2 | 3.51e-1 | 1.11e-3 | 79594 | 9/9 | Photometry \| Synth.Spectrum |
| LOri028 | Kurucz | 3750 | 4.00 | 0.00 | 1.26e+2 | 1.58e-1 | 5.87e-11 | 1.85e-13 | 0.49 | 4.00e+2 | 2.93e-1 | 9.22e-4 | 79594 | 9/9 | Photometry \| Synth.Spectrum |
| LOri029 | NextGen | 3100 | 4.5 | 0 | 7.28e+3 | 1.94e-20 | 9.01e-11 | 2.54e-13 | 0.40 | 4.00e+2 | 4.49e-1 | 1.27e-3 | 35634 | 6/10 | Photometry \| Synth.Spectrum |
| LOri030 | NextGen | 3700 | 4.5 | 0 | 2.15e+2 | 6.10e-21 | 6.39e-11 | 2.22e-13 | 0.48 | 4.00e+2 | 3.19e-1 | 1.11e-3 | 79594 | 9/9 | Photometry \| Synth.Spectrum |
| LOri031 | NextGen | 3800 | 4.5 | 0 | 2.77e+2 | 5.65e-21 | 6.52e-11 | 2.24e-13 | 0.47 | 4.00e+2 | 3.25e-1 | 1.12e-3 | 79594 | 9/9 | Photometry \| Synth.Spectrum |
| LOri032 | NextGen | 3700 | 4.5 | 0 | 1.70e+2 | 5.76e-21 | 6.09e-11 | 2.10e-13 | 0.48 | 4.00e+2 | 3.04e-1 | 1.05e-3 | 79594 | 9/9 | Photometry \| Synth.Spectrum |
| LOri033 | NextGen | 3700 | 4.5 | 0 | 7.12e+2 | 6.25e-21 | 6.37e-11 | 2.69e-13 | 0.46 | 4.00e+2 | 3.17e-1 | 1.34e-3 | 79594 | 9/9 | Photometry \| Synth.Spectrum |
| LOri034 | NextGen | 3000 | 4.0 | 0 | 1.77e+4 | 2.27e-20 | 8.66e-11 | 2.16e-13 | 0.36 | 4.00e+2 | 4.32e-1 | 1.08e-3 | 35634 | 6/10 | Photometry \| Synth.Spectrum |
| LOri035 | NextGen | 3700 | 4.5 | 0 | 1.61e+2 | 5.09e-21 | 5.35e-11 | 1.82e-13 | 0.48 | 4.00e+2 | 2.67e-1 | 9.09e-4 | 79594 | 9/9 | Photometry \| Synth.Spectrum |

**Figure C.6**: Several rows of the "master-table" with all the fittings.

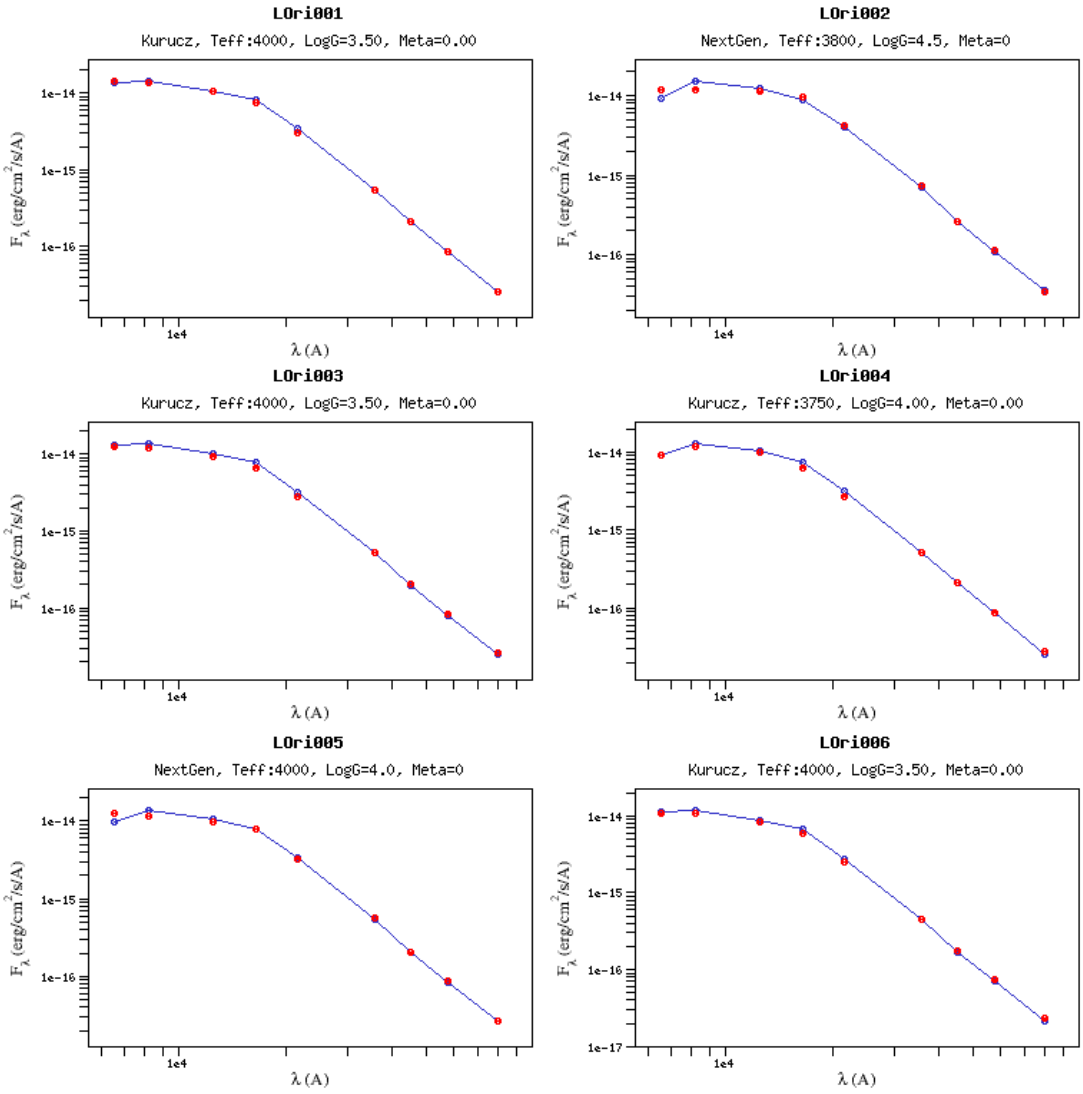


**Figure C.7**: First page from the graphical results output.

LOri086

| Model | $T_{eff}$ | LogG | Metallicity | $X^2$ | $M_d$ | $F_{tot}$ | $\Delta F_{tot}$ | $F_{obs}/F_{tot}$ | D (pc) | $L_{bol}/L_{sun}$ | $\Delta L_{bol}/L_{sun}$ | $\lambda_{last}$ | $N_{fit}/N_{tot}$ | Action |
|---|---|---|---|---|---|---|---|---|---|---|---|---|---|---|
| **NextGen** | **3400** | **4.5** | **0** | **9.18e+1** | **1.08e-21** | **8.14e-12** | **4.09e-14** | **0.49** | **4.00e+2** | **4.06e-2** | **2.04e-4** | **79594** | **9/9** | Best \| See \| |
| NextGen | 3500 | 4.5 | 0 | 1.40e+2 | 9.38e-22 | 8.06e-12 | 4.09e-14 | 0.49 | 4.00e+2 | 4.02e-2 | 2.04e-4 | 79594 | 9/9 | Best \| See \| |
| NextGen | 3600 | 4.0 | 0 | 2.41e+2 | 9.16e-22 | 8.48e-12 | 4.09e-14 | 0.47 | 4.00e+2 | 4.23e-2 | 2.04e-4 | 79594 | 9/9 | Best \| See \| |
| NextGen | 3700 | 4.0 | 0 | 2.91e+2 | 8.09e-22 | 8.44e-12 | 4.09e-14 | 0.47 | 4.00e+2 | 4.21e-2 | 2.04e-4 | 79594 | 9/9 | Best \| See \| |
| NextGen | 3500 | 4.0 | 0 | 3.68e+2 | 1.02e-21 | 8.45e-12 | 4.09e-14 | 0.47 | 4.00e+2 | 4.21e-2 | 2.04e-4 | 79594 | 9/9 | Best \| See \| |
| Kurucz | 3500 | 3.50 | 0.00 | 5.98e+2 | 2.88e-2 | 8.10e-12 | 4.09e-14 | 0.49 | 4.00e+2 | 4.04e-2 | 2.04e-4 | 79594 | 9/9 | Best \| See \| |
| Kurucz | 3500 | 4.00 | 0.00 | 1.18e+3 | 2.67e-2 | 7.81e-12 | 4.09e-14 | 0.51 | 4.00e+2 | 3.89e-2 | 2.04e-4 | 79594 | 9/9 | Best \| See \| |
| Kurucz | 3500 | 4.50 | 0.00 | 1.99e+3 | 2.46e-2 | 7.50e-12 | 4.09e-14 | 0.53 | 4.00e+2 | 3.74e-2 | 2.04e-4 | 79594 | 9/9 | Best \| See \| |
| Kurucz | 3750 | 3.50 | 0.00 | 3.14e+3 | 1.77e-2 | 7.34e-12 | 4.09e-14 | 0.54 | 4.00e+2 | 3.66e-2 | 2.04e-4 | 79594 | 9/9 | Best \| See \| |
| Kurucz | 3750 | 4.00 | 0.00 | 3.70e+3 | 1.70e-2 | 7.20e-12 | 4.09e-14 | 0.55 | 4.00e+2 | 3.59e-2 | 2.04e-4 | 79594 | 9/9 | Best \| See \| |
| DUSTY00 | 2500 | 4.5 | 0 | 1.01e+4 | 2.94e-21 | 7.10e-12 | 4.09e-14 | 0.56 | 4.00e+2 | 3.54e-2 | 2.04e-4 | 79594 | 9/9 | Best \| See \| |
| DUSTY00 | 2500 | 4.0 | 0 | 1.02e+4 | 2.93e-21 | 7.12e-12 | 4.09e-14 | 0.56 | 4.00e+2 | 3.55e-2 | 2.04e-4 | 79594 | 9/9 | Best \| See \| |
| DUSTY00 | 2500 | 3.5 | 0 | 1.03e+4 | 2.92e-21 | 7.13e-12 | 4.09e-14 | 0.56 | 4.00e+2 | 3.56e-2 | 2.04e-4 | 79594 | 9/9 | Best \| See \| |
| DUSTY00 | 2400 | 4.5 | 0 | 1.16e+4 | 3.23e-21 | 6.85e-12 | 4.09e-14 | 0.58 | 4.00e+2 | 3.41e-2 | 2.04e-4 | 79594 | 9/9 | Best \| See \| |
| DUSTY00 | 2400 | 4.0 | 0 | 1.17e+4 | 3.20e-21 | 6.88e-12 | 4.09e-14 | 0.58 | 4.00e+2 | 3.43e-2 | 2.04e-4 | 79594 | 9/9 | Best \| See \| |
| COND00 | 1800 | 4.0 | 0 | 1.63e+4 | 7.24e-21 | 5.80e-12 | 4.09e-14 | 0.69 | 4.00e+2 | 2.89e-2 | 2.04e-4 | 79594 | 9/9 | Best \| See \| |
| COND00 | 1800 | 4.5 | 0 | 1.64e+4 | 7.33e-21 | 5.83e-12 | 4.09e-14 | 0.68 | 4.00e+2 | 2.91e-2 | 2.04e-4 | 79594 | 9/9 | Best \| See \| |
| COND00 | 1800 | 3.5 | 0 | 1.65e+4 | 7.12e-21 | 5.78e-12 | 4.09e-14 | 0.69 | 4.00e+2 | 2.88e-2 | 2.04e-4 | 79594 | 9/9 | Best \| See \| |
| COND00 | 1600 | 3.5 | 0 | 1.68e+4 | 1.01e-20 | 5.47e-12 | 4.09e-14 | 0.73 | 4.00e+2 | 2.73e-2 | 2.04e-4 | 79594 | 9/9 | Best \| See \| |
| COND00 | 1700 | 4.0 | 0 | 1.70e+4 | 8.45e-21 | 5.63e-12 | 4.09e-14 | 0.71 | 4.00e+2 | 2.81e-2 | 2.04e-4 | 79594 | 9/9 | Best \| See \| |

**Figure C.8**: Example of the "small table" showing the 20 best fits for an individual object (LOri086).

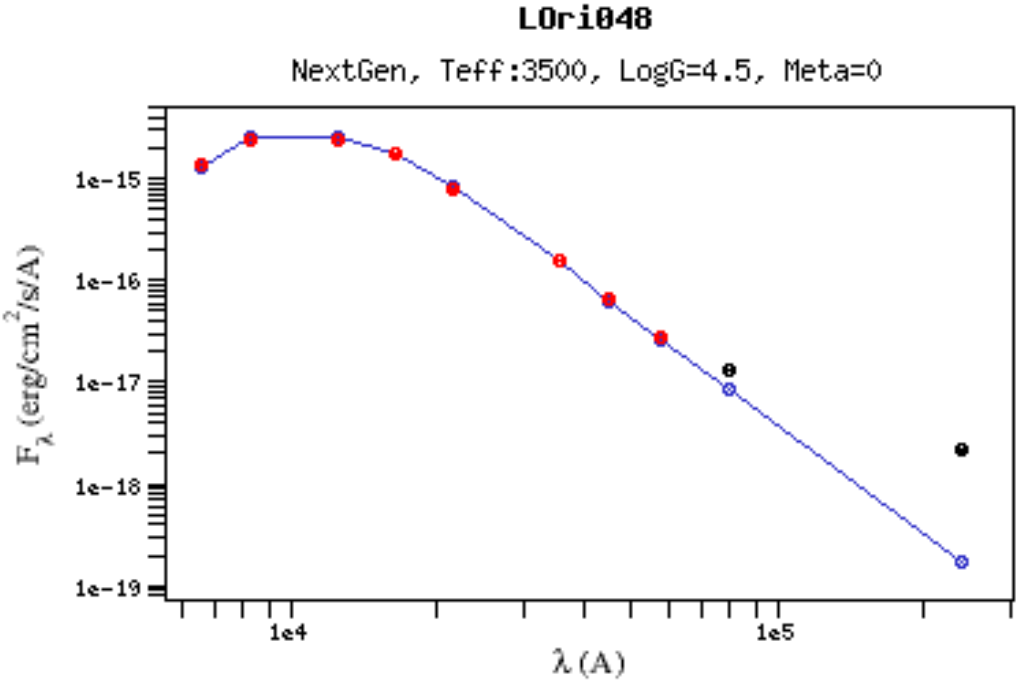


**Figure C.9**: Graphical output from VOSA for a source with infrared excess (LOri048). The black dots highlight those data points not considered when performing the fitting process.

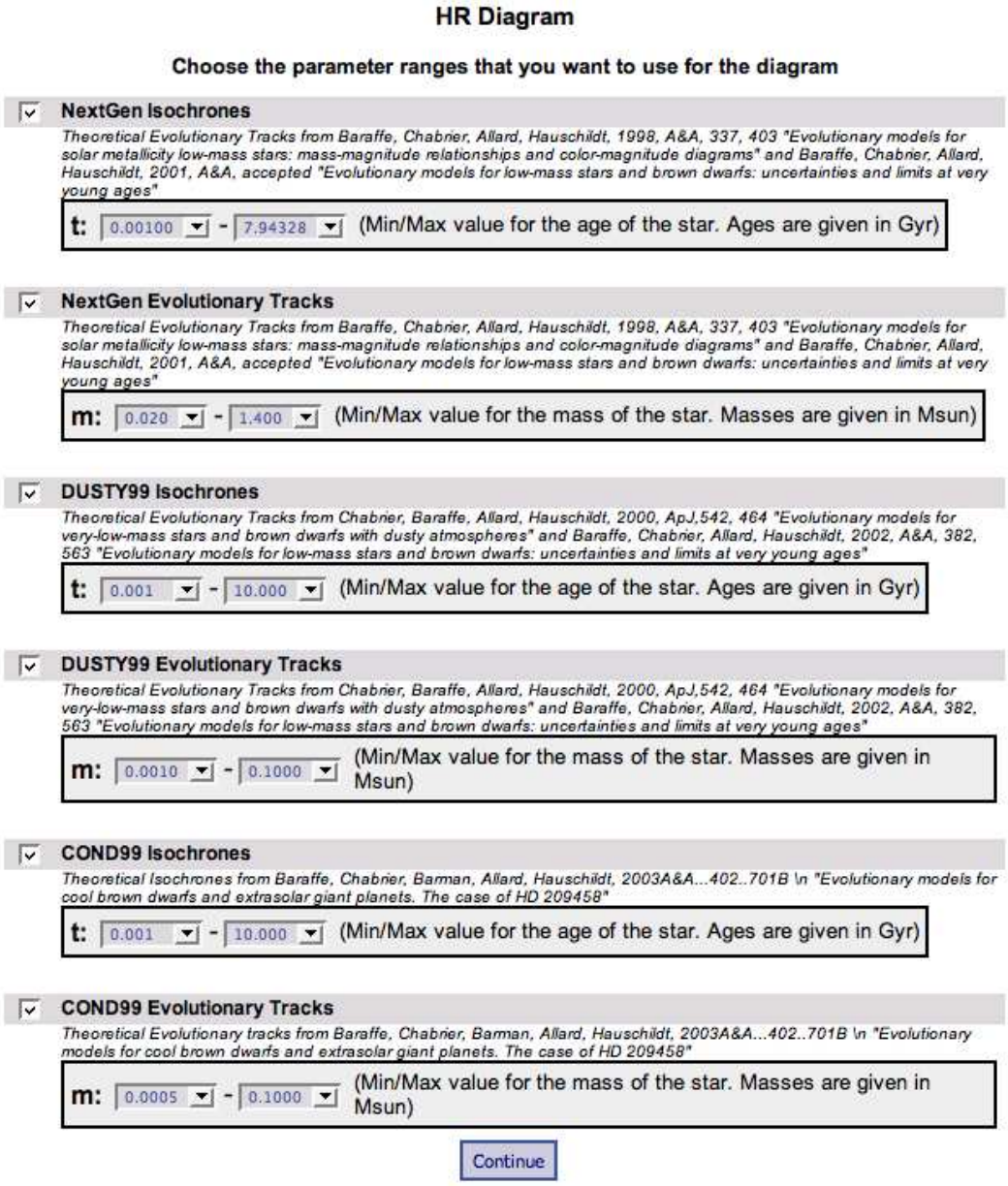


**Figure C.10**: Range of parameters queried for each collection of isochrones and evolutionary tracks.

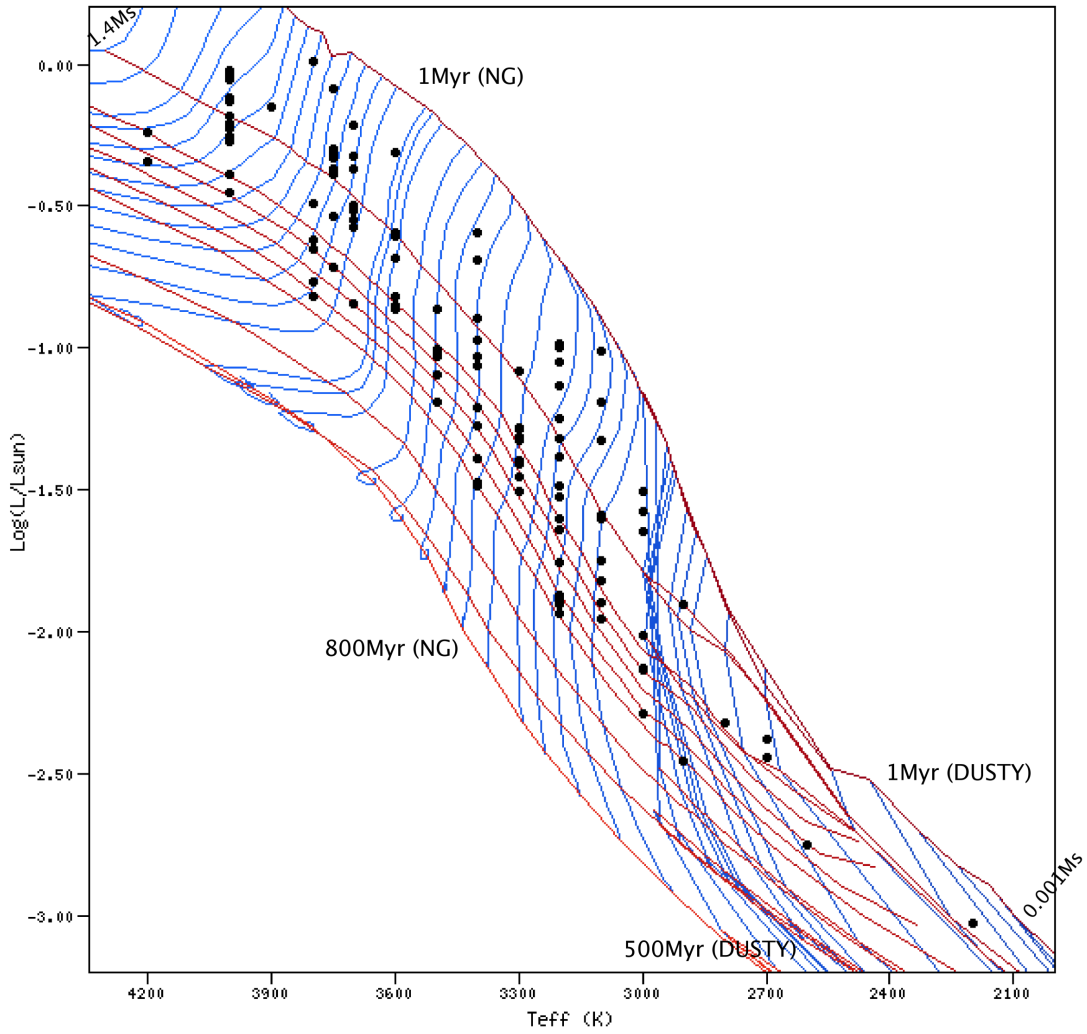


**Figure C.11**: HR diagram of the members of Collinder 69 for which no infrared excess was detected. Isochrones corresponding to ages of 1, 5, 10, 12.5, 16, 20, 25, 50, 100 and 800 Myrs are displayed for the NextGen collection, and those corresponding to ages of 1, 5, 10, 50, 100,120 and 500 Myr for the DUSTY collection. Evolutionary tracks are also displayed for masses between $0.001M_{\odot}$ and $1.4M_{\odot}$ (including both, NextGen and DUSTY collections).

# Bibliography

Adams, F. C., Lada, C. J., & Shu, F. H. 1987, ApJ, 312, 788

Allard, F., Guillot, T., Ludwig, H.-G., et al. 2003, in IAU Symposium, Vol. 211, Brown Dwarfs, ed. E. Martín, 325–+

Allen, L. E., Calvet, N., D'Alessio, P., et al. 2004, ApJS, 154, 363

Andre, P. & Montmerle, T. 1994, ApJ, 420, 837

Andre, P., Ward-Thompson, D., & Barsony, M. 1993, ApJ, 406, 122

Baraffe, I., Chabrier, G., Allard, F., & Hauschildt, P. 1998, VizieR Online Data Catalog, 333, 70403

Baraffe, I., Chabrier, G., Allard, F., & Hauschildt, P. H. 2002, A&A, 382, 563

Baraffe, I., Chabrier, G., Barman, T. S., Allard, F., & Hauschildt, P. H. 2003, A&A, 402, 701

Barrado y Navascués, D. 2006, A&A, 459, 511

Barrado y Navascués, D., Bayo, A., Morales-Calderón, M., et al. 2007a, A&A, 468, L5

Barrado y Navascués, D., Béjar, V. J. S., Mundt, R., et al. 2003, A&A, 404, 171

Barrado y Navascués, D., García López, R. J., Severino, G., & Gomez, M. T. 2001, A&A, 371, 652

Barrado y Navascués, D. & Martín, E. L. 2003, AJ, 126, 2997

Barrado y Navascués, D., Mohanty, S., & Jayawardhana, R. 2004a, ApJ, 604, 284

Barrado y Navascués, D., Stauffer, J. R., Bouvier, J., Jayawardhana, R., & Cuillandre, J.-C. 2004b, ApJ, 610, 1064

Barrado y Navascués, D., Stauffer, J. R., Morales-Calderón, M., et al. 2007b, ApJ, 664, 481

Barrado y Navascués, D., Zapatero Osorio, M. R., Martín, E. L., et al. 2002, A&A, 393, L85

Basri, G. 1997, Memorie della Societa Astronomica Italiana, 68, 917

Basri, G., Mohanty, S., Allard, F., et al. 2000, ApJ, 538, 363

Béjar, V. J. S., Martín, E. L., Zapatero Osorio, M. R., et al. 2001, ApJ, 556, 830

Bessell, M. S. 1991, AJ, 101, 662

Bildsten, L., Brown, E. F., Matzner, C. D., & Ushomirsky, G. 1997, ApJ, 482, 442

Bontemps, S., Andre, P., Terebey, S., & Cabrit, S. 1996, A&A, 311, 858

Bouvier, J., Stauffer, J. R., Martin, E. L., et al. 1998, A&A, 336, 490

Bouy, H., Huelamo, N., Barrado y Navascues, D., et al. 2009a, ArXiv e-prints

Bouy, H., Huélamo, N., Martín, E. L., et al. 2009b, A&A, 493, 931

Bromm, V. & Larson, R. B. 2004, ARA&A, 42, 79

Burgasser, A. J. 2002, PhD thesis, AA(CALIFORNIA INSTITUTE OF TECHNOLOGY)

Burgasser, A. J., Kirkpatrick, J. D., Brown, M. E., et al. 2002, ApJ, 564, 421

Burgasser, A. J., Tinney, C. G., Cushing, M. C., et al. 2008, ApJ, 689, L53

Burrows, A., Marley, M., Hubbard, W. B., et al. 1997, ApJ, 491, 856

Caballero, J. A., López-Santiago, J., de Castro, E., & Cornide, M. 2009, AJ, 137, 5012

Calvet, N., Muzerolle, J., Briceño, C., et al. 2004, AJ, 128, 1294

Cambresy, L., Epchtein, N., Copet, E., et al. 1997, A&A, 324, L5

Casagrande, L., Flynn, C., & Bessell, M. 2008, MNRAS, 389, 585

Chabrier, G. & Baraffe, I. 1997, A&A, 327, 1039

Chabrier, G., Baraffe, I., Allard, F., & Hauschildt, P. 2000, ApJ, 542, 464

Chen, H., Myers, P. C., Ladd, E. F., & Wood, D. O. S. 1995, ApJ, 445, 377

Cohen, M., Wheaton, W. A., & Megeath, S. T. 2003, AJ, 126, 1090

Comerón, F., Fernández, M., Baraffe, I., Neuhäuser, R., & Kaas, A. A. 2003, A&A, 406, 1001

Comerón, F., Neuhäuser, R., & Kaas, A. A. 2000, A&A, 359, 269

Cruz, K. L. & Reid, I. N. 2002, AJ, 123, 2828

Danks, A. C. & Dennefeld, M. 1994, PASP, 106, 382

Dolan, C. J. & Mathieu, R. D. 1999, AJ, 118, 2409

Dolan, C. J. & Mathieu, R. D. 2001, AJ, 121, 2124

Dolan, C. J. & Mathieu, R. D. 2002, AJ, 123, 387

Duerr, R., Imhoff, C. L., & Lada, C. J. 1982, ApJ, 261, 135

Dunham, M. M., Crapsi, A., Evans, II, N. J., et al. 2008, ApJS, 179, 249

Epchtein, N., Deul, E., Derriere, S., et al. 1999, A&A, 349, 236

Fazio, G. G., Hora, J. L., Allen, L. E., et al. 2004, ApJS, 154, 10

Fernández, M. & Comerón, F. 2001, A&A, 380, 264

Finkbeiner, D. P. 2003, ApJS, 146, 407

Fitzpatrick, E. L. 1999, PASP, 111, 63

Geballe, T. R., Knapp, G. R., Leggett, S. K., et al. 2002, ApJ, 564, 466

Gomez, M. & Lada, C. J. 1998, AJ, 115, 1524

Gómez, M. & Persi, P. 2002, A&A, 389, 494

González Hernández, J. I., Caballero, J. A., Rebolo, R., et al. 2008, A&A, 490, 1135

Goodman, J. 1993, ApJ, 406, 596

Hartmann, L. 1999, Physics Today, 52, 60

Hartmann, L., Hewett, R., & Calvet, N. 1994, ApJ, 426, 669

Hartmann, L., Megeath, S. T., Allen, L., et al. 2005, ApJ, 629, 881

Hauck, B. & Mermilliod, M. 1998, A&AS, 129, 431

Høg, E., Fabricius, C., Makarov, V. V., et al. 2000, A&A, 355, L27

Indebetouw, R., Mathis, J. S., Babler, B. L., et al. 2005, ApJ, 619, 931

Irwin, M. & Lewis, J. 2001, New Astronomy Review, 45, 105

Jansen, F., Lumb, D., Altieri, B., et al. 2001, A&A, 365, L1

Jayawardhana, R., Ardila, D. R., Stelzer, B., & Haisch, Jr., K. E. 2003a, AJ, 126, 1515

Jayawardhana, R., Luhman, K. L., D'Alessio, P., & Stauffer, J. R. 2002a, ApJ, 571, L51

Jayawardhana, R., Mohanty, S., & Basri, G. 2002b, ApJ, 578, L141

Jayawardhana, R., Mohanty, S., & Basri, G. 2003b, ApJ, 592, 282

Joergens, V. & Guenther, E. 2001, A&A, 379, L9

Jones, H. R. A., Longmore, A. J., Jameson, R. F., & Mountain, C. M. 1994, MNRAS, 267, 413

Kenyon, S. J. & Hartmann, L. 1995, ApJS, 101, 117

Kirkpatrick, J. D., Henry, T. J., & McCarthy, Jr., D. W. 1991, ApJS, 77, 417

Kirkpatrick, J. D., Reid, I. N., Liebert, J., et al. 1999, ApJ, 519, 802

Kirkpatrick, J. D., Reid, I. N., Liebert, J., et al. 2000, AJ, 120, 447

Lada, C. J. 1987, in IAU Symposium, Vol. 115, Star Forming Regions, ed. M. Peimbert & J. Jugaku, 1–17

Lada, C. J., Muench, A. A., Luhman, K. L., et al. 2006, AJ, 131, 1574

Lawson, W. A., Feigelson, E. D., & Huenemoerder, D. P. 1996, MNRAS, 280, 1071

Leggett, S. K. 1992, ApJS, 82, 351

Leggett, S. K., Allard, F., Berriman, G., Dahn, C. C., & Hauschildt, P. H. 1996, ApJS, 104, 117

Leggett, S. K., Allard, F., Dahn, C., et al. 2000, ApJ, 535, 965

Leggett, S. K., Allard, F., Geballe, T. R., Hauschildt, P. H., & Schweitzer, A. 2001, ApJ, 548, 908

Lonsdale, C. J., Smith, H. E., Rowan-Robinson, M., et al. 2003, PASP, 115, 897

Luhman, K. L. 1999, ApJ, 525, 466

Luhman, K. L., Adame, L., D'Alessio, P., et al. 2007, ApJ, 666, 1219

Luhman, K. L., Stauffer, J. R., Muench, A. A., et al. 2003, ApJ, 593, 1093

Makovoz, D. & Khan, I. 2005, in Astronomical Society of the Pacific Conference Series, Vol. 347, Astronomical Data Analysis Software and Systems XIV, ed. P. Shopbell, M. Britton, & R. Ebert, 81–+

Margulis, M. & Snell, R. L. 1989, ApJ, 343, 779

Martin, E. L. 1997, A&A, 321, 492

Martín, E. L., Delfosse, X., Basri, G., et al. 1999, AJ, 118, 2466

Martín, E. L., Dougados, C., Magnier, E., et al. 2001, ApJ, 561, L195

Martín, E. L. & Magazzù, A. 1999, A&A, 342, 173

Martin, E. L., Rebolo, R., & Zapatero-Osorio, M. R. 1996, ApJ, 469, 706

Mason, K. O., Breeveld, A., Much, R., et al. 2001, A&A, 365, L36

Massey, P. 2003, ARA&A, 41, 15

Maury, A. C. & Pickering, E. C. 1897, Annals of Harvard College Observatory, 28, 1

Maxted, P. F. L., Jeffries, R. D., Oliveira, J. M., Naylor, T., & Jackson, R. J. 2008, MNRAS, 385, 2210

McMahon, R. G., Walton, N. A., Irwin, M. J., et al. 2001, New Astronomy Review, 45, 97

Miyazaki, S., Komiyama, Y., Sekiguchi, M., et al. 2002, PASJ, 54, 833

Mohanty, S. & Basri, G. 2003, ApJ, 583, 451

Mohanty, S., Basri, G., & Jayawardhana, R. 2005, Astronomische Nachrichten, 326, 891

Mohanty, S., Jayawardhana, R., & Barrado y Navascués, D. 2003, ApJ, 593, L109

Mohanty, S., Jayawardhana, R., Huelamo, N., & Mamajek, E. 2007, ApJ, in press

Morales-Calderón, M. 2008, PhD thesis, UNIVERSIDAD AUTÓNOMA DE MADRID

Morgan, W. W., Keenan, P. C., & Kellman, E. 1943, An atlas of stellar spectra, with an outline of spectral classification (Chicago, Ill., The University of Chicago press [1943])

Mouschovias, T. C. 1991, NATO ASIC, Proc. 342, 449

Murdin, P. & Penston, M. V. 1977, MNRAS, 181, 657

Muzerolle, J., Hartmann, L., & Calvet, N. 1998, AJ, 116, 455

Muzerolle, J., Luhman, K. L., Briceño, C., Hartmann, L., & Calvet, N. 2005, ApJ, 625, 906

Myers, P. C., Adams, F. C., Chen, H., & Schaff, E. 1998, ApJ, 492, 703

Myers, P. C. & Ladd, E. F. 1993, ApJ, 413, L47

Nakajima, T., Oppenheimer, B. R., Kulkarni, S. R., et al. 1995, Nature, 378, 463

Natta, A. & Testi, L. 2001, A&A, 376, L22

Natta, A., Testi, L., Comerón, F., et al. 2002, A&A, 393, 597

Natta, A., Testi, L., Muzerolle, J., et al. 2004, A&A, 424, 603

Natta, A., Testi, L., & Randich, S. 2006, A&A, 452, 245

Neuhaeuser, R., Wolk, S. J., Torres, G., et al. 1998, A&A, 334, 873

Oliva, E. & Origlia, L. 1992, A&A, 254, 466

Oppenheimer, B. R., Kulkarni, S. R., Matthews, K., & Nakajima, T. 1995, Science, 270, 1478

Padoan, P. & Nordlund, Å. 2002, ApJ, 576, 870

Padovani, P., Allen, M. G., Rosati, P., & Walton, N. A. 2004, A&A, 424, 545

Pasquini, L., Avila, G., Blecha, A., et al. 2002, The Messenger, 110, 1

Perryman, M. A. C., Lindegren, L., Kovalevsky, J., et al. 1997, A&A, 323, L49

Pickering, E. C. 1890, Annals of Harvard College Observatory, 27, 1

Pontoppidan, K. M., Dullemond, C. P., van Dishoeck, E. F., et al. 2005, ApJ, 622, 463

Rebolo, R., Martin, E. L., & Magazzu, A. 1992, ApJ, 389, L83

Reid, I. N., Burgasser, A. J., Cruz, K. L., Kirkpatrick, J. D., & Gizis, J. E. 2001, AJ, 121, 1710

Reid, I. N., Hawley, S. L., & Gizis, J. E. 1995, AJ, 110, 1838

Reid, I. N., Kirkpatrick, J. D., Gizis, J. E., et al. 2000, AJ, 119, 369

Reipurth, B. & Clarke, C. 2001, AJ, 122, 432

Rieke, G. H., Young, E. T., Engelbracht, C. W., et al. 2004, ApJS, 154, 25

Sacco, G. G., Franciosini, E., Randich, S., & Pallavicini, R. 2008, A&A, 488, 167

Santiago, B. X., Gilmore, G., & Elson, R. A. W. 1996, MNRAS, 281, 871

Schiavon, R. P., Barbuy, B., Rossi, S. C. F., & Milone, A. 1997, ApJ, 479, 902

Scholz, A., Geers, V., Jayawardhana, R., et al. 2009, ApJ, 702, 805

Shu, F. H., Adams, F. C., & Lizano, S. 1987, ARA&A, 25, 23

Shu, F. H., Najita, J., Ruden, S. P., & Lizano, S. 1994, ApJ, 429, 797

Siess, L., Dufour, E., & Forestini, M. 2000, A&A, 358, 593

Skrutskie, M. F., Cutri, R. M., Stiening, R., et al. 2006, AJ, 131, 1163

Strüder, L., Briel, U., Dennerl, K., et al. 2001, A&A, 365, L18

Terebey, S., Shu, F. H., & Cassen, P. 1984, ApJ, 286, 529

Testi, L., Natta, A., Oliva, E., et al. 2002, ApJ, 571, L155

Tinney, C. G., Mould, J. R., & Reid, I. N. 1993, AJ, 105, 1045

Tsalmantza, P., Kontizas, E., Cambrésy, L., et al. 2006, A&A, 447, 89

Turner, M. J. L., Abbey, A., Arnaud, M., et al. 2001, A&A, 365, L27

Vacca, W. D., Cushing, M. C., & Rayner, J. T. 2003, PASP, 115, 389

Ventura, P., Zeppieri, A., Mazzitelli, I., & D'Antona, F. 1998, A&A, 331, 1011

Wade, C. M. 1958, Australian Journal of Physics, 11, 388

Wainscoat, R. J., Cohen, M., Volk, K., Walker, H. J., & Schwartz, D. E. 1992, ApJS, 83, 111

White, R. J. & Basri, G. 2003, ApJ, 582, 1109

Wilking, B. A., Greene, T. P., & Meyer, M. R. 1999, AJ, 117, 469

York, D. G., Adelman, J., Anderson, Jr., J. E., et al. 2000, AJ, 120, 1579

Young, K. E., Harvey, P. M., Brooke, T. Y., et al. 2005, ApJ, 628, 283

Zapatero Osorio, M. R., Béjar, V. J. S., Bihain, G., et al. 2008, A&A, 477, 895

Zapatero Osorio, M. R., Béjar, V. J. S., Pavlenko, Y., et al. 2002, A&A, 384, 937

Zhang, C. Y., Laureijs, R. J., Chlewicki, G., Wesselius, P. R., & Clark, F. O. 1989, A&A, 218, 231